Formation of carbonate mounds in the Porcupine Basin, offshore Ireland: evaluating transport of substrates for microbial processes from deep sources using numerical simulation and organic geochemistry

Dipl.-Geol.

Jochen Naeth

aus Aachen

Von der Fakultät VI – Bauingenieurwesen und Angewandte Geowissenschaften
der Technischen Universität Berlin
zur Erlangung des akademischen Grades eines Doktors der
Naturwissenschaften
– Dr. rer. nat. –
genehmigte Dissertation

Promotionsausschuss:

Vorsitzender:	Prof. Dr. Johannes H. Schroeder
Berichter:	Prof. Dr. Brian Horsfield
Berichter:	Prof. Dr. Ralf Littke (RWTH Aachen)
Berichter:	Prof. Dr. Wilhelm Dominik

Tag der wissenschaftlichen Aussprache: 17.11.2003

Berlin 2004

D83

Acknowledgment

This dissertation was carried out in the framework of the EU-Project “Geomound”. I would like to thank Prof. Brian Horsfield who initiated the project, supervised this study and helped to direct the research towards success by numerous discussions and informative reviews of reports, presentations and manuscripts. Prof. Ralf Littke is acknowledged for petrographical supervision and for reviewing this dissertation.

This work would not have been possible without the most patient help and support of Dr. Rolando di Primio at the GFZ during the evaluation of the basin model and the preparation of several abstracts, reports, manuscripts and last but not least this thesis.

Thanks are extended to all my colleagues at the GFZ, in particular to Dr. Volker Dieckmann who helped me much on the kinetics, to Dr. Kai Mangelsdorf for the discussions and analytical help on the biomarkers. Also gratefully acknowledged are my colleagues Thomas Fischer, Raingard Haberer, Marina Kloppisch and Volkmar Neumann for the numerous discussions on partially non scientific issues and who have made my time in Jülich and Berlin so enjoyable.

My thanks go to the head of the institut Prof. G. H. Schleser at the FZJ. I would like to thank Dr. Rainer G. Schaefer at FZJ for his support on the geochemical analysis and organisational questions. Also the Technical Staff at the FZJ especially Franz Leistner and Helmut Willsch are acknowledged for their support in developing and establishing the static and dynamic headspace gas chromatography. Also I would like to thank W. Benders for his help in preparation and accomplishment of the organic petrology.

Acknowledged is the help of all Geomound partners especially to Prof. J. P. Henriet (University of Gent) for the Project Coordination, Prof. Patrick M. Shannon (University of Dublin) and his co-workers Wayne Bailey, Angela McDonnell and Vikram Unnithan for their help on the seismic sections and a good time in Dublin.

I am grateful to IES Jülich, who allowed me to use their software during my time at the FZJ and the support of Prof. Dr. D. H. Welte, Dr. Thomas Hantschel, Christof Keuser and Dr. Björn Wygralla in building the model and for the possibility to work for IES. My thanks go to all my former colleagues for this time.

This thesis would never have been completed without the help and support of my parents. Also I would like to thank for the invaluable assistance of my siblings Angelika, Bernd und Gudrun, of my godmother Angela Koelman and of all my friends Christian Brinzer, Tanja Freudenreich, Eva Gerick, Michael Weißleder and Dirk Wynands who always managed to get my mind off scientific problems. Last but not least heartfelt thanks to Ina Zellmann for being there when I needed it most.

Deutsche Zusammenfassung

Diese Dissertation beschäftigt sich mit dem Zusammenhang von aktiver Kohlenwasserstoffleckage und dem Wachstum von Tiefseekorallen am Kontinentalrand des Nordatlantiks. Gegenstand der Untersuchung sind rezente und begrabene Karbonathügel im Porcupine Becken, 200km westlich von Irland. Die Karbonathügel sind bis zu 3 km lang und 600 m hoch und auf zwei Provinzen begrenzt, der Hovland-Magellan-mound Provinz am nördlichen und der Belgica-mound Provinz am östlichen Hang des Beckens. Die Form der Hügel variiert von hauptsächlich gestreckt bis kreisförmig. Sie bestehen hauptsächlich aus Korallen, Karbonatkrusten und fein gekörnten klastischen Sedimenten.

Um den möglichen Bezug von Kohlenwasserstoffleckage und Korallenwachstum zu evaluieren, wurden 2D Beckenmodellierungen sowie die geochemische Analyse von Sedimenten aus Schwerkraftkernen benutzt. Zwei Nord-Süd und eine Ost-West verlaufende seismische Linien erstrecken sich von der Hovland-Magellan zur Belgica-mound Provinz. Vitrinitreflexionsdaten, Bohrlochtemperaturen und Apatit-Spaltspurdaten von sechs in der Nähe liegende Explorations-bohrungen wurden zur Kalibrierung der Versenkungs- und Temperaturgeschichte herangezogen.

Die Temperaturgeschichte wurde anhand der geologischen Geschichte des Porcupine-Beckens rekonstruiert mit Wärmefluß-Peaks im Jura und in der Kreide (rifting) sowie im Paleozän (Island Hot-Spot). Die Höhe der Wärmefluß-Peaks wurde anhand des Spreizungsfaktors beta ermittelt. Die Kalibrierung der Temperaturgeschichte zeigte, dass alle drei thermischen Ereignisse benötigt werden um einen zufriedenstellenden Abgleich von modellierten und gemessenen Daten zu erzeugen. Für die Modellierung der Migrationsgeschichte ist die Rekonstruktion der Paläogeometrie unumgänglich. Paläowassertiefenkarten wurden für jeden Zeitschritt entwickelt um unnatürliche Strukturen während der Versenkungsrekonstruktion zu vermeiden.

Jurassischen und ältere Schichten enthalten potentielle Muttergesteine bestehend aus hautsächlich marinem und lakustrinem Kerogen. Kretazische und tertiäre Schichten enthalten marines und deltaisches organisches Material. Da keine Muttergesteinsproben vorhanden waren, wurden Asphaltene aus Rohölen des Connemara Ölfeldes gewonnen und zur Beschreibung der pauschal-kinetischen Prozesse von Kerogen zu Kohlenwasserstoffen benutzt. Zusätzlich wurden veröffentlichte kompositionelle Kinetiken zur Simulation der Öl- und Gasgeneration und –migration sowie dem Phasenverhalten während der Migration benutzt.

Die Modellierungsergebnisse zeigen, dass jurassische und ältere Muttergesteine im gesamten Becken reif bis überreif sind. Die kretazischen Schichten sind im Beckeninneren reif bis unreif und an den Flanken unreif. Die tertiären Sedimente bleiben im gesamten Becken unreif. Die Kohlenwasserstoffgenese begann in der späten Kreide für die tief versenkten Schichten. Basierend auf den Berechnungen mit der kompositionellen Kinetik generiert das jurassische Muttergestein ungesättigtes Öl im Ölfenster, in höheren

Reifestadium hingegen Gaskondensat. Die modellierten Phasenseparation liegt zwischen 2000 und 4000 m. Oberhalb dieses Teufenbereiches dominiert die Migration freien Gases. Die Migration wird bestimmt durch Schwerkraft bedingten Auftrieb und ist hauptsächlich vertikal, nur die Aptischen und tertiären deltaischen Schichten leiten den Kohlenwasserstoffffluss an den Beckenrand. Kohlenwasserstoffleckage wird für große Bereiche des Beckens vorhergesagt, wobei keine offensichtliche Fokussierung hinsichtlich der Hovland-Magellan-mound Provinz erfolgt. Als Grund dafür kann die seismische Auflösung herangezogen werden. Zudem ist die Migration ein drei-dimensionaler Prozess der in einem 2D-Modell nur unzureichend berechnet werden kann. Die 3D Karten basierte Modellierung der tertiären Schichten zeigt eine Übereinstimmung von vermuteten Ölspills und Karbonathügeln. Hingegen erfolgt in der Belgica-mound Provinz eine deutlich Fokussierung von Kohlenwasserstoffen auf die Karbonathügel beeinflusst durch das Auskeilen kretazischer und tertiärer Sande. Diese Modellierungsergebnisse konnten mit Hilfe geochemischer Analytik an Sedimentproben von Schwerkraftkernen nicht nachvollzogen werden. Biomarker für methanotrophe Bakterien sowie migrierte Kohlenwasserstoffe konnten nicht gefunden werden, leichte Kohlenwasserstoffe wurden nur in Spuren gefunden.

Die Ergebnisse dieser Untersuchungen basierend auf der Beckenmodellierung zeigen einen deutlichen Zusammenhang zwischen den Karbonathügeln und Kohlenwasserstoffleckage für beide Provinzen. Die geochemischen Untersuchungen konnten diese Ergebnisse nicht bestätigen wobei zurücksichtigen ist, dass die Schwerkraftkerne nicht die Schichten an der Karbonathügelbasis erreichen und somit nur eine Kohlenwasserstoffleckage für die letzten 1 Millionen Jahre ausgeschlossen werden kann.

Abstract

The goal of this study is to assess whether deep coral mound growth on the continental slope of the north Atlantic is related to active hydrocarbon leakage. The objects of interest are numerous buried and non-buried carbonate mounds in the Porcupine Basin, 200 km offshore Ireland. Mounds with a size of up to 3 km length and a maximum height of about 600 m have been found in two mound provinces, the Hovland-Magellan mound province on the northern slope and the Belgica mound province on the eastern slope of the basin. The shape of the mounds varies from mostly elongated to circular and mounds consist mainly of corals, carbonate crusts and fine grained clastic sediments.

To evaluate the possible link between hydrocarbon leakage and mound growth 2D basin modelling in combination with geochemical analysis of sediments from gravity cores was used. Two north-south trending seismic lines with an intersecting east-west line cover the Hovland-Magellan mound province and reach the border of the Belgica mound area. Six close by exploration wells were used for calibration of the burial and thermal history using vitrinite reflectance, bottom hole temperatures and apatite fission track data.

The temperature history was defined based on the geologic evolution of the Porcupine basin, assuming heat flow peaks in Jurassic/Cretaceous times (rifting) and in the Paleocene (Iceland plume). The magnitude of the heat flow peaks was determined using the stretching factor beta for each point of the basin. Calibration of the thermal history indicated that both the rifting and plume effects were required in order to reproduce all calibration data satisfactorily. For fluid flow simulation a correct geometric reconstruction of the modelled sections was required. The paleo-geometry was defined by means of estimated paleo-water depth profiles for each time step, which were then introduced to the model to prevent unrealistic structures during burial.

Possible source rocks in the Porcupine Basin are found in the Jurassic and older strata containing mainly marine to lacustrine kerogen types. Cretaceous and Tertiary sequences contain marine to delta plain, coaly organic matter. As no source rock samples were available asphaltene kinetics determined on oil samples from the Connemara oil field were used for bulk kinetic characterisation of hydrocarbon generation. Additionally published compositional kinetic data sets were used for the simulation of oil and gas generation and petroleum phase behaviour.

Modelling results indicate that Jurassic and older source rocks are mature to overmature throughout the basin. Cretaceous strata is immature to mature in the central part of the basin and immature on the flanks. The Tertiary sequence remains immature over the entire basin. Hydrocarbon generation started in Late Cretaceous times for the deepest sequences. Based on the compositional kinetic model used, the Upper Jurassic source rock generates undersaturated black oil while in the oil window, with gas condensate dominating at higher maturities. Phase separation was modelled to occur during migration at depth ranges between 2000 and 4000m. Upon phase separation the migration of the free gas phase

dominates over that of the oil, such that gas is the main migrating fluid in the shallower intervals. Migration is mainly buoyancy driven and vertical, only Aptian and Tertiary deltaic layers direct hydrocarbon flow out of the basin. Modelling predictions over the entire basin indicate gas breaking through to the seafloor but without any obvious focussing of hydrocarbon leakage towards the Hovland-Magellan mound province. This lack of focussing could be a problem related to either lack of sufficient stratigraphic detail in the model or related to the inadequacy of using a 2D model for the simulation of an essentially 3D process. Map based 3D modelling of the tertiary layers indicates a coincidence of possible spill points and mound occurrence. Never the less, that the model predicts significant focussing of gas migration towards the Belgica mounds where a pinch out of Cretaceous and Tertiary layers beneath the mound area is observed. The inferred focussing of gas migration towards the Belgica mounds could, however, not be confirmed by geo-chemical methods, as no enhanced methane contents could be found in the gravity cores. Only traces of methane and light hydrocarbons were identified whereas no biomarkers for methanotrophic bacteria or migrated hydro-carbons could be observed.

The results from this study indicate that a link between hydrocarbon leakage and carbonate mound growth is feasible in the case of the Belgica and the Hovland Magellan mound province using basin modelling. The geochemical analysis did not confirm these results as the gravity cores did not penetrate the Pre-Pliocene sediments and do therefore only show no active hydrocarbon seepage for the last million year.

Contents

Figures:

Tables:

1 Introduction

1.1 Carbonate Mounds and Seepage Phenomena

Carbonate mounds of varying size and shape are found in a variety of locations. Carbonate mounds (stromatolites) built up by cyanobacteria are known since the Late Precambrian (Monty, 1995). In the Early Paleozoic the huge diversity in microbial and biodetrital fabrics with abundant mound-building calcified microbes, calcified coralline and green algae and a variety of Paleozoic benthic invertebrates played a role in mound construction (Bosence and Bridges, 1995). It is important to mention that photosynthesis was not essential for the precipitation of carbonates, which is controlled by the properties of the bacterial membranes. These ensure calcium transportation and binding following two metabolic pathways that alter the physico-chemical environment toward increased alkalinization: the nitrogen cycle and the sulphur cycle, which are described in detail by Castanier et al. (2000).

During mid- to Late Ordovician the development of reefs and typical stromatactoid mud-mounds was caused by the dramatic rise of large skeletal metazoans and higher algae (Monty, 1995). Lower Devonian carbonate mounds (kess-kess) of the Moroccan Anti-Atlas are related to carbonate precipitation from hydrothermal fluids (Mounji et al., 1998). Sponges dominate the Frasnian carbonate mounds in Belgium in the Upper Devonian (Monty, 1995). Early Carboniferous carbonate mounds are described from Belgium (Figure 1-1), Ireland, English Midlands, North America, central Asia and North Africa. They are built of a sequence of bacterial derived mud and macroskeletal crinoid, bryozoan and brachiopod components (Henriet et al., 2002). For these mounds, which developed around fault-controlled basinal highs or in deep ramp environments well below the photic zone, no satisfactory explanation of occurrence and distribution has been found (Lees and Miller, 1995). Mud mounds in the Permo-Triassic vary in their composition consisting of newly evolved calcisponges, microbial crusts and sessile foraminifera coated by microbial encrustations (Pratt, 1995). Bosence and Bridges (1995) reported a decline in the abundance and diversity of microbial mounds from the Triassic to the Cretaceous. From the mid-Cretaceous onwards microbial fabrics are only known as components to metazoan framework reefs (Pratt, 1995). Most Cenozoic mud-mounds are of biodetrital origin though microbial components might have remained significant in deeper water (Monty, 1995).

In the past carbonate mounds were normally associated with warm tropical waters (Bathurst, 1975) but nowadays modern cool-water carbonates accumulate in seawater that is generally colder than 20°C (James, 1997). The use of submersibles and towed underwater camera systems (de Mol et al., 2002) has led to the discovery of cold water carbonate build-ups in a wide range of regions including the Cobb Seamount, northeast Pacific (Farrow and Durant, 1985), the southeast Brazilian continental slope (Viana et al., 1994), the West Florida Slope (Neumann et al., 1977), the Bahama Bank slopes (Mullins et al., 1981), the Blank Plateau (Stetson et al., 1963), the Rockall Bank (Wilson, 1979), the Porcupine Bank (Scoffin and Bowes, 1988), the Faeroe Islands (Frederiksen et al., 1992), offshore mid-Norway (Mortensen et al., 1995) and Norwegian fjords (Stromgren, 1974). A review of cool water

corals settings is given in James and Clarke (1997). In recent years a number of extensive provinces of carbonate build-ups have been recorded in deep water (typically 450 – 900 m) within the Porcupine Seabight and the Rockall Trough in the North Atlantic (Henriet et al., 1998; Hovland et al., 1994; Wilson, 1979).

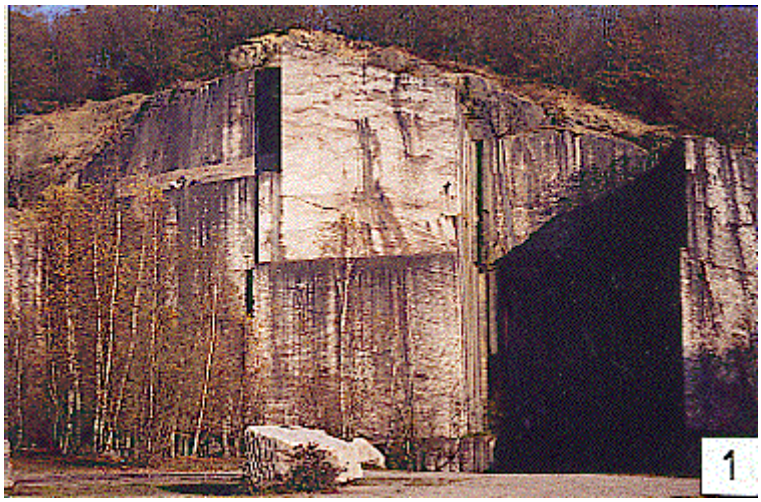

Figure 1-1: The Beauchâteau mud mound (outcrop in closed mine) of the Petit-Mont Membre near Senzeilles (Belgium) (Henriet et al., 2002)

Several models have been proposed for the origin of mounds including hydrothermal venting, hydrocarbon seepage, basin hydrography and ocean currents, iceberg drop stones and whale carcasses.

Hydrothermal venting is known from mid-ocean ridges and back-arc basins in the Pacific Indian and Atlantic oceans (Elder, 1965). Most are found at an average depth of about 2100 m in areas of seafloor spreading along the Mid-Ocean Ridge System (Heezen and Tharp, 1977).

Corliss et al. (1979) explained the origin of hydrothermal vents along the Mid-Ocean Ridge. Based on the concepts of plate tectonics, tectonic plates move apart and create cracks and crevices in the ocean floor. Seawater seeps into these openings and is heated by magma, that lies beneath the Earth's crust. As the water is heated, it rises and seeks a path back out into the ocean through an opening in the seafloor. This heated water (up to 400°C) dissolves and transports many elements including sulphur and economically important metals, such as copper, zinc and gold, carrying them to the sea floor, where they precipitate as sulphide and sulphate minerals. The vent sites are often marked by the occurrence of chimney structures termed “black-smokers” (Figure 1-2) where hot fluids, carrying sulphide minerals, form distinctive plumes and “white-smokers”, where colder fluids with high concentrations of calcium, barium, sulfur and other elements are vented through anhydrite tubes. Around these vent sites live highly specialised animal communities. Tubeworms, bivalves, gastropods and crustaceans live in a hostile environment of complete darkness, extreme pressure, and vent water temperatures that range from 10°C to 400°C (Figure 1-3).

Figure 1-2: Black smokers, photo taken with the R/V Atlantis (University of Delaware, 2003)

The occurrence, size, mineralogy and geologic setting of hydrothermal fields on mid-ocean ridges is controlled by many variables, including crustal permeability, magma supply, depth of heat source, sea floor depth, crustal thickness, crustal composition, spreading rate, and the spatial and temporal history of volcanic and tectonic activity (Langmuir et al., 1997). To constrain the relative importance of these parameters Langmuir et al. (1997) examined the Lucky Strike hydrothermal field in the North Atlantic which has only small variations in spreading rate but large variations in axial depth, crustal thickness and basalt composition due to the influence of the Azores and Iceland hot spots on the ridge. Multiple hydrothermal vents occur over an area of at least 300 m by 700 m with morphologies ranging from flanges to chimneys. Fluid compositions vary geographically and are not simply related to cooling or mixing processes suggesting an important substrate contribution to the chemical compositions of hydrothermal fluids and their associated mineral deposits. In the Lucky Strike area the fluid characteristics are a result from a combination of slow spreading rate and substrate control.

Kelley et al. (2001) described the 500 m long Mothra hydrothermal field, which is the largest venting site in areal extent on the Endeavour segment of the Juan de Fuca Ridge. Within this field, there are at least five actively venting sulfide complexes, spaced 40 to 200 m apart.

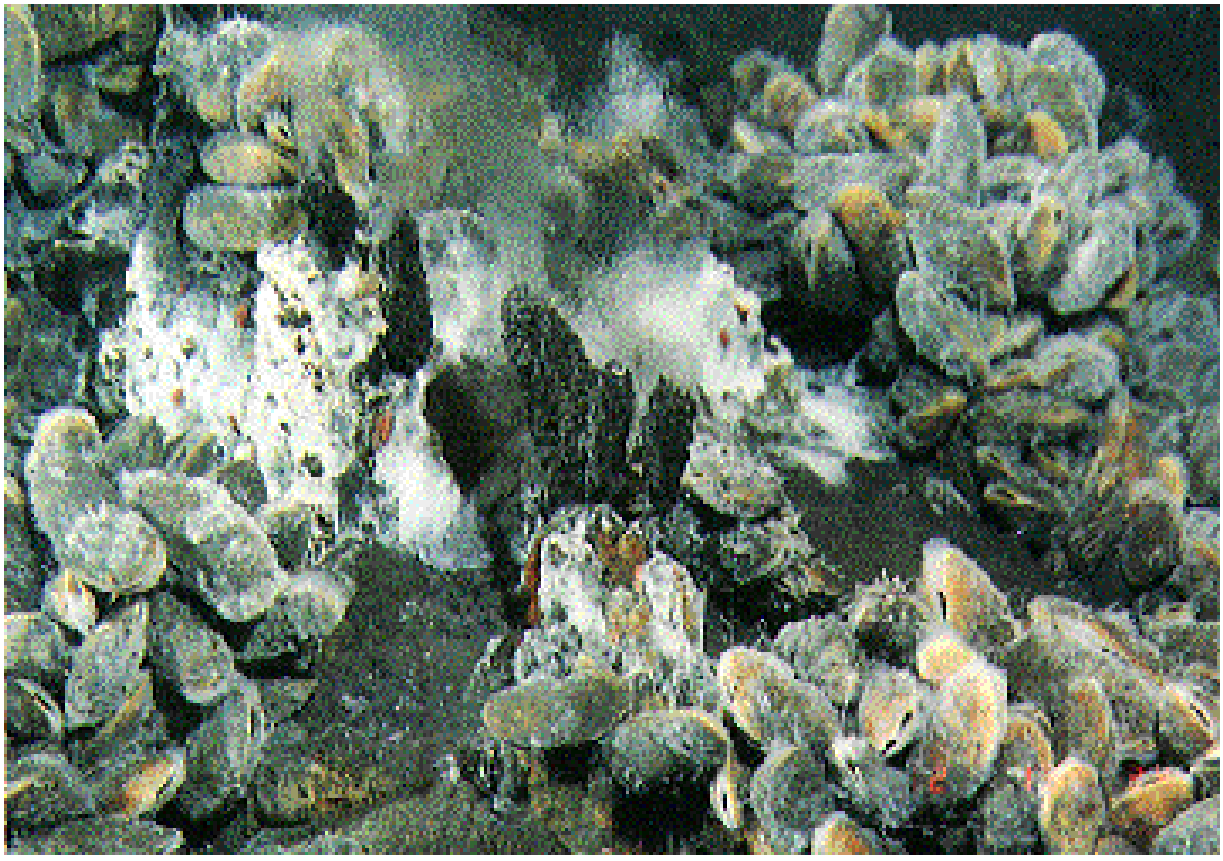

Figure 1-3: Chimney and hydrothermal vent community at Suiyo seamount, Izu-Ogasawara (Bonin) Islands, 1400 m deep (Jamstec, 2003)

The clusters are composed of multiple steep-sided pinnacles that rise up to 20 m above the seafloor. Most of the sulfide structures are awash in diffusely venting fluids (30-200 °C) that support rich and diverse macrofaunal and microbial communities. The linear arrays of sulfide complexes delineate a zone of active faulting near the western wall of the axial valley. This fault network serves as the conduit for the rising fluids.

Toshitaka et al. (2001) described the chemical characteristics of hydrothermal fluids in the Indian Ocean. The end member fluid of the hydrothermal Kairei field, located north of the Rodrigues Triple Junction, Central Indian Ridge, has a similar chemical composition to the hydrothermal fluids sampled from sediment-starved mid-ocean ridges in the Pacific and the Atlantic oceans. This suggests typical interactions between hot fluid and mid-ocean basalts in the sub seafloor reaction zone. Deposits of sulphide and sulphate minerals are formed at these sites from vents where circulated seawater reacts with hot, recently cooled magma feeding huge biological communities.

In 1978 clam shells were observed in the Galapagos Rift from the submersible “Cyana” which resembled the large *Vesicomydae* clams which cluster around active hydrothermal vents (Francheteau et al., 1981). Since then benthic communities associated with deep-sea hydrothermal vents have been studied intensively (Lutz and Kennish, 1993).

Faunal assemblages similar to those at the Galapagos Rift (Lonsdale, 1977) have been sampled at other hydrothermal vent locations along the East Pacific Rise, in the Guaymas Basin, along the Gorda, Juan de Fuca and Explorer ridges, in the western Pacific at the Marian Trough, Manus Back-Arc Basin, Lau Basin, North Fiji Basin and Okinawa Trough and along the Mid-Atlantic Ridge (Both et al., 1986; Bouchet and Waren, 1991; Desbruyères et al., 1991; Desbruyères and Laubier, 1989; Fujikura et al., 1991; Grassle, 1986; Grassle et al., 1986; Hashimoto et al., 1991; Hawkins et al., 1990; Hessler and Lonsdale, 1991; Jones, 1985; Juniper et al., 1990; Kimura et al., 1988; Lutz and Kennish, 1993; McMurray, 1990; Miura and Ohta, 1991; Rona, 1980; Southward, 1991; Tunnicliffe, 1991; Tunnicliffe, 1992; van Dover and Berg, 1988; van Dover and Hessler, 1990). Dense megafaunal and macrofaunal populations at some vent sites in the eastern Pacific were found on the Explorer Ridge and on the East Pacific Rise (Ballard et al., 1986; Crane, 1985; Crane et al., 1985; Lutz, 1984; Lutz and Kennish, 1993; Southward, 1991; Tunnicliffe, 1991; Tunnicliffe et al., 1986). Fowler and Tunnicliffe (1997) described communities of giant white crabs, and a variety of tubeworms at hydrothermal vents. Van Dover et al. (1994) discovered the vent shrimp *Rimicaris exoculata* which lacks normal shrimp eyes but was found to have a novel photoreceptor. As sunlight penetrates not farther than a few hundred feet down no natural light is present at the vent sites. However, the shrimps use ambient light which is emitted by high-temperature black smokers and flange pools on the Juan de Fuca Ridge (White et al., 2000). The emitted light is of long wavelengths (700-1000 nm) and corresponds well to thermal radiation from a body at the same temperature as the vents/flanges. Flange pools do not exhibit excess visible light over that for a thermal source, suggesting that the light at smokers is caused by mechanisms related to turbulence, mixing, or precipitation (White et al., 2000).

Without sunlight no photosynthesis takes place in the deep sea meaning that vent species rely not on photons from the sun but on chemosynthesis (van Dover et al., 1994). Microbes oxidize the hydrogen sulfide that diffuses out of the vents providing nutrients for animals higher up the food chain (Harder, 1997). Some creatures, such as the molluscs feast on the bacteria directly; others, including predatory fish, dine on animals that have eaten or otherwise made use of the microbes; still others, like tubeworms, host the microorganisms in their tissues in exchange for organic compounds that the bacteria fashion from the vent chemicals and seawater.

Hydrocarbon seepage is the transfer of hydrocarbons from the Earth interior across the sediment-water interface (Horvitz, 1939). Offshore springs and emanations of fluids from coastal sediments were reported since at least the days of the Romans (Schlüter, 2002) and the concept that hydrocarbons migrate from subsurface accumulations and mature source rocks to near-surface sediments is well documented all over the world e.g. (Abrams, 1996; Drozd, 1983; Horvitz, 1939; Horvitz, 1969; Horvitz, 1980; Horvitz, 1981; Horvitz, 1985a; Horvitz, 1985b; Kennicutt and Brooks, 1988; Price, 1986) (Figure 1-4). A review of hydrocarbon seepage occurrence and mechanisms is given in Schumacher and Abrams (1996).

Figure 1-4: Petroleum seep with oil and gas rising to the surface. The seep began after the 1994 Northridge earthquake in the North Sulphur Mountain Area of Ojai oil field, Ventura County, CA. Photo by Mulqueen (2003).

The presence of hydrocarbons is essential for hydrocarbon leakage processes. Hydrocarbons are expelled from the source rock and migrate through carrier beds into a reservoir (Matthews, 1996). Based on the accumulated hydrocarbon mass its buoyancy pressure in the reservoir increases and when buoyant pressure overcomes the cap rocks capillary entry pressure hydrocarbons migrate from the reservoir into the seal. Finally, within the seal, the hydrocarbons move through discrete pathways of one or more continuous threads or by diffusion until they encounter a carrier bed. This breaks the continuous hydrocarbon tread at each carrier unit, constraining the buoyant force to reservoir-seal couplets. As the hydrocarbons migrate vertically through the section, they continuously reequilibrate into gas and oil phases to the new pressure-temperature conditions (di Primio et al., 1998). In the course of upward movement of a fluid phase separation will eventually happen and continue to occur as long as pressure and temperature are reduced (England et al., 1987). As phase separation of a liquid and gaseous phase are not the only processes occurring, the reequilibration of the fluid to its new pressure and temperature conditions can be expected to lead also to a precipitation of a solid phase out of the liquid due to changes in solubility. These phases are often partitionated into different accumulation sites due to difference in migration pathways (spillage of oil and capillary leakage of gas or oil). The rates of leakage through the sequence of seals between the source rock and the earth's surface control the pattern of hydrocarbon accumulations along the secondary migration route and

both the magnitudes and spatial properties of surface seepage (Matthews, 1996). Additional migration occurs along faults and fractures, through highly permeable discontinuities, or by means of diffusion (Schowalter, 1976). Link (1952) studied worldwide occurrence of seeps and concluded that they occur dominantly along high-permeability pathways such as faults, fractures, unconformities and pore networks in outcropping reservoirs. Additionally, they can be related to structural features such as sea floor highs, subsurface highs, diapirs, faults, unconformities, and spill points which may result from structural failure of trapping components (Abrams, 1996). Unfortunately, unequivocal petroleum seepage does not usually occur directly above prospects, but is found at the end of migration pathways often tens or even hundreds of kilometres away (Hunt, 1979).

Seeps vary in shape, size and form including halo (Doughnut), apical (focal), crescent, or linear (straight-line) shapes (Abrams, 1996). Pockmark structures, mud volcanoes, mud ridges, large sediment slides deposits (Kaluza and Doyle, 1996) and authigenic carbonate crusts and slabs are also surface expressions of the activity of hydrocarbon seeps (Diaz-del-Rio et al., 2003; Ivanov et al., 2000).

Pockmarks occur worldwide on the floors of all oceans and some lakes in water depths ranging from shallow waters to depths of thousands of meters (Kelley et al., 1994). These authors describe an active pockmark field with 160 pockmarks per km^2 in Belfast Bay, Maine. Another pockmark field is the subject of Vogt et al (1990). It occupies a strip about 1.3 km wide and 50 km long between Greenland and Spitzbergen underlain by methane hydrates. The roughly conical depressions are about 350 m in diameter and up to 35 m deep and cover fields up to 1000 km^2 (Vogt et al., 1994). Sea-bed pockmarks are thought to be formed when methane gas is explosively vented, e.g. when methane hydrate decomposes (Paull et al., 1995).

Mud volcanoes are similar to pockmarks but include the transport of sediment (mud). They have been discovered around the globe by various authors and an overview of their occurrence is summarized in Milkov (2000). Figure 1-5 shows the distribution of mud volcanoes.

The size of mud volcanoes ranges from a few centimeters to a few kilometers wide, or small pools to hills up to a few hundred meters in height (Figure 1-6). They correspond to morphological spots of highly focused gas, water, and fluidized sediments outflows and are associated with highly pressurized source regions at depth (Brown, 1990). To understand the dynamics of the tectonic system driving the mud volcanism Milkov (2000) proposes the following controls:

1. Geologic reasons including (a) thick sedimentary cover (8–22 km), mainly composed of terrigenous sediments; (b) the presence of plastic shale layers in the subsurface; (c) a rock density inversion; (d) the occurrence of gas accumulations in the deep subsurface; (e) abnormally high formation pressure.

2. Tectonic reasons: (a) the rapid subsidence of the sedimentary cover due to the high sediment accumulation rate or by overriding thrust sheets; (b) the occurrence of diapiric or anticlinal folds; (c) the occurrence of faults; (d) lateral tectonic compression; (e) seismic activity; (f) isostatic processes.

3. Geochemical reasons: (a) petroleum generation in the deep subsurface; (b) the dehydration of clay minerals.

4. Hydrogeological reasons, i.e. fluid flow along fracture zones.

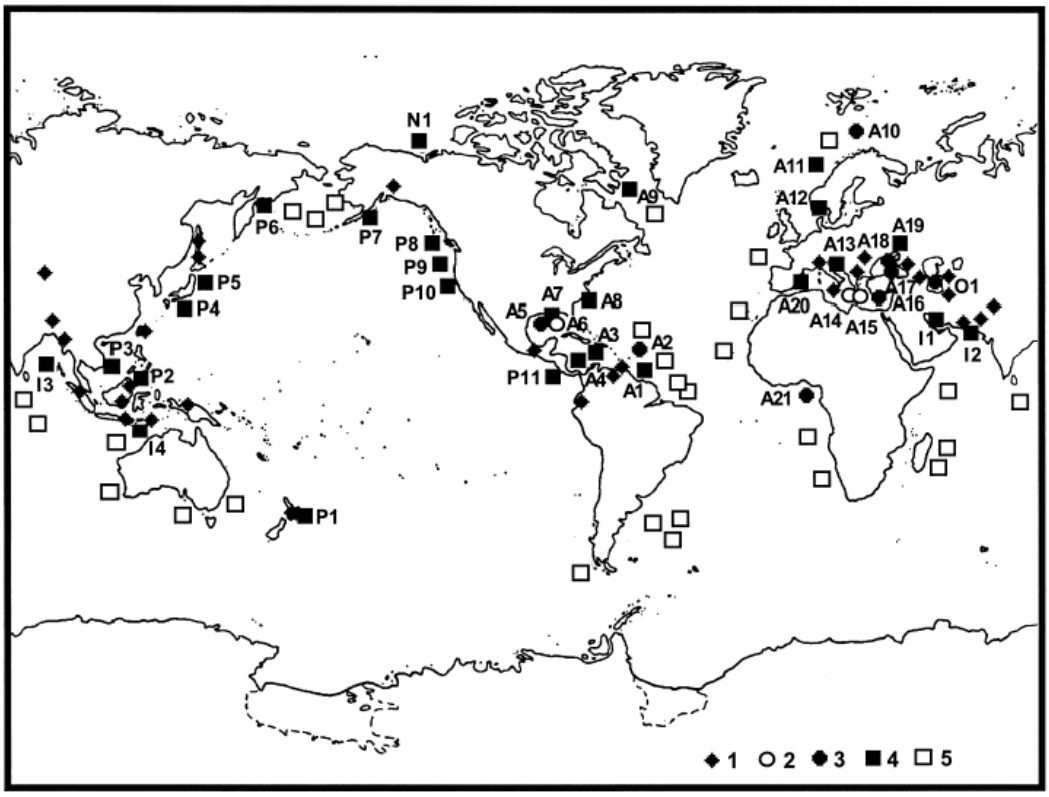

Figure 1-5: Map showing the worldwide locations of mud volcanoes: 1) after Rakhmanov, 1987, 2) without gas hydrates, 3) hydrate bearing, 4) inferred submarine mud volcanoes and 5) possible sediment diapirs mapped by Lancelot and Embley (1997) (after Milkov, 2000)

Many of these reasons are closely related to each other or require the presence of each other. Regularities in the spatial distribution of known and inferred submarine mud volcanoes are attributed to two key reasons by Milkov (2000): first the high sediment accumulation rate at passive continental margins and in the abyssal parts of Mediterranean seas and second the lateral tectonic compression at active continental margins. In addition, plastic clay layers must be present for mud volcanoes to form. The formation of mud volcanoes has been considered as a result of the destruction of deep gas accumulations (Shnukov et al., 1971),

the piercing of the surface by shale diapirs (Higgins and Saunders, 1973), the rise of fluidized mud along faults (Yakubov and Rakhmanov, 1978) and the decomposition of gas hydrates (Reed et al., 1990).

Figure 1-6: Mud volcano near Baku (Azerbaidjan) (van der Meer, 2003)

Authigenic carbonates are precipitated as crusts or concretions at the sediment/water interface above or near sites of hydrocarbon leakage (Ritger et al., 1987). Stakes et al. (1999b) analysed hydrocarbon derived samples of authigenic carbonate collected from Monterey Bay petrographically and observed carbonate-cemented sandstones, micritic carbonate precipitates with a terrigenous component, or carbonate veins within host rocks. Shell fragments, organic carbon debris and pyrite were present in the authigenic carbonate sediments. The formation of the authigenic carbonate is associated with high amounts of bicarbonate released by the process of anaerobic methane oxidation.

Michaelis et al. (2002) reported massive microbial mats covering up to 4 m high carbonate build-ups, which prosper at methane seeps in anoxic waters of the northwestern Black Sea shelf. The mats consist of densely aggregated archaea and sulphate-reducing bacteria. Vast amounts of microbial biomass may accumulate in an anoxic marine environment because of the use of methane as an electron donor for sulphate reduction and as organic carbon source for cell synthesis.

Although no anaerobic methanotroph has ever been isolated, biogeochemical studies have shown that the overall process involves a transfer of electrons from methane to sulphate (Hoehler et al., 1994; Iversen and Jørgensen, 1985). The isotopic and genetic signature of the microbial biomass in environments enriched with methane shows that this transfer is probably mediated by a microbial consortium that includes archaea and sulphate-reducing bacteria (Boetius et al., 2000; Hinrichs et al., 1999). Hinrichs and Boetius (2002) described

the processes of anaerobic oxidation of methane known so far in detail. Based on the observations of Barnes and Goldberg (1976) sulphate was suggested to be the terminal electron acceptor for anoxic methane oxidation: $CH_4 + SO_4^{2-} \rightarrow HCO_3^- + HS^- + H_2O$. This reaction becomes favourable at in situ conditions in marine sediments based on thermodynamic models but yields only a free energy of –25 kJ per mol methane consumed, which is only approximately half the energy required for the formation of ATP (Hoehler et al., 1994).

Different approaches and subreactions were used to explain this reaction occurring under thermodynamic unfavourable conditions (Hinrichs and Boetius, 2002). Different possible electron shuttles e.g. hydrogen, acetate or methanol were tested but, at present, only the transfer of formate resulted in free energy gain (Sørensen et al., 2001). Members of the order Methanobacterials and Methanococcales use formate for methanogensis but no member of the order Methanosarcinales is known to utilize formate. On the basis of the current knowledge a reversal of methanogenisis on the basis of known enzymes for the anaerobic oxidation of methane appears attractive (Hinrichs and Boetius, 2002). In the case of methanogenesis, some of the enzymes of methanogens used for the reduction of CO_2 to CH_4 are operating in reverse in the oxidative pathway of the sulphate-reducing archaeon Archaeoglobus (Nauhaus et al., 2002). The final enzymatic step in methane production involves the protonation of methyl-nickel by the enzyme methyl-CoM reductase and is considered irreversible (Hoehler and Alperin, 1996). Therefore it is likely that other, yet unknown enzymes are involved. This is the subject of ongoing research. Even though the process is not understood in the last detail it is obvious that microbial anaerobic oxidation of sedimentary organic matter and methane occurs. This bacterial flora is the basis for a complex local food-web involving micro-organisms, filter-feeders and scavengers (Grassle, 1985). Such hydrocarbon-derived, vent-related carbonate hardgrounds or build-ups are typical by-products of microbial chemosynthesis and have been termed chemoherms (Roberts and Aharon, 1994). This stable substrate can be used by corals to settle and grow e.g. *Lophelia pertusa* (Wilson, 1979) acting as the foundation of a carbonate mound.

The remarkable abundance of giant tubeworms (*Vestimentiferans*) and large bivalves (i.e. *Vesicomydae*, *Mytilidae*) is one of the most striking features of cold seep communities and described extensively in Sibuet and Olu-Le Roy (1998) and (2002). The large faunal communities are based on the symbiotic associations between bacteria, which take the energy from chemosynthesis of methane and sulphide, and invertebrate hosts. Three common symbioses are 1. Pogonogphoran tubeworms which keep their sulphur-oxidising symbionts in a specialised organ, the trophosome; 2. Species of bivalve families which host their symbionts in the gill tissue: 3. some sponge species which host methanotroph symbionts extra- and intra-cellularly. Up to date a total number of 61 species are known and show the high diversity of the chemosynthesis-based fauna in cold seep environments as compared to the known species of the same phyla at hydrothermal vents (Sibuet and Olu-Le Roy, 2002). The cold seep species show a great endemism at species level but not at genus level. For example *Mytilidae* bivalves are restricted to a bathymetric range of 400 – 2000 m water depth, the *Vesicomydae* bivalves species are observed down to 5800 m in the Japan

Trenches (Juniper and Sibuet, 1987) and Peru Trench (Olu-Le Roy et al., 1996a). As shown for the *Vesicomydae* species Barry et al. (1997) suggested that differences in bathymetry, the habitat and sulphide and methane concentration can influence the species composition due to differences in species biology and physiology such as symbiotic associations (methanotrophic and/or sulphur-oxidising bacteria) and physiological characteristics such as sulphide binding affinity. Different fluid flow and habitat influences the type of communities composed by distinct species of *Vesicomyidae* bivalves and/or *Mytiladae* bivalves (Olu-Le Roy et al., 1996b) indicating that several species can live together owing to their different physiological adaptions and different environmental preferences. Biodiversity of cold seep communities reflects the biotope variability in space and probably also in time (Sibuet and Olu-Le Roy, 2002).

The literature show numerous case studies involving hydrocarbon seepage in the build up of bioherms (Abrams, 1996; Ahr and Stanton, 1999; Aref, 1998; Bosence and Bridges, 1995; Cavagna et al., 1999; Coles et al., 1996; Han and Suess, 1989; Henrich et al., 1995; Henrich et al., 1996; Hovland, 1990; Hovland et al., 1994; Hovland et al., 1998; Hovland et al., 1987; James, 1997; James and Clarke, 1997; Kopaska-Merkel and Haywick, 2001; Lein et al., 2002; Monty, 1995; Mounji et al., 1998; O'Brien et al., 2002; Peckmann et al., 1999; Rad et al., 1996; Ritger et al., 1987; Roberts, 1998; Roberts and Aharon, 1994; Stakes et al., 1999a; Wu et al., 1999).

O'Brien et al. (2002) showed recently, that the Ashmore Reef and other genetically rich carbonate seed bank systems are closely associated spatially with active hydrocarbon systems. They used assorted remote sensing data, satellite synthetic aperture radar, Landsat, water column geochemical sniffer, airborne laser fluorosensor, seismic data and seafloor sediment sampling to investigate the benthic communities in the Timor sea in Australia. Their interpretations suggest that the reefs and the build-ups formed by a sequential process involving hydrocarbon seepage induced by collision-related faulting. This triggered localised small seafloor biological carbonate communities which ultimately formed topographically positive features keeping up with the rising sea-level as the most favourable conditions for initial reef colonisation probably occurred during periods of relatively low sea-level, when the areas around the reefs were located at much shallower water depths (<40 m) than today and ample sunlight reached the seafloor (O'Brien et al., 2002).

Hovland et al. (1998) discovered recently large coral banks, mud-mounds and pockmarks at water depths between 220 and 310 m on the continental shelf off mid-Norway associated with the Heidrun Oil field. The seabed consists of sub-glacial till containing silty, sandy clay and gravel. The banks consist of the framework builder coral *Lophelia* and can be divided into three zones, the base consisting of dead *Lophelia* branches colonized mainly by sponges, an intermediate zone consisting of a mixture of mainly dead and a few live scattered corals with decreasing sediment content and the upper zone. This zone is dominated by dense aggregations of live *Lophelia pertusa* (Wilson, 1979). Hovland et al. (1998) showed, based on geophysical, visual, geochemical and radiocarbon analysis that the coral banks form as a consequence of local fertilization by micro-seeped hydrocarbons. The

coral banks, which have been there for at least 8000 years, can be related to the occurrence of light hydrocarbons. However, the biological processes were not distinguished in detail in the sense of the discovery of methanotrophic bacteria.

Using *Lophelia* as the framework builder of carbonate mounds the basin ***hydrography and ocean currents*** become important as *Lophelia* and other deepwater corals are promoted by high current speed (Genin et al., 1986). The deepwater coral *Lophelia pertusa* is widely distributed from the Faeroe shelf (Frederiksen et al., 1992), Norway (Ancellin, 1957), Ireland and continental Europe (Le Danois, 1948), West Africa (Allen and Wells, 1962) and the Mexican Gulf (Ludwick and Walton, 1957). Recent research shows also discoveries of Lophelia at Symour Island, Gulf coast, Hinakura (New Zealand), at Lake Ferry, the Mediterrainen sea, the Aegean Sea, the Florida Strait and outer Blake Plateau (Freiwald, 2002).

Prerequisites for the occurrence of deep-water coral build ups are the attachment on a hard substrate and the association with permanently or episodically strong currents (Freiwald, 2002). The Planula larva – which as yet has never been found – needs a hard substrate for settling and metamorphosis. Hardground formation can be the result of condensed sedimentation, cementation of sediments by changes in groundwater geochemistry and hydrocarbon seepage. In high energy conditions at the seafloor, the cementing material is derived from the overlying seawater and/or groundwater and precipitates due to changes in the pH (Molenaar and Zijlstra, 1997). Another reason for hardground formation are methane oxidizing bacteria under anaerobic conditions creating carbonate crusts e.g. on hydrocarbon seepage areas (Boetius et al., 2000; Hovland et al., 1987).

Lophelia, which lacks photosymbionts in their soft tissue (Freiwald, 2002), is found in water depths ranging from 0 – 6200 m with temperatures from -1 – 29°C (Stanley and Cairns, 1988). They can exist in seasonally eutrophicated environments and produce 30 –100 cm high massive, dendroid and bushy skeletal colonies. The architectural stability of the framework increases significantly as the neighbouring branches commonly grow together. The growth and preservation of the corals is influenced by the current strength, food supply and by sediment-infill. Environments with high currents and high suspension-load in the water result in mud-supported seafloor elevations whereas low suspension-load in the water results in framework-support mounds. Freiwald (2002) concludes that the knowledge of the biology, distribution and environmental controls of *Lophelia pertuas* as a biospecies and reef constructor is quite poor.

High current speed is necessary at least periodically to keep suitable settling surfaces clear from fine grained sediment and to keep the corals from silting over (Frederiksen et al., 1992). In addition higher current speeds provide a higher food particle supply. Therefore, *Lophelia* is preferentially found on topographic highs such as submerged moraine ridges, clay ridges, spurs, outcropping rocks, and artificial substrates. ***Iceberg rafted sediments and drop stones*** randomly deposited over a basin provide also a suitable ground for Lophelia to settle and may provide the initial take-off for mound growth (Freiwald et al., 1999). Similarly the

exposed skeletons of ***whale carcasses*** are colonised by chemosynthetically based communities similar to those occurring around vents initiating a point for longer-term changes in palaeoproductivity and mound growth (Gooday and Rathburn, 1999).

1.2 The Geomound Project

The “Geomound” project, belonging to the “Fifth Framework Program” of the European Union, was designated to explore the formation of giant carbonate mounds along the Atlantic ocean continental slope lying in water depths ranging from 600 to 1000 m (Henriet et al., 1998). The area under investigation in this study is the Porcupine Basin, a thick succession of Late Palaeozoic to recent sediments lying beneath the bathymetric depression of the Porcupine Seabight offshore Ireland in the Atlantic Ocean (Figure 1-7), where numerous carbonate mounds have been recognized (Croker and O'Loughlin, 1998; de Mol et al., 2002; Henriet et al., 2002; Hovland et al., 1994; Scoffin and Bowes, 1988). Of special interest are the major complex mound provinces: the “Hovland” and “Magellan” mound provinces on the northern slope of the Porcupine Seabight and the “Belgica” mound province on the eastern slope. Numerous buried and surface mounds have been discovered by seismic surveying over the Hovland- and Magellan provinces and on a survey with the R/V Belgica in 1997 (Henriet et al., 1998).

The underlying petroleum system of the Porcupine Basin consists of a marine/lacustrine type Jurassic source rock, Aptian and Cenozoic carriers sealed by Cretaceous and Cenozoic shales (Croker and Shannon, 1987). Accumulations of oil are found in the Connemara oil field in the northern part of the Porcupine Basin trapped in tilted Jurassic fault blocks. Hovland (1990) showed that associations of mounds in the Porcupine Basin with interpreted faults and underlying petroleum accumulations in some cases appear to point to a genetic link between the carbonate reefs and the seepage of hydrocarbons. A sniffer survey in the Porcupine Basin by Oilsearch plc. showed a good correlation of fluorescence on the sea surface with the underlying mound provinces (McDonnell, 2001). McDonnell (2001) stated that all buried mounds root on the mid Miocene horizon C20 and the surface mounds on the C10-horizon of Pliocene age. Migration of hydrocarbons is possible along faults from underlying reservoirs, or as a result of cap rock failure or due to diffusion (Hovland, 1990). As diffusion is a dispersive process, faults, cap rock failure and topography are the main features, which can focus fluid flow in a limited area (Figure 1-8). There, the migrating hydrocarbons may have been utilised by methanotrophic bacteria leading to hardground formation, the base for coral growth. No faults are present beneath the build-ups, pointing to in-situ generated diagenetic rather than catagenetic substrates if indeed a genetic association exists between the mounds and expelled fluids from the geosphere. De Mol (2002) pointed out that the genesis and initial control of mound growth in the Porcupine Basin can be related to hydrocarbon seeps. But in recent geological times the major development of the Porcupine coral banks was most likely controlled by oceanic circulation and dynamics in water masses and nutrient supply.

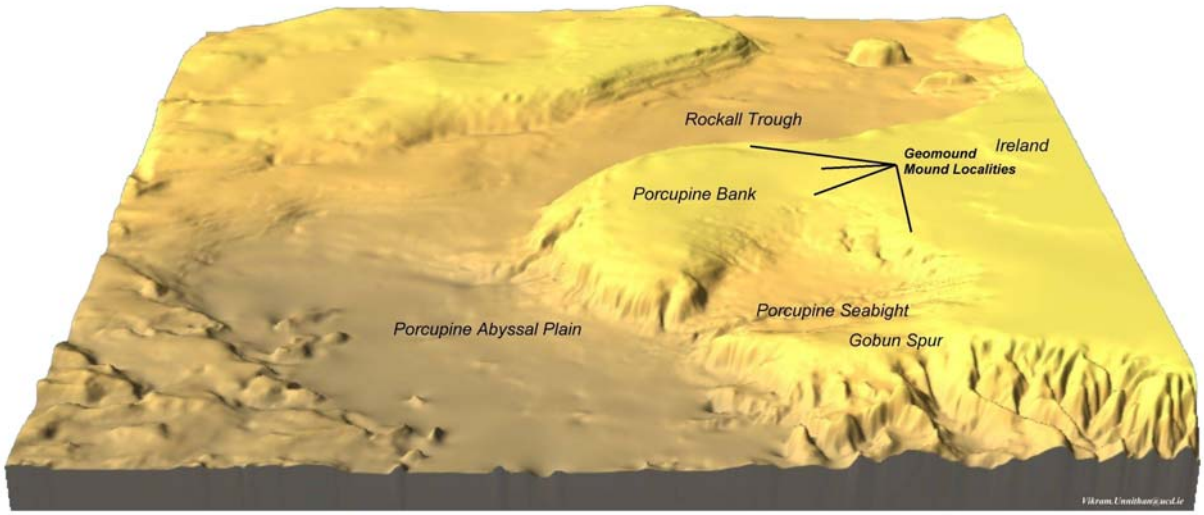

Figure 1-7: Porcupine Basin located offshore Ireland in the Atlantic Ocean including mound areas (Unnithan, 2000)

1.3 Goals and Approach

The task was to integrate the timing, amount and composition of pertinent hydrocarbon generation processes and assess whether migration is focussed towards the carbonate mounds. In other word, it was sought to determine if the mounds form a “coupled” system with the fluid flow processes of underlying strata. The chemical, physical and biological processes involved include the formation of hydrocarbon gases and low molecular weight fluids from macromolecular starting materials, their transport through porous media and/or retention on mineral surfaces, their accumulation in traps, their episodic expulsion to the surface and their utilisation as substrates by bacteria must all be taken into account.

Two methods were used to achieve this goal, numerical basin modelling and geochemical analysis of sediment samples. Numerical simulations, developed for industrial hydrocarbon exploration purposes, were used to examine hydrocarbon formation. Structural, stratigraphic and geochemical data were merged with the results of the interpretation of well logs. Additional experimental results of petrophysical property determinations on available sediment samples were used for seal property evaluation. The organic chemical signatures of light hydrocarbons and biomarkers were measured in long cores (ca. 30 m) from the mound areas using gas chromatography and mass spectrometry for identification of a possible thermogenic origin.

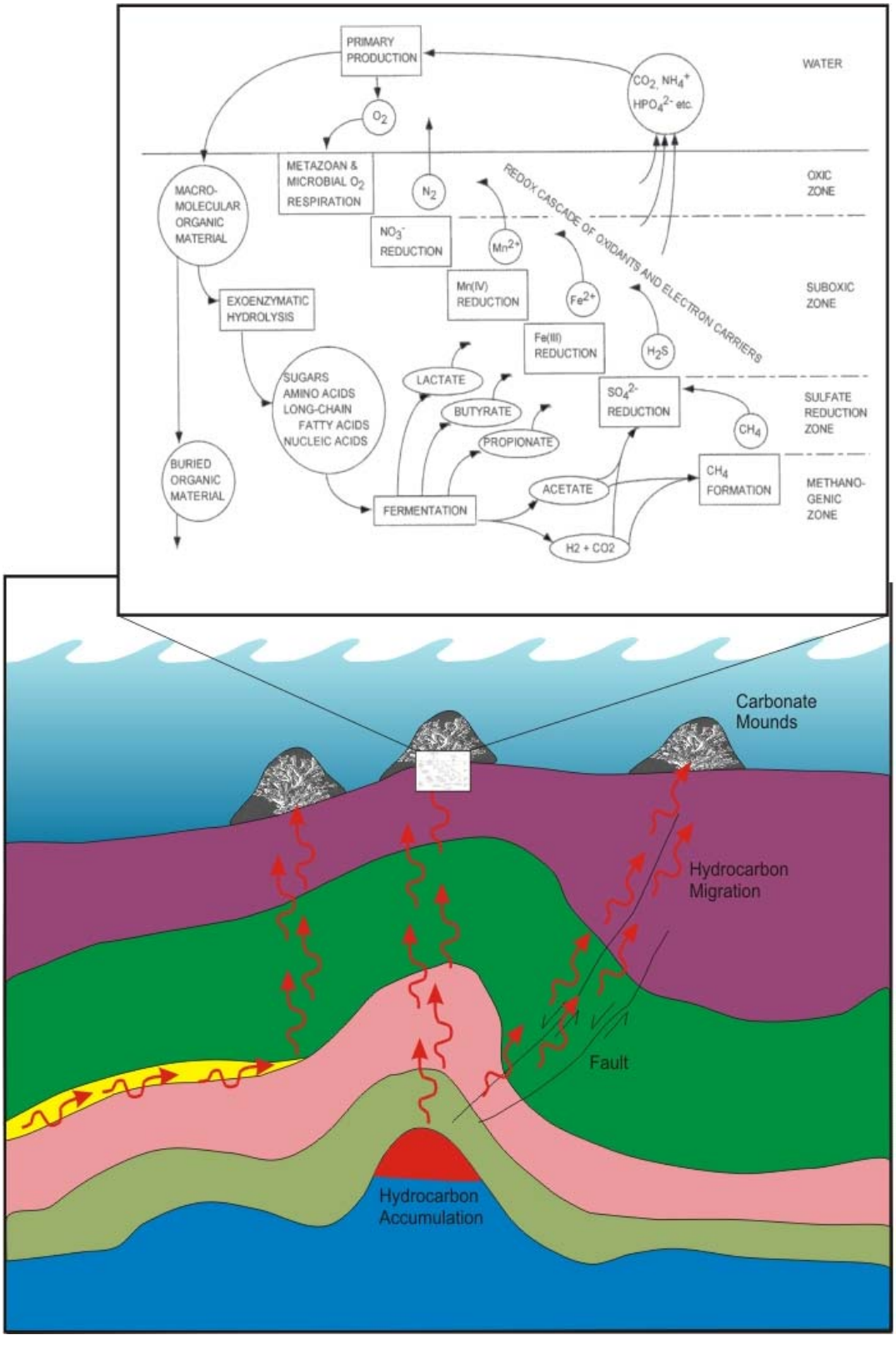

Figure 1-8: Carbonate mound formation mechanism based on focussed hydrocarbon flow through pinch outs, cap rock failure and faults. Hydrocarbon reduction pathways at the sediment water interface are stated on top modified from Boetius et al. (2002)

2 Study Area

2.1 Geology of the Porcupine Basin

The Porcupine Basin is a north-south trending basin lying 150-250 km offshore western Ireland in the Atlantic margin. It is approximately 270 km in length and 60 - 100 km in width (Moore, 1993). The Porcupine Basin can be divided into three major elements, the Main Porcupine Basin, the North Porcupine Basin and the Porcupine Seabight (Figure 2-1). The North Porcupine Basin is a small sub-basin separated from the Main Porcupine Basin to the south by an east-west trending basement ridge at the approximate latitude 53°N (Naylor and Shannon, 1982). The Main Porcupine Basin is bounded to the north by the Slyne Ridge, to the west by the Porcupine High and to the east by the Irish Mainland Shelf. It merges with the Seabight Basin to the south and with the Porcupine Abyssal Plain to the southwest. Water depths in the Main Porcupine Basin range from 300 m to more than 2000 m in the south (Moore and Shannon, 1995) .

Carbonate mounds developed during the Late Cenozoic (Henriet et al., 1998; Hovland et al., 1994; Wilson, 1979). They occur in the Hovland- and Magellan provinces and the Belgica mound province in deep water (typically 700-1200 m) (de Mol et al., 2002). For the purposes of the present study the Hovland and Magellan mounds, which occur in the same general region and which are largely distinguished by being either predominantly surface (Hovland) or buried (Magellan) mounds (Huvenne et al., in press.), are treated as a single province (Hovland-Magellan). The carbonate mounds appear to root on the Pliocene C10 and mid-Miocene C20 horizons (McDonnell, 2001).

2.1.1 Structural and Tectonic Setting

Most basins in the Atlantic Margin region developed in response to episodic crustal extension and resultant multiple rift events during Permo-Triassic to Early Cretaceous times (Croker and Shannon, 1987; Shannon and Naylor, 1998; Shannon et al., 1995; Sinclair, 1995; Tate, 1993; Walsh et al., 1999). Plate reconstructions indicate the Porcupine Basin as one of a series of intra-cratonic basins on the southeastern margin of the developing North Atlantic rift system. This long-lived zone of crustal weakness finally evolved into the northeast Atlantic Ocean with the commencement of sea-floor spreading and the separation of Greenland from northwest Europe during earliest Eocene times (Moore, 1993).

During the late Jurassic (Figure 2-2), active rifting took place in many of the basins in northwest Europe, including the North Sea graben system, the Slyne-Erris Troughs, the Porcupine and the Celtic Sea basins (Shannon, 1991b). Prior to the Cretaceous opening of the North Atlantic, the basins along the present day western seaboard of the British Isles linked southwestwards into basins on the Newfoundland shelf, such as the Jeanne d'Arc and Scotian basins (Fowler and McAlpine, 1995). During this phase of extension, a series of northwest – southeast trending lineaments became active as transfer zones along the length of the rift system.

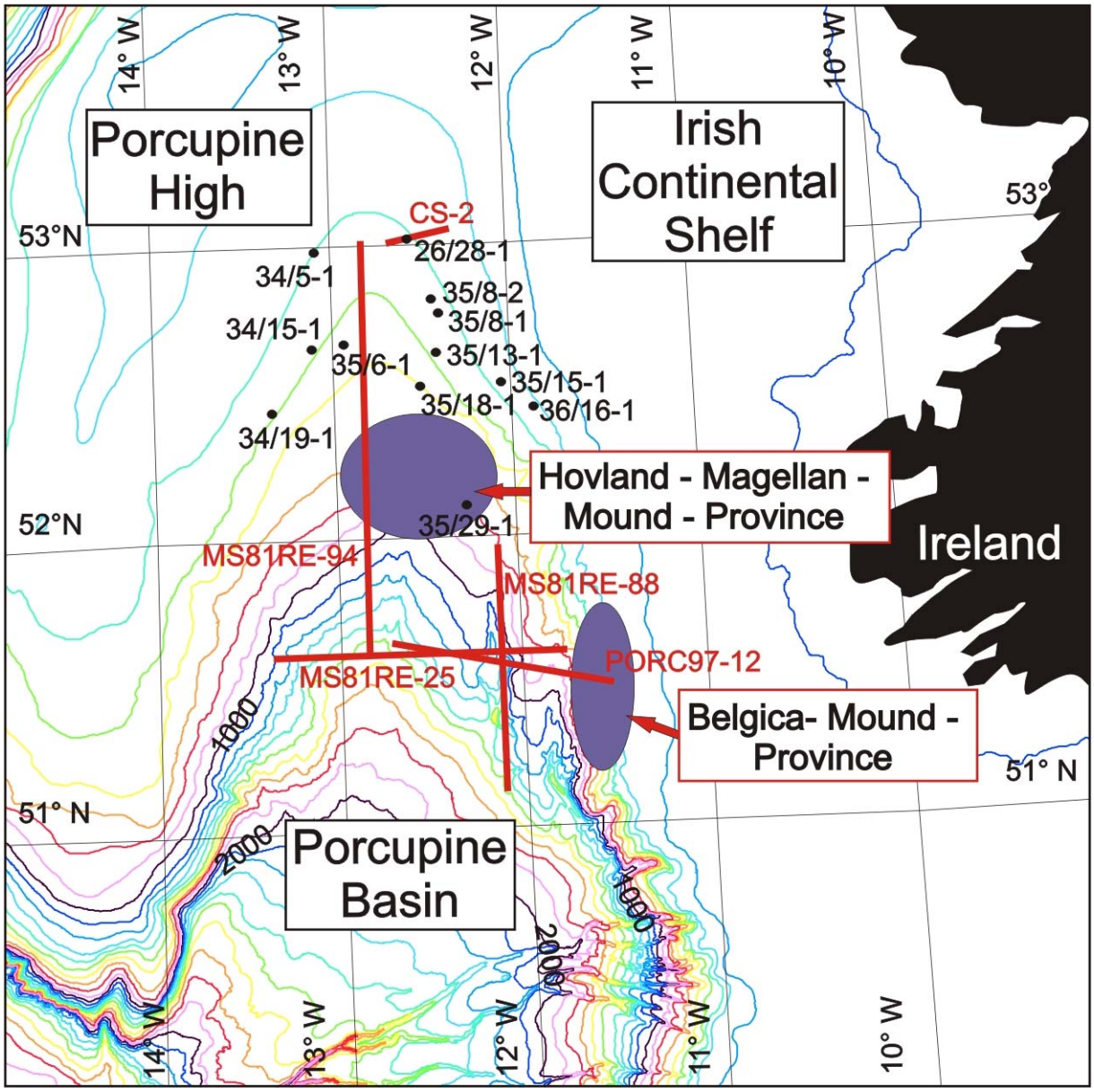

Figure 2-1: The Porcupine Basin including the location of mound provinces, wells and seismic lines; bathymetric contours are in 100 m intervals

Late Jurassic rifting was followed by Late Jurassic - Early Cretaceous thermal collapse and the establishment of passive sedimentation in the Porcupine Basin, with a gradual infilling of the deep-water late Jurassic basin. A similar history is seen in the North Sea and Celtic Sea basins. During the subsequent mid Cretaceous rift phase, the zone of active rifting extended from the Rockall Trough in the southwest through the Faeroe-Shetland and Møre basins into the Vøring Basin to the northeast. Clastic sediment influx occurred at this time in the Porcupine Basin where synrift accommodation space was generated through selective fault reactivation (Corfield et al., 1999). An igneous province in the Porcupine Seabight Basin and adjacent shelf west of Ireland records repeated episodes of intrusive and extrusive igneous activity, from the mid-Jurassic to late Oligocene (Tate and Dobson, 1988). The 150 km long

Porcupine Median Volcanic Ridge is interpreted to be extrusive in the South, but progressively intrusive northwards.

The latest Aptian and Albian deltaic package is interpreted as reflecting a rift episode (Shannon et al., 1993). This rift phase was accompanied by the opening of the North Atlantic and Bay of Biscay and the anti-clockwise rotation of Iberia resulting in a basin flank uplift occurring in Aptian to Albian times (Ziegler, 1981). Extension along the northeast rift zone was accommodated by movement along the previously established set of northwest – southeast trending transfer zones. A transition to passive thermal subsidence followed in the Porcupine Basin. During the Late Cretaceous (Campanian/Maastrichtian) seafloor spreading began in the Labrador Sea and the widespread sea level highstands at this time resulted in extensive chalk deposition (Moore and Shannon, 1995). The latest Cretaceous onset of spreading in the Labrador Sea was succeeded by the initiation of the spreading in the Norwegian-Greenland Sea in the Early Eocene (Knott et al., 1993). The culmination of these events led to the separation of North America and Greenland followed by the break-up of Greenland and Eurasia. Complete continental separation between Greenland and Eurasia did not occur until near the Palaeocene – Eocene transition (Roberts and Aharon, 1994). The earliest Cenozoic strata is marked by a notable marine regression and a subsequent transgressive phase. Influences of the complete continental separation between Greenland and Eurasia in the Palaeocene – Eocene transition (Roberts and Aharon, 1994) on the Porcupine region include underplating beneath Scotland (Brodie and White, 1995), Iceland plume effects (Joppen and White, 1990), eustacy and ridge-push from sea floor spreading west of Hatton Continental Margin (Shannon, 1993).

During Late Palaeocene times a major magma plume became established beneath the rift zone centred over present day southeast Greenland. The development of this hot-spot during the Palaeocene led to thermal uplift of a large area including northern Britain, the central and northern North Sea and much of Greenland. This thermal uplift was episodic with periods of hinterland uplift leading to the shedding of large quantities of clastics into the surrounding basins (Ziegler, 1981). The phases of uplift were accompanied by the extrusion of massive volumes of basalt lava over the Rockall and Faeroe platforms, southeast Greenland and the Jan Mayen and More areas. The active rift zone shifted to the northwest of the Rockall Plateau, continuing through the Møre and Vøring basins. The Faeroe-Shetland Basin became an arm of this rift system (Jacqué and Thouvenin, 1975) (Figure 2-2).

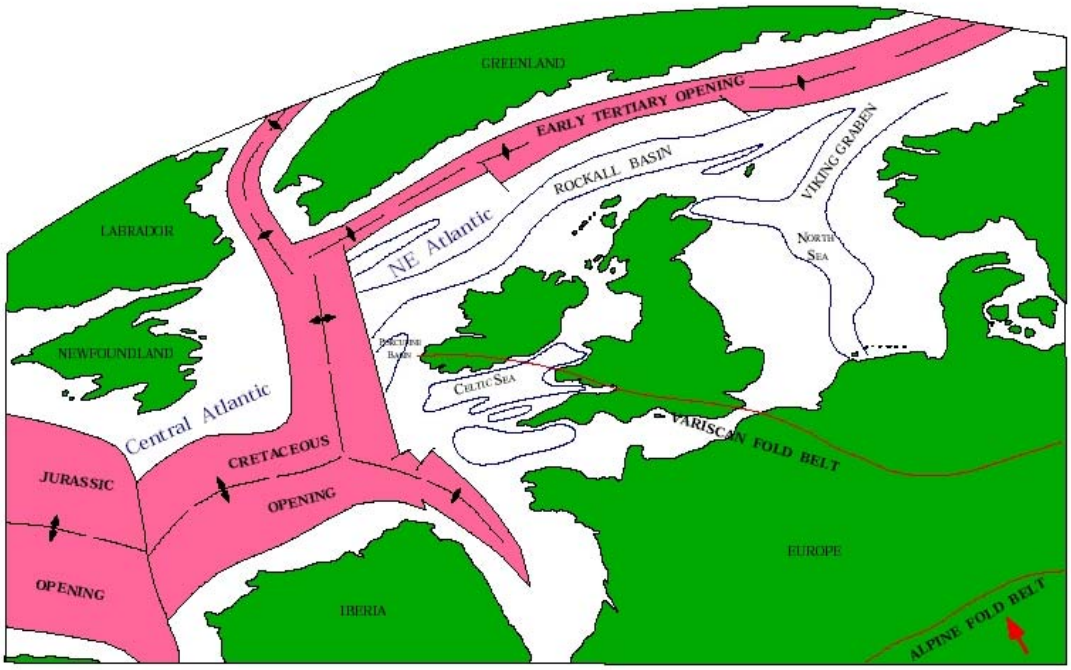

Figure 2-2: Scheme of northward progression of Atlantic sea-floor spreading (Mc Donnell, 2001)

Cenozoic sediments were deposited during generally rising sea levels. This broad pattern was interrupted on numerous occasions by relative sea-level falls. The three main unconformities are of latest Eocene – Early Oligocene (C30), mid-Miocene (C20) and Early Pliocene (C10) age (McDonnell and Shannon, 2001). During the Early Cenozoic a regressive succession, punctuated by minor transgressions, marks a major interruption in the general post-rift thermal subsidence pattern of the region. This regression, possibly triggered by lithospheric thermal effects ridge push stresses and/or alpine deformation pulses, resulted in Palaeocene to Eocene deltaic and submarine fan deposition, with submarine channel trends indicating that sediment was sourced mainly from the Porcupine High to the north and west. The fan deposits are identified at Paleocene-Oligocene and Miocene levels (Shannon, 1993). A significant seismic marker is the Mid-Miocene C20 horizon (McDonnell and Shannon, 2001). The submarine fan deposits are interbedded with mudstones (Shannon, 1993). The thick prograding shelf and deltaic sands in the Porcupine Basin are of Early to Middle Eocene age, deposited during a period of relative high sea level when sediments became trapped on the shelf. These sands were derived from platform areas of the Irish Shelf and Porcupine Ridge, which may have suffered compressive uplift as a result of the initiation of spreading in the northeast Atlantic. The Neogene reflects shale-dominated marine deposition, with the development of slope failure features (Unnithan et al., 2001) and contourite drifts. During Late Cenozoic to recent times there was a lack of significant marginal sediment input in the Porcupine Basin.

The Jeanne d'Arc basin shares a similar Jurassic tectonic evolution to the Porcupine Basin (Sinclair, 1995). The basin is situated in the northeastern Grand Banks area, off the east coast of Newfoundland, eastern Canada (Fowler, 1995). This basin was formed as a result of the Mesozoic extensional rift tectonics which produced the North Atlantic Ocean (McAlpine, 1990). Seafloor spreading between the central Grand Banks and Iberia began in early Aptian time, while farther north, between Flemish Cap and Goban Spur, spreading began by at least late Albian time resulting in the separation from the Porcupine Seabight (Dick et al., 1989). Slow regional subsidence during the Late Cretaceous and Cenozoic resulted in a relatively undisturbed and thin cover of fine-grained marine shelf deposits (Fowler, 1995).

Specific questions to answer for the modelling were:

- how did heat flow evolve through time?
- what was the influence of the Iceland Plume?
- which were the critical petroleum system elements?
- what were the major phases of hydrocarbon generation and migration?
- what are the limiting factors on hydrocarbon migration pathways?

2.1.2 Stratigraphy

2.1.2.1 Pre-Devonian (Crystalline Basement)

This interval is very poorly known, rocks of this age having only been confirmed by two wells within the basin. Croker and Klemperer (1989) reported that the Shell 26/26-1 well terminated in schist-gneiss of probable Dalradian age, and the Phillips 26/30-1 well encountered granite/granodiorite of probable Caledonian or older age (Croker and Shannon, 1987). Auffret et al. (1987) reported that metamorphic and crystalline basement rocks – in detail mica schists and gneisses – crop out on the western flank of the Porcupine Ridge. Lewisian basement is known from the northwest of the Porcupine Ridge (Naylor and Shannon, 1982). The Elf 34/5-1 well terminated in white, indurated, very fine grained quartzite, which, although undated, is of a similar facies type to many Dalradian quartzites seen onshore in west and northwest Ireland (Holland, 1981). Lower Palaeozoic sediments crop out to the south, on the Goban Spur (Auffret et al., 1987).

2.1.2.2 Devonian and Carboniferous

The Devonian and Carboniferous sequences represent the economic basement in the Porcupine Basin and have been encountered in a number of wells (Croker and Shannon, 1987). Onshore, the thick eastwest trending Munster Basin contains Devonian red beds of a thickness greater than 6 km with rapid thinning northwards (Naylor and Sevastopulo, 1979). Again with an eastwest trend the overlying Carboniferous succession is a southerly

thickening wedge of marine sediments of Fammennian - Namurian age in the South Munster Basin (Naylor and Anstey, 1987). From the limited amount of well data available the sequence is sub-divided into a lower poorly dated Devonian - Lower Carboniferous clastic-dominated sequence, and a widespread Upper Carboniferous coal-bearing succession, which might be a good source for gas and condensate (Croker and Shannon, 1987). The lower sequence is encountered in a number of wells close to the basement ridge between the North Porcupine Basin and the Main Porcupine Basin and comprises fluvial, deltaic and occasionally shallow marine facies. Croker and Klemperer (1989) report that some very reflective sequences on seismic sections of possible Carboniferous age are seen in Chevron well 36/16-1 penetrating over 1400m of Carboniferous strata.

The Upper Carboniferous succession encountered in most wells is of continental-brackish habitat and of Namurian through Stephanian age. Four main sequences have been recognised within it (Croker and Shannon, 1987):

(1) Namurian - early Westphalian B: a delta front sequence up to 500 m thick, comprising coarsening-up sandstones separated by thick shales.

(2) Late Westphalian B - early Westphalian C: up to 400 m of abundant coal beds and interbeds of thin sandstones and shales, with some thicker fining-up sandstone cycles. A swampy delta top environment is envisaged with some fluvial point bar development.

(3) Late Westphalian C - Westphalian D: 650 m of thick alluvial fan sheet sandstones, distributory mouth bar and possibly offshore bar sandstones and shales with occasional thin freshwater limestones.

(4) Stephanian: variable thickness due to pre-Middle Jurassic erosion. It is best developed on the western margin of the basin and is thin, or absent, towards the northern and eastern flanks. It is shale dominated with some thin limestones, sandstones and rare coals.

2.1.2.3 Permian and Triassic

The major sediment supply for the Permian and Triassic succession is from the eroded Hercynian Mountains to the south (Shannon, 1991a). A relatively thin Autunian succession conformably follows the Stephanian sequence in the Deminex 34/15-1 well. This is a shale dominated succession with anhydrite traces (Croker and Shannon, 1987) and is only deposited locally.

Triassic strata have only been encountered in the North Porcupine sub-basin in well BP 26/22-1A. It consists of a massive beach sandstone unit overlain by a stacked series of shallow marine glauconitic sand bars. This is in turn overlain by an evaporite-bearing shale sequence (Figure 2-3).

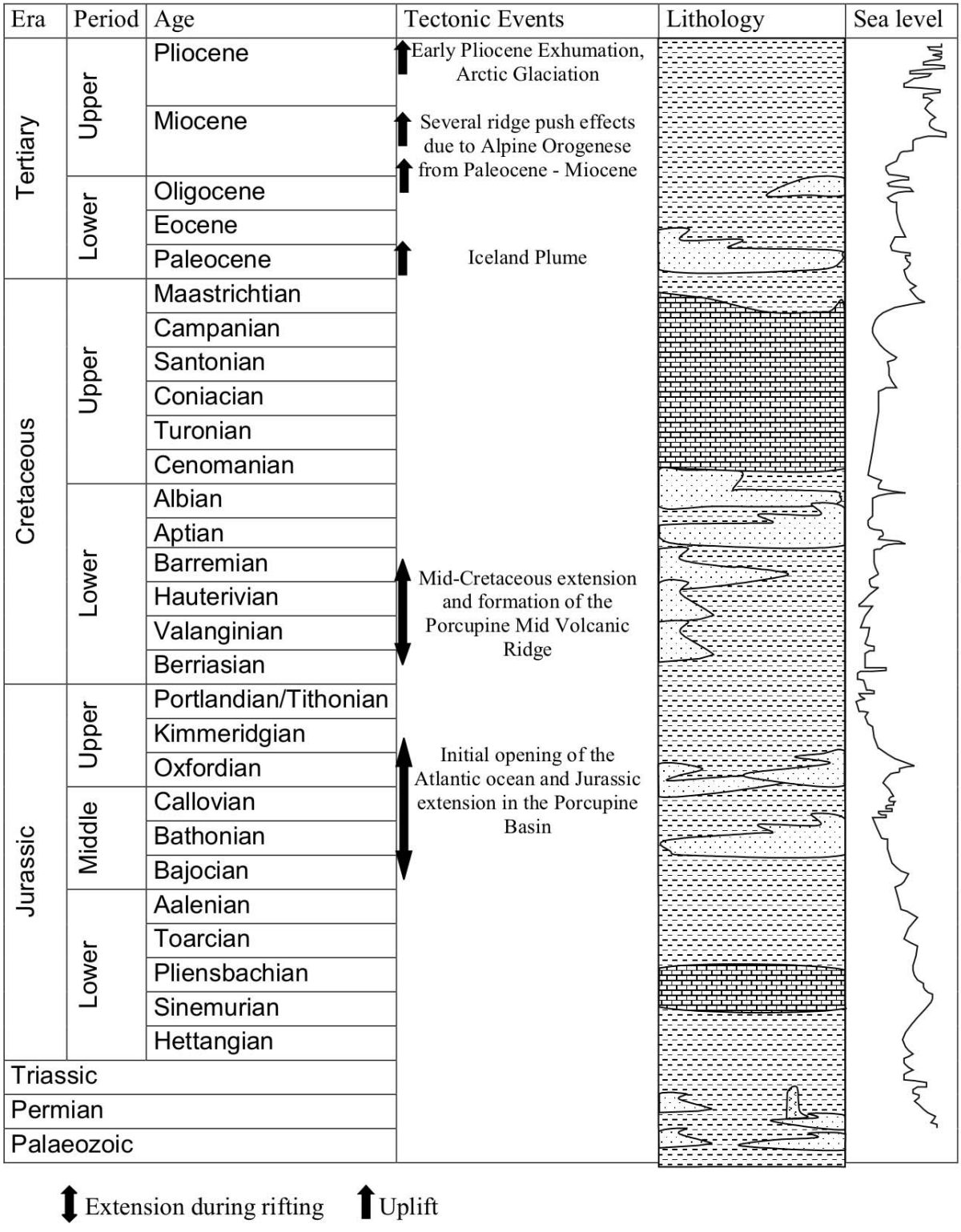

Figure 2-3:Schematic stratigraphy of the Porcupine Basin

2.1.2.4 Lower Jurassic (Liassic)

The Lower Jurassic (Liassic) is only locally preserved and onlaps the irregular underlying topography. The spread out basins are thought to be similar to those of the Upper Triassic (Shannon, 1991a). Liassic strata have only been proven in the North Porcupine Basin where they are of marine facies. The sequence consists of interbedded limestones, shales and occasional siltstones of Rhaetian and Hettangian age, with good petroleum generating potential in some horizons. The sequence is open marine in the Gulf 26/21-1 well while the presence of dolomite in the BP 26/22-1A well may be indicative of a shallow marine environment (Croker and Shannon, 1987).

2.1.2.5 Middle and Upper Jurassic

Middle Jurassic strata of continental affinity mostly rest unconformably on older strata such as the Upper Carboniferous (Naylor and Sevastopulo, 1979), though Ziegler (1981) has reported continental Middle Jurassic clays and minor sandstones lying conformably on the Lower Jurassic in some wells. The oldest Middle Jurassic rocks encountered in most wells in the basin are Bajocian-Bathonian in age. Initial Middle Jurassic sedimentation was continental, with the prominant source area lying to the north with possible minor ones on the eastern and western margins of the basin represented by fluvial, floodplain and lacustrine shales, siltstones and sandstones (Croker and Klemperer, 1989). The fluvial strata debouch southwards and probably grade into deltaic and marine strata in the southern part of the basin (Shannon, 1991a). The sequence is thicker and shalier in the vicinity of the Elf 35/2-1 and Deminex 34/15-1 wells, suggesting more rapid subsidence with less clastic input (Croker and Shannon, 1987). By the end of Callovian times the Middle Jurassic sequence had inundated most of the upstanding areas within the basin except the ridge at the northern end of the main Porcupine Basin (Croker and Shannon, 1987); marine conditions existed in the central and southern parts of the basin, with non-marine conditions present in the north.

Upper Jurassic strata conformably overlie Middle Jurassic sediments in the Porcupine Basin and consist of a northward transgressing marine facies of shales with interbedded sandstones and limestones (Croker and Klemperer, 1989). All upstanding blocks within the basin were submerged by Kimmeridgian times (Croker and Shannon, 1987). Marine shale units in the Kimmeridgian and occasionally the Tithonian have good to excellent oil and gas potential. The Kimmeridgian is regarded as the single most important source rock interval in the basin and is the most probable source for the oil in the Middle and Upper Jurassic reservoirs of the Connemara field. A detailed geochemical study has shown that oils from the Porcupine and Jeanne d'Arc basins were not sourced only from a typical, fully marine Upper Jurassic Kimmeridge Clay Formation equivalent (Butterworth et al., 1999). Rather, these oils are thought to be coderived from Upper Jurassic shale and a Middle Jurassic non-marine source interval. The results indicate that oil from the Porcupine Basin resembles that of the Jeanne d'Arc Basin, eastern Canada (Butterworth et al., 1999).

Oxfordian to Tithonian strata have been encountered in most wells drilled in the basin with a broad range of depositional environments developed in the overall setting of a regional sea-level rise (Croker and Shannon, 1987). The transgressive facies moved progressively northwards throughout the Late Jurassic. Different conditions existed towards the basin margins than in the basin centre, with fluvial conditions giving way to thick (up to 350 m), coarse, wedge-shaped alluvial fans seen on the western margin in Deminex well 34/15-1. Towards the centre of the basin the Phillips 35/8-2 well encountered a deep-water turbidite of Kimmeridgian age. The overlying Middle Tithonian shales represent tranquil marine deposits (Croker and Shannon, 1987).

The Late Cimmerian unconformity and condensed section consists of sediments of latest Jurassic to earliest Cretaceous age. The unconformity cuts across tilted Jurassic fault blocks at the basin margins in a similar way to the classic hydrocarbon structures of the Brent and Ninian oilfields in the North Sea (Morton et al., 1988).

2.1.2.6 Cretaceous

Up to 5 km of Cretaceous strata are preserved in the Porcupine Basin and it rests with angular unconformity upon tilted fault blocks composed of Jurassic and older strata (Shannon et al., 1993). It was deposited during a time of overall sea-level rise with some sea - level falls at approximately Berriasian and Late Aptian times represented by onlap (Moore, 1993). The Cretaceous sediments vary from deep marine claystones in the central part, to fault-bounded clastic fans and prograding deltaic sequences towards the eastern and northern margins (Shannon and Naylor, 1998). Rising sea level culminated in the development of the chalk facies in Upper Cretaceous to lowermost Cenozoic times (Cenomanian-Danian). The chalk is thickest on the basin axis and thins northwards towards the basin ridge separating the North Porcupine Basin from the Main Porcupine Basin and starts thickening immediately north of this ridge (McDonnell, 2001). The formation of the Porcupine Median Volcanic Ridge as interpreted by Roberts et al. (1981) and Masson and Miles (1986) and is associated with an episode of rifting during the Valanginian to Barremian interval which is discussed in detail in chapter 2.1.2.8.

2.1.2.7 Cenozoic

The Cenozoic was also deposited during generally rising sea levels. This broad pattern was interrupted on numerous occasions by relative sea-level falls indicated by the three main unconformities of latest Eocene – Early Oligocene (C30), mid-Miocene (C20) and Early Pliocene (C10) age (McDonnell and Shannon, 2001). During the Early Cenozoic a regressive succession, resulted in Paleocene and Eocene deltaic and submarine fan deposition, with submarine channel trends indicating that sediment was sourced mainly from the Porcupine High to the north and west. This sequence is dominated by four stacked deltaic episodes prograding from north to south with deep marine shales in the south. Deep marine mounded submarine fans often lie beyond penecontemporaneous environments. Sand deposition in the Porcupine Basin occurred principally during Middle to Late Eocene times. In Oligocene

and Neogene times, sediment build-ups developed towards the margins and sedimentation appears to have been principally influenced by oceanographic circulation patterns. Lower Cenozoic coaly, lignitic and shaly deltaic sequences have good gas potential. The Oligocene and Miocene sequences are composed of deep marine, generally mudstone deposits. There is evidence of substantial instability and the main features of these sequences are large-scale soft sediment slump deposits on the basin margins. Some deep marine channels are also present as is some continental slope progradation. Also groups of buried and none buried carbonate mounds have been discovered in the Hovland-Magellan- and the Belgica-mound area. The mounds are up to 2 km in diameter, with heights of 250 m (Henriet et al., 1998). Gravity cores on the mounds recovered deep-water colonial coral debris (Lophelia sp.) with interbedded sandy and muddy layers. During Late Cenozoic to recent times there was a lack of significant marginal sediment input in the Porcupine Basin while Neogene sediment input continued locally in the Hebrides region of the Rockall Basin.

2.1.2.8 Igneous Rocks

Seismic and well data show evidence of considerable igneous activity, the oldest one known being a minor ash fall deposit in the Upper Jurassic of BP well 26/28-1 (MacDonald et al., 1987). Most of the activity is correlated to the Cenozoic extrusives reported from the northeastern area of Quadrant 35 where Tate mapped four major North-East – South-West trending features, together with a number of smaller isolated plugs with Early Palaeocene to late Oligocene age (Tate and Dobson, 1988). Substantial quantities of basic to intermediate volcanics occur in the Miocene of Shell well 35/13-1, while further intrusions and associated sills of unknown composition occur in the southwest of Quadrant 44 (Tate and Dobson, 1988). Sills and Dykes have been noted on a considerable number of seismic lines: most commonly they intruded into Lower Cretaceous sequences.

A major gravity and magnetic anomaly on the eastern edge of the basin just to the south of latitude 53°, has been interpreted by Riddihough and Max (1976) as a large basic intrusive centre, the Brendan Igneous Complex. In the absence of well penetration it has not been dated, but Tate and Dobson (1988) consider a late Cretaceous age as most likely. This igneous centre is postulated to feed many of the Cenozoic dykes and sills in the Main Porcupine Basin. A second linear anomaly within the southern part of the basin and extending into the Porcupine Seabight is interpreted by Roberts et al. (1981) and Masson and Miles (1986) as a buried volcanic ridge, the Porcupine Median Volcanic Ridge, which is coeval with an episode of rifting during the Valanginian to Barremian interval in the Porcupine and Goban Spur Basins. It was discovered on line MS81–61 (Merlin Survey 1981) just to the west of Phillips well 35/8-1 and also reported from the Lower Cretaceous of Quadrant 43 (Tate et al., 1993). The large, elongate volcanic median ridge with a NNE-SSW trend, at least 150 km long and up to 25 km wide, lies subparallel to, and broadly coincident with, the axis of the Porcupine Basin. Its age has been further constrained by using its reversed magnetization (Young et al., 2000), which is thought to must predate the Cretaceous normal polarity period extending from the Aptian to Early Campanian. Seismic stratigraphy shows

that the ridge consists of three discrete layers of which only the first pertains to the northern intra-Jurassic extension. Layer 1 is a homogenized core region, layer 2 comprises a narrow outer zone surrounding the core and layer 3 is a marginally developed wedge-shaped zone of more parallel and continuous reflectors inclined at higher angles than layers 1 and 2. However, there is no clear seismic evidence for Late Cretaceous igneous activity in the Porcupine Seabight Basin.

Specific questions to answer for the modelling were:

- what is the vertical and lateral distribution of sandstones, shales and limestones?
- what are the petrophysical properties concerning heat and fluid transport?
- what are the source rock and reservoir rock distribution?

2.1.3 Petroleum System Elements

The occurrence of petroleum in the Connemara Oil Field and detection of oil and gas shows in other areas shows that all four elements of the petroleum system namely source, reservoir, seal and trap are in place in the Porcupine Basin. The petroleum system is defined as a natural system containing an active source rock, oil and gas and all the geologic elements and processes that are essential for hydrocarbon formation and accumulation (Magoon and Dow, 1994). Appropriate relative timing of formation of these elements and the processes of generation, migration and accumulation are necessary for hydrocarbons to accumulate and be preserved. The components and critical timing relationships of a petroleum system can be displayed in a chart that shows geologic time along the horizontal axis and the petroleum system elements along the vertical axis.

The physical properties and exact chemical composition of generated hydrocarbons varies from one locality to another based on the differences in source rocks and geological evolution. For determination of the petroleum composition various analysis can be carried out e.g. physical, thermal, electrical, and optical property testing methods as well as spectroscopic, chemical, fractionation, and chromatographic methods. Petroleum reservoir fluids are usually classified into five fluid categories: dry gas, wet gas, gas condensate, volatile oil and black oil (Rhodes et al., 1992). The first three of these are in gaseous state at reservoir conditions and gas and wet gas are distinguished by their content of light hydrocarbons. Gas condensates contain significant amounts of C_{5+} components depending on the PVT conditions meaning that with decreasing pressure the amount of condensing liquids increases. The reservoir oils are classified as either black oil or volatile oil based on the gas to oil ratio (GOR). The solution GOR is the amount of dissolved gas that will evolve from the oil as the pressure is reduced to atmospheric from some higher pressure. GOR is usually expressed in units of SCFgas/STB oil. A GOR of about 750 SCF/STB is a good indicator for the demarcation between these two oil types with black oils having the lower GOR (Rhodes et al., 1992). Reservoir fluid properties are usually plotted in a pressure-

temperature diagram for a specific composition. Depending on reservoir temperature, a fluid can be defined as an oil or a gas. An oil exhibits a bubblepoint pressure at saturated conditions, while a gas condensate exhibits a dewpoint pressure.

For exploration purposes the estimation of generated hydrocarbons is the main task. For the forecast of recoverable reserves material balance equations or decline curve analysis to production history curves are applied (Slatt et al., 1992). For example in a depletion type reservoir, the solution gas to oil ratio is sometimes plotted versus cumulative oil production (Garb and Smith, 1987) and in the case of a good straight-line relationship the curve can be used for recovery predictions.

The calculation of hydrocarbon generation and migration in the Porcupine Basin is one main task of this study, therefore the petroleum system elements are listed in the following section.

2.1.3.1 Source Rocks

Several publications suggest potential hydrocarbon source rock intervals occur in the Carboniferous to the Cenozoic (Butterworth et al., 1999; Croker and Shannon, 1987; Croker and Shannon, 1995; Moore and Shannon, 1995). In four wells in the Connemara oil field migrated hydrocarbons were encountered and several others had oil and gas shows. The lacustrine / marine Upper Jurassic source rock sequence has been documented as the best oil-prone source rock. It contains good to excellent oil and gas source potential with TOC values about 3-4 % at maximum (Croker and Shannon, 1987; Shannon et al., 1995). Also, Middle Jurassic shales have locally good oil and gas potential with TOC values up to 1.8 % (Shannon and Naylor, 1998) but are along with Ryazanian to Aptian marine shales of an amorphous oil-prone type of minor importance. Aptian – Albian shales with TOC values of up to 2.7 % have fair oil-generating potential. In the Lower Cenozoic immature coaly, lignitic and shaly deltaic sequences have gas potential with TOC values of up to 50.5 %.

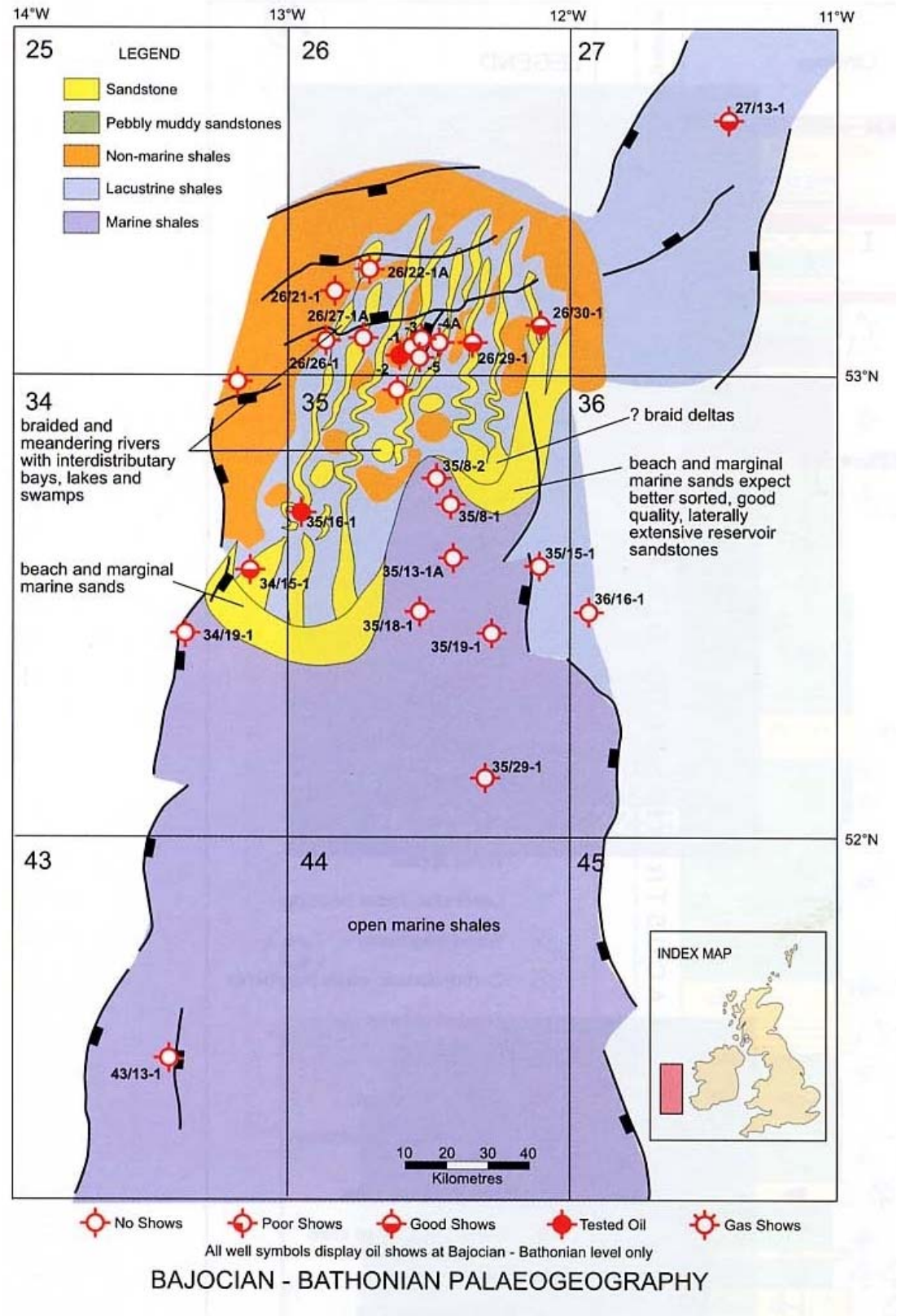

Figure 2-4: Generalized Middle Jurassic paleogeographical reconstructions of the Porcupine Basin (Butterworth et al. 1999)

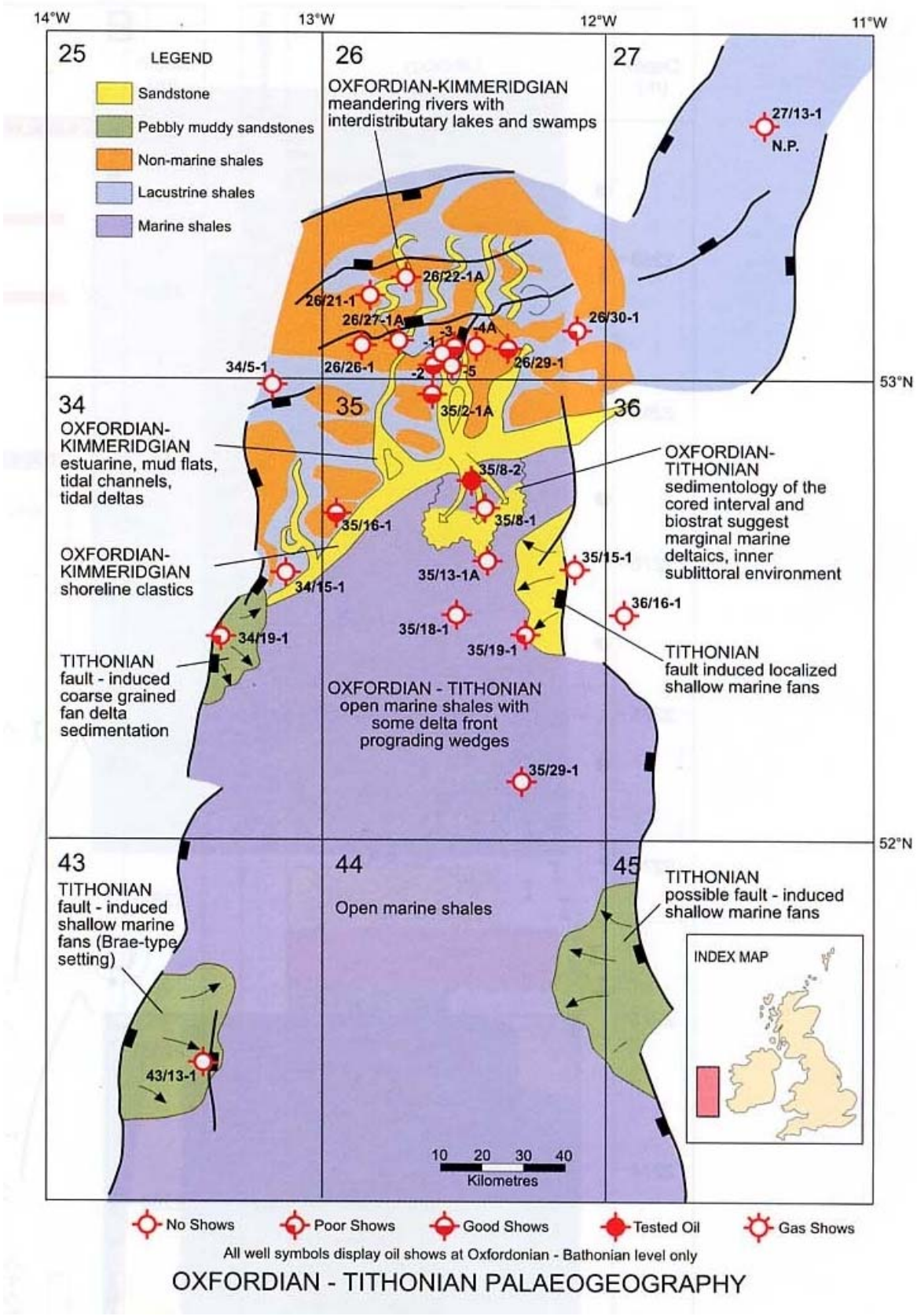

Figure 2-5: Generalized Late Jurassic paleogeographical reconstructions of the Porcupine Basin (Butterworth et al. 1999)

Reconstruction of the paleo environment of the Porcupine Basin (Figure 2-4, Figure 2-5) indicate that non-marine conditions prevailed in the northern part of the basin from at least Bathonian until well into Kimmeridgian age whereas the southern part was fully marine (Butterworth et al., 1999). Fluvial and costal plain channel sandstones are interbedded with lacustrine shales and sandstone deltas. This entire facies assemblage (Butterworth et al., 1999) reflects a periodic development of shallow lakes with preservation of sand-prone lacustrine deltas and periodic algal blooms. These lacustrine shales are excellent oil-prone source rocks with TOC values from 1.5 – 4 % and HI > 500 and can be related to lacustrine shales in the Jeanne d'Arc Basin, offshore Newfoundland, Canada. Potential source rocks of Kimmeridgian age were there deposited in the Egret Member of the Rankin Formation (McAlpine, 1990). Oil and gas discoveries have been made in clastic Late Cretaceous sediments.

2.1.3.2 Reservoir Rocks

Upper Carboniferous deltaic layers provide up to 200 m of sandstones with net/gross ratios within the range 0.1-0.5, and porosities typically around 5-15 % but occasionally ranging up to 20 %. Permo-Triassic strata with generally limited areal distribution in the Porcupine Basin contain a net sandstone thickness of 150 m, with an average porosity of 22 % in the north of the basin.

The Middle Jurassic succession in the northern part of the Porcupine Basin has a gross thickness of 250–400 m with net sandstone/gross thickness ratios of up to 0.25. Porosities average at 17-22 % and permeabilities are typically in the order of tens to hundreds of mD. Approximately 200 m thick Oxfordian to lower Kimmeridgian continental to marginal-marine packages with a net sandstone/gross thickness ratio of approximately 0.25, porosities averaging 19 % and permeabilities in the order of tens to several hundreds of mD are found along the margins of the Porcupine Basin. On the western margin of the basin Tithonian clastic fans have gross sandy intervals of approximately 350 m and a net/gross ratio sometimes in excess of 0.5 and porosities about 12-15 %. Thin Cretaceous reservoirs were drilled in the pre-Aptian of the Porcupine Basin, the thickest sequence of Cretaceous reservoir rocks are the Late Aptian to Albian, deltaic and overlying shallow-marine sandy succession with drilled thicknesses up to 366 m, while net/gross ratios are typically in excess of 0.5 and porosities average 25-30 % located in the shelf and marginal areas. Lower Cenozoic deltaics contain about 200 m of net sandstones with porosities of up to 39 %.

The Mesozoic and the Cenozoic succession in the Porcupine Basin contain sandstone reservoirs at various levels, some of which are of limited areal distribution. These sequences have also been drilled in the northwest offshore basins (Shannon and Naylor, 1998). Numerous carrier beds in the Cenozoic might channel flow of seeping hydrocarbons. McDonnell (2001) proposed a model where Oligocene contourite deposits provided a fluid seepage pathway from beneath assuming that this succession has a coarser grained component than the adjacent basinal mudstone succession. Seismic investigation indicates a strong spatial coincidence between carbonate mounds and the extent of underlying

contouritic deposits which are assumed to be sand-prone, which is supported in well 35/18-1. The underlying Eocene and Paleocene deltaic sequence is assumed to be the hydrocarbon source. Fluids may have seeped through the sandy contourite deposits towards the mound area. Additionally to the Oligocene contourite deposits strong coincidence is seen between mound locations and a Miocene (C20-horizon) contouritic package.

2.1.3.3 Cap Rocks

Mesozoic and Cenozoic layers include adequate thicknesses of shales to provide efficient cap rocks for the sandstone reservoirs (Shannon and Naylor, 1998). The Aptian sand is sealed by an Albian mudstone, the Miocene sand deposits are overlain by Miocene contourite deposits and Pliocene basinal mudstones. In the Connemara oil field, the Jurassic reservoir is sealed by the juxtaposed Cretaceous mudstones and overlying Upper Jurassic shales.

2.1.4 Traps and Exploration Plays

Extensional episodes lead to four different play types for hydrocarbon accumulation (Shannon and Naylor, 1998), tilted fault-block structures, Jurassic, Cretaceous and Cenozoic clastic fans, Cretaceous and Cenozoic deltas and Upper Cretaceous stratigraphic traps shown in Figure 2-6.

Tilted fault-block structures are most clearly developed along the basin margins. The Carboniferous fault-block structures are best developed along the eastern margin and Upper Carboniferous deltaic sandstones are sealed by interbedded shales or by overlying Cretaceous shales. Source rocks are recorded in the Carboniferous coaly sequence. Along the western basin margin and towards the northern part of the Porcupine Basin Jurassic syn-rift tilted fault-block structures occur with Middle and Upper Jurassic fluvial sandstones and submarine fans as reservoir units and interbedded shales as source and cap rocks.

In Block 26/28 BP Petroleum Development Limited (Ireland) discovered oil in well 26/28-1, later delineated to the Connemara oil field (MacDonald et al., 1987). The rotated, extensional-fault-block structure contains oil-bearing reservoirs. During the late Jurassic episode crustal extension formed the fault-block with an average dip of approximately 20 degrees, which was followed by deposition of the volumetrically most important Bajocian to Kimmeridgian reservoir sandstone. In part it is coeval with deposition of the shallower Kimmeridgian to Early Tithonian reservoir sandstone. Fault movement largely ceased during the Early Cretaceous. From Barreminan to Aptian times the rift topography was progressively infilled by marine mudstones. During Cenozoic times the larger faults were reactivated. Jurassic source-rock maturation could have been achieved during the Late Cretaceous in the deeper parts of the Porcupine Basin. The volume of oil within the western segment of the Block 26/28 structure is estimated to be approximately 120 million stock tank barrels with an additional 75 million stock tank barrels within the eastern segment.

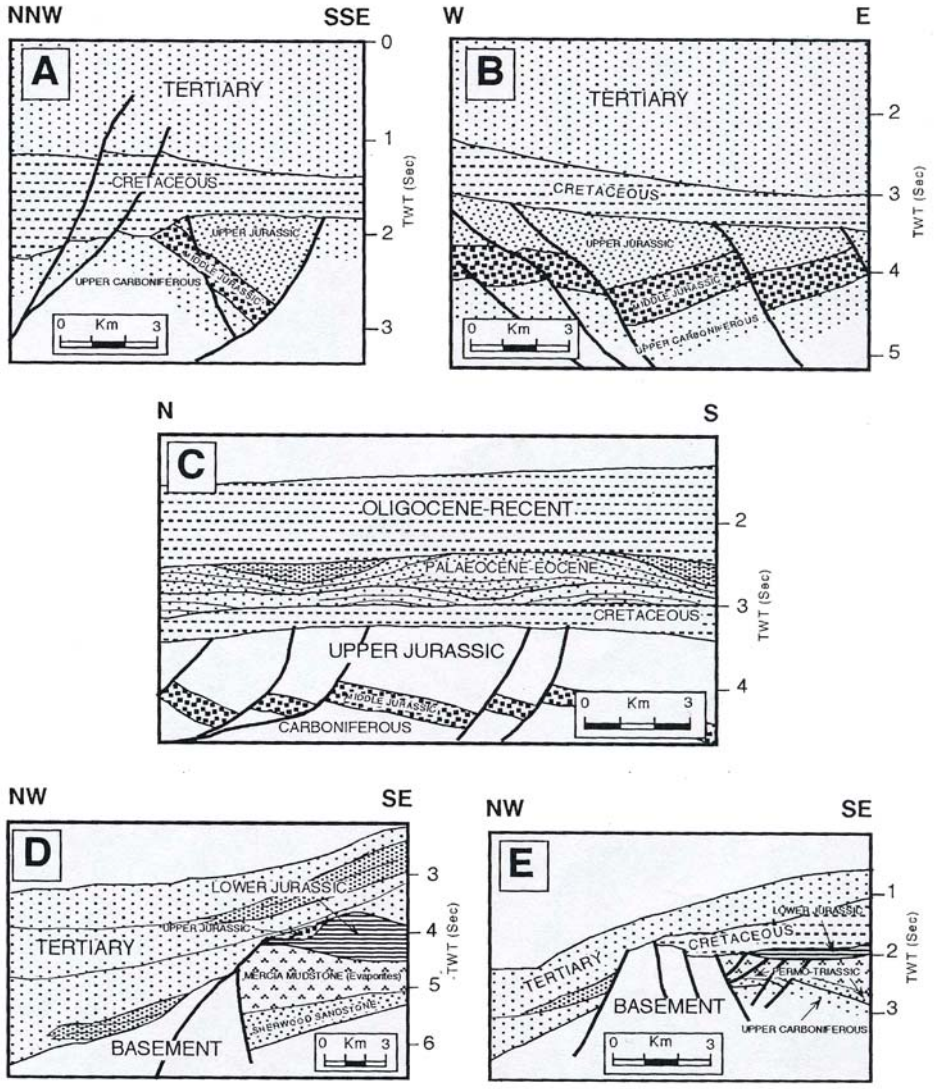

Figure 2-6: Play types with A: rotated and tilted fault blocks, B: basin edge tilted fault blocks, C: deltaic stratigraphic traps, D: stratigraphic traps adjecent to Basement and E: stratigraphic traps on basement horsts (Croker et Shannon, 1995)

Jurassic, Cretaceous and Cenozoic clastic fans developed along the basin margins and intrabasinal highs with an either stratigraphic or fault related closure. Upper Jurassic fault-controlled fan deltas are sourced from Upper Jurassic shales and sealed by Lower Cretaceous shales. Cretaceous submarine fans are topographically controlled, when sand-prone sediment gravity flows preferentially focussed into the topographic residual footwall lows developed during Early Cretaceous thermal subsidence in the basin. The Late Palaeocene submarine fans are also stratigraphically controlled. They are charged from the basin centre by mature Jurassic and Cretaceous shales or Carboniferous coals and sealed by distal fan or overbank shales.

Cretaceous and Cenozoic deltas occur especially in the northern and eastern parts of the basin during the Lower Cretaceous (Aptian-Albian) and also in the northern part of the basin

in the Lower Cenozoic (Palaeocene-Eocene). Top-seal is provided by overlying delta-top and marine shaly strata and the source rocks are most likely Jurassic or Cretaceous shales in the central part of the basin.

Upper Cretaceous stratigraphic traps are marked by a series of mounded, circular to slightly elongate structures at the top of Cretaceous chalk succession which are interpreted as possible biohermal reefal buildups. They are onlapped and draped by uppermost Cretaceous and lowermost Cenozoic strata. These structures could be sourced by deeper, mature Jurassic or Cretaceous shales.

Specific questions to answer for the modelling were:

- what are the source rock properties (richness, quality, maturity)?
- what are the reservoir rock properties – how do these control not only occurrence of petroleum but also surface manifestations?
- what are the cap rock properties?
- what are the trap properties?

3 Choice of Methods and Samples

3.1 Numerical Basin Modelling

Numerical basin modelling, developed in the first instance for hydrocarbon exploration purposes, is based on the description and calculation of all geological processes during the evolution of sedimentary basins (Poelchau et al., 1997). The task of the simulation is to predict the occurrence and composition of petroleum in time and space. Important for that task is the reconstruction of all chemical and physical processes which means, e.g. that it is not only important to know the time of sedimentation of a potential source rock but also to know the generation history, migration processes and possible traps (Tissot, 1969). All these processes have to be recognized and understood especially in chronological order; then to be described in a numerical model to simulate the formation and retention of a hydrocarbon accumulation up to the present day. This workflow allows quantitative statements on the geological and thermal evolution of the study area.

It is almost impossible to observe geological processes directly because of their low speed over geological time frames. For the simulation a lot of information has to be gathered and brought into the right chronological order and described mathematically using physical and chemical laws. Especially the interaction of the different processes requires an iterative calculation of all parameters.

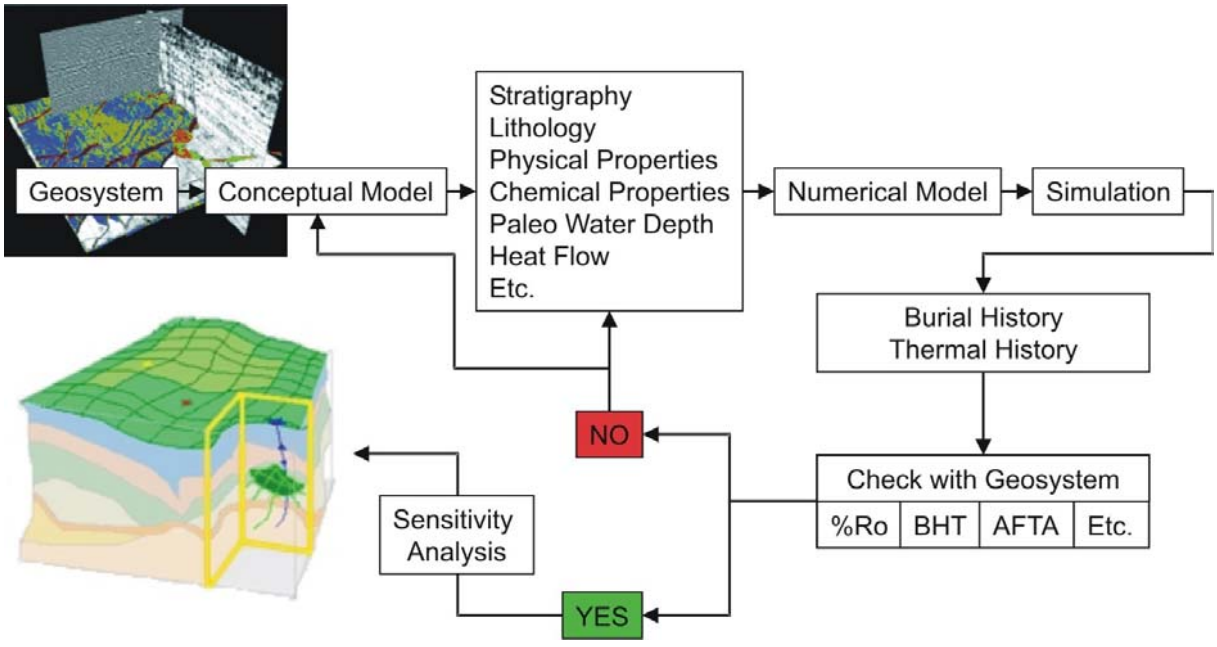

Figure 3-1: Principles of numerical simulation

The principles of numerical simulation are shown in Figure 3-1. Starting with the Geosystem, which is the study area, a conceptual model is developed. The evolutionary history of a geologic sedimentary basin consists of a sequence of events in time during which a large

number of physical processes have acted on the basin materials in three-dimensional space. The computer simulation requires the quantification of all defining parameters, and the conceptual model provides the temporal framework, which is needed to structure the input data (Wygrala, 1988).

The conceptual model is a formulation of the principal elements of a basin history suitable for numerical treatment (discretization) (Welte and Yalcin, 1987). It must be based on the interpretation of conventional geologic, geophysical, and geochemical observational data placed in a temporal framework. Stratigraphic analysis provides the most crucial input to the conceptual model. From such analysis, basin history is subdivided into an uninterrupted sequence of events, of specified age and duration, which take place during the evolution of the basin. Each stratigraphic event represents a time span during which one of three basic geologic processes prevailed, i.e., accumulation of a layer (deposition), non-deposition (hiatus), or uplift and erosion (unconformity). Similarly, structural and tectonic events, such as folding, faulting, fracturing, salt piercement, may be included in the conceptual model when reasonable geologic age limits and durations can be assigned. The resulting conceptual model of the geologic basin history provides the numerical “pattern,” both physical and temporal, which provides the essential input for the basin simulation programme. Evaluation of input data implies defining the physical stratigraphy, chronology, and the physical properties of the basin-fill materials, identifiying the post-depositional processes, their timing, and their kinetics.

Clearly, stratigraphic history modelled as a sequence of events is the most basic and common requirement for the design of all basin models (Welte et al., 1997). However, the conceptual model has certain shortcomings when used in more advanced basin modelling systems where a multitude of postdepositional processes are considered which can change or add parts of the stratigraphic section. This concerns, for instance, diagenetic alteration of only parts of selected layers such that a new physical stratigraphic entity is created long after deposition. Other examples are interstratal hydrothermal deposits or intrusive sills. A second problem is the rigid time frame of a limited number of events extending over the entire cross section. Advanced finite element modelling systems are capable of much higher and varying time and space resolution that can be adjusted to local differences in geologic details.

The numerical model is based on ideas and experience gained from working with the basin simulation programs PDI-PC™ and PetroMod™ developed by IES Juelich. IES started 1975 with the development of one dimensional (1D) maturity modelling (Tissot and Espitalié, 1975). Under the assumption of the change in lithology properties during compaction and decompaction the simulation allows a continuous recalculation of density, porosity and permeability in geological time. These iterative calculations lead to the burial history and with the integration of heat flow data to temperature history of a number of layers or a single horizon. In contrast to the first models, which were based on a constant temperature gradient, present day thermophysical parameters like heat conductivity and capacity are calculated in dependence of lithology and grade of compaction. Therefore a calculation of the change in temperature with the change in depth is possible and leads to a more precise

temperature history, which is very important with respect to hydrocarbon generation. Small changes in temperature can have significant effects on the generation of hydrocarbons (Tissot and Welte, 1984).

This technique was used to calculate the temperature history, the generation of oil and gas and petrophysical rock properties but could not predict the migration and accumulation of hydrocarbons. Therefore two-dimensional (2D) methods have been developed since 1980 to take the spatial dimension into account (Wygrala, 1988). Now it was possible to calculate and display the generation, migration and accumulation of hydrocarbons through time along profiles (Clayton and Hay, 1994; Magoon and Dow, 1994). In addition to the previous described calculations 2D-modelling techniques are able to simulate lateral heat flow and heat flow altered by aquifers. These parameters can change the migration and accumulation of hydrocarbons as well as the temperature. Since 2000 a modelling software to calculate processes in time and three dimensions has become available.

For this project the simulation program PetroMod^{TM} (version 7.1) from IES GmbH Juelich was used. The program uses a forward modelling approach to calculate the geological and thermal evolution of a profile in depth and time. For a 2D – simulation, the profile has to be divided into dimensional and time units. Vertical Gridlines define the lateral resolution of the profile. The event ages define the temporal resolution. To set a time frame for the geological evolution of the basin a series of complete chronostratigraphic events is necessary. The gridlines and events set up a net of finite elements in which the input and results from the simulation are stored numerically. Especially important is that there is a direct exchange of data, which enables a simulation of lateral geological processes such as migration of fluids and heat flux.

After the numerical model is defined and the architecture or geometry of the basin is adjusted the input data has to be defined. Evaluation of input data means defining the physical stratigraphy, chronology, and the physical properties of the basin-fill materials, identifying the postdepositional processes, their timing, and their kinetics, to finding the various temperature and maturation measures needed for calibration of the model and the final output of burial and temperature history and hydrocarbon generation (Figure 3-1). These parameter assignments are just a first approximation. The label “shaly sand” points to a collection of parameter values (density, thermal conductivity, heat capacity, compressibility, etc.), which may be typical for the average “shaly sand”. The particular layer may have actual values far from that average, and perhaps closer to another lithology with a different label. What counts are the values of physical properties that are assigned to a given lithology (Poelchau et al., 1999). These can be default values suggested by the program or user-defined values given through actual measurements. In most modelling areas rock samples are rare and default values are commonly taken.

Once all input data is defined the simulation is started. In principle a simulation is the reconstruction of a temperature- and pressure field over time in the chosen geological system under consideration of conductive and convective heat flux as well as radioactive

heat sources. Pressure calculation is based on compaction and pressure of fluids. The compaction of a sedimentary layer is a function of the compressibility and the effective stress which is the difference between the maximum stress (vertical stress) and the pore pressure (Bjørlykke, 1997). An increase in the overburden load or due to reduction in pore pressure constrains effective stress resuming in compaction. Pressure is divided into a lithostatic, hydrostatic and pore pressure compound (Lee and Deming, 2002). As long as the pores of the sedimentary column are interconnected and ultimately open to the surface and there is sufficient permeability, the fluids inside the pore space are under normal hydrostatic pressure (Welte et al., 1997). Lithostatic pressure is attained when the pore fluid carries the entire load of the overlying water-saturated sediment column. Interstitial fluid pressures in sediments vary between hydrostatic and lithostatic pressures (Figure 3-2) and are controlled by the radius of the pores, gravity acceleration, the height of the hydrocarbon column, the density of the fluids, the interfacial tensions between hydrocarbons and water, temperatures and thermal conductivity of the rock (Bjørlykke, 1997; Poelchau et al., 1999; Tissot and Welte, 1984). Overpressure and fracturing of rocks are also considered during the simulation. Calculation of thermal maturation of organic matter and generation of hydrocarbons is based on chemical kinetics in combination with the calculated temperature history and will be described later. The temperature history itself results from the burial history in a temperature field changing over time. These interactions are calculated in an iterative process. The simulation is a forward modelling method, starting from the oldest defined geological section and resulting in a continuous chronological process to the youngest event.

After the simulation, the output has to be checked against the “real Geosystem” (Figure 3-1). A geologic system is complex because of the many interactions of the multitude of geologic, physical, and chemical processes taking place. A similar complexity exists in the basin simulation system that tries to imitate the geologic reality. To achieve this, the conceptual model is calibrated by comparing the simulation results with measured or observed data (Poelchau et al., 1999; Yalcin et al., 1997). Data that can be used for the calibration include the thickness of the different units, porosity, pressures, temperatures, and maturity distribution (usually expressed by vitrinite reflectance values) (Leischner et al., 1993; Noeth et al., 2002). The calibration process is based on modifications of the conceptual model by adjusting the input parameters until an acceptable match has been reached between measured data and simulation results. However, geological, physical and chemical rules should not be violated during this procedure. The calibration procedure helps narrowing the range of those parameters that cannot be measured directly. Typical examples for such parameters are the paleo heat flow history, duration of erosional and depositional events, original thickness of eroded units, and lithology of the eroded units (McCuen, 1973).

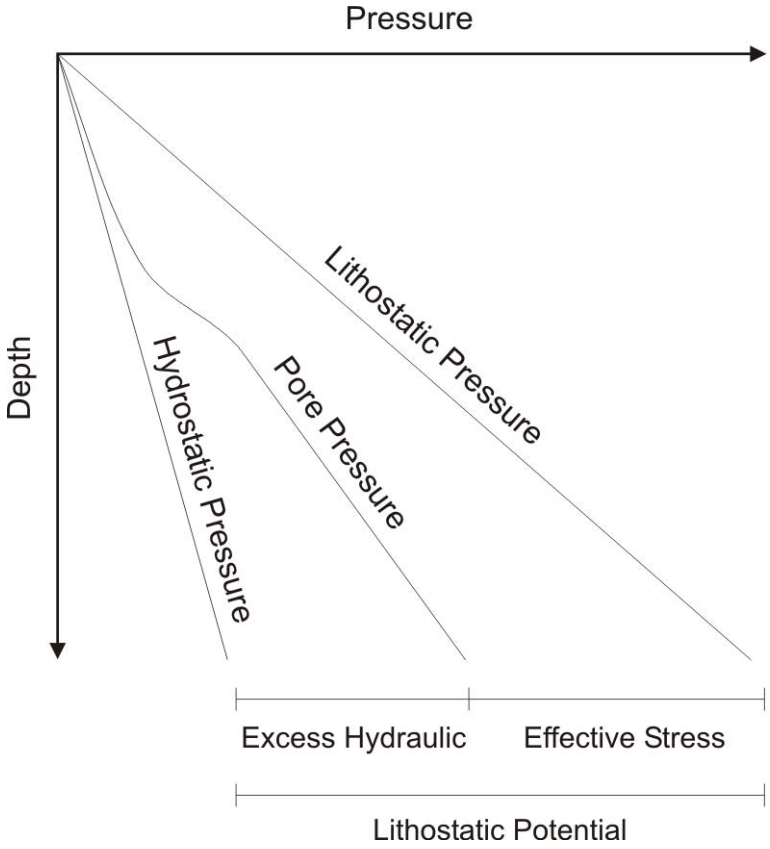

Figure 3-2: Relation between hydrostatic, pore and lithostatic pressure (modified after Welte et al., 1987)

It is important to note that the calibration procedure, i.e. the modifications of the conceptual model, is independent of the simulation run: the calibration parameters, which have to be matched with the simulation results, are not used as input parameters or as boundary conditions for the calculation. The calibration procedure of the model requires therefore an iterative change of input parameters within reasonable ranges. In this sense, the calibration procedure is not a mathematical fitting routine as other authors tried to approach the problem (Lerche, 1990). A study therefore requires careful tracing of the behaviour of various variables using sensitivity analysis.

3.1.1 Modelling Hydrocarbon Formation

Assessing the temporal and spatial limits of petroleum migration in sedimentary basins is one of the most fundamental problems in basin modelling (Schenk et al., 1997b, and references cited therein). Hydrocarbons are generated from macromolecular organic matter due to thermal degradation during burial. The multitude of chemical reactions involved are unknown in detail and irreversible (Welte, 1965). Chemical reaction kinetics describe the formation of oil and gas from kerogen. Total petroleum generation is first described by bulk kinetics making no distinction between oil and gas, and product yields at various levels of conversion or maturity. Compositional kinetics are then used to describe the rate at which organic matter

decomposes into oil and gas and finer subdivisions of these compounds or compound-classes. Such resolution is required in order to determine the yields and timing of generation of dry gas (C_1, methane), wet gas (C_2-C_4), light oil (C_5-C_{14}) and normal oil (C_{15+}) as well as to explain the first oil formed and expelled from source rocks and also to predict GOR and gas wetness at varying temperatures or maturities (Jarvis and McKenzie, 1980).

Kinetic data are derived from source rocks using different techniques e.g. Rock-Eval type or closed (MSSV type analysis) system pyrolysis experiments (Schenk et al., 1997a). The most common way of gathering kinetic data for gross petroleum generation is by programmed-temperature open-system pyrolysis (Schaefer et al., 1990). Open system pyrolysis simulates the behaviour of a source rock that would expel volatile compounds into a cool trap as soon as they are generated (Ungerer, 1989). Therefore an estimation of the exact amounts should not be expected since heavy compounds are not volatilized (Ungerer, 1989). Modelling closed system pyrolysis results in identical pre-exponential factors and rather similar gross hydrocarbon potential vs. activation energy distributions but open-system pyrolysis may overestimate the genetic potential of source rocks (Schenk and Horsfield, 1993). During closed-system experiments two factors cause lower yields, first the extent of secondary cracking reactions and secondly the tar condensation in the analysis system. Despite of the activation energy distributions only the yields were affected based on the assumption that the proportions of tar-forming vs. non-tar-forming products are in balance (Schenk and Horsfield, 1993). The role of water in closed-system pyrolysis is controversial (Ungerer, 1989). Comparing open, high pressure and hydrous pyrolysis shows that empirically the degree of pyrolysis severity to form volatile products in open pyrolysis is similar to that required to form an expelled oil phase in hydrous pyrolysis (Burnham, 1995). As an effect of the differences in pressure, the yields of hydrocarbons from open pyrolysis are close to those from hydrous pyrolysis, but hydrous pyrolysis tends to assist the separation of hydrocarbons from polar materials. But independent from the pyrolysis method is the assessment of the timing of petroleum generation (Schenk and Horsfield, 1993).

The success of hydrocarbon formation predictions depends strongly on how closely the samples analysed resemble the actual source rocks (di Primio et al., 2000). In a basin it is difficult to assess, which source rock generated which petroleum due to vertical and lateral source facies changes and migration. In cases where source rock samples are absent asphaltenes derived from oil samples can be used instead. Asphaltenes are organic macromolecular aggregates and are assumed to bear close structural similarities to their precursor kerogens. This structural signature is carried within asphaltenes expelled from source rocks during petroleum migration, hence kinetic information derived from oil asphalthenes can be used as an alternative to source rock kerogen kinetics (di Primio et al., 2000).

Bulk kinetics require the application of “gross” kinetic concepts, whereby molecular precursors of oil and gas are replaced by so-called bulk petroleum or gross hydrocarbon potentials which are fractions of total product yields (Tissot and Espitalié, 1975). These potentials are assumed to be more or less simultaneously transformed into hydrocarbons

during natural evolution or pyrolysis. This process is described by the sum of n parallel pseudoreactions based on the Arrhenius equation:

$$k = f(T) = A \cdot e^{(-E/RT)}$$

with k being the reaction rate constant, A the pre-exponential frequency factor, E the activation energy, R the ideal gas constant and T the absolute temperature. The reaction rate constant k strongly increases with temperature T and is therefore a parameter for the speed of the reaction (Schaefer, 1999). Upon burial, the transformation of the sedimentary organic matter can be described by a multitude of parallel and consecutive reactions, which are unknown in detail, but are recognized to be quasi-irreversible and controlled by chemical kinetics (Dieckmann et al., 1998). Kinetic laws represent a mathematical link between high temperature – short time and low temperature – long time configurations, and allow an extrapolation from laboratory to natural heating conditions. The kinetic analysis method used is based on the mathematical model described by Schaefer et al. (1990). It describes the hydrocarbon generation rate versus temperature, or geological time, assuming a number of first-order parallel reactions with respective activation energies and a single pre-exponential “Arrhenius”-factor.

Bulk kinetics constrain all data to a single set of kinetic parameters, which limits its capability to predict early oil generation or the broad dry gas generation window. Compositional kinetic data, which measures the rate of kerogen decomposition into specific chemical moieties, provides detailed kinetic parameters and hydrocarbon yields for each of these fractions (Jarvis and McKenzie, 1980). Further, these data show that the gas window varies among and within kerogen types, as do the condensate and oil windows. In addition these data explain the formation of early oil, i.e., the oil present in low to early oil window maturity source rocks. Compositional kinetics have been defined by several authors: (Abu-Ali et al., 1999; Béhar et al., 1997; Burnham, 1989; Dieckmann et al., 1998; Pepper and Corvi, 1995; Tissot et al., 1987; Ungerer, 1989; Vandenbroucke et al., 1999).

Since the main objective of the study was to reconstruct the migration pathways of gas to the surface, a description of gas generation and gas volumes evolving from phase separation of migrating petroleum was required. The newest basin modelling packages allow the possibility to model petroleum composition during hydrocarbon generation as well as the phase behaviour of the fluid during migration The compositional kinetic models (see above) available to date have never been tested with respect to phase prediction, and in fact recent results (di Primio and Skeie, in press) indicate that the compositional schemes are inadequate for correct phase behaviour modelling. Compositional kinetics developed by di Primio et al. (2002) divide the bulk fraction into nine compounds or subfractions. Six characterise the gas phase behaviour (C_1-C_6) and three the high molecular weight fraction (C_7+ A,B,C). These models are compatible with standard PVT data and calibrated to natural fluid compositions.

3.1.2 Migration Mechanisms of Hydrocarbons

The movement of hydrocarbons from their source into reservoir rocks is called migration (Welte et al., 1997). The movement of newly generated hydrocarbons out of their source rock is termed primary migration. The further movement of the hydrocarbons into the reservoir rock in a hydrocarbon trap or other area of accumulation is termed secondary migration. Tertiary migration is the movement of petroleum out of previously formed hydrocarbon accumulations (Hunt, 1996). Migration typically occurs from a structurally low area to a higher area because of the buoyancy force of hydrocarbons in comparison to the surrounding water phase. The subsequent process of migration is governed by supply of hydrocarbons and the combined effect of pressure, buoyancy and capillary forces. The process of secondary migration, in which oil and gas are transported from the source rocks, through water saturated sedimentary carrier rocks, to a trap or reservoir can be described in terms of the gravity driven penetration of a low-density non-wetting fluid through a porous medium saturated with a wetting fluid. Migration can be local or can occur along distances of hundreds of kilometres in large sedimentary basins, and is critical to the formation of a viable petroleum system (Demaison and Huizinga, 1991).

Migration of hydrocarbons can be modelled by various approaches which are Darcy flow, flowpath or ray tracing, invasion percolation modelling and by hybrid methods (Welte et al., 2000). The Darcy flow concept is based on the multiphase Darcy flow law using the assumption that permeability and fluid viscosity functions control migration. Darcy's law describes a linear relationship between volumetric flow rate (Darcy velocity) and pressure (head or potential) gradient and has been the fundamental principle in flow and transport processes in porous media (Wu, 2002) and is valid for laminar flow (Tissot and Welte, 1984). But several mechanisms such as separate phase flow, diffusion, solution and dissolution of gas in oil and water and chemical cracking simultaneously influence and define the complex migration process (Mann et al., 1997). To describe the flow of each phase in the presence of other phases and the interactions of the various compounds mathematically the multiphase version of Darcy's law is required:

$$v_{\mathrm{p}} = -\frac{K k_{\mathrm{rp}}}{\mu_{\mathrm{p}}}(\nabla P_{\mathrm{p}} - \rho_{\mathrm{p}}\mathbf{g})$$

where the subscript p labels the phase, v is the Darcy velocity (volume of phase p flowing per unit area per unit time), K is the absolute permeability (when only one phase is flowing), P is the pressure, ρ is the density, μ is the viscosity, g is the acceleration due to gravity, and k_r is the relative permeability (Jackson and Blunt, 2002). Newest analysis introduce elliptic regions into solutions of the governing three-phase flow equations in the limit of negligible capillary pressure which suggests that numerical solutions of three-phase flow, even at large length-scales where capillary forces are small, must properly account for capillary pressure to be physically meaningful and reproduce the correct sequence of saturation changes (Jackson and Blunt, 2002).

Using the multiphase Darcy flow enables the calculation of the different migration velocities of gas, oil and water. The PVT-conditions, describing pressure and temperature-derived changes in the dissolution and exsolution behaviour of hydrocarbons during migration, determine the composition of the fluids based on the multicomponent definition. Coupling of the multiphase Darcy flow and the fluid composition at every time step at every gridpoint is the essence of a compositional migration model. For flow modelling two approaches are used, the reservoir modelling approach, which uses the detailed capillary pressure concept and operates on a small scale of metres to tens of metres, and the basin modelling approach which uses larger cells of a few hundreds of meters size, focussing more on compaction, lithology, fluid property variations, gas segregation and diffusion (Hantschel et al., 2000). In high-resolution models, Darcy flow modelling requires long processing times.

The multiphase Darcy flow equation system assumes that at any given saturation, each fluid flows in its own set of flow channels and exerts negligible shear stress on the other fluid (Carruthers and van Wijngaarden, 2000). In contrast invasion percolation modelling is based on the concept that the balance between gravity and capillary forces controls migration over geologic time scales. Viscous forces can be ignored due to the low flow rates. Calculations are much faster than Darcy flow but the dynamic framework is still missing entirely in the invasion percolation approach, which is needed to quantify thermal and overpressure histories and the timing and amounts of hydrocarbon generation (Hantschel et al., 2000).

Flowpath or ray tracing models use well-defined carrier systems and are based on buoyancy as the principal driving force for migration. Processes as overpressure generation, pressure controlled compaction and multi-dimensional effects are not taken into account but the model can determine complex and detailed filling and spilling histories, meniscus heights and mixing in reservoirs. The flowpath method is able to handle more realistically scaled, high-resolution data better than the Darcy flow method (Sylta et al., 1998).

Using flowpath modelling, fluid flow is modelled as a purely geometrical phenomenon (Hantschel et al., 2000). The driving force for migration is buoyancy assuming that a capillary pressure threshold is exceeded and the entire carrier rock can be treated as flow conducting. The map is subdivided into drainage areas and the petroleum in each drainage area is moved to its proper reservoir assuming that migration occurs instantaneously relative to the geologic time scale and physical interactions during migration are negligible. Such methods are also called ray tracing, map-based, surface-based or 2.5D models (Sylta, 1991). In this case, all of the petroleum starts migrating in one drainage area following the flowpaths towards the reservoir, which is mapped as a closure defined by the topographic position in relation to the surrounding drainage area. When a reservoir is completely filled spilling takes place. Possible spill flowpaths into the bordering drainage areas can be calculated from the map structure. The main advantage of flowpath modelling is rapid processing (Hantschel et al. 2000). Maps can be modelled quickly retaining detailed geometric information but loosing the completeness of the physical model of petroleum migration. It cannot be used for more complex migration processes because paleo-geometry and physical effects such as

interactions of the migrating and the migrated components with the bulk system are not taken into account.

Hybrid methods use a combination of two of the formerly described methods. The hybrid method of the Petromod^{TM} simulator-module uses a link from Darcy Flow to flowpath which is activated during every time loop throughout the geologic history of a model (Hantschel et al., 2000). This enables fast calculations of flow processes in efficient carriers without losing the dynamic framework provided by the full physics calculations. The grid used for the complex Darcy flow calculations can be sampled and the data exchanged with the original high-resolution grid at every timestep, which reduces calculation times while the realistic geometric representation of the hydrocarbon system is retained.

3.2 Collection of Samples and Data

Possible source rocks, possible carrier and reservoir rocks, cap rocks and fresh oil samples were collected in co-operation with the Geomound partners. Criteria for selection of samples were based on the needs for the numerical simulation described above (section 3.1). These needs can be divided into four main topics:

1. Chronostratigraphic-Structural Framework
2. Facies, Lithology
3. Temperature
4. Geochemistry

The required information types are briefly summarized and their need explained. At the end of this section, Table 3-1 shows the rock and oil samples taken. Information gathered on special topics, e.g. temperature, are discussed in the appropriate section.

Chronostratigraphic-Structural Framework

The Petroleum Affairs Division in Dublin provided topographic, structural and depositional maps. A total of 30 exploration wells have been drilled in the basin by a variety of oil companies (Croker and Shannon, 1995). The data from these wells was mainly derived from composite and petrophysical logs as well as core descriptions and core samples.

To understand the underlying geology of the area cross sections and seismic lines were very important. In cooperation with the Marine and Petroleum Research Group at University College Dublin (UCD) published seismic lines from the MS 81-survey (shot by the Merlin Geophysical Company in 1981) were selected (Figure 2-1). The survey itself contained 84 eastwest dip lines and 22 northwest strike lines. The strike line spacing is 7 km with the dip lines spaced 3-4 km apart. The total coverage of the survey is 5568.3 km. From this survey three lines were chosen: two north-south strike lines (RE94 and RE88) and one east-west

dip line (RE25). RE94 runs across the Hovland-Magellan mound province to the centre of the basin where the basin deepens to a water depth of approximately 2000 m. Line RE88 runs parallel to the Belgica mound area on the eastern flank of the Porcupine Basin. The east-west line RE25 connects both lines and ends close by the Belgica mound area on its eastern end. All three lines were interpreted by UCD and made available for basin modelling. Up to 13 horizons were given in the first interpretation of the seismic section containing following horizons: 1. Seabed; 2. Mid-Miocene; 3. Lower-Miocene; 4. Base Miocene; 5. Base Oligocene; 6. Base Cenozoic; 7. Base Chalk; 8. Base Albian Sand; 9. Base Aptian; 10. Sills; 11. Volcanic Centre; 12. Base Cretaceous; 13. Base Mid-Jurassic (Figure 3-3, Figure 3-4 and Figure 3-5).

Using the Landmark format the data set was imported into the PetroMod^{TM} interpretation module Seistrat. During the ongoing modelling process it became obvious, that stratigraphic resolution in higher detail as well as the presence of visible mounds on the seismics was needed. Therefore line PORC97-12, which crosses lines RE25 and RE88 was chosen as on this line also mound SP46 is visible (Figure 3-7). The PORC-lines were shot in the framework of the seventh Training-through-Research international cruise of the R/V Professor Logachev in the northeast Atlantic in July - August 1997 (Croker and O'Loughlin, 1998).

For stratigraphic purposes also line CS2 in the Connemara field was included as well 26/28-1 is on the line and gas chimneys and pockmarks visible on the seismics are evidence of the active hydrocarbon system (Figure 3-6). Line CS2 was generated out of a 3D seismic set acquired in 1998 by Statoil Exploration (Ireland) and its partners. The high quality data set extends down to 6 s TWT with inline and crossline spacings of 12.5 m and a vertical resolution of ca. 4 ms TWT and covers a volume of about 1040 km^2.

Information on stratigraphy, ages and information concerning events of sedimentation, hiatus and erosion in combination with the regional tectonic regime was taken from several papers e.g. (Croker and Klemperer, 1989; Moore, 1993; Moore and Shannon, 1992; Shannon et al., 1995) and provided in published and internal reports by PAD. This information is summarised in section 4.1 of this thesis.

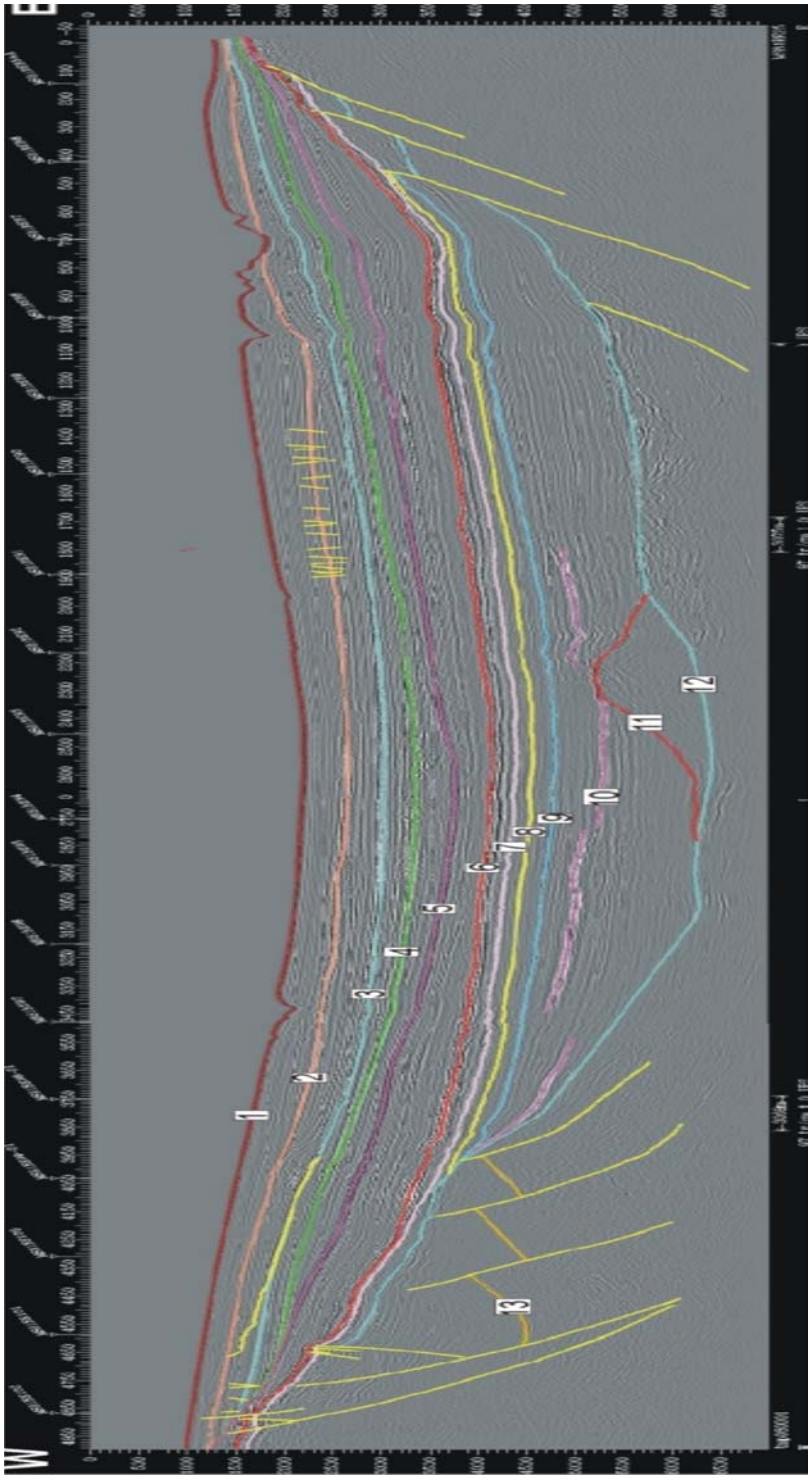

Figure 3-3: Profile MS81RE-25 including horizons: seabed (1), Mid-Miocene (2), Lower-Miocene (3), Base Miocene (4), Base Oligocene (5), Base Cenozoic (6), Base Chalk (7), Base Albian Sand (8), Base Aptian (9), Sills (10), Volcanic Centre (11), Base Cretaceous (12) and Base Mid-Jurassic (13)

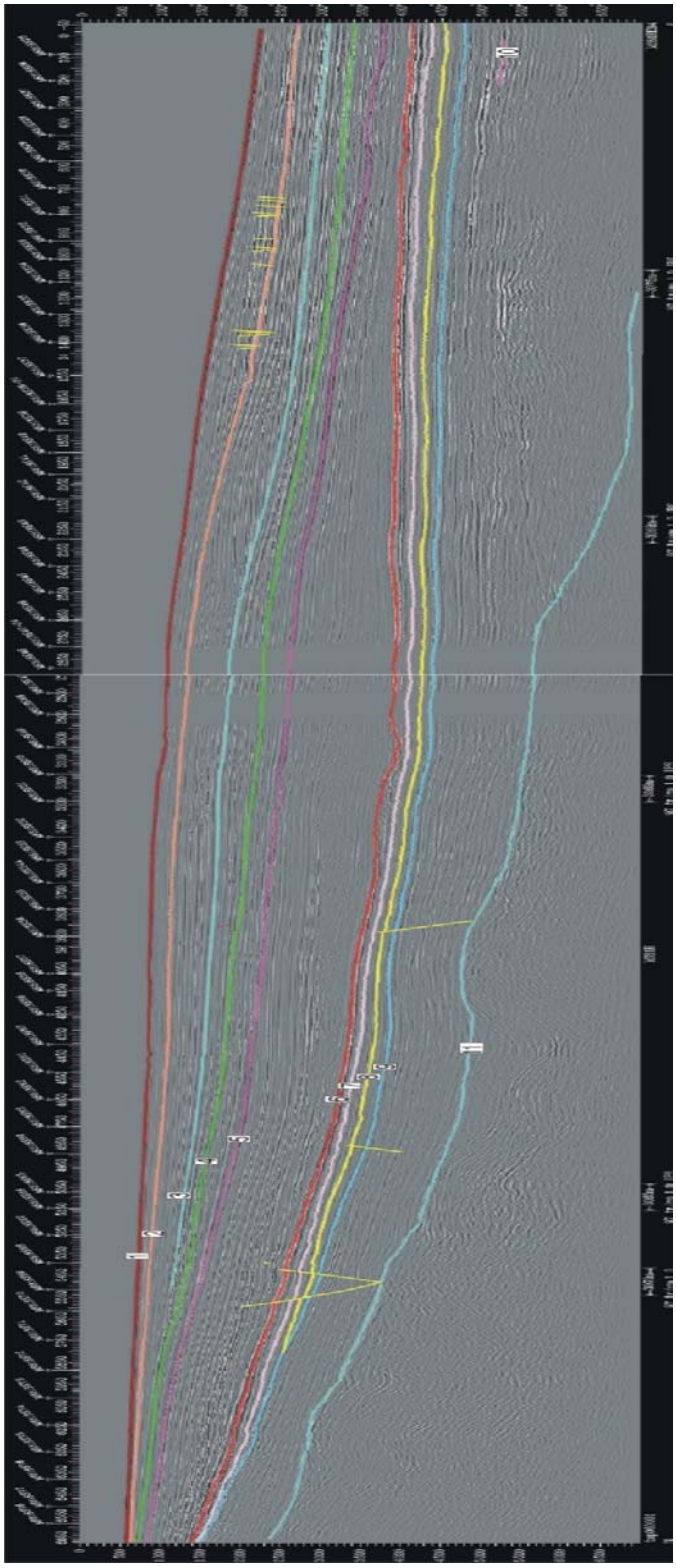

Figure 3-4: Profile MS81RE-94 including horizons: seabed (1), Mid-Miocene (2), Lower-Miocene (3), Base Miocene (4), Base Oligocene (5), Base Cenozoic (6), Base Chalk (7), Base Albian Sand (8), Base Aptian (9), Sills (10), Base Cretaceous (11)

Figure 3-5: Profile MS81RE-94 including horizons: seabed, Mid-Miocene, Lower-Miocene, Base Miocene, Base Oligocene, Base Cenozoic, Base Chalk, Base Albian Sand, Base Aptian, Sills, Volcanic Centre, Base Cretaceous and Base Mid-Jurassic

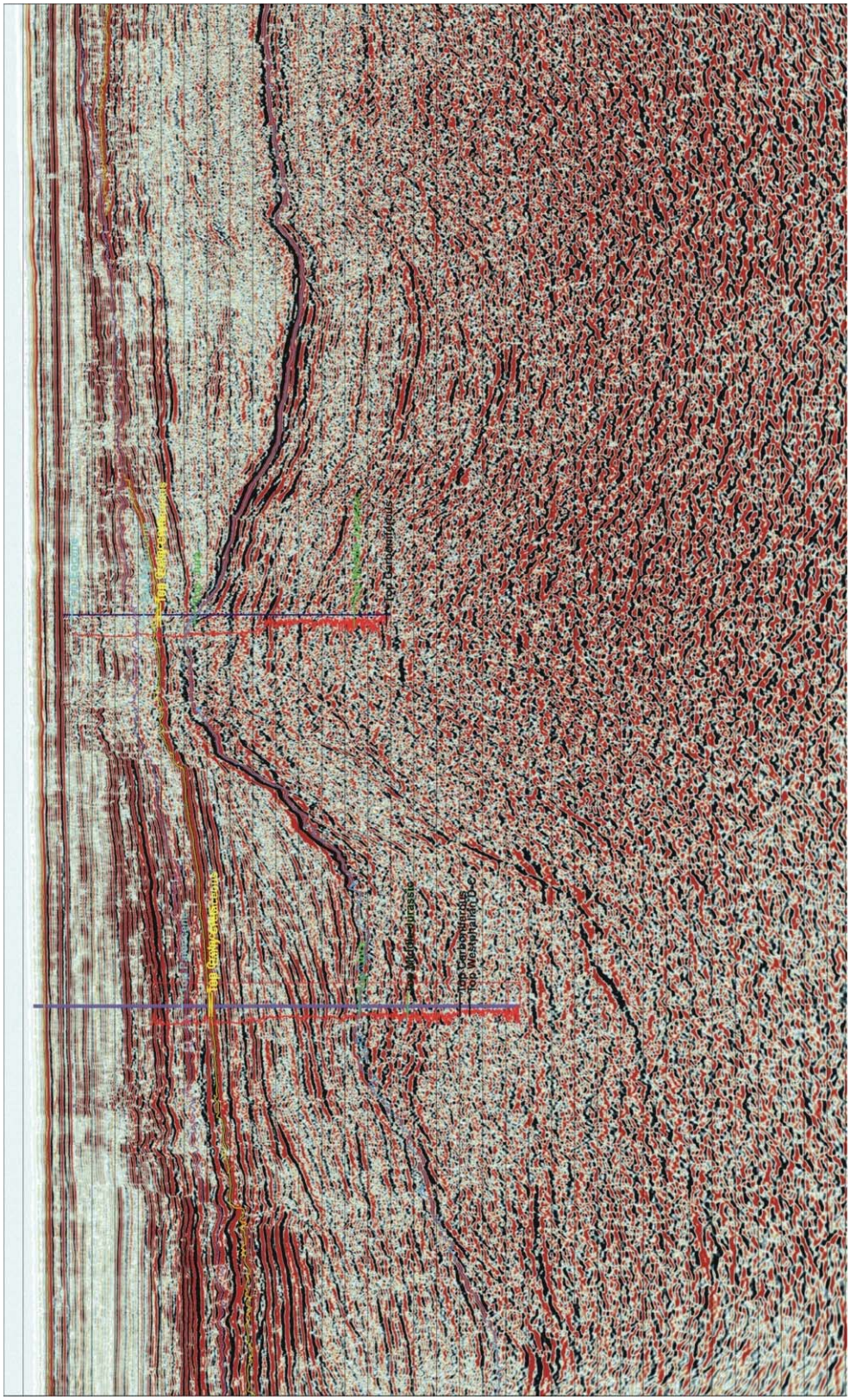

Figure 3-6: Profile CS2 in the Connemara Oil Field

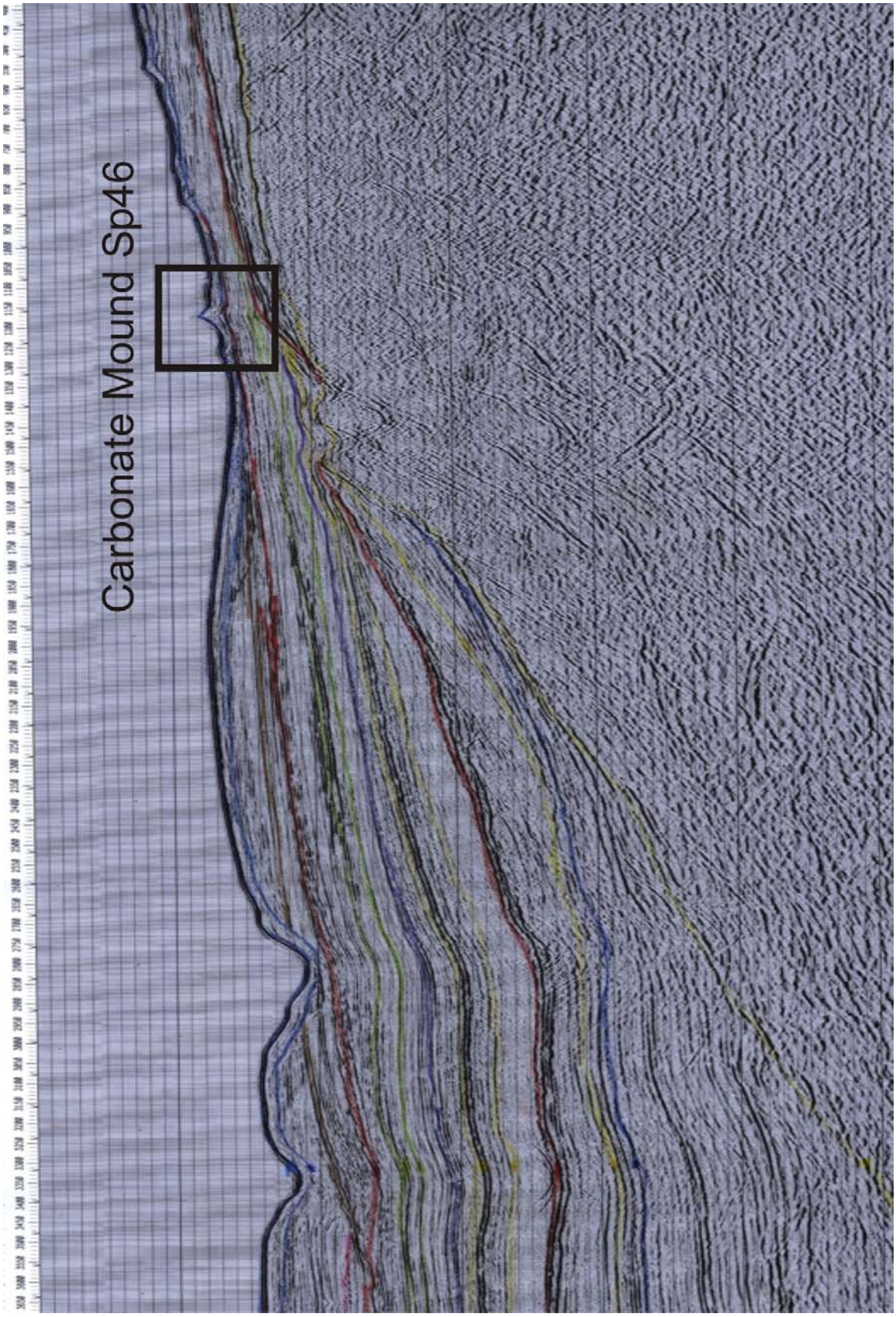

Figure 3-7: Profile PORC97-12 including carbonate mound SP46

Facies, Lithology

Facies and lithology are characteristics that require definition for every single stratigraphic element. There are several ways to describe the facies and the lithology and assign properties. Combined well logs with gamma, sonic, electric and density measurements provided information on the lithological column drilled in the well. This can be verified by core samples and cuttings described during the drilling process. Most of this information was again provided by PAD. 38 core samples were taken from released wells and are listed in Table 3-1.

Detailed information regarding sediment depositional conditions was needed to assess paleo-water depths. The water depth during deposition is of interest for determination of the compaction, temperature and pressure histories. In addition paleo-water depth is a boundary condition for the paleo-geometry of the basin, which is important for the reconstruction of migration and accumulation of hydrocarbons through geologic time.

Information on present and past porosity and permeability was required in order to describe the burial history and calibrate compaction. Compaction is the largely irreversible process of sediment volume reduction due to overburden loading, grain rearrangement (packing), grain solution, etc., and can be described primarily as a function of pore space (porosity) reduction (Poelchau et al., 1997). The reduction of the solids volume plays only a minor role. Bulk compressibility describes compaction as a function of stress. As the pore space is filled with fluids, which must be expelled during the compaction process, the ability of the sediment to transmit fluids, or permeability, is the additional controlling parameter in the compaction process. In order to model compaction the general path of porosity, permeability and compressibility decrease with depth must be known.

Temperature

The burial, temperature and pressure histories combined with the lithologic information mainly control the porosity, permeability, thermal conductivity, heat capacity and density evolution in the system. Temperature data are the most readily available data for calibration, albeit usually restricted to present time (Yalcin et al., 1997). The most commonly used temperature parameters are present-day bottom hole temperatures (BHT) and borehole temperature logs. BHT temperatures should be corrected for circulation of cooler drilling or completion fluids. Corrected BHT's were provided by PAD. A similar kind of data are temperatures from drill steam tests (DST) or formation tests (FT). These were available together with formation pressures.

Temperature logs can be a source of good temperature data if they have been run after the well has been shut in for a sufficiently long time (weeks or months) to reach a state near equilibrium. Such temperature data are usually close to real formation temperatures but tend be lower than DST extrapolated temperatures in the lower part of the well and higher in the upper part (Foerster and Merriam, 1999).

Simulated present – day temperature is controlled by the recent heat flow, surface temperature, and by thermal conductivity of the underlying and overlying layers. It is not affected by the heat flow history except for the most recent part. Therefore, present - day temperature is fairly simple to match, but the match has little significance for the thermal history of the basin. Indicators for actual paleo-temperatures for various geologic events are required for reconstruction of the heat flow history. Inorganic paleo-temperature indicators provide such additional constraints. Certain geothermometers such as fluid inclusion or fission track analysis can furnish maximum fluid temperatures or fix points on the time-temperature scale and are useful for supplementary control (Leischner et al., 1993).

For reconstruction of the paleo-temperatures apatite fission-track analysis provides information regarding the magnitude and timing of heating events. The annealing of fission tracks in apatite and the resulting effect on fission-track ages and track-lengths can be used to reconstruct the thermal history of basins from deposition and burial of sediments through subsequent cooling related to uplift and erosion (Naeser, 1993).

Geochemistry

Geochemical and organic petrologic analysis provide data on maturity, the type and amount of organic matter. Vitrinite reflectance is the most widely used parameter to evaluate the maturity of the source rock and is the primary calibration parameter for modelling temperature history (Taylor et al., 1998). Although vitrinite reflectance is the most commonly available and routinely measured maturation parameter used for calibration, it is not always the best. In some situations vitrinite reflectance may be altered by weathering, bitumen retention, or microbial alteration (Taylor et al., 1998). In oxic environments (e.g., some carbonates) vitrinite reflectance can be too high. Also, there are some lithologies in which vitrinites are rare or absent. In these cases other organic parameters can be used instead.

Another group of organic maturation parameters is based on the isomerization and aromatisation of certain organic compounds in the source rock bitumen or crude oil. One such commonly applied parameter is the Methylphenantrene Index or MPI (Radke and Welte, 1983) which has been correlated with vitrinite reflectance.

Pyrolysis (Rock-Eval) Tmax values are an alternative maturation parameter but values are kerogen type dependent (Espitalié et al. 1984).

3.2.1 Samples

The sample sets taken for geochemical and petrophysical analysis can be divided into three types: core material from exploration wells, core material from gravity cores and oil samples. The core material was mainly used for total carbon and source rock potential analysis, the gravity core material for geochemical analysis of active seeping hydrocarbons and the oils for source rock characterisation (Figure 3-8). Sample location is given in Figure 3-9.

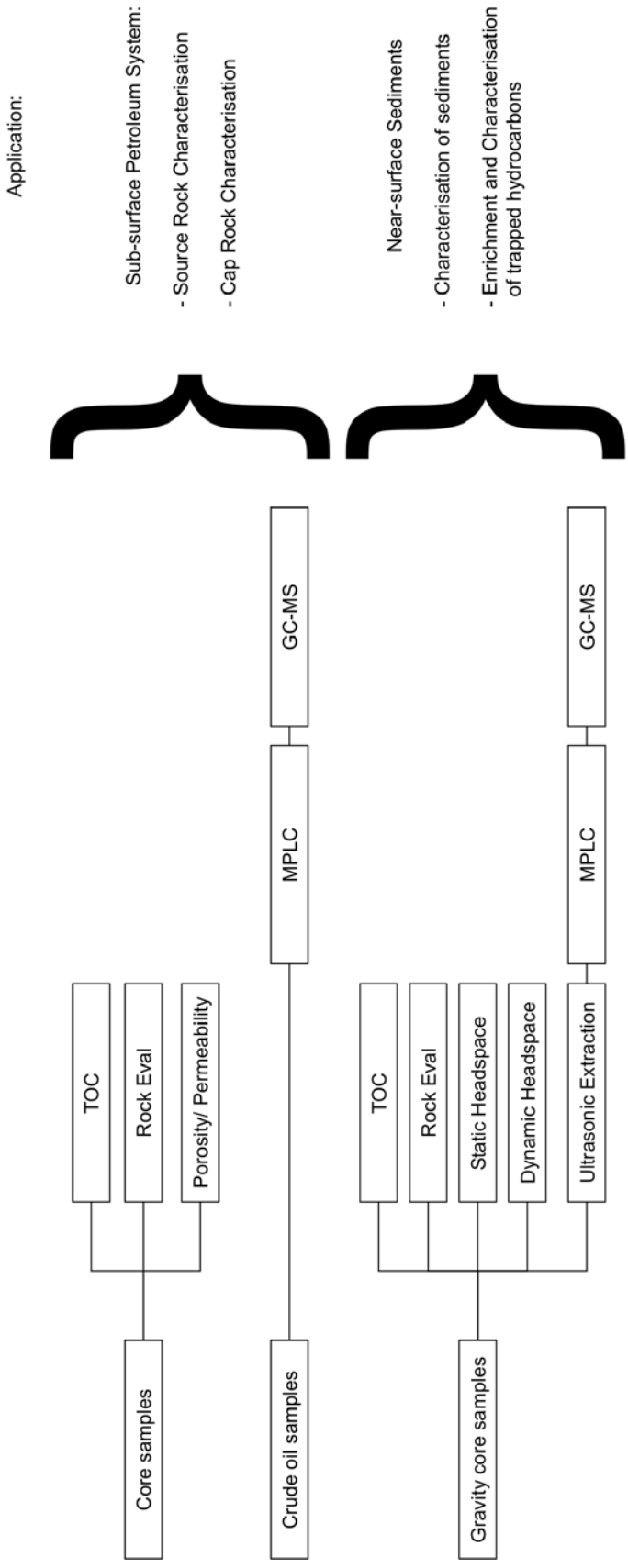

Figure 3-8: Samples and analysis

3.2.1.1 Well Samples

In cooperation with the Petroleum Affairs Division in Dublin 38 core samples were taken. The wells were, due to commercial interests, mainly located in the northern part of the basin. Sample selection was based on several criteria: determination of source rock characteristics and petrophysical character of carrier and cap rocks. A limiting factor was the proximity to the mound areas and the availability of core material as a total of only 40 m core material out of 25 wells was collected. Boxes from 8 wells were opened and core slices of about 3 cm thickness taken for further analysis as listed in Table 3-1 and in Appendix I.

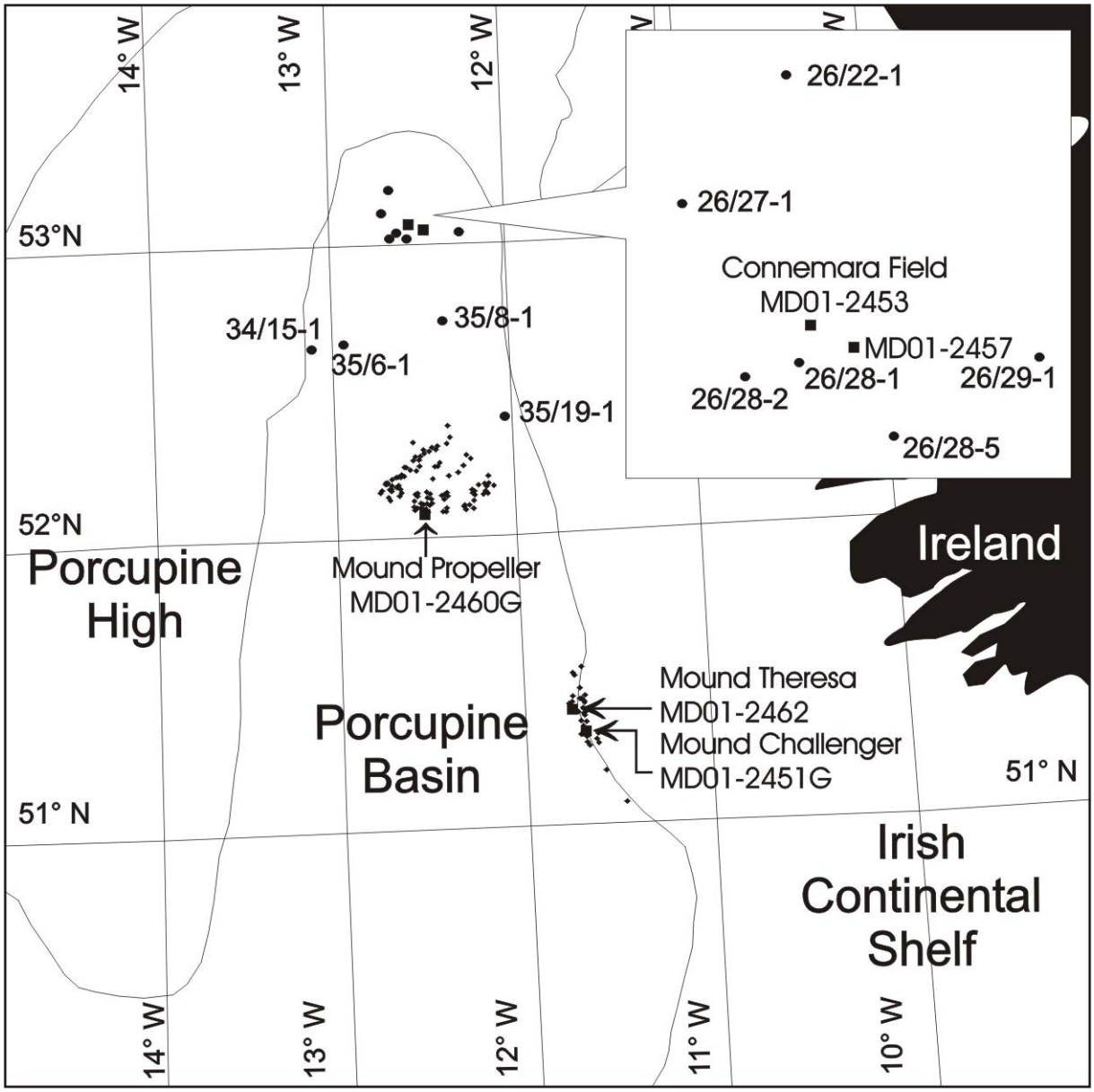

Figure 3-9: Sample location, squares show location of gravity cores

The sampled source rocks were used for characterisation of the quantity and quality of the organic matter, the type of organic matter and its hydrocarbon potential. The organic matter type also provides information on the depositional environment, which can be useful in determining the paleo-geometry and the paleo-waterdepth. Kinetic parameters measured on source rock kerogen or petroleum asphaltenes provide a prediction of the timing and rate of hydrocarbon generation and expulsion.

Petrophysical characterisation of carrier rocks allows an understanding of migration processes whereas cap rock analysis provides information on reservoir seal quality.

FZJ-number	Well	Depth (m.s.l.)	Period/Age	Potential Source Rock	Potential Cap Rock	Potential Reservoir Rock
49713	26/22-1A	2005.4	Bathonian to Hettangian		X	
49714	26/22-1A	2006.4	Bathonian to Hettangian			X
49715	26/22-1A	2006.7	Bathonian to Hettangian		X	
49716	26/22-1A	2009.6	Bathonian to Hettangian		X	
49717	26/27-1B	2506.6	Carboniferous		X	
49718	26/27-1B	2661.6	Carboniferous	X		
49719	26/28-1	2255.5	Early Kimmeridgian - Oxfordian		X	
49720	26/28-1	2256.0	Early Kimmeridgian - Oxfordian			X
49721	26/28-1	2263.4	Early Kimmeridgian - Oxfordian	X		
49722	26/28-1	2426.0	Bathonian		X	
49723	26/28-1	2426.7	Bathonian	X		
49724	26/28-1	2428.0	Bathonian	X		
49725	26/28-1	2429.8	Bathonian	X		
49726	26/28-2	2093.3	Bathonian			X
49727	26/28-5	2402.0	Bathonian	X		
49728	26/28-5	2403.2	Bathonian	X		
49729	26/28-5	2766.6	Bathonian		X	
49730	26/29-1	1782.0	Bajocian to Bathonian		X	
49731	26/29-1	1782.8	Bajocian to Bathonian		X	
49732	26/29-1	1786.3	Bajocian to Bathonian		X	
49733	26/29-1	1833.4	Late Westfalian C	X		
49734	26/29-1	1781.4	Bajocian to Bathonian			X
49735	34/15-1	4441.3	Stephanian		X	
49736	35/6-1	3954.0	Bajocian to Bathonian		X	
49737	35/6-1	3955.3	Bajocian to Bathonian		X	
49739	35/8-1	1711.8	Lower Eocene	X		
49740	35/19-1	5014.0	Late Berriasian		X	

Table 3-1: Core samples specific for source, reservoir and cap rock characterization

3.2.1.2 Gravity Core Samples

Three sets of gravity core samples were collected in the second year of this study. The main sample set was taken on the research cruise of the French vessel Marion Dufresne (Figure 3-9). The second sample set was sub sampled from material taken on the Atalante cruise by dive-robots. The last sampling procedure took place in Gif-sur-Yvette at CNRS where one core from the Marion Dufresne cruise was re-sampled to ensure that no gas was lost during filling and splicing of samples into the storage systems onboard.

The research vessel Marion Dufresne (operated by IFREMER in Brest) collected sixteen long gravity cores in the Porcupine area on its cruise from 27.08.2001 to 13.08.2001. Seven of the cores taken within the Porcupine areas are gravity cores of lengths varying between 0.5-14m, the nine remaining cores are calypso gravity cores with a maximum penetration of almost 30 meters. Five cores were sub sampled for geochemical analysis, two cores from the Connemara field (MD01-2453 & MD012457), one each from Therese mound (MD01-2462), from Propeller mound (MD01-2460G) and from Challenger mound (MD01-2451G) (Figure 3-9). The sampling procedure had to be carried out as soon as the core arrived on deck and was cut into 1.5 m sections (Table 3-2). The top of each section was chosen as sampling interval.

For the two different analytical procedures different sized containers were chosen: for static headspace analysis material was placed in glass vials (22.5 cm^3), whereas material for the dynamic headspace analysis was stored in metal cans (120 cm^3). Each container was filled up to 2/3 with the sediment and the bactericide sodium azide (NaN_3) added in 1% aqueous solution. Then clean water was added leaving a 2 cm headspace. After cleaning of the rim, the cans were sealed, inverted and stored in a deep freezer at minus 80°C. The glass vials were closed using a septum and metal cap by using a special hand crimper, and then placed horizontally in the deep freezer. Placed on dry ice in cooling boxes the samples were then brought to the Research Centre Juelich for further analysis.

The second sample set was taken during a visit in IFREMER. The same sampling procedure was used to sub sample three slabs (Dive 125-3 CL1 on Therese mound & Dive 128-06 on Challenger mound) taken by a submersible robot and one 40 cm long core (PL127-05 CT05 from Therese mound).

For the third sample set the core section 15-16.5 m from gravity core MD01-2462 was completely frozen with liquid nitrogen. A 30 cm section was sawed out from the middle part of the section, the core material crushed with a hammer and filled into cans and vials as described before.

FZJ-number	Depth[m]	Depth [msl]	FZJ-number	Depth[m]	Depth [msl]
MD01-2451G (Mound Challenger 51°22/11°43)			**MD01-2460G (Mound Propeller 52°09/12°46)**		
50166	0	762	50208	0	710
50167	1.5	763.5	50209	1.5	711.5
50168	3	765	50210	3	713
50169	4.5	766.5	50211	4.5	714.5
50170	6	768	50212	6	716
50171	7.5	769.5	50213	7.5	717.5
50172	9	771	50214	9	719
50173	10.5	772.5	50215	10.5	720.5
50174	12	774	50216	12	722
			50217	13.5	723.5
MD01-2453 (Connemara 53°04/12°31)					
50175	0	359	**MD01-2462 (Mound Theresa 51°25/11°46)**		
50176	1.5	360.5	50218	1.5	873.5
50177	3	362	50219	3	875
50178	4.5	363.5	50220	4.5	876.5
50179	6	365	50221	6	878
50180	7.5	366.5	50222	7.5	879.5
50181	9	368	50223	9	881
50182	10.5	369.5	50224	12	884
50183	12	371	50225	10.5	882.5
50184	13.5	372.5	50226	13.5	885.5
50185	15	374	50227	15	887
50186	16.5	375.5	50228	16.5	888.5
50187	17.8	376.8	50229	18	890
50188	17.8	376.8	50230	19.5	891.5
50189	17.8	376.8	50231	21	893
50190	17.8	376.8	50232	22.5	894.5
50191	17.8	376.8	50233	24	896
50192	17.8	376.8	50234	25.5	897.5
50193	17.8	376.8	50235	27	899
50194	17.8	376.8	50236	28.5	900.5
50195	17.8	376.8			
			Atalante Cruise (sub-sampling at Ifremer)		
MD01-2457 (Connemara 53°04/12°31)					
50196	0	360	**Dive 125-3 CL1 (Mound Theresa)**		
50197	1.5	361.5	50237		
50198	3	363	50238		
50199	4.5	364.5	50239		
50200	6	366			
50201	7.5	367.5	**Dive 128-06 (Mound Challenger)**		
50202	9	369	50240		
50203	10.5	370.5	50241		
50204	12	372	50242		
50205	13.5	373.5	50243		
50206	15	375	50244		
50207	16.5	376.5	50245		
CNRS (second sampling of core MD01-2462)			**Core PL127-05 CT05**		
50526	15.5	887.5	50528		
50527	air from the laboratory				

Table 3-2: Sample set for geochemical analysis

3.2.1.3 Oil Samples

During commercial drilling in the 1970's and 80's oil shows and stains were observed in some wells close to the Connemara oil field (Croker and Shannon, 1987). Only a few of the drill stem test samples have been left over such that only five oils from wells 26/28-1 & 26/28-2 were provided by PAD for further analysis of geochemical composition, biomarker fingerprints and for kinetic modelling.

FZJ-number	Well	DST-number	Depth (m.s.l.)	API (deg)
49851	26/28-1	DST 1 - 1563	2310.0	32
49852	26/28-1	DST 2 - 1556	2250.0	38
49853	26/28-1	DST 3 - 1559	2000.0	34
49854	26/28-2	DST 2 - 1552	2149.0	39
49855	26/28-2	DST 3 - 1568	2183.0	41

Table 3-3: Oil samples

3.3 Geochemical Analyses

Organic geochemistry concerns the fate of all organic compounds in the geosphere as a whole (Killops and Killops, 1993). Organic matter is incorporated into sediments and preserved for geological periods involving biochemical and geochemical transformations. Changes in the organic matter can be observed, characterized and quantified by using organic petrology and organic geochemical methods to assess the depositional environment, maturity and quality of a given source rock.

For determination of quality, maturation and depositional environment of potential source rocks the total organic carbon content (TOC) and Rock Eval parameters of samples were measured. The oil samples (Schaefer et al., 2002) and the extracts of samples from the gravity cores of the Marion Dufresne cruise were separated into compound classes by medium pressure liquid chromatography (MPLC). The different fractions were further analysed by capillary gas chromatography and coupled gas chromatography and mass spectroscopy. Headspace gases from sealed samples were also analysed using capillary gas chromatography and coupled gas chromatography and mass spectroscopy.

3.3.1 Organic Petrology

Vitrinite originates from the lignin and cellulose of plant cell walls. The determination of vitrinite reflectance has been used to assess the rank and maturation of coals and sedimentary organic matter for more than 30 years (Taylor et al., 1998). There are three stages of maturity of source rocks: diagenesis, catagenesis and metagenesis (Radke et al., 1997).

Diagenesis (< 0.5% Rr)

During early diagenesis no thermal cracking reactions occur because the increase in temperature and time has not been sufficient. Only biogenic gas is generated by bacteria. When depth and temperature have increased to a sufficiently high level during later diagenesis, oxygen loss from kerogen is particularly important and results in CO_2 and H_2O formation. The first petroleum products liberated by this transformation include mostly heteroatomic (N, S, O)-compounds of high molecular weight, particularly asphaltenes and resins (Tissot and Welte, 1984). A certain amount of thermogenic gas might also be generated, especially from organic matter of type II (Muscio et al., 1994).

Catagenesis (0.5 – 2.0% Rr)

As temperature continues to increase, strong chemical bonds are broken. Hydrocarbon molecules, and particularly aliphatic chains, are produced from kerogen and from the previously generated N, S, O – compounds (Horsfield and Rullkoetter, 1994). Trace amounts of geochemical fossils, which were formerly entrapped in the kerogen matrix or linked by various bonds are also found. Most of the new hydrocarbons generated during the main zone of oil generation have a medium to low molecular weight. They have no characteristic structure or specific distribution, contrary to the geochemical fossils, which are progressively diluted by these new hydrocarbons. Liquid oil generation is accompanied by formation of significant amounts of gas. Typical gas-oil ratios for mature type II kerogen sourced petroleums are 0.2 – 0.4 kg/kg (Tissot and Welte, 1984).

Metagenesis (> 2.0% Rr)

After most labile material has been eliminated, a structural reorganization occurs in kerogen, with the development of a higher degree of ordering. However, in this stage no significant amounts of hydrocarbons are generated from kerogen except for some methane. Large amounts of methane may result from cracking of source rock hydrocarbons and of reservoired liquid petroleum (Durand, 1980; Dieckmann et al., 1998; Horsfield et al., 1991; Schenk et al., 1997b).

For organic petrologic analyses the rock samples were cut in pieces of 3 cm^3 and fixed in a cold mounting epoxy resin with the measuring surface perpendicular to the layering. This surface was ground (300-1200 Grit Size SiC paper) and stepwise polished with a diamond suspension with a decreasing grain size of 6, 4 & 1 µm. Afterwards the samples could be used for petrological analyses.

Vitrinite reflectance analysis was performed using a Zeiss universal microscope with a 40/0.85 oil immersion objective, total magnification was 600x. The incident light wavelength of 546 nm was used for determination of type, proportion and optical properties. For each sample at least fifty measurements were recorded with the exception of samples, which

contained only low amounts of vitrinites. According to microscopic observation, the indigenous histograms were interpreted resulting in a mean value (Rr) and a standard deviation.

Observations under blue excitation (365 – 450 nm) were used to determine the characteristics of the liptinites. Liptinites consist of sporine, cutine, suberine, resins, waxes, fats and oils of vegetable origin (Stach et al. 1982). The liptinites are auto-luminescent when irradiated with long-wave UV or blue light. This is a helpful method to evaluate the amount of liptinites, which are often hard to see in normal light and to characterize the type of liptinite. Especially algae are easier to identify in fluorescent light.

3.3.2 Apatite Fission Track Data Analysis (AFTA)

Apatite Fission track analysis provides a method for the estimation of the thermal history of sedimentary basins (Naeser, 1993). This method uses fission tracks, which are zones of intense damage caused by fission fragments travelling through a dielectric solid. As ^{238}U has, as compared to other naturally occurring isotopes, sufficiently short fission half-life of $4.5x10^9$ years it produces significant numbers of spontaneous tracks over a time period of geologic interest (Fleischer et al., 1975). ^{238}U is found in common minerals and mostly used for AFTA-analysis in apatites and zircons. It fissions spontaneously at a constant rate. The fission track age is a combination of the number of spontaneous tracks intersecting a polished mineral surface and the amount of uranium. Heating of a mineral containing spontaneous fission tracks to a sufficiently high temperature causes the etchable damage zones to become progressively shorter and to ultimately disappear, a process called “annealing”. This annealing process differs in the temperature range for different minerals. At temperatures above 120°C all fission tracks in apatites are rapidly lost, while above 60°C, the length of tracks begin to decline from their original length in excess of 14.5 µm (Green et al., 1989). The annealing of fission tracks in apatite over the temperature range 60-120°C makes them ideal for unravelling the amount of exhumation as kinetics of annealing are known, allowing a quantitative assessment of the timing and amount of uplift and is used to reconstruct the thermal history of sedimentary rocks from deposition and burial through subsequent cooling related to uplift and erosion (Naeser, 1993). This technique can also be used to localize temperature anomalies related to intrusions or the penetration of hot fluids. In the Porcupine Basin McCulloch (1993) provided a data set of 6 AFTA measurements of core samples from well 26/28-1, which were used for heat flow history calibration.

3.3.3 TC, TOC and Sulphur Analysis

The contents of Total Organic Carbon (TOC), Total Carbon (TC) and Total Sulphur (TS) were determined via a LECO^{TM} carbon analyser IR 112. For Total Organic Carbon determination 100 mg of each sample was wetted with ethanol and then treated with hydrochloric acid (25%) and heated at 70°C for 24 hrs. prior to analysis in order to remove inorganic carbon. Analyses were performed at 1000°C in an oxygen atmosphere in duplicate. TC and TS were determined on the same instrument but without previous treatment with

HCl. The detection of the oxides of carbon by an infrared detector allowed the calculation of TOC, TC and TS as weight-percent of the rock sample. The content of carbonate ($CaCO_3$) can be calculated by subtracting TOC from TC and multiplying by the atomic proportion of carbon to the corresponding carbonate molecule as shown below, the result is expressed as percent calcium carbonate or dolomite:

In the case of calcium carbonate $CaCO_3$/C -> (40+12+3*16)/12 = 8.33

$\%CaCO_3$ = (TC – TOC) * 8,33

In the case of dolomite $Ca,Mg(CO_3)_2$/C -> ((40+24)/2+12+3*16)/12 = 7.66

$\%CaCO_3$ = (TC – TOC) * 7.66

3.3.4 Rock-Eval Pyrolysis

Rock-Eval Pyrolysis (Espitalié et al., 1985; Espitalié et al., 1977) was used to determine the type of organic matter and to predict bulk petroleum generation characteristics of source rocks. The analyses were carried out using a Rock Eval II instrument from Delsi Instruments S.A. Samples of ground whole rock weighing up to 100 mg are heated at 300°C for 3-4 minutes to distil freely occurring organic matter, followed by programmed pyrolysis at 25°C/min to 550°C to pyrolyse macromolecular organic matter, both in a helium atmosphere. Products released from the sample are detected by a flame ionisation detector (FID), which responds to organic compounds, and a thermal conductivity detector (TCD), which is used to detect carbon dioxide. The first peak (S1) represents milligrams of hydrocarbons that can be thermally distilled from one gram of rock. The second peak (S2) represents milligrams of hydrocarbons generated by pyrolytic degradation of the kerogen in one gram of rock. The third peak (S3) represents milligrams of carbon dioxide generated from one gram of rock during temperature programming up to 390°C. During pyrolysis, the temperature is monitored by a thermocouple. The temperature at which maximum rate of S2 occurs is called Tmax.

The hydrogen index (HI) corresponds to the quantity of pyrolyzable organic compounds (or hydrocarbons, HC) measured as FID-signal corresponding to S2 normalized to the total organic carbon in the sample (mg HC/g TOC). The oxygen index (OI) corresponds to the quantity of carbon dioxide measured as TCD-signal corresponding to S3 normalised to the TOC (mg CO_2/g TOC). The production index (PI) is defined as ratio S1/(S1+S2).

3.3.5 Hydrocarbon Generation Kinetics

Modern basin analysis uses kinetic models (chapter 3.1.1) to predict the extent of petroleum generation within potential source rocks from high-molecular weight kerogen (Pepper and Corvi, 1995). Kinetic data is usually determined on source rocks or kerogen concentrates using different techniques e.g. Rock-Eval or MSSV-experiments (Horsfield et al., 1991; Radke et al., 1997; Schaefer et al., 1990; Schenk et al., 1997b). Due to the absence of

source rock samples asphaltene kinetics from crude oil derived asphaltenes were used instead.

Asphaltene kinetics were determined at Humble Instruments & Services, Inc. USA. The methodology is described in di Primio and Horsfield (1996). Asphaltenes were precipitated from the oils using C_7 as solvent for 24 hrs and a filter of 0.22 µm. The asphaltenes then were subjected to programmed-temperature open-system pyrolysis (Horsfield et al., 1994). The samples were analysed at multiple heating rates with precise temperature measurements (Jarvie pers. comm.). The instrumentation used for bulk kinetic analysis is Humble Instruments' SR Analyzer Kinetics WorkStation, which is operated under the following conditions: initial temperature of 250°C (actual) for 5 minutes; heating rates at 1, 5, 15, 30, or 50°C/minute (nominal) and a final temperature of 600°C (actual) for 2 minutes. The fastest and slowest heating rates were completed in duplicate when there was sufficient sample material.

Kinetic results were computed using the Kinetics2000 programme and the following results are reported: discrete Ea distribution with free A factor, discrete with fixed A factor, Gaussian, Gaussian with free reaction order, and nucleation models. The calculated activation energy distribution and single frequency factor were used for modelling the generation of hydrocarbons in the Porcupine basin.

3.3.6 Ultrasonic Extraction and Medium Pressure Liquid Chromatography (MPLC)

Ultrasonic extraction was performed using a modified method described in Blanco et al. (1992). The freeze-dried sediment was crushed to < 200µm and inserted into a glass flask with 150 ml solvent mixture of methanol/dichloromethane (1:99). The glass flask was immersed in an ultrasonic bath and kept there for 15 min. Then the solution was filtered under a weak vacuum using a glass fibre filter. The residue was washed out using 100 ml of the solvent and repeating the ultrasonic extraction and filtering twice. The filtrate was isolated from the solvent using a Zymark TurboVap. The total extracts were separated into aliphatic hydrocarbons, aromatic hydrocarbons and heterocompounds using medium pressure liquid chromatography (MPLC) after the method described by Radke et al. (1980).

3.3.7 Gas Chromatography – Mass Spectrometry Analysis

The composition of organic matter in marine surface sediments can be related to a number of different sources (Killops and Killops, 1993; Peters and Moldowan, 1993). These sources include the autochthonous production of organic material in the overlaying water column and in the surface sediment layers (e.g. by phytoplankton, zooplankton, benthic organisms and bacteria) and the allochthonous organic matter from the adjacent continent (e.g. terrestrial plant material transported by river discharge or wind into the marine sediments). Furthermore the assemblage of organic matter components is biased by microbial and chemical alteration and degradation within the sediment (diagenetic processes). Additionally migrated mobile oil

and gas components from ancient deeper sediment layers can contribute to the organic matter composition.

In the scope of this study it was of special interest to resolve whether those seeping fossil hydrocarbons (oil or gases) may have induced the formation of carbonate hardgrounds on the seafloor on which corals initially could colonised to form subsequently the huge carbonate mounds observed in this area (Hovland, 1990). Methanotrophic bacteria using methane as a carbon source and producing carbonate may have played an important role in this hardground forming process. The analysis of molecular biomarkers is an appropriate tool to prove the occurrence of those microbial communities and of migrated fossil hydrocarbons in the sediments of the Porcupine Basin.

GC-MS analysis were carried out on an Agilent 6890 GC interfaced with a Finnigan MAT95XL mass spectrometer. The GC is equipped with a 50 m SGE BPX5 Fused Silica column, 0.25mm inner diameter and coated with 5% phenyl (equivalent) / 95% methyl polysilphenylene / siloxane phase as the stationary phase (3µm film thickness). The GC runs on a temperature program from 50-340°C column temperature using helium (1 ml/min) as carrier gas. Full scan measurements on the Finnigan MAT95XL mass spectrometer were acquired for m/z 50-600 at a scan rate of 1s/d, a scan cycle time of 1.1s and a source temperature of 230°C.

3.3.8 Static Headspace Gas Chromatography

Analysis of headspace gas was performed in order to assess whether the gas is of biogenic or thermogenic origin. For this purpose gas composition and the gas isotopic signature was required. For static headspace analysis, the sealed vials, containing 5-14 g of sediment, were removed from the fridge and left for two hours to adapt to room temperature. In the Hewlett Packard Series II 5890 gas chromatograph with a Perkin Elmer Turbomatrix 40 auto sampler, the vials were heated up to 80°C for 30 min. After equilibration of hydrocarbons in the gas phase at elevated temperature an aliquot of the headspace gas was injected into the gas chromatograph. In view of the high vapour pressure of the gaseous hydrocarbons at 80°C the measured concentrations reflect nearly total yields of the headspace and the “associated” gas. Therefore, the determination of individual distribution coefficients had not to be carried out.

The gas chromatographic system consists of a fused silica column (Macherey & Nagel) of 60 m length, 0.25 mm inner diameter, coated with Optima 1 silicone elastomer as the stationery phase (1 µm film thickness) run at a column temperature programme (30°C (hold for 10 min), linear heating rate 3°C/min up to 90°C (hold for 8 min)), 1:20 split ratio, using helium as carrier gas. Methane and higher-molecular weight hydrocarbons were determined by this capillary gas chromatographic system using a flame ionisation detector (FID). Compounds, which are low-molecular-weight hydrocarbons (C_1-C_7) were quantified using a mixture of C_1-C_5 as an external standard.

3.3.9 Dynamic Headspace Gas Chromatography

The dynamic headspace technique uses a purge and trap system (Schaefer et al., 2003). This system consists of the sample, the purge and trap sampler system PT1 (Köhnen-Willsch, Jülich) and the capillary gas chromatograph HP6890 of Agilent (Figure 3-10). The sample material was stored in iron cans and kept under liquid nitrogen. For the analysis, the cans were opened when still frozen and small parts splitted off with a hammer and 3 –7 g sample material put into glass vials with 10 ml volume and closed as quickly as possible with a septum and a cap. The vial was then heated for the analysis up to 90°C for one hour.

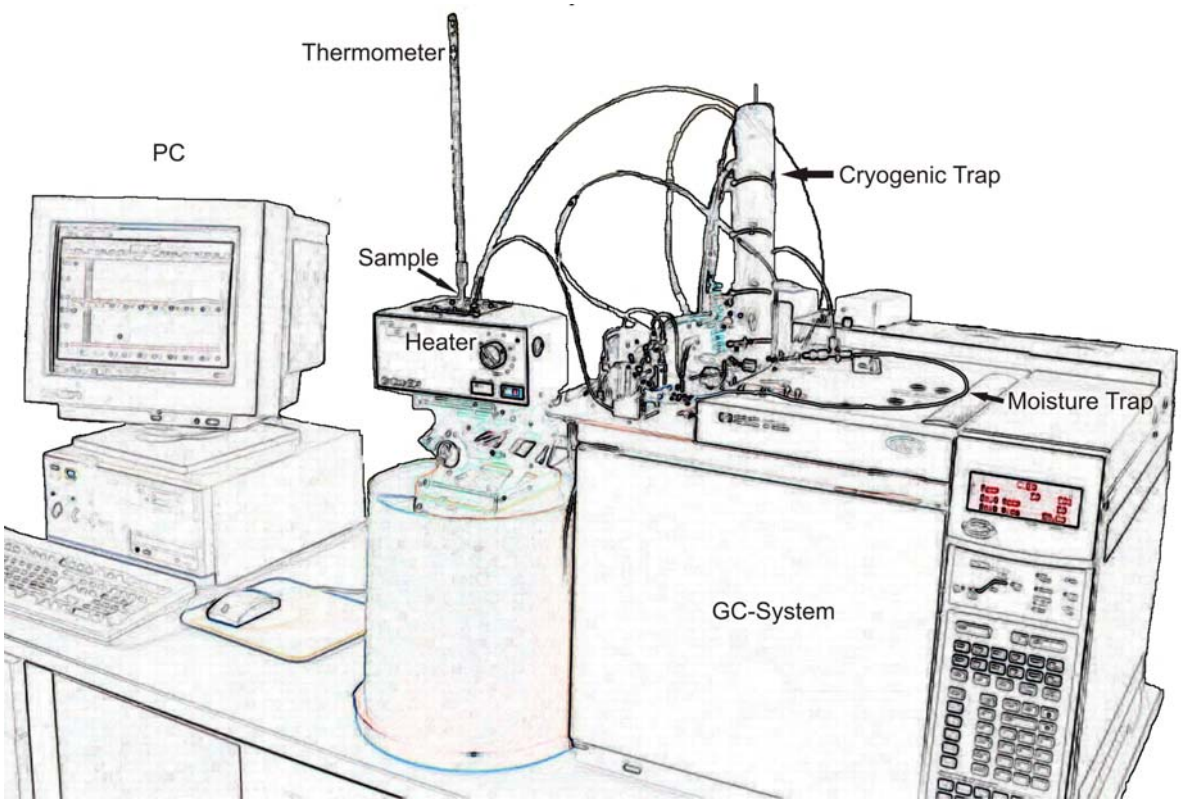

Figure 3-10: Dynamic headspace system

During the analysis the vial was purged with Helium. The outgoing gas mixture was directed through a PermaPur moisture trap into a two-step liquid nitrogen cooled trap. The first unit of the trap consists of a 1/8 inch GLT-high grade steal tube filled with glass spheres to trap C_{2+} molecules. The second unit is filled with a polymer absorbing the C_1 molecules. The trap was cooled to –100°C during vial purging for five minutes. After that the flow direction through the trap was inverted and the trap was heated up to 100°C to remove the hydrocarbons and analyse them in a HP 6890 Series gas chromatograph. The GC was equipped with a 60 m Optima Fused Silica column (Macherey & Nagel), 0.25 mm inner diameter and coated with Optima 1 silicone elastomer as the stationary phase (1 µm film thickness) run at 30°C column temperature programme (30°C (hold for 35 min), linear heating rate 3°C/min up to

60°C (hold for 5 min)). Methane and higher-molecular weight hydrocarbons were determined using a flame ionisation detector (FID). The chromatographic data were acquired and quantitated by a MULTICHROM chromatography data system, Labsystems.

Compound identification and quantitation were performed using a C_1 to C_4 hydrocarbon mixture as an external standard. In addition, the polar compounds have been identified by combination of the purge and trap system with gas chromatography/mass spectrometry (GC/MS) using a Finnigan MAT 95SQ mass spectrometer. Full scan measurements were acquired for m/z 14-150 at a scan rate of 0.3 s/d, a scan cycle time of 0.509 s and a source temperature of 260°C. The column was the same as described above for the static headspace methodology.

3.4 Petrophysical Properties

The petrophysical properties of fine grained lithologies control the migration of hydrocarbons in sedimentary basins (Welte et al., 1997). The degree of sediment compaction in sedimentary basins is a function of burial depth and varies predominantly based on the grain size distribution, mineralogical composition and pore fluid compositions and pressure regimes (Bjørlykke and Høeg, 1997). As migrating hydrocarbons can be trapped by an impermeable or a very low permeable barrier porosity and permeability measurements were carried out on four potential cap rock samples. Wood's low pressure mercury-porosimetry system was used for porosity measurements and permeabilities were measured at the Technical University of Aachen (Hildenbrand et al., 2001).

3.4.1 Permeability Measurements

To determine the permeability fluid flow measurements were performed in triaxial flow cells designed for confining pressures up to 50 MPa (500 bar), axial load of up to 100 kN and maximum temperatures up to 350° C. The cells accommodate cylindrical sample plugs of 28.5 mm diameter and a maximum length of approximately 30 mm. Sample plugs were placed between two porous stainless steel disks and two stainless steel pistons equipped with boreholes for fluid introduction and removal. The outer surface of the sample/piston arrangement is sealed with a double-layered sleeve. The inner sleeve consists of lead foil (0.15 mm thickness); for the outer layer either thin-walled copper or aluminium tubes are used. Application of a confining pressure of at least 300 bar ensures a tight seal around the sample plugs.

In the present study, single-phase flow experiments were performed to determine the absolute permeability of the samples supplied. Normal tap water was used as the penetrating fluid phase. Constant fluid pressure was applied at the upstream side and the fluid volume forced through the sample as a result of the pressure gradient was measured at the downstream side of the pressure cell. The pressure at the downstream side was atmospheric. At the end of the experiment Darcy's law was used to calculate the permeability of the rock samples.

3.4.2 Porosity Measurements

Sample porosity was measured with a Wood's low-pressure mercury-porosimeter. A small dried plug drilled from the sample is inserted in a cell which is then filled with mercury and placed in the Quantachrome Autoscan-60 porosimeter SP-10LV. Mercury (Hg) is a none wetting fluid and therefore pressure is needed to inject Hg into porous material. This pressure depends on the pore throat size through which pore is filled. The equivalent pore radius r was computed according to the capillary pressure equation (Rootare, 1970; Washburn, 1921):

$$r = \frac{2\gamma\cos\theta}{P_c}$$

where Pc is the capillary pressure, γ is the interfacial tension ($\gamma Hg/air=0.471 Nm^{-1}$) and θ the wetting angle ($\theta Hg/air=140°$). According to this equation the radius of pores accessible to mercury depends on the pressure applied. From the amount of mercury and known weight of the sample, the density of the sample can be determined by following equation:

$$\rho_G = \frac{\rho_{Hg}\, M_P}{Z_{Hg}+M_P-Z_{HG,}}$$

ρ_G = density of sample
ρ_{Hg} = density of mercury
M_P = sample weight
Z_{Hg} = weight of cell filled with mercury
M_P-$Z_{HG,P}$ = weight of cell filled with mercury and sample

The volume of mercury entering the pore system of the rock sample then is plotted as a function of pressure on a logarithmic scale (Hg intrusion curve). The pressure at which mercury starts to penetrate the largest pores of the pore system after correction for surface roughness effects is denoted as entry pressure. The two other characteristic pressure values correspond to the inflexion point of the sigmoidal capillary pressure curve and the intersection of the tangent to this inflexion point with the logarithmic pressure axis. The inflexion point marks the pressure at which the incremental rate of intrusion of mercury with increasing pressure is highest and, in terms of pore size distribution, it represents the most prominent pore radius. And the other pressure is termed breakthrough pressure or threshold pressure (Katz and Thompson, 1987). This pressure may also be determined from the pressure corresponding to 10% Hg-saturation (e.g. Schlömer and Krooss, 1997; Schowalter, 1979).

4 Geological Reconstruction of the Porcupine Basin – Basin Modelling

4.1 Conceptual Model

The conceptual model defines the relationship and temporal framework between the actual geology and the input data for the numerical simulation (Welte et al., 1997). The first step of the conceptual model construction is the subdivision of the lithostratigraphic sequence into geochronological entities called “events”. Each event represents a defined time interval during which deposition, erosion or non-deposition occurred. Parameters required as input for the simulation must be defined for each of the events. These include, in the case of PetroMod^{TM}, parameters such as age, thickness, porosity, lithology and physical properties (e.g. density, compressibility, permeability, thermal conductivity and heat capacity). In addition, data on bathymetry, sediment-air or sediment-water interface temperatures, and heat flow into the sedimentary column during each event are required as input. The basic conceptual model is presented in Table 4-1. For each horizon name, the age, lithology, environment, sea level and tectonic events are given beginning with the Jurassic sequences.

The five 2D -profiles shown in Figure 2-1 were subdivided vertically into layers, each representing stratigraphic or lithological units. The stratigraphic units were taken from the interpreted seismic profiles and document times of sedimentation. Thirteen horizons were interpreted, ranging from seabed to Base Mid-Jurassic. Units below the Mid-Jurassic could not be traced over any significant distance because of poor seismic resolution. These units were tied to wells in the vicinity of the Connemara oil field and, for the purposes of the modelling, were assumed to be of constant thickness throughout the entire basin.

The tectono-stratigraphic evolution of the basin was based on key publications presented in Shannon et al. (in press), most notably Croker and Klemperer (1989), Tate (1993) and McDonnell and Shannon (2001). It is structured in an uplift phase in Early Permian times following the Variscan Orogeny followed by subsidence which is only interrupted by three successive phases of uplift in the Late Jurassic, Early Cretaceous and Cenozoic. The phases of uplift are associated with erosional events. During uplift-related erosion in the Late Jurassic, approximately 600 m of sediment were removed (PAD internal report). Associated with the onset of regional marine currents and basin deepening at the end of the Late Eocene - Early Oligocene C30 unconformity, approximately 250 m of sediment and at the end of the Oligocene approximately 200 m of sediment were eroded (PAD internal report). At the end of the Cretaceous a period of non-sedimentation occurred. 5 ma after deposition of the Cretaceous marine outer neritic chalks, the Palaeocene uplift was characterized by prograding deltas and growing terrestrial influence (Moore and Shannon, 1992).

Horizon name	Age		Lithology	Environment	sea-level	Palaeo-water Depth	tectonic events
	from	to				at well 26/28-1	
Pliocene (C10)	5.3	0.0	mudstone	low energy shelf to basinal mudstone succession, base of mounds		0->500	
Miocene sills	20.3		Basalt			0->500	
Mid Miocene (C20)	14.8	5.3	mudstone	high energy contourite depositon and slump surfaces		0->500	Alpine deformation pulse and ridge push effects
Base Mio	23.8	14.8	mudstone - occasional sandstones	basinal		0-500	
Erosion	26.0	23.8			200 m		
Oligocene (C30)	33.7	26.0	mudstone	contourite deposition	relative sea-level fall	0-200	
Erosion	43.0	33.7			250 m		
Eocene	54.8	43.0	mudstone	submarine fan development		0-60	
Paleocene/Eocene	56.0	54.8	coaly-sandy-shaly	shelf to basinal deposition, marginal clastic input (basin floor fans and deltaics)		0-61	Iceland plume related uplift
Hiatus	60.9	56.0					
Chalk	71.3	60.9	marl	marine outer neritic chalkes	eustatic sea-level fall	<60-200	
Base Albian Sands	112.0	71.3	sandstone	marginal to shallow marine		0-200	
Base Aptian	121.0	112.0	mudstone	southward prograding turbidites		0-500	
Volcanic ridge	142.0	135.0	Basalt				
Base Cretaceous	142.0	121.0	mudstone	southward prograding fans	fault related subsidence	0-500	rifting during Mid-Cretaceous
Uppper Jurassic	180.0	142.0	mudstone	marine to lacustrine	fault related subsidence	0->200	rifting during Late Jurassic
Lower Jurassic	205.0	180.0	mudstone	deep marine		>200	

Table 4-1: Conceptual model of the Porcupine Basin

Absolute ages were needed for each event (Table 4-1). Because of a paucity of data for the Porcupine Basin ages were taken from the newest publication of the Geological Society of America (1999) and combined with the available absolute age determinations from Tate and Dobson (1988).

The basin geometry determines the depositional environment and the type of sediment deposited during each event. Reconstruction of the basin geometry is based on PAD data for the paleo water depth and will be presented in section 4.2. The basic conceptual model is presented in Table 4-1. For each horizon name the age, lithology, environment, sea level and tectonic events is given beginning with the Jurassic sequences. Older strata are not taken into account, as stratigraphic units cannot be resolved on the seismic interpretations.

An additional important and usually overriding influence on fluid flow is provided by faults. There are three stacked fault systems in the Cenozoic found within the 3D seismic data (Bailey et al., subm.). The lowest fault system comprises large (up to km-scale displacement) Jurassic to Early Cretaceous syn-rift growth faults. Throughout the basin these faults strike predominantly N-S and locally NE-SW. They define the present-day structure of the Porcupine Basin. The majority of these faults is buried by up to 3 s TWT of sediment, but a few show post-Cretaceous reactivation and extend up to the Miocene or Pliocene succession.

Between the Base Tertiary and Base Oligocene (C30) reflections systems of N-S trending intraformational faults with a max. displacement < ca. 250 m were found. These faults are organised in well-defined systems, located above the Jurassic-Cretaceous syn-rift basin margins, within packages of submarine fan deposits. Their location along the basin margins and their time of formation suggest that they are the product of significant differential Eocene subsidence and compaction of the Basin (Bailey et al., submitted).

Paleogene and Neogene layers contain polygonal faults in localised packages throughout the basin often occurring in submarine fan sequences. One of these packages is present in the 3D seismic data set, in a mudstone-dominated Eocene sequence. It is also truncated by the C30 unconformity. Polygonal faults in mudstone-dominated sequences in the North Sea Basin are interpreted as the result of the volumetric contraction during compactional dewatering (Cartwright and Lonergan, 1996). Layer-parallel volumetric contraction or in other words shrinkage, causes isotropic tensional stresses, which are large enough to cause failure. Based on the evaporation of pore fluids and coupled bulk volume change, desiccation cracks form in muddy sediment. As the shrinkage stresses are approximately of radial distribution polygonal joints and fissures develop. The low permeabilities of the mudstones impede the expulsion of pore fluids during burial, which causes increased pore fluid pressure. This increased excess pore fluid pressure trigger the failure during early burial. The response to the dewatering may have been an increase in the shrinkage force, causing more failure and the continued growth of the fault system as long as the rock mass contracted volumetrically for the first 500 – 1000 m of burial. With increasing burial and decreasing pore fluids the fault system ceases to be an important dewatering valve, which becomes inactive beneath a threshold depth.

The fault systems of the Porcupine Basin have been described in detail by Bailey et al. (submitted) and also briefly in Huvenne et al. (in press.) and were incorporated into the model.

For the conceptual model, the Upper Jurassic strata was defined as the main source rock with TOC values of 4 % and a Hydrogen Index (HI) of 550 mgHC/gTOC. Additionally source rock properties were assigned to the Middle Jurassic with TOC values of 1.8 % and a Hydrogen Index of 550 mgHC/gTOC, based on data provided in Croker and Shannon (1987) and Shannon and Naylor (1998).

4.2 Burial History Reconstruction

4.2.1 Definition of Basin Geometry

Changes in topographic elevation due to erosion or tectonic processes also affect the evolution of flow systems at the basin scale (Bachu and Underschultz, 1995). For example, the trapping of hydrocarbons in the petroleum system of the Williston-, Powder River- and Denver Basins is the result of paleotopographic control (Thomas, 1991) and migration pathways have varied through time due to tilting and truncation (Goldsmith, 1998). As far as

petroleum migration is concerned a correct reconstruction of the geometric evolution of the model is required as changes in carrier structure through time will significantly alter drainage patterns (Kjennerud and Sylta, 2001). The basin geometry at any given time step is defined by the thickness of the sedimentary sequences at that time step and the paleo water depth. In a basin model the surface topography represents the upper boundary condition with respect to present and paleo geometry. In submarine settings paleo water depths of every event are critical input data for correctly reconstructing petroleum migration. Therefore, paleo water depth maps were introduced for every time step modelled. As shown in the conceptual model (Table 4-1), paleo water depth values exist for the northern margin of the basin, but throughout the basin only little detailed paleo-depth information is available. The only really reliable data are from the deltaic strata in the Early Cenozoic and in the Mid-Cretaceous, together with the local lacustrine facies of the Middle Jurassic and the fluvial strata of the Middle and part of the Upper Jurassic. In most other instances the interpretations are poorly constrained. Even where they are constrained, this constraint is only valid for local areas. For example in extensional settings the environments will vary at any one time from non-marine to marine depending on the location within the rift system. Therefore, the present day geometry of individual layers with paleo-depositional information was used to calculate the paleo geometry by scaling the present day depth of each mapped top to the known paleo water depth of these layers at well positions. Additionally, information on paleobathymetric values, trends and basin shape based on the paleobathymetric reconstruction of the North Sea by Kjennerud and Sylta (2001) were used for the adjustment of the paleo water depth.

At the intersections of the three lines (Figure 4-1) the thickness of any layer and its respective paleo water depth must be identical. For control the burial histories at the line intersections were compared. The burial history is a one-dimensional shot where the depth is plotted against the age in a diagram. The burial depth is controlled by the water depth and the sedimentary load.

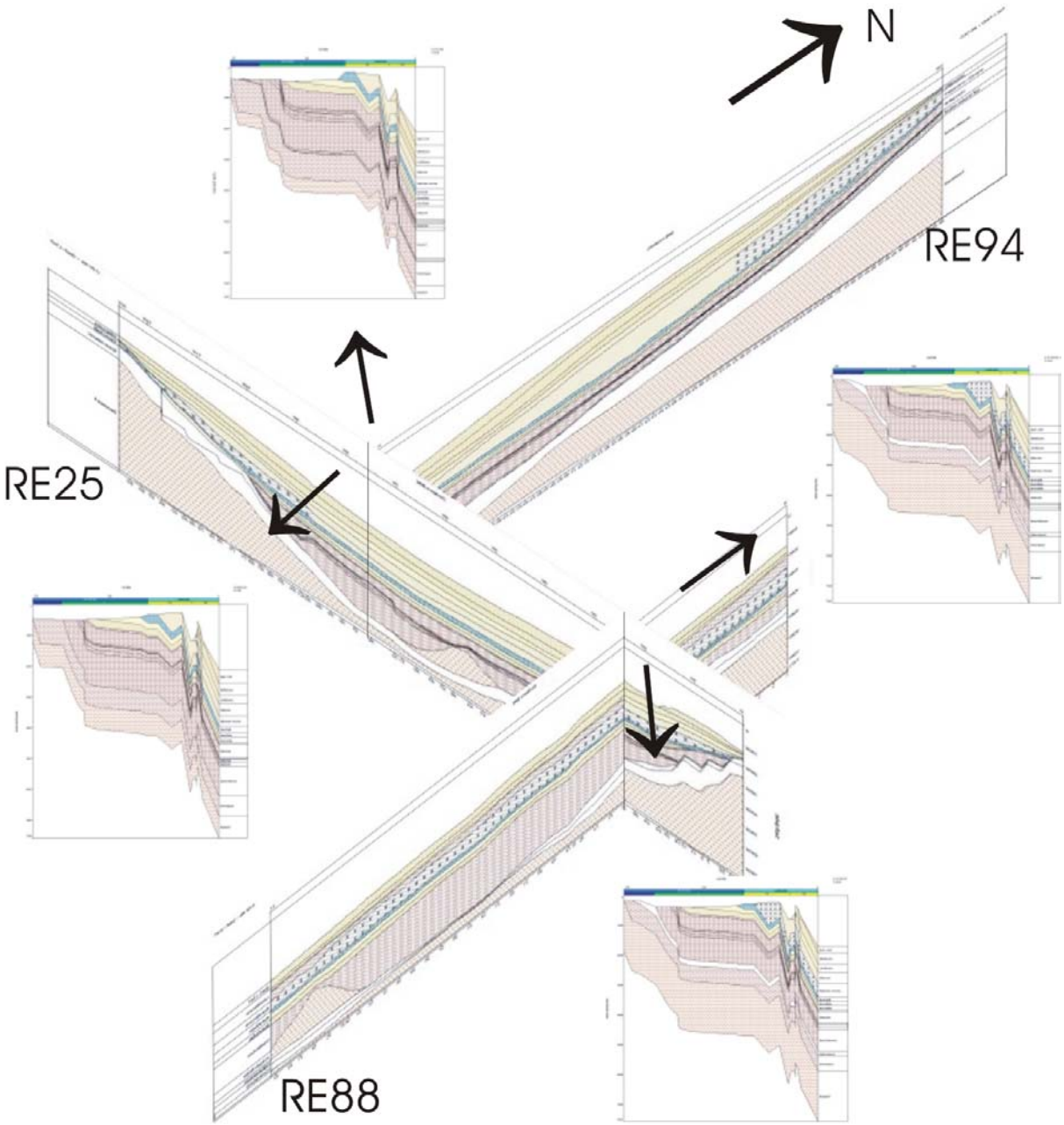

Figure 4-1: Basin geometry at intersection of the seismic lines

Figure 4-2 shows the burial history of line RE94 at the intersection with line RE25. After the Late Jurassic and Mid-Cretaceous fault controlled subsidence the basin was progressively filled with sediment until the Palaeocene uplift. The following phases of uplift are related to the Iceland Plume and ridge push effects and/or alpine deformation pulses. After the Porcupine Basin was uplifted, renewed burial started and continues until the present day situation. This general burial history is similar for all three lines.

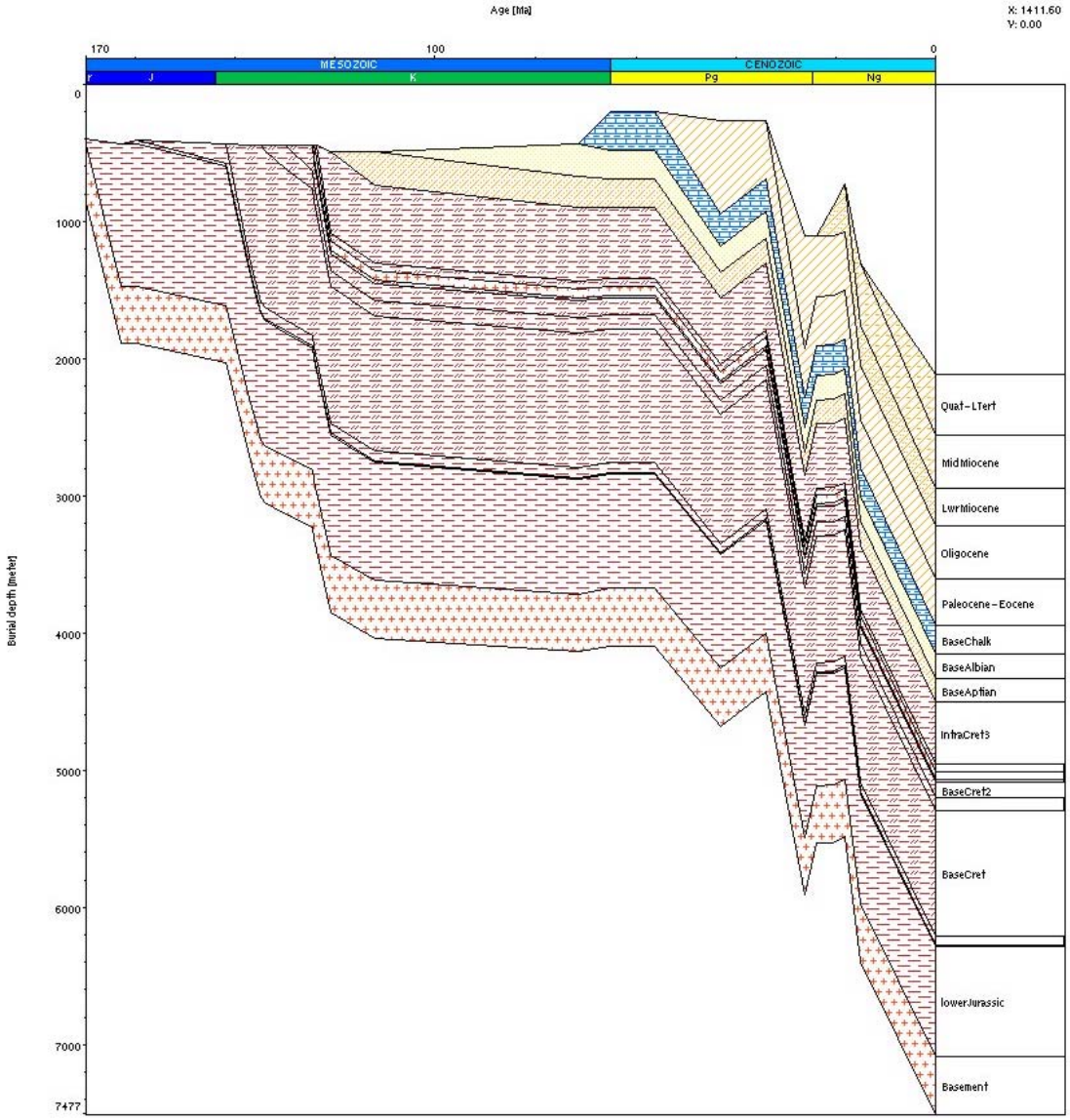

Figure 4-2: Burial history of profile RE94 at intersection with profile RE25

Line RE94 was used as the starting point for calibration as all wells with calibration data are close to the line. At the intersection with line RE25 the burial histories were compared and paleo water depth values were correlated to those of line RE94 (Figure 4-1). The third line RE88 crosses line RE25 with no well control. Therefore values at intersection with line RE25 were used.

4.2.2 Compaction Modelling versus Poro/Perm-measurements

The results of the mercury porosimetry measurements were used to determine the total porosity and capillary sealing efficiency of the cap rock samples 49724, 49728, 49729 and 49740. Table 4-2 documents the matrix density, the bulk density and the porosity of the four measured samples. The porosity of the samples ranges from 3 – 8% and is, as expected,

very low and decreases with depth. A similar evolution is seen in the permeabilities, which also decrease with increasing sample depth. The permeability coefficients of the four samples range from $2*10^{-20}$ m^2 (20 nDarcy) down to $6.6*10^{-22}$ m^2. (0.66 nDarcy). This is very low and the mudstones can be described as tight and would act as good sealing rocks.

Sample	Depth [m]	Permeability [Darcy]	Matrix density [g/cm^3]	Bulk density [g/cm^3]	Porosity [%]
49724	2428.0	$2.2 \cdot 10^{-9}$	2.71	2.55	6
49728	2403.2	$2.0 \cdot 10^{-8}$	2.81	2.6	7.6
49729	2766.6	$7.3 \cdot 10^{-9}$	2.63	2.5	5.2
49740	5014.0	$6.7 \cdot 10^{-10}$	2.79	2.7	3.2

Table 4-2: Permeability and porosity for selected samples

Porosity – Permeability relationships for limestone and shales investigated by different authors are shown in Figure 4-3 including IES standard data (Wygrala, 1989). Permeability generally decreases with decreasing porosity during burial. Generalizations covering all types of lithologies are not possible as the number of variables e.g. grain size, packing, fracturing, cementation, etc. is too large. Therefore a definition of specific porosity – permeability relationship for each type of lithology is necessary and shown for limestone, shale and siltstone in Figure 4-3. IES standard data for shales are given in Table 4-3.

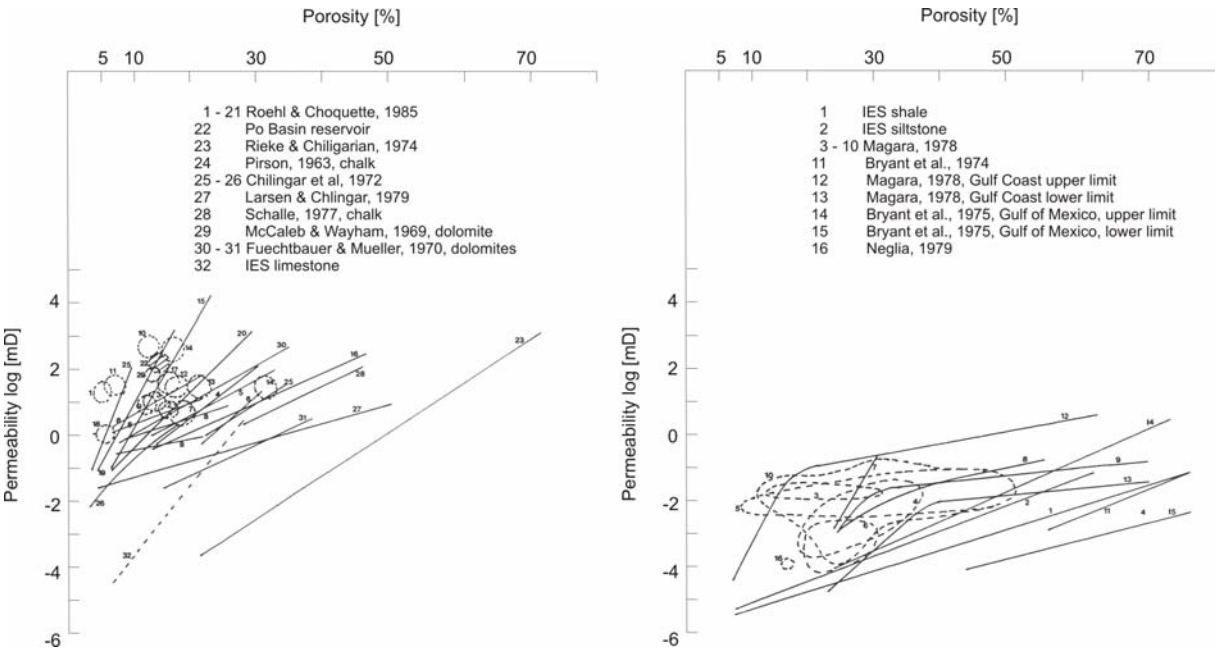

Figure 4-3: Porosity - permeability relationship for limestones and shales (Wygrala, 1989)

	Density	Initial Porosity	Thermal Conductivity	Thermal Conductivity	Heat Capacity	Heat Capacity	Permeability	Permeability
			at 20°C	at 100°C	at 20°C	at 100°C	at 5% Porosity	at 75% Porosity
	[kg/m3]		[W/m/K]	[W/m/K]	[kcal/kg/K]	[kcal/kg/K]	log [mD]	log [mD]
SHALE	2680	0.65	1.98	1.91	0.213	0.258	-5.5	-1
SHALEsilt	2677	0.62	2.05	1.94	0.21	0.254	-5.35	-0.7
SHALEcarb	2655	0.62	1.5	1.43	0.212	0.258	-5.5	-1
SHALEevap	2630	0.47	2.93	2.61	0.21	0.247	-8	-4
SHALEsand	2674	0.57	2.32	2.12	0.205	0.248	-4.5	0
SHALEcalc	2688	0.52	2.22	2.09	0.208	0.248	-2.5	8.5
SHAL&SAND	2669	0.52	2.65	2.38	0.197	0.236	-4	3
SHAL&SILT	2674	0.59	2.09	1.97	0.207	0.251	-5.25	-0.5
SHAL&LIME	2695	0.53	2.39	2.24	0.208	0.246	-5	6
SHALEtuff	2675	0.6	2.21	2.1	0.205	0.248	-5.5	-1

Table 4-3: IES standard data for shales

IES standard data for lithologies were used for the facies assignment, as only few measurements of actual samples exist. For sensitivity analysis, all stratigraphic units, as described in the conceptual model (Table 4-1), of profile RE94 were modified to unique units consisting of only sand, silt or shale to model compaction under the same boundary conditions.

The porosities and permeablities of the measured samples were very low indicating an efficient cap rock. These petrophysical properties are influenced by the initial deposited material, the grain size, water content and diagenetic processes controlled by the load of the overburden, temperature and water column and mechanical compaction (Giles, 1997). Due to the limited amount of sample material available the measured samples were not petrographically analysed regarding their cementation history. As the measured porosity of 3 – 8% seems to be very low compared to calculated porosities of 10 – 15% (shale to limestone) a secondary loss of porosity due to cementation seems most likely. This is confirmed by MacDonald et al. (1987) who observed calcite and dolomite cements in Jurassic sediments due to the Early Cretaceous transgression. However, the sealing efficiency of rocks is controlled by the capillary entry pressure, the permeability and relative permeability and the extent of diffusive losses through the fluid-saturated pore space (Schlömer and Krooss, 1997).

The permeability is divided into a lateral (horizontal) and a vertical component. The core samples were measured perpendicular to the layering and the determined permeability is comparable to the vertical permeability. Figure 4-4 shows the modelled horizontal and vertical permeabilities and the measured permeabilities on line PORC97-12 in the Connemara oil field close to well 26/28-1. The high permeability peaks at 2900 m, 3900 m and 4700 m depth are based on the sandy Miocene, calcareous Chalk and sandy Aptian layer. The measured permeabilities fit in the range of the calculated horizontal and vertical permeabilities but do not perfectly fit as expected the calculated vertical permeabiltity, which indicates that the samples were not perfectly perpendicular cored to the bedding.

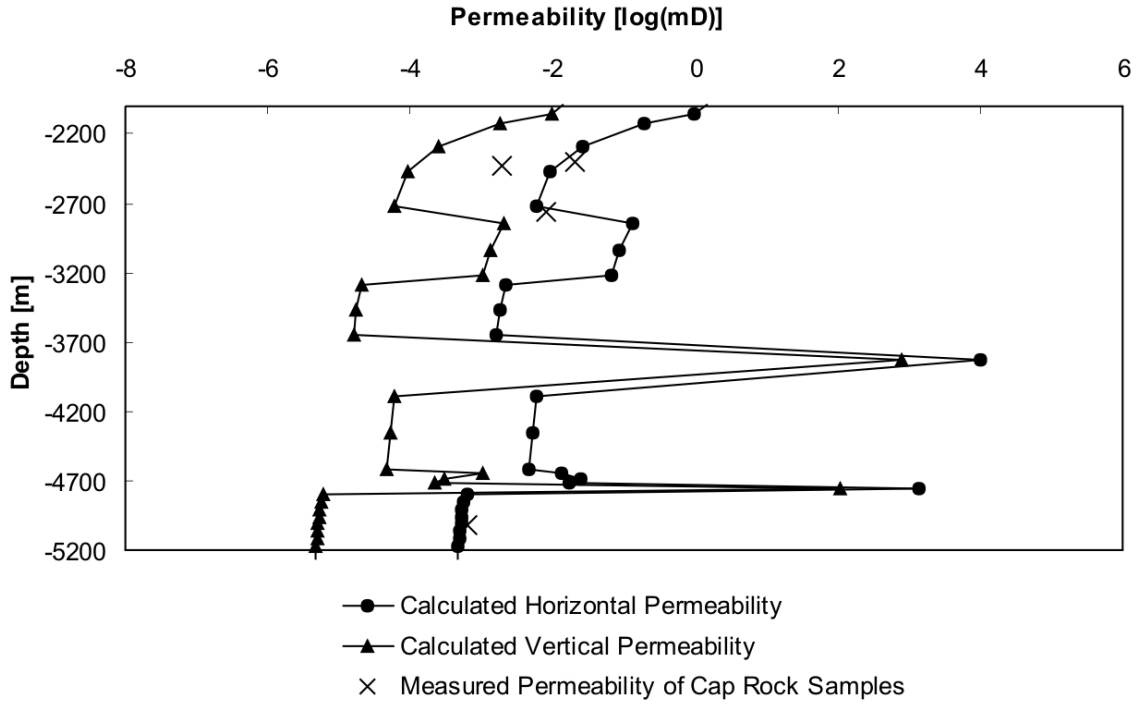

Figure 4-4: Modelled and measured permeability

Keeping in mind that the four samples are only a snapshot of the geological situation for a distinct layer in the well we can assume that the lithologies chosen in the conceptual model are confirmed by the permeability measurements of the core samples. A second way to confirm the taken lithologies is to analyse the pressure regime and compare it to measurements taken on wells.

4.2.3 The Pressure Regime

Few pressure data from the drilled wells, which can be compared to the modelling results, exist. Figure 4-5 shows the calculated lithostatic, hydrostatic and pore pressures (s. section 3.1) in comparison to measured pressure data from wells 26/28-1, 26/28-2, 35/6-1 and 35/15-1. The lithostatic and hydrostatic pressures are as expected in a narrow range for all modelled cases. The pore pressure increases at approximately 5500 m depth at the sediment – basement – boundary due to the properties of the basement as it is assumed to be impermeable in the IES standard data. The measured values are all hydrostatic indicating that there is no overpressure in this area. The modelled results for the pore pressure indicate the predominance of hydrostatic pressure conditions. Combining these observations with the permeability and porosity observations the lithological properties of the chosen facies in the conceptual model fit the measurements and observations made in the basin. No overpressure is observed in the Porcupine Basin.

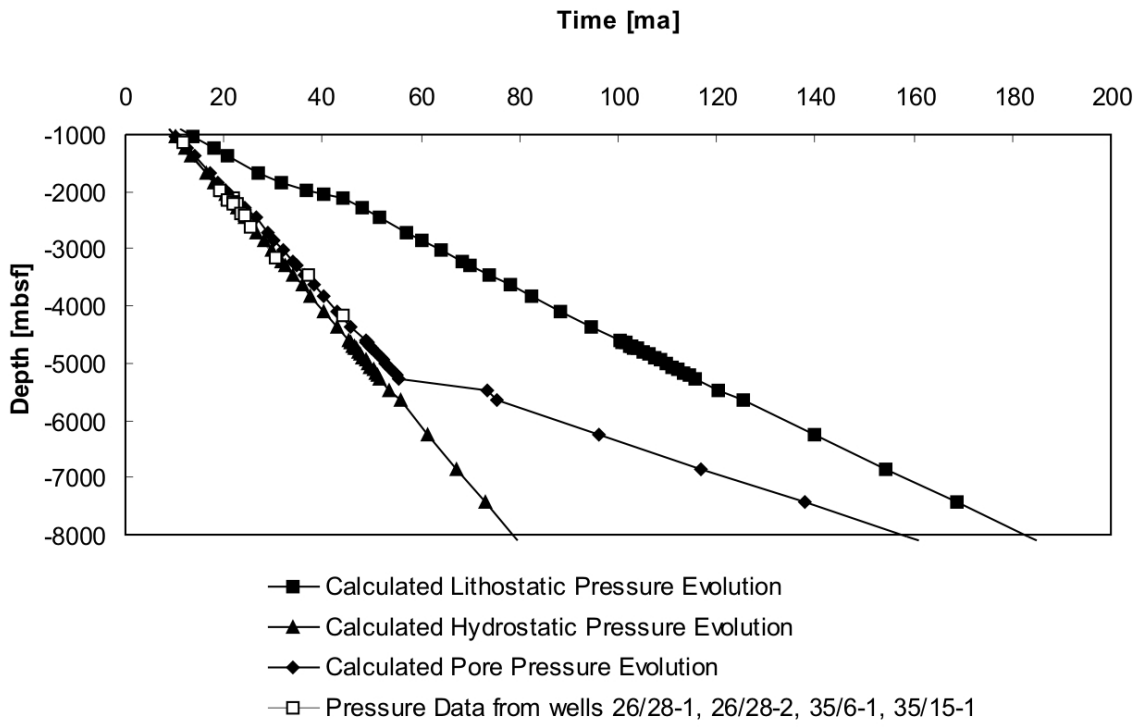

Figure 4-5: Pressure regime in the Porcupine Basin based on modelled lithostatic, hydrostatic and pore pressure as compared to the available calibration data

4.3 Thermal History Reconstruction

Calibration of a basin model consists of the comparison of measured data with predicted values of calibration data. Following the reconstruction of the basin geometry, the thermal history was developed using the following calibration data: vitrinite reflectance, bottom hole temperatures and apatite fission track data. The thermal evolution of sedimentary basins is calculated using the basal heat flow evolution, which varies as a function of crustal extension, stretching or compression.

4.3.1 Levels of Maturity from Vitrinite Reflectance

Combined published and measured maturity data from 8 wells were available. Evolution of vitrinite reflectance as a function of depth is illustrated in Figure 4-6 for the wells studied, the data is also presented in Table 4-5. These wells are all located in the vicinity of profile RE94. Locations are given in Figure 2-1. Histograms for in-house measured data are given in Appendix 2.

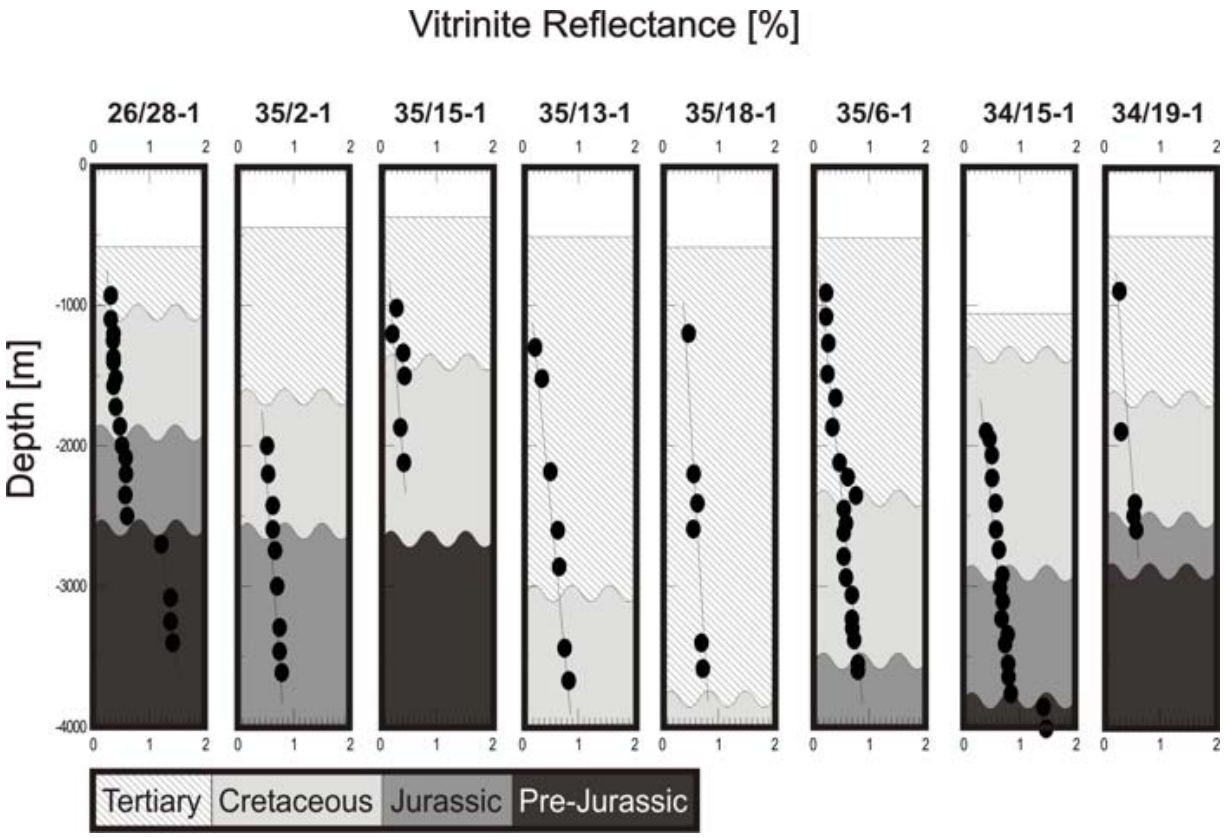

Figure 4-6: Vitrinite reflectance measured in wells close to Line RE94

The abundance of indigenous vitrinites was very low in the samples studied. Reworked vitrinites are of higher rank, mostly 1.2 – 1.7 % Rr, and made a significant contribution to all

samples. They are derived from uplifted and eroded areas most likely from sediments of Pre-Jurassic age.

Generally, maturity increases with depth and age of stratigraphic units. The trend observed starts from very low and immature values in the Cenozoic and increases to mature values of about 1 – 1.3 % in Cenozoic, Cretaceous and Jurassic successions – depending on the well location – and highly mature to overmature values in the Pre-Jurassic sequences. As a generalisation the maturity trends imply that organic matter at 2500 m depth has attained the onset of oil window maturity (Rr = 0.5%) and that at 4000 m depth late maturity stage (Rr = 1%) was reached.

In BP well 26/28-1 and Deminex well 34/15-1 the trend is disturbed due to the erosion of Pre-Jurassic and Jurassic sediments. At the discordance there is a step of 0.3 % in reflectance. In order to correctly reconstruct the burial history the thickness of eroded material must be determined since it forced the Pre-Jurassic to a deeper part of the basin with higher temperatures, which explains the increased reflectance values. However, this was not performed, as the seismics do not penetrate the Pre-Jurassic sediments.

The deepening of the basin from north to south is clearly seen in the Cenozoic succession. In BP well 26/28-1 the Cenozoic contains 400 m of sediment, in Amoco well 35/18-1 already 3000 m are found. Therefore sediments of the same age have undergone different degrees of maturation because their burial and hence temperature histories were different.

Additionally, sills of Cenozoic age and the Volcanic Ridge disturb the normal maturity evaluation of the basin. The formation of the Volcanic Ridge is a consequence of the active rifting in the Porcupine Basin, which has a major impact on the heat flow history of the basin. Therefore the influence on the maturity evolution of the organic matter is discussed later in the development of the heat flow history of the basin. Sills of at maximum 20 m thickness intruded into the Cretaceous strata (Tate and Dobson, 1988) and add, depending on their thickness and composition, additional energy to the system. However, this additional heat pulse is locally very limited as the heat affects the intruded sediment only at a distance corresponding to half of the thickness of the sill. Peters et al. (1983) showed for black shales from the Cape Verde Rise, which were penetrated by hot diabase sills during the Miocene that the hydrocarbon generation was restricted to within about 10 meters of the shale/sill contacts. This has no basin wide effect on the hydrocarbon generation. Therefore the influence of the sills is negligible in the Porcupine Basin.

Vitrinite reflectance was measured on rock samples from exploration wells drilled in the 1960's and 70's. Measured reflectance data and reported reflectance data by PAD as well as literature data correlate well and trends in different boreholes are similar giving confidence in a relatively low error. However, vitrinite reflectance can be suppressed by weathering, bitumen retention, or microbial alteration (Taylor et al., 1998). In oxic environments (e.g. carbonates) vitrinite reflectance can be too high. As mudstones are the dominating lithology

in the Porcupine basin only minor error is expected and the vitrinite reflectance can be used as the most reliable calibration parameter.

4.3.2 Bottom Hole Temperatures

Figure 4-7 shows a simplified plot of the temperature gradients from the seabed datum (5°C assumed) to the deepest corrected temperatures from the PAD data set. The bottom hole temperature data were acquired from wireline logs, were reprocessed and corrected with the aid of mud log information and Horner Plots using following expression:

$$(T_1+T_2)/T_2$$

T_1 is the cooling time which is the time taken to drill the last 10 m of borehole prior to circulating bottoms-up and pulling out to run logs. T_2 is the warming time, which is the recovery time since mud circulation stopped to the time at which the logging tool is in position. The stabilised formation temperature at a given measurement depth is obtained by extrapolating a regression line through the temperature points to the y-axis such that $(T_1+T_2)/T_2 = 1$. The circulation time varies between 0.5 to 10 hours for the wells drilled in the Porcupine Basin (PAD internal reports).

Wells 26/28-1, 35/6-1, 35/8-2, 35/13-1, 35/15-1 and 35/18-1 were used for calibration. They show an average geothermal gradient from 20 – 30°C/km based on the different sedimentation rates as condensed sedimentation occurred on the flanks and thicker sediments were deposited in the faster subsiding basin center.

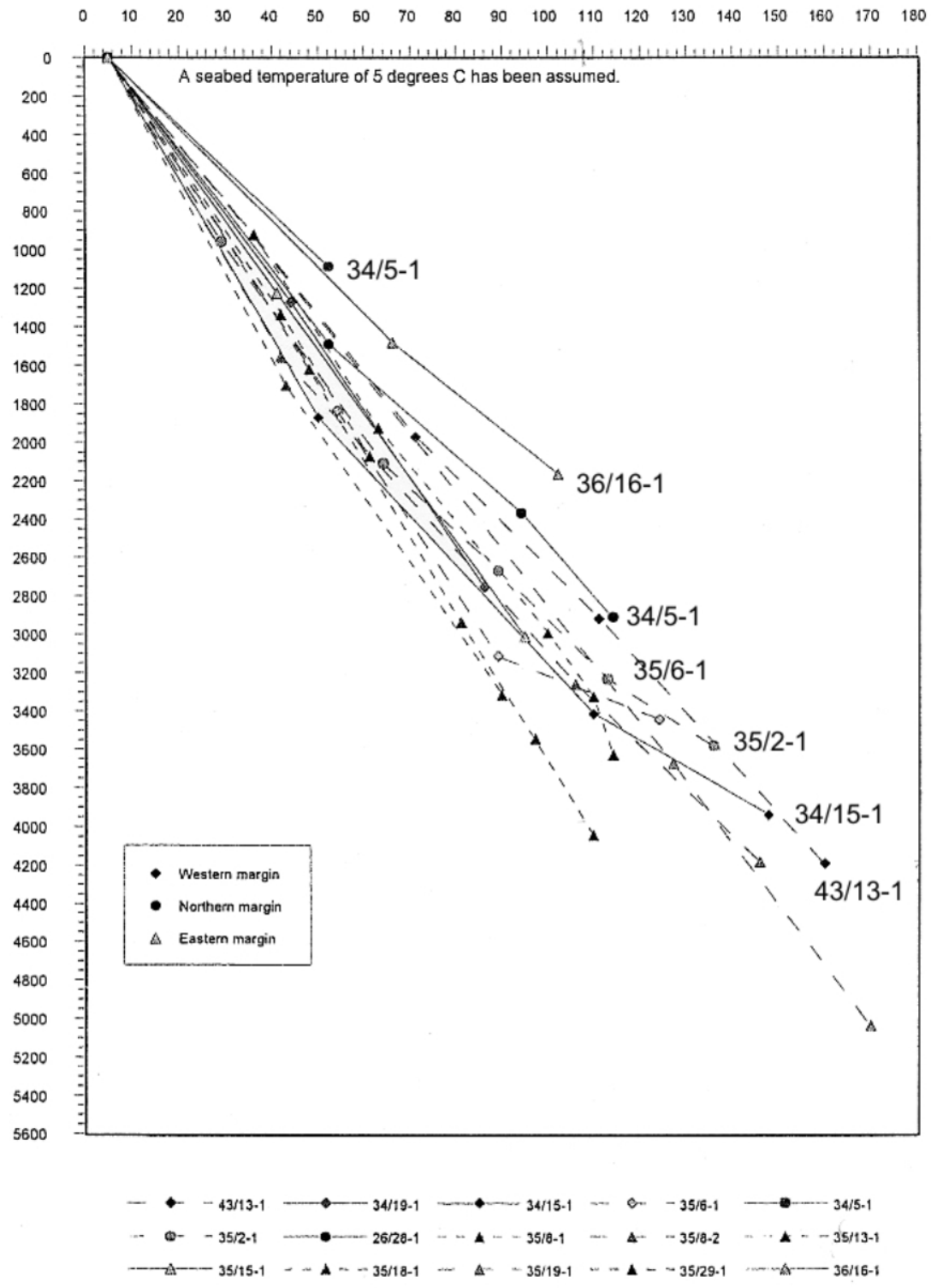

Figure 4-7: BHT-data from PAD internal reports (1996)

4.3.3 Apatite Fission Track Data (AFTA)

The apatite fission track data used was from McCulloch (1993). The data set was measured in borehole 26/28-1 and is shown in Figure 4-8. The deepest samples (PB10, PB11) are presently at their maximum burial temperatures. The age and maximum temperatures for each sample are summarized in Table 4-4.

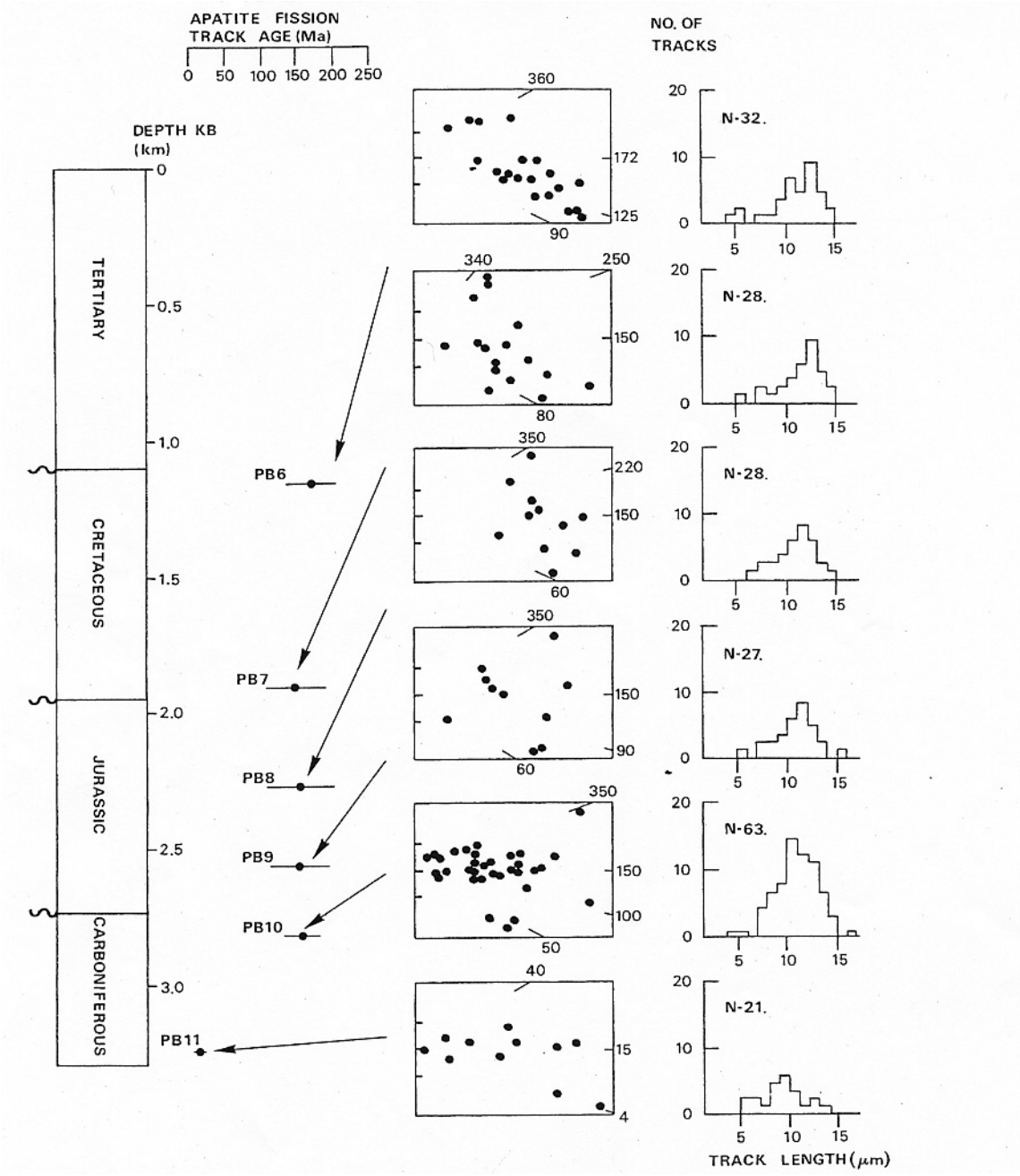

Figure 4-8: AFTA-data (McCulloch, 1993)

Sample number	Fission track age	Max. temperature
	[ma]	[°C]
PB6	172.0 ± 34.8	> 80
PB7	152.2 ± 36.0	> 80
PB8	154.1 ± 44.0	~ 90
PB9	155.4 ± 42.6	~ 90
PB10	158.3 ± 24.2	> 100
PB11	10.2 ± 5.2	~ 120

Table 4-4: AFTA-data (McCulloch, 1993)

4.3.4 Heat Flow Evolution

As a first approximation for the thermal history reconstruction the determination of present day heat flow was performed. The basic simplistic assumption in this first case was that heat flow had remained constant during the evolution of the basin. This was later modified as described later in the text.

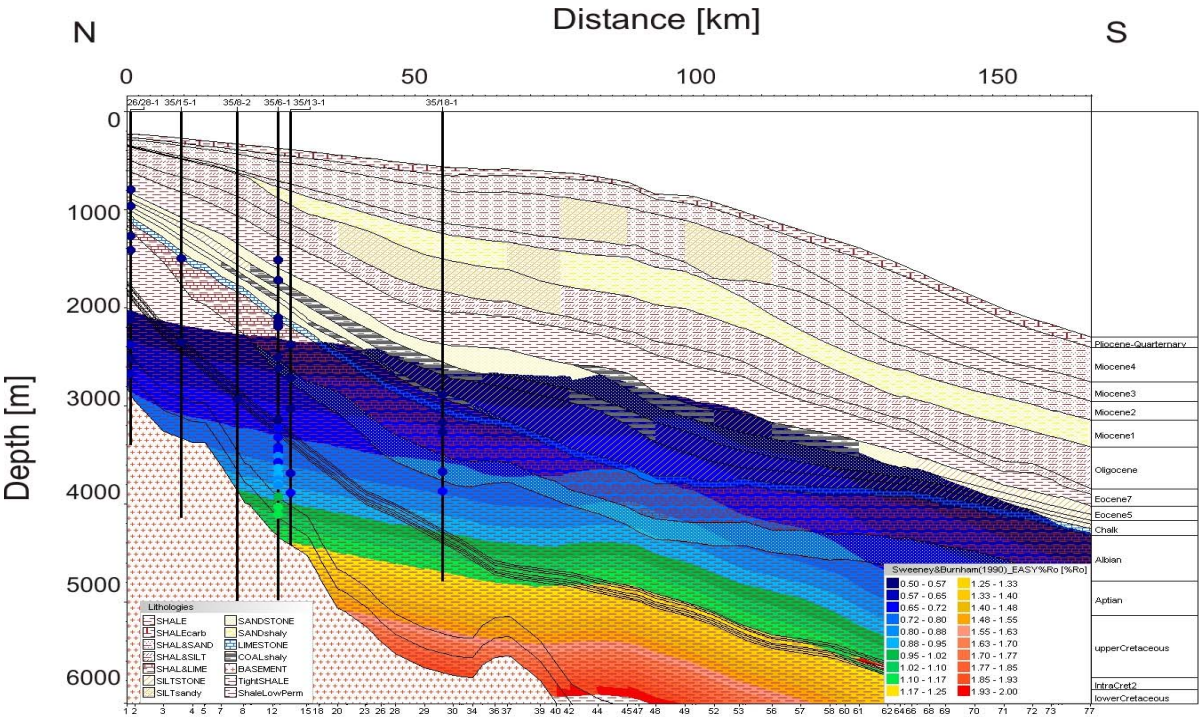

Figure 4-9: Line RE94 with calibration wells and Easy Rr overlay

The six wells close to line RE94 were used for present day calibration (Figure 4-9). Vitrinite reflectance is shown in the maturity assessment in this section and corrected bottom hole temperatures were taken from PAD internal reports. A constant heat flow of 58 mW/m^2, fitting best the calibration data was used for further heat flow modelling (Figure 4-10, Figure 4-11). Figure 4-11 shows the calibrated values for vitrinite reflectance and bottom hole

temperatures for wells 35/18-1, 35/15-1, 35/13-1, 35/8-2, 35/6-1 and 26/28-1 for a constant heat flow of 58 mW/m^2. The measured vitrinite reflectances fit the modelled ones well in all wells. At the same time the measured BHT are a bit lower than the modelled temperatures. This phenomenon is described by Foerster and Merriam (1999). Bottom hole temperatures are difficult in that it takes a long time for the water column in the borehole to equilibrate with the surrounding rock temperature. To correct these effects Horner plots were used by PAD, but it is commonly known that measured data tend to be a little lower than the actual bottom hole temperatures. Therefore the fit of the calibration data for vitrinite reflectance and BHT as shown in the calibration plots is reasonable and the assumption of a recent heat flow of 58 mW/m^2 is justified.

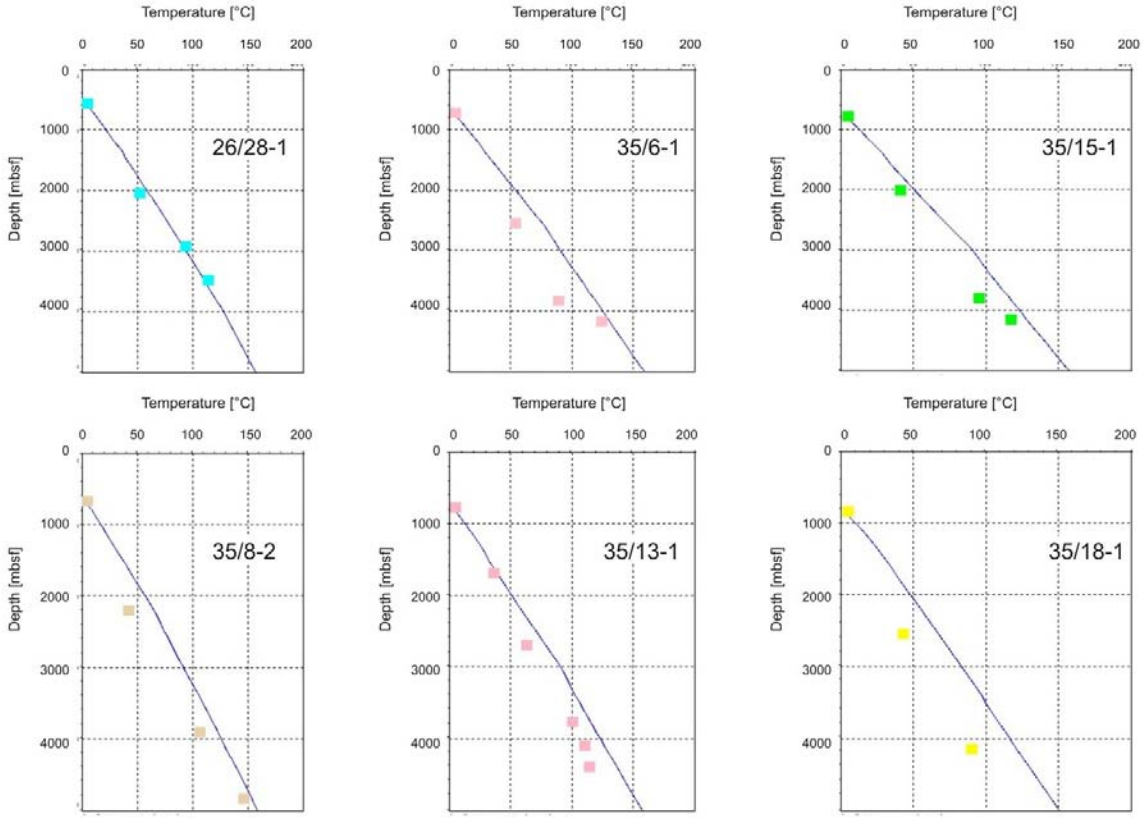

Figure 4-10: Calibration data (solid squares) plotted against modelled temperatures (straight line) for the six calibration wells 26/28-1, 35/6-1, 35/15-1, 35/8-2, 35/13-1 and 35/18-1

However, as discussed in the section tectonostratigraphic evolution of the Porcupine Basin, additional heating events are known on from the Jurassic, Cretaceous and Cenozoic. To take those into account, different heat flow scenarios were developed. The first scenario was based on Jurassic and Cretaceous rifting and for the second heat flow scenario additional heat was added during the Iceland plume event.

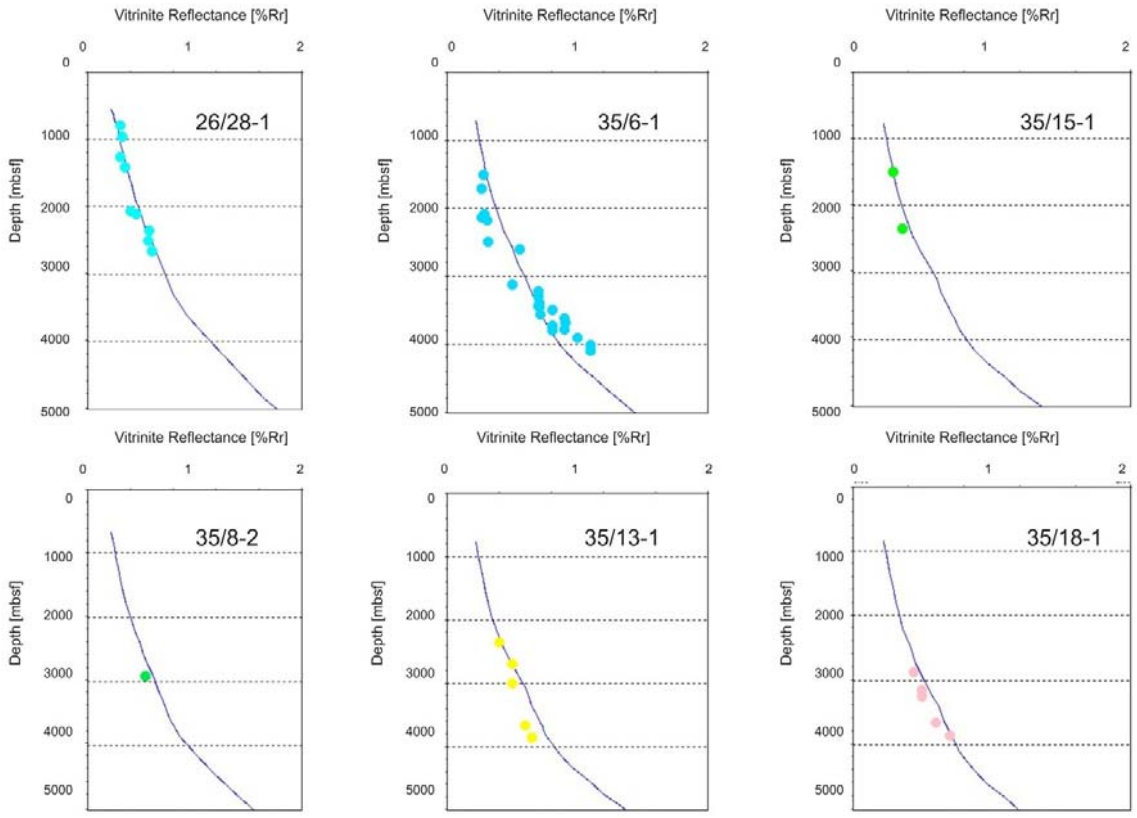

Figure 4-11: Calibration data (solid squares) plotted against modelled vitrinite reflectance (straight line) for the six calibration wells 26/28-1, 35/6-1, 35/15-1, 35/8-2, 35/13-1 and 35/18-1

The heat flow scenarios applied in this study are shown in Figure 4-12. The heights of the double peak during Jurassic and Cretaceous times were determined by the amount of stretching of the basin as expressed by the β-factor. Rifting lasted about 40-60 ma years (Croker and Shannon, 1987) starting in the Middle Jurassic and ending in the Cretaceous with a second short pulsed event leading to the evolution of the Median Porcupine Ridge. For the entire Jurassic event, lithospheric stretching of up to β = 5.5 was coincident with crustal extension on normal faults of ca. 20%. By assuming that Jurassic rifting continued into Cretaceous time a reduced lithosphere stretching factor of up to β = 2.3 is predicted (Baxter et al., 2001). Tate (1993) developed a β-factor map for the Jurassic, which is shown in Figure 4-13. Superposition of the locations of the modelled lines gives a β-factor for every point of each line. Using the McKenzie (1978) approach a distinct heat flow and thermal decay was assigned to every β-factor determining thus the height of the corresponding heat flow peaks.

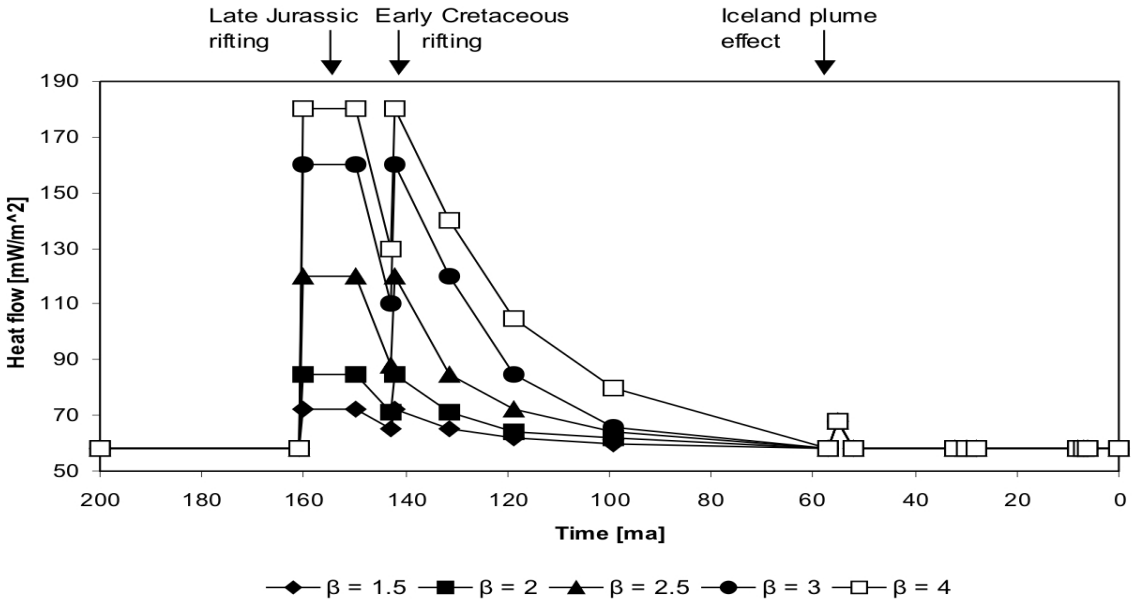

Figure 4-12: Heat flow depending on rifting events and stretching magnitude as described by the stretching value β (s. Figure 4-13)

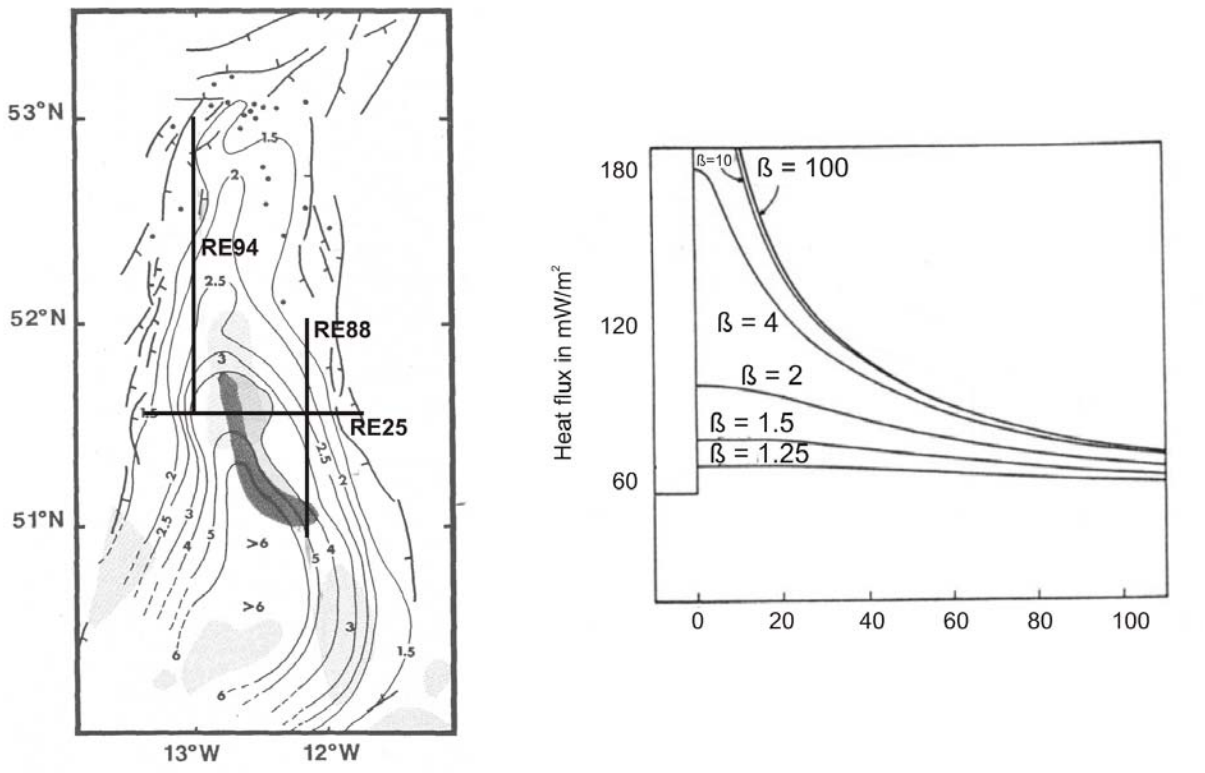

Figure 4-13: β - factor map of Tate et al. (1993) with modelled line locations and the modified McKenzie (1978) stretching factor – heat flow relationship

The modelled lines were divided into segments according to the map (Figure 4-13) and heat flow values consistent to β-factors 1.5, 2, 2.5, 3, 4 and 5 were assigned. The maximum heat flow of 180 mW/m^2 is assigned to the β-factor 5 decreasing to 58 mW/m^2 at a β-factor of 1 (Figure 4-13).

The additional heat flux input of the Iceland plume was relatively low because of the distance of the Porcupine Basin to the plume and was taken into account with a peak of 10 mW/m^2 for a duration of one million years (Figure 4-13). Apatite fission track data give the maximum temperature for the Cenozoic which is plotted as an overlay on the calculated burial depth (Figure 4-14). The influence of the Iceland plume can be seen in the increasing temperature for the Paleocene, which fits the AFTA data very well.

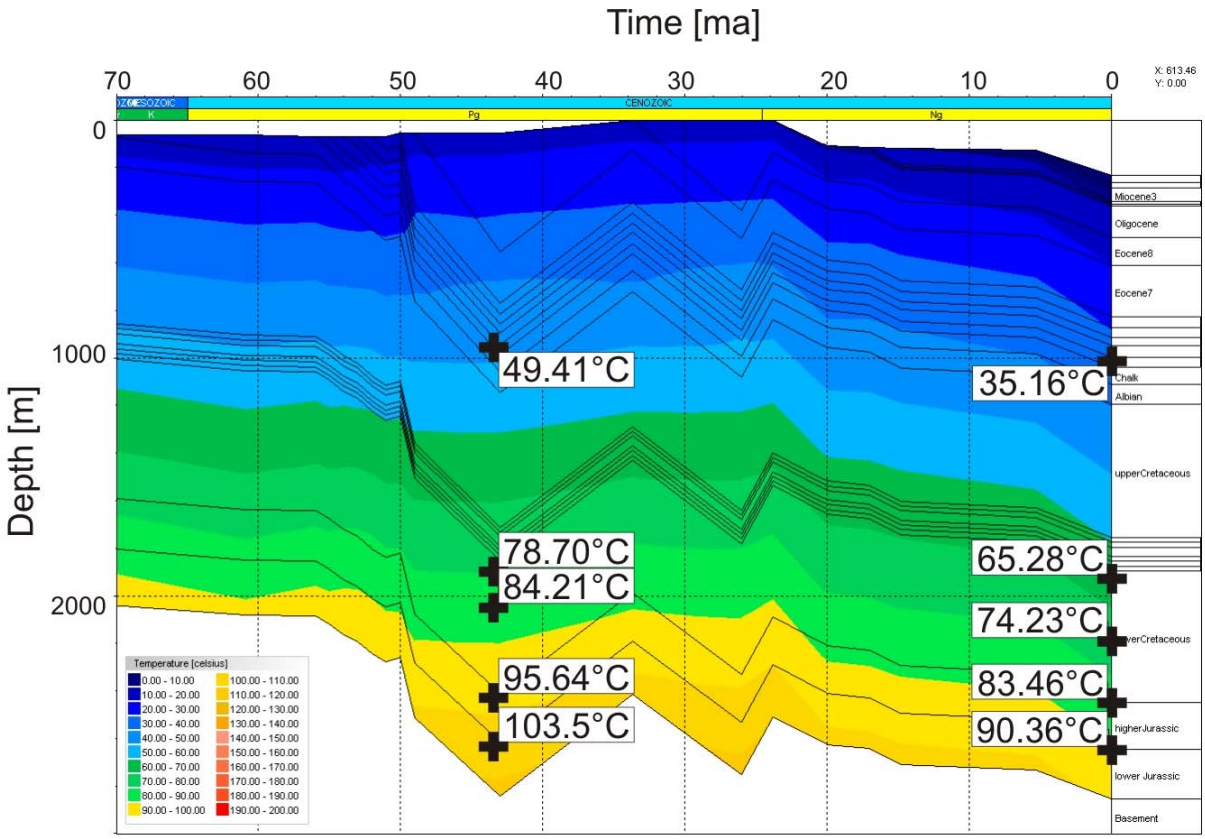

Figure 4-14: Modelled present and paleo temperatures (Paleocene) of well 26/28-1. Results at Paleocene time are influenced by the Iceland plume heat pulse and compared favourably to AFTA maximum paleotemperatures reported by McCulloch et al. (1993). Location of temperature points corresponds to McCullochs samples PB6 - PB10 from top to bottom, PB11 is of Carboniferous age and in the stratigraphic basement of the model.

Using vitrinite reflectance, BHT data and AFTA data the heat flow history consisting of a heat flow peak in Jurassic and Early Cretaceous times plus the influence of the Iceland plume shows the best correlation to the known geological history as well as available calibration data and was therefore used for the analysis of hydrocarbon generation and migration.

The development of the heat flow history itself is a crucial part in the model building. Surface heat flow values are composed of two components, a deep mantle derived component and a radioactive decay component which is important in continental areas (Giles, 1997). The radioactive component generated within the sediment column and crust varies with lithology, shales being in general more radioactive than sands and consequently generating more heat. Given that in general the gross basin lithology does not change rapidly, there is no reason to expect the total heat flow to vary rapidly over a few kilometres, heat flow should vary slowly with position. Exceptions to this rule exist where local geometric factors are important, for instance above or below a highly conductive lithology such as salt or coal or adjacent to a large step in crystalline basement or in the vicinity of intrusions.

In the Porcupine Basin the model of Jarvis and McKenzie (1980) for rift basins, which takes the stretching of crust and lithosphere into account, was used for determination of the basic heat flow history of the basin. In addition the influence of the Iceland plume and Cenozoic sills were included in the heat flow history. The rifting in Jurassic and Cretaceous times is extensively discussed by Baxter (2001). Tate (1993) performed stretching analysis of the Porcupine Basin providing a basis for the two models of Baxter et al. (2001). The first model of Baxter et al. (2001) describes a dominant Mid-Late Jurassic rift with observed upper-crustal faulting of ca. 20% extension and associated lithosphere extension up to β=5.5. The second model assumes a Mid-Jurassic rifting with ca. 20% extension that continued into Early Cretaceous time with additional upper-crustal faulting of ca. 10% extension and deeper lithosphere extension up to β=2.3.

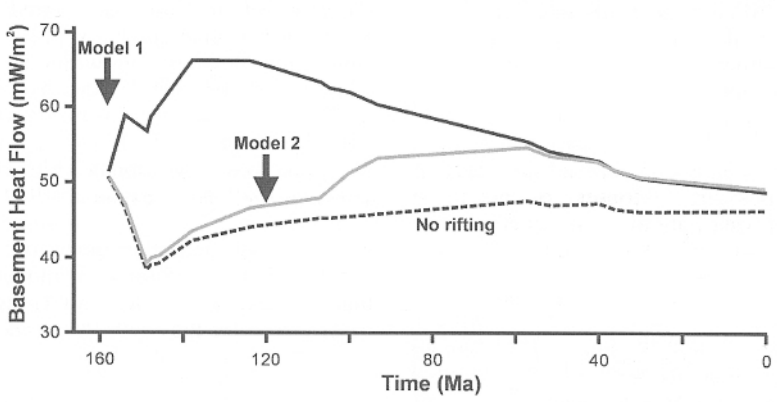

Figure 4-15: Heat flow models used by Baxter et al. (2001)

Both of these models show a distinct discrepancy between predicted lithosphere stretching and the magnitude of extension observed on upper-crustal faults. However, seismic data quality in the centre of the basin renders this inconclusive at present. Both of the above

models fit within the bounds of crustal thickness measurements and a preferential model is not obvious. Heat flow predictions for the Early Cenozoic are similar and fit the present day situation as well as our model results with a present day heat flux of 58 mW/m^2.

Two aspects seem to support the first model, one is the overall geological scheme and the second are the oils found in the Connemara oil field. Looking at the geological setting the evolution of the Porcupine Basin at Jurassic and Cretaceous times including the evolution of the Volcanic Ridge support the idea of a high heat flow input. Dean et al. (1997) described rifting events from the Jurassic to the Paleocene in the Faeroe-Shetland Basin north of the Rockall Trough. They estimated heat flow pulses up to 140 mW/m^2 depending on the rift duration for the Faeroe-Shetland Basin, which is comparable to the assumption of a heat, flow of 180 mW/m^2 for the Porcupine Basin as extension and active rifting took place in this basin.

Another difficult part of the heat flow history is the determination of the effect of the Iceland Plume. Following Edwards (2002) the extent of the influence of the Iceland plume on the Hatton-Rockall troughs, which are geographically closer to the Iceland Plume, remain problematical. A review of different authors shows different magnitudes of the impact on the Porcupine Basin. Paleocene uplift and intrusions in the Rockall Trough seem to support a pulse of the Iceland Plume (Lundin and Doré, 2002). Following the approach of Nadin et al. (1997) the assumption of a rise in heat-flow of 10 mW/m^2 seems plausible. Modelling of the temperature history including the Iceland Plume pulse at Paleocene age matched the apatite fission track data and supports the assumption of a short pulse of 10 mW/m^2.

4.3.5 Maturity Evaluation

Modelling results show that Jurassic and older source rocks in the basin are mature to overmature in a range of 0.7 – >4.7% Rr and a temperature range from 95 – 260°C, starting with low values on the flanks and higher maturity in the middle of the basin, due to the greater burial depth (Figure 4-16). Figure 4-9 shows the calculated vitrinite reflectance from 0.5 to 2% Rr for line RE94. Cretaceous strata are immature to mature in the central part of the basin and immature on the flanks. Vitrinite reflectance ranges in between 0.3 – 4.6 % Rr and temperatures between 40 – 240°C. Transformation ratios, which will be discussed later, show a total conversion (TR = 1) in the central part of the basin below 4500 m. As far as the Cenozoic sequence is concerned, immaturity is maintained over the entire basin and no transformation from kerogen to hydrocarbons has taken place so far. Vitrinite reflectance is at a maximum of 0.4 % Rr and temperatures range between 4 – 70°C.

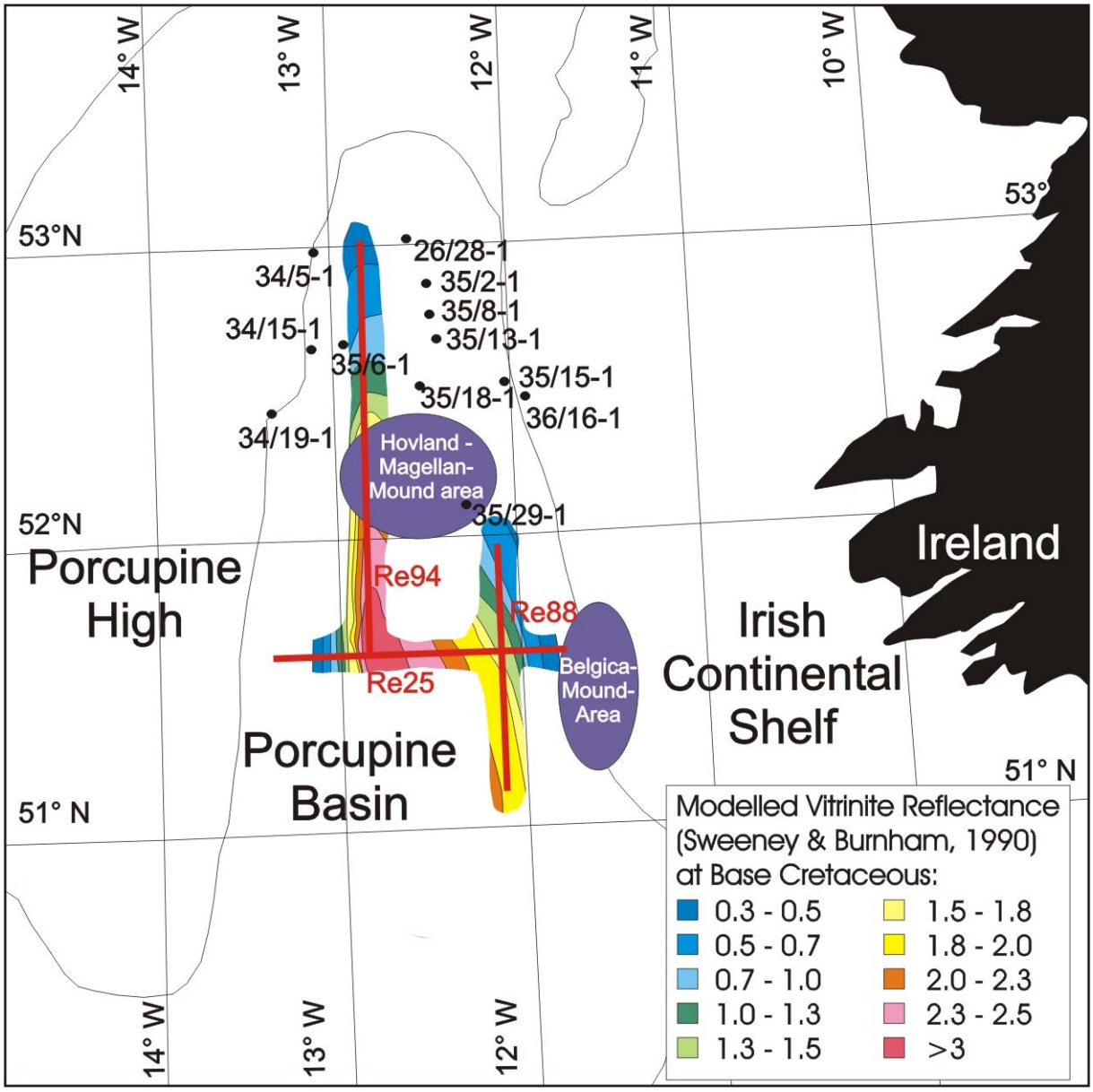

Figure 4-16: Maturity map of the Base Cretaceous based on the 2D modelling results of the profiles RE25, RE88 and RE94

4.4 Organic Matter Characterisation

To calculate and model hydrocarbon generation several input data are needed, first the source rock properties itself and second the burial and thermal evolution. The burial and thermal histories were tested and calibrated in the previous section and as a result the maturity distribution in the Porcupine Basin was calculated. This leaves the Jurassic section as the main source rock interval because the Cenozoic section is immature and the Cretaceous section has only poor source rock potential. The pre-Jurassic strata cannot be resolved on the seismics and must therefore be neglected.

Source rock properties needed for the model are the quantity of organic material expressed by the total organic carbon (TOC), the quality of organic matter expressed by the Hydrogen Index evaluated with the Rock-Eval analysis and the type of kerogen. The type of kerogen is based on the composition as different compositions yield different amounts and hydrocarbon compositions as e.g. a type III kerogen yield mainly gas in contrast to an oil-prone type II kerogen. In the following, first the known oil composition is described, which provides information on the composition and original properties of the source rock, then the source rock properties are evaluated and summarized for the model input.

The conversion of kerogen to oil and gas is controlled by reaction kinetic processes as stated in section 3.1.1. The available kinetic approaches are presented, and gathered information from literature is compared to asphaltene and compositional kinetics.

From literature and already from section 2.1.3.1 it is known that the lacustrine / marine Upper Jurassic source rock sequence has been documented as the best oil-prone source rock. It contains good to excellent oil and gas source potential with TOC values about 3-4 % at maximum (Croker and Shannon, 1987; Shannon et al., 1995). Additionally, Middle Jurassic shales have locally good oil and gas potential but are of minor importance as the amount of kerogen is only up to 1.8 % (Shannon and Naylor, 1998). However, the choice of samples available for this study provided very restricted samples for the Upper Jurassic but gave the opportunity to characterize samples from Middle Jurassic sequences.

4.4.1 Oil Composition

Several of the wells drilled in the Porcupine Basin showed oil and gas shows (Croker and Shannon, 1995). Oil has been discovered and sampled in wells 35/8-1, 35/8-2 and 26/28-1 in the Connemara oil field. Data from PAD were used and combined with newly acquired data and compared to an extensive study on Porcupine and Jeanne d'Arc basin oils by Butterworth et al. (1999).

Reports from PAD Dublin focus on the crude oils obtained from well 26/28-1, 35/8-1 and 35/8-2. DST-2 oil from well 26/28-1 oil is found in Kimmeridgian-Oxfordian sandstone, DST-3 in sandstones of Portlandian age. API gravities from these Jurassic oils range from 31 – 37°. DST-3 oils show high NI/V ratios, which seem consistent with a marginal, marine or lacustrine source whereas DST-2 oil shows particularly low NI/V ratios and is comparable with oils generated from non-marine higher plant organic matter.

Only DST-2 sample (2245-2268 m) from Kimmeridgian-Oxfordian sandstones was available for chromatographic analyses to PAD. Bulk compositional analysis by open column liquid chromatography indicates the DST-2 crude oil to be paraffinic or paraffinic-naphthenic and moderately waxy. The whole oil and C_{15+} saturates chromatograms are characterised by n-alkanes extending out to C_{35}. Odd carbon numbered members predominate in the C_{21}-C_{29} range and at C_{17}. The baseline is slightly elevated due to naphthenic material. In combination with the pristane/phytane, Pr/C_{17} and Ph/C_{18} ratios suggest an organic source facies

composed of algal and higher land plant matter and a depositional environment compatible with marginal marine/marine conditions. This observation is supported the carbon isotope ($\delta^{13}C$) data of the saturates, aromatics, resins and asphaltenes displaying a slight dog leg in the aromatics fraction and provide relatively light isotope values. Based on the palaeoenvironmental considerations, compatible source rock candidates could include Late Jurassic and/or Early Cretaceous intervals containing prospective Type II (sapropelic) kerogen assemblages that have attained thermal maturity levels in excess of Rr 0.6-0.7%.

Maturation of the oil is given by the aromatic compound distributions which suggest a moderately mature oil with a methylphenanthrene index-1 (MPI-1) yielding an equivalent vitrinite reflectance maturity of Rc 0.78% for the source rock. The methylphenanthrene ratio (MPR) provides a higher maturity of Rc 0.89%. The GC-MS data suggest a lower maturity of Rc 0.70%.

Chromatographic analysis of the aromatic organosulphur compound shows the benzothiophene class of compounds to be absent with the exception of a very minor dibenzothiophene (DBT) peak. In comparison, North Sea crude oils frequently display a full suite of methyldibenzothiophene (MDBT) compounds associated with generation from a fully marine anoxic source facies. This indicates that the 26/28-1 crude oil has been generated from a different facies to that of a typical North Sea Kimmeridgian source rock. The whole oil chromatogram includes a full suite of light to medium molecular weight compounds without evidence of biodegradation or water washing.

Results of the analysis of five Jurassic oils E49851, E49852, E49853, E49854 and E49855 carried out at the Forschungszentrum Jülich are reported in Schaefer et al. (2002). The API gravities range between 31.4 and 42.2°. The saturated hydrocarbons indicate a not fully mature crude oil based on the Light Hydrocarbon Index (LHCPI). The Carbon Preference Index ($CPI_{25\text{-}31}$) ranges between 1.08 – 1.10. Calculated vitrinte reflectance ranges between 0.78 – 0.84 %. The chromatograms of the triterpanes indicate a deposition of the source rock under marine shelf sub-oxic conditions indicated by the occurrence of diahopanes.

4.4.1.1 Porcupine and Jeanne d'Arc Oil – Source Rock correlation

Compositional analyses of Porcupine Basin and Jeanne d'Arc Basin oils were used by Butterworth et al. (1999) to correlate oils from both basins and predict source facies characteristics. The Upper Jurassic source rock from the Porcupine Basin is isotopically similar to the Egret Member extract from the Jeanne d'Arc Basin.

The Porcupine oils, along with some Jeanne d'Arc Basin oils, show the lowest marine algal C_{30} sterane input. The C_{30} steranes are used to calculate an ARCO lacustrine indicator. This ratio confirms that there is an additional lacustrine component to the non-marine or marginal marine source contributors of the Porcupine Basin oils. Very high dinosterane contents in the Porcupine and Jeanne d'Arc Basin oils correlate well with many of the low maturity Lower

and Middle Jurassic source rock extracts. In summary, the geochemical characteristics of the oils from both are indicative of mixed non-marine and marine input.

However oil compositions from both basins are in sharp contrast to the traditional marine Upper Jurassic Kimmeridge Clay Formation source rocks of the North Sea. The Porcupine Basin oils tend to differ from the classical North Sea oils in many ways: they have similar to lower sulphur contents (including dibenzothiophenes, DBT), lower rearranged steranes, isotopically lighter saturate hydrocarbons relative to aromatic hydrocarbons, higher gammacerane contents, higher 4α-methylstigmastanes relative to C_{29}stigmastanes, higher to slightly higher ARCO lacustrine biomarker indicators, slightly higher wax content, distinctly lower C_{30} marine steranes, lower hopane/sterane ratios, lower to similar bisnorhopane contents, and generally a lower thermal maturity (Butterworth et al., 1999).

4.4.2 Source Rock Evaluation

To determine the source rock properties 38 core samples from 8 wells were taken as listed in Table 3-1. The samples are core slices of about 3 cm thickness and were used for characterisation of the quantity and quality of the organic matter, the type of organic matter and its hydrocarbon potential. The organic matter type also provides information on the depositional environment, which can be useful in determining the paleo-geometry and the paleo-waterdepth. Kinetic parameters measured on source rock kerogen or petroleum asphaltenes provide a prediction of the timing and rate of hydrocarbon generation and expulsion.

Potential source rock intervals were presented in the previous section. In the following examples for the different intervals are described and the properties of distinct source rocks are determined and listed below, the complete description can be found in Appendix I. A first evaluation of the results of elemental analysis and Rock-Eval pyrolysis is presented and the results compared to those of the Jeanne d'Arc basin and typical North Sea source rocks.

Four Pre-Jurassic samples of Carboniferous age were taken from the cores. Figure 4-17 show samples 49717 from well 26/27-1B (2506.6 msl) and 49735 from well 34/15-1 (4441.3 msl), which consist of a thinly bedded, glauconitic, slightly carboniferous grey mudstone with some siderite concretions.

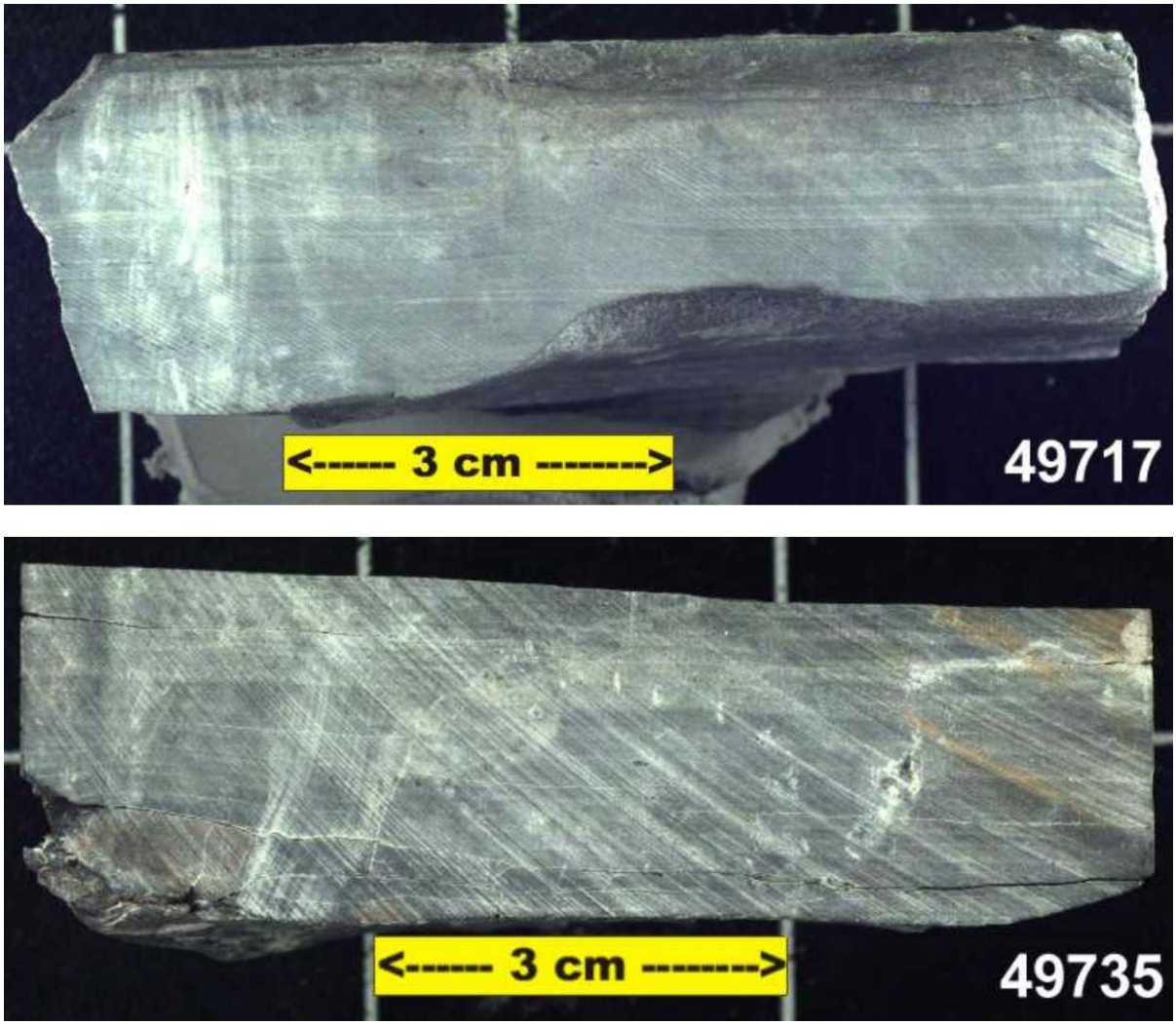

Figure 4-17: Carboniferous core samples 49717 and 49735

The Lower Jurassic samples shown in Figure 4-18 consists of greenish-grey laminated mudstones presented in samples 49713 (2005.4 msl) and 49715 (2006.7 msl) and an interbedded sandstone 49714 (2006.4 msl) from well 26/22-1A. The argillaceous to carbonaceous mudstone is of grey – green color and contains sideritic concretions and striae. The sandstone is light grey to yellow, moderate sorted and quarzitic with subordinate feldspar and jasper.

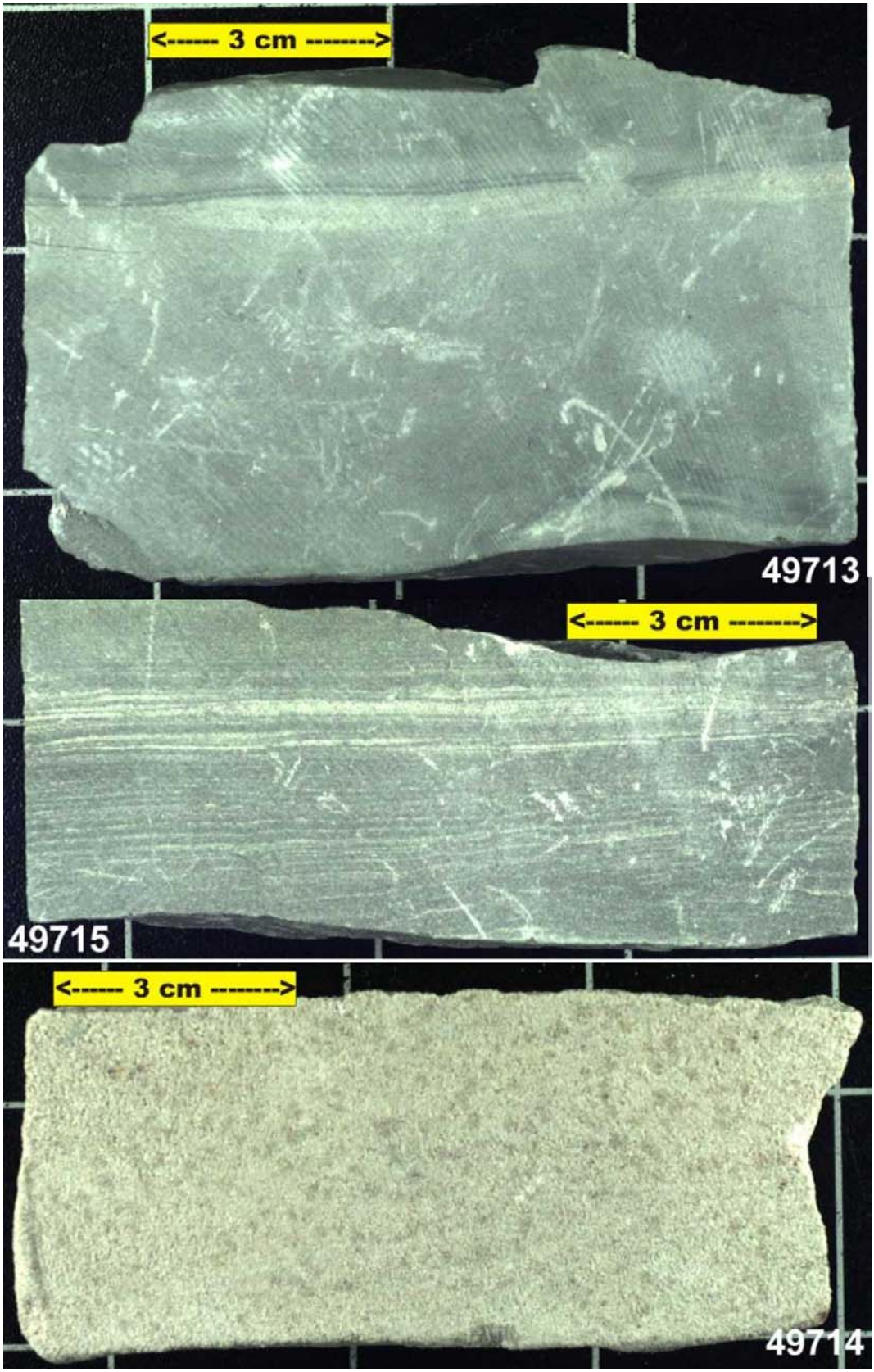

Figure 4-18: Lower Jurassic samples 49713, 49714 and 49715

Middle Jurassic samples are shown in Figure 4-19 and represented by the sandstone samples 49726 (2093.3 msl) from well 26/28-2 and 49730 (1782.0 msl) from well 26/29-1 and two mudstone samples 49736 (3954.0 msl) and 49737 (3955.3 msl) from well 35/6-1. The sandstone samples are different in their appearance. Sample 49726 is of yellow to pale brown color, fine grained, angular rounded, moderately sorted, good visible porosity with some patchy carbonaceous cements, a visible cross-bedding and oil stains. In contrast interlaminated sandstone sample 49730 is of light grey to reddish color, very fine grained, well sorted, slightly carbonaceous with no visible porosity. The mudstone samples are of light to dark grey color, laminated, crossbedded and interbedded with carbonaceous beds and containing siderite concretions. Sample 49736 is less silty and more carbonaceous than sample 49737.

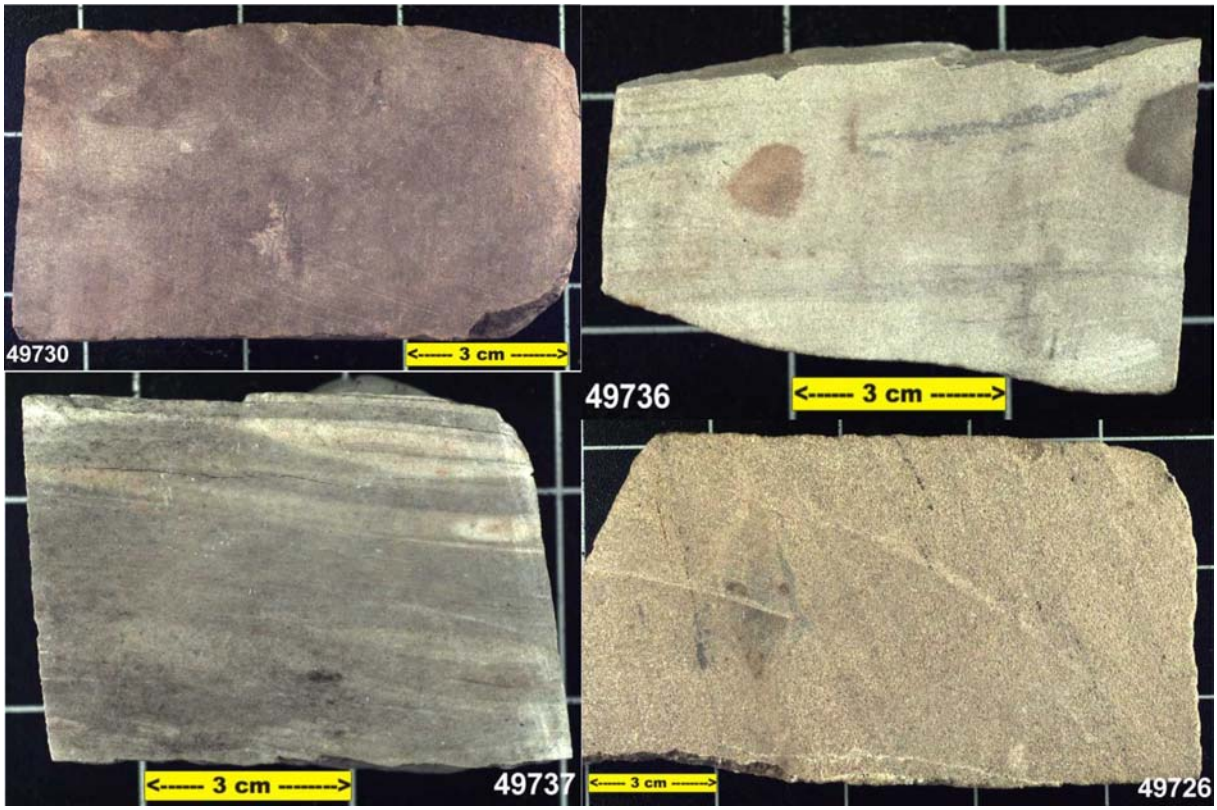

Figure 4-19: Middle Jurassic samples 49726, 49730, 49736 and 49737

The Upper Jurassic strata are presented by a sandstone sample 49720 (2256.0 msl) and a mudstone sample 49721 (2263.4 msl) from well 26/28-1 (Figure 4-20). The mudstone sample 49721 is of medium grey colour, slightly silty and carbonaceous, laminted and with visible bioturbation in the upper part. The sandstone sample 49720 is of light to dark brown colour, fine grained, good sorted, with a good visible porosity and containing oil stains.

Figure 4-20: Upper Jurassic samples 49720 and 49721

The Cretaceous section is represented by sample 49740 (5015.9 msl) from well 35/19-1 (Figure 4-21). The silty claystone is dark grey to dark greenish grey, glauconitic, carbonaceous, laminated and contains some siderite concretions.

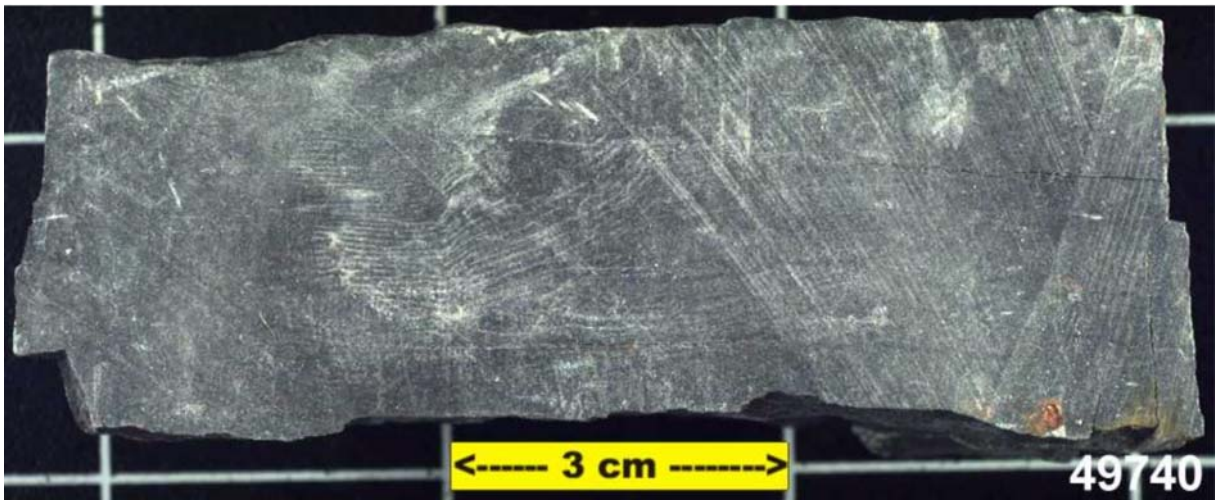

Figure 4-21: Cretaceous samples 49740

The Cenozoic samples 49738 (1711.8 msl) and 49739 (1711.9 msl) are taken from well 35/8-1 (Figure 4-22). They are of very rotten appearance due to the storage conditions. As far as recognizable the samples are a very fine layered/laminated claystone, very carbonaceous and some interbedded sands.

Figure 4-22: Cenozoic samples 49738 and 49739

For the source rock analysis the mudstone samples were used as they are stratigraphically close to the source rocks and the composition of the organic matter is expected to be similar to the source rock properties based on sequence stratigraphy concepts (Miall, 1997). The

sandstone samples were thought for the extraction of the organic matter, which is e.g. described by the oil stains, but the due to the low amount of organic matter (section 4.4.2.2) not used.

4.4.2.1 Petrographyical Analysis

Petrograhphical analysis were carried out on every available well sample as listed in Table 3-1 (Appendix II). Due to the low content of organic matter a petrographical characterization of the organic matter in form of a maceral analysis could not be performed. An example is presented in Figure 4-23, which shows a mudstone from the Late Jurassic.

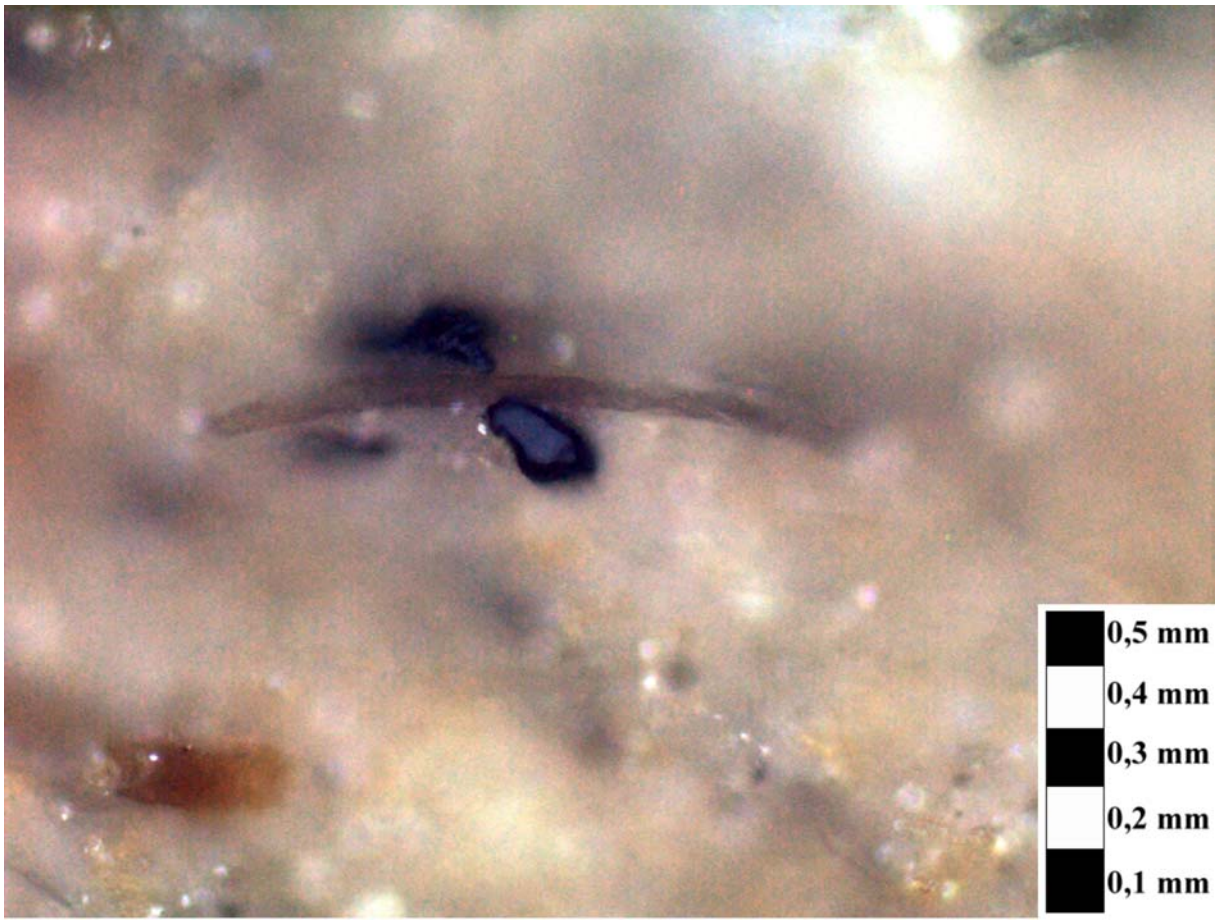

Figure 4-23: A microscopic view (600x magnification) of the Late Jurassic potential source rock sample 49728 showing a small vitrinite particle in the middle of the photo

However, analysis under fluorescent light was successful for one sample of Kimmeridgian age. In the case of the sample 49719 bodies of the algae *Botryococcus* were found indicating type I kerogen and a lacustrine depositional setting.

The measurement of the vitrinite reflectance was possible for samples 49713, 49715, 49717,49718, 49718, 49719, 49722, 49723, 49724, 49727, 49728, 49729, 49733, 49735, 49739 and 49740. Figure 4-24 shows the histogram of sample 49728 with a vitrinite

reflectance of 0.55%. The peak at 1.2% Rr shows either a reworked vitrinite or a fusinite. The Jurassic sample 49728 is taken from well 26/28-5 in the Connemara field where the Jurassic section did not experience deep burial and just reached the oil window. The results for all samples are listed in Table 4-5 and incorporated in Figure 4-6. Again, due to the low amount of organic matter the analyses were very difficult as in some cases it was even not possible to measure 50 points per sample. However, the measured vitrinite reflectances confirm the published data sets for the given depth intervals (Figure 4-6).

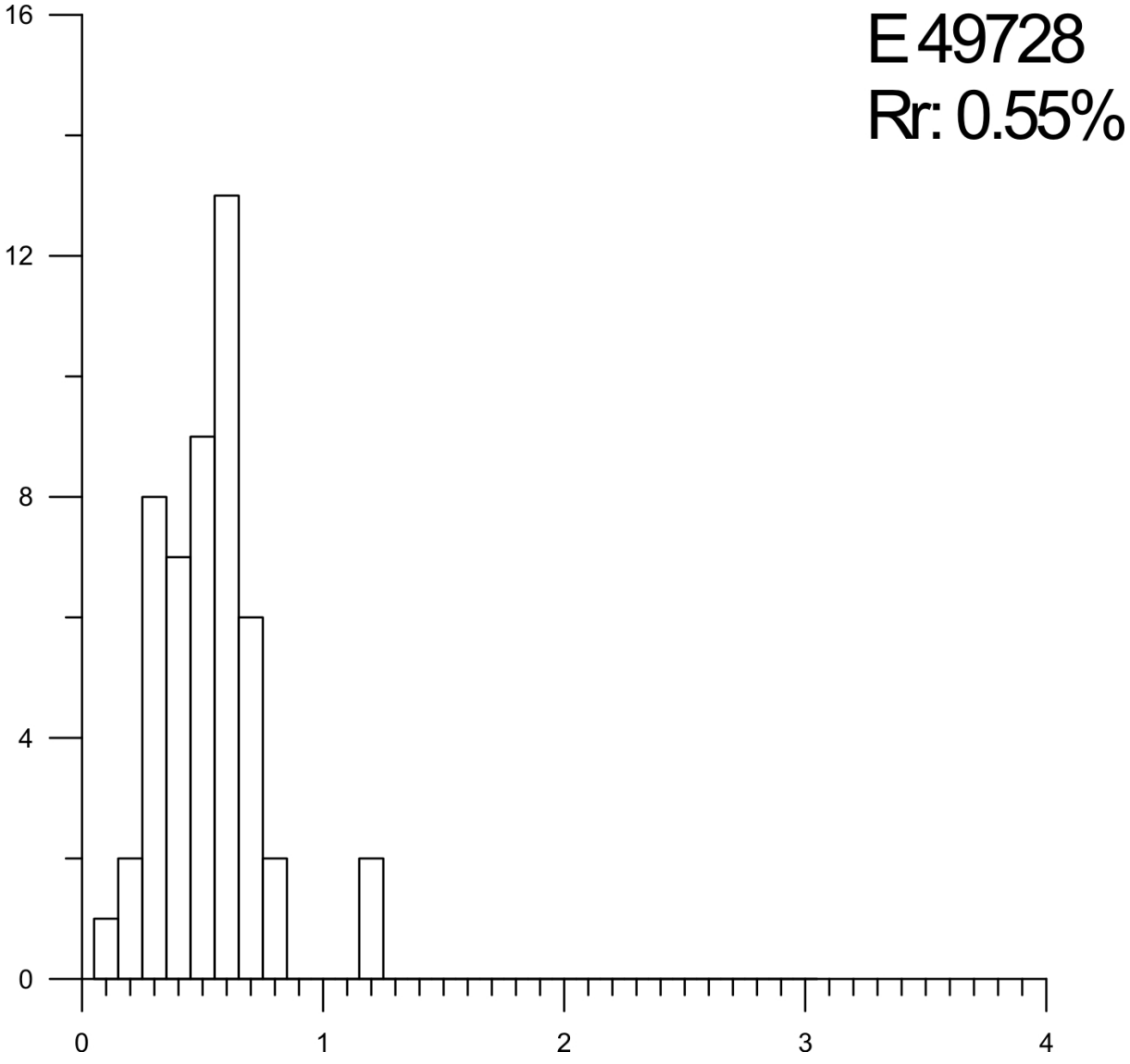

Figure 4-24: Histogram for the vitrinite reflectance for Jurassic sample 49728

4.4.2.2 Elemental analysis and Rock-Eval pyrolysis

Elemental and Rock Eval analysis were used to evaluate source rock properties. The screening data set including TOC, TC, $CaCO_3$, TS, S1, S2, S3, Tmax, PI, HI, OI and Rr is presented in Table 4-5.

TOC- and Rock-Eval-analysis were carried out on all core samples. Generally the content of organic carbon is very low, below 4% in this data set. In most cap- and carrier-rocks the content of organic carbon is below 1%. TOC contents for the Jurassic source rock formations range between 0.5 and 2.1 % TOC.

The Rock Eval S1 parameter represents the fraction of the original genetic potential, which has been effectively transformed into hydrocarbons, the quantity S2 represents the residual genetic potential which has not yet been used to generate hydrocarbons. Both S1 and S2 values are influenced by the amount and type of organic matter present in the rock sample. Due to the relatively low TOC contents in the samples analysed, the S2 peak was very weak and broad and the Tmax-values could only be assigned with a larger uncertainty than with higher TOC values.

Sample	Well	Depth	TOC	TC	CaCO3	TS	S1	S2	S3	Tmax	PI	HI	OI	R_r
		(m)	%	%	%	%	mg HC/g sample	mg HC/g sample	mg CO2/g sample	°C	S1 / (S1+S2)	mg HC/g TOC	mg CO2/g TOC	(%)
49713	26/22-1A	2005.4	0.22	0.23	0.07	0.03	0.04	0.19	0.04	519	0.18	84.88	17.45	1.20
49714	26/22-1A	2006.4	0.09	0.20	0.91	0.02	0.01	0.22	0.19	546	0.05	247.95	212.47	
49715	26/22-1A	2006.7	0.21	0.22	0.08	0.03	0.04	0.30	0.02	514	0.11	145.27	10.55	1.40
49716	26/22-1A	2009.6	0.11	0.55	3.71	0.05	0.02	0.18	0.60	444	0.10	167.93	566.80	
49717	26/27-1B	2506.6	0.18	0.17	0.00	0.02	0.03	0.20	0.00	497	0.14	112.27	0.00	1.50
49718	26/27-1B	2661.6	0.75	0.78	0.19	0.02	0.01	0.41	0.03	493	0.03	55.13	3.57	0.90
49719	26/28-1	2255.5	0.38	0.45	0.58	0.03	0.07	0.39	0.33	520	0.15	101.24	85.87	0.70
49720	26/28-1	2256.0	0.67	0.80	1.02	0.07	5.89	2.39	0.45	410	0.71	355.37	67.16	
49721	26/28-1	2263.4	0.50	0.79	2.38	0.03	0.09	0.19	0.19	491	0.32	37.18	37.75	
49722	26/28-1	2426.0	0.36	1.78	11.79	0.08	0.02	0.18	0.70	431	0.11	50.87	194.22	0.60
49723	26/28-1	2426.7	0.53	1.64	9.28	0.09	0.03	0.33	0.55	428	0.07	63.59	103.90	0.70
49724	26/28-1	2428.0	0.46	1.39	7.76	0.17	0.02	0.37	0.46	427	0.04	80.90	100.46	0.60
49725	26/28-1	2429.8	0.50	1.45	7.89	0.13	0.02	0.46	0.57	429	0.03	90.71	113.80	
49726	26/28-2	2093.3	0.52	2.51	16.54	1.77	5.35	1.20	0.43	405	0.82	228.66	82.63	
49727	26/28-5	2402.0	2.08	2.73	5.37	1.85	0.11	6.95	0.64	429	0.02	334.36	30.59	0.60
49728	26/28-5	2403.2	1.19	2.97	14.83	0.41	0.05	3.05	1.36	428	0.02	257.06	114.89	0.55
49729	26/28-5	2766.6	0.25	0.63	3.15	0.02	0.01	0.11	0.84	500	0.07	46.44	339.63	0.60
49730	26/29-1	1782.0	0.07	0.25	1.47	0.01	0.01	0.33	0.70	540	0.04	465.14	981.21	
49731	26/29-1	1782.8	0.07	0.39	2.60	0.01	0.01	0.19	1.07	544	0.06	251.10	1439.22	
49732	26/29-1	1786.3	0.08	0.10	0.18	0.03	0.01	0.38	0.08	493	0.02	494.89	109.14	
49733	26/29-1	1833.4	1.84	3.87	16.95	0.05	0.33	2.11	0.47	431	0.13	114.83	25.87	0.70
49734	26/29-1	1781.4	0.07	0.09	0.17	0.01	0.01	0.26	0.12	503	0.05	364.46	168.45	
49735	34/15-1	4441.3	0.20	2.44	18.63	0.07	0.01	0.06	0.93	483	0.14	29.23	465.42	1.80
49736	35/6-1	3954.0	0.13	1.42	10.72	0.02	0.08	0.08	0.40	485	0.47	65.98	314.63	
49737	35/6-1	3955.3	0.16	0.86	5.80	0.02	0.06	0.08	0.77	430	0.42	48.01	478.35	
49739	35/8-1	1711.8	1.92	2.03	0.87	0.74	0.10	1.28	1.46	414	0.07	66.87	76.26	0.34
49740	35/19-1	5014.0	0.40	0.73	2.71	0.08	0.01	0.09	0.20	497	0.10	22.72	49.68	1.30

Table 4-5: Screening Data Set

The quality of the organic matter in all samples was assessed by Rock-Eval analysis. An increase of the Tmax values with depth was observed. A plot of Tmax against the vitrinite reflectance (Figure 4-25) shows as expected higher Tmax-values at higher maturity, but a large variation exists at high Tmax and Rr-values due to the very low TOC content.

The Tmax-values are dependent on the type of kerogen. Areas of type I and III kerogen are shaded grey in Figure 4-25 using the approach of Tissot et al. (1987). The Cenozoic and Cretaceous samples plot in the area of type III kerogen, which shows a terrestrial origin of the organic matter. This fits the observation of Cenozoic coaly layers in the prograding deltaic structures.

Within the Jurassic samples a large diversity in the type of kerogen was observed. Some of the samples fit into the lacustrine type I kerogen group, whereas one sample has a terrestrial

origin (Figure 4-25), however most of these samples contain reworked vitrinite. Further characterisation is shown in the HI vs. OI – diagram (Figure 4-26).

The Westphalian sample 49735 has a relatively low Tmax and a high vitrinite reflectance (1.80 % Rr) and plots in the type III area, which indicates a terrestrial environment. This also fits the geological observation of Westphalian coal beds.

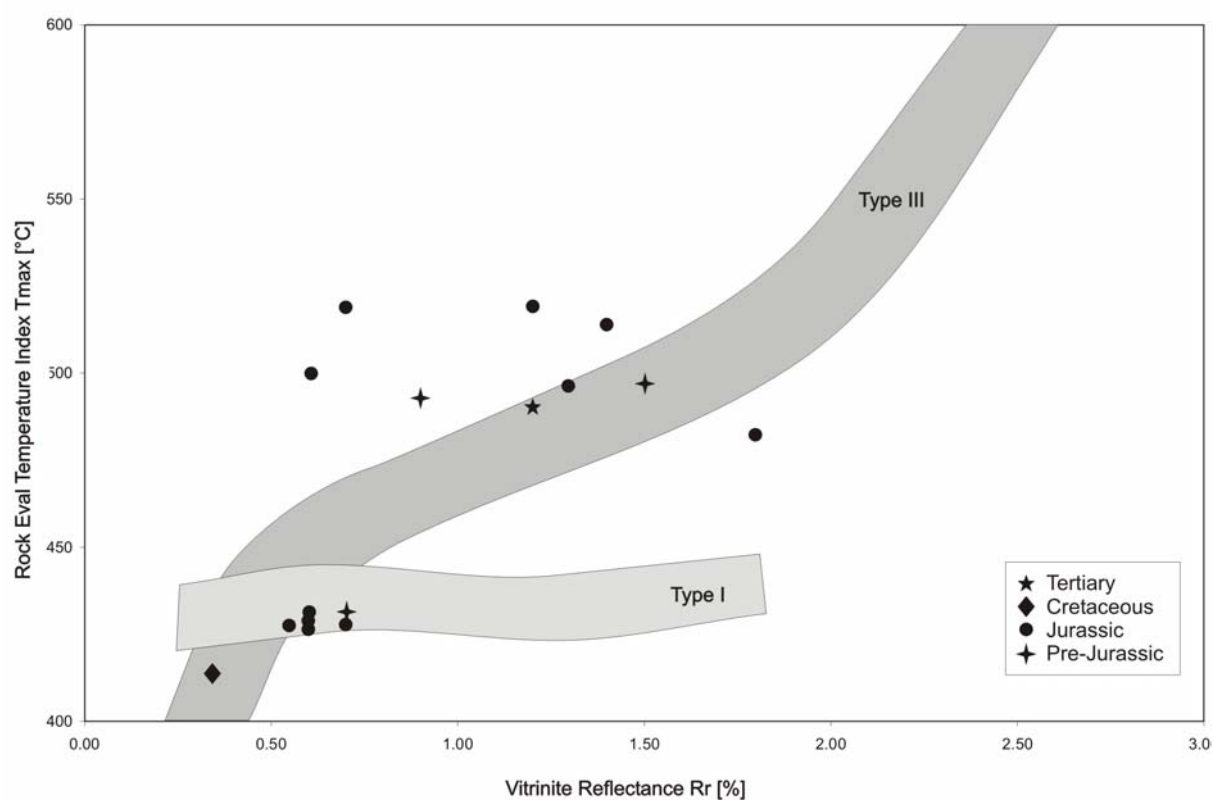

Figure 4-25: Relationship between the temperature index Tmax and the vitrinite reflectance after Tissot et al. (1987)

The production index PI = S1/(S1+S2) was used to characterize the level of evolution of the organic matter. Except for samples 49720, 49721 and 49728 the PI is very low, which can be interpreted either as for an indication of immaturity (low S1 due to non generation) or of effective petroleum expulsion (Espitalié et al., 1977). The Kimmeridgian sample 49720 has a high S1, indicating either generation of hydrocarbons or impregnation, the Kimmeridgian sample 49721 and the Bathonian sample 49728 have low S1 values indicating either immaturity or effective petroleum expulsion.

The type of kerogen is characterized in a HI versus OI – diagram (Espitalié et al., 1985) and also in a S2 versus TOC – diagram (Horsfield et al., 1994) (Figure 4-26). Cretaceous and Cenozoic units are only represented by one sample for each stratigraphic unit. Both samples are a type III kerogen and back up the observations of a deltaic environment with terrestrial

influence. Type III kerogens mostly generate gas and almost no oil (Horsfield and Rullkoetter, 1994).

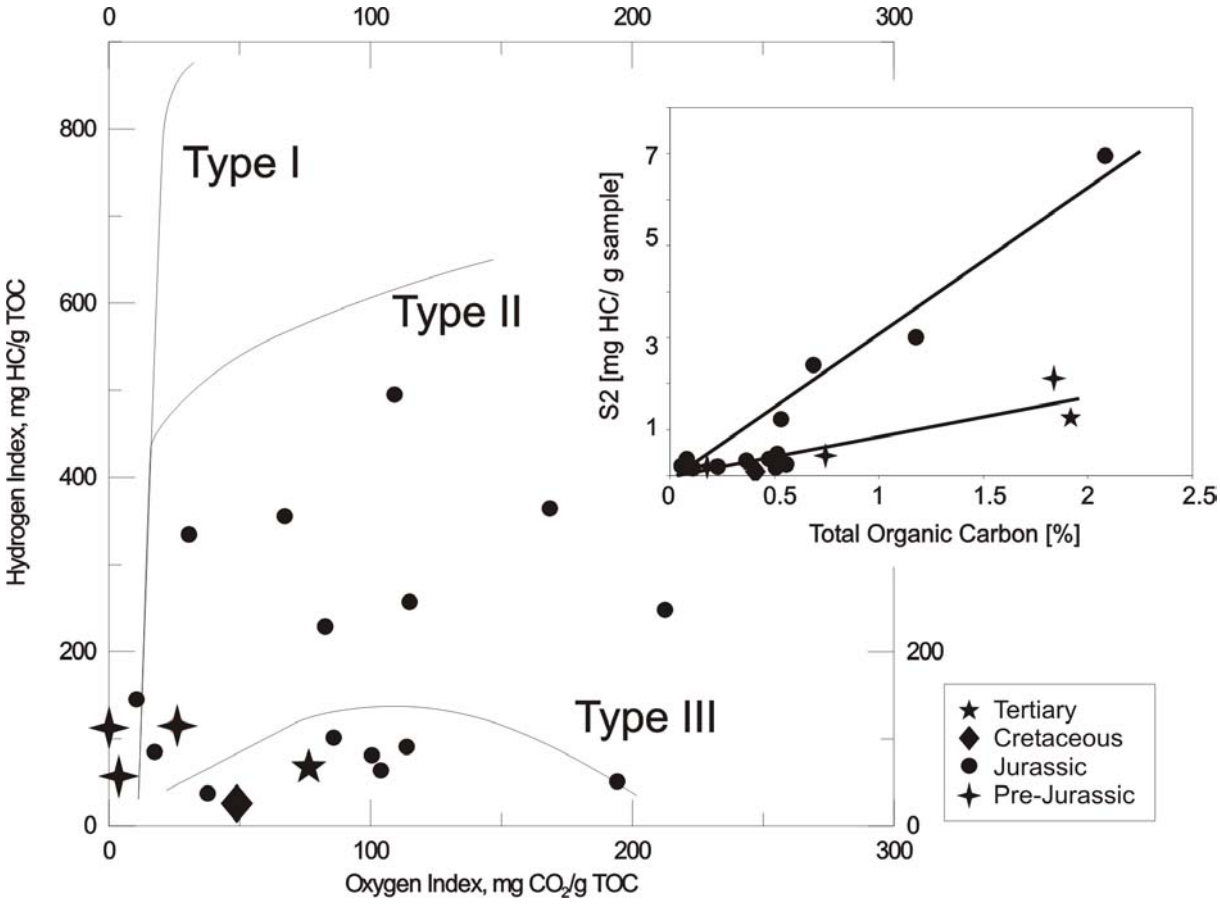

Figure 4-26: Kerogen type discrimination on the basis of Rock Eval parameters Hydrogen Index (HI) and Oxygen Index (OI), S2 and TOC

The Pre-Jurassic samples are very low in both HI and OI making recognition of original kerogen type impossible using the HI versus OI - diagram. In the S2 – TOC – diagram it becomes obvious that the samples of Westphalian age follow a kerogen type III trend which also can be confirmed by the observations in Figure 4-25.

The Jurassic samples are a mixture of type II and type III kerogen (Figure 4-26). This confirms the changes in sea level and transition from terrestrial to marine environments. Kerogen of type I is usually found in anoxic lacustrine settings. Pure type I kerogens are not detected in the HI vs. OI – diagram but observed in the Tmax vs. Rr – diagram (Figure 4-25). This indicates a mixture of the three types of kerogens, which is confirmed by geochemical biomarker analysis by Butterworth et al. (1999). They indicated a mixed lacustrine / marine environment for the Upper Jurassic.

In the Jurassic section, no maturity trends were recognised. The samples 49732 and 49734 are in between Type II and Type III but are at a depth of approximately 1780 m, a vitrinite

reflectance of 0.70 % Rr and a Tmax of almost 500 °C. Sample 49722 is from a depth of 2430 m and has a vitrinite reflectance of 0.60 % Rr and a Tmax of 431 °C. There is no difference in maturity from the point of vitrinite reflectance, therefore the Jurassic must consist of different types of kerogen, indicated by the difference in the Tmax values.

A clear trend fitting the palaeo geographic framework cannot be seen in Figure 4-26. The kerogen type seems to be independent from lithology and age. Reasons may be the relatively large distance in between the wells of about tens of kilometres and the structure of the basin. Some wells e.g. Chevron 36/6-1 are on the shallow flanks and others e.g. Amoco 35/18-1 in the deeper, more central part of the basin. Therefore the same lithologies undergo different stages of maturity and due to the distance between the wells there may be changes in facies, which, due to the low number of samples of the same stratigraphic unit, cannot be reasonably proven.

General remarks on the type of kerogen can be made about the Jurassic sequence. The absence of a type I influence in the measured samples is limited to the sample selection as no source rocks could be sampled. Literature data from Shannon et al. (1995) and Butterworth et al. (1999) indicate a type I/II mixture for the Jurassic sequences whereby type I is the dominant feature. The Cretaceous and Cenozoic contain type III kerogen. These observations confirm the terrestrial input of organic matter due to erosion in the hinterland and uplift and low sea-level phases.

4.4.2.3 Source rock properties in the Jeanne d'Arc Basin

Numerous literature citations showed that the Hibernia Field oil of the Jeanne d'Arc Basin is sourced solely by the Kimmeridgian Egret member of the Rankin Formation (Arthur et al. 1982, von der Dick 1989, Fowler & Brooks 1990, Williamson 1992, Huang et al. 1994). The Lower to Middle Egret member consists of calcareous shales, which are rich in amorphous, liptinitic oil-prone organic matter. Kerogen mixtures of type II to I have an average TOC of 3-4.5% and HI of 500-600 (Figure 4-27).

Other potential source intervals are the Bathonian – Oxfordian Voyager Formation and the Kimmeridgian – Tithonian Jeanne d'Arc Formation. These formations represents more oxidic depositional environments characterized by a terrigenous-rich marginal facies (Dick et al., 1989). Shannon et al. (1995) document a series of rhythmically laminated Upper Jurassic lacustrine shales, which appear to be very similar to algal lacustrine oil-prone shales of the Porcupine Basin. Microscopic examination of the organic matter of the Egret Member indicates that it is predominately amorphous (lamalginite) throughout the basin. Mature samples are usually heavily bitumen-stained (Fowler, 1995).

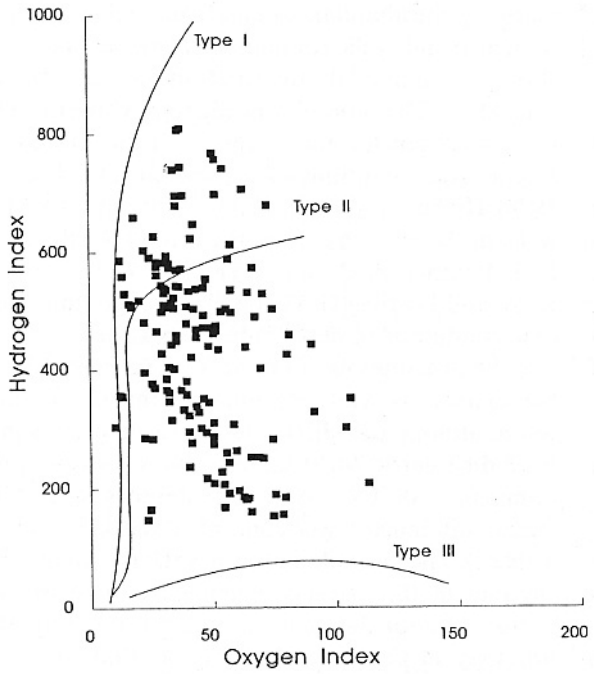

Figure 4-27: Source rock properties of the Egret Member

4.4.2.4 Typical North Sea Jurassic source rock properties

The Jurassic of the North Sea contains the main source rock intervals including the dominant source interval Upper Jurassic - basal Cretaceous Kimmeridge Clay and Borglum-Draupne Formations (UK and Norwegian nomenclature respectively) (Cornford, 1998). The Lower Jurassic, absent in the offshore areas, was deposited in fluvodeltaic environments. It is mainly gas-prone with an average TOC of 2% and a Hydrogen Index up to 500 mg/g TOC for the laminated lithologies (Cornford, 1972; Ebukanson, 1985; Thomas, 1993).

Middle Jurassic source rock deposition is limited (Ziegler, 1982). Oil-prone, algal-rich deltaic shales and coals are only found in the Inner Moray Firth Basin (Mckenzie and Quigley, 1988), the Yorkshire-Sole Pit Trough area (Hancock and Fisher, 1981), the Moray Firth Basin (e.g. Maher, 1981) the Viking Graben (Eynon, 1981) and the Horda, Egersund and North Danish basins (Koch, 1983). Coals are shown as minor components in theses sequences (Parry et al., 1981). The Middle Jurassic shales commonly have TOC values as high as 5% whereas in the coal-measure sequences the TOC values fluctuate considerably.

The Upper Jurassic contains the dominant oil (and associated condensate and gas) source rock of the North Sea, found in the Kimmeridge Clay, Borglum and Draupne Formation. The regional distribution of Upper Jurassic source rocks has been reviewed in terms of average TOC values and kerogen type in the context of the paleogeography of the western Tethys by Baudin (1995). The Draupne Formation contains predominantly marine kerogen with relatively elevated sulphur contents (Erdmann, 1999). Stratigraphically, the Kimmeridge Clay

overlies the Oxfordian Heather Formation. The Oxfordian shales are generally reported as fair to rich gas-prone kerogen type II source rocks with TOC values ranging from 2-9% (Cornford, 1998) They are also of marine kerogen type and are characterized by higher amounts oxygen functional groups as the Draupne Formation and a similar alkyl-chainlength distribution (Erdmann, 1999). Erdmann (1999) concluded that the Draupne Formation is a marine kerogen with a strong aliphatic hydrocarbon signature whereas the Heather Formation has a high proportion of aromatic hydrocarbons and phenols due to increased terrigenous organic matter content.

The Kimmeridge clay formation contains the major oil source rocks of the North Sea (Field, 1985). It accumulated in a series of grabens and basins formed during a Kimmeridgian phase of rifting. The Triassic graben system of northwestern Europe was polarised to a few major rifts such as the North Sea Rift, Polish-Danish Troughs, the Porcupine Trough and the Celtic Sea-Bristol Channel and Western Approaches Basins (Ziegler, 1978). The Kimmeridge formation can be subdivided into two sequences of the more organic rich unit “hot shale” and overlaying “cold shale” (Cornford, 1998). The hot shale mudrock facies was characterized by high concentrations of vanadium, uranium and selenium relative to the surrounding sediments. Ramanampisoa and Radke (1995) found organic cycles on a 30 ka scale, with correlations between TOC and “orange structureless kerogen”. Subjected to Rock Eval pyrolysis, the kerogen mixture generally plots as a type II oil-prone kerogen (Barnard et al., 1981). TOC values range from 2-8% and Hydrogen Index up to 600 mg/g TOC. The characteristics of the formation vary considerably but in general, the rocks deposited in the basin centre will tend to contain the best kerogen quality and also be the most deeply buried as subsidence and burial progress to the present day (Cornford, 1995).

4.4.3 Modelling Parameters

The availability of source rock samples was very limited as it was not possible to sample the best source rock facies. Source rock properties from the surrounding rocks were measured and this helped to classify the source rock potential based on sequence stratigraphic concepts as the over- and underlying strata of the source rock were deposited in a sequential order respective to the changes in environments from e.g. a deep basin to a shallow basin with a deltaic sequence (Miall, 1990). Therefore it was possible to narrow down the Jurassic source rock to a mixture of type I and type II kerogen caused by changes in sea level and transition from marine to lacustrine deltaic to environments (Shannon, 1991a). This observation is also confirmed by geochemical biomarker analysis by Butterworth et al. (1999) showing a mixed lacustrine marine environment for the Upper Jurassic. This Upper Jurassic sequence can additionally be compared to the Kimmeridge Clay formation, which is the major oil source rocks of the North Sea (Field, 1985). The kerogen mixture generally plots as a type II oil-prone kerogen (Barnard et al., 1981) with TOC values ranging from 2-8% and Hydrogen Index up to 600 mg/gTOC. Source rock properties of the Egret member from the Jeanne d’Arc basin show similar values. Additionally the analysis of the crude oil composition and biomarkers show evidence of a mixture of type I / II kerogen as origin. Based on the

information gathered from in-house analysis, Porcupine, Jeanne d'Arc and North Sea source rocks the Upper Jurassic strata was defined as the main source rock. The TOC was fixed to 4 % and the Hydrogen Index (HI) to 550 mg/gTOC. Additionally source rock properties were assigned to the Lower Jurassic with TOC values of 1.8 % and a Hydrogen Index of 550 mg/gTOC based on data derived from actual samples out of the Porcupine Basin provided in Croker and Shannon (1987) and Shannon and Naylor (1998).

4.4.3.1 Hydrocarbon Reaction Kinetics

To calculate the generation of hydrocarbon two prerequisites are necessary, the source rock properties as evaluated in the previous section and a mathematical description of the transformation processes, which are described in reaction kinetics. These are approximations derived from pyrolysis experiments as discussed in section 3.1.1. Two different sets of kinetics can be used in the Petromod^{TM} programme: bulk kinetics and compositional kinetics. Bulk kinetics constrain all data to a single set of kinetic parameters whereas compositional kinetic data provides detailed kinetic parameters and hydrocarbon yields for each of these fractions based on the decomposition of kerogen into specific chemical moieties.

In the case of the Porcupine Basin no kinetic data sets describing the conversion of kerogen to hydrocarbons have been published. In the tectonic analogue Jeannne d'Arc Basin M. Fowler (per. comm.) determined kinetic data for the Egret Member, which could not be used within the Petromod^{TM} Input module due to incomplete and inconsistent data.

In addition no source rock samples were available for this study as described in section 4.4.2. As a conclusion no kinetic data set could be measured. Therefore kinetic data was derived from asphaltenes from crude oil samples DST-1 and DST-2 from well 26/28-1 and provided a first bulk kinetic data set. Asphaltenes can be used instead of source rock material as they bear close structural similarities to their precursor kerogens (section 3.1.1). The kinetic data set derived from the asphaltenes was compared and combined with published kinetic data sets from oils worldwide. The published kinetic data sets used are those of Pepper and Corvi (1995) and those of (di Primio et al., 2002) labelled RdPII & RdPIII, which were developed for typical North Sea Oils.

4.4.3.2 Asphaltene kinetics

As previously discussed (section 3.1.1), in the absence of source rock samples, asphaltenes derived from oil samples can be used instead for the determination of kinetic parameter. Two of the five Jurassic oils taken on wells in the Connemara oil field were selected for asphaltene kinetics analysis. The original FID-traces are plotted in Figure 4-28. The measured and fitted curves by the program Kinetics2000 are shown in Figure 4-29.

Sample	Well	DST	Depth [m]
E49851	26/28-1	DST1-1563	2328-2329.5
E49854	26/28-2	DST2-1552	2245-2268

Table 4-6: Oil samples used for determination of asphaltene-kinetics

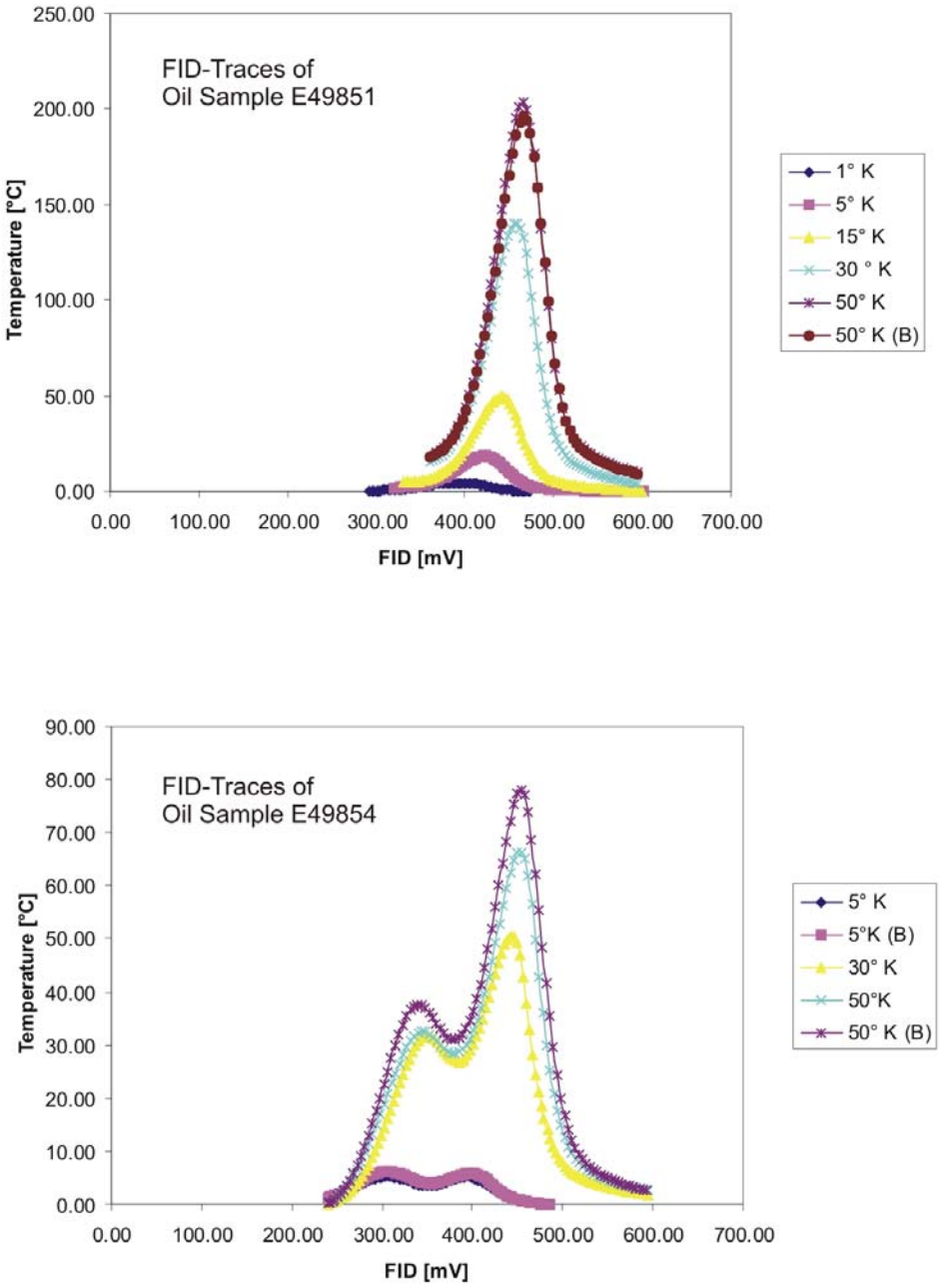

Figure 4-28: Original FID-traces

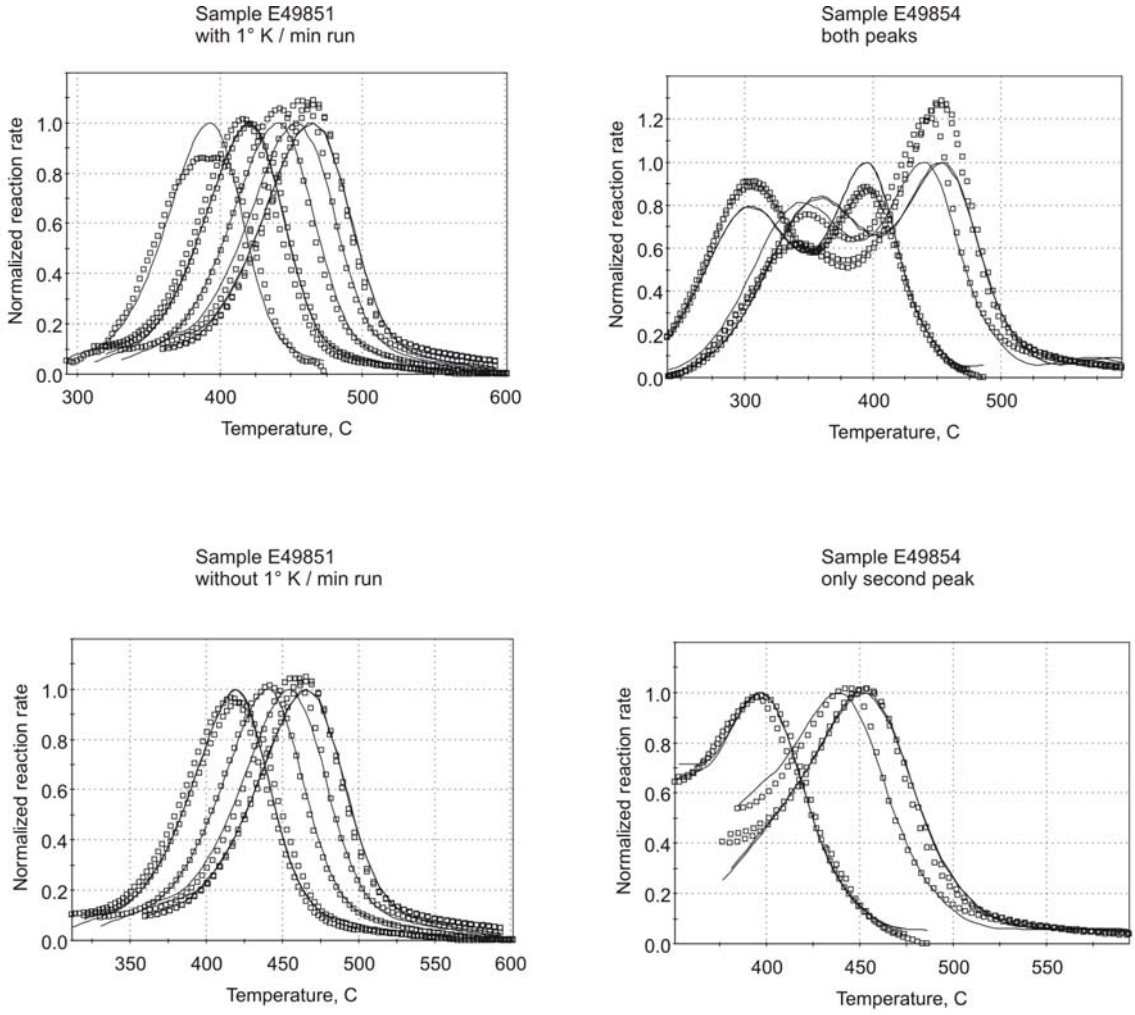

Figure 4-29: Fitted asphaltene kinetics

Figure 4-28 and Figure 4-29 show clearly that there is an unnatural bimodal distribution for sample E49854 giving no usable results for the calculation of the kinetic results. Figure 4-29 also shows the calculated kinetic parameters in- and excluding the 1°K/min run. For further calculation the kinetic parameters from oil E49857 including the 1°K/min run were used. The activation energy distribution and frequency factor of Oil E49851 fit the generally observed range of kinetics of asphaltenes and marine source rocks.

Sample E49854 showed a bimodal activation energy distribution indicating the likelihood of resin contamination of the asphaltene fraction (Figure 4-31). For further use only the kinetics of oil E49851 were used.

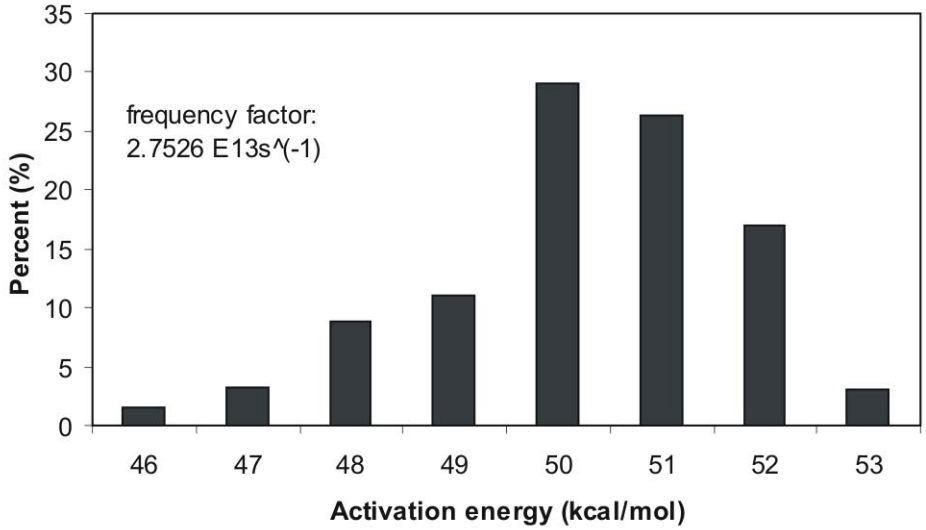

Figure 4-30: Distribution of asphaltene fraction for sample E49851

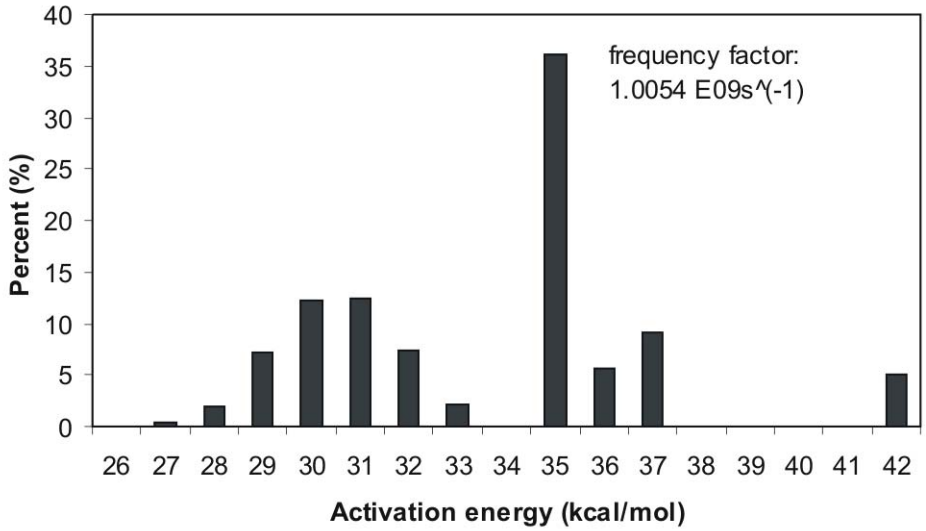

Figure 4-31: Distribution of asphaltene fraction for sample E49854

As discussed in di Primio et al (2000), asphaltene kinetics seem to be representative for the maturity interval in which the oil from which the asphaltenes were taken, was generated. Given a calibrated temperature history, asphaltene kinetics can be used to determine the temperature at which the oil was generated and expelled, but it is still unclear whether asphaltenes contain the entire description of kerogen degradation. Therefore a kinetic data set consisting of at least an oil and gas compound are needed.

4.4.3.3 Compositional kinetics

Compositional kinetic data as described in section 3.1.1, provides detailed kinetic parameters and hydrocarbon yields for each fraction. Accordingly, in view of the fact that a compositional description of the products generated was necessary for the detailed migration modelling (including phase behaviour) compositional kinetics from Pepper & Corvi (1995) were used as a first approximation for oil and gas generation modelling. These kinetics divide the kerogen into five global organofacies: A: aquatic marine, siliceous or carbonate/evaporate; B: aquatic marine, siliciclastic; C: aquatic, non-marine, lacustrine; D: terrigenous, non-marine, waxy, resins; E: terrigenous, non-marine, waxy; F: terrigneous, non-marine, wax-poor. Based on the classification of the kerogen types in the Porcupine Basin discussed earlier the type B kerogen properties can be used for the Jurassic source rocks and type F kerogen kinetics for the Cenozoic coal beds. The kinetic properties for oil and gas generation are displayed in Figure 4-32. However, this compositional kinetic data set uses only two components, a gas and an oil component to calculate hydrocarbon generation.

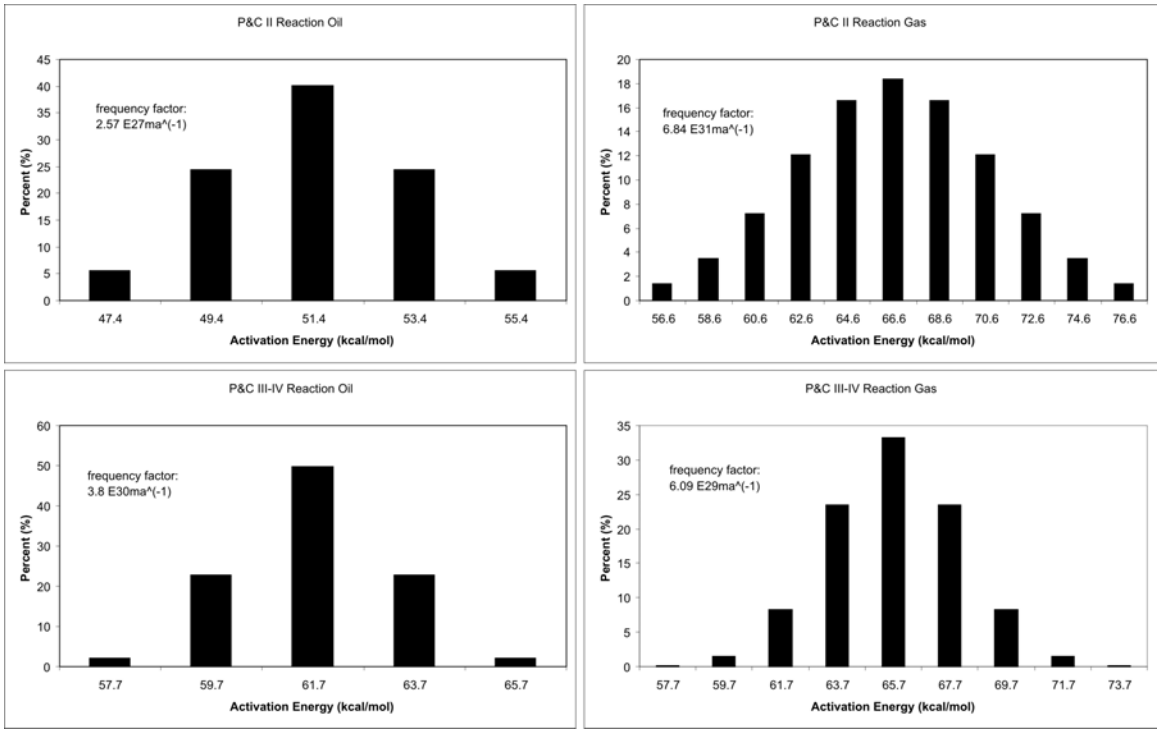

Figure 4-32: Kinetic data set for oil and gas of kerogen type II and III-IV (Pepper and Dodd, 1995)

As discussed previously, the correct simulation of hydrocarbon migration requires a correct description of hydrocarbon phase behaviour. The compositional models of di Primio et al. (2002) represent tuned kinetic data sets (tuned to natural fluid properties from the North Sea), which are the first of their kind to allow the correct simulation of petroleum phase behaviour during migration, applying equation of state (EOS) based algorithms available in

the basin modelling software used. The type II and III compositional kinetics used are shown in Figure 4-33.

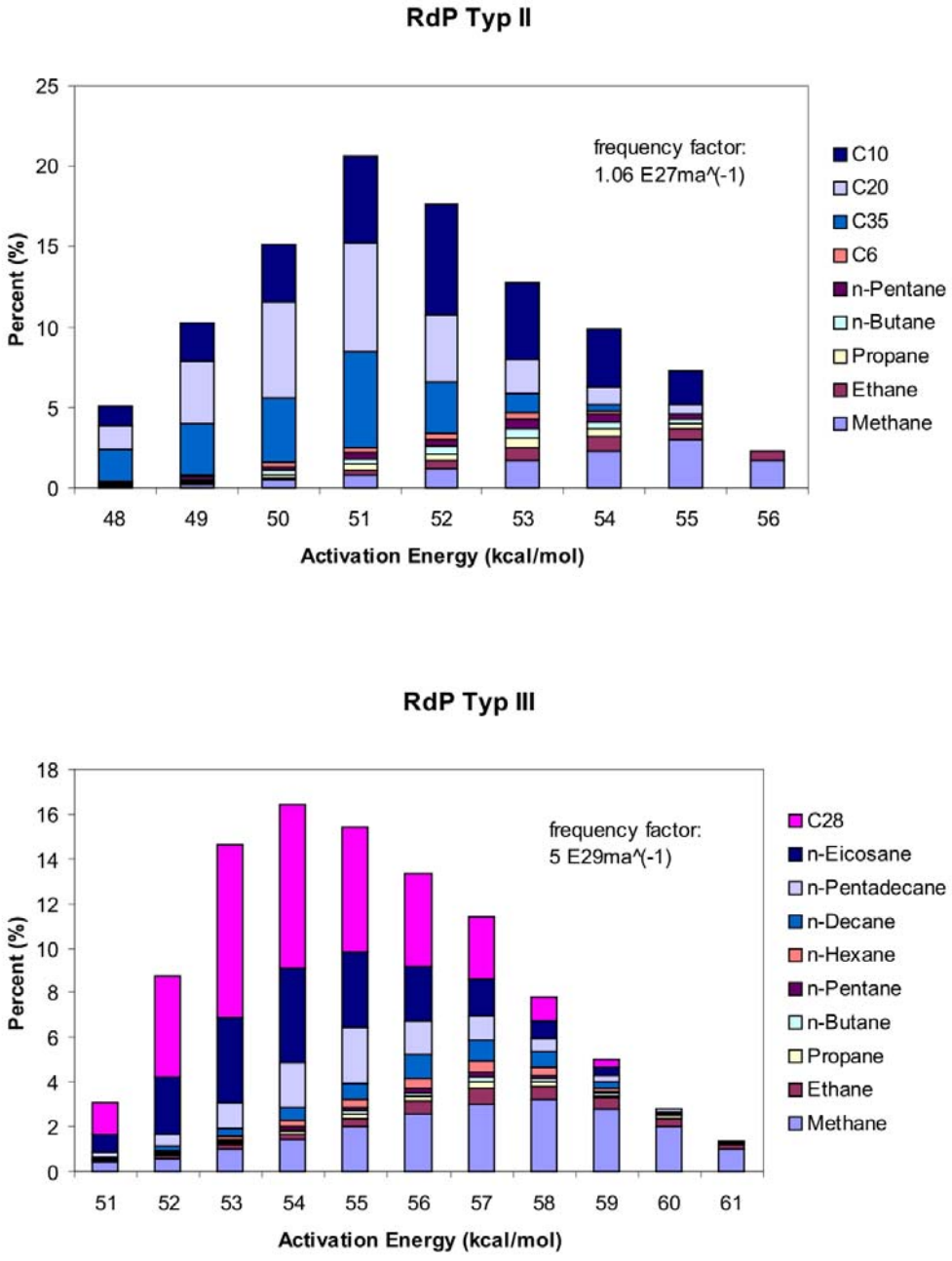

Figure 4-33: Kinetic data for the RdP kinetics

In-source secondary cracking was taken into account using the secondary gas kinetics of Dieckmann et al. (1998). Cracking of oil to gas can take place as the petroleum system evolves, either during late generation in the source rock or in the reservoir (Blanc and Connan, 1994). Closed-system pyrolysis and kinetic modeling by Horsfield et al. (1991) showed that the onset of in-reservoir gas generation from an oil acquired from the Norwegian

North Sea Central Graben might occur between 170°C and 190°C, which is about 20°C – 30°C higher than oil to gas cracking in the source rock. Schenk et al. (1997a) confirmed that oil to gas cracking is very unlikely to take place at temperatures less than 160°C independent from the crude oil type or the geological heating conditions. Dieckmann et al. (1998) showed that oil to gas cracking in-source occurs at about 1.2%Rr vitrinite reflectance and that predicted temperature ranges of secondary oil to gas cracking are around 30°C lower than those derived from isothermal and non-isothermal pyrolysis of produced oils, which demonstrates obviously a fundamental difference between in-source and in-reservoir secondary cracking. This might be due, among others, to the catalytic activities of kerogen residues in source rocks (Dieckmann et al., 1998). Comparing open and closed-system pyrolysis provides strong evidence that in the case of marine source rocks the overlap between primary oil generating and secondary oil cracking reactions is negligible as secondary oil generation starts essentially after the former have come to an end (Dieckmann et al., 1998). Simple stoichiometric relationships were used for cumulative MSSV evolution of liquid and gaseous compounds. This kinetic model of secondary cracking was applied exclusively to the liquid phase compounds assuming that for reasons of hydrogen balance only 70% of cracked C_{6+} compounds are converted into gas and 30% into pyrobitumen. The compound generated by secondary cracking was methane. In Petromod™, which uses the same kinetics for in-source and in-reservoir cracking, residual hydrocarbon saturation remaining behind in a source rock is fixed to a value of 5% of the litholigies porosity. Accordingly cracking of this residual provides only minor proportions of additional gas.

Figure 4-34 shows the transformation ratio for the Jurassic source rock sequence of profile MS81RE-94. Whatever the assumed sample is, 100% conversion of kerogen is predicted for Jurassic material buried below 4000 m and a partial conversion for material above 4000 m. Even in the shallowest parts of the basin, Jurassic kerogen produced at minimum 30% hydrocarbons. Generation of hydrocarbons started in Mid-Cretaceous times for the Jurassic sequences shown in Figure 4-34, and is related to the high heat flow occurring during the rifting event. Generation continues up to present day with the exception of periods of uplift in the Late Cretaceous and Miocene. Generation rates increased in the Oligocene and Miocene due to faster subsidence. The main transformation processes for Jurassic source rocks are finished before 45 ma according to the kerogen type II kinetics of Pepper and Corvi (1995), whereas a kerogen type III kinetic model (Pepper and Corvi, 1995) is still sensitive to subsidence in the last 45 ma. As the Cretaceous only contains low amounts of organic matter only negligible amounts of early hydrocarbons can be expected for the deeper buried parts. Variations in the evolution of hydrocarbon generation for the different kinetic datasets used reflect differences in the organic matter used for kinetic analysis.

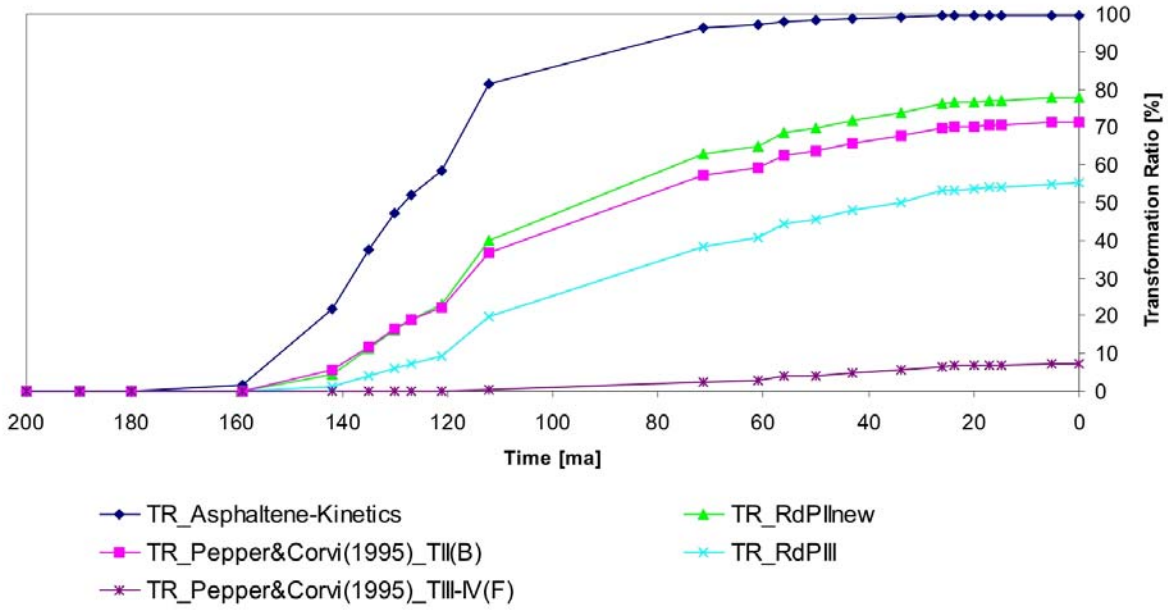

Figure 4-34: Transformation ratios of used kinetics for the Upper Jurassic source rock for the central part of the Porcupine Basin, profile MS81RE-94

The close match of predictions concerning onset of hydrocarbon generation from the asphaltene and compositional kinetic models was taken as an indication that the compositional kinetic schemes behaved similar and hence were the preferred kinetic dataset for the purposes of this study. Since the RdP kinetics predicted nearly identical conversion, timing and rates as the corresponding Pepper and Corvi kinetics, and as the RdP kinetics allowed a better compositional resolution for phase behaviour modelling these were selected for further hydrocarbon generation and migration modelling. The transformation ratios for the single compounds are plotted with regard to the vitrinite reflectance in Figure 4-35.

Figure 4-35 is taken from the Upper Jurassic source rock on the profile CS-2 from the Connemara area. The source rock is, with a calculated present day vitrinite reflectance of 1.2, still in the gas window. During the Middle to Late Jurassic the source rock reached the oil window and the kerogen started to expel hydrocarbons corresponding predominantly to the liquid phase namely C_6, C_{10+}, C_{20+} and C_{35+}, which show almost total conversion at present day. The transformation of methane and ethane look similar to the other ones and follow the scheme as stated for the total transformation ratios influenced by the various heat flow pulses as explained for Figure 4-34. However, these compounds reach a transformation ratio of about 70% as the kerogen is just at the beginning of the gas window based on the calculated vitrinite reflectance.

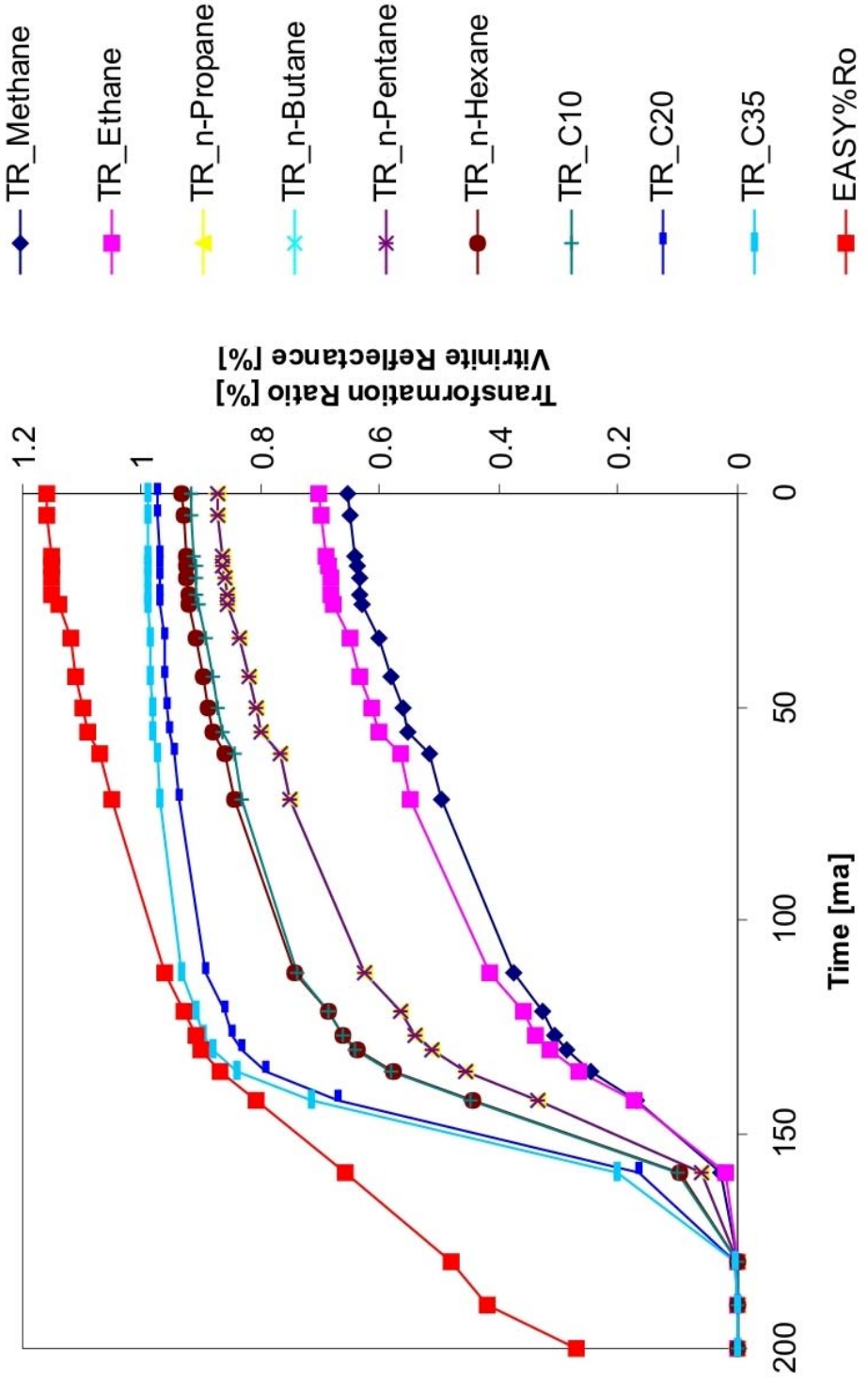

Figure 4-35: Transformation ratios of single compounds of the RdPII kinetic and calculated vitrinite reflectance for the Upper Jurassic source rock in vicinity of the Connemara area calculated of line CS-2

4.5 Migration

For the three regional seismic lines (RE94, RE88 and RE25) (Figure 4-36, Figure 4-37, Figure 4-38) modelled hydrocarbon flow was simulated across the basin in the time steps 205, 180, 142, 121, 112, 71.3, 60.9, 56, 54.8, 43, 33.7, 23.8, 5.3 ma and present day. The modelled migration shows essentially buoyancy-driven migration pathways over the entire basin.

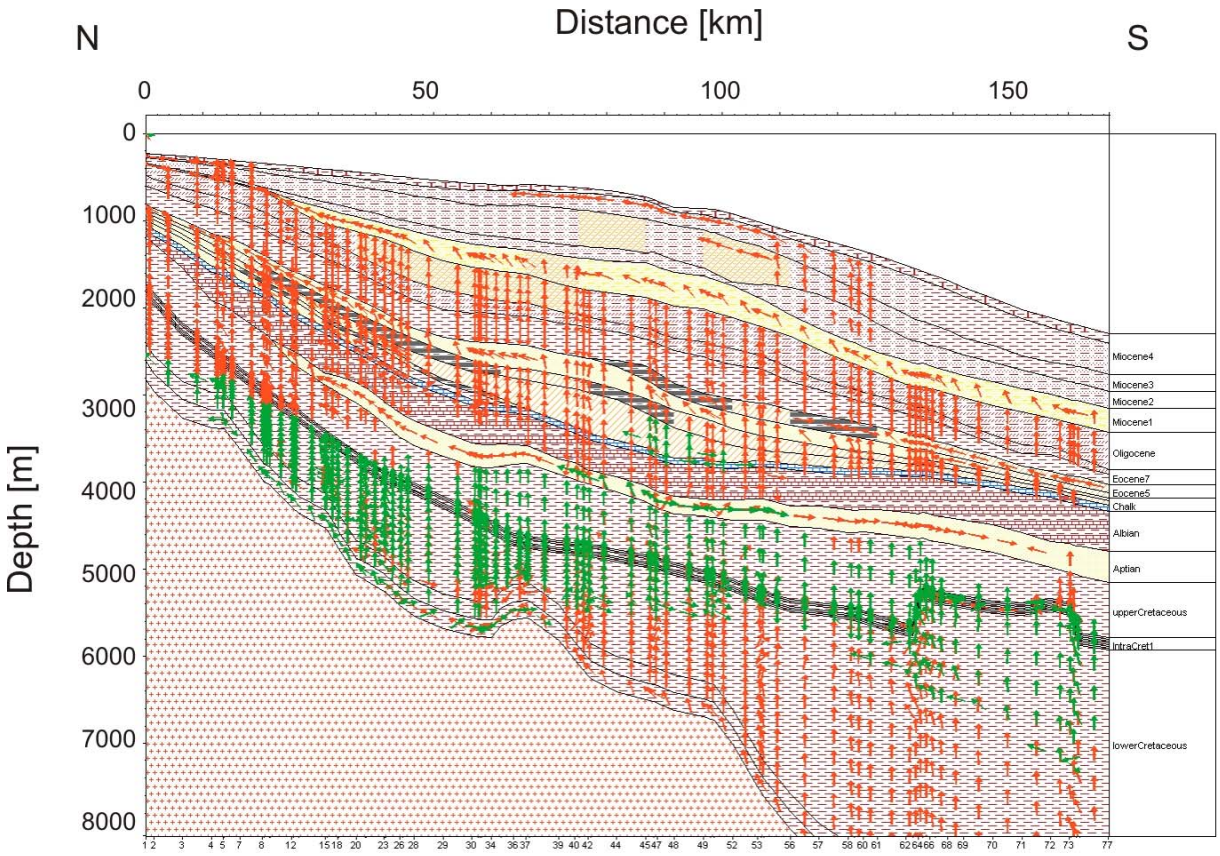

Figure 4-36: Present day configuration of modelled gas (red vectors) and oil (green vectors) flow along profile RE94

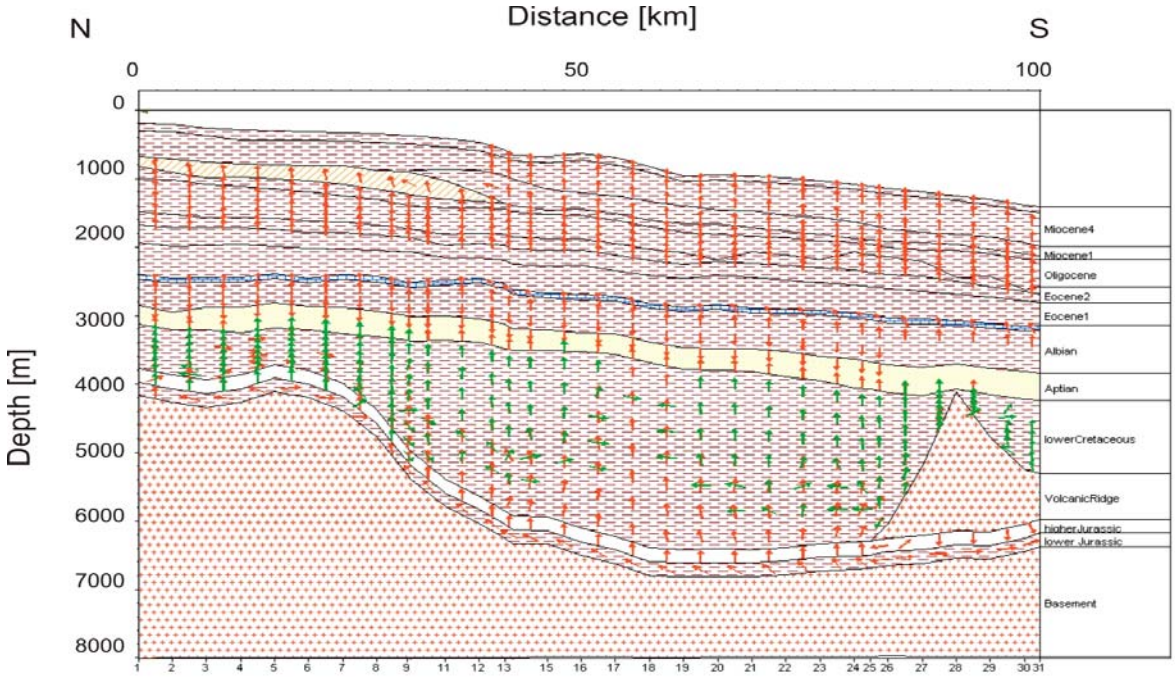

Figure 4-37: Present day configuration of modelled gas (red vectors) and oil (green vectors) flow along profile RE88

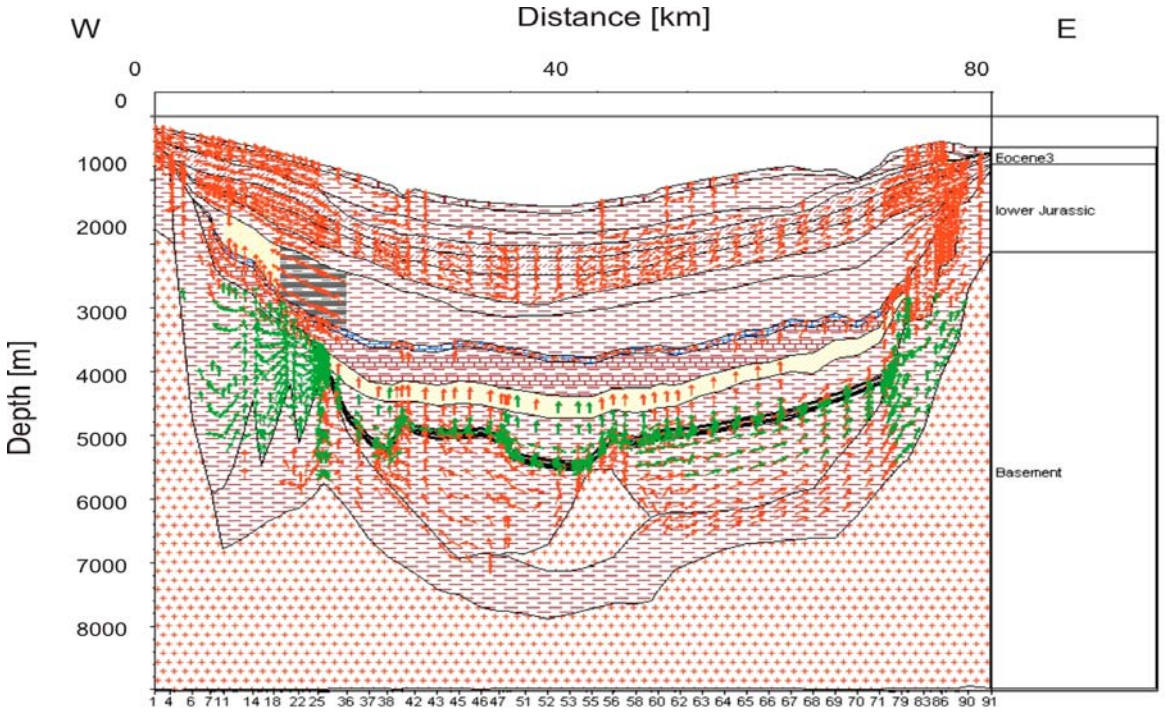

Figure 4-38: Present day configuration of modelled gas (red vectors) and oil (green vectors) flow along profile RE25

When Jurassic organic matter enters the oil window during the Mid-Cretaceous, migration of hydrocarbons starts. In the central part of the basin early-generated Jurassic gas of negligible volumetric amounts (section 4.4.3.3) migrates mainly vertically through to the surface whereas towards the end of the Cretaceous this area generates liquid hydrocarbons, which also start to migrate vertically. This scheme continues through Aptian and Albian times. Phase separation, predicted by the use of compositional kinetics, is observed in the depth of 2000 - 4000 m sub seafloor over the entire basin (Figure 4-39, Figure 4-40, Figure 4-41). During Albian times oil and gas accumulates in the Aptian sandy layer, which is sealed by the Late Cretaceous marl. Some hydrocarbons are modelled to remain in the Albian sandy layer up to present day. Other hydrocarbons migrate through the marl at locations where the hydrocarbon column height leads to capillary failure of the cap rock or where changes in the paleogeometry, controlled by the loading by the Eocene delta, resulting in the Miocene sandy sequences forming major migration pathways. If the Albian sandy layer is continuous throughout the basin it seems to be the main migration pathway due to its relatively high permeability (about 3 D) and porosity (about 17%) (data derived from modelling results at 3000 mbsf on profile PORC97-12).

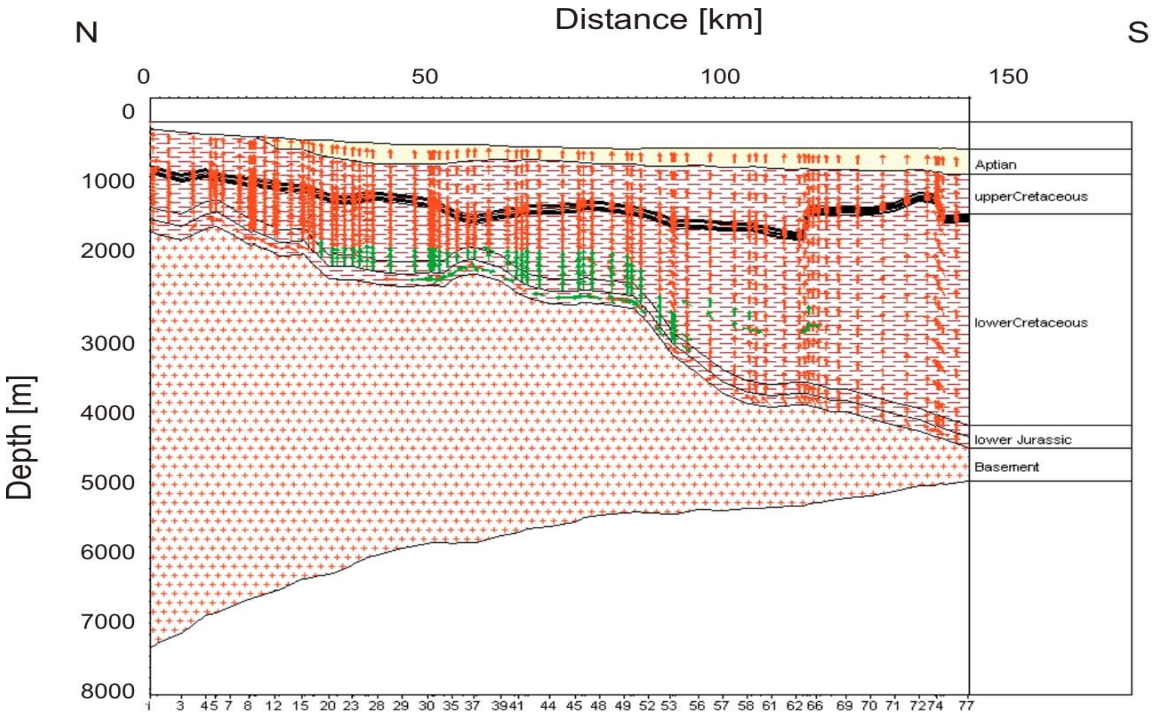

Figure 4-39: Aptian configuration of modelled gas and oil flow along profile RE94

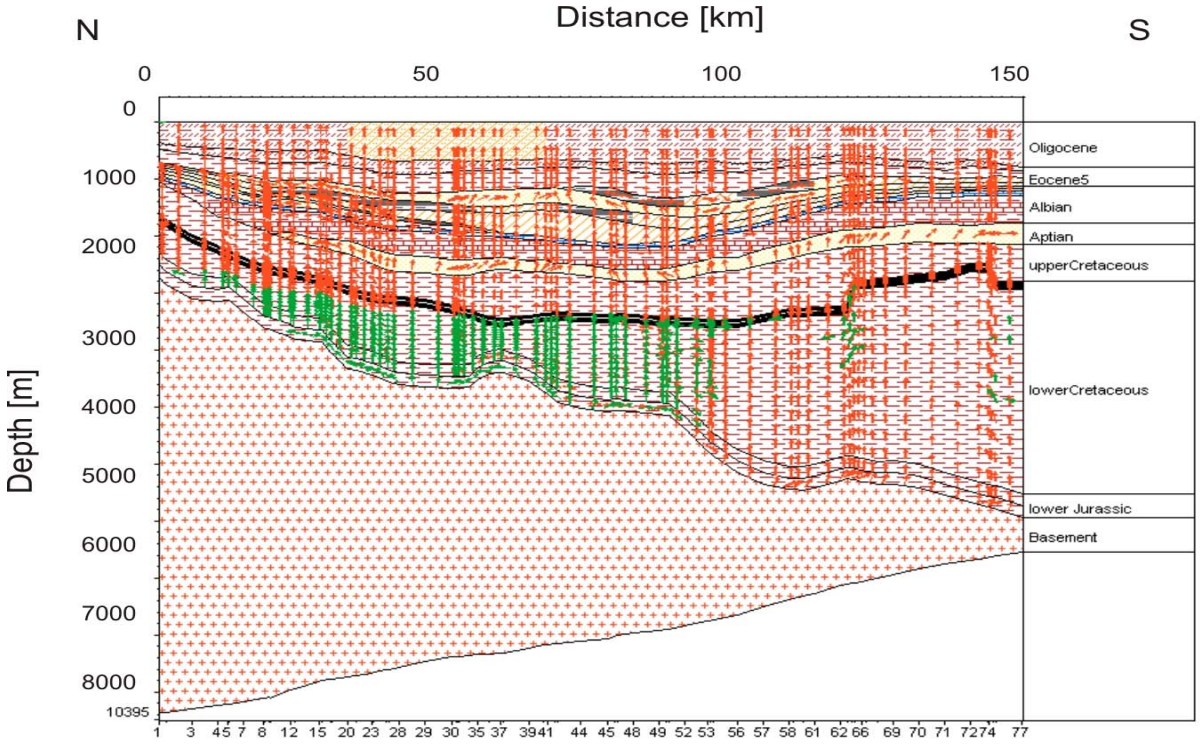

Figure 4-40: Oligocene configuration of modelled gas and oil flow along profile RE94

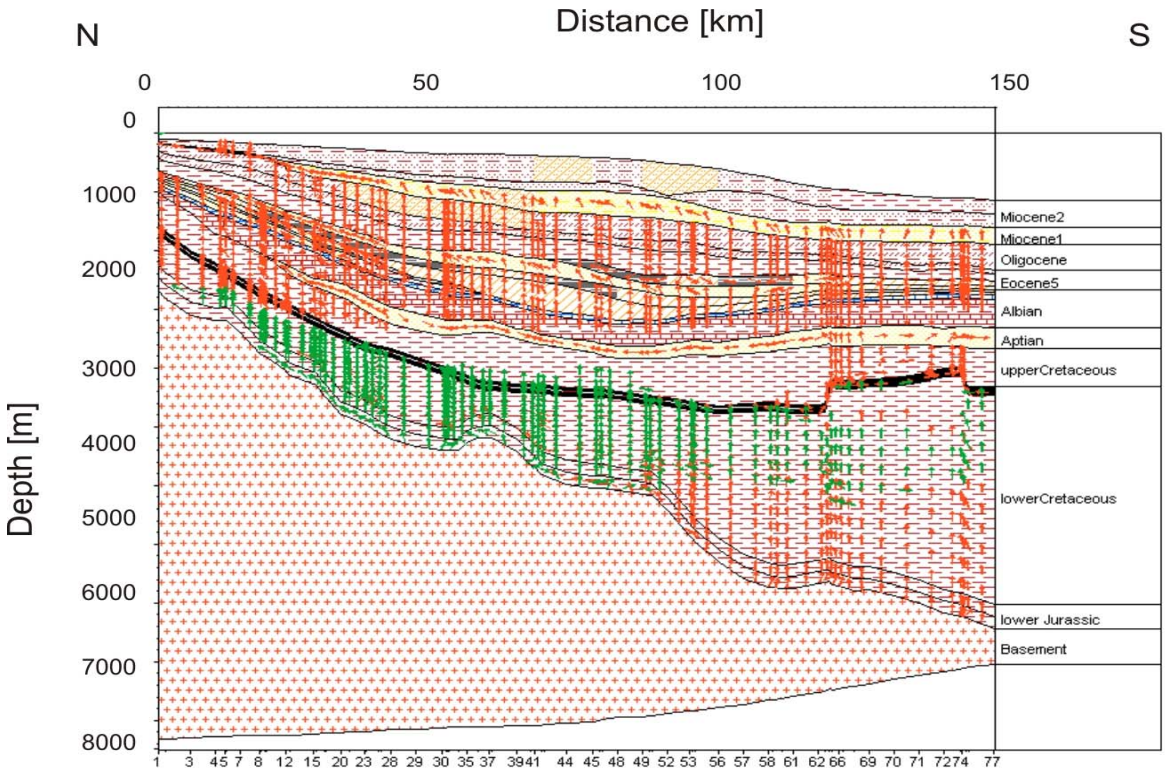

Figure 4-41: Miocene configuration of modelled gas and oil flow along profile RE94

During the Eocene migration was more active in the northern part of the basin due to the additional loading and enhanced generation following burial under the prograding delta front. Migration remained mainly vertical except for movement along the Albian and Miocene layers. The end of the Eocene was marked by an aggressive marine erosion due to the onset of marine currents associated with a major change in regional basin morphology followed by renewed subsidence during Oligocene times, but migration follows the same general pattern.

Igneous intrusions of earliest and latest Cretaceous to Paleocene and Eocene age in Cretaceous units locally generated some hydrocarbons, which migrated into the Albian layer and from there into traps or laterally out of the model. Later in the Miocene migration still remained vertical with some focussing of hydrocarbon flow through Miocene slump structures and polygonal faulted sediments (see detailed discussion below). Late Miocene and Early Pliocene sedimentation was marked by strong subsidence in the southern part of the basin, concentrating generation and migration of hydrocarbons into that area with again mainly vertical migration.

The properties of the Cenozoic faults were modelled as permeable and impermeable for fluid flow in sensitivity runs but have no distinct effect on the migration pattern in the Cenozoic sediments. Migration patterns in the high-resolution lines modelled are discussed in the following sections.

4.5.1 Line PORC97-12

Detailed stratigraphic information was derived from the seismic interpretation of line PORC97-12. The line terminates in the basin centre and displays the geological setting at and below the Belgica mound province. The presence and visibility of mound SP46 on the seismics is of obvious advantage in the attempt to reconstruct hydrocarbon migration pathways and check for a link between surface leakage and mound occurrence as it gives a good chance of modelling migration processes from the kitchen area to the mounds. Paleo water depth maps and the heat flow history were assigned using the reconstructed burial and thermal histories. Figure 4-42 shows the model using the conceptual model input parameters and migration results. Vectors for oil migration are shown in green, vectors representing gas migration are marked red.

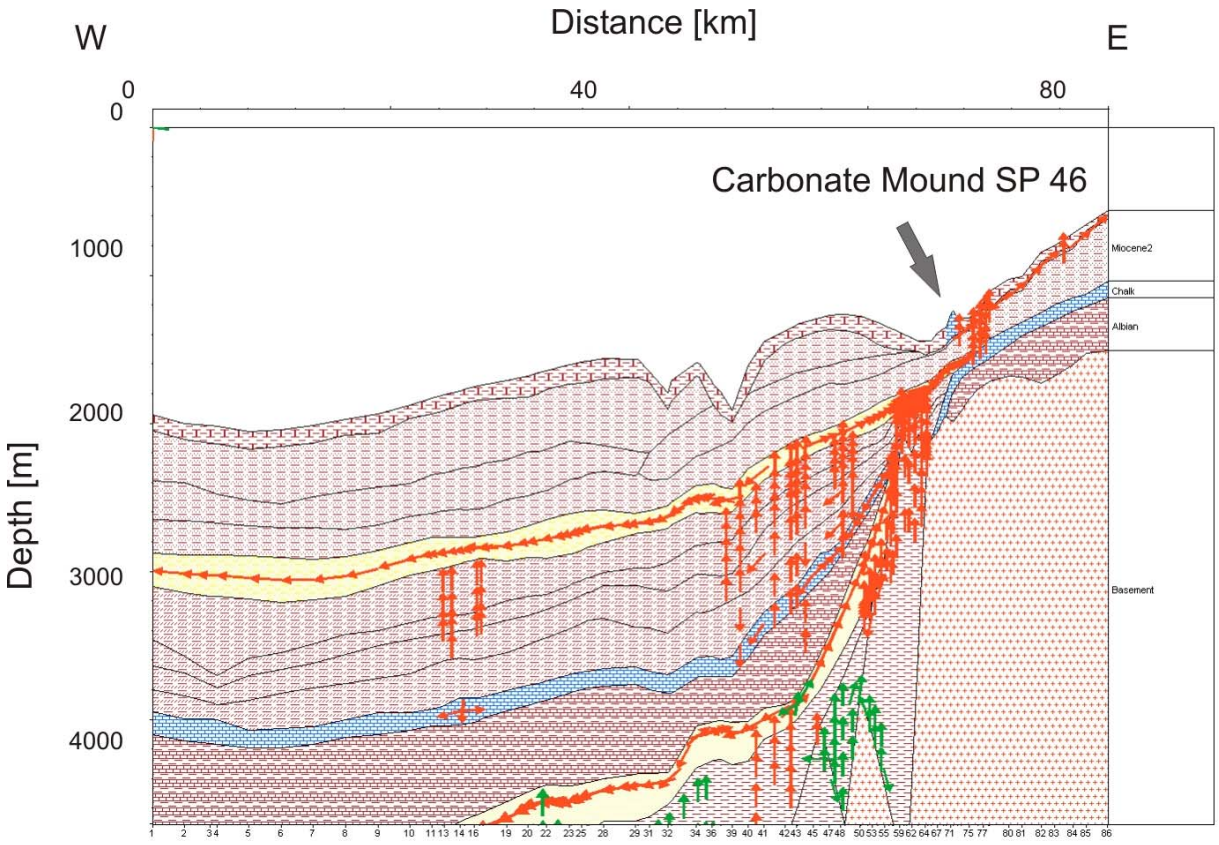

Figure 4-42: Modelled gas (red vectors) and oil (green vectors) migration along Aptian and Miocene sand layers (yellow) on profile PORC97-12 towards the carbonate mound SP46

Modelling of the migration processes was based on the compositional kinetic predictions. Hydrocarbon generation started in Early Cretaceous from the Upper Jurassic source rock, which is overmature in the centre of the basin at the present day. Migration towards the eastern flank of the basin started in the Early Cretaceous. Shaly and muddy sequences seal the Aptian sandy layers, which act as a high permeable migration pathway. These Aptian sand layers pinch out on the basement on the eastern flank and could form a stratigraphic trap. The Late Cretaceous is marked by the deposition of chalk with a more or less constant thickness. Cenozoic sequences consist mainly of muddy lithologies with a decreasing thickness towards the eastern flank. The influence of the Paleocene Iceland Plume and alpine orogenesis led to basin uplift and to the deposition of the Miocene marine sand from the shoreline above the basement high on the eastern flank to the basin centre. Following thermal decay rapid subsidence dominated and deep marine environments evolved, characterised by the deposition of shaly, silty sequences. These lithologies have not been confirmed by drilling and are assigned according to the conceptual model, observation of well data and the general scheme of deposition in the Atlantic ocean described by Cornford (1998).

However, the Aptian facies is deposited under marine shelf conditions with deltaic facies along the northern and southeastern margin of the basin including occasional deep marine turbidites, clastic fans and fault scarps (Croker and Shannon, 1987; Croker and Shannon, 1995; Moore and Shannon, 1991; Moore and Shannon, 1992; Shannon, 1993). Therefore the assumption of a high permeable layer in the Aptian seems reasonable but is not confirmed, as no wells are located in this vicinity.

Description of the Miocene sediments is based on Shannon (1992) who describes deep marine and also deltaic and fan deposits in the Early Cenozoic sequences. From the Miocene onwards, sedimentation was dominated by drift deposition in which slumping occurred (Huvenne et al., 2002). These drift deposits and even more the deltaic sequences can also be associated with high permeable layers, e.g. clastic channel fill sediments (Moore and Shannon, 1991). Therefore the occurrence of a high permeable Miocene layer is justified.

This network of Aptian deltaic layers and fan type sediments as well as the Miocene channel fill sediments are able to focus hydrocarbon flow towards the mound but detailed seismic interpretation has to be done on these stratigraphic units. As an example (Garland et al., 1999) described the reservoir heterogeneity in the sand-rich submarine fan in the Miller Field, which is located in the Viking Graben (Figure 4-43). The Miller fan is a sandy submarine fan system of Kimmeridgian age consisting of lobe abandonment facies and numerous thin shales. Fluid flow in the environment is influenced by the different lithologies and compaction rates based on the deposition of the turbidites and the locations of the lobe core vs. lobe fringe. Even very thin shales were shown to have a great importance to fluid flow. But these features are of meter – tens of meter scale and difficult to interpret on the seismics.

In the Porcupine Basin the Miocene and Aptian sequences also contain turbidites and deltaic structures of meters in dimension, which are of importance for fluid flow analysis. The seismic resolution of the section is similar to that in the Miller fan and therefore exact predictions of the pathways are not possible. In the Belgica mound area the focus of flow is obviously based on and influenced by the structural pinch outs of carrier layers. But predictions for the Hovland-Magellan mound area based on the available seismics show only a broad pattern of focused fluid flow towards the mound area, a detailed 3D seismic investigation would provide more detail on needed structures as channels and deltaic features.

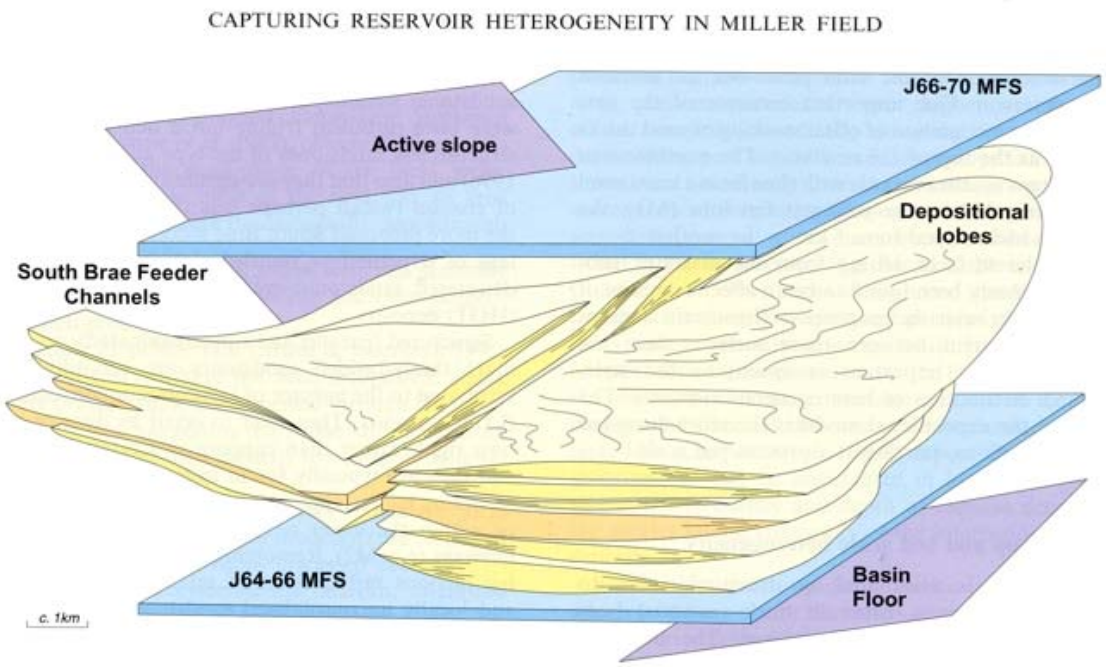

Figure 4-43: Miller fan schematic architecture (Garland et al. 1999)

The petroleum composition predicted by the compositional kinetics used is characterised by high gas contents due to the relatively elevated maturity of the source rocks. Such gas-rich fluids quickly become saturated during upward migration and separate into oil and gas. In the modelling software used the phase behaviour of the fluids is calculated using an equation of state. The predicted volumetrics and physical properties of the coexisting hydrocarbon phases are such that, under the conditions modelled, gas migrates preferentially as compared to oil. The difference in migration rates and fluid mobility between oil and gas increases with decreasing pressure. In the upper 2000 meters of the sedimentary section studied gas migration is the dominant process. Migration pathways are, as shown before, the Aptian and Miocene sand layers. Hydrocarbons are trapped in the pinch out of the Albian sand layer on the eastern basement high. Low capillary entry pressures of the thin Late Albian shales, Late Cretaceous chalks and weakly consolidated Cenozoic mudstones direct hydrocarbon flow into the Miocene sand layer. A reactivation of the Jurassic rotated block bounding faults during the Early Cenozoic might also open migration conduits, but are not necessary to model the leakage into the Miocene sand layer.

As no well control was available in the Belgica region it was impossible to check the model parameters (lithologies, stratigraphy, etc.) as well as its predictions regarding sediment porosities, permeabilities or capillary entry pressures. Accordingly the results concerning focussing of hydrocarbon leakage remain questionable. The main uncertainties are the sediment properties, as the permeability contrast between carrier and cap rock is the main controlling element for hydrocarbon leakage. Therefore, in order to test our predictions in the

Belgica area, the Connemara study area, which contains good well control and known gas leakage, was used as a test case.

4.5.2 Connemara Line CS2

4.5.2.1 Migration Pathways and Seepage Phenomena

Connemara line CS2 runs across well 26/28-1 and shows evidence of gas chimneys and pockmarks on the seafloor. The presence of an active petroleum system is confirmed by the discovery well 26/28-1.

The basin geometry in the Connemara area is controlled by the structural high consisting of rotated Jurassic fault blocks and older sequences. The sedimentary sequence in well 26/28-1 starts with sediments of Devonian age overlain by Carboniferous coaly sequences. An unconformity follows with sedimentation starting again in the middle Jurassic and continuing to present. The Albian sand layer has a maximum thickness of about 200 m at the basin centre. This sequence is overlain by thin shales of about 50 m thickness at maximum, the Late Cretaceous chalk deposits and Cenozoic shaly and sandy sequences. The geometry is controlled by the tilted Jurassic fault blocks. Sediments in well 26/28-1 show evidence of sediments up to Devonian age overlain by Carboniferous coaly sequences and sedimentation again starting in the middle Jurassic.

The geometrical configuration, burial and thermal histories were adjusted to the setup used in the regional lines studied. Hydrocarbon generation and migration was predicted using compositional kinetics. The Jurassic source rocks remain immature in this cross section due to shallow burial. But, as observed in the results from lines RE94, RE25, RE88 and PORC97-12, the hydrocarbon kitchen is located further towards the basin centre which is outside of line CS2. To analyse the hydrocarbon flowpaths the presence of hydrocarbons is required. Therefore, Jurassic source properties were also assigned hypothetically to the deeper Carboniferous sequences which leads to an adequate generation of hydrocarbons. The modelled petroleum composition is based on the RDPII compositional kinetics. Fluids generated by the source rocks migrate vertically into the Jurassic carrier beds and then laterally until they reach the structurally highest position (Figure 4-44). These Jurassic sandstones are sealed by overlying Cretaceous sediments and by juxtaposition across rift-related faults, therefore hydrocarbons accumulate in the fault-bound structures of the Jurassic-Cretaceous rotated blocks. One of these structural traps was drilled in well 26/28-1 and the coincidence of predicted and discovered hydrocarbons supports the modelling parameters used. When the hydrocarbon column in the accumulations exceeds the capillary entry pressure of the cap rock lithologies leakage occurs. In the younger sequences the main migrating fluid is gas. The location of the main leakage sites directly above the structural closures in the model fits the location of the observed gas chimneys. Modelled seepage through to the seafloor also indicate an appropriate amount of gas is generated to lead to pockmarks (Figure 4-44).

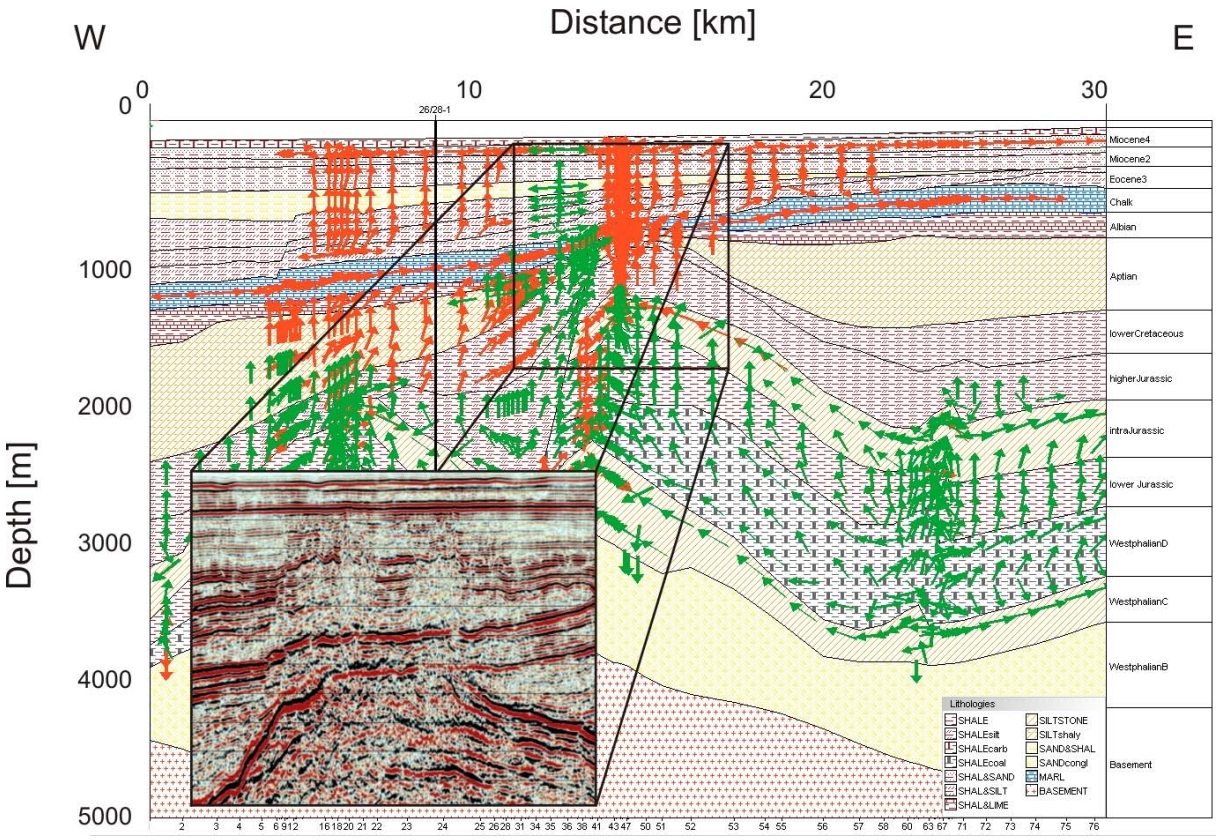

Figure 4-44: Profile CS2 through the Connemara field showing well 26/28-1 and modelled gas (red vectors) and oil (green vectors) flow as well as the gas chimneys and pockmarks observed in the seismics

The properties of the boundary faults were modelled as open (permeable) and closed (impermeable) faults in sensitivity runs. The fault properties have no effect on the migration pattern itself; only the volumes of migrating hydrocarbons are slightly different. Therefore, the capillary failure of the cap rock is considered as the main controlling factor for hydrocarbon migration in the Porcupine Basin.

Regarding the compositional predictions of the kinetic models used (RDPII and III), the Connemara section is an ideal location for also assessing their value. Predicted compositions of accumulations can be compared to the earlier described physical oil samples. Measured API gravities between 30-36° and a methane content of below 18%for the Connemara field indicate a black oil (section 4.4.1), which is predicted by the model with an API gravity of 35°. Based upon available seismic, well information, estimation of reservoir size and the volume of oil discovered in well 26/28-1 MacDonald et al. (1987) determined 195 million barrels of light, paraffinic, waxy oil low in sulphur content in place plus additional 40 – 80 MMBO estimated by Scotchman (2001).

As the modelled distributions of hydrocarbon accumulations and gas chimneys fit the present-day observations we can assume that the used lithologic descriptions and compaction behaviour correctly reproduces the natural system, and that extrapolations of the

same lithologic properties to shallower settings such as the Belgica region is reasonable. Therefore, the modelled migration pathways for the line PORC97-12 in the Belgica mound province are assumed to describe the natural processes effectively.

4.5.2.2 Testing Migration Models

For the analysis of migration in the Porcupine Basin the migration calculation method is an important point to discuss. Migration calculations in the PetroMod^{TM} simulation module are possible as pure Darcy flow, flowpath or ray tracing, Invasion percolation modelling and by hybrid methods (Hantschel et al., 2000). In contrast to the Darcy flow concept, flowpath or ray tracing models use well defined carrier systems. The hybrid method uses a link from Darcy Flow to flowpath modelling. Compared to Darcy flow, the hybrid method shows a more realistically migration history based on fast calculations of flow processes in efficient carriers without losing the dynamic framework. Comparison of results from pure Darcy and hybrid methods in the Porcupine Basin shows that the migration patterns within the Aptian and Miocene sand layers are different depending on the chosen method.

Figure 4-45 shows the profile CS2 through the Connemara field. The blue overlay shows the saturation of lithologies with gas, vectors in green represent oil and in red gas migration. The background picture was modelled using the hybrid method. Both, the Aptian and the Miocene high permeable layer show gas saturations up to 30% whereas in the model using Darcy flow (bottom right in Figure 4-45) no gas saturation is observed. As a result, gas chimneys on the left side (white square on the background picture) are only observed using the hybrid method based on the higher column height in the Miocene sand enabling a spilling towards the surface through the younger sediments. Hydrocarbons in the Aptian and Miocene sand layer migrate faster using the hybrid method and generate therefore larger accumulations, larger column heights and therefore more focussed leakage-points. In contrast the Darcy flow concept concentrates more on compaction, lithology and fluid property variations, gas segregation, diffusion and pressure and temperature derived changes in the dissolution and exsolution behaviour of hydrocarbons during migration which result in a smearing and slowing down of migration pathways in high permeable layers (Hantschel et al., 2000). For the simulation of in-reservoir movements the Darcy approach seems to be more realistic but for the observation of large-scale migration patterns, which is the aim in this study, the hybrid method is the appropriate methodology.

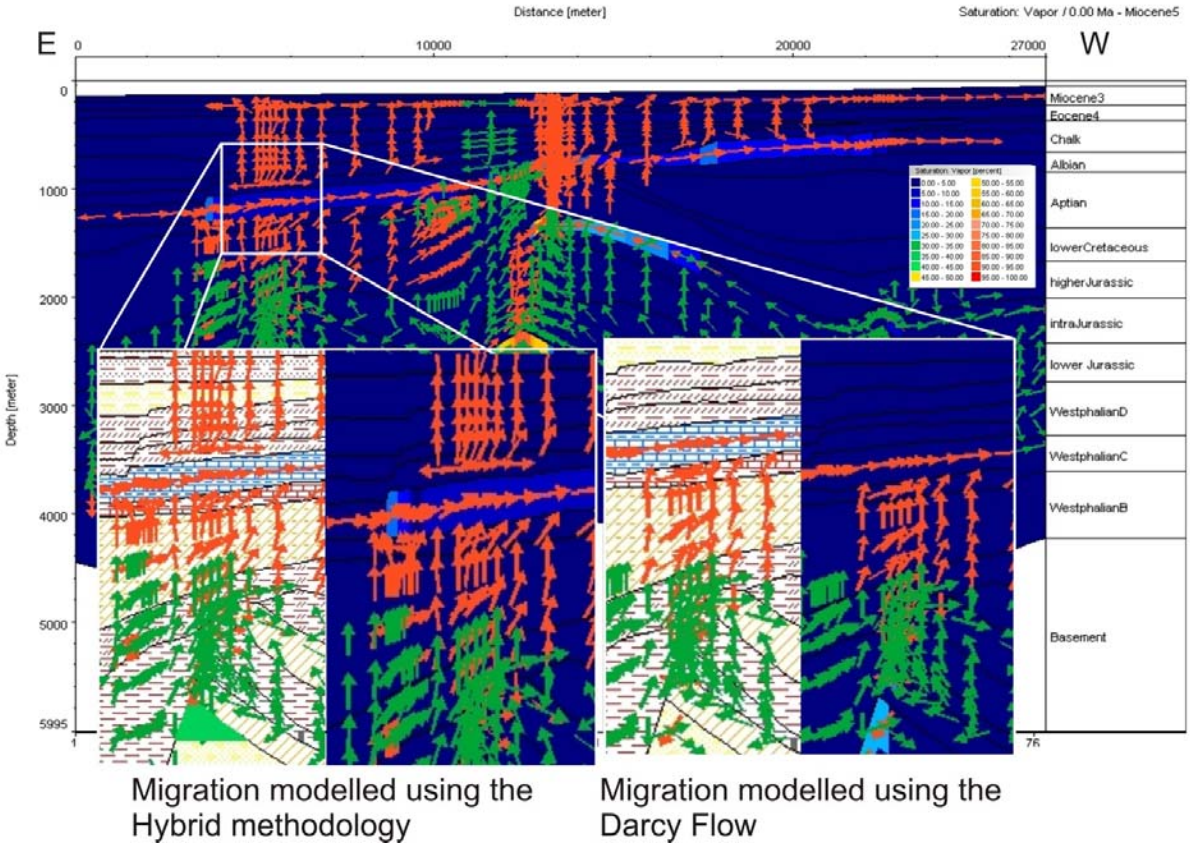

Figure 4-45: Migration modelled using hybrid and Darcy flow with gas saturation overlay

The physical and chemical properties of the Aptian and Miocene layers determine the migration pattern in the Porcupine Basin. Migration in the Porcupine Basin is mainly buoyancy driven as overpressure can be excluded from modeling results and well data. Therefore capillary failure of cap rock lithologies due to hydrocarbon column heights (Clayton and Hay, 1994) is the main leakage mechanism. The capillary entry pressures are lower in high permeable layers and are therefore the preferential migration pathways (Clayton and Hay, 1994).

4.5.3 Hovland-Magellan mound province

4.5.3.1 2D-Modelling

The Hovland-Magellan mound province is located in the central part of line RE94. Due to the location of the line no mounds are observed in the seismics. The set up for the line is the same as described above. Again vertical migration due to capillary leakage is the main migration pattern. Additional migration pathways are the Aptian and Miocene sands, which direct hydrocarbon flow out of the modelled line. No obvious focussing of hydrocarbons towards the mound area was predicted by the model (Figure 4-36) although gas migrates beneath the Pliocene layer in the mound area.

Early Cenozoic deltaic sequences, slump structures and Late Cenozoic contourites have been proposed to focus hydrocarbon migration towards the mound area (McDonnell, 2001) (Figure 4-46).

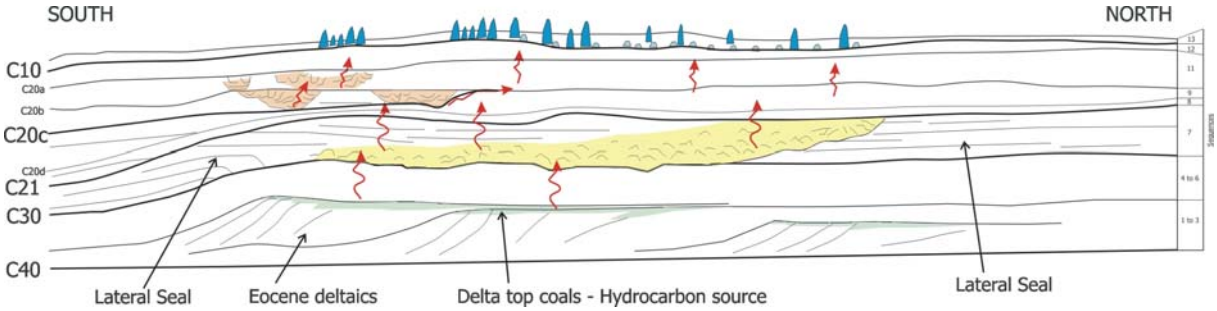

Figure 4-46: Model for hydrocarbon migration through the Cenozoic section (McDonnell, 2001)

The Oligocene and Miocene contourite deposits are assumed to have a coarser grained component than the adjacent basinal mudstone succession and can therefore provide a fluid seepage pathway from beneath. In well 35/18-1, which is with 20 km closest in distance to the mound area, a thin sand-prone Late Oligocene succession was drilled and supports the assumption of sandy contourite deposits. In the model of McDonnell (2001) the underlying Eocene and Paleocene coaly delta top facies is thought to be a likely hydrocarbon source. However, this study showed that the Cenozoic section is immature over the entire basin (section 4.3.5), however hydrocarbon supply from deeper sources took place in this model as shown in Figure 4-42.

Incorporation of these structures into the model, as shown in Figure 4-42, did not result in any obvious focussing of hydrocarbons towards the mound area (Figure 4-47). The model resolution did not allow a detailed recognition of the underlying strata. Therefore the lack of focus in the modelled flow patterns is probably a problem of seismic resolution and also of two dimensional modelling as the structure and topography of layers directs flow laterally and can influence the fluid flow in a 3D sense. A full 3D seismic survey was not available for this study. However, maps of the Oligocene (C30), Miocene (C20), Mid-Miocene and Pliocene (C10), based on the MS81 seismic survey and mapped in the framework of the EU Fifth Framework STRATAGEM project, were available for this study. These maps were used for drainage area calculations based on the present day topography of the layers to analyse possible flow patterns.

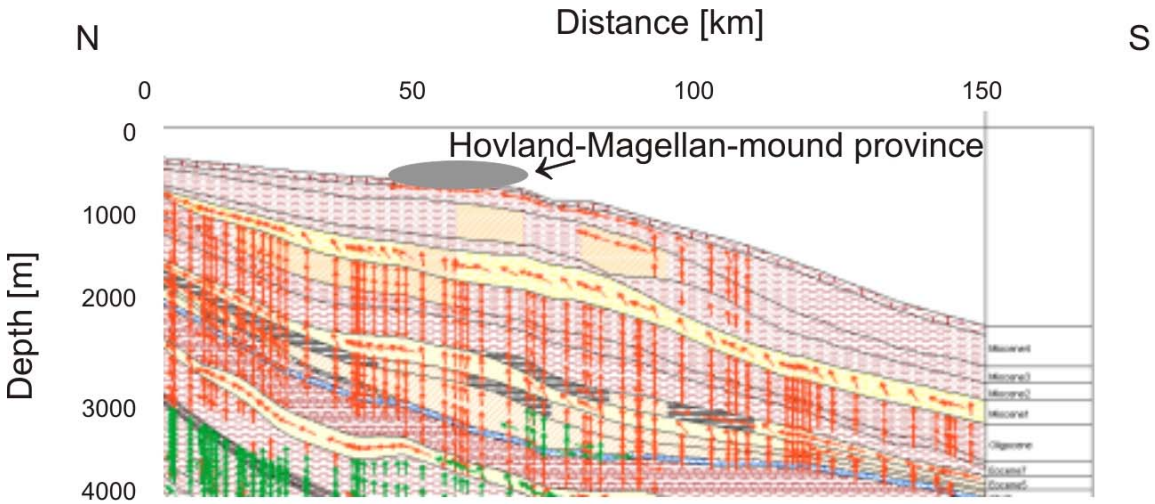

Figure 4-47: Gas migration towards the Hovland-Magellan mound province with no significant flow through the high permeable contourite deposits (light brown) after the model from McDonnell (2001)

4.5.3.2 Drainage Area Modelling

Using flow path modelling, fluid flow is modelled as a purely geometrical problem (Hantschel et al. 2000). The driving force for migration is buoyancy assuming that a carrier rock capillary threshold pressure is exceeded and the entire carrier then can be treated as flow conducting. A carrier map is subdivided into drainage areas and the petroleum in each drainage area is moved to its proper reservoir assuming that migration occurs instantaneously relative to the geologic time scale and physical interactions with the sediment and fluids during migration are negligible. Such methods are also called ray tracing, map-based, surface-based or 2.5D models (Sylta, 1991). In this case, all of the petroleum starts migrating in one drainage area following the flowpaths towards the reservoir, which is mapped as a closure defined by the topographic position in relation to the surrounding drainage area. When a reservoir is completely filled spilling takes place. Possible spill flowpaths into the bordering drainage areas can be calculated from the map structure (Figure 4-48). The calculation of the drainage areas of the four maps provides the drainage area boundaries and closures based on the present day topography. The closures demonstrate areas of possible hydrocarbon accumulations. Hydrocarbon leakage takes place at either spill points or above the closures, providing that hydrocarbon column heights are sufficiently high to overcome cap rock capillary threshold pressures. If mound growth is hydrocarbon related one would expect mound locations to be geographically associated to these closures.

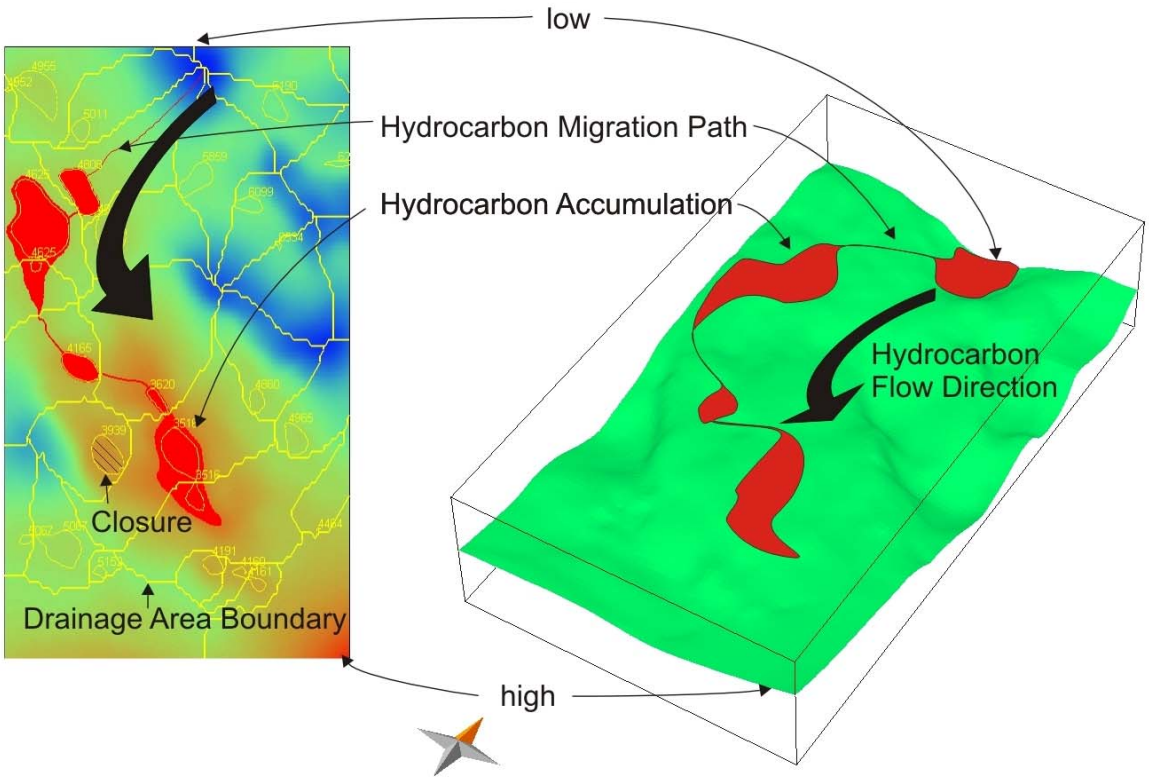

Figure 4-48: Theoretical background of drainage area modelling showing a map in 3D-view with hydrocarbon migration pathways and accumulations on the right. On the left a map view including migration pathways, accumulations and drainage area boundaries and closures

Drainage area modelling was performed on the four Oligocene to Pliocene maps available. Figure 4-49 shows the result of all drainage areas, Figure 4-50, Figure 4-51, Figure 4-52 and Figure 4-53 show the results for the single four maps. The calculation of the drainage areas of the four maps provided the drainage area boundaries and closures based on the present day topography. The closures demonstrate areas of possible hydrocarbon accumulations. Hydrocarbon leakage takes place at either spill points or above the closures, providing that hydrocarbon column heights are sufficiently high to overcome cap rock capillary threshold pressures (Brown, 2000). If mound growth is hydrocarbon related one would expect mound locations to be geographically associated to these closures.

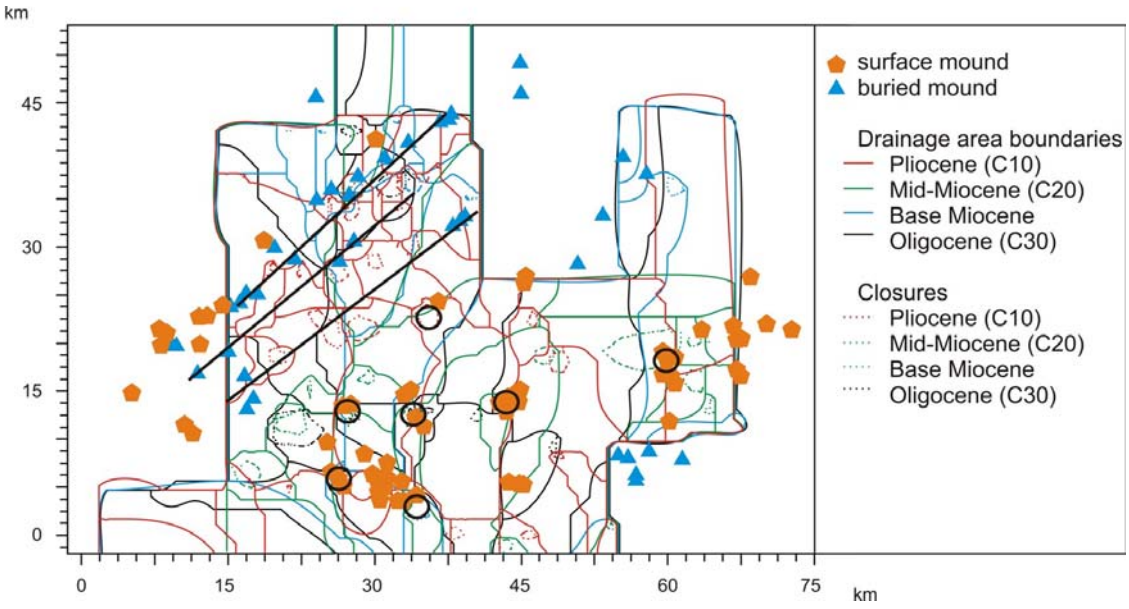

Figure 4-49: Results from the drainage area analysis, coincidence of surface mounds and closures are marked by black circles, the trend seen in the buried mounds is marked by the black lines.

Figure 4-49 shows the superposition of all mapped boundaries and closures as well as the positions of buried and surface mounds in the Hovland-Magellan area. This Figure shows a high degree of coincidence of mound location and closures for the surface mounds marked by the black circles. Almost every group of mounds is related to a closure. However, the coincidence is limited by the rough resolution of the maps and the limited areal distribution. Coincidence of mound location and underlying closure is best for the central parts of the maps, where the map quality is best but will be analysed in detail in the following section.

From Figure 4-49 no coincidence of mounds and closures was observed for the buried mounds. However, mound locations display roughly a northeast-southwest trend, which runs parallel to most of calculated drainage area boundaries. This could indicate a link to a deeper structure, which could be a structural or stratigraphic feature such as observed beneath the Belgica mound province.

It is important to mention that the calculation of the drainage areas is influenced by the boundaries of the maps and nearly one third of the mounds lie outside of the maps. Another limiting factor is that the discovery and mapping of mounds is still in process and numerous new mounds have been found on a 3D-survey (Huvenne et al., in press). The following plots present a detailed analysis of every map and eventual correlation to the mounds (Figure 4-50, Figure 4-51, Figure 4-52 and Figure 4-53).

Figure 4-50 shows the drainage areas and closures calculated for the Oligocene C30 horizon. In the central part of the C30 map three cases of coincidence between closures and surface mounds can be observed. In the eastern part of the map no coincidence is observed,

which may be related to the rough resolution of the data. The buried mounds however align along the drainage area boundaries.

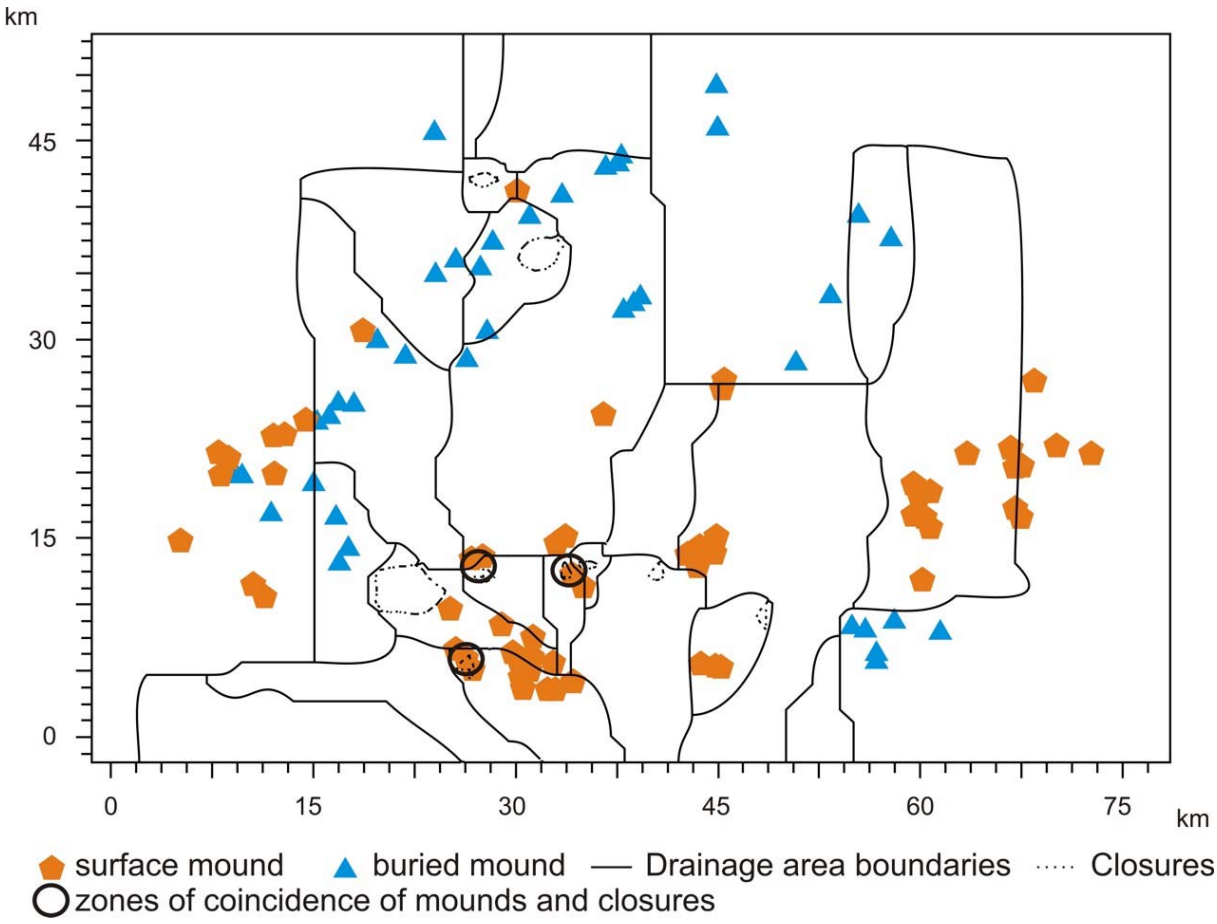

Figure 4-50: Results from the drainage area analysis for the C30 – map

In the case of the Base-Miocene map (Figure 4-51) two cases of coincidence of closures and occurrences of surface mounds are observed in the southern-central part of the basin. In the eastern middle part of the map, a cluster of mounds lies in the middle of a drainage area but based on the areal extent of the drainage area, the related closure far in the northeastern part is questionable. The buried mounds again align along the drainage area in the central part of the mapped area. Here, coincidence of buried mound occurrence and drainage area boundary is very good.

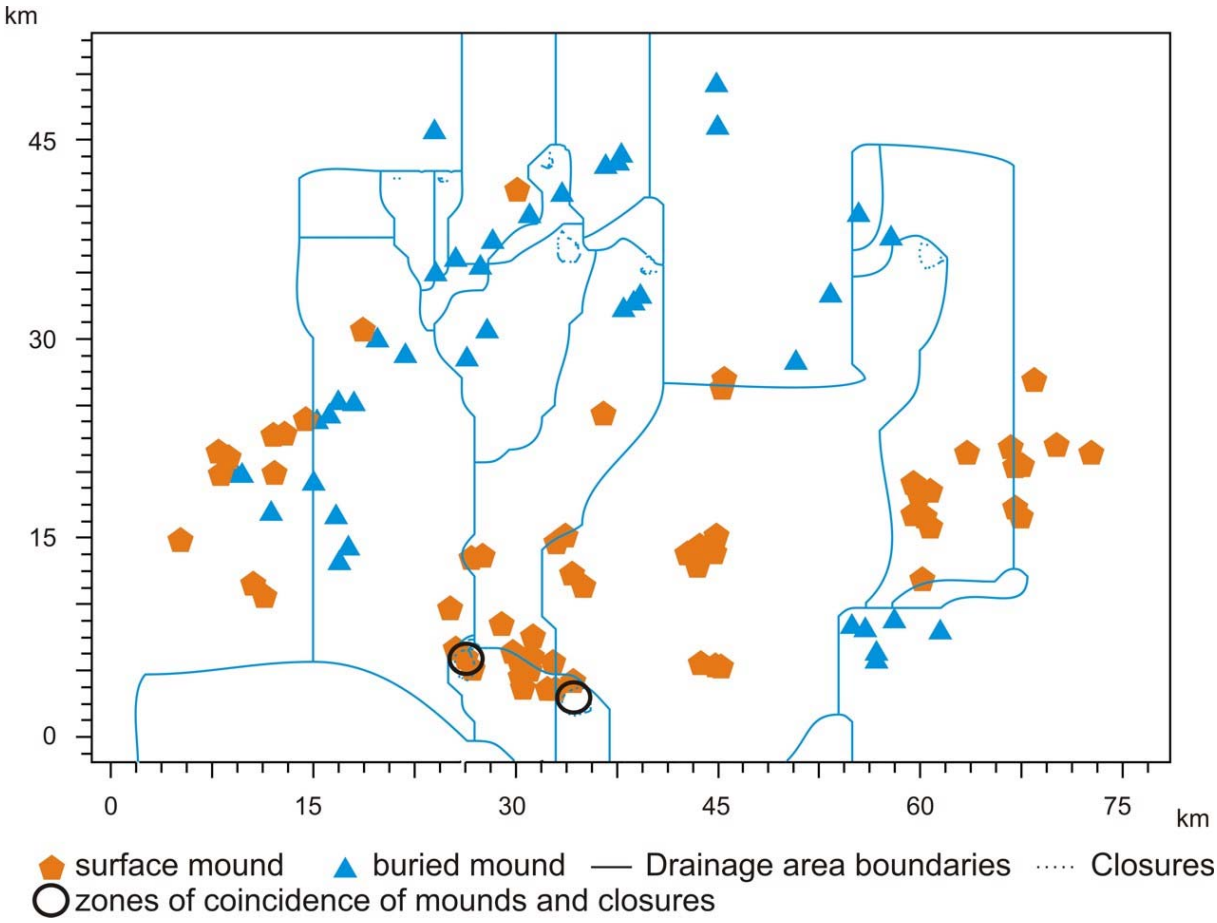

Figure 4-51: Results from the drainage area analysis for the Base-Miocene – map

The map of the C20 horizons shows a distribution of closures and drainage area boundaries, which is similar to the one from the C30 horizon. This time there are four cases of coincidence of mound occurrence and closures, which is the highest for all maps. Interestingly the coincidence in the eastern part of the map is very good. The topographic structure is derived from 2D seismics and it would be necessary to see the underlying sediment facies distribution as the mounds then could be related to the contourites described by McDonnell (2001). However, based on the topography no confirmation of the occurrence of contourites can be drawn. Another explanation can be provided by the fact that the mounds produce a velocity pull up in the seismics which might influence the seismic mapping and explain the good coincidence of surface mounds and the C20 horizon. However, this pull up effect would be very local and certainly not influence the definition of drainage areas.

For the buried mounds, which root on this horizon, almost no coincidence can be found except for some mounds which are again aligned to the drainage boundaries in the northern middle part of the map.

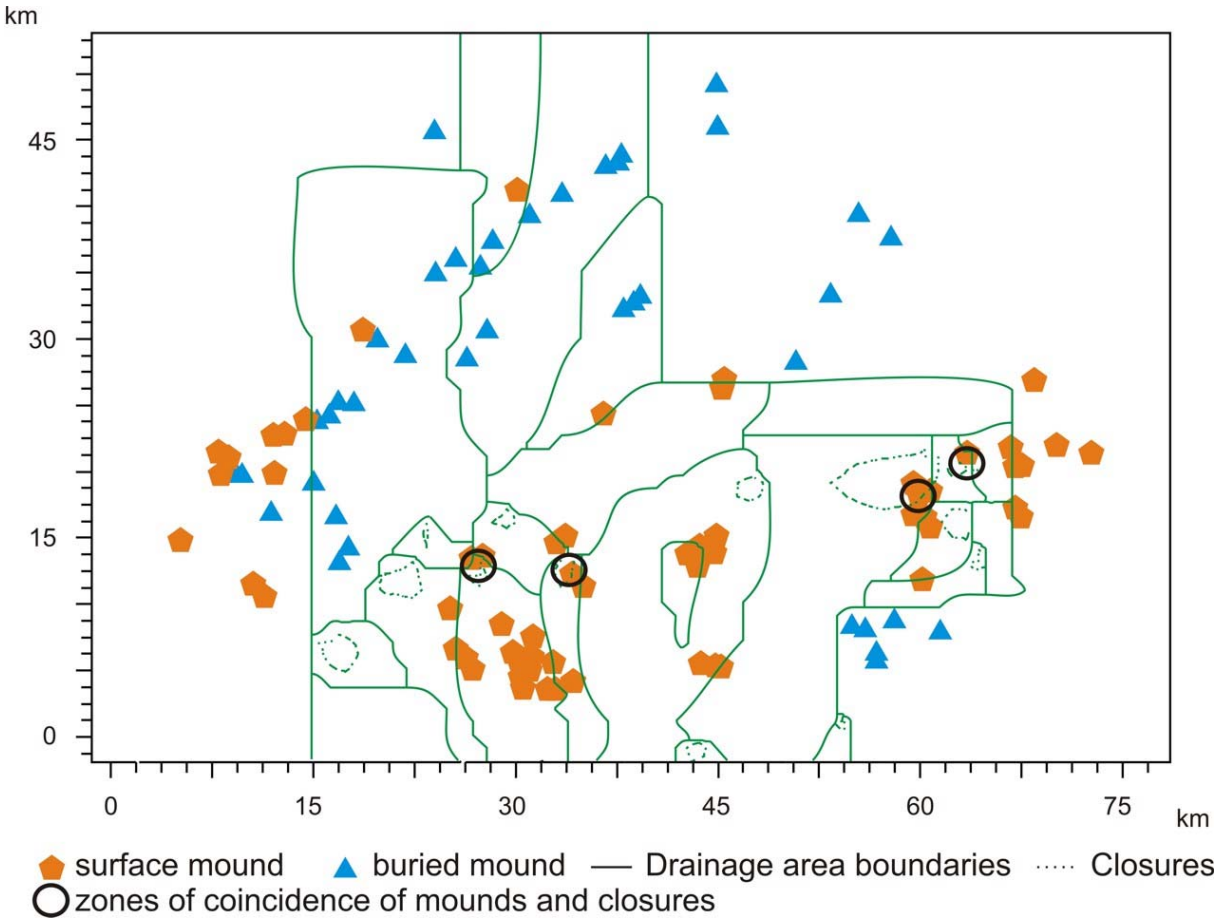

Figure 4-52: Results from the drainage area analysis for the C20 - map

Astonishingly, the C10 map, which is the base of the surface mounds show almost no coincidence of closures and occurrence of surface mounds but a close relation between the mounds and the drainage area boundaries. As the mounds compact the underlying sediment more intensely due to their mass, this could explain their position at the drainage area boundaries (the area in between is less consolidated and of higher elevation). Therefore the given topography is not reliable with respect to the paleotopography.

The buried mounds show a good coincidence to some closures in the northern part of the map, which is definitely an artefact of the seismic mapping. The mounds are elevated features in the topography. This, of course, results in bias in the calculation of the drainage areas and closures.

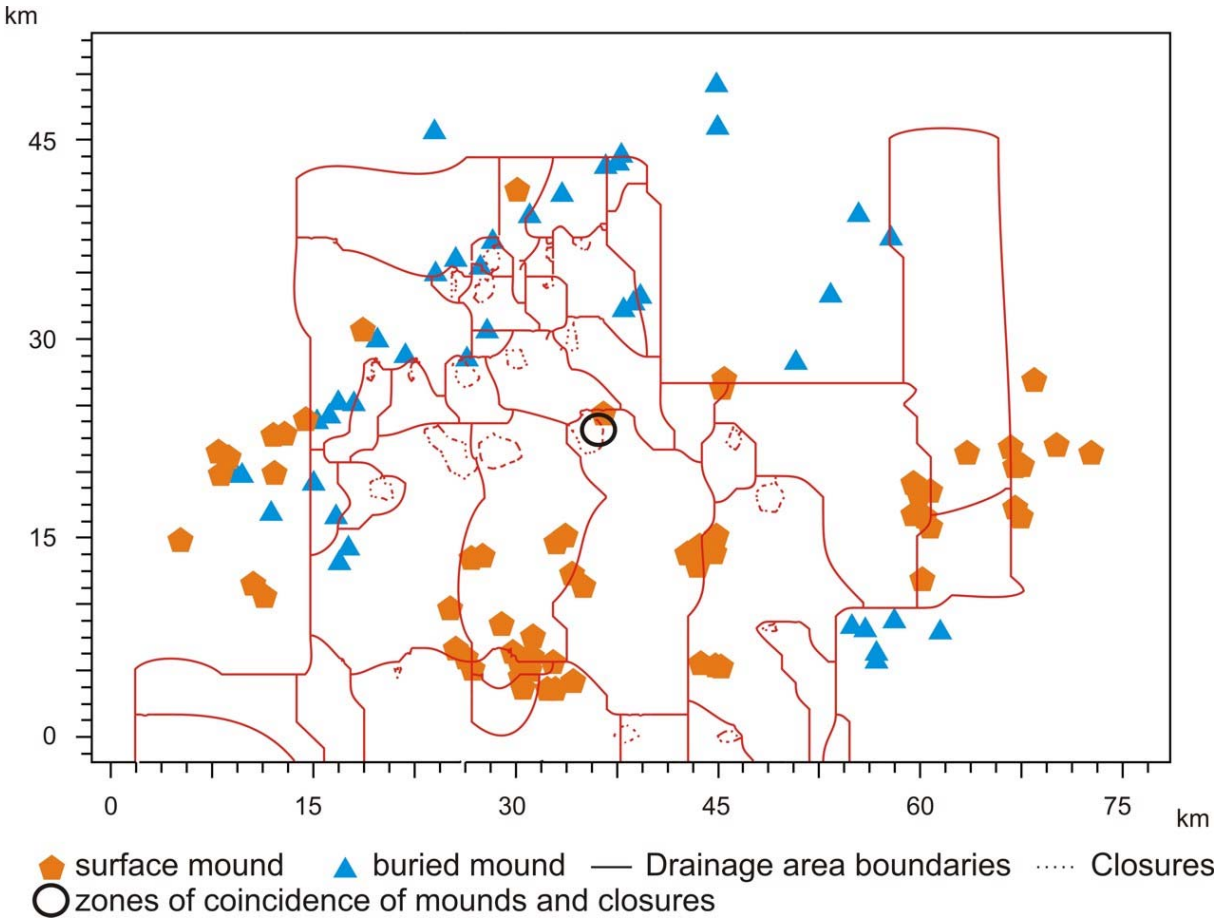

Figure 4-53: Results from the drainage area analysis for the C10 - map

One result from the drainage area analysis is that the surface mounds can be related mainly to the closures of the C30 and C20 maps. From the maps the contourites described by McDonnell (2001) could not be identified which is more a problem of the mapping than of the model.

However, the buried mounds cannot be related to closures but follow roughly a northeast-southwest trend parallel to the drainage area boundaries. This indicates a deeper structure, maybe in the form of a pinch out of a sandy layer like shown for the Belgica mound area (section 4.5.1), or a fan-type like deposit described for the Miller fan (Figure 4-43). From the available data set no clear evidence is found but a strong indication that a deeper structure focuses hydrocarbon flow towards the buried mound area.

5 Checking Predictions – Organic Geochemistry

Modelling results indicate a link between the leakage of hydrocarbons and mound growth. A direct identification of migrated thermal hydrocarbons was, in addition, attempted on the gravity cores taken during the Marion Dufresne cruise 2001. Gravity cores were taken from the tops and flanks of the mounds as well from sediments between the mounds, but not from hardgrounds. The cores penetrated the sediment up to 28.5 mbsf in the case of the Therese mound (MD01-2462) and at maximum 17 mbsf for the cores on mound Challenger (MD01-2451G), Propeller (MD01-2460G) and in the Connemara area (MD01-2453 and MD01-2457). The cores on the mounds site consist of mudstones, often dominated by a framework of the coral *Lophelia*, which makes up 70% and more of the core. No detailed core description exists as the cores were only cut into 1.5 m segments and sampled at the open ends but not opened (cut in half) entirely to remain the structure for x-ray analysis by other Geomound-partners. The cores taken on mound sites did not penetrate through the entire mounds as the mound are about 200 m high, so that the base of the mounds could not be detected and sampled. The cores in the vicinity of the Connemara Oil field consist of a very sticky grey mudstone. These cores also have not been opened in regard of following investigations and therefore again no lithologic description exists. The two carried out geochemical methods used on this samples were gas analysis and biomarker analysis.

5.1 Static Headspace Analysis

In a first run, the C_1-C_7 compounds were determined in all vials and cans from Therese mound (core MD01-2462) by the static headspace - gas chromatography method. Results are presented along side with TOC- & sulfur measurements in Table 5-1. Mainly methane was found in most samples in a range from 0-6 vpm, which is very low and only slightly above the content in air of around 1.8 vpm (Whiticar, 1994). The methane, which was in the air during sampling, was replaced by CO_2 during storage on dry ice, as the septa appeared not to be tight at –80°C. The complete headspace of the vial was replaced by CO_2 after 3-4 days of storage. While the measured methane can be assumed to represent in situ methane which was released from the sediment during analysis. Absolute contents of hydrocarbons determined in these analysis must be treated with caution. Parallel to these analysis the 17 cans from the Therese mound were analysed for the same purpose by Applied Petroleum Technology AS, Norway showing also only traces of methane (Table 5-1).

Part of the core from Therese mound MD01-2462 was sampled again at CNRS in January 2002 to prove that no methane was lost by splitting and splicing the sediment into small parts on board of the Marion Dufresne. The splitting of the sediment was necessary to fill the sediments into the vials. The core from a depth of 15 m was chosen, as it is the middle part of the entire core of 28 m length. It had remained at 4°C in a cooling room since being taken and was still of muddy consistence. The 1.5 m long core from 15 to 16.5 mbsf was completely cooled in liquid nitrogen to prevent gas to escape during opening of the core and to simplify the sampling procedure. After consolidation of the core the central 30 cm of the core were crushed with a hammer and sediment fragments were immediately sealed in vials

and cans and allowed to equilibrate to room temperature. Headspace gas chromatography analysis showed the same low methane contents as measured before on the samples taken on board (Table 5-1).

Sample	Methane [vpm]	Ethane [vpm]	i-Butane ? [vpm]	TOC [%]	S [%]
MD01-2451G (Mound Challenger 51°22/11°43)					
E50166	5.1	0.0	0.0	0.17	0.03
E50167	3.8	0.0	0.0	0.23	0.25
E50168	3.0	0.0	0.0	0.23	0.35
E50169	0.0	0.0	0.0	0.22	0.29
E50170	2.1	0.0	0.0	0.34	0.18
E50171	1.0	0.0	0.0	0.37	0.16
E50172	0.4	0.0	0.0	0.31	0.19
E50173	3.6	0.0	0.0	0.17	0.20
E50174	0.9	0.0	0.0	0.22	0.17
MD01-2453 (Connemara 53°04/12°31)					
E50175	5.9	0.0	0.0	0.16	0.03
E50176	2.6	0.0	0.0	0.38	0.05
E50177	2.7	0.0	0.0	0.27	0.16
E50178	2.6	0.0	0.0	0.22	0.13
E50179	1.7	0.0	0.0	0.29	0.12
E50180	1.6	0.0	0.0	0.29	0.11
E50181	1.7	0.0	0.0	0.40	0.07
E50182	1.6	0.0	0.0	0.42	0.05
E50183	1.6	0.0	0.0	0.41	0.04
E50184	2.2	0.0	0.0	0.54	0.09
E50185	2.8	0.0	0.0	0.54	0.07
E50186	1.9	0.0	0.0	0.23	0.04
MD01-2457 (Connemara 53°04/12°31)					
E50196	5.2	0.0	0.0	0.24	0.03
E50197	3.1	0.0	0.0	0.40	0.41
E50199	1.9	0.0	0.3	0.35	0.09
E50200	1.9	0.0	0.0	0.32	0.55
E50201	1.1	0.0	0.0	0.30	0.40
E50202	1.3	0.0	0.0	0.38	0.26
E50203	2.7	0.0	0.0	0.39	0.07
E50204	2.1	0.0	0.0	0.36	0.04
E50205	1.5	0.0	0.0	0.39	0.03
E50206	1.4	0.0	0.0	0.50	0.08
E50207	1.3	0.0	0.0	0.45	0.07
MD01-2460G (Mound Propeller 52°09/12°46)					
E50208	1.5	0.0	0.0	0.26	0.03
E50209	1.5	0.0	0.0	0.23	0.09
E50210	1.4	0.0	0.0	0.10	0.04
E50211	1.5	0.0	0.0	0.15	0.05
E50212	1.4	0.0	0.0	0.14	0.06
E50213	1.5	0.0	0.0	0.27	0.18
E50214	1.3	0.0	0.0	0.23	0.19
E50215	1.3	0.0	0.0	0.15	0.12
E50216	1.3	0.0	0.0	0.20	0.18
E50217	2.1	0.0	0.0	0.21	0.13
MD01-2462 (Mound Theresa 51°25/11°46)					
E50218	3.7	0.0	0.0	0.24	0.05
E50219	3.7	0.0	0.0	0.20	0.05
E50220	4.2	0.0	0.0	0.22	0.29
E50221	5.2	0.0	0.0	0.24	0.05
E50222	4.6	0.0	0.0	0.11	0.03
E50223	2.2	0.0	0.0	0.25	0.08
E50224	3.2	0.8	0.6	0.10	0.04
E50225	1.3	0.0	0.0	0.16	0.09
E50526	0.7	0.4	0.4	0.15	0.14
E50227	1.5	0.0	0.0	0.35	0.14
E50228	1.0	0.0	0.0	0.43	0.17
E50229	2.0	0.0	0.0	0.37	0.14
E50230	1.7	0.0	0.0	0.17	0.09
E50231	1.0	0.0	0.0	0.19	0.17
E50232	2.1	0.0	0.0	0.30	0.27
E50233	1.8	0.0	0.0		
E50234	1.6	0.0	0.0	0.11	0.03
E50235	1.6	0.0	0.0	0.12	0.06

Sample	Methane [vpm]	Ethane [vpm]	i-Butane ? [vpm]	TOC [%]	S [%]
MD01-2462 (Mound Theresa 51°25/11°46) - second sampling at CNRS					
E5026/1	0.8	0.3	0.3	0.13	0.10
E5026/2	0.7	0.4	0.4	0.25	0.19
E5026/3	0.2	0.3	0.3	0.18	0.17
E5026/4	0.6	0.3	0.3	0.24	0.14
E5026/5	1.1	0.4	0.3	0.19	0.14
E5026/6	0.9	0.6	0.3	0.16	0.14
E5026/7	0.8	0.0	0.2	0.21	0.16
E5026/8	0.9	0.5	0.4	0.16	0.14
Air taken at the laboratory at CNRS					
E50527/1	2.0	0.0	0.0		
E50527/2	2.0	0.0	0.0		
Dive 125-3 CL1 (Mound Theresa)					
E50237	4.4	0.0	0.0	0.06	0.02
E50238	4.9	0.0	0.0	0.06	0.02
E50239	5.3	0.0	0.0	0.06	0.02
Dive 128-06 (Mound Challenger)					
E50240	5.1	0.0	0.6	0.25	0.03
E50241	4.4	0.0	0.7	0.20	0.03
E50242	4.1	0.0	0.0	0.23	0.03
E50243	4.8	0.0	0.4	0.19	0.02
E50244	5.2	0.0	0.3	0.20	0.03
E50245	4.3	0.0	0.0	0.21	0.02
Atalante Cruise (PL127-05 CT05)					
E50528	2.3	0.7	1.4	0.32	0.15
E50528	1.8	0.5	1.4	0.37	0.21
E50528	2.1	0.6	1.6	0.38	0.17
Samples measured by Aptec					
50218					
50219	21.0				
50220	16.0				
50221	18.0				
50222					
50223	3.0				
50224	4.0				
50227	6.0				
50228	9.0				
50229					
50230					
50231	8.0				
50232					
50233	47.0				
50234					
50235	0.4				
50236	13.0				

Table 5-1: Results from the static headspace analysis showing the results from the initial cores taken on the MD-cruise 2001 on the left side and results of the resampled cores, samples from other cruises and of the samples measured by Aptec on the right side

Other gases were found in a few samples but in even lower amounts (Table 5-1). Ethane and possibly i-butane were found in the cores from Connemara field (MD01-2457), Therese Mound (MD01-2462) and Challenger Mound (Dive 128-06) in concentrations below 1 vpm. Contents of the samples E50526/1-8 (sub-sampling at CNRS) of ethane and i-butane are only slightly higher than the detection limit and were therefore not taken into account.

TOC and sulfur contents were also very low not showing any significant accumulation of organic rich material. Figure 5-1 shows the TOC content plotted versus the depth. The cores from the Connemara vicinity MD01-2453 and MD01-2457 show a similar depth trend with low surface TOC-values, an increase at 1.5 mbsf, and a decrease of TOC up to 9 mbsf, an increase up to 15 mbsf and a decrease up to the end of the core. The content of sulphur plotted versus depth (Figure 5-2) shows a similar trend with two high peaks at 1.5 and 7.5 mbsf. However, the variations are in between 0.2% TOC respectively 0.4% sulphur. Taking the instrumental error of the Leco instrument of ± 5% to the errors possibly made during homogenisation of the sediment the variations making this trends are questionable.

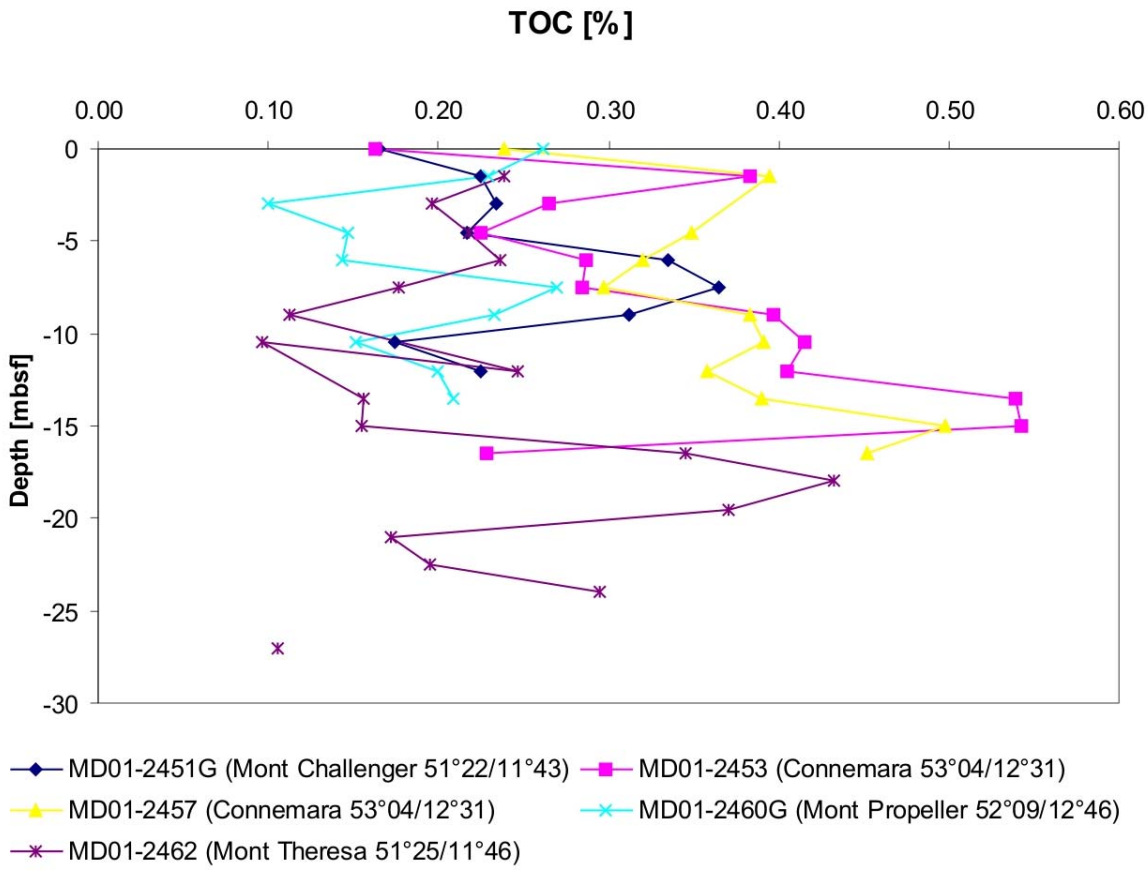

Figure 5-1: TOC plotted versus depth for the cores MD01-2451G, MD01-2453, MD01-2457, MD01-2460G and MD01-2462

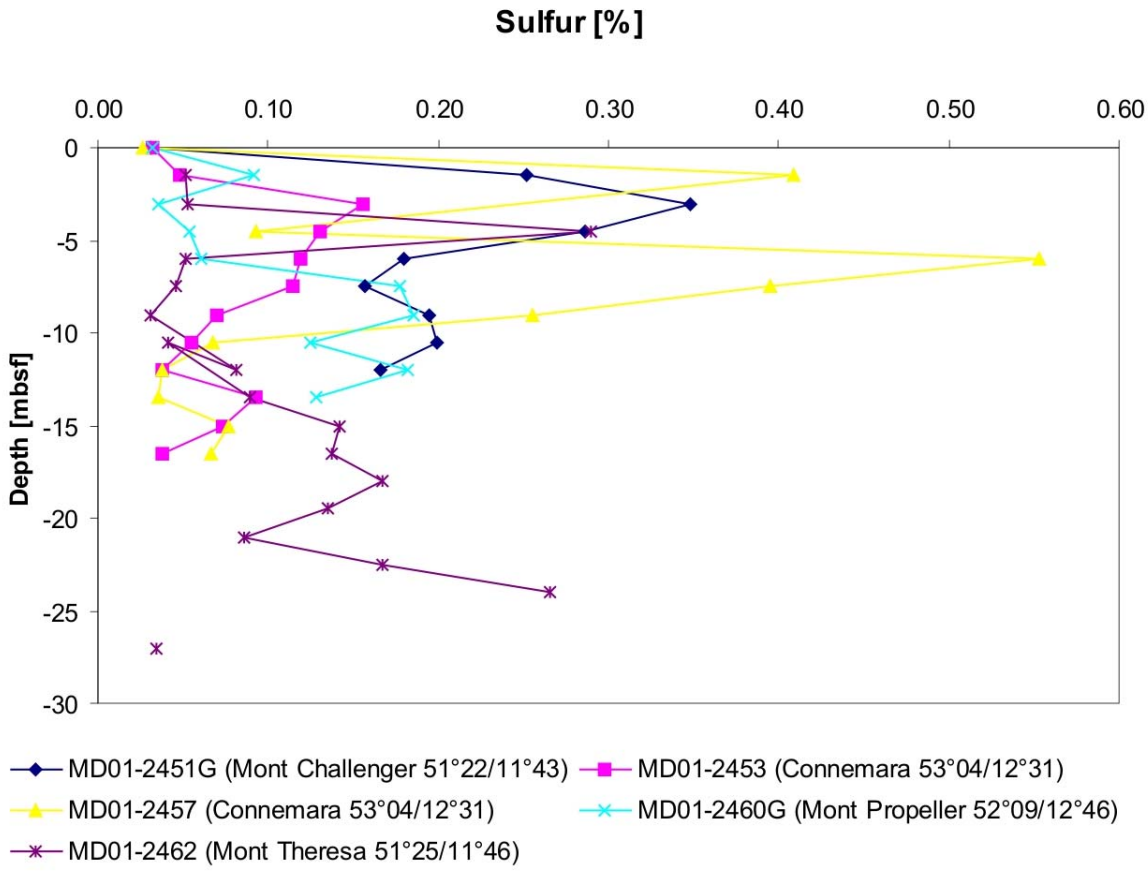

Figure 5-2: Sulfur content plotted versus depth for the cores MD01-2451G, MD01-2453, MD01-2457, MD01-2460G and MD01-2462

The trends for the TOC contents measured on cores MD01-2451G, MD01-2460G and MD01-2462 on the mound sites are similar except of the surface samples. In the case of Mound Challenger the TOC contents are higher than the ones from Mound Theresa and Propeller. The trends from the mound site varies to the one from the Connemara field as that the TOC content is a bit lower and oppositional to the one from the mound sites. This can be caused by the corals from the mound site. If the content of corals is high, the mud content is low and the overall TOC content is low. Therefore the low content of TOC can be an indication of coral dominated sediment. As the variations of TOC are low the organic matter seems to be incorporated into the mud and derived from marine or terrestrial material. No layers were found which had exceptional high values, which could indicate hydrocarbon accumulations or precipitations.

For further investigation, the relationship between the methane content and TOC content can be used to investigate whether the methane can be a cracking product during analysis or be related to high TOC contents or if it is of natural origin. A plot of methane content against the TOC content implies two families (Figure 5-3). Family I is characterized by low TOC contents and high methane contents, Family II by high TOC contents and low methane contents. The

expected relationship between high TOC and high methane contents could not be detected. Therefore the methane can be considered to be in situ in the sediment. Interestingly, family I consists of near seafloor samples from a depth of 0 – 3 mbsf. But as all of the measured values are somehow close to the detection limit this relationship is questionable.

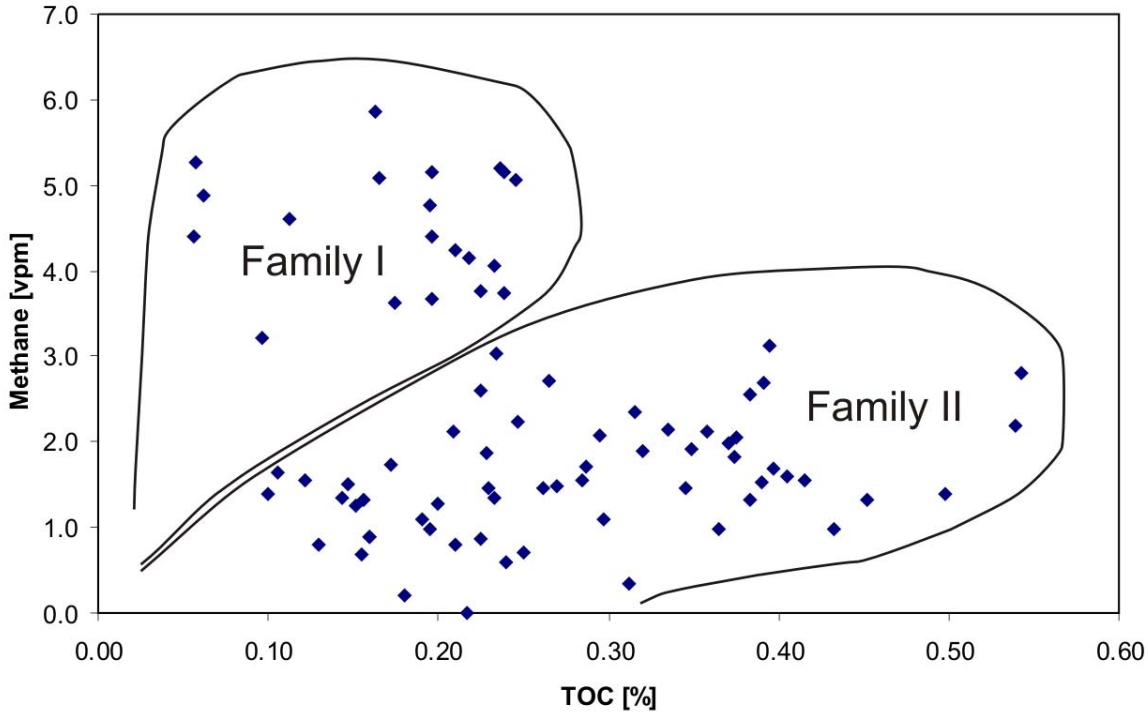

Figure 5-3: Relationship between TOC content and methane content

5.2 Purge and Trap

Samples from gravity cores MD01-2451 and Dive 128-06 (Belgica mound province), MD01-2460G (Hovland-Magellan mound province) and cores MD01-2453 and MD01-2457 (Connemara Oil field) were also analysed using the purge and trap headspace chromatography apparatus. This differs from static headspace in that the vials were purged with helium for five minutes, resulting in an exchange of the headspace for 5 times. The outgoing gas was trapped with the help of liquid nitrogen. During that time all light hydrocarbons should be able to migrate out of the sediment into the headspace. Test measurements with longer purging times using comparable samples yielded no higher methane contents indicating that five minutes is an appropriate purging time. The overall contents of light hydrocarbons are expected to be higher as in the static headspace and traces of additional hydrocarbons are expected to be detected and resolved based on the purge and trap process.

A total of 26 substances were determined. Identification was done by coupling the purge and trap system with a mass-spectrometer and by injecting standards (Schaefer et al., 2003). Gas concentration data are reported for a series of hydrocarbons given in order of elution (Table 5-2): methane, ethene, ethane, propene, propane, U-1a/b, methylpropane, methylpropene +1-butene, n-butane, trans-2-butene, cis-2-butene, methylbutane, 1-pentene, furane, n-pentane, dimethylsulphide, U-2, U-3, U-4, 1-hexene, 2-methylfurane, n-hexane, 3-methylfurane, U-5, U-6 and benzene is given in Figure 5-4. U1-6 are six peaks, which have not been identified so far.

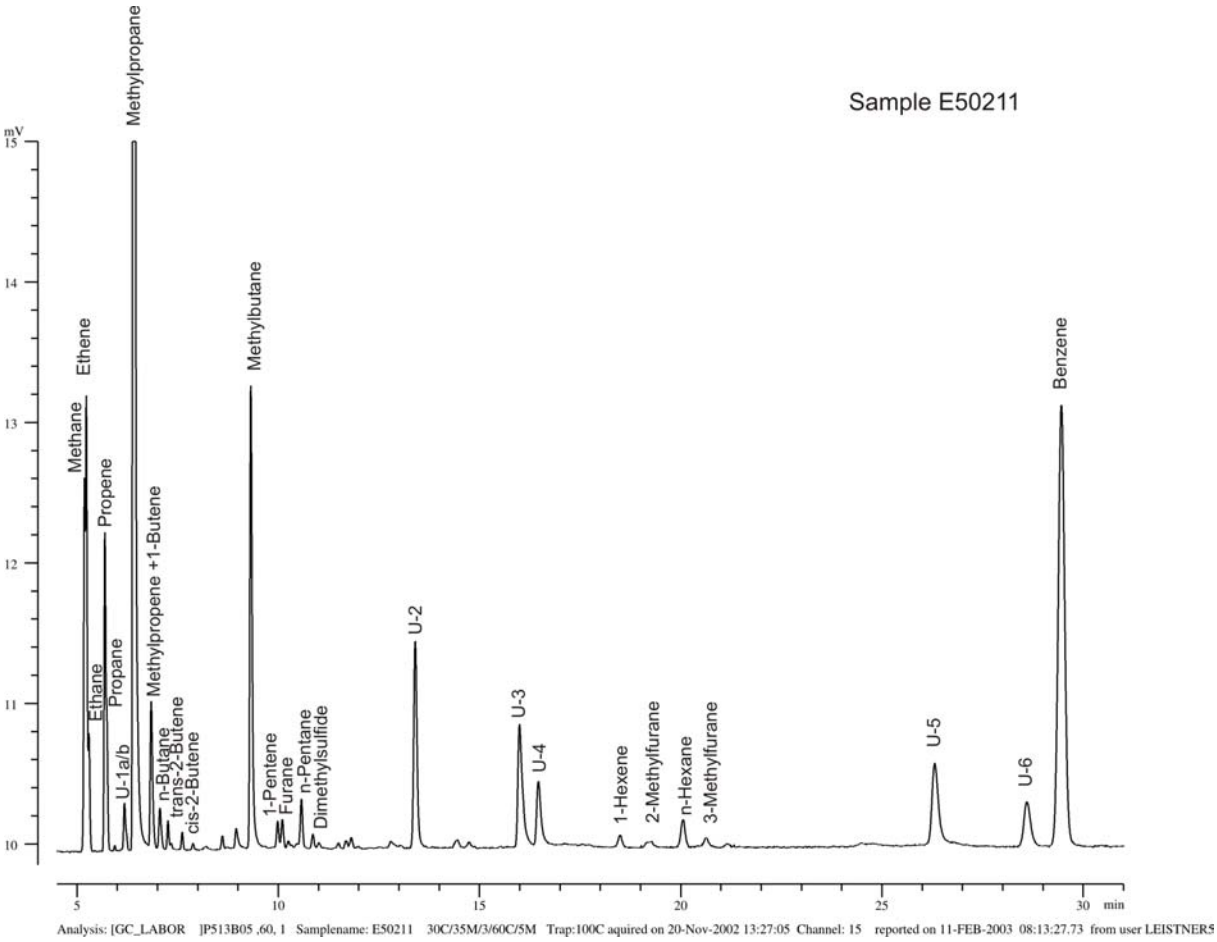

Figure 5-4: Gas chromatogram of sample E50211 from the Belgica mound province with identified peaks

Samples	Depth [mslf]	Methane [ng/g rock]	Ethene [ng/g rock]	Ethane [ng/g rock]	Propene [ng/g rock]	Propane [ng/g rock]	U-1a/b [ng/g rock]	Methylpropane [ng/g rock]	Methylpropene +1-butene [ng/g r	n-Butane [ng/g rock]	trans-2-Butene [ng/g rock]	cis-2-Butene [ng/g rock]	Methylbutane [ng/g rock]	1-Pentene [ng/g rock]	Furane [ng/g rock]	n-Pentane [ng/g rock]	Dimethylsulfide [ng/g rock]	U-2 [ng/g rock]	U-3 [ng/g rock]	U-4 [ng/g rock]	1-Hexene [ng/g rock]	2-Methylfurane [ng/g rock]	n-Hexane [ng/g rock]	3-Methylfurane [ng/g rock]	U-5 [ng/g rock]	U-6 [ng/g rock]	Benzene [ng/g rock]
MD01-2451G (Mound Challenger 51°22/11°43)																											
E50166	0.00	4.72	1.11	0.94	4.77	2.25	0.23	8.11	0.41	0.24	0.22	0.03	0.90	0.14	0.25	0.66	0.28	4.55	0.66	0.23	0.12	0.00	0.12	0.05	0.37	0.22	3.50
E50167	-1.50	3.15	6.19	1.37	1.90	0.72	0.30	18.40	1.34	0.38	0.15	0.11	1.95	0.17	0.68	0.27	0.04	1.15	1.17	0.44	0.09	0.13	0.20	0.13	0.60	0.34	5.18
E50168	-3.00	1.71	0.40	0.21	0.34	0.13	0.12	7.03	0.25	0.09	0.07	0.04	0.59	0.04	0.12	0.08	0.08	0.25	0.46	0.14	0.03	0.04	0.07	0.04	0.14	0.08	7.57
E50169	-4.50	1.75	1.42	0.49	0.89	0.64	0.29	14.51	0.59	0.29	0.13	0.07	1.84	0.13	0.18	0.35	0.00	1.11	1.27	0.49	0.08	0.08	0.33	0.09	0.61	0.36	8.41
E50170	-6.00	2.91	1.46	0.78	0.77	0.70	0.36	12.37	0.62	0.26	0.13	0.09	1.05	0.13	0.11	0.28	0.29	0.68	0.67	0.26	0.07	0.06	0.19	0.07	0.44	0.28	1.87
E50171	-7.50	2.71	3.08	1.43	1.50	1.39	0.78	20.29	1.11	0.50	0.18	0.10	2.67	0.22	0.20	0.53	0.06	2.04	1.72	0.80	0.12	0.14	0.40	0.11	1.29	0.91	5.08
E50172	-9.00	3.37	1.34	0.84	0.65	0.81	0.46	10.78	0.46	0.29	0.10	0.05	1.32	0.14	0.11	0.33	0.00	0.58	0.90	0.34	0.00	0.00	0.22	0.00	0.37	0.25	3.81
E50173	-10.50	1.76	1.10	0.56	0.52	0.48	0.36	8.16	0.41	0.20	0.08	0.04	0.81	0.07	0.06	0.22	0.16	0.68	0.47	0.16	0.05	0.04	0.14	0.05	0.35	0.25	4.39
E50174	-12.00	3.01	1.03	0.60	0.65	0.50	0.37	9.84	0.41	0.19	0.09	0.05	0.92	0.09	0.06	0.21	0.00	0.39	0.82	0.27	0.05	0.05	0.11	0.05	0.35	0.17	2.04
MD01-2453 (Connemara 53°04/12°31)																											
E50175	0.00	4.43	2.78	1.03	1.53	0.58	1.45	9.38	1.40	0.36	0.15	0.09	1.31	0.17	0.38	0.30	2.37	0.51	0.83	0.28	0.11	0.16	0.22	0.29	0.38	0.12	2.23
E50176	-1.50	1.76	4.59	0.77	1.61	0.51	0.23	19.64	0.88	0.23	0.16	0.09	1.70	0.11	0.69	0.17	0.04	0.96	1.23	0.39	0.06	0.09	0.16	0.12	0.60	0.33	4.37
E50177	-3.00	1.20	7.01	0.58	1.85	0.44	0.06	25.51	1.50	0.28	0.33	0.20	2.00	0.15	2.83	0.30	0.03	1.16	1.59	0.52	0.11	0.13	0.25	0.07	0.92	0.32	2.23
E50178	-4.50	1.64	3.91	0.81	1.23	0.59	0.17	10.53	0.80	0.30	0.12	0.08	1.11	0.16	0.39	0.31	0.05	0.49	0.99	0.20	0.06	0.09	0.23	0.17	0.24	0.12	5.67
E50179	-6.00	1.51	3.01	0.56	1.37	0.48	0.21	17.66	0.90	0.25	0.14	0.10	1.63	0.13	0.58	0.21	0.00	2.05	1.23	0.41	0.11	0.14	0.21	0.13	0.35	0.31	4.55
E50180	-7.50	0.61	4.96	0.77	1.72	0.40	0.11	28.85	1.26	0.28	0.24	0.14	1.73	0.12	2.71	0.31	0.00	0.63	0.89	0.41	0.09	0.09	0.25	0.05	0.61	0.25	2.39
E50181	-9.00	1.69	4.27	0.94	1.90	0.66	0.39	18.73	1.09	0.31	0.16	0.09	2.03	0.14	0.46	0.23	0.06	1.11	1.20	0.49	0.08	0.12	0.21	0.16	0.60	0.29	2.54
E50182	-10.50	1.40	3.55	0.79	1.88	0.57	0.41	17.32	1.04	0.33	0.17	0.09	1.52	0.14	0.69	0.28	0.00	0.71	1.15	0.29	0.07	0.09	0.19	0.13	0.38	0.20	8.32
E50183	-12.00	0.58	1.10	0.00	0.73	0.00	0.10	37.63	2.26	0.50	0.38	0.24	1.93	0.25	3.19	0.67	0.00	0.38	0.69	0.53	0.18	0.06	0.47	0.05	1.13	0.18	3.89
E50184	-13.50	1.00	4.76	0.67	1.56	0.51	0.16	16.05	0.88	0.25	0.05	0.07	1.31	0.09	0.66	0.24	0.00	1.03	0.75	0.35	0.09	0.09	0.18	0.05	0.81	0.50	2.34
E50185	-15.00	2.77	4.13	0.87	1.97	0.71	0.30	15.90	0.98	0.36	0.18	0.09	1.38	0.17	0.66	0.33	0.05	0.71	1.19	0.38	0.14	0.12	0.24	0.10	0.45	0.24	5.71
E50186	-16.50	1.90	2.72	0.57	0.93	0.36	0.13	13.10	0.57	0.19	0.11	0.07	0.88	0.08	0.78	0.15	0.00	0.42	1.09	0.24	0.04	0.08	0.11	0.08	0.25	0.13	2.89
MD01-2457 (Connemara 53°04/12°31)																											
E50196	0.00	3.39	1.66	0.80	0.66	0.51	1.41	10.80	0.88	0.30	0.16	0.07	1.59	0.12	0.41	0.38	2.42	1.42	1.03	0.38	0.15	0.24	0.28	0.30	0.44	0.32	2.37
E50197	-1.50	3.50	2.34	0.53	1.34	0.37	0.13	11.35	0.72	0.16	0.13	0.07	1.05	0.07	0.47	0.10	0.02	0.52	1.02	0.28	0.06	0.10	0.08	0.11	0.34	0.17	2.18
E50198	-3.00	1.96	2.92	0.75	1.40	0.45	0.25	20.66	0.76	0.23	0.15	0.10	1.72	0.10	0.92	0.19	0.00	0.78	1.88	0.47	0.06	0.08	0.14	0.10	0.45	0.26	4.06
E50199	-4.50	2.81	4.22	1.03	2.15	0.68	0.28	12.47	1.40	0.39	0.21	0.14	0.98	0.21	0.54	0.35	0.07	0.47	1.08	0.23	0.11	0.15	0.24	0.19	0.22	0.13	5.47
E50200	-6.00	0.90	4.10	0.73	1.59	0.54	0.19	15.66	1.02	0.28	0.15	0.10	1.50	0.16	0.45	0.25	0.00	0.71	1.42	0.40	0.10	0.11	0.19	0.14	0.45	0.26	6.95
E50201	-7.50	0.71	3.70	0.64	1.42	0.47	0.25	13.00	0.88	0.24	0.13	0.09	1.18	0.14	0.55	0.21	0.07	0.68	1.10	0.32	0.12	0.19	0.22	0.18	0.32	0.22	4.63
E50202	-9.00	1.81	3.08	0.60	1.56	0.51	0.24	10.33	0.91	0.23	0.12	0.09	0.91	0.12	0.38	0.19	0.04	0.49	0.76	0.19	0.07	0.08	0.13	0.10	0.29	0.17	4.41
E50203	-10.50	0.97	4.47	0.85	1.52	0.62	0.28	14.53	0.84	0.32	0.13	0.09	1.48	0.11	0.46	0.27	0.00	0.67	1.25	0.34	0.06	0.08	0.17	0.09	0.43	0.23	2.07
E50204	-12.00	1.75	3.39	0.79	1.55	0.54	0.34	13.82	1.03	0.30	0.14	0.08	1.24	0.14	0.41	0.23	0.06	0.59	1.08	0.33	0.11	0.16	0.22	0.23	0.34	0.18	5.59
E50205	-13.50	1.61	4.21	1.22	1.44	0.94	0.41	14.19	0.82	0.55	0.16	0.10	1.25	0.12	0.64	0.47	0.00	0.44	0.82	0.28	0.09	0.08	0.22	0.09	0.19	0.16	5.39
E50206	-15.00	1.06	4.64	0.80	1.66	0.58	0.26	15.10	0.89	0.32	0.18	0.10	1.36	0.12	0.76	0.29	0.00	0.75	0.86	0.36	0.10	0.09	0.22	0.09	0.60	0.28	3.95
E50207	-16.50	1.10	3.48	0.55	1.68	0.50	0.35	16.83	0.92	0.26	0.15	0.08	1.57	0.15	0.57	0.27	0.33	0.84	1.18	0.47	0.10	0.12	0.23	0.10	0.65	0.28	9.49
MD01-2460G (Mound Propeller 52°09/12°46)																											
E50208	0.00	2.54	1.81	0.56	1.25	0.52	0.17	11.92	0.88	0.28	0.15	0.10	1.30	0.15	0.20	0.35	0.05	0.82	1.04	0.36	0.17	0.18	0.31	0.17	0.57	0.34	7.01
E50209	-1.50	3.08	1.99	0.62	1.33	0.63	0.20	7.76	0.84	0.31	0.15	0.09	0.93	0.13	0.11	0.38	0.07	0.48	0.81	0.19	0.09	0.08	0.33	0.09	0.29	0.19	2.14
E50210	-3.00	1.66	0.50	0.32	0.33	0.23	0.07	7.69	0.27	0.12	0.08	0.05	0.55	0.09	0.08	0.14	0.00	0.24	0.41	0.14	0.00	0.00	0.10	0.05	0.18	0.08	6.69
E50211	-4.50	1.58	2.12	0.53	1.50	0.59	0.33	21.90	1.06	0.32	0.16	0.10	3.31	0.21	0.22	0.40	0.05	2.04	1.80	0.93	0.17	0.15	0.39	0.16	1.55	0.89	8.33
E50212	-6.00	2.81	1.51	0.66	0.65	0.39	0.14	11.53	0.49	0.17	0.10	0.06	1.27	0.07	0.10	0.17	0.04	0.97	0.73	0.33	0.06	0.08	0.13	0.08	0.57	0.35	3.17
E50213	-7.50	2.03	3.20	0.73	1.65	0.76	0.35	11.93	1.04	0.37	0.16	0.11	1.55	0.21	0.20	0.45	0.13	0.86	1.25	0.37	0.17	0.16	0.42	0.20	0.58	0.31	3.75
E50214	-9.00	0.60	5.39	0.76	1.21	0.43	0.09	13.18	0.90	0.20	0.16	0.09	1.32	0.10	0.62	0.21	0.05	0.90	0.64	0.38	0.09	0.08	0.19	0.09	0.70	0.41	2.69
E50215	-10.50	1.23	0.77	0.20	0.53	0.21	0.10	7.33	0.32	0.12	0.09	0.04	0.69	0.08	0.10	0.17	0.04	0.46	0.72	0.19	0.09	0.11	0.24	0.07	0.25	0.12	21.65
E50216	-12.00	1.24	2.61	0.61	0.73	0.50	0.23	8.16	0.47	0.26	0.08	0.06	0.99	0.08	0.14	0.24	0.00	0.53	0.85	0.27	0.09	0.11	0.22	0.15	0.41	0.24	2.96
E50217	-13.50	1.27	1.53	0.42	0.80	0.40	0.25	11.86	0.48	0.28	0.11	0.07	1.40	0.11	0.16	0.32	0.00	0.74	1.15	0.42	0.10	0.14	0.25	0.14	0.52	0.31	11.30
Dive 128																											
E50240		6.04	3.35	1.41	2.53	0.80	1.04	12.38	2.27	0.50	0.20	0.13	1.91	0.27	0.38	0.41	1.98	0.87	0.95	0.32	0.15	0.16	0.25	0.34	0.30	0.16	4.02
E50241		2.41	4.86	0.96	1.71	0.59	0.86	34.42	2.56	0.38	0.33	0.21	4.55	0.11	3.56	0.60	11.00	2.53	1.63	0.87	0.26	0.58	0.35	0.64	2.61	0.73	4.38
E50242		5.07	1.32	0.68	0.76	0.44	0.69	6.42	0.57	0.22	0.10	0.06	0.89	0.10	0.23	0.23	1.35	0.35	0.51	0.14	0.06	0.13	0.16	0.23	0.23	0.10	3.82
E50243		4.14	1.59	0.72	0.82	0.48	1.05	12.13	0.68	0.26	0.13	0.07	1.62	0.09	0.35	0.32	2.24	0.54	0.85	0.28	0.10	0.09	0.20	0.26	0.34	0.13	3.40
E50244		3.39	2.40	0.94	0.97	0.59	1.36	10.21	0.98	0.32	0.16	0.07	1.78	0.10	0.48	0.33	3.29	0.78	0.73	0.24	0.13	0.14	0.18	0.28	0.35	0.12	3.26
E50245		3.59	1.30	0.52	0.48	0.35	0.77	7.64	0.30	0.16	0.08	0.03	1.12	0.05	0.09	0.16	1.17	0.36	0.57	0.25	0.05	0.05	0.12	0.11	0.31	0.10	1.48

Table 5-2: Quantitative composition of light hydrocarbons of the samples analysed in the Purge & Trap gas chromatograph

Peak integration gave quantitative amounts of the substances for all samples from all locations (Table 5-2). Generally, the amounts are very low for most compounds although the vials were purged for 5 min. For the interpretation of the gases an important assumption is that the gas composition of the samples reflect the in situ gas composition of the sampled stratigraphic interval. Lorenson et al. (1999) stated that the headspace extraction technique is very concentration dependant as gases which are well below saturation conditions in situ can be measured realistically whereas gases near of above saturation exsolve rapidly during recovery. Therefore it can be concluded that the samples have undergone some degassing before analysis and that the reported concentrations are minimum concentrations. A second

limitation in the interpretation of the peaks is the heating period (1 h at 90°C) of the vials prior to the analysis as new compound formation can already occur above 30°C (Mills, pers. comm.). However, measurements at room temperature yielded no results. Plotting the amounts of the concentrations (on a logarithmic scale) versus depth shows no depth trends for the single substances (Figure 5-5, Figure 5-6, Figure 5-7 and Figure 5-8). For all four cores it is obvious that the content of methylpropene is two orders of magnitude higher than that of most of the other components, which gives a first indication for bacterial activity. Benzene, methane and ethene are also one order of magnitude higher than the rest of the substances.

The high quantity of benzene is very interesting and can be caused by two reasons, a contamination from a solvent used for cleaning of the sampling devices or as a natural solute in water. McAuliffe (1980) described the solubilities of crude oil compounds namely normal alkanes and aromatic hydrocarbons in water. Benzene has the highest solubility in water and could therefore be used as indication of an underlying petroleum accumulation. Additionally to benzene compounds with higher carbon number e.g. toluene, dimethylbenzenes and so on are found but due to the measurement duration of the dynamic headspace gaschromatography of 30 min not detected in the samples from the Porcupine Basin. As the benzene content of the sediment samples from the Connemara area (MD01-2451G and MD2453) is not higher than the one from the mound sites (MD01-2457 and MD01-2460G) it can be interfered that the benzene concentration is not related to the petroleum accumulation in the Connemara oil field but to an overall background. This implies that petroleum is present basin wide which is confirmed by a study of Burtell and Jones (1996). They use the content of benzene as an effective indictor for the distance of a petroleum reservoir. In the Gulf of Mexico, the benzene content of brines from typical oil reservoirs ranges from about 5 to 20 ppm. Around the accumulations benzene and related aromatic constituents form a plume, which increases in distance from the reservoir. Thereby the distance to an oil reservoir is directly proportional to the log of benzene concentration. For a distance of 20 km they estimate a benzene concentration of 0.1 ppm. In the case of the Porcupine Basin, where the contents are similar for all wells and range between 0.002 to 0.009 ppm (2-9 ng/g rock), the benzene content can be considered as the background from a far away or long existing petroleum accumulation.

Methane and ethane can indicate either thermogenic or biogenic gas. To determine the origin, normally isotiopic ratios are used, but due to the absence of those, other gas ratios were calculated. Ratios of gas component concentrations are used as diagnostic parameters for distinguishing biogenic or thermogenic origins (Kvenvolden and Lorenson, 2000; Lorenson et al., 1999; Whiticar, 1994). The ratios are explained in the following: Lorenson et al. (1999) used the C1/(C2+C3) for the analysis of headspace gas from the Mallik gas hydrate. Bacterial gas is associated with C1/(C2+C3) over or near 1000, thermogenic gas ratios are less than 100. The ratios are normally associated to the carbon isotopes but as no isotope measurements were available in the Porcupine Basin, the ratios can still be used as an indication.

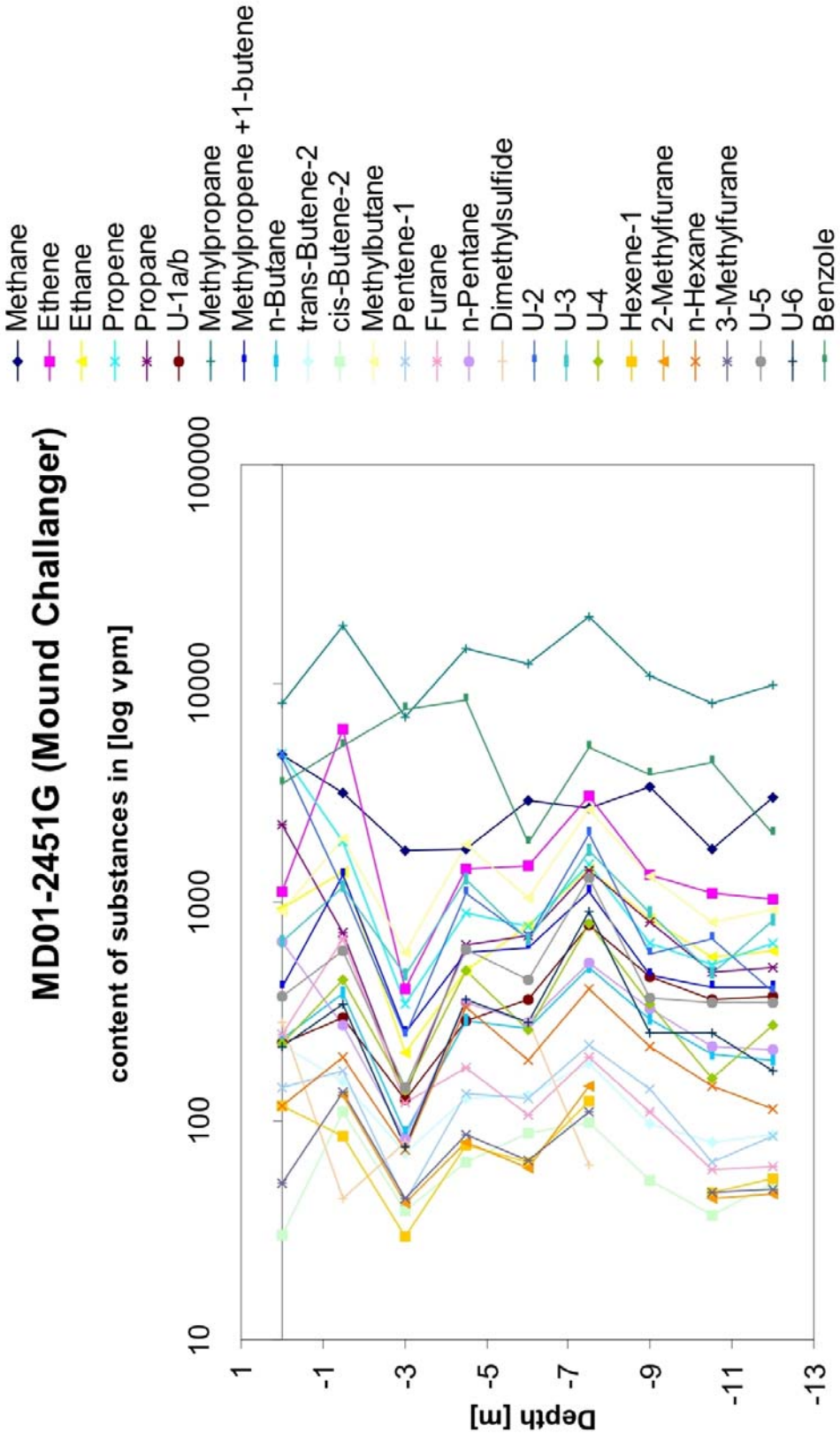

Figure 5-5: Compounds vs. depth plots for gravity core MD01-2451G

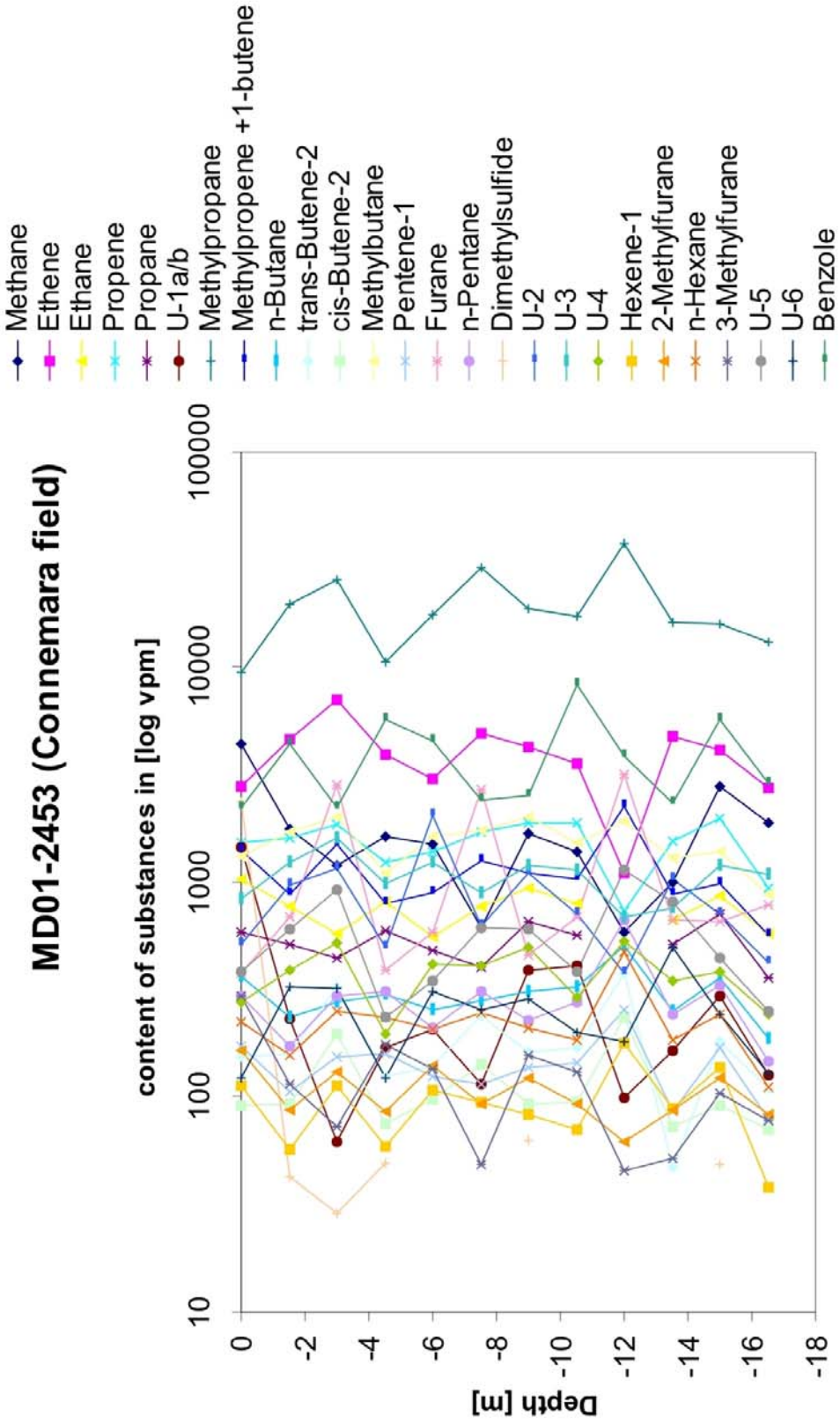

Figure 5-6: Compounds vs. depth plots for gravity core MD01-2453

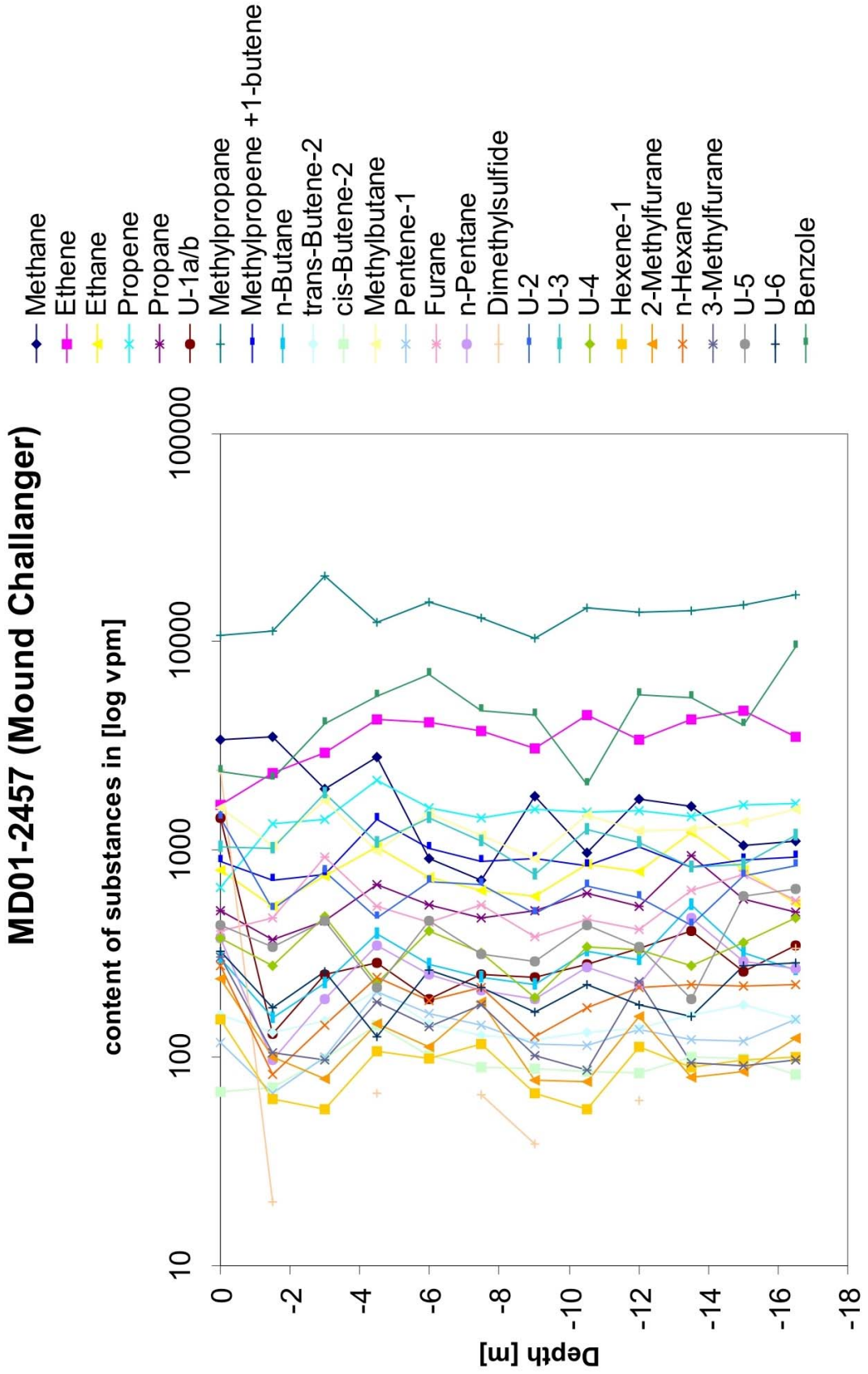

Figure 5-7: Compounds vs. depth plots for gravity core MD01-2457

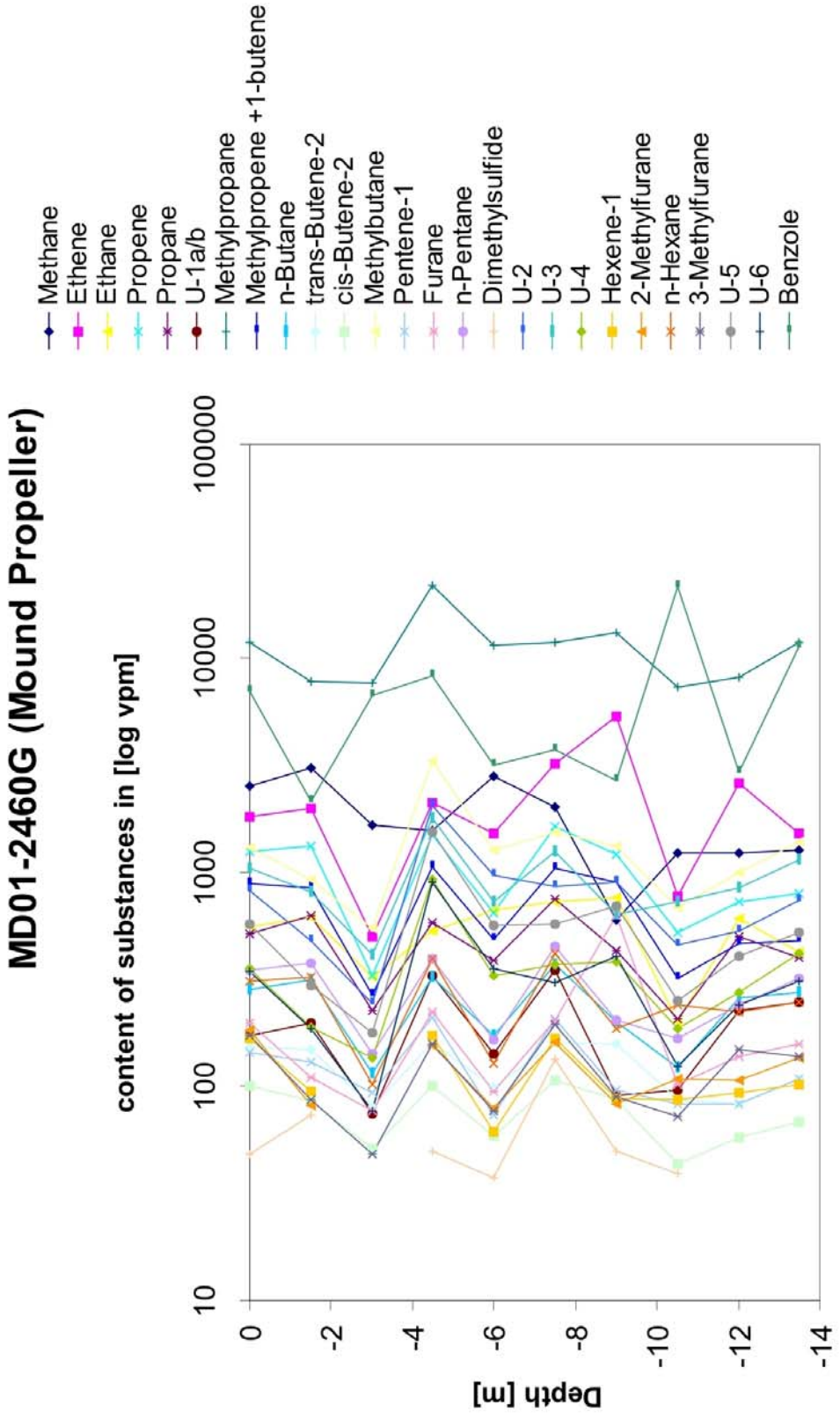

Figure 5-8: Compounds vs. depth plots for gravity core MD01-2460G

Samples	Depth [msfl]	C1/(C2+C3) (Lorenson)	iC4/nC4 (Lorenson)	Gas wetness (Whiticar) (C2+C3+iC4+nC4)/(C1+C2+C3 +iC4+nC4)*100	saturated/unsaturated ((Methane+Ethane+Propane+ Methylpropane+n-Butane+ Methylbutane)/(Ethene+Propene + Methylpropene+1-butene+ trans-2-Butene+cis-2-Butene))	Ethane/Ethene	Propane/Propene	Methylbutane/Furane
MD01-2451G (Mound Challenger 51°22/11°43)								
E50166	0.00	1.48	34.08	70.97	0.52	0.84	0.47	3.64
E50167	-1.50	1.50	48.29	86.91	0.19	0.22	0.38	2.85
E50168	-3.00	5.07	79.41	81.35	0.24	0.51	0.38	4.88
E50169	-4.50	1.55	50.71	90.10	0.16	0.35	0.71	10.48
E50170	-6.00	1.96	46.78	82.92	0.28	0.54	0.91	9.90
E50171	-7.50	0.96	40.19	89.69	0.21	0.46	0.93	13.65
E50172	-9.00	2.04	36.64	79.07	0.36	0.63	1.24	11.99
E50173	-10.50	1.68	40.60	84.27	0.27	0.51	0.93	13.59
E50174	-12.00	2.74	52.27	78.70	0.33	0.58	0.77	14.72
MD01-2453 (Connemara 53°04/12°31)								
E50175	0.00	2.74	25.73	71.93	0.39	0.37	0.38	3.50
E50176	-1.50	1.37	83.73	92.33	0.11	0.17	0.32	2.46
E50177	-3.00	1.18	91.61	95.71	0.07	0.08	0.24	0.71
E50178	-4.50	1.17	35.05	88.20	0.19	0.21	0.48	2.87
E50179	-6.00	1.45	69.78	92.61	0.11	0.19	0.35	2.80
E50180	-7.50	0.52	102.62	98.03	0.05	0.15	0.23	0.64
E50181	-9.00	1.05	60.75	92.44	0.13	0.22	0.35	4.42
E50182	-10.50	1.03	53.00	93.16	0.12	0.22	0.30	2.20
E50183	-12.00		75.09	98.50	0.02	0.00	0.00	0.61
E50184	-13.50	0.85	63.52	94.58	0.10	0.14	0.33	1.97
E50185	-15.00	1.76	44.36	86.55	0.19	0.21	0.36	2.10
E50186	-16.50	2.05	69.89	88.22	0.16	0.21	0.38	1.12
MD01-2457 (Connemara 53°04/12°31)								
E50196	0.00	2.59	36.10	78.55	0.32	0.48	0.77	3.91
E50197	-1.50	3.89	72.79	77.98	0.27	0.23	0.27	2.24
E50198	-3.00	1.63	89.93	91.87	0.12	0.26	0.33	1.86
E50199	-4.50	1.65	31.78	83.83	0.23	0.24	0.31	1.82
E50200	-6.00	0.71	55.51	95.01	0.10	0.18	0.34	3.34
E50201	-7.50	0.65	53.45	95.26	0.10	0.17	0.33	2.16
E50202	-9.00	1.63	45.69	86.54	0.19	0.20	0.33	2.38
E50203	-10.50	0.66	44.98	94.38	0.12	0.19	0.41	3.18
E50204	-12.00	1.32	46.56	89.80	0.16	0.23	0.35	3.00
E50205	-13.50	0.75	25.92	91.31	0.19	0.29	0.65	1.94
E50206	-15.00	0.77	46.83	94.09	0.12	0.17	0.35	1.78
E50207	-16.50	1.04	63.62	94.29	0.10	0.16	0.30	2.72
MD01-2460G (Mound Propeller 52°09/12°46)								
E50208	0.00	2.37	42.14	83.94	0.22	0.31	0.41	6.63
E50209	-1.50	2.47	24.71	75.16	0.35	0.31	0.47	8.38
E50210	-3.00	3.01	66.64	83.44	0.25	0.64	0.69	7.16
E50211	-4.50	1.41	67.87	93.67	0.10	0.25	0.39	14.80
E50212	-6.00	2.67	66.58	81.95	0.26	0.44	0.60	13.28
E50213	-7.50	1.36	32.09	87.17	0.20	0.23	0.46	7.58
E50214	-9.00	0.50	65.12	96.05	0.09	0.14	0.35	2.12
E50215	-10.50	3.02	60.09	86.44	0.18	0.26	0.39	6.76
E50216	-12.00	1.12	31.26	88.47	0.20	0.23	0.68	7.18
E50217	-13.50	1.55	42.82	91.06	0.15	0.28	0.50	8.82

Table 5-3: Ratios calculated from gas concentrations of the gravity core samples

Kvenvolden and Lorenson (2000) also showed that the ratios of iC_4/nC_4 are less than 1 in the case of thermogenic origin of a gas. The gas wetness was used after Whiticar (1994) and is defined as (C2 + C3 + iC4 + nC4) / (C1 + C2 + C3 + iC4 + nC4)*100. The relative proportions of C1-C4 n-alkanes can be used as an initial classification of natural gas as higher homologs are abundant in bacterial gas. Kvenvolden (2000) showed the same for ratios of saturated to unsaturated alkanes, ethane to ethene and propane to propene ratio. Values below 0.5 indicate dry gas, which can indicates bacterial gas but isotopic investigations are needed to confirm this. Additionally, a ratio of methylbutane to furane was set up as the visible investigation of the peak size in the chromatograms indicated that the content of methylbutane seems to be contrariwise to the content of furan. The ratios are presented in Table 5-3.

The C1/(C2+C3) ratio varies between 0.5 and 5.0 (Table 5-3) and indicates a clear thermogenic gas (Lorenson et al., 1999). The gas wetness with an average of 88 also indicates a thermogenic origin of the hydrocarbons based on the classification of Haworth et al. (1985).

However, the methylpropane (iso-butane)/n-butane ratio with an average about 54 shows clear evidence of bacterial activity. The traces of ethane, ethene, propane, propene, butane and pentane which have been formed by microbial fermentation processes also indicate the presence of bacteria (Hunt, 1984). Kvenvolden and Lorenson (2000) measured also methane, ethane, ethene, propane, propene, isobutene, n-butane, neopentane, isopentane, n-pentane, cyclopentane, neohexane, isohexane, n-hexane, and isoheptane in clearly biogenic gases on cores of Leg 164 on the southeastern North American continental margin. In contrast to the measurements of Kvenvolden and Lorenson (2000) the contents of ethene, propene, n-butane, neopentane, isopentane, n-pentane, cyclopentane, neohexane, isohexane, n-hexane, and isoheptane in the Porcupine cores were negligible. The ratio of propane to propene ranges from 0.2 to 0.9 indicating a mixture of thermogenic and biogenic origin. A similar behaviour shows the ethane to ethene ratio, which varies between 0.1 and 0.8.

Interestingly the propane/propene and ethane/ethene ratios are higher in the cores from the mound areas MD01-2451G from Mound Challenger and MD01-2460G from Mound Propeller than in the cores in the Connemara area. This can be related to higher bacterial activity due to the living and dead corals in the mound areas.

Dimethylsulfides are produced by marine algae (Steinke et al., 2002). Dacey and Wakeham (1986) described mesozooplankton grazing on dimethylsulfide-producing microalgae on oil slicks. In the Porcupine Basin dimethylsulfide was only found in higher concentrations in the seafloor sediments in the Connemara oil field - with underlying gas chimneys - indicating the presence of marine algae feeding on weak microseeping hydrocarbons, which can be controlled by diffusion (van der Meer et al., 2002).

Furans have been described by various authors, e.g. (Baldock and Smernik, 2002; Bartoschek et al., 2000; Marynowski et al., 2001). Baldock et al. 2002 described the conversion of O alkyl C to aryl and O.aryl furan-like structures in *Pinus resinosa* wood caused by increasing temperatures for example during forest fires. Dioxins and furans are also described to be emitted during combustion, Marynowski et al. (2001) described furans as pyrolysis products. As a conclusion, the occurrence of furans could indicate the impact of terrigenous transported material. In contrast Bartoschek et al. (2000) described the N-Carboxymethanofuran (carbamate) formation from unprotonated mehtanofuran (MFR) and CO_2 as the first reaction in the reduction of CO_2 to methane in methanogenic archea. Therefore furan could indicate the presence of archea.

Plotting the methylbutane-furane ratio versus depth shows that the ratio increases with depth in core MD01-2451 but shows no similar trend in the three other cores (Figure 5-9). This is astonishing as core MD01-2451G is located in the Connemara area and one would expect a similar result for the nearby core MD01-2457. Finding an explanation would require more work, which is not possible due to the limited amount of time for this study, as this can be seen as a promising idea for future work.

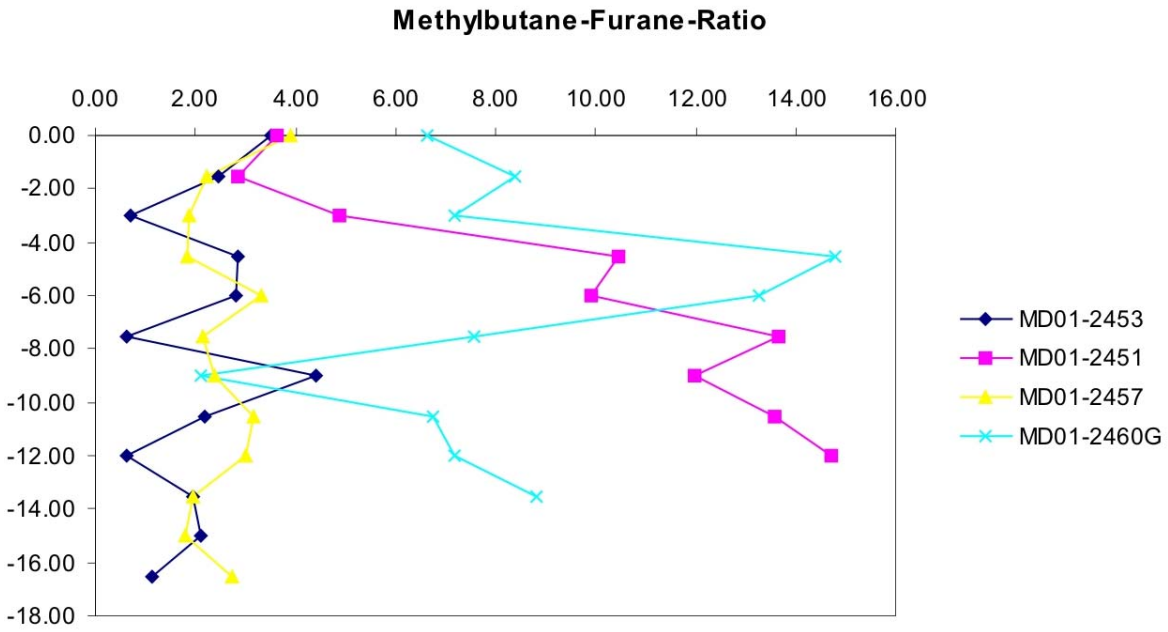

Figure 5-9: Methylbutane-Furane-Ratio

The results, obtained on the sediments for the gravity cores of the Marion Dufresne cruise are problematic in their interpretation. In areas typical for hydrocarbon seepage values of about 10's to 100's of ppm for methane are commonly found in the sediment. These measurements are usually made directly on site. Onboard methane measurements during

ODP-legs show in sediments directly overlying gas hydrates on the Bahamas low to no methane concentrations in the first 20 – 30 m of the sediment column (Kvenvolden et al., 1989; Kvenvolden and McDonald, 1989; McDonald et al., 1989; Vuletich et al., 1989; Whiticar and Faber, 1989a; Whiticar and Faber, 1989b). As the sampled long cores are typically about 16 m this lack of high gas concentrations could be a natural effect indicating that the penetration of the cores was not deep enough to reach sedimentary layers with enhanced methane contents. The sampling method itself provided some pit-falls, which complicated determination of the gas composition.

Measurements by the static and dynamic headspace gas chromatographic technique showed only traces of gases. The low amount of gas can have two reasons: first the gas can be lost on the way from the sea floor to the deck of Marion Dufresne and further on to FZJ, secondly there may be no methane or other light hydrocarbons in the sediment. The loss of gas during travel time from sea floor to the ship can't be excluded but the sampling procedure seemed to prevent much gas from escaping. The core entered the sediment with a velocity of 1 m/s. In the middle part of the core the sediment seemed to be undisturbed. The sediment consisted of a coral network with a filling of carbonaceous clay or mudstone. These lithologies have a very low permeability and there were no signs of gas-escape structures. Also no extraordinary bubbles were seen when the cores were taken out of the water. In addition in the core of mound Therese (MD01-2462) a strong H_2S smell was recognised when the sediment was forced out of the core liner. The ongoing degassing during sampling indicates that a total loss of all light hydrocarbons seems to be unlikely.

Furthermore, the samples were frozen at –80°C prior to and during transport. During the storage on dry ice the headspace of the vials was replaced by CO_2 due to leaky seals. But the results of the analysed cans have shown only slightly higher gas contents, taking the higher amount of the sediment into account. On the other hand the measured gas content of the vials represents the amount of gas, which was trapped in the sediment in situ. No bias due to atmospheric methane during the sampling procedure is expected.

Combined with the observations from the Caracole Cruise in august 2001, where a methane sniffer tool was brought to the sea floor and failed to detect even traces of methane it seems that there is no or only very little active leakage of hydrocarbons at present (J.-C. Caprais pers. comm.). This is confirmed by the dynamic headspace gas chromatographic analysis, which also showed no clear evidence of hydrocarbon seepage. However, McDonnell and Shannon (2001) showed that the mounds root on the mid Miocene (C20) respectively Pliocene (C10) horizon. As mound growth is supposed to be triggered by hydrocarbon seepage, indications should be found in the pre-Pliocene sediments, which have not been penetrated by the gravity cores. However, purge and trap headspace analysis showed that the amounts of light hydrocarbons are very low eliminating the idea of active hydrocarbon macroseepage. However, an indication of both thermogenic and biogenic gas is given by various ratios and presence of individual substances. A final estimation could be provided by isotopic characterization of the gases.

Carbon isotopes were determined on sample 50167 from Mound Challenger at a depth of 1.5 mbsf. The analysis was done on a Finnigan MAT DeltaXP, Isotope Ratio Mass Spectrometer (Applied Petroleum Technology AS, Norway). The hydrocarbon contents were below detection limit. Therefore only carbon isotopes of CO_2 could be determined and yielded a $\delta^{13}C$-value of 15.5. Martini et al. (1999) showed that gas, taken from the New Albany Shale in the Illinois Basin, is clearly of microbial origin when $\delta^{13}C$ of the CO_2 is higher than 10, which implies a microbial origin of the CO_2 in the core from Mound Challenger.

5.3 Biomarker Analysis

Sediment samples 50170 (6 mbsf) and 50174 (12 mbsf) from mound Challenger (Belgica mound province), 50184 (13.5 mbsf) and 50206 (15 mbsf) from the Connemara field as well as 50208 (0 mbsf) and 50213 (7.5 mbsf) from mound Propeller (Hovland-Magellan mound province) were analyzed with regard to their molecular biomarker composition using the analytical method described in Mangelsdorf et al. (2000). Special molecular indicators (biomarkers) for anaerobic methanotrophs are archaeol or hydroxyarchaeol (Hinrichs et al., 1999) and some isoprenoids like crocetane and pentamethylicosane (PMI) (Elvert et al., 1999; Thiel et al., 1999). Useful indicators for oil-derived hydrocarbons are 17a-hopanes and steranes as well as aromatic steranes and diamondoids (Shimoyama and Yabuta, 2002).

The free lipid fractions of the investigated sediment samples are characterized by a large variety of organic compounds of marine, terrestrial and bacterial sources typical for continental slope sediments (Mangelsdorf, pers. comm.). They comprise n-alkanes, n-alcohols, sterols, n-fatty acids and hopanoids. The n-alkanes occur in the range from C_{14} to C_{33}. Their distribution is dominated by long-chain n-alkanes from C_{23} to C_{33} with a maximum mostly at n-C_{29} and a strong odd-over-even carbon number predominance, indicating the immature character of these compounds. The observed n-alkane composition is typical of an origin from epicuticular waxes of higher land plants (Eglinton and Hamilton, 1967) and represents therefore terrestrial derived organic material in the investigated sediments. The presence of terrigenous organic material is confirmed by the occurrence of long-chain n-alcohols in the carbon number range of C_{22} to C_{30} and by the appearance of some C_{29}-sterols (e.g. 24 Ethylcholest-5 en-3b ol (b-sitosterol)) in the Connemara sediments. The n-alcohol distributions show their maximum mostly at C_{26} and a strong even-over-odd carbon number predominance, which is also typical of epicuticular waxes of higher land plants (Eglinton and Hamilton, 1967). Organic matter of marine origin is indicated by n-fatty acids with 14, 16 and 18 carbon atoms and some C_{27}- and C_{28}-sterols (e.g. 24-Methylcholesta-5,22E-dien-3b-ol (diatomsterol)). Saturated and unsaturated fatty acids in the low carbon number range are presumably derived mainly from algae (Cranwell, 1974) and diatomsterols is a main sterol in diatoms (Volkman, 1986) and also present in other microalgae, such as haptophytes and cryptophytes (Volkman et al., 1998). Hopenes (e.g. Hop-17(21)-ene) and hopanes in their biogenic 17b, 21b-configuration represent bacterial biomass in all investigated sediments. However, special microbial biomarkers for methanotrophic microbial communities, as mentioned above, are not detectable. Although hopanes in their mature most stable 17a,

21b-configuration could be detected in all sediments, the total hopane distribution as well as the absence of other oil biomarkers seems not to support the presence of migrated oil-derived hydrocarbons in the sediments investigated.

6 Conclusions

Basin Modelling

- A total of five 2D cross sections, based on seismic data, were modelled in this study. The seismic profiles RE25, RE94 and RE88 were used for the development of a regional understanding of basin evolution, whereas a refined interpretation of RE94 as well as lines PORC97-12 and CS2 were used for the detailed migration modelling.

- A conceptual model for the Porcupine Basin was developed under consideration of input parameters such as age, thickness, porosity, lithology and physical properties. The burial and thermal history of the Porcupine Basin was reconstructed dating the extension of the basin to Late Jurassic and mid-Cretaceous and to the Paleocene based on the influence of the Iceland Plume. Early Cenozoic uplift was taken into account.

- The Upper Jurassic strata was defined as the main source rock. For the basin modelling TOC values of 4 % and a Hydrogen Index (HI) of 550 mgHC/gTOC were used. Additional source rock properties were assigned to the Lower Jurassic with TOC values of 1.8 % and a hydrocarbon index of 550 mgHC/gTOC.

- Modelling results suggest that Jurassic and older source rocks are mature to overmature throughout the basin. Cretaceous strata are immature to mature in the central part of the basin and immature on the flanks. The Cenozoic sequence remains immature over the entire basin.

- Hydrocarbon generation started in Late Cretaceous times for the deepest Jurassic sequences. Based on the compositional kinetic model used, the Upper Jurassic source rock generates undersaturated black oil within the oil window, while gas condensate dominates at higher maturities. Phase separation was modelled to occur during migration at depth ranges between 2000 and 3000m (depending on the fluid composition). Upon phase separation the migration of the free gas phase dominates over that of the oil, such that gas is the main migrating fluid in the shallower intervals.

- Migration is mainly buoyancy driven and vertical. The only way to direct hydrocarbon flow out of the basin is along Aptian and Cenozoic sand horizons. Modelling predictions over the entire basin indicate gas breaking through to the seafloor.

- Fractures and faults are limited to local areas in Jurassic and Early Cenozoic sediments. Although the properties of the faults remain unknown, sensitivity studies with permeable and impermeable faults indicate that the fluid flow pattern does not change significantly due to migration along these faults. Overall, fluid flow through the pore framework is the favoured transport mechanism. Permeability changes could direct fluid flow but no obvious evidence was found.

Organic Geochemistry

- Core samples from exploration wells were used for micropetrographic maturity investigation and source rock and oil analysis. The measured vitrinites reflectance values fitted well in the range of the published data and were used for the calibration of the model. Source rock samples could not be sampled but the over- and underlying strata were analysed and confirmed more or less the published data of marine to lacustrine type Jurassic source rock. The analysis of the crude oils revealed the same results.

- Gravity core samples from carbonate mounds were taken on the cruise of R/V Marion Dufresne 2001 and trapped light hydrocarbons were analysed with the static and dynamic headspace gas chromatography. The overall content of light hydrocarbons in the sediment is very low and not in the range typical of leakage related sediments. However, traces of thermogenic-derived hydrocarbons were detected.

- Additionally biological markers were determined on the gravity core samples. They showed evidence of normal marine sediments but no evidence of migrated oils nor of biomarkers indicating methanotrophic bacteria.

Carbonate Mounds

- On the line PORC97-12 representing the geology in the Belgica mound province, the model predicts a significant focussing of gas migration towards the Belgica mounds where a pinch out of Cretaceous and Cenozoic layers beneath the mound area is observed.

- In the 2D studies of the Hovland-Magellan mound province no obvious focussing of hydrocarbon leakage towards the Hovland-Magellan mound province was observed. This lack of focussing could be a problem related to either lack of sufficient stratigraphic detail in the model or related to the inadequacy of using a 2D model for the simulation of an essentially 3D process.

- Using drainage area analysis (map based flow modelling) the locations of surface mounds in the Hovland-Magellan mound province correlate significantly well with mapped closures in the Oligocene (C30), Base Miocene, Mid-Miocene (C20) and Pliocene (C10) indicating the likelihood of a link between preferred sites of leakage and mound location. By contrast, the locations of buried mounds in this area follow mapped drainage boundaries pointing towards a possible link to a deeper structural feature focussing hydrocarbons towards the mound area.

- Geochemical analysis indicate a thermogenic origin of hydrocarbons in the Pliocene – recent sediments but could not show a clear evidence of hydrocarbon leakage. However, a limitation to this method is that the cores do not penetrate pre-Pliocene sediments as the mounds root on the Pliocene unconformity and as hydrocarbon

leakage is supposed to trigger mound growth evidence of leakage should be found in the pre-Pliocene sediments.

- The results of this study suggest that in addition to pockmarks and mud volcanoes, deep water carbonate mounds are surface expressions of the underlying active petroleum system.

7 References

Abrams, M.A., 1996. Distribution of subsurface hydrocarbon seepage in near-surface marine sediments, Hydrocarbon migration and its near-surface expression. American Association of Petroleum Geologists, Tulsa, OK, United States, pp. 1-14.

Abu-Ali, M.A., Rudkiewicz, J.L.L., McGillivray, J.G. and Béhar, F., 1999. Paleozoic petroleum system of central Saudi Arabia. GeoArabia (Manama), 4(3): 321-336.

Ahr, W.M. and Stanton, R.J., 1999. Common characteristics of frameless carbonate mounds, Geological Society of America, 1999 annual meeting. Geological Society of America (GSA), Boulder, CO, United States, pp. 241.

Allen, J.R.L. and Wells, J.W., 1962. Holocene coral banks and subsidence in the Niger delta. Journal of Geology, 70(4): 381-397.

Ancellin, J., 1957. Observations sur la faune et les fonds de pêche de quelques secteurs de la Manche et des mers nordiques. Revue des travaux de l'institut des pêches Maritimes, 21: 4.

Aref, M.A.M., 1998. Biogenic carbonates; are they a criterion for underlying hydrocarbon accumulations? An example from the Gulf of Suez region, Egypt. AAPG Bulletin, 82(2): 336-352.

Auffret, G.A. et al., 1987. Geologie de escarpements de Porcupine et de Goban (NE Atlantique). Resultats de la plonge CYAPORC. Comtes Rendus de L'Academie des Sciences, 304: 1003-1008.

Bachu, S. and Underschultz, J.R., 1995. Large-scale underpressuring in the Mississippian-Cretaceous succession, southwestern Alberta Basin. AAPG Bulletin, 79(7): 989-1004.

Bailey, W.R., Shannon, P.M., Walsh, J.J. and Unnithan, V., submitted. The spatial distributions of faults and deep sea carbonate mounds in the Porcupine Basin, offshore Ireland. Marine and Petroleum Geology.

Baldock, J.A. and Smernik, R.J., 2002. Chemical composition and bioavailability of thermally altered Pinus resinosa (Red pine) wood. Organic Geochemistry, 33(9): 1093-1109.

Ballard, R.D., Francheteau, J., Juteau, T., Rangin, C. and Normack, W., 1986. East Pacific Rise at 21°N: The volcanic, tectonic, and hydrothermal processes of the central axis. Earth and Planetary Science Letters, 55: 1-10.

Barnes, R.O. and Goldberg, E.D., 1976. Methane production and consumption in anoxic marine sediments. Geology (Boulder), 4(5): 297-300.

Barry, J.P., Kochevar, R.E. and Baxter, C.H., 1997. The influence of pore-water chemistry and physiology in the distribution of vesicomyid clams at cold seeps in Monterey Bay: Implications for patterns of chemosynthetic community organization. Limnol Oceanogr, 42: 318-328.

Bartoschek, S., Vorholt, J.A., Thauer, R.K., Geierstanger, B.H. and Griesinger, C., 2000. N-Carboxymethanofuran (carbamate) formation from mehtanofuran and CO_2 in mehtanogenic archea, Thermodynamics and kinetics of the spontaneous reaction. Eur. J. Biochem., 267: 3130-3138.

Bathurst, R.G.C., 1975. Diagenetic fabrics in some British Dinantian limestones, Sedimentary rocks; concepts and history. Dowden Hutchinson & Ross Inc., Stroudsburg, Pa., United States.

Baudin, F., 1995. Depositional controls on Mesozoic source rocks in the Tethys, Paleogeography, paleoclimate, and source rocks. American Association of Petroleum Geologists, Tulsa, OK, United States, pp. 191-213.

Baxter, K., Buddin, T., Corcoran, D.V. and Smith, S., 2001. Structural modelling of the south Porcupine Basin, offshore Ireland: implications for the timing, magnitude and style of crustal extension. In: P.M. Shannon, P.D.W. Haughton and D.V. Corcoran (Editors), The Petroleum Exploration of Ireland's Offshore Basins. Geological Society Special Publication, pp. 275-290.

Béhar, F., Vandenbroucke, M., Tang, Y., Marquis, F. and Espitalié, J., 1997. Thermal cracking of kerogen in open and closed systems: determination of kinetic parameters

and stoichiometric coefficients for oil and gas generation. Organic Geochemistry, 26(5/6): 321-339.
Bjørlykke, K., 1997. An overview of factors controlling rates of compaction, fluid generation and flow in sedimentray basins.
Bjørlykke, K. and Høeg, K., 1997. Effects of burial diagenesis on stresses, compaction and fluid flow in sedimentary basins. Marine and Petroleum Geology, 14(3): 267-276.
Blanc, P. and Connan, J., 1994. Preservation, degradation, and destruction of trapped oil, The petroleum system; from source to trap. American Association of Petroleum Geologists, Tulsa, OK, United States, pp. 237-247.
Blanco, C.G., Prado, J.G., Guillen, M.D. and Borrego, A.G., 1992. Preliminary results of extraction experiments in an oil shale, Collected papers from the Seventh annual meeting of the Society for Organic Petrology. Pergamon, Oxford-New York, International, pp. 313-316.
Boetius, A. et al., 2002. Microbial Systems in Sedimentary Environments of Continental Margins. In: G. Wefer et al. (Editors), Ocean Margin Systems. Springer-Verlag, pp. 479-495.
Boetius, A. et al., 2000. A marine microbial consortium apparently mediating anaerobic oxidation of methane. Nature (London), 407(6804): 623-626.
Bosence, D.W.J. and Bridges, P.H., 1995. A review of the origin and evolution of carbonate mud-mounds. Spec. Publs int. Ass. Sediment., 23: 3-9.
Both, R. et al., 1986. Hydrothermal chimneys and associated fauna in the Manus Back Arc Basin, Papua, New Guinea. Eos, Transactions, American Geophysical Union, 67: 489-490.
Bouchet, P. and Waren, A., 1991. Ifremeria nautilei, Nouveau gastéropode d'èvents hydrothermaux, problement associé à des bactéries symbiotiques. C. R. Acad. Sci, 312(3): 495-501.
Brodie, J. and White, N., 1995. The link between sedimentary basin inversion and igneous underplating. In: J.G. Buchanan and P.G. Buchanan (Editors), Geological Society Special Publications. Geological Society of London, London, pp. 21-38.
Brown, A., 2000. Evaluation of possible gas microseepag mechanisms. AAPG Bulletin, 84(11): 1775-1789.
Brown, K.M., 1990. The nature and hydrogeologic significance of mud diapirs and diatremes for accretionary systems, Special section on the Role of fluids in sediment accretion, deformation, diagenesis, and metamorphism in subduction zones. American Geophysical Union, Washington, DC, United States, pp. 8969-8982.
Burnham, A.K., 1989. A simple kinetic model of petroleum formation and cracking. Lawrence Livermore National Laboratory Report UCID- 21665: 11p.
Burnham, A.K., 1995. Relationship between hydrous and ordinary pyrolysis, Composition, geochemistry and conversion of oil shales. D Reidel Publishing Company, Dordrecht-Boston, Netherlands, pp. 211-227.
Burtell, S.G. and Jones, V.T., III, 1996. Benzene content of subsurface brines can indicate proximity of oil, gas. Oil and Gas Journal, 94(23): 59-64.
Butterworth, P., Holba, A., Hertig, S., Hughes, W. and Atkinson, C., 1999. Jurassic non-marine source rocks and oils of the Porcupine Basin and other North Atlantic margin basins. In: A.J. Fleet and S.A.R. Boldy (Editors), Petroleum Geology of Northwest Europe: Proceedings of the 5th Conference, pp. 471-486.
Carruthers, D.J. and van Wijngaarden, M.d.L., 2000. Modelling viscous-dominated fluid transport using modified invasion percolation techniques, Proceedings of Geofluids III; third international conference on Fluid evolution, migration and interaction in sedimentary basins and orogenic belts. Elsevier, Amsterdam-New York, International, pp. 669-672.
Cartwright, J.A. and Lonergan, L., 1996. Volumetric contraction during the compaction of mudrocks: a mechanism for the development of regional-scale polygonal fault systems. Basin Research, 8: 183-193.

Castanier, S., Le, M.L.G. and Perthuisot, J.P., 2000. Bacterial roles in the precipitation of carbonate minerals, Microbial sediments. Springer, Berlin, Federal Republic of Germany.

Cavagna, S., Clari, P. and Martire, L., 1999. The role of bacteria in the formation of cold seep carbonates: geological evidence from Monferrato (Tertiary, NW Italy). Sedimentary Geology, 126: 253-270.

Clayton, C.J. and Hay, S.J., 1994. Gas migration mechanisms from accumulation to surface. Bulletin of the Geological Society of Denmark, 41: 12-23.

Coles, G.P., Ainsworth, N.R., Whatley, R.C. and Jones, R.W., 1996. Foraminifera and Ostracoda from Quaternary carbonate monds associated with gas seepage in the Porcupine Basin, Offshore Western Ireland. Revista Espanola de Micropaleontologia, XXVIII(2): 113-151.

Corfield, S., Murphy, N. and Parker, S., 1999. The structural and stratigraphic framework of the Irish Rockall Trough. In: A.J. Fleet and S.A.R. Boldy (Editors), Petroleum geology of Northwest Europe. Geological Society of London, London, pp. 407-420.

Corliss, J.B. et al., 1979. Submarine thermal springs on the Galapagos Rift. Science, 203(4385): 1073-1083.

Cornford, C., 1998. Source rocks and hydrocarbons of the North Sea.; 4, Petroleum geology of the North Sea; basic concepts and recent advances. Blackwell Science Geology & Petroleum Geology, Oxford, United Kingdom.

Crane, K., 1985. The distribution of geothermal fields along the mid-ocean ridge; an overview, Hydrothermal vents of the eastern Pacific; an overview. INFAX Corporation for the Biological Society of Washington, Vienna, VA, United States, pp. 3-18.

Crane, K. et al., 1985. The distribution of geothermal fields on the Juan de Fuca Ridge. Jgr, Journal of Geophysical Research. B. 90(1): 727-744.

Cranwell, P.A., 1974. Monocarboxylic acids in lake sediments; indicators, derived from terrestrial and aquatic biota, of paleoenvironmental trophic levels. Chemical Geology, 14(1-2): 1-14.

Croker, P. and Klemperer, S.L., 1989. Structure and Stratigraphy of the Porcupine Basin: Relationships to Deep Crustal Structure and the Opening of the North Atlantic. AAPG Memorial, 46: 445-459.

Croker, P.F. and O'Loughlin, O., 1998. A catalogue of irish offshore carbonate mud mounds. TTR-7 Post Cruise Conference on Carbonate Mud Mounds and Cold Water Reefs: 1-13.

Croker, P.F. and Shannon, P.M., 1987. The evolution and hydrocarbon prospectivity of the Porcupine Basin, Offshore Ireland. In: J. Brooks and K. Glennie (Editors), Petroleum Geology of North West Europe - Proceedings of the 3rd Conference on Petroleum Geology of North West Europe. Graham & Trotman, London/Dordrecht/Boston, pp. 633-642.

Croker, P.F. and Shannon, P.M., 1995. The Petroleum Geology of Ireland's Offshore Basins: introduction. Geological Society Special Publication, 93: 1-8.

Dacey, J.W.H. and Wakeham, S.G., 1986. Oceanic dimethylsulfide: production during zooplankton grazing on phytoplankton. Science, 233: 1314-13416.

de Mol, B. et al., 2002. Large deep-water coral banks in the Porcupine Basin, southwest of Ireland, European North Atlantic Margin (ENAMII); quantification and modelling of large-scale sedimentary processes. Elsevier, Amsterdam, Netherlands, pp. 193-231.

Dean, K., McLachlan, K. and Chambers, A., 1997. Rifting and the development of the Faeroe-Shetland Basin. In: A.J. Fleet and S.A.R. Boldy (Editors), Petroleum Geology of Northwest Europe, Proceedings of the 5th Conference, London, pp. 534-544.

Demaison, G. and Huizinga, B.J., 1991. Genetic classification of petroleum systems. AAPG Bulletin, 75(10): 1626-1643.

Desbruyères, D., Alayse-Danet, A.M. and Ohta, S., 1991. Deep-sea hydrothermal communities in two southwestern back-arc basins (the North Fiji and Lau basins):

Composition microdistribution and food web, paper presented at 6th Deep-Sea Bilogy Symposium, Univ. of Copenhagen.
Desbruyères, D. and Laubier, L., 1989. Raralvinella hessleri, New species of Alvinellidae (Polychaeta) from Mariana Back-Arc Basin hydrothermal vents. Proc. Biol. Soc. Wash., 102: 761-767.
di Primio, R., Dieckmann, V. and Mills, N., 1998. PVT and phase behaviour analysis in petroleum exploration. Org. Geochm., 29(1-3): 207-222.
di Primio, R. and Horsfield, B., 1996. Predicting the generation of heavy oils in carbonate/ evaporitic environments using pyrolysis methods, Proceedings of the 17th international meeting on Organic chemistry; Part III, Origin of natural gases; petroleum geochemistry, impact of organic geochemistry on exploration; migration and expulsion of oil and gas. Pergamon, Oxford-New York, International, pp. 999-1016.
di Primio, R., Horsfield, B. and Guzman-Vega, M.A., 2000. Determining the temperature of petroleum formation from the kinetic properties of petroleum asphaltenes. Nature, 406: 173-176.
di Primio, R., Skeie, J.E. and Horsfield, B., 2002. Compositional modelling of hydrocarbon generation and migration: A case study from the Tampen Spur, Norway. Schriftenreihe der Deutschen Geologischen Gesellschaft, GEO 2002, Planet Erde: Vergangenheit, Entwicklung, Zukunft: 269.
Diaz-del-Rio, V. et al., 2003. Vast fields of hydrocarbon-dervied carbonate chimneys related to the accretionary wedge/olistostrome of the Gulf of Cádiz. Marine Geology, 196: 1-24.
Dick, H.v.d., Meloche, J.D., Dwyer, J. and Gunther, P., 1989. Source-Rock Geochemistry and Hydrocarbon Generation in the Jeanne D'Arc Basin, Grand Banks, Offshore Eastern Canada. Journal of Petroleum Geology, 12(1): 51-68.
Dieckmann, V., Schenk, H.J., Horsfield, B. and Welte, D.H., 1998. Kinetics of petroleum generation and cracking by programmed-temperature closed-system pyrolysis of Toarcian Shales. Fuel, 77(1/2): 23-31.
Drozd, R., 1983. The Bullmoose Mine Project. CIM Bulletin (1974), 76(853): 54-59.
Durand, S.C., 1980. Thermogravimetric analysis and associated techniques applied to kerogens, Kerogen; insoluble organic matter from sedimentary rocks. Ed Technip, Paris, France.
Edwards, J.W.F., 2002. Development of the Hatton - Rockall Basin, North - East Atlantic Ocean. Marine and Petroleum Geology, 19: 193-202.
Eglinton, G. and Hamilton, R.J., 1967. Leaf epicuticular waxes. Science, 156: 1322-1335.
Elder, J.W., 1965. Physical process in geothermal areas, Chapter 8, Terrestrial heat flow.
Elvert, M., Suess, E. and Whiticar, M.J., 1999. Anaerobic methane oxidation associated with marine gas hydrates; superlight C-isotopes from saturated and unsaturated C20 and C25 irregular isoprenoids. Naturwissenschaften, 86(6): 295-300.
England, W.A., MacKenzie, A.S., Mann, D.M. and Quigley, T.M., 1987. The movement and entrampment of petroleum fluids in the subsurface. Journal of the Geological Society, London, 144: 327-347.
Erdmann, M., 1999. Gas Generation from Overmature Upper Jurassic Source Rocks, Northern viking Graben. PhD-thesis Thesis, 128 pp.
Espitalié, J., Deroo, G. and Marquis, F., 1985. La pyrolyse Rock-Eval et ses applications. Deuxième partie: Interprétation des paramèters. Rev. Inst. Fr. Pét., 40: 755-784.
Espitalié, J. et al., 1977. Méthode rapide de caractérisation des roches mères de leur potential petrolier et de leur degré d'evolution. Rev. Inst Fr. Petr., 32: 23-42.
Farrow, G.E. and Durant, G.P., 1985. Carbonate-basaltic sediments from Cobb Seamount, Northeast Pacific; zonation, bioerosion and petrology. Marine Geology, 65(1-2): 73-102.
Fleischer, R.L., Price, P.B. and Walker, R.M., 1975. Nuclear Tracks in Solids - Principles and Applications. University of California Press, Berkeley, 605 pp.

Foerster, A. and Merriam, D.F., 1999. Problems and potential of industrial temperature data from a cratonic basin environment. In: A. Foerster and D.F. Merriam (Editors), Geothermics in basin analysis, pp. 35-59.
Fowler, C.M.R. and Tunnicliffe, V., 1997. Hydrothermal vent communities and plate tectonics. Endeavour, New Series, 21(4): 164-168.
Fowler, M.G. and McAlpine, K.D., 1995. The Egret Member, a Prolific Kimmeridgian Source Rock from Offshore Eastern Canada. In: B. Katz (Editor), Petroleum Source Rocks. Springer-Verlag, New York, pp. 111-130.
Francheteau, J. et al., 1981. First manned submersible dives on the East Pacific Rise at 21 degrees N (project RITA); general results. Marine Geophysical Researches, 4(4): 345-379.
Frederiksen, R., Jensen, A. and Westerberg, H., 1992. The distribution of the Scleractinian Coral *Lophelia Pertusa* around the Faroe Islands and the Relation to internal tidal mixing. Sarsia, 77: 157-171.
Freiwald, A., 2002. Reef-Forming Cold-Water Corals. In: G. Wefer et al. (Editors), Ocean Margin Systems. Springer-Verlag, pp. 365-385.
Freiwald, A., Wilson, J.B. and Henrich, R., 1999. Grounding Pleistocene icebergs shape recent deep-water coral reefs. Sedimentary Geology, 125: 1-8.
Fujikura, K., Hashimoto, J. and Okutani, T., 1991. Preliminary account of gastropods associated with hydrothermal vents and cold seeps aound Japan, paper presented at 6th Deep-Sea Bilogy Symposium, Univ. of Copenhagen.
Garb, F.A. and Smith, G.L., 1987. Estimation of oil and gas reserves. In: H.B. Bradley (Editor), Petroleum Engineering Handbook. Society of Petroleum Engineers, pp. 4-40.
Garland, C.R., Haughton, P., King, R.F. and Moulds, T.P., 1999. Capturing reservoir heterogeneity in a sand-rich submarine fan, Miller Field, Petroleum geology of Northwest Europe; proceedings of the 5th conference. The=Geological Society of London, London, United Kingdom, pp. 1199-1208.
Genin, A., Dayton, P.K., Lonsdale, P.F. and Spiess, F.N., 1986. Corals on seamount peaks provide evidence of current acceleration over deep-sea topography. Nature, 322: 59-61.
Giles, M.R., 1997. Diagenesis: A Quantitative Perspective, Imolications for Basin Modelling and Rock Property Prediction. Kluwer Academic Publishers, Dordrecht, 526 pp.
Gooday, A.J. and Rathburn, A.E., 1999. Temporal variability in living deep-sea benthic Foraminifera; a review. In: F.M. Gradstein and G.J. van der Zwaan (Editors), Ordering the fossil record; challenges in stratigraphy and paleontology; selected papers from a symposium held in honour of the 75th birthday of Cor Drooger. Earth-Science Reviews. Elsevier, Amsterdam, pp. 187-212.
Grassle, J.F., 1985. Hydrothermal vent animals; distribution and biology. Science, 229: 713-717.
Grassle, J.F., 1986. The evology of deep-sea hydrothermal vent communities. Advances in Marine Biology, 23: 301-362.
Grassle, J.F., Humphris, S.E., Rona, P.A., Thompson, G. and van, D.C.L., 1986. Animals at Mid-Atlantic Ridge hydrothermal vents, AGU 1986 fall meeting and ASLO winter meeting. American Geophysical Union, Washington, DC, United States, pp. 1022.
Green, P.F. et al., 1989. THermal annealing of fission tracks in apatite, 4. Quantitative modelling techniques and extension to geological timescales. Chem. Geol., 79: 155-182.
Han, M.W. and Suess, E., 1989. Subduction induced pore fluid venting and the formation of authigenic carbonates along the Cascadia continental margin: Implications for the global Ca-Cycle. Palaeogeography, Palaeoclimatology, Palaeoecology, 71: 97-118.
Hantschel, T., Kauerauf, A.I. and Wygrala, B., 2000. Finite element analysis and ray tracing modeling of petroleum migration, Thematic set on hydrocarbon migration. Elsevier, Oxford, United Kingdom, pp. 815-820.

Harder, J., 1997. Anaerobic methane oxidation by bacteria employing ^{14}C-methane uncontaminated with ^{14}C-carbon monoxide. Marine Geology, 127(1-2): 12-23.
Hashimoto, J., Fujikura, K. and Ohta, S., 1991. Vent communities around Japan, paper presented at 6th Deep-Sea Bilogy Symposium, Univ. of Copenhagen.
Hawkins, J.W., Lonsdale, P.F., Macdougall, J.D. and Volpe, A.M., 1990. Petrology of the axial ridge of the Mariana Trough backarc spreading center, The Mariana Trough; special section. Elsevier, Amsterdam, Netherlands, pp. 226-250.
Haworth, J.H., Sellens, M. and Whittaker, A., 1985. Interpretation of hydrocarbon shows using light (C_1 -C_5) hydrocarbon gases from mud-log data. AAPG Bulletin, 69(8): 1305-1310.
Heezen, B.C. and Tharp, M., 1977. World Ocean Floor.
Henrich, R. et al., 1995. Controls on Modern Carbonate Sedimentation on Warm-temperate to Arctic Coast, Shelves and Seamounts in the Northern Hemisphere: Implications for Fossil Counterparts. Facies, 32: 71-108.
Henrich, R. et al., 1996. Nordic Cold-Water Carbonates: Occurrences and Controls. In: J. Reitner, F. Neuweiler and F. Gunkel (Editors), Global and Regional Controls on Biogenic Sedimentation. I. Reef Evolution, Research Reports. Göttinger Arb. Geol. Paläont., Göttingen, pp. 35-52.
Henriet, J.P., Guidard, S. and Team, O.P., 2002. Carbonate Mounds as a Possible Example for Microbial Activity in Geological Processes. In: G. Wefer et al. (Editors), Ocean Margin Systems. Springer-Verlag, pp. 439-455.
Henriet, J.P. et al., 1998. Gas hydrates may help build reefs. Nature, 391(12): 648-649.
Hessler, R.R. and Lonsdale, P., 1991. Bogeography of Marinaa Trough hydrothermal vent communities. Deep Sea Res., 38: 185-199.
Higgins, G.E. and Saunders, J.B., 1973. Mud volcanoes - their nature and origin: contribution to the geology and paleobiology of the Carribbean and adjacent areas. Verh. Naturforsch. Geschel. Basel, 84: 101-152.
Hildenbrand, A., Angabini, A. and Krooss, B., 2001. Permeability measurements on rock samples from the Porcupine Basin, RWTH Aachen, Lehrstuhl für Geologie, Geochemie und Lagerstätten des Erdöls und der Kohle.
Hinrichs, K.U. and Boetius, A., 2002. The Anaerobic Oxidation of Methane: New Insights in Microbial Ecology and Biogeochemistry. In: G. Wefer et al. (Editors), Ocean Margin Systems. Springer-Verlag, pp. 457-477.
Hinrichs, K.U., Hayes, J.M., Sylva, S.P., Brewer, P.G. and DeLong, E.F., 1999. Methane-consuming archaebacteria in marine sediments. Nature (London), 398(6730): 802-805.
Hoehler, T.M. and Alperin, M.J., 1996. Anaerobic methane oxidation by a methanogen-sulfate reducer consortium: geochemical evidence and biochemical considerations. In: M.E. Lidstrom and F.R. Tabita (Editors), Microbial Growth on C_1 Compounds. Kluwer Academic Publisher, Dordrecht, pp. 326-333.
Hoehler, T.M., Alperin, M.J., Albert, D.B. and Martens, C.S., 1994. Field and laboratory studies of methane oxidation in an anoxic marine sediment; evidence for a methanogen-sulfate reducer consortium. Global Biogeochemical Cycles, 8(4): 451-463.
Holland, C.H., 1981. A Geology of Ireland. Scottish Academic Press., Edinburgh, 335 pp.
Horsfield, B. et al., 1994. Organic geochemistry of freshwater and alkaline lacustrine sediments in the Green River Formation of the Washakie Basin, Wyoming, U.S.A, Advances in organic geochemistry 1993; proceedings of the 16th international meeting on Organic geochemistry. Pergamon, Oxford-New York, International, pp. 415-440.
Horsfield, B. and Rullkoetter, J., 1994. Diagenesis, catagenesis, and metagenesis of organic matter, The petroleum system; from source to trap. American Association of Petroleum Geologists, Tulsa, OK, United States, pp. 189-199.

Horsfield, B., Schenk, H.J., Mills, N. and Welte, D.H., 1991. An investigation of the in-reservoir conversion of oil to gas: compositional and kinetic findings from closed-system programmed-temperature pyrolysis. Advances in Organic Geochemistry, 19(1-3): 191-204.
Horvitz, L., 1939. On geochemical prospecting; I. Geophysics, 4(3): 210-228.
Horvitz, L., 1969. Hydrocarbon geochemical prospecting after thirty years, Unconventional methods in exploration for petroleum and natural gas. Southern Methodist University, Dallas, TX, United States.
Horvitz, L., 1980. Near-surface evidence of hydrocarbon movement from depth, Problems of petroleum migration. American Association of Petroleum Geologists, Tulsa, OK, United States, pp. 241-269.
Horvitz, L., 1981. Hydrocarbon geochemical prospecting after forty years. Unconventional Methods in Exploration for Petroleum and Natural Gas, 2: 83-95.
Horvitz, L., 1985a. Geochemical exploration for petroleum. Science, 229(4716): 821-827.
Horvitz, L., 1985b. Hydrocarbon geochemical exploration after fifty years. Unconventional Methods in Exploration for Petroleum and Natural Gas.
Hovland, M., 1990. Do carbonate reefs form due to fluid seepage? Terra nova, 2: 8-18.
Hovland, M., Croker, P.F. and Martin, M., 1994. Fault-associated seabed mounds (carbonate knolls?) off western Ireland and north-west Australia. Marine and Petroleum Geology, 11: 232-246.
Hovland, M., Mortensen, P.B., Brattegard, T., Strass, P. and Rokoengen, K., 1998. Ahermatypic Coral Banks off Mid-Norway: Evidence for a Link with Seepage of Light Hydrocarbons. Palaios, 13: 189-200.
Hovland, M., Talbot, M.R., Qvale, H., Olaussen, S. and Aasberg, L., 1987. Methane-Related Carbonate Cements in Pockmarks of the North Sea. Journal of Sedimentary Petrology, 57(5): 881-892.
Hunt, J.M., 1979. Petroleum geochemistry and geology. W.H. Freemand and Company, San Francisco, 617 pp.
Hunt, J.M., 1984. Generation and migration of light hydrocarbons. Science, 226(4680): 1265-1270.
Hunt, J.M., 1996. Petroleum Geochemistry and Geology. W. H. Freeman and Company, New York, 743 pp.
Huvenne, V. et al., in press. The Magellan mound province in the Porcupine Basin. In: J.P. Henriet and C. Dullo (Editors), North Atlantic carbonate mounds: clues towards their genesis, development and significance. Springer-Verlag.
Huvenne, V., Croker, P.F. and Henriet, J.P., 2002. A refreshing 3D view of an ancient sediment collapse and slope failure. Terra Nova, 14: 33-40.
Ivanov, M.K. et al., 2000. Goals and principal result of the TTR-9 cruise. Final Porc. Int. Conf. Geological Porcesses on European continental Margins, Granada, Spain, UNESCO IOC Workshop Report 168: 3-4.
Iversen, N. and Jørgensen, B.B., 1985. Anerobic methane oxidation rates at the sulfate-methane transition in marine sediments from Kattegat and Skagerrak (Denmark). Limnol Oceanogr, 30: 944-955.
Jackson, M.D. and Blunt, M.J., 2002. Elliptic regions and stable solutions for three-phase flow in porous media. Transport in Porous Media, 48(3): 249-269.
Jacqué, M. and Thouvenin, J., 1975. Lower Tertiary Tuffs and Volcanic Activity in the North Sea. In: A.W. Woodland (Editor), Petroleum and the Continentla Shelf of North-west Europe, London, pp. 455-465.
James, N.P., 1997. The cool-water carbonate depositional realm, Cool-water carbonates. SEPM (Society for Sedimentary Geology), Tulsa, OK, United States, pp. 1-20.
James, N.P. and Clarke, J.A.D., 1997. Cool-Water Carbonates. SEPM Special Publication, 56.
Jarvis, G.T. and McKenzie, D.P., 1980. Sedimentary Basin Formation with finite extension rates. Earth and Planetary Science Letters, 48: 42-52.

Jones, M.L., 1985. Hydrothermal vents of the eastern Pacific: An overview. Bull. Biol. Soc. Wash. 6, 547 pp.

Joppen, M. and White, R.S., 1990. The Structure and Subsidence of Rockall Trough From Two-Ship Seismic Experiments. Journal of Geophysical Research, 95(B12): 19821-19837.

Juniper, S.K. and Sibuet, M., 1987. Cold seep benthic communities in Japan subduction zones: Spatial organization, trophic strategies and evidence for temporal evolution. Mar. Ecol Prog. Ser., 40: 115-126.

Juniper, S.K., Tunnicliffe, V. and Desbruyères, D., 1990. Reginal-scale features of northeast Pacific, East Pacific Rise, and Gulf of Aden vent communities. In: G.R. McMurray (Editor), Gorda Ridge, A Seafloor Spreading Center in the United States' Exclusive Economic Zone. Springer-Verlag, pp. 965-967.

Kaluza, M.J. and Doyle, E.H., 1996. Detecting fluid migration in shallow sediments; continental slope environment, Gulf of Mexico, Hydrocarbon migration and its near-surface expression. American Association of Petroleum Geologists, Tulsa, OK, United States, pp. 15-26.

Katz, A.J. and Thompson, A.H., 1987. Quantitative prediction of permeability and electrical conductivity in porous rock, Abstracts of papers presented at the 56th annual international SEG meeting. Society of Exploration Geophysicists, Tulsa, OK, United States, pp. 378.

Kelley, D.S., Delaney, J.R. and Yoerger, D.R., 2001. Geology and venting characteristics of the Mothra hydrothermal field, Endeavour Segment, Juan de Fuca Ridge. Geology (Boulder), 29(10): 959-962.

Kelley, J.T., Dickson, S.M., Belknap, D.F., Barnhardt, W.A. and Henderson, M., 1994. Giant sea-bed pockmarks; evidence for gas escape from Belfast Bay, Maine. Geology (Boulder), 22(1): 59-62.

Kennicutt, M.C., II and Brooks, J.M., 1988. Relation between shallow sediment bitumens and deeper reservoired hydrocarbons, offshore Santa Maria Basin, California, U.S.A. Applied Geochemistry, 3(6): 573-582.

Killops, S.D. and Killops, V.J., 1993. An Introduction to Organic Geochemistry. Longman Scientific and Technical, New York.

Kimura, M. et al., 1988. Study of topography, hydrothermal deposits and animal colonies in the middle Okinawa Trough hydrothermal areas using the submersible Shinkai 2000 system. Deep Sea Res., 5: 224-244.

Kjennerud, T. and Sylta, O., 2001. Application of quantitative palaeobathymetry in basin modelling, with reference to the northern North Sea. Petroleum Geoscience, 7(4): 331-341.

Knott, S.D., Burchell, M.T., Jolley, E.J. and Fraser, A.J., 1993. Mesozoic to Cenozoic plate reconstructions of the North Atlantic and hydrocarbon plays of the Atlantic margins. In: J.R. Parker (Editor), Petroleum Geology of Northwest Europe: Proceedings of the 4th Conference. The Geological Society, London, pp. 953-974.

Kopaska-Merkel, D.C. and Haywick, D.W., 2001. Carbonate mounds: sedimentation, organismal response and diagensis. Sedimentary Geology, 145: 157-159.

Kvenvolden, K.A., Golan, B.M., McDonald, T.J., Pflaum, R.C. and Brooks, J.M., 1989. Hydrocarbon gases in sediment of the Voring Plateau, Norwegian Sea, Proceedings of the Ocean Drilling Program, Norwegian Sea; covering Leg 104 of the cruises of the Drilling Vessel JOIDES Resolution, Bremerhaven, Germany, to St John's, Newfoundland, Sites 642-644, 19 June 1985-23 August 1985. Texas A & M University Ocean Drilling Program, College Station, TX, United States, pp. 319-326.

Kvenvolden, K.A. and Lorenson, T.D., 2000. Methane and other hydrocarbon gases in sediment from the southeastern North American continental margin, Proceedings of the Ocean Drilling Program; volume 164; scientific results; gas hydrate sampling on the Blake Ridge and Carolina Rise; covering Leg 164 of the cruises of the drilling vessel JOIDES Resolution, Halifax, Nova Scotia, to Miami, Florida, sites 991-997, 31

October-19 December 1995. Texas A & M University Ocean Drilling Program, College Station, TX, United States, pp. 29-36.
Kvenvolden, K.A. and McDonald, T.J., 1989. Organic geochemistry on Leg 104, Proceedings of the Ocean Drilling Program, Norwegian Sea; covering Leg 104 of the cruises of the Drilling Vessel JOIDES Resolution, Bremerhaven, Germany, to St John's, Newfoundland, Sites 642-644, 19 June 1985-23 August 1985. Texas A & M University Ocean Drilling Program, College Station, TX, United States, pp. 291-307.
Langmuir, C. et al., 1997. Hydrothermal vents near a mantle hot spot; the Lucky Strike vent field at 37 degrees N on the Mid-Atlantic Ridge. Earth and Planetary Science Letters, 148(1-2): 69-91.
Le Danois, E., 1948. Les profundeurs de la mer. Trente ans de recherches sur la faune sous-marine au large des côtes de France. Payot: 303-321.
Lee, Y. and Deming, D., 2002. Overpressures in the Anadarko Basin, southwestern Oklahoma; static or dynamic? AAPG Bulletin, 86(1): 145-160.
Lees, A. and Miller, J., 1995. Waulsortian banks, Carbonate mud-mounds; their origin and evolution. Blackwell, Oxford, International, pp. 191-271.
Lein, A.Y., Ivanov, M.V., Pimenov, N.V. and Gulin, M.B., 2002. Geochemical Peculiarities of the Carbonate Constructions Formed during Microbial Oxidation of Methane under Anerobic Conditions. Microbiology, 71(1): 78-90.
Leischner, K., Welte, D.H. and Littke, R., 1993. Fluid inclusions and organic maturity parameters as calibration tools in basin modelling, Basin modelling; advances and applications; proceedings of the Norwegian Petroleum Society conference. Elsevier, New York, International, pp. 161-172.
Lerche, I., 1990. Philosophies and strategies of model building. In: T.A. Cross (Editor), Quantitative dynamic stratigraphy, pp. 21-44.
Link, W.K., 1952. Significance of oil and gas seeps in world oil exploration. Bulletin of the American Association of Petroleum Geologists, 36(8): 1505-1540.
Lonsdale, P., 1977. Structural geomorphology of a fast-spreading rise crest; the East Pacific Rise near 3 degrees 25'S. Marine Geophysical Researches, 3(3): 251-293.
Lorenson, T.D., Whiticar, M.J., Waseda, A., Dallimore, S.R. and Collett, T.S., 1999. Gas composition and isotopic geochemistry of cuttings, core, and gas hydrate from the JAPEX/ JNOC/ GSC Mallik 2L-38 gas hydrate research well, Scientific results from JAPEX/ JNOC/ GSC Mallik 2L-38 gas hydrate research well, Mackenzie Delta, Northwest Territories, Canada. Geological Survey of Canada, Ottawa, ON, Canada, pp. 143-163.
Ludwick, J.C. and Walton, W.R., 1957. Shelf-edge calcareous prominences in northeastern Gulf of Mexico. Bulletin of the American Association of Petroleum Geologists, 41(9): 2054-2101.
Lundin, E. and Doré, A.G., 2002. Mid-Cenozoic post-breakup deformation in the 'passive' margins bordering the Norwegian-Greenland Sea. Marine and Petroleum Geology, 19: 79-93.
Lutz, R.A., 1984. Deep-sea hydrothermal vents: Oases on the ocean floor. In: D. Calhoun (Editor), 1985 Yearbook of Science and the Future, Encyclopaedia Britannica, pp. 226-242.
Lutz, R.A. and Kennish, M.J., 1993. Ecology of deep-sea hydrothermal vent communities; a review. Reviews of Geophysics, 31(3): 211-242.
MacDonald, H., Allan, P.M. and Lovell, J.P.B., 1987. Geology of oil accumulation in Block 26/28, Porcupine Basin, Offshore Ireland. In: J. Brooks and K. Glennie (Editors), Petroleum Geology of North West Europe. Graham & Trotman, pp. 643-651.
Magoon, L.B. and Dow, W.G., 1994. The Petroleum System. In: L.B. Magoon and W.G. Dow (Editors), The petroleum system - from source to trap. AAPG Memoir, pp. 3-24.
Mangelsdorf, K., Guentner, U. and Rullkoetter, J., 2000. Climatic and oceanographic variations on the California continental margin during the last 160 kyr. Organic Geochemistry, 31(9): 829-846.

Mann, U. et al., 1997. Petroleum migration; mechanisms, pathways, efficiencies and numerical simulation. In: D.H. Welte, B. Horsfield and D.R. Baker (Editors), Petroleum and basin evolution; insights from petroleum geochemistry, geology and basin modeling. Springer, Berlin, Federal Republic of Germany.

Martini, A.M., Walter, L.M., McIntosh, J.C. and Budai, J.M., 1999. Identification of Microbial Methane Deposist via Core Analysis, Ninth Annual V. M. Goldschmidt Conference, Cambridge.

Marynowski, L., Czechowski, F. and Simoneit, B.R.T., 2001. Phenylnaphthalenes and polyphenyls in Palaeozoic source rocks of the Holy Cross Mountains, Poland. Organic Geochemistry, 32(1): 69-85.

Masson, D.G. and Miles, P.R., 1986. Structure and Development of Procupine Seabight Sedimentary Basin, Offshore Southwest Ireland. The Amereican Association of Petroleum Geologists Bulletin, 70(5): 536-548.

Matthews, M.D., 1996. Migration; a view from the top, Hydrocarbon migration and its near-surface expression. American Association of Petroleum Geologists, Tulsa, OK, United States, pp. 139-155.

McAlpine, K.D., 1990. Mesozoic stratigraphy, sedimentary evolution, and petroleum potential of the Jeanne d'Arc basin, Grand Banks of Newfoundland. Geol. Surv. Can. Pap., 89(17): 1-50.

McAuliffe, C.D., 1980. Oil and gas migration; chemical and physical constraints, Problems of petroleum migration. American Association of Petroleum Geologists, Tulsa, OK, United States, pp. 89-107.

McCuen, R.H., 1973. The role of sensitivity analysis in hydrologic modeling. Journal of Hydrology, 18(1): 37-53.

McDonald, T.J., Kennicutt, M.C., II, Brooks, J.M. and Kvenvolden, K.A., 1989. Organic matter at sites 642, 643, and 644, ODP Leg 104, Proceedings of the Ocean Drilling Program, Norwegian Sea; covering Leg 104 of the cruises of the Drilling Vessel JOIDES Resolution, Bremerhaven, Germany, to St John's, Newfoundland, Sites 642-644, 19 June 1985-23 August 1985. Texas A & M University Ocean Drilling Program, College Station, TX, United States, pp. 309-317.

McDonnell, A., 2001. Comperative Tertiary Basin Development in the Porcupine and Rockall Basins. unpublished PhD thesis National University of Ireland Thesis, University College of Dublin, Dublin, 201 pp.

McDonnell, A. and Shannon, P.M., 2001. Comparative Tertiary stratigraphic evolution of the Porcupine and Rockall Basins. In: P.M. Shannon, P.D.W. Haughton and D.V. Corcoran (Editors), The Petroleum Exploration of Ireland's Offshore Basins. Geological Society, pp. 323-345.

McKenzie, D., 1978. Some Remarks on the Development of Sedimentary Basins. Earth and Planetry Science Letters, 40: 25-32.

McMurray, G.R., 1990. Gorda Ridge, A Seafloor Spreading Center in the United States' Exclusive Economic Zone, 311 pp.

Miall, A.D., 1990. Principles of Sedimentary Basin Analysis. Springer-Verlag, New York, 668 pp.

Miall, A.D., 1997. The Geology of Stratigraphic Sequences. Springer, Berlin-Heidelberg.

Michaelis, W. et al., 2002. Microbial reefs in the Black Sea fueled by anaerobic oxidation of methane. Science, 297(5583): 1013-1015.

Milkov, A.V., 2000. Worldwide distribution of submarine mud volcanoes and associated gas hydrates. Marine Geology, 167: 29-42.

Miura, T. and Ohta, S., 1991. Two olychaete species from the deep-sea hydrothermal vent in the middle Okinawa Trough. Zool. Sci, 8: 383-387.

Molenaar, N. and Zijlstra, J.J.P., 1997. Differential early diagenetic low-Mg calcite cementation and rhythmic hardground development in Campanian-Maastrichtian chalk. Sedimentary Geology, 109(3-4): 261-281.

Monty, C.L.V., 1995. The rise and nature of carbonate mud-mounds: an introductory actualistic approach. Spec. Publs int. Ass. Sediment., 23: 11-48.
Moore, J.G., 1993. A Seismic and Sequence Stratigraphic Study of the Cretaceous and Tertiary Succesions of the Porcupine Basin, offshore Ireland. Phd Thesis, University College Dublin, Dublin, 254 pp.
Moore, J.G. and Shannon, P.M., 1991. Slump structures in the Late Tertiary of Porcupine basin, offshore Ireland. Marine and Petroleum Geology, 8: 184-197.
Moore, J.G. and Shannon, P.M., 1992. Palaeocene-Eocene deltaic sedimentation, Porcupine Basin, offshore Ireland - a sequence stratigraphic approach. First Break, 10(12): 461 - 469.
Moore, J.G. and Shannon, P.M., 1995. The Cretaceous succession in the Porcupine Basin, offshore Ireland: facies distribution and hydrocarbon potential. In: P.F. Croker and P.M. Shannon (Editors), The Petroleum Geology of Ireland's Offshore Basins. Geological Society Special Publication, 93, pp. 345-370.
Mortensen, P.B., Hovland, M., Brattegard, T. and Farestveit, R., 1995. Deep water bioherms of the scleractinian coral Lophelia pertusa (L.) at 64 N on the Norwegian Shelf: structure and associated emgafauna. Sarsia: 145-158.
Morton, A.C. et al., 1988. Early Tertiary volconic rocks in Well 163/6-1A, Rockall Trough. In: A.C. Morton and L.M. Parson (Editors), Early Tertiary Vocanism and the Opening of the NE Atlantic, Geological Society Special Publication No. 39, pp. 293-308.
Mounji, D., Bourque, P.A. and Savard, M.M., 1998. Hydrothermal origin of Devonian conical mounds (kess-kess) of Hamar Lakhdad Ridge, Anti-Atlas, Morocco. Geology (Boulder), 26(12): 1123-1126.
Mullins, H.T., Newton, C.R., Heath, K. and Vanburen, H.M., 1981. Modern Deep-Water Coral Mounds north of little Bahama bank: Criteria for Recognition of deep-water coral bioherms in the rock record. Jorunal of Sedimentary Petrology, 51(3): 999-1013.
Muscio, G.P.A., Horsfield, B. and Welte, D.H., 1994. Occurrence of thermogenic gas in the immature zone; implications from the Bakken in-source reservoir system, Advances in organic geochemistry 1993; proceedings of the 16th international meeting on Organic geochemistry. Pergamon, Oxford-New York, International, pp. 461-476.
Nadin, P.A., Kusznir, N.J. and Cheadle, M.J., 1997. Early Tertiary plume uplift of the North Sea and Faeroe-Shetland basins. Earth and Planetry Science Letters, 148: 109-127.
Naeser, N.D., 1993. Apatite fission-track analysis in sedimentary basins - a critical appraisal. In: A.G. Doré (Editor), Basin Modelling: Advances and Applications. NPF Special Publication, pp. 147-160.
Nauhaus, K., Boetius, A., Krüger, M. and Widdel, F., 2002. In vitro demonstration of anaerobic oxidation of methane coupled to sulphate reduction in sediment from a marine gas hydrate area. Environmental Microbiology, 4(5): 296-305.
Naylor, D. and Anstey, N.A., 1987. A reflection study of the Porcupine Basin, offshore Ireland. Irish Journal of Earth Sciences, 8: 187-210.
Naylor, D. and Sevastopulo, G.D., 1979. The Hercynian "Front" in Ireland. Krystalinikum, 14: 77-90.
Naylor, D. and Shannon, P.M., 1982. The Geology of Offshore Ireland and West Britain. Graham & Trotman Ltd., London, 161 pp.
Neumann, A.C., Kofoed, J.W. and Keller, G.H., 1977. Lithoherms in the Straits of Florida. Geology (Boulder), 5(1): 4-10.
Noeth, S., Thomsen, R.O. and Littke, R., 2002. A method for assessing statistical significance and incertainties for calibraton of 1D thermal basin maturation models. AAPG Bulletin, 86(3): 417-431.
O'Brien, G.W. et al., 2002. Influence of hydrocarbon migration and seepage on benthic Communities in the Timor Sea, Australia. Second Proof, 3(4): 225-240.
Olu-Le Roy, K., Duperret, A., Sibuet, M., Foucher, J.P. and Fiala-Médioni, A., 1996a. Structure and distribution of codl seep communities along the Peruvian active margin: Relationship to geological and fluid patterns. Mar. Ecol Prog. Ser., 132: 109-125.

Olu-Le Roy, K., Sibuet, M., Harmegnies, F., Foucher, J.P. and Fiala-Médioni, A., 1996b. Spatial distribution of diverse cold seep communities living on various diapiric structures of the southern Barbados prism. Prog. Oceanogr., 38: 347-376.

Paull, C.K., Ussler, W., III, Borowski, W.S. and Spiess, F.N., 1995. Methane-rich plumes on the Carolina continental rise; associations with gas hydrates. Geology (Boulder), 23(1): 89-92.

Peckmann, J. et al., 1999. Cold seep deposits of Beauvoisin (Oxfordian, southeastern France) and Marmorito (Miocene; northern Italy): microbially authignic carbonates. In Journ Earth Sciences, 88: 60-75.

Pepper, A.S. and Corvi, P.J., 1995. Simple kinetic models of petroleum formation. Part I: oil and gas generation from kerogen. Marine and Petroleum Geology, 12(3): 291-319.

Pepper, A.S. and Dodd, T.A., 1995. Simple kinetic models of petroleum formation. Part II: oil - gas cracking. Marine and Petroleum Geology, 12(3): 321-340.

Peters, K.E. and Moldowan, J.M., 1993. The biomarker guide; interpreting molecular fossils in petroleum and ancient sediments. Prentice Hall, Englewood Cliffs, NJ, United States, 363 pp.

Peters, K.E., Whelan, J.K., Hunt, J.M. and Tarafa, M.E., 1983. Programmed pyrolysis of organic matter from thermally altered Cretaceous black shales. AAPG Bulletin, 67(11): 2137-2146.

Poelchau, H.S., Baker, D.R., Hantschel, T., Horsfield, B. and Wygrala, B.P., 1997. Basin Simulation and the Design of the Conceptual Model. In: D.H. Welte, B. Horsfield and D.R. Baker (Editors), Petroleum and Basin Evolution, pp. 3-62.

Poelchau, H.S., Zwach, C., Hantschel, T. and Welte, D.H., 1999. Effect of oil and gas saturation on simulation of temperature history and maturation. In: D.F. Merriam and A. Foerster (Editors), Geothermics in basin analysis. Kluwer Academic/Plenum Publishers, New York, NY, United States.

Pratt, B.R., 1995. The origin, biota and evolution of deep-water mud-mounds. Spec. Publs int. Ass. Sediment., 23: 49-123.

Price, L.C., 1986. A critical overview and proposed working model of surface geochemical exploration, Unconventional methods in exploration for petroleum and natural gas IV. Inst Study Earth and Man South, Methodist Univ.

Rad, U.v. et al., 1996. Authigenic carbonates derived from oxidized methane vented from the Makran accretionary prism off Pakistan. Marine Geology, 136: 55-77.

Radke, M., Horsfield, B., Littke, R. and Rullkoetter, J., 1997. Maturation and petroleum generation, Petroleum and basin evolution; insights from petroleum geochemistry, geology and basin modeling. Springer, Berlin, Federal Republic of Germany.

Radke, M. and Welte, D.H., 1983. The methylphenanthrene index (MPI); a maturity parameter based on aromatic hydrocarbons. In: M. Bjoroey et al. (Editors), Proceedings of the International Meeting on Organic Geochemistry. Chichester, New York, pp. 504-512.

Radke, M., Willsch, H. and Welte, D.H., 1980. Preparative Hydrocarbon Group Type Determination by Automated Medium Pressure Liquid Chromatography. Anal. Chem., 52: 406-411.

Reed, D.L., Silver, E.A., Tagudin, J.E., Shipley, T.H. and Vrolijk, P., 1990. Relations between mud volcanoes, thrust deformation, slope sedimentation, and gas hydrate, offshore North Panama. Marine and Petroleum Geology, 7(1): 44-54.

Rhodes, E.G. et al., 1992. Reservoir engineering methods, Development geology reference manual. American Association of Petroleum Geologists, Tulsa, OK, United States, pp. 503-541.

Riddihough, R.P. and Max, M.D., 1976. A geological framework for the continental margin to the west of Ireland. Geological Journal, 11(Part 2): 109-120.

Ritger, S., Carson, B. and Suess, E., 1987. Methane-derived authigenic carbonates formed by subduction-induced pore-water expulsion along the Oregon/ Washington margin; with Suppl. Data 87-02. Geological Society of America Bulletin, 98(2): 147-156.

Roberts, D.G., Masson, D.G., Montadert, L. and De, C.O., 1981. Continental margin from the Porcupine Seabight to the Armorican marginal basin, Petroleum geology of the continental shelf of North-West Europe; Proceedings of the second conference. Heyden and Son, London, United Kingdom.

Roberts, H.H., 1998. Evidence of episodic delivery of fluids and gases to the seafloor and impacts of delivery rate on surficial geology (Gulf of Mexico), American Association of Petroleum Geologists 1998 annual meeting. American Association of Petroleum Geologists and Society of Economic Paleontologists and Mineralogists, Tulsa, OK, United States.

Roberts, H.H. and Aharon, P., 1994. Hydrocarbon-derived carbonate buildups of the northern Gulf of Mexico continental slope; a review of submersible investigations. In: P. Aharon (Editor), In: Hydrocarbon seeps and vents. Geo-Marine Letters, pp. 135-148.

Rona, P.A., 1980. TAG hydrothermal field; Mid-Atlantic Ridge crest at latitude 26 degrees N, Metallogenesis at oceanic spreading centres. Geological Society of London, London, United Kingdom, pp. 385-402.

Rootare, H.M., 1970. A review of mercury porosimetry. Perspectives in Powder Metallurgy, 5: 225-253.

Schaefer, R.G., 1999. Petroleum Kinetic Modeling. In: C.P. Marshall and R.W. Fairbridge (Editors), Encyclopedia of Geochemistry. Kluwer Academic Publishers, Dordrecht, Netherlands, pp. 499-500.

Schaefer, R.G., Disko, U. and Willsch, H., 2002. Organic-Geochemical Characterization of Crude Oils from the Connemara Field Area, offshore Ireland, Part A: High-molecular-weight hydrocarbons, FZJ/ICG-4 Interner Bericht Nr. 500202.

Schaefer, R.G., Schenk, H.J., Hardelauf, H. and Harms, R., 1990. Determination of gross kinetic parameters for petroleum formation from Jurassic source rocks of different maturity levels by means of laboratory experiments, Advances in Organic Geochemistry 1989; Part I, Organic Geochemistry in Petroleum Exploration. Pergamon, pp. 115-120.

Schaefer, R.G., Willsch, H., Leistner, F. and Naeth, J., 2003. Determination of low-molecular-weight organic compounds in sediments of the Porcupine Basin by means of a dynamic headspace technique. Data report. FZJ/ICG-V Internal Report No. 500203.

Schenk, H.J., Di Primio, R. and Horsfield, B., 1997a. The conversion of oil into gas in petroleum reservoirs. Part 1: Comparative kinetic investigation of gas generation from crude oils of lacustrine, marine and fluviodeltaic origin by programmed-temperature closed-system pyrolysis. Org. Geochm., 26(7/8): 467-481.

Schenk, H.J. and Horsfield, B., 1993. Kinetics of petroleum generation by programmed-temperature closed- versus open-system pyrolysis. Geochimica et Cosmochimica Acta, 57(3): 623-630.

Schenk, H.J., Horsfield, B., Krooss, B., Schaefer, R.G. and Schwochau, K., 1997b. Kinetics of Petroleum Formation and Cracking. In: D.H. Welte, B. Horsfield and D.R. Baker (Editors), Petroleum and Basin Evolution, pp. 233-269.

Schlömer, S. and Krooss, B., 1997. Experimental characterization of the hydrocarbon sealing efficiency of cap rocks. Marine and Petroleum Geology, 14: 565-580.

Schlüter, M., 2002. Fluid Flow in Continental Margin Sediments. In: G. Wefer et al. (Editors), Ocean Margin Systems. Springer-Verlag, pp. 205-217.

Schowalter, T., 1976. The Mechanics of secondary hydrocarbon migration and entrapment. The Wyoming Geological Association Earth Science Bulletin, 9(4): 1-43.

Schowalter, T.T., 1979. Mechanics of secondary hydrocarbon migration and entrapment. AAPG Bulletin, 63(5): 723-760.

Schumacher, D. and Abrams, M.A., 1996. Hydrocarbon migration and its near-surface expression, 66;. American Association of Petroleum Geologists, Tulsa, OK, United States, 446 pp.

Scoffin, T.P. and Bowes, G.E., 1988. The facies distribution of carbonate sediments on Porcupine Bank, Northeast Atlantic, Non-tropical shelf carbonates; modern and ancient. Elsevier, Amsterdam, Netherlands, pp. 125-134.

Scotchman, I.C., 2001. Petroleum geochmistry of the Lower and Middle Jurassic in Atlantic margin basins of Ireland and the UK. In: P.M. Shannon, P. Haughton and D.V. Corcoran (Editors), The Petroleum Exploration of Ireland's Offshore Basins. Geological Society, London, Special Publications, 188, pp. 31-60.

Shannon, P.M., 1991a. The development of Irish offshore sedimentary basins. Journal of the Geological Society, London, 148: 181 - 189.

Shannon, P.M., 1991b. Irish offshore basins: geological development and petroleum plays. In: A.M. Spencer (Editor), Generation, accumulation, and production of Europe's hydrocarbons. Special Publications of the European Association of Petroleum Geoscientists, Oxford, pp. 99-109.

Shannon, P.M., 1992. Early Tertiary submarine fan deposits in the Porcupine basin, offshore Ireland. In: J. Parnell (Editor), Basins on the Atlantic Seaboard: Petroleum Geology, Sedimentology and BAsin Evolution. Geological Society Special Publication, pp. 351-373.

Shannon, P.M., 1993. Submarine Fan Types in the Porcupine Basin, Ireland. In: A.M. Spencer (Editor), Generation, Accumulation and Production of Europe's Hydrocarbons III, Special Publication of the European Association of Petroleum Geoscientists No. 3. Springer-Verlag, Berlin Heidelberg, pp. 112-120.

Shannon, P.M., Moore, J.G., Jacob, A.W.B. and Makris, J., 1993. Cretaceous and Tertiary basin development west of Ireland, Petroleum geology of Northwest Europe; Proceedings of the 4th conference. The=Geological Society of London, London, United Kingdom, pp. 1057-1066.

Shannon, P.M. and Naylor, D., 1998. An Assessment of Irish offshore Basins and Petroleum Plays. Journal of Petroleum Geology, 21(2): 125-152.

Shannon, P.M., Williams, B.P.J. and Sinclair, I.K., 1995. Tectonic controls on Upper Jurassic to Lower Cretaceous reservoir architecture in the Jeanne d'Arc Basin, with some comparisons from the Porcupine and Moray Firth Basin. In: P.F. Croker and P.M. Shannon (Editors), The Petroleum Geology of Ireland's Offshore Basin. Geological Society Special Publications, pp. 467-490.

Shimoyama, A. and Yabuta, H., 2002. Mono- and bicyclic alkanes and diamondoid hydrocarbons in the Cretaceous/ Tertiary boundary sediments at Kawaruppu, Hokkaido, Japan. Geochemical Journal, 36(2): 173-189.

Shnukov, E.F. et al., 1971. Mud volcanism and ore formation. Naukova Dumka (in Russian).

Sibuet, M. and Olu-Le Roy, K., 1998. Biogeography, biodiversity and fluid dependence of deep-sea cold seep communities at active and passive margins. Deep Sea Res., 45: 517-567.

Sibuet, M. and Olu-Le Roy, K., 2002. Cold Seep Communities on Continetal Margins: Structure and Quantitative Distribution Relative to Geological and Fluid Venting Patterns. In: G. Wefer et al. (Editors), Ocean Margin Systems. Springer-Verlag, pp. 235-251.

Sinclair, I.K., 1995. Sequence stratigraphic response to Aptian-Albian rifting in conjugate margin basins: a comparisons of the Jeanne d'Arc Basin, offshore Newfoundland, and the Porcupine Basin, offshore Ireland. In: R.A. Scrutton, M.S. Stoker, G.B. Shimmield and A.W. Tudhope (Editors), The Tectonics, Sedimentation and Palaeoceanography of the North Atlantic Region. Geological Society Special Publications, pp. 29-49.

Slatt, R.M. et al., 1992. Geological methods, Development geology reference manual. American Association of Petroleum Geologists, Tulsa, OK, United States, pp. 261-354.

Sørensen, K.B., Finster, K. and Ramsing, N.B., 2001. Thermodynamic and kinetic requirements in anaerobic methane oxidizing consortia exclude hydrogen, acetate and methanol as possible electron shuttles. Microbal Ecology, 42(1): 1-10.
Southward, E.C., 1991. Three new species of Pogonophora, including two vestimentiferans, from hydrothermal sites in the Lau Back-Arc Basin (southwest Pacific Ocean). J. Nat. Hist., 25: 859-881.
Stakes, D.S., Orange, D., Paduan, J.B., Salamy, K.A. and Maher, N., 1999a. Cold-seeps and authigenic carbonate formation in Monterey Bay, California. Marine Geology, 159: 93-109.
Stakes, D.S., Orange, D.L., Paduan, J.B., Salamy, K.A. and Maher, N., 1999b. Cold-seeps and authigenic carbonate formation in Monterey Bay, California. Marine Geology, 159(1-4): 93-109.
Stanley, G.D., Jr. and Cairns, S.D., 1988. Constructional azooxanthellate coral communities; an overview with implications for the fossil records. Palaios, 3(2): 233-242.
Steinke, M., Malin, G. and Liss, P.S., 2002. Trophic Interactions in the Sea: An Ecological Role for Climate Relevant Volatiles? J. Phycol., 38: 630-638.
Stetson, T.R., Hersey, J.B. and Knott, S.T., 1963. Shallow structures of the Blake Plateau. Transactions - American Geophysical Union, 44(1): 64.
Stromgren, T., 1974. The use of a weighted arithmetic mean for describing the sediments of a landlocked basin (Borgenfjorden, Western Norway). Deep-Sea Research and Oceanographic Abstracts, 21(2): 155-160.
Sylta, O., Pedersen, J.I. and Hamborg, M., 1998. On the vertical and lateral distribution of hydrocarbon migration velocities during secondary migration, Dating and duration of fluid flow and fluid-rock interaction. Geological Society of London, London, United Kingdom, pp. 221-232.
Tate, M., White, N. and Conroy, J.-J., 1993. Lithospheric Extension and Magmatism in the Porcupine Basin West of Irland. Journal of Geophysical Research B, 98: 13905-13923.
Tate, M.P., 1993. Structural framework and tectono-stratigraphic evolution of the Porcupine Seabight Basin, offshore western Ireland. Marine and Petroleum Geology, 10: 95-123.
Tate, M.P. and Dobson, M.R., 1988. Syn- and post-rift igneous activity in the Porcupine Seabight Basin and adjacent continental margin of W of Ireland. In: A.C. Morton and L.M. Parson (Editors), Early Tertiary Vocanism and the Opening of the NE Atlantic, Geological Society Special Publication No. 39, pp. 309-334.
Taylor, G.H. et al., 1998. Organic Petrology. Gebrüder Borntraeger, 704 pp.
Thiel, V. et al., 1999. Highly isotopically depleted isoprenoids: Molecular markers for ancient methane venting. Geochemica et Cosmochimica Acta, 63(23/24): 3959-3966.
Thomas, G.E., 1991. Paleotopography and hydrocarbon accumulation; Williston, Powder River, and Denver basins, AAPG Rocky Mountain Section meeting. American Association of Petroleum Geologists, Tulsa, OK, United States, pp. 1142.
Tissot, B., 1969. Premieres donnees sur les mecanismes et la cinetique de la formation du petrole dans les sediments; simulation d'un schema reactionnel sur ordinateur. Revue de l'Institut Francais du Petrole, 24(4): 470-501.
Tissot, B. and Espitalié, J., 1975. L'évolution thermique de la matière organique des sédiments: application d'une simulation mathématique. Revue l'Institute francais du pétrole, 30: 743-777.
Tissot, B.P., Pelet, R. and Ungerer, P., 1987. Thermal history of sedimentary basins, maturation indices, and kinetics of oil and gas generation. AAPG Bulletin, 71(12): 1445-1466.
Tissot, B.P. and Welte, D.H., 1984. Petroleum Formation and Occurrence. Springer Verlag, Berlin.

Toshitaka, G. et al., 2001. Chemical characteristics of newly discovered black smoker fluids and associated hydrothermal plumes at the Rodriguez triple junction, Central Indian Ridge. Earth and Planetry Science Letters, 193: 371-379.
Tsunogai, U. et al., 1994. Peculiar features of Suiyo Seamount hydrothermal fluids, Izu-Bonin Arc; differences from subaerial volcanism. Earth and Planetary Science Letters, 126(4): 289-301.
Tunnicliffe, V., 1991. The biology of hydrothermal vents: Ecology and evolution. Oceanogr. Mar. Biol., 29: 319-407.
Tunnicliffe, V., 1992. Hydrothermal-vent communities of the deep sea. Am. Sci., 80: 336-464.
Tunnicliffe, V. et al., 1986. Hydrothermal vents of Explorer Ridge, northeast Pacific. Deep Sea Res., 33: 401-412.
Ungerer, P., 1989. State of the art of research in kinetic modelling of oil formation and expulsion. Advances in Organic Geochemistry, 16(1-3): 1-25.
Unnithan, V., O'Reilly, B.M., Readman, P.W., Jacob, A.W.B. and Kenyon, N., 2001. Slope failure features on the margins of the Rockall Trough. In: P.M. Shannon, P.D.W. Haughton and D.V. Corcoran (Editors), The Petroleum Exploration of Ireland's Offshore Basins. Geological Society, pp. 455-465.
van der Meer, F., van Dijk, P., van der Werff, H. and Yang, H., 2002. Remote sensing and petroleum seepage: a review and case study. Terra Nova, 14: 1-17.
van Dover, C.L. and Berg, C.J., Jr., 1988. Recruitment of marine invertebrates to hard substrates at deep-sea hydrothermal vents, AGU 1988 spring meeting. American Geophysical Union, Washington, DC, United States, pp. 303.
van Dover, C.L. et al., 1994. Light at deep sea hydrothermal vents. Eos, Transactions, American Geophysical Union, 75(4): 44-45.
van Dover, C.L. and Hessler, R.R., 1990. Spatial variation in faunal composition of hydrothermal vent communities on the East Pacific Rise and Galapagos spreading center. In: G.R. McMurray (Editor), Gorda Ridge, A Seafloor Spreading Center in the United States' Exclusive Economic Zone. Springer-Verlag, pp. 253-264.
Vandenbroucke, M., Béhar, F. and J.L., R., 1999. Kinetic modelling of petroleum formation and cracking: implications from the high pressure/high temperature Elgin Field (UK, North Sea). Organic Geochemistry, 30: 1105-1125.
Viana, M.S.S., Mabesoone, J.M. and Neumann, V.H., 1994. Lacustrine phases in the Araripe Basin (NE Brazil), 14th International Sedimentological Congress; abstracts. International Association of Sedimentologists Comparative Sedimentology Division, Utrecht, Netherlands, pp. S6.11-S6.12.
Vogt, P.R., Crane, K., Sundvor, E., Max, M.D. and Pfirman, S.L., 1994. Methane-generated(?) pockmarks on young, thickly sedimented oceanic crust in the Arctic; Vestnesa Ridge, Fram Strait. Geology (Boulder), 22(3): 255-258.
Volkman, J.K., 1986. A review of sterol markers for marine and terrigenous organic matter. Organic Geochemistry, 9(2): 83-99.
Volkman, J.K. et al., 1998. Microalgal biomarkers; a review of recent research developments, Advances in organic geochemistry 1997; proceedings of the 18th international meeting on Organic geochemistry; Part II, Biogeochemistry. Pergamon, Oxford-New York, International, pp. 1163-1179.
Vuletich, A.K., Threlkeld, C.N. and Claypool, G.E., 1989. Isotopic composition of gases and interstitial fluids in sediment of the Voring Plateau, ODP Leg 104, Site 644, Proceedings of the Ocean Drilling Program, Norwegian Sea; covering Leg 104 of the cruises of the Drilling Vessel JOIDES Resolution, Bremerhaven, Germany, to St John's, Newfoundland, Sites 642-644, 19 June 1985-23 August 1985. Texas A & M University Ocean Drilling Program, College Station, TX, United States, pp. 281-283.
Walsh, A. et al., 1999. Petroleum geology of the Irish Rockall Trough; a frontier challenge. In: A.J. Fleet and S.A.R. Boldy (Editors), Petroleum Geology of Northwest Europe. The Geological Society of London, London, pp. 433-444.

Washburn, E.W., 1921. Note on a method of determining the distribution of pore sizes in a porous material. Proceedings of the National Academy of Science, 7: 115-116.
Welte, D.H., 1965. Relation between petroleum and source rock. AAPG Bulletin, 49: 2246-2268.
Welte, D.H., Hantschel, T., Wygrala, B.P., Weissenburger, K.S. and Carruthers, D.J., 2000. Aspects of petroleum migration modelling. Journal of Geochemical Exploration, 69-70: 711-714.
Welte, D.H., Horsfield, B. and Baker, D.R., 1997. Petroleum and Basin Evolution. Springer-Verlag, Berlin, 534 pp.
Welte, D.H. and Yalcin, M.N., 1987. Formation and occurrence of petroleum in sedimentary basins as deduced from computer aided basin modelling. In: R.K. Kumar, P. Dwivedi, V. Banerjie and V. Gupta (Editors), Petroleum geochemistry and exploration in the Afro-Asian region, pp. 17-23.
White, S.N. et al., 2000. Variations in ambient light emission from black smokers and flange pools on the Juan de Fuca Ridge. Geophysical Research Letters, 27(8): 1151-1154.
Whiticar, M.J., 1994. Correlation of natural gases with their sources, The petroleum system; from source to trap. American Association of Petroleum Geologists, Tulsa, OK, United States, pp. 261-283.
Whiticar, M.J. and Faber, E., 1989a. Carbon, hydrogen, and oxygen isotope distribution in the interstitial fluid of ODP Leg 104, Holes 642B, 642D, 643A, Voring Plateau, Norwegian Sea, Proceedings of the Ocean Drilling Program, Norwegian Sea; covering Leg 104 of the cruises of the Drilling Vessel JOIDES Resolution, Bremerhaven, Germany, to St John's, Newfoundland, Sites 642-644, 19 June 1985-23 August 1985. Texas A & M University Ocean Drilling Program, College Station, TX, United States, pp. 285-289.
Whiticar, M.J. and Faber, E., 1989b. Molecular and stable isotope composition of headspace and total hydrocarbon gases at ODP Leg 104, sites 642, 643, and 644, Voring Plateau, Norwegian Sea, Proceedings of the Ocean Drilling Program, Norwegian Sea; covering Leg 104 of the cruises of the Drilling Vessel JOIDES Resolution, Bremerhaven, Germany, to St John's, Newfoundland, Sites 642-644, 19 June 1985-23 August 1985. Texas A & M University Ocean Drilling Program, College Station, TX, United States, pp. 327-334.
Wilson, J.B., 1979. 'Patch' development of the deep-water coral *Lophelia Pertusa* (L.) on Rockhall Bank. Journal of the Marine Biological Association U.K., 59: 165-177.
Wu, G., Zhang, B., Bian, L. and Liu, J., 1999. Preliminary study of carbonate mud-mounds, Middle-Upper Ordovician, Tazhong area, Xinjiang, China. Acta Sedimentologica Sinica, 17(2): 198-203.
Wu, Y.S., 2002. Numerical simulation of single-phase and multiphase non-Darcy flow in porous and fractured reservoirs. Transport in Porous Media, 49(2): 209-240.
Wygrala, B.P., 1988. Integrated computer-aided basin modeling applied to analysis of hydrocarbon generation history in a northern Italian oil field. In: L. Mattavelli and L. Novelli (Editors), Advances in Organic Geochemistry 1987; Part I, Organic Geochemistry in Petroleum Exploration; Proceedings of the 13th International Meeting on Organic Geochemistry. Organic Geochemistry, pp. 187-197.
Wygrala, B.P., 1989. Integrated study of an oil field in the southern Po Basin, Northern Italy. PhD Thesis, Universität Köln, Köln, 217 pp.
Yakubov, A.A. and Rakhmanov, R.R., 1978. Mud volcanoes of the Andaman and the Nicobar Islands and their tectonic position. Transactions (Doklady) of the U S S R, Academy of Sciences: Earth Science Sections. 239(1-6): 81-82.
Yalcin, M.N., Littke, R. and Sachsenhofer, R.F., 1997. Thermal history of sedimentary basins, Petroleum and basin evolution; insights from petroleum geochemistry, geology and basin modeling. Springer, Berlin, Federal Republic of Germany.

Young, E.F., Aldridge, J.N. and Brown, J., 2000. Development and validation of a three-dimensional curvilinear model for the study of fluxes through the North Channel of the Irish Sea. Continental Shelf Research, 20: 997-1035.

Ziegler, P.A., 1981. Evolution of sedimentary basins in NW Europe. In: L.V. Illing and G.S. Hobson (Editors), The Geology of the Continental Shelf of NW Europe. Heyden & Son Ltd., London, pp. 3-39.

8 Appendix

8.1 Appendix I: Samples and Geochemical Data

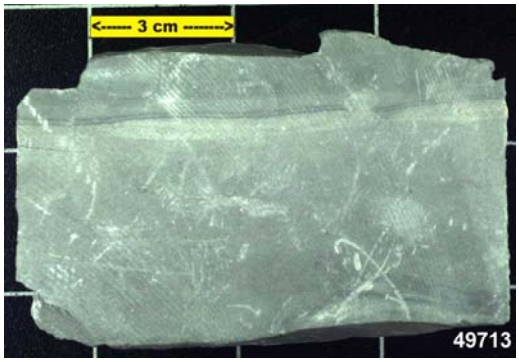

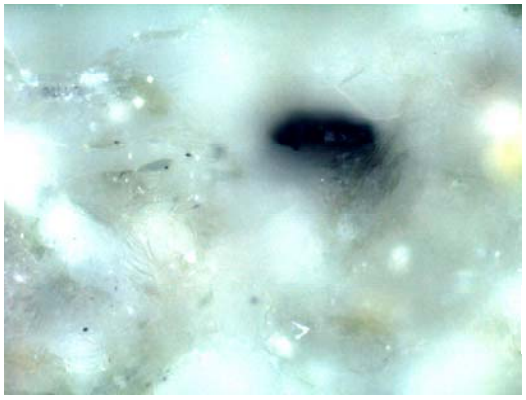

Sample :	49713
Depth:	- 2005,4 m
Stratigraphy:	Bath. – Hett.
R_r:	1,2
TOC:	0,22 %
TC:	0,23 %
$CaCO_3$:	0.07 %
TS:	0,03 %
S1:	0,04 mg HC/g
S2:	0,19 mg HC/g
S3:	0,04 mg HC/g
T_{max}:	519 °C
PI:	0,18
HI:	85
OI:	17

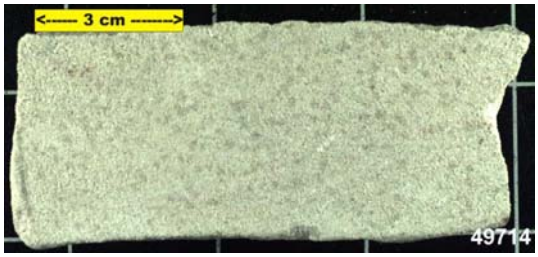

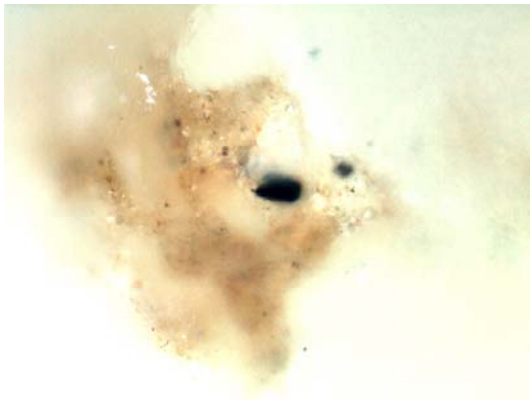

Sample :	49714
Depth:	- 2006,4 m
Stratigraphy:	Bath. – Hett.
R_r:	nicht meßbar
TOC:	0,09 %
TC:	0,20 %
$CaCO_3$:	0.91 %
TS:	0,02 %
S1:	0,01 mg HC/g
S2:	0,22 mg HC/g
S3:	0,19 mg HC/g
T_{max}:	546 °C
PI:	0,05
HI:	248
OI:	212

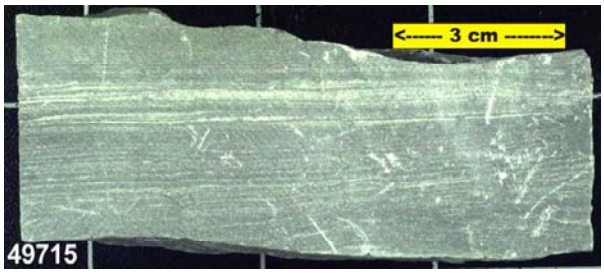

Sample :	49715
Depth:	- 2006,7 m
Stratigraphy:	Bath. – Hett.
R_r:	1,4
TOC:	0,21 %
TC:	0,22 %
$CaCO_3$:	0.08 %
TS:	0,03 %
S1:	0,04 mg HC/g
S2:	0,30 mg HC/g
S3:	0,02 mg HC/g
T_{max}:	514 °C
PI:	0,11
HI:	145
OI:	11

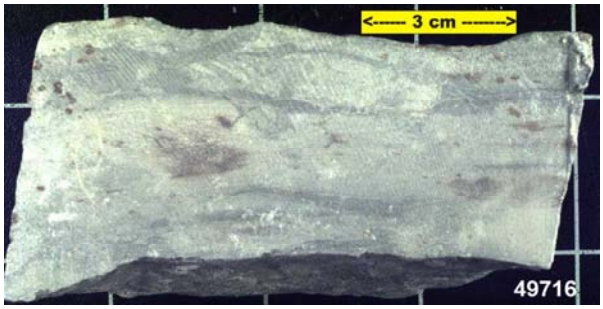

Sample :	49716
Depth:	- 2009,6 m
Stratigraphy:	Bath. – Hett.
R_r:	nicht meßbar
TOC:	0,11 %
TC:	0,55 %
$CaCO_3$:	3.71 %
TS:	0,05 %
S1:	0,02 mg HC/g
S2:	0,18 mg HC/g
S3:	0,60 mg HC/g
T_{max}:	444 °C
PI:	0,10
HI:	168
OI:	567

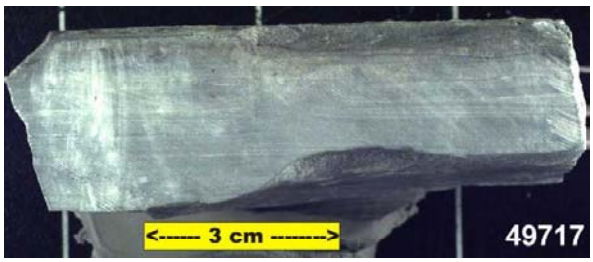

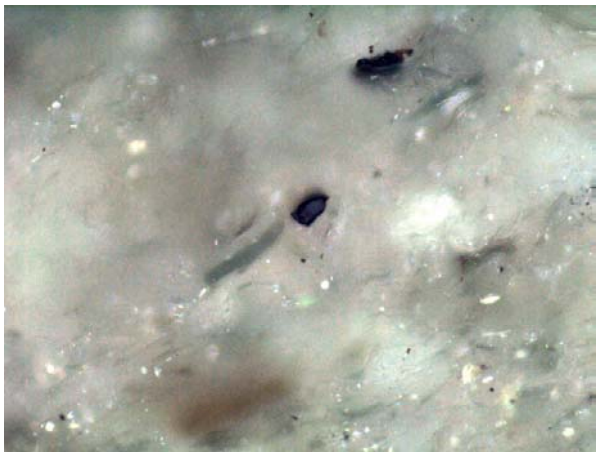

Sample :	49717
Depth:	- 2506,6 m
Stratigraphy:	Carbon.
R_r:	1,5
TOC:	0,18 %
TC:	0,18 %
$CaCO_3$:	0.00 %
TS:	0,02 %
S1:	0,03 mg HC/g
S2:	0,20 mg HC/g
S3:	0,00 mg HC/g
T_{max}:	497 °C
PI:	0,14
HI:	112
OI:	0

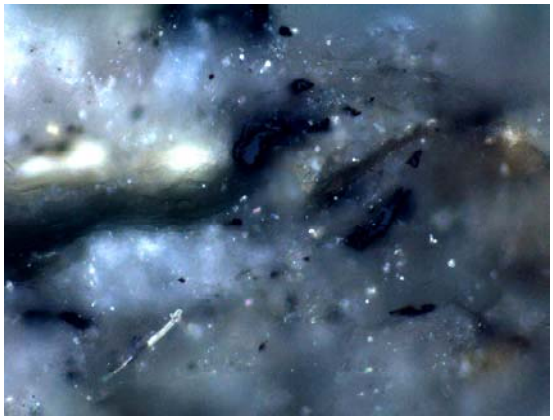

Sample :	49718
Depth:	- 2661,6 m
Stratigraphy:	Carbon.
R_r:	0,9
TOC:	0,75 %
TC:	0,78 %
$CaCO_3$:	0.20 %
TS:	0,02 %
S1:	0,01 mg HC/g
S2:	0,41 mg HC/g
S3:	0,03 mg HC/g
T_{max}:	493 °C
PI:	0,03
HI:	55
OI:	4

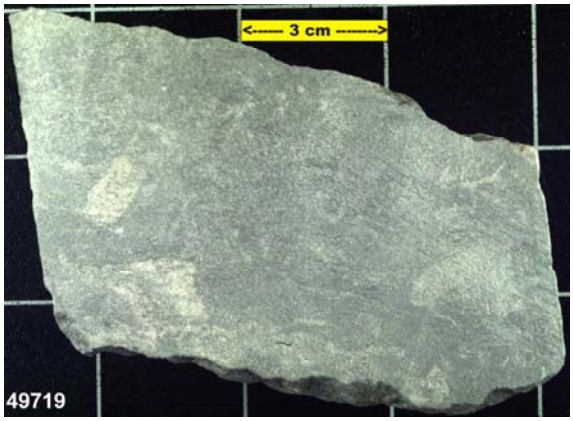

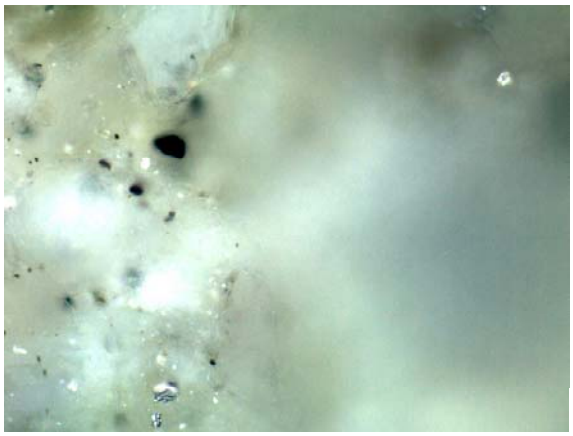

Sample :	49719
Depth:	- 2255,5 m
Stratigraphy:	Kimm. – Oxf.
R_r:	0,7
TOC:	0,38 %
TC:	0,45 %
$CaCO_3$:	0.58 %
TS:	0,03 %
S1:	0,07 mg HC/g
S2:	0,39 mg HC/g
S3:	0,33 mg HC/g
T_{max}:	520 °C
PI:	0,15
HI:	101
OI:	86

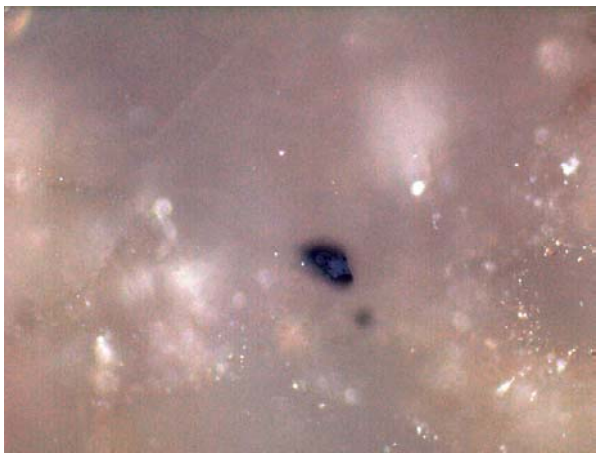

Sample :	49720
Depth:	- 2256,0 m
Stratigraphy:	Kimm. – Oxf.
R_r:	nicht meßbar
TOC:	0,67 %
TC:	0,80 %
$CaCO_3$:	1.02 %
TS:	0,07 %
S1:	5,89 mg HC/g
S2:	2,39 mg HC/g
S3:	0,45 mg HC/g
T_{max}:	410 °C
PI:	0,71
HI:	355
OI:	67

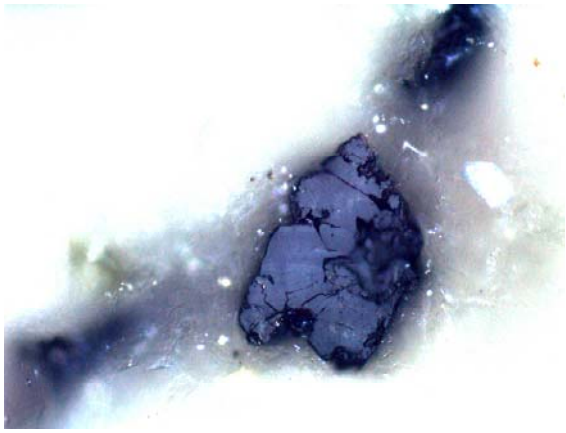

Sample :	49721
Depth:	- 2263,4 m
Stratigraphy:	Kimm. – Oxf.
R_r:	1,2
TOC:	0,50 %
TC:	0,79 %
$CaCO_3$:	2.38 %
TS:	0,03 %
S1:	0,09 mg HC/g
S2:	0,19 mg HC/g
S3:	0,19 mg HC/g
T_{max}:	491 °C
PI:	0,32
HI:	37
OI:	38

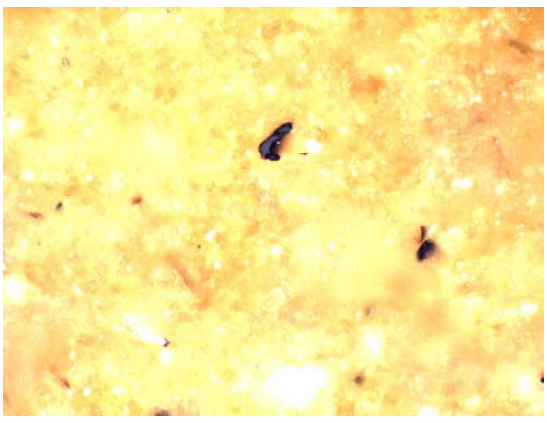

Sample :	49722
Depth:	- 2462,0 m
Stratigraphy:	Bath.
R_r:	0,6
TOC:	0,36 %
TC:	1,78 %
$CaCO_3$:	11.79 %
TS:	0,08 %
S1:	0,02 mg HC/g
S2:	0,18 mg HC/g
S3:	0,70 mg HC/g
T_{max}:	431 °C
PI:	0,11
HI:	51
OI:	194

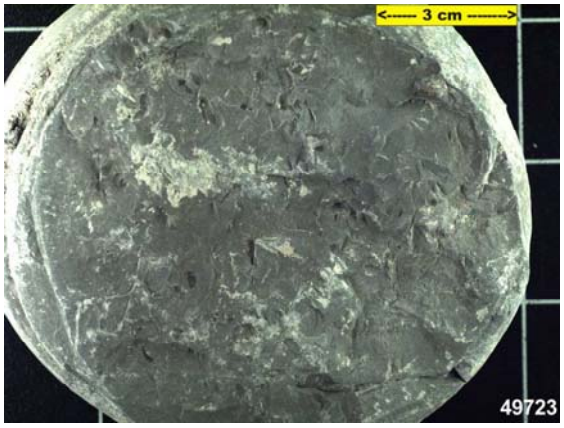

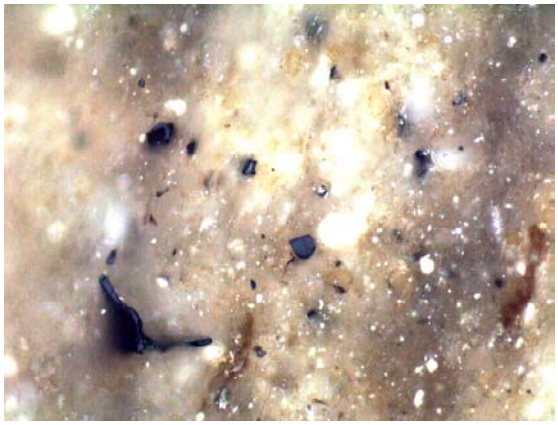

Sample :	49723
Depth:	- 2426,7 m
Stratigraphy:	Bath.
R_r:	0,7
TOC:	0,53 %
TC:	1,64 %
$CaCO_3$:	9.28 %
TS:	0,10 %
S1:	0,03 mg HC/g
S2:	0,33 mg HC/g
S3:	0,55 mg HC/g
T_{max}:	428 °C
PI:	0,07
HI:	64
OI:	104

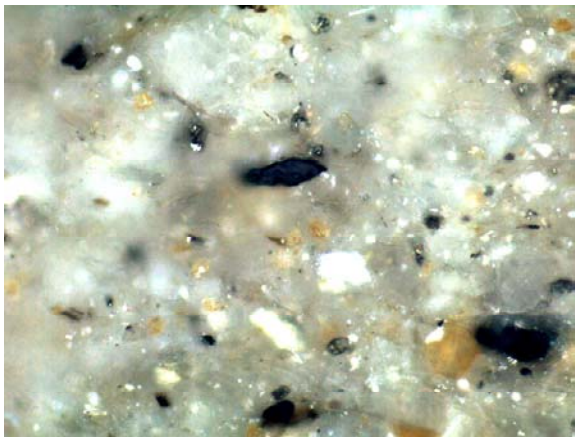

Sample :	49724
Depth:	- 2428,0 m
Stratigraphy:	Bath.
R_r:	0,6
TOC:	0,46 %
TC:	1,39 %
$CaCO_3$:	7.76 %
TS:	0,17 %
S1:	0,02 mg HC/g
S2:	0,37 mg HC/g
S3:	0,46 mg HC/g
T_{max}:	427 °C
PI:	0,04
HI:	81
OI:	100

Sample :	49725
Depth:	- 2429,8 m
Stratigraphy:	Bath.
R_r:	nicht meßbar
TOC:	0,50 %
TC:	1,45 %
$CaCO_3$:	7.79 %
TS:	0,13 %
S1:	0,02 mg HC/g
S2:	0,46 mg HC/g
S3:	0,57 mg HC/g
T_{max}:	429 °C
PI:	0,03
HI:	91
OI:	114

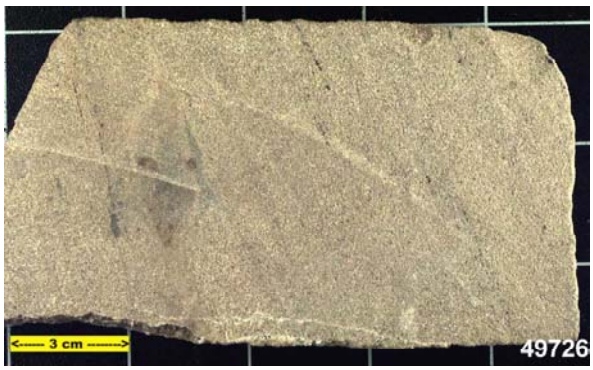

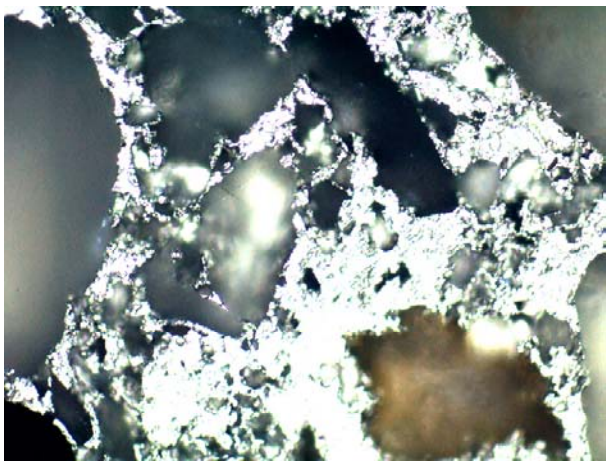

Sample :	49726
Depth:	- 2093,3 m
Stratigraphy:	Bath.
R_r:	nur Inertinit
TOC:	0,52 %
TC:	2,51 %
$CaCO_3$:	16.54 %
TS:	1,77 %
S1:	5,35 mg HC/g
S2:	1,20 mg HC/g
S3:	0,43 mg HC/g
T_{max}:	405 °C
PI:	0,82
HI:	229
OI:	83

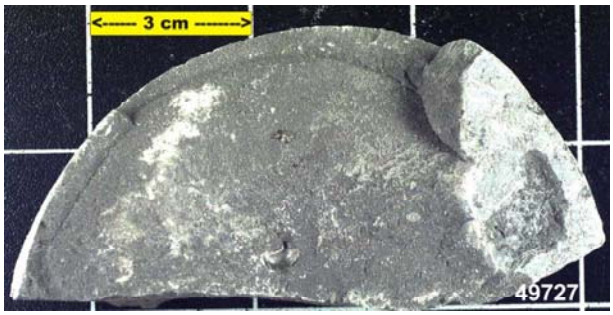

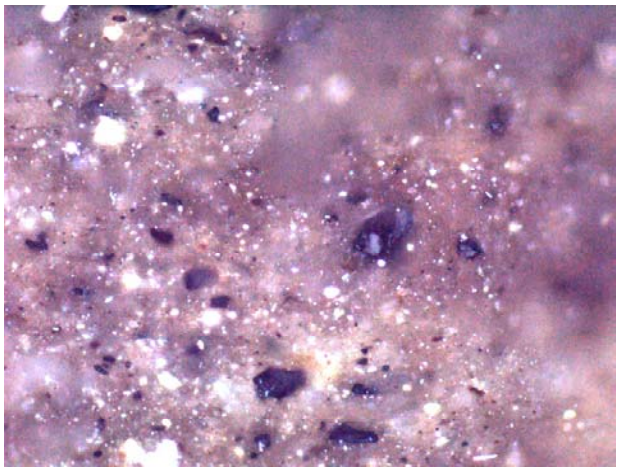

Sample :	49727
Depth:	- 2402,0 m
Stratigraphy:	Bath.
R_r:	0,6
TOC:	2,08 %
TC:	2,73 %
$CaCO_3$:	5.37 %
TS:	1,85 %
S1:	0,11 mg HC/g
S2:	6,95 mg HC/g
S3:	0,64 mg HC/g
T_{max}:	429 °C
PI:	0,02
HI:	334
OI:	31

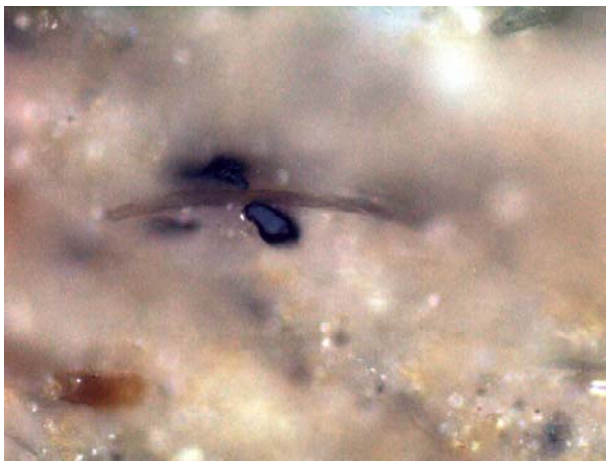

Sample :	49728
Depth:	- 2403,2 m
Stratigraphy:	Bath.
R_r:	0,55
TOC:	1,19 %
TC:	2,97 %
$CaCO_3$:	14.83 %
TS:	0,41 %
S1:	0,05 mg HC/g
S2:	3,05 mg HC/g
S3:	1,36 mg HC/g
T_{max}:	428 °C
PI:	0,02
HI:	257
OI:	115

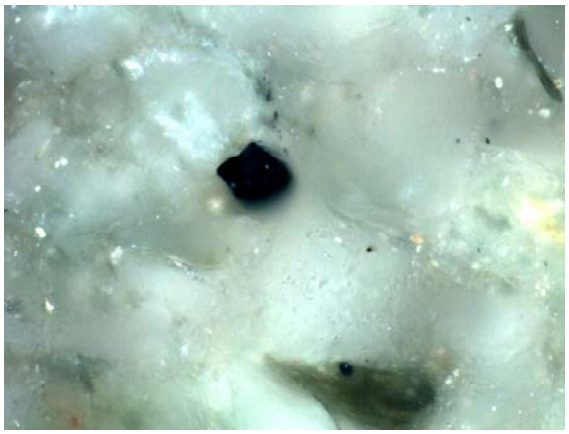

Sample :	49729
Depth:	- 2766,6 m
Stratigraphy:	Bath.
R_r:	0,6
TOC:	0,25 %
TC:	0,63 %
$CaCO_3$:	3.15 %
TS:	0,02 %
S1:	0,01 mg HC/g
S2:	0,11 mg HC/g
S3:	0,84 mg HC/g
T_{max}:	500 °C
PI:	0,07
HI:	46
OI:	340

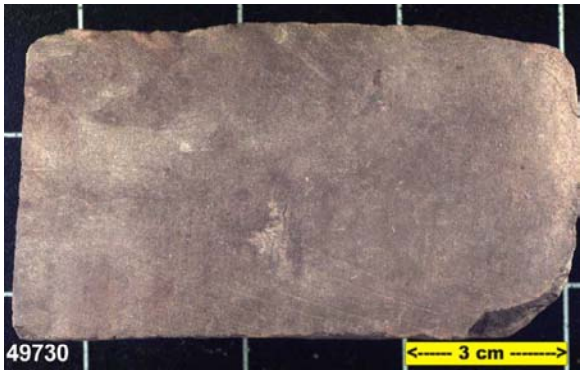

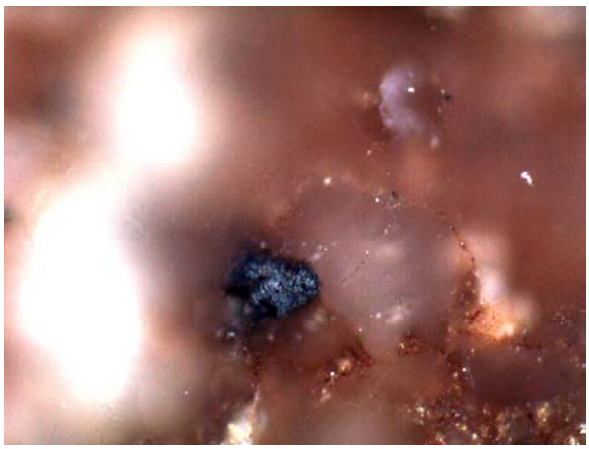

Sample :	49730
Depth:	- 1782,0 m
Stratigraphy:	Baj. – Bath.
R_r:	nicht meßbar
TOC:	0,07 %
TC:	0,25 %
$CaCO_3$:	1,47 %
TS:	0,02 %
S1:	0,01 mg HC/g
S2:	0,33 mg HC/g
S3:	0,70 mg HC/g
T_{max}:	540 °C
PI:	0,04
HI:	465
OI:	981

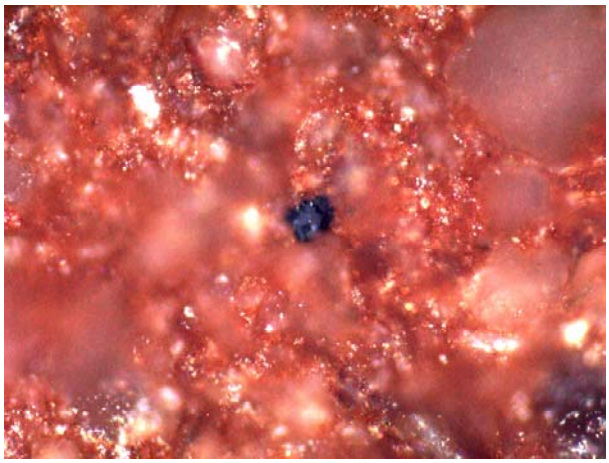

Sample :	49731
Depth:	- 1782,8 m
Stratigraphy:	Baj. – Bath.
R_r:	nicht meßbar
TOC:	0,07 %
TC:	0,39 %
$CaCO_3$:	2.60 %
TS:	0,01 %
S1:	0,01 mg HC/g
S2:	0,19 mg HC/g
S3:	1,07 mg HC/g
T_{max}:	544 °C
PI:	0,06
HI:	251
OI:	1439

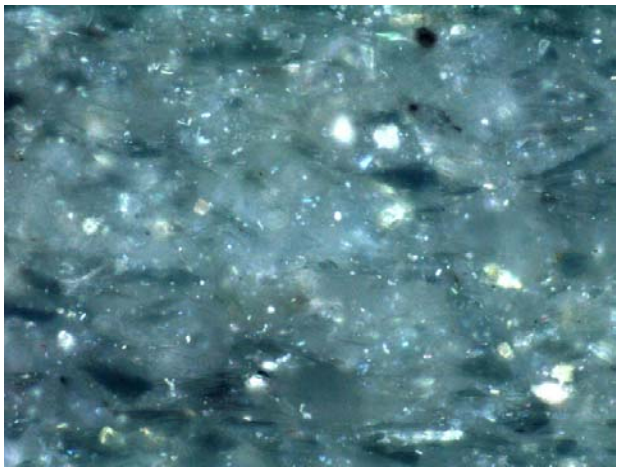

Sample :	49732
Depth:	- 1786,3 m
Stratigraphy:	Baj. – Bath.
R_r:	nicht meßbar
TOC:	0,08 %
TC:	0,10 %
$CaCO_3$:	0.18 %
TS:	0,03 %
S1:	0,01 mg HC/g
S2:	0,38 mg HC/g
S3:	0,08 mg HC/g
T_{max}:	493 °C
PI:	0,02
HI:	495
OI:	109

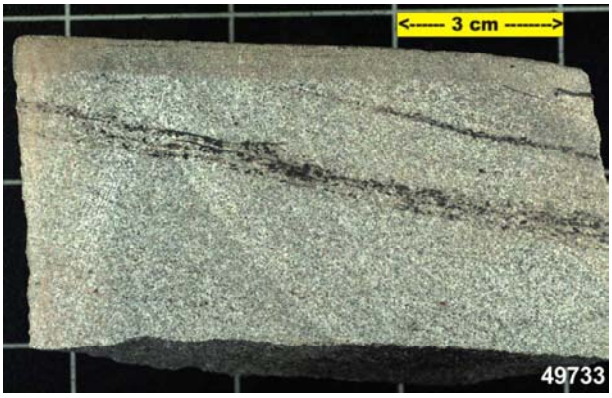

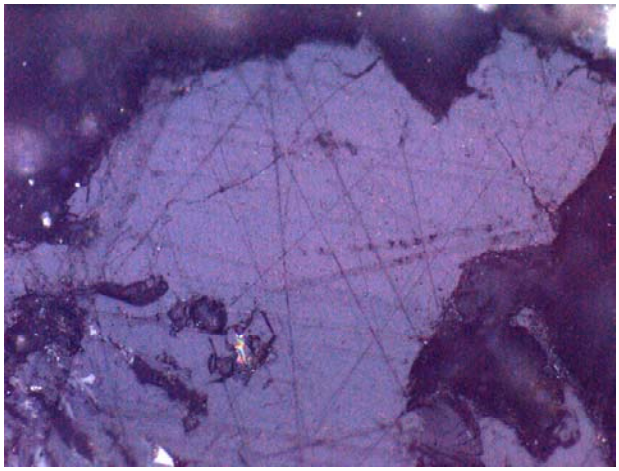

Sample :	49733
Depth:	- 1833,4 m
Stratigraphy:	Westf. C
R_r:	0,7
TOC:	1,84 %
TC:	3,87 %
$CaCO_3$:	16.95 %
TS:	0,05 %
S1:	0,33 mg HC/g
S2:	2,11 mg HC/g
S3:	0,47 mg HC/g
T_{max}:	431 °C
PI:	0,13
HI:	115
OI:	26

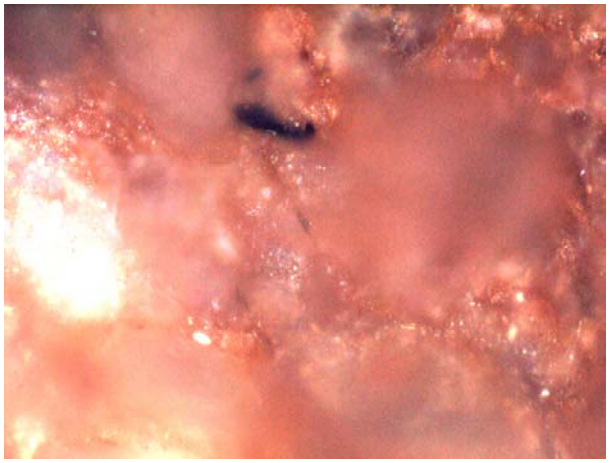

Sample :	49734
Depth:	- 1781,4 m
Stratigraphy:	Baj. – Bath.
R_r:	nicht meßbar
TOC:	0,07 %
TC:	0,09 %
$CaCO_3$:	0.17 %
TS:	0,01 %
S1:	0,01 mg HC/g
S2:	0,26 mg HC/g
S3:	0,12 mg HC/g
T_{max}:	503 °C
PI:	0,05
HI:	364
OI:	168

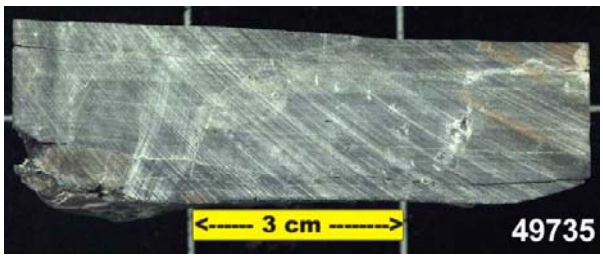

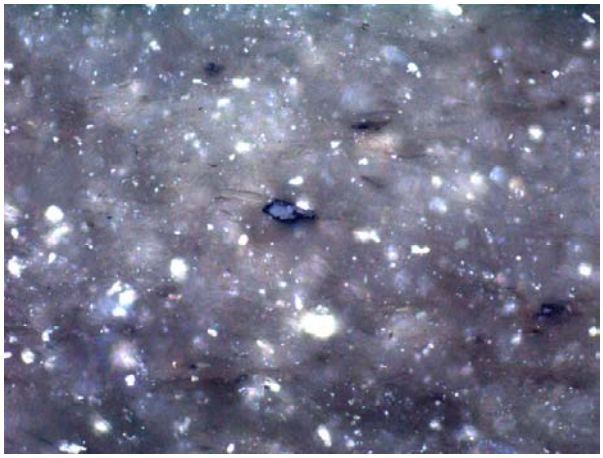

Sample :	49735
Depth:	- 4441,3 m
Stratigraphy:	Steph.
R_r:	1,8
TOC:	0,20 %
TC:	2,44 %
$CaCO_3$:	18.63 %
TS:	0,07 %
S1:	0,01 mg HC/g
S2:	0,06 mg HC/g
S3:	0,93 mg HC/g
T_{max}:	373 °C
PI:	0,14
HI:	29
OI:	465

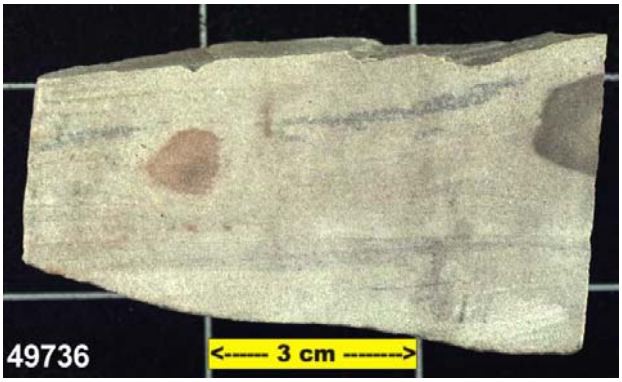

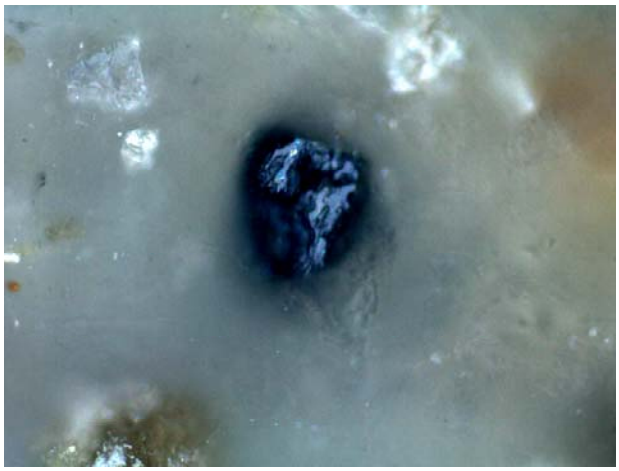

Sample :	49736
Depth:	- 3954,0 m
Stratigraphy:	Baj. – Bath.
R_r:	nicht meßbar
TOC:	0,13 %
TC:	1,42 %
$CaCO_3$:	10.72 %
TS:	0,02 %
S1:	0,08 mg HC/g
S2:	0,08 mg HC/g
S3:	0,40 mg HC/g
T_{max}:	348 °C
PI:	0,47
HI:	66
OI:	315

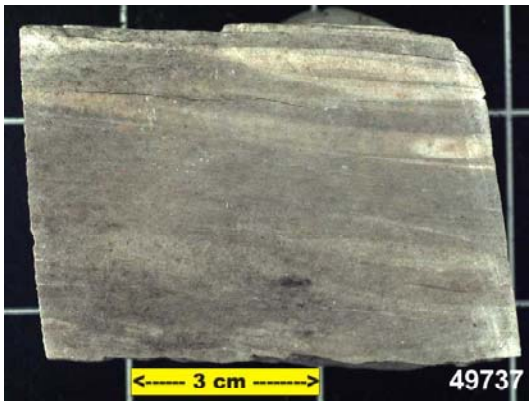

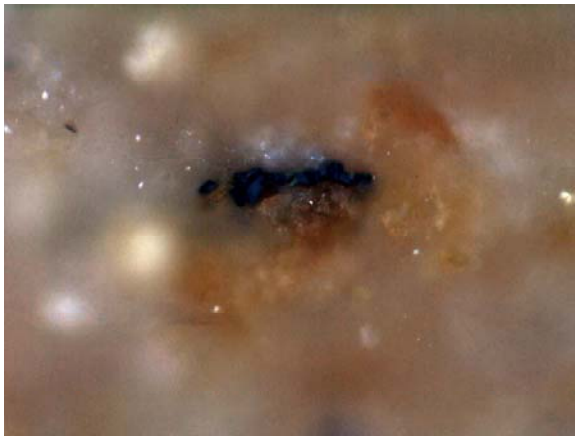

Sample :	49737
Depth:	- 3955,3 m
Stratigraphy:	Baj. – Bath.
R_r:	nicht meßbar
TOC:	0,16 %
TC:	0,86 %
$CaCO_3$:	5.80 %
TS:	0,02 %
S1:	0,06 mg HC/g
S2:	0,08 mg HC/g
S3:	0,77 mg HC/g
T_{max}:	352 °C
PI:	0,42
HI:	48
OI:	478

Sample :	49738
Depth:	- 1710,7 m
Stratigraphy:	Lo. Eocene
R_r:	
TOC:	
TC:	
$CaCO_3$:	
TS:	
S1:	
S2:	
S3:	
T_{max}:	
PI:	
HI:	
OI:	

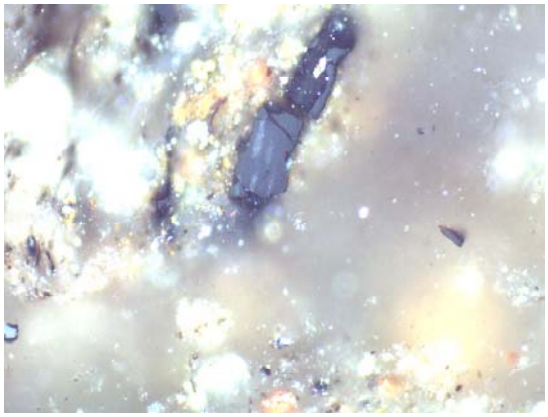

Sample :	49739
Depth:	- 1711,8 m
Stratigraphy:	Lo. Eocene
R_r:	0,34
TOC:	1,92 %
TC:	2,03 %
$CaCO_3$:	0.87 %
TS:	0,744 %
S1:	0,10 mg HC/g
S2:	1,28 mg HC/g
S3:	1,46 mg HC/g
T_{max}:	414 °C
PI:	0,07
HI:	67
OI:	76

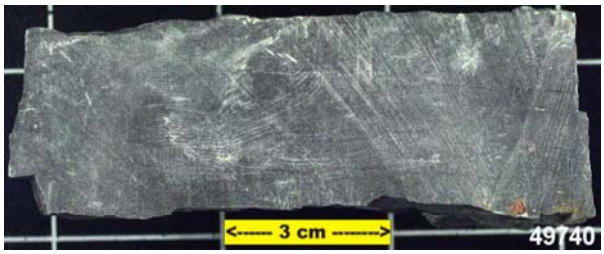

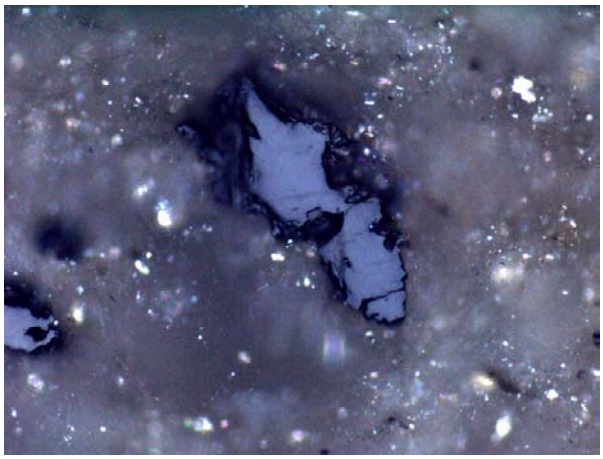

Sample :	49740
Depth:	- 5014,0 m
Stratigraphy:	Early Cret.
R_r:	1,3
TOC:	0,40 %
TC:	0,73 %
$CaCO_3$:	2.71 %
TS:	0,08 %
S1:	0,01 mg HC/g
S2:	0,09 mg HC/g
S3:	0,20 mg HC/g
T_{max}:	497 °C
PI:	0,10
HI:	23
OI:	50

8.2 Appendix II: Vitrinite Reflectance

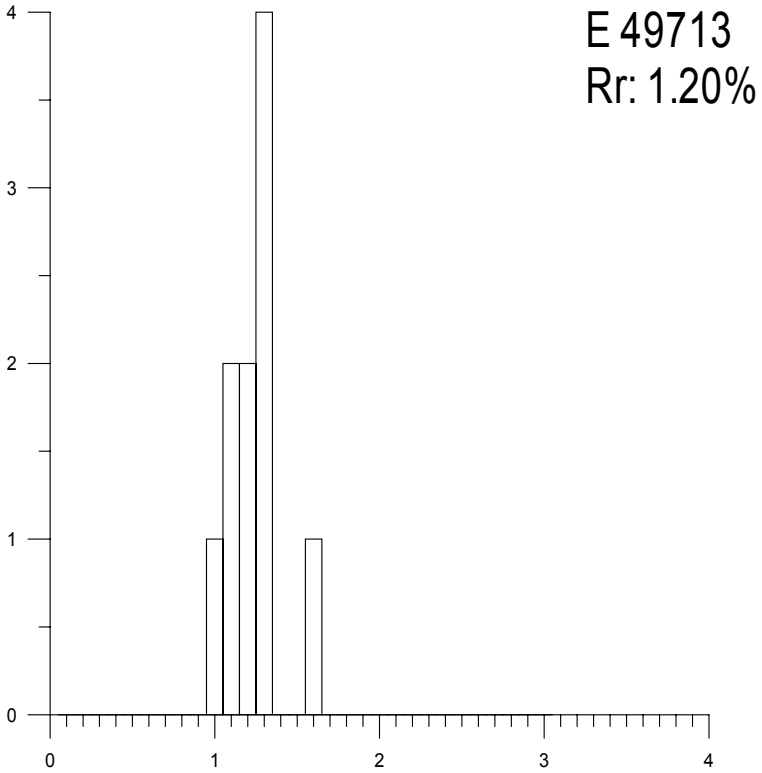

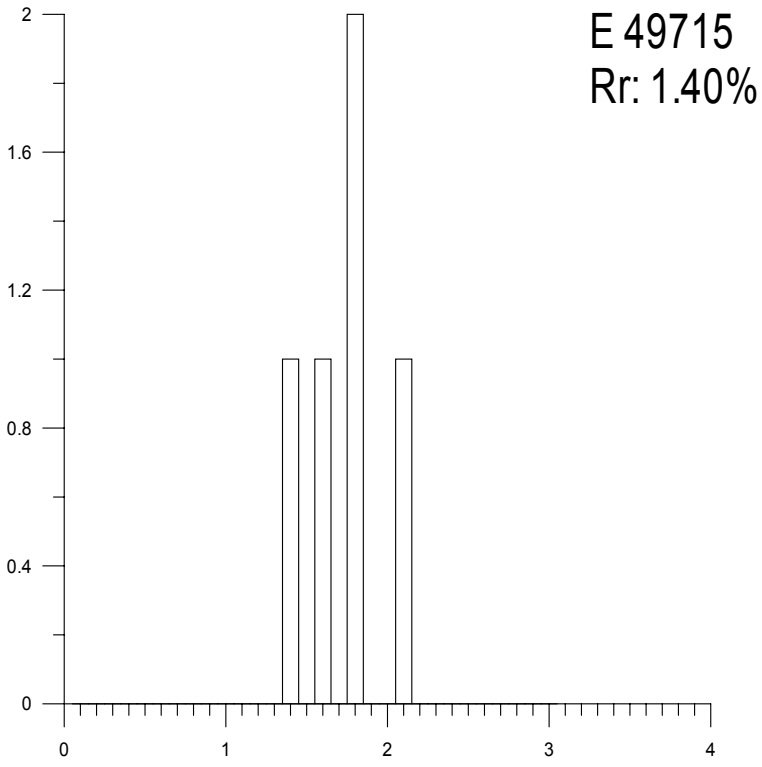

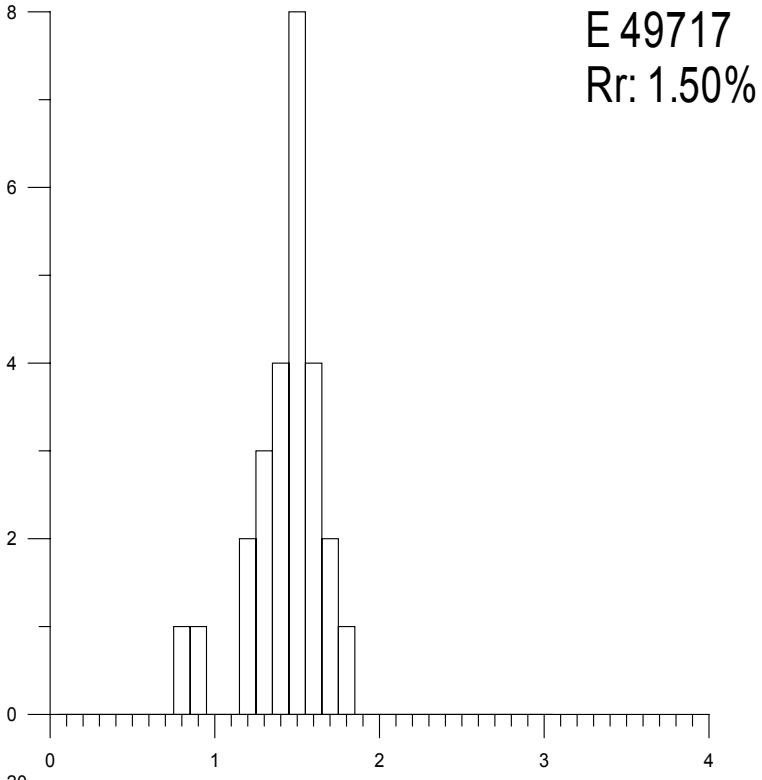
E 49717
Rr: 1.50%
8
6
4
2
0
0
1
2
3
4

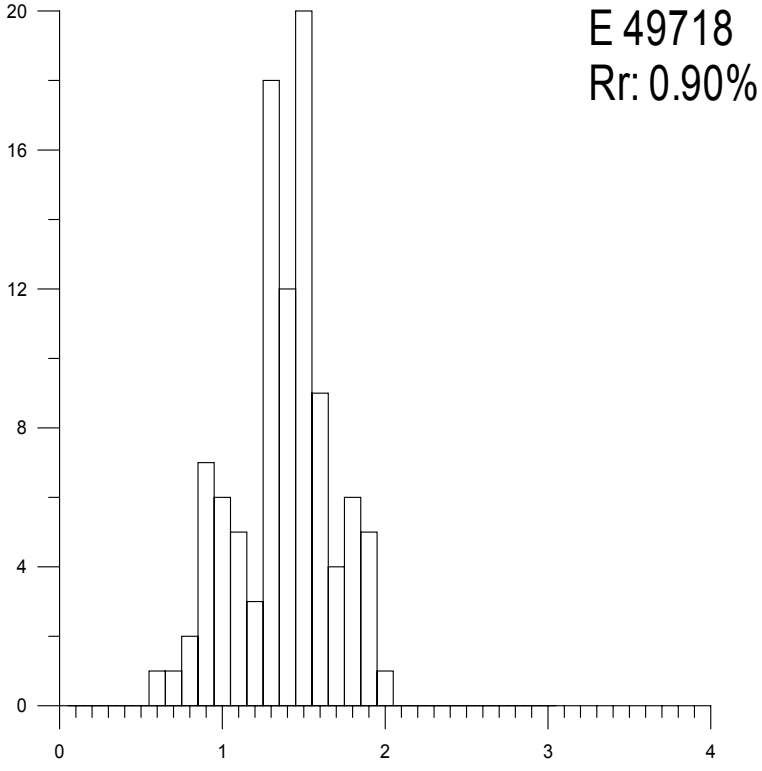
E 49718
Rr: 0.90%
20
16
12
8
4
0
0
1
2
3
4

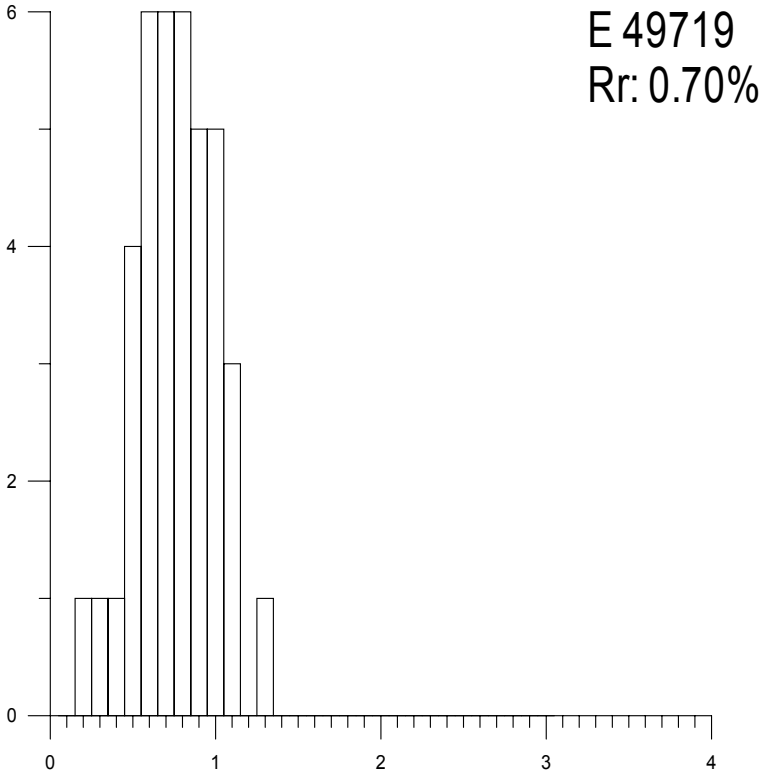
E 49719
Rr: 0.70%
6
4
2
0
0
1
2
3
4

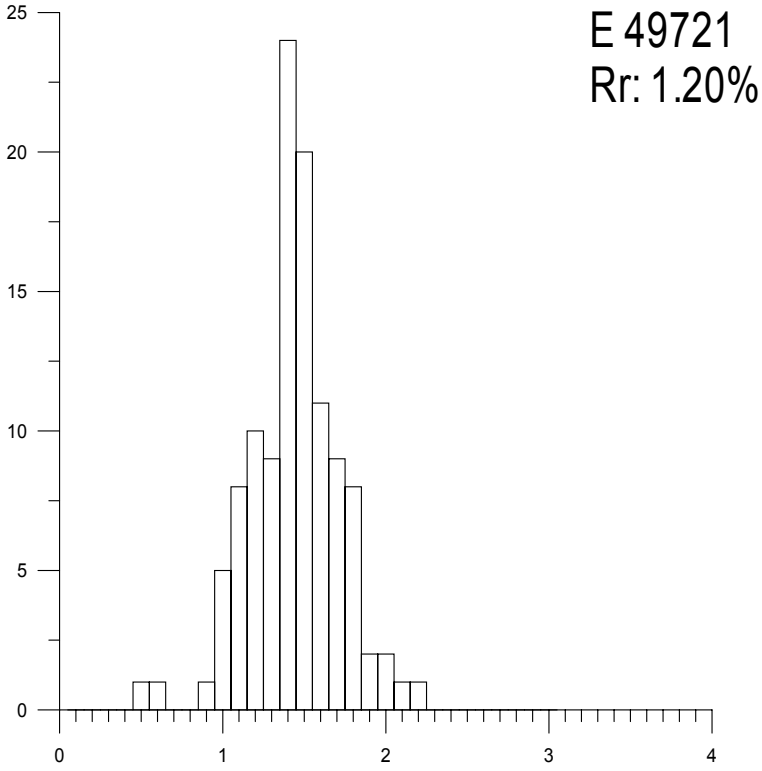
E 49721
Rr: 1.20%
25
20
15
10
5
0
0
1
2
3
4

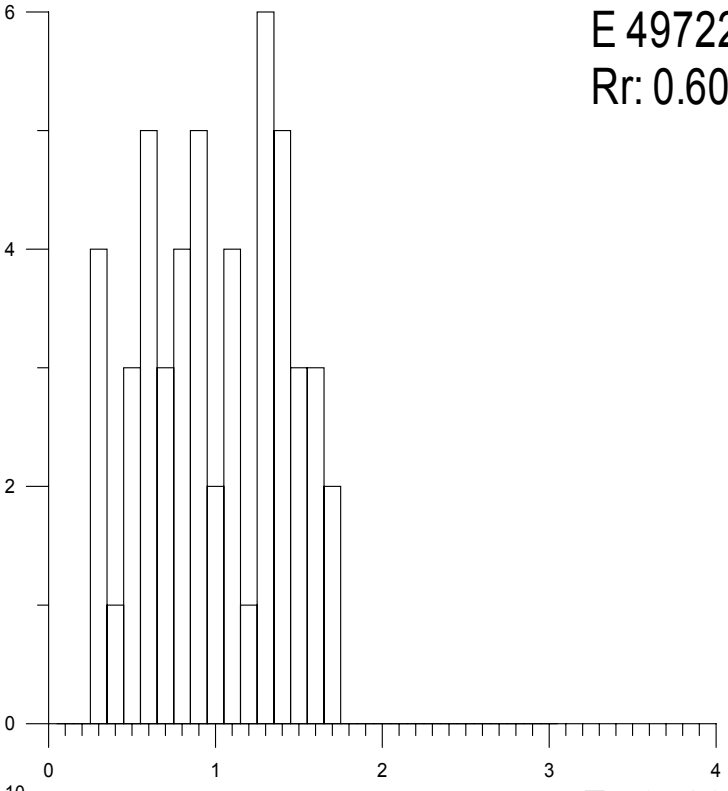
E 49722
Rr: 0.60%
6
4
2
0
0
1
2
3
4

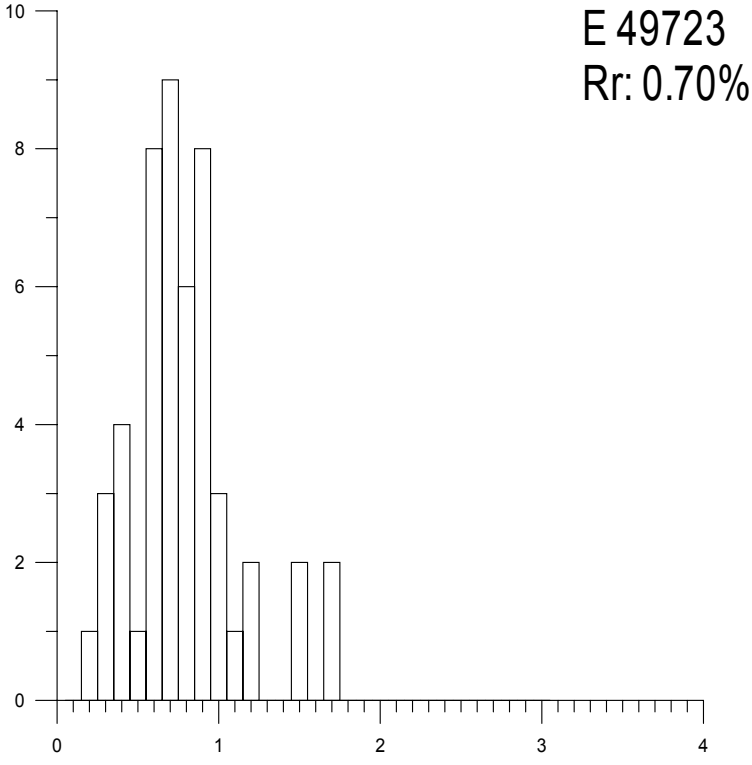
E 49723
Rr: 0.70%
10
8
6
4
2
0
0
1
2
3
4

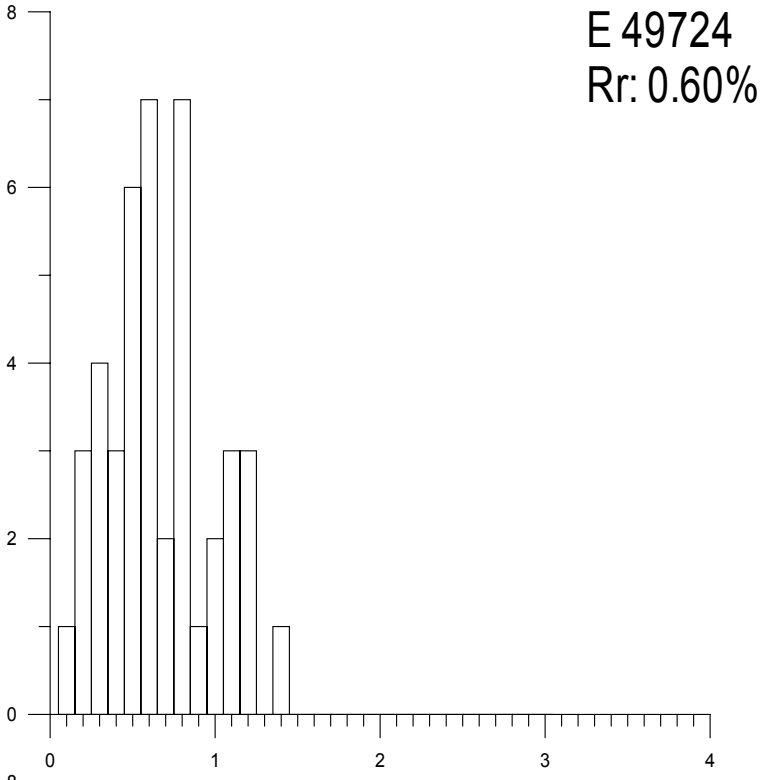
E 49724
Rr: 0.60%
8
6
4
2
0
0
1
2
3
4

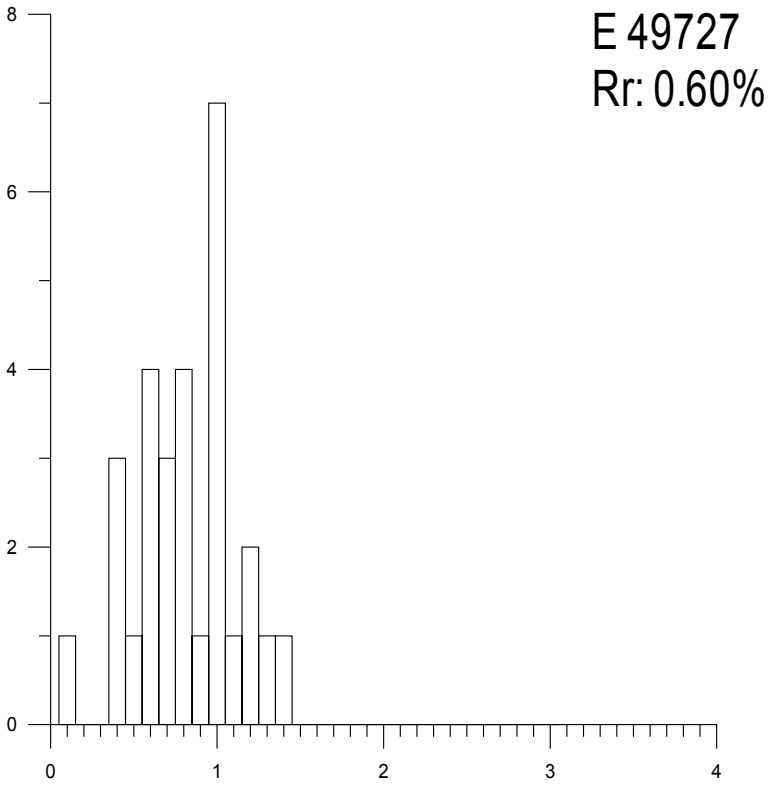
E 49727
Rr: 0.60%
8
6
4
2
0
0
1
2
3
4

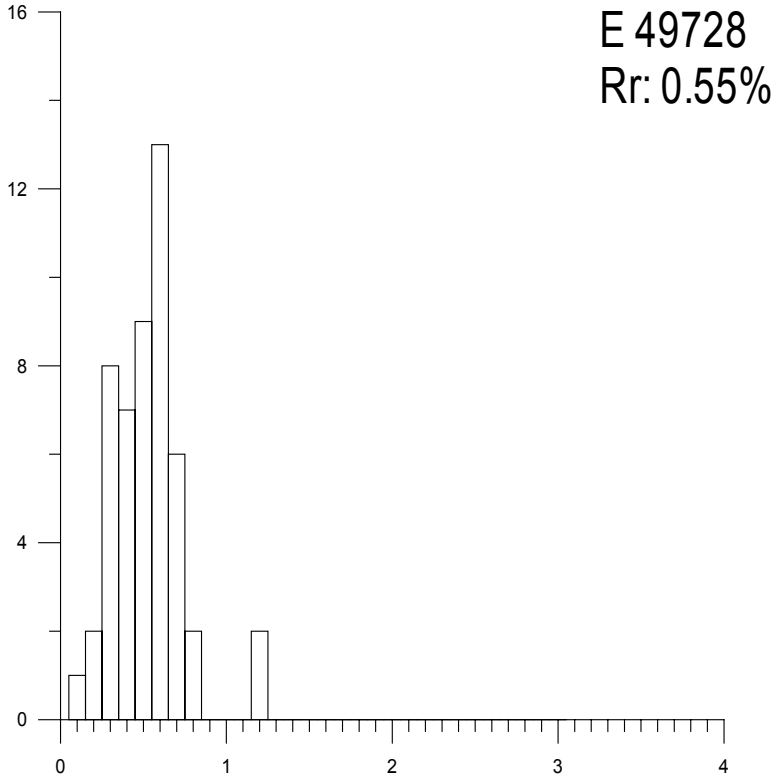
E 49728
Rr: 0.55%
16
12
8
4
0
0
1
2
3
4

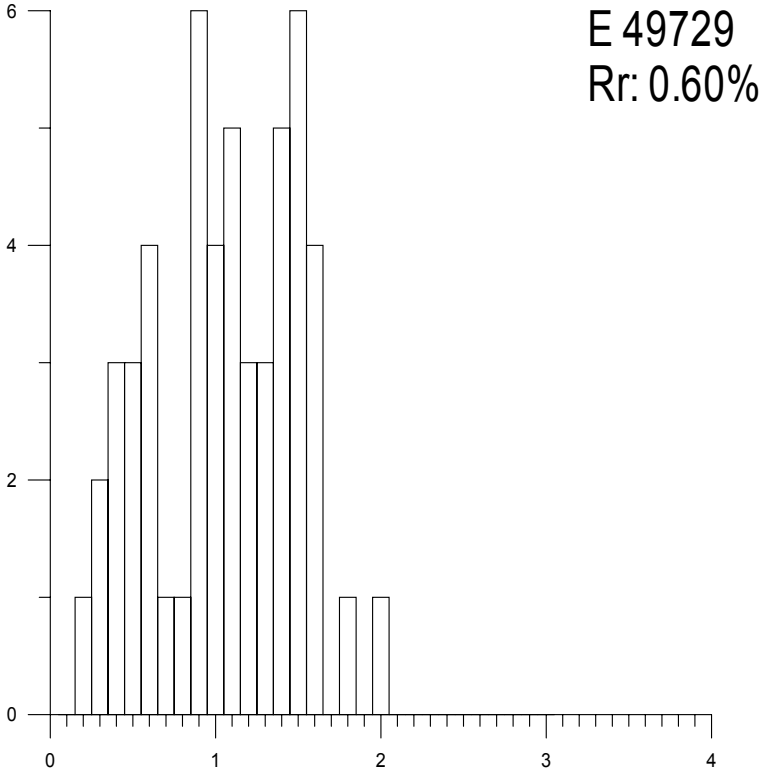
E 49729
Rr: 0.60%
6
4
2
0
0
1
2
3
4

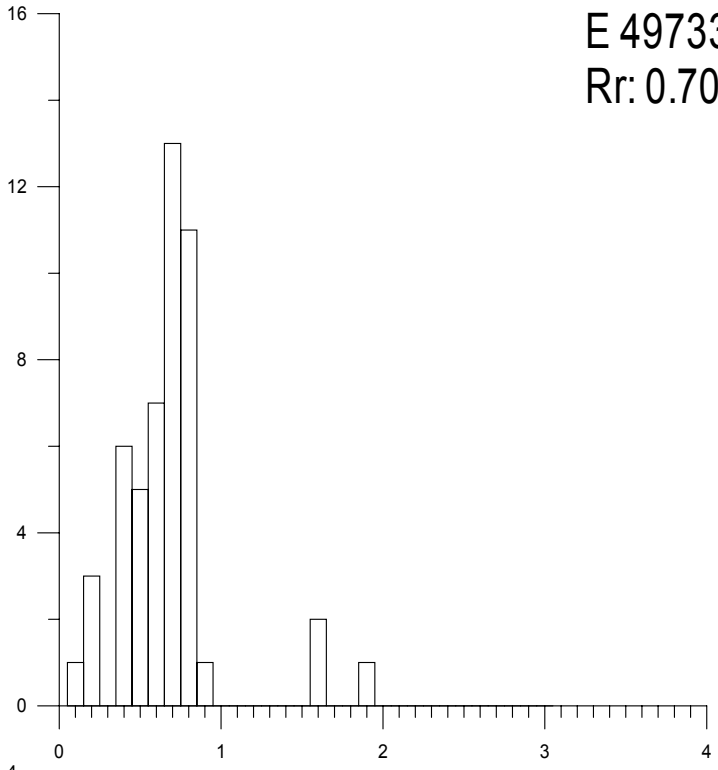
E 49733
Rr: 0.70%
16
12
8
4
0
0
1
2
3
4

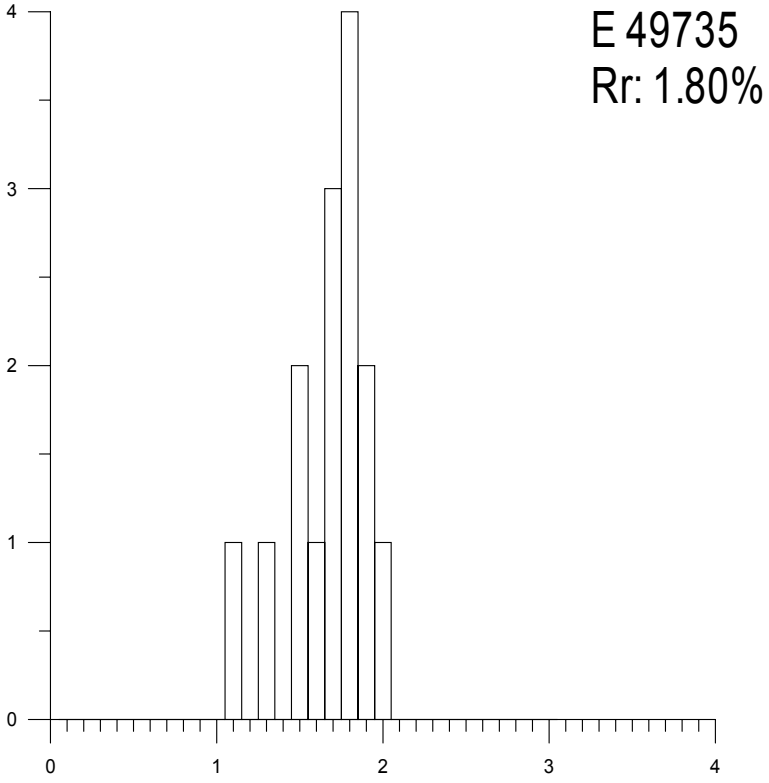
E 49735
Rr: 1.80%
4
3
2
1
0
0
1
2
3
4

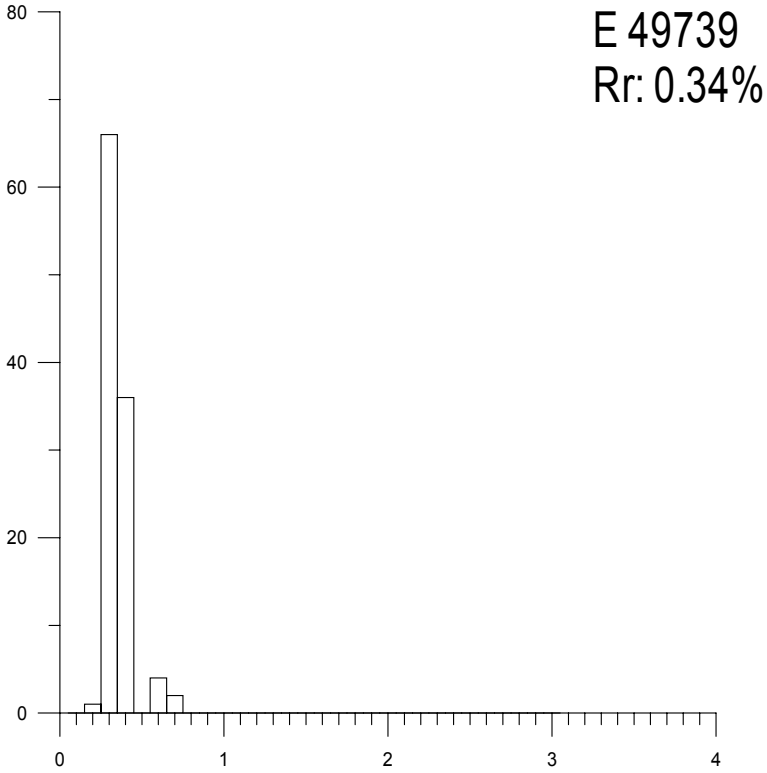
E 49739
Rr: 0.34%
80
60
40
20
0
0
1
2
3
4

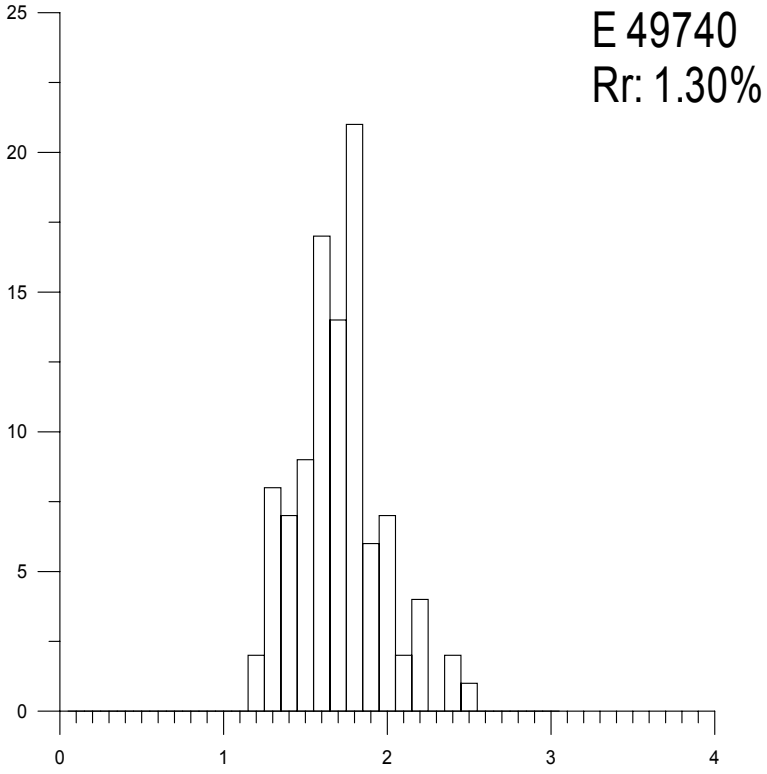
E 49740
Rr: 1.30%
25
20
15
10
5
0
0
1
2
3
4

8.3 Appendix III: Input-Data for Calibration Wells

well 26/28-1

Depth	Vitrinite reflectance	Depth	Bottom Hole Temperatures
[mbsf]	[Rr]	[mbsf]	[°C]
960	0.33	560	5
790	0.31	2049	52
1260	0.31	2925	94
1410	0.35	3475	114
2060	0.40		
2110	0.46		
2360	0.58		
2510	0.57		
2660	0.60		

well 35/8-2

Depth	Vitrinite reflectance	Depth	Bottom Hole Temperatures
[mbsf]	[Rr]	[mbsf]	[°C]
2918	0.54	669	5
		2201	42
		3904	106
		4831	146

well 35/15-1

Depth	Vitrinite reflectance	Depth	Bottom Hole Temperatures
[mbsf]	[Rr]	[mbsf]	[°C]
1493	0.29	781	5
2343	0.36	2007	41
		3795	95
		4154	117

well 35/18-1

Depth	Vitrinite reflectance	Depth	Bottom Hole Temperatures
[mbsf]	[Rr]	[mbsf]	[°C]
2869	0.44	837	5
3149	0.5	2545	43
3249	0.5	4150	90
3649	0.6		
3849	0.7		

well 35/6-1

Depth	Vitrinite reflectance	Depth	Bottom Hole Temperatures
[mbsf]	[Rr]	[mbsf]	[°C]
1509	0.28	722	5
1712	0.27	2554	54
2087	0.29	3837	89
2134	0.27	4165	124
2181	0.31		
2493	0.32		
2603	0.56		
3118	0.50		
3212	0.70		
3306	0.70		
3400	0.71		
3431	0.70		
3446	0.71		
3493	0.81		
3556	0.72		
3618	0.90		
3681	0.91		
3728	0.81		
3759	0.81		
3775	0.90		
3790	0.81		
3900	1.00		
4009	1.10		
4087	1.10		

well 35/13-1

Depth	Vitrinite reflectance	Depth	Bottom Hole Temperatures
[mbsf]	[Rr]	[mbsf]	[°C]
2364	0.4	771	5
2704	0.5	1692	36
3014	0.5	2692	63
3664	0.6	3764	100
3864	0.65	4098	110
		4396	114

8.4 Appendix IV: Static Headspace Chromatograms

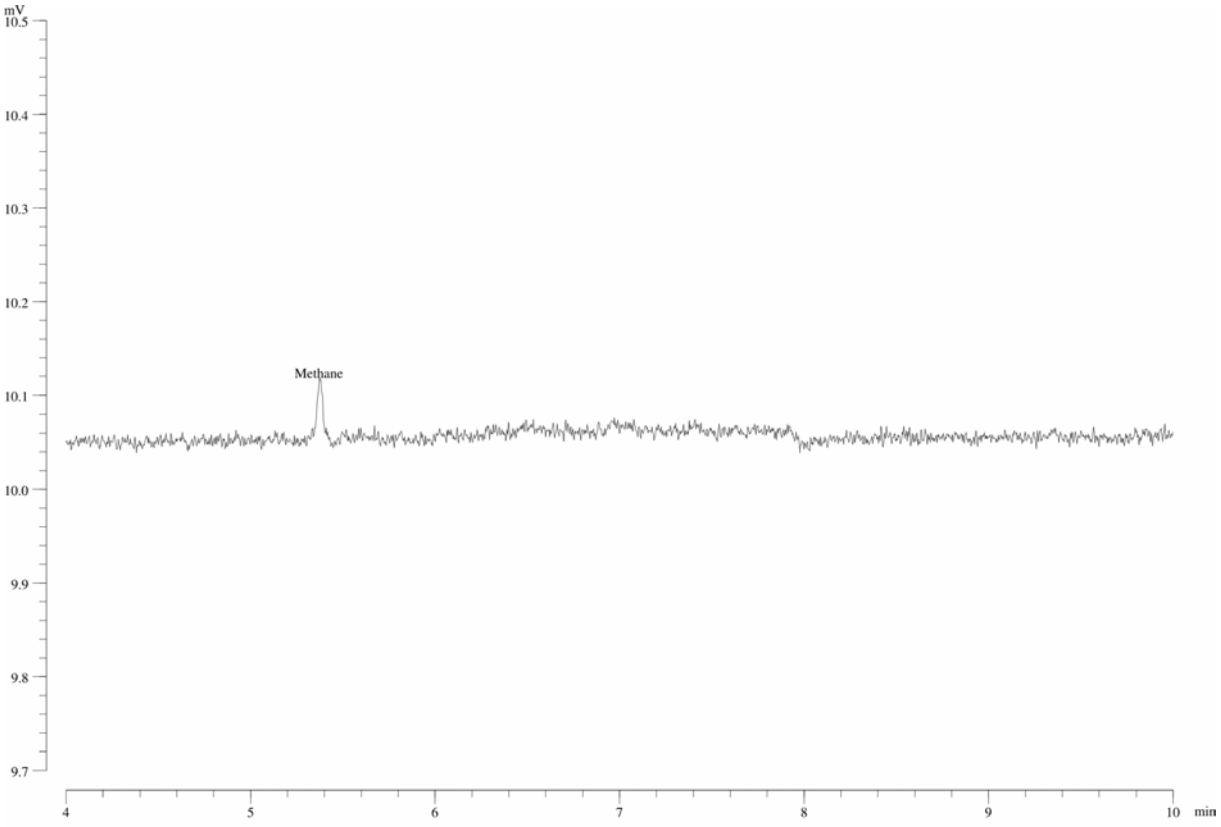

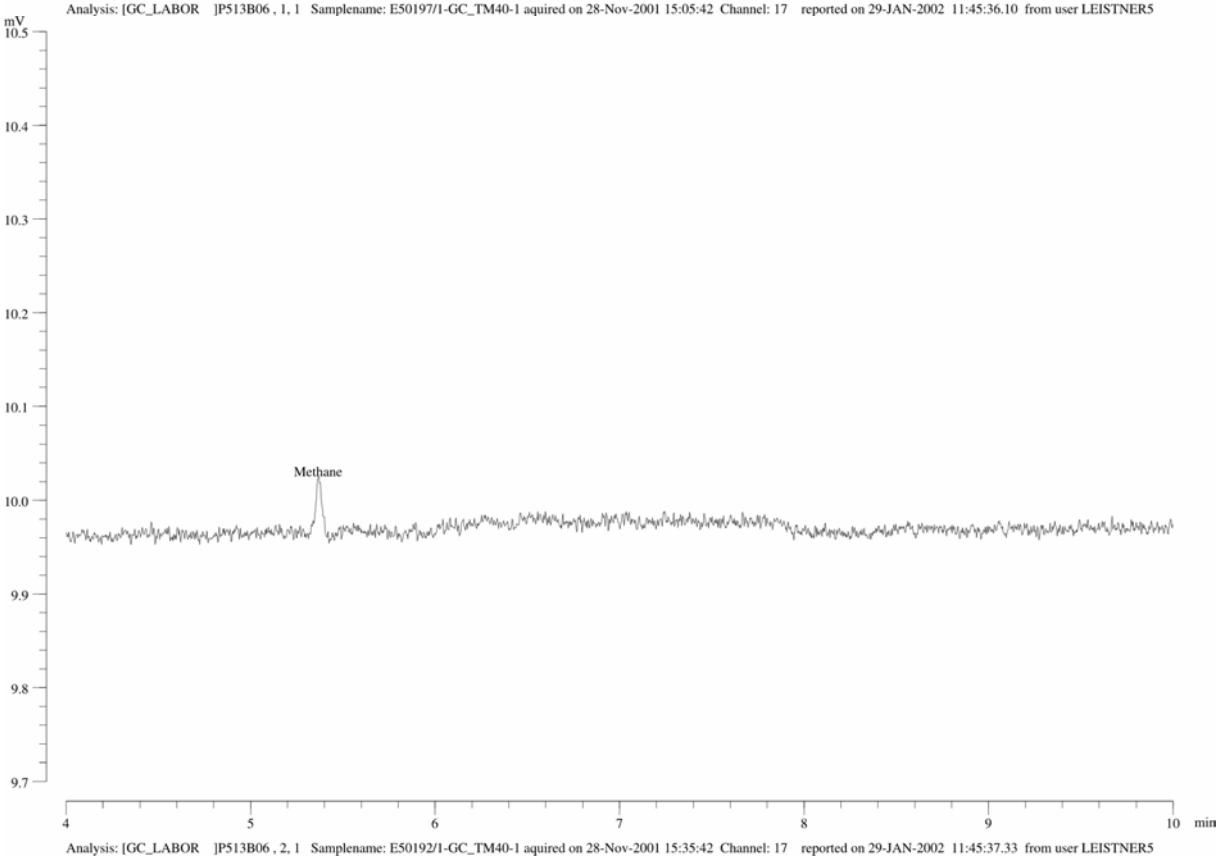

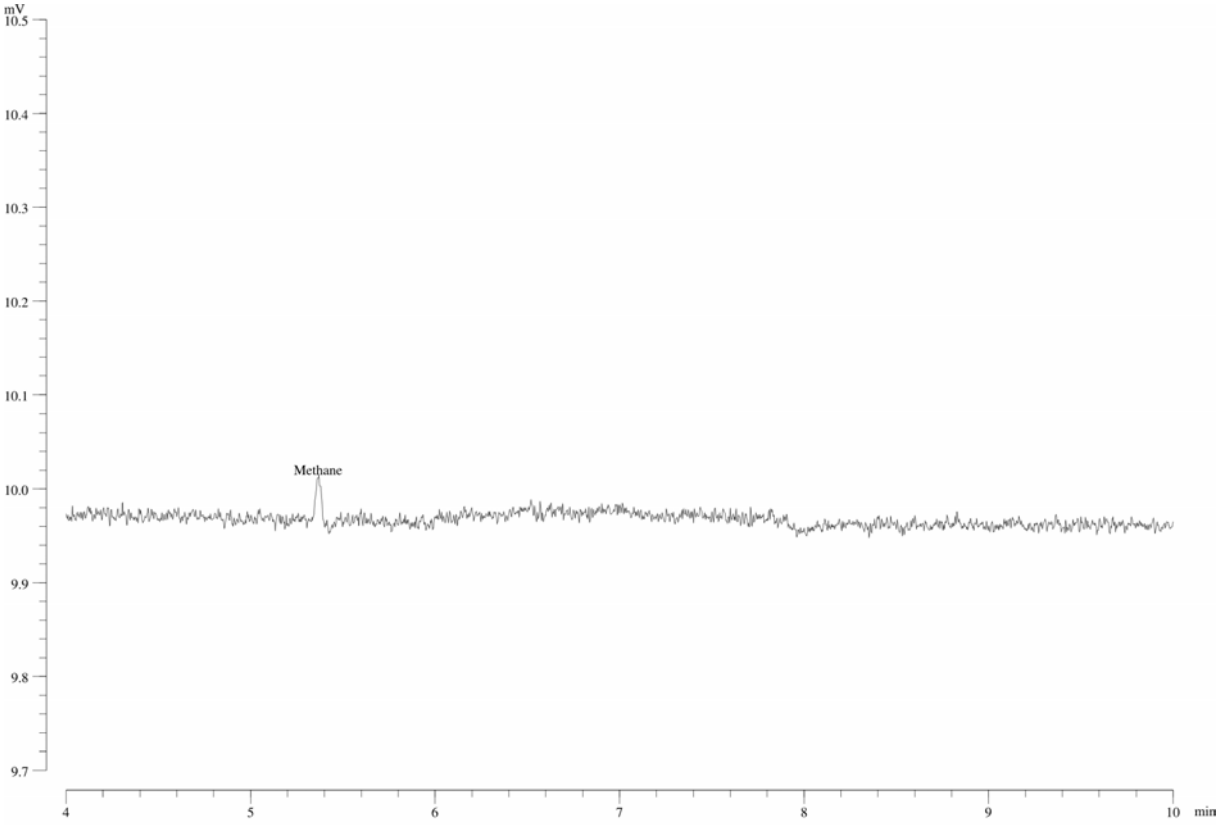

Analysis: [GC_LABOR]P513B06 , 3, 1 Samplename: E50190/1-GC_TM40-1 aquired on 28-Nov-2001 16:05:42 Channel: 17 reported on 29-JAN-2002 11:45:38.43 from user LEISTNER5

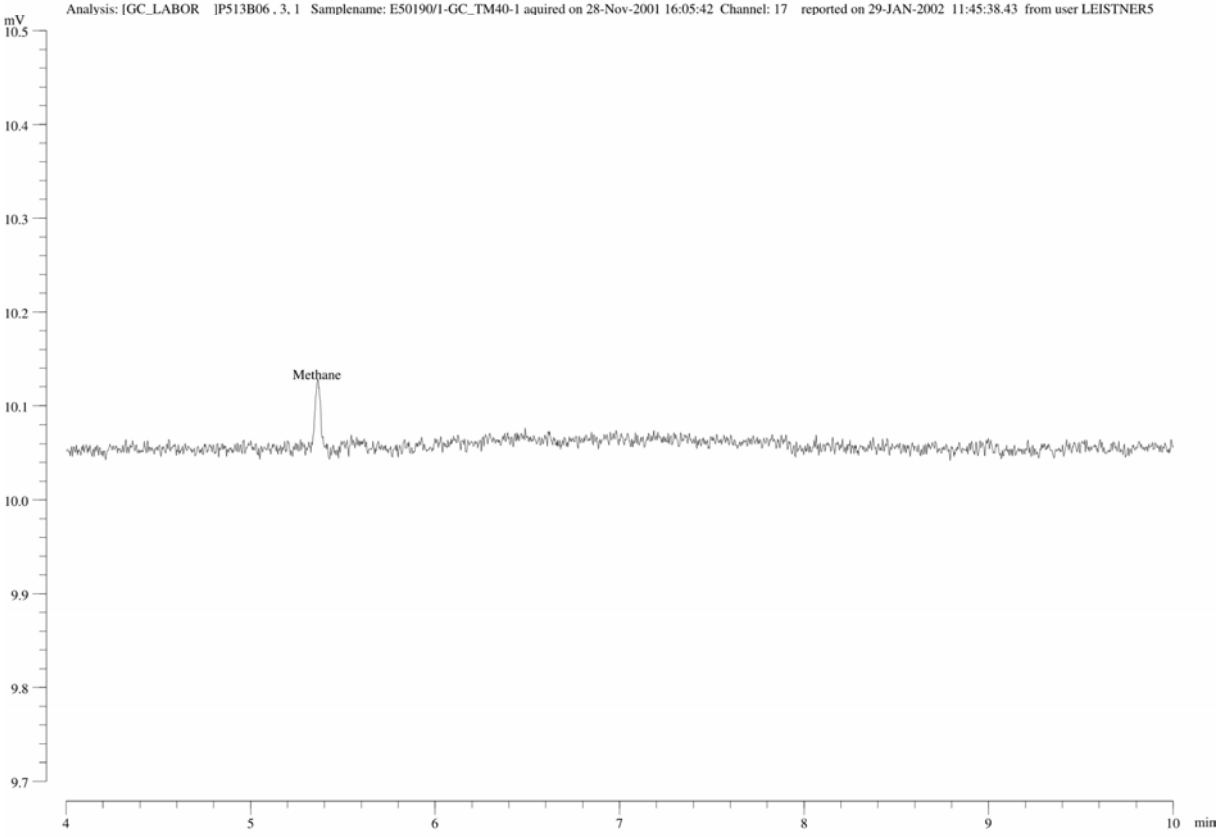

Analysis: [GC_LABOR]P513B06 , 4, 1 Samplename: E50189/1-GC_TM40-1 aquired on 28-Nov-2001 16:35:41 Channel: 17 reported on 29-JAN-2002 11:45:39.51 from user LEISTNER5

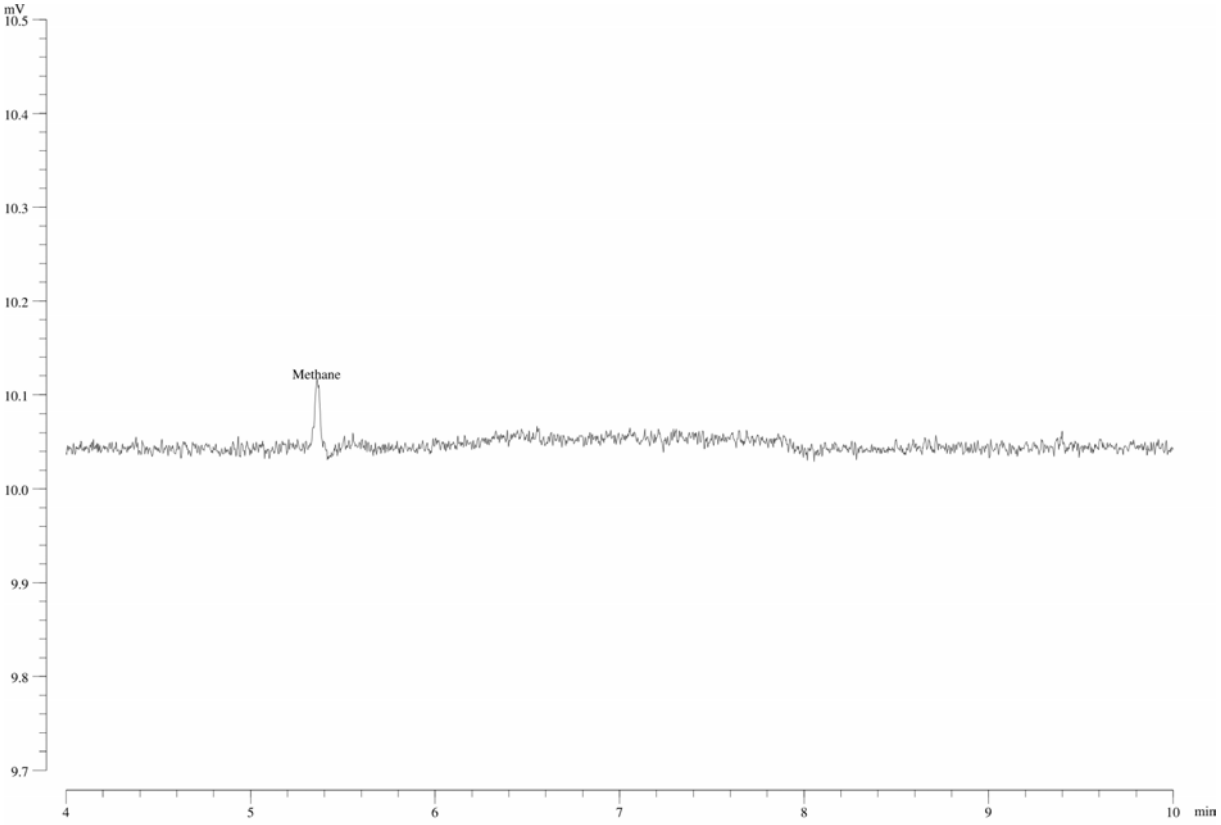

Analysis: [GC_LABOR]P513B06 , 5, 1 Samplename: E50188/1-GC_TM40-1 aquired on 28-Nov-2001 17:05:41 Channel: 17 reported on 29-JAN-2002 11:45:40.60 from user LEISTNER5

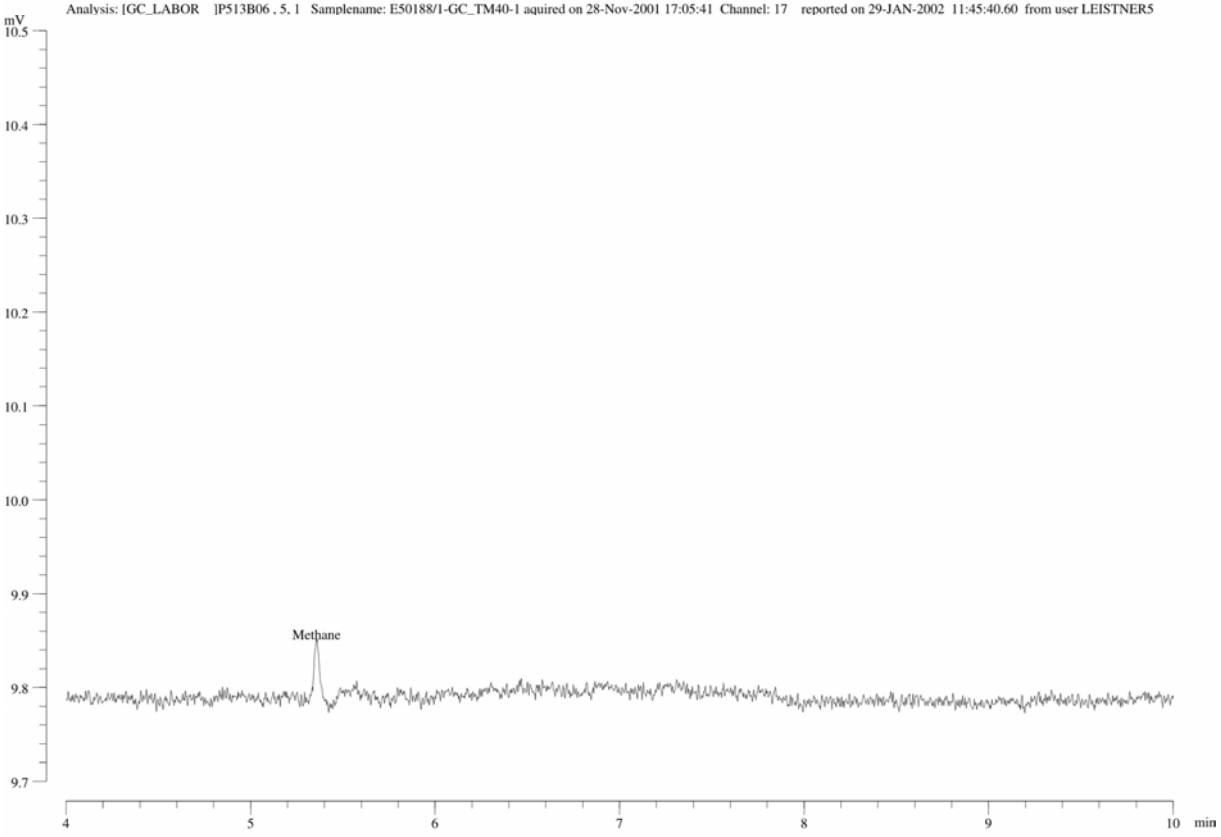

Analysis: [GC_LABOR]P513B06 , 6, 1 Samplename: E50187/1-GC_TM40-1 aquired on 28-Nov-2001 17:35:41 Channel: 17 reported on 29-JAN-2002 11:45:41.64 from user LEISTNER5

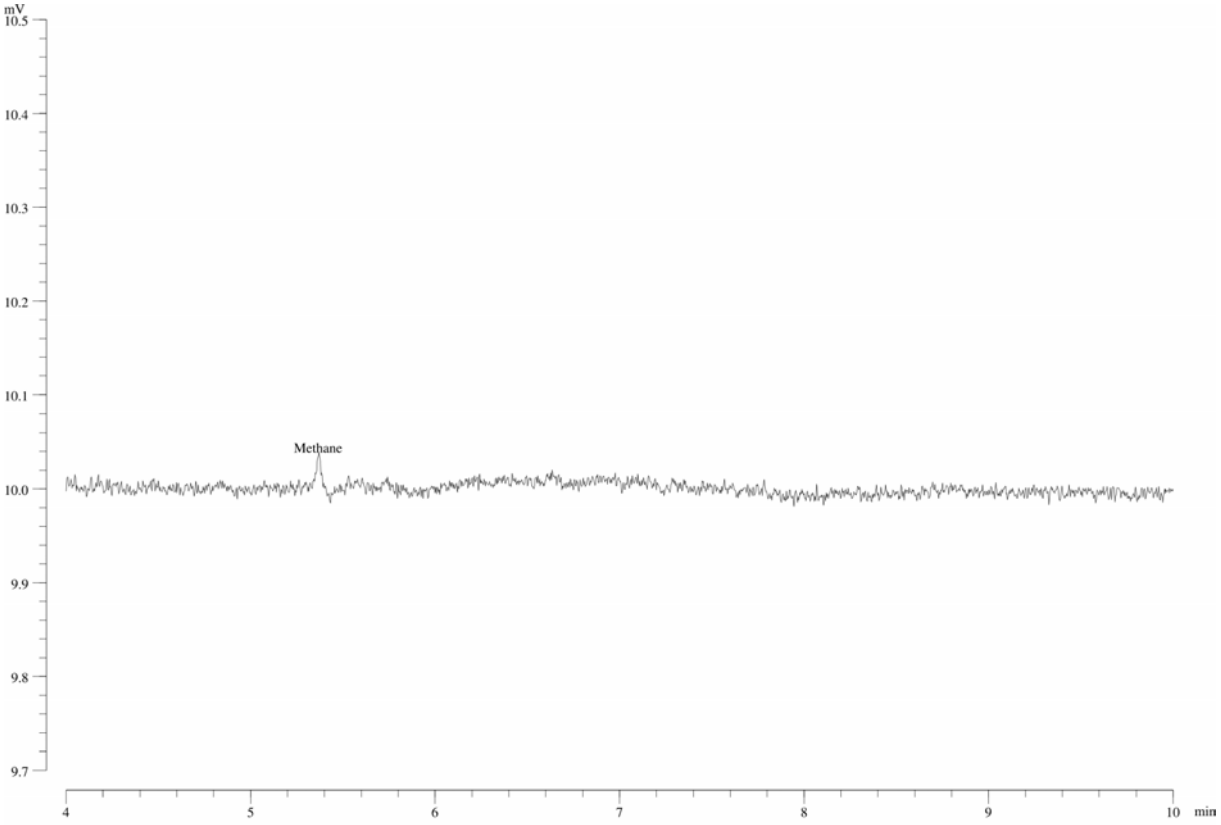

Analysis: [GC_LABOR]P513B06 , 7, 1 Samplename: E50174/1-GC_TM40-1 aquired on 28-Nov-2001 18:05:41 Channel: 17 reported on 29-JAN-2002 11:45:42.72 from user LEISTNER5

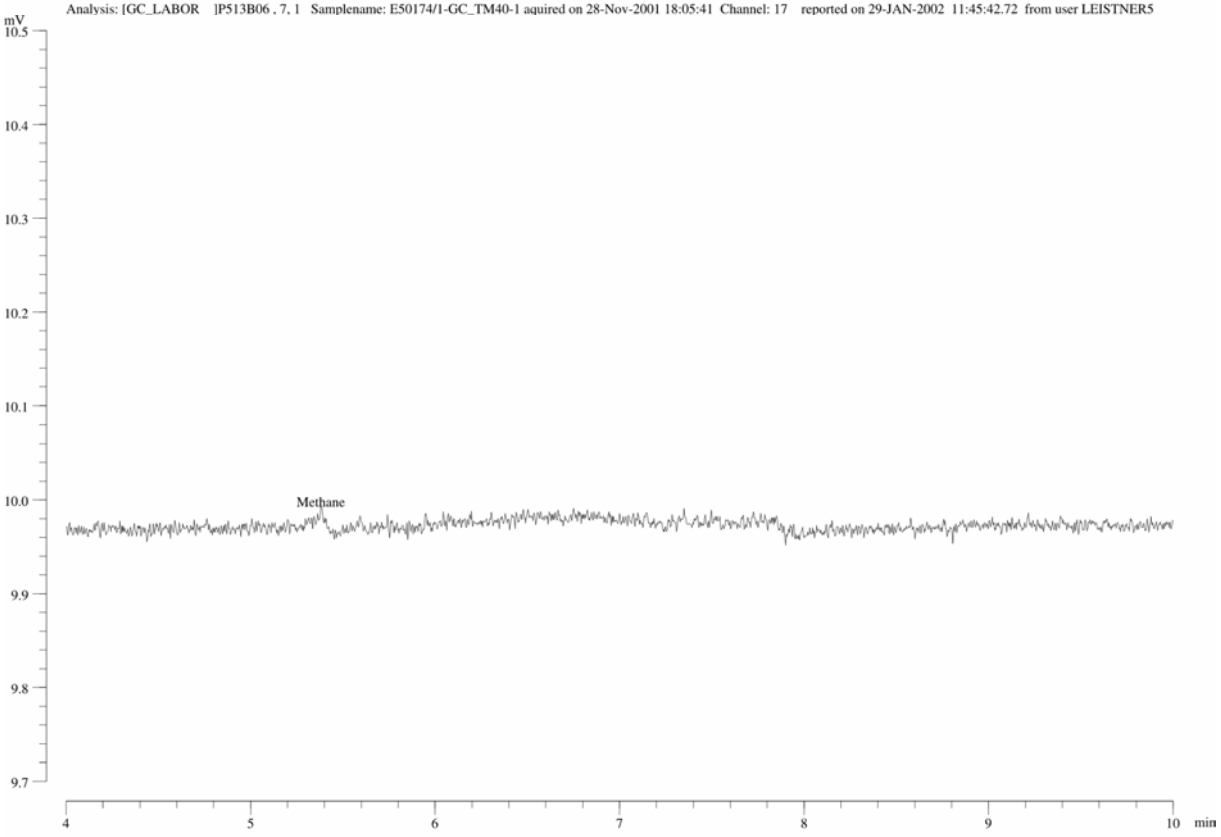

Analysis: [GC_LABOR]P513B06 , 8, 1 Samplename: E50172/1-GC_TM40-1 aquired on 28-Nov-2001 18:35:41 Channel: 17 reported on 29-JAN-2002 11:45:44.01 from user LEISTNER5

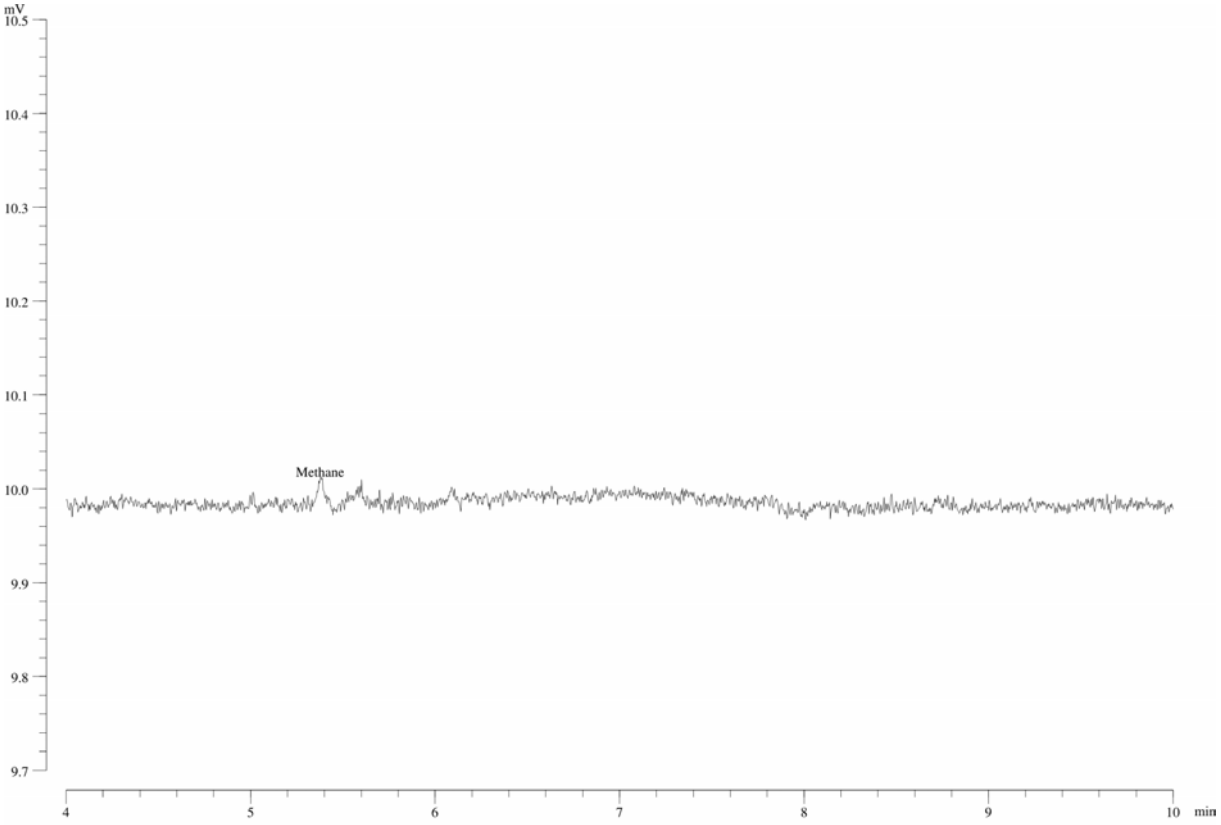

Analysis: [GC_LABOR]P513B06 , 9, 1 Samplename: E50171/1-GC_TM40-1 aquired on 28-Nov-2001 19:05:41 Channel: 17 reported on 29-JAN-2002 11:45:45.06 from user LEISTNER5

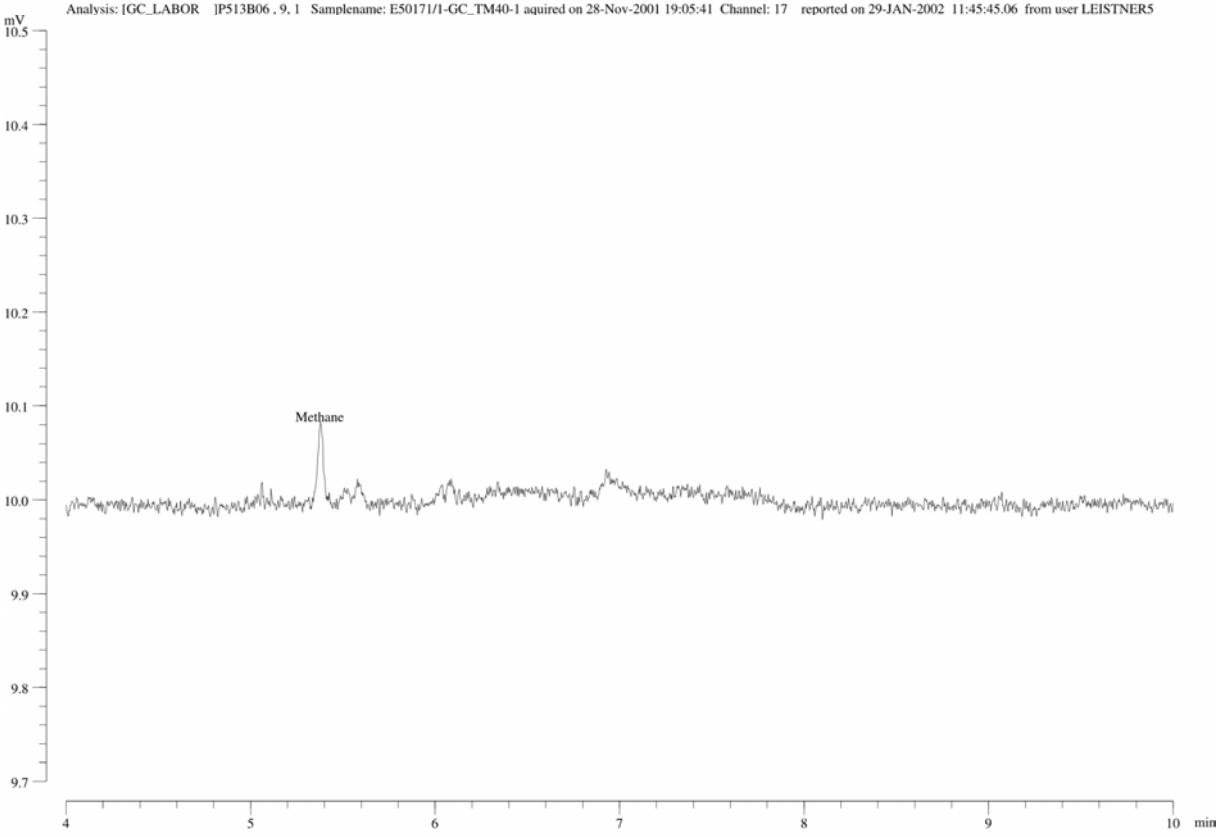

Analysis: [GC_LABOR]P513B06 ,10, 1 Samplename: E50170/1-GC_TM40-1 aquired on 28-Nov-2001 19:35:41 Channel: 17 reported on 29-JAN-2002 11:45:46.09 from user LEISTNER5

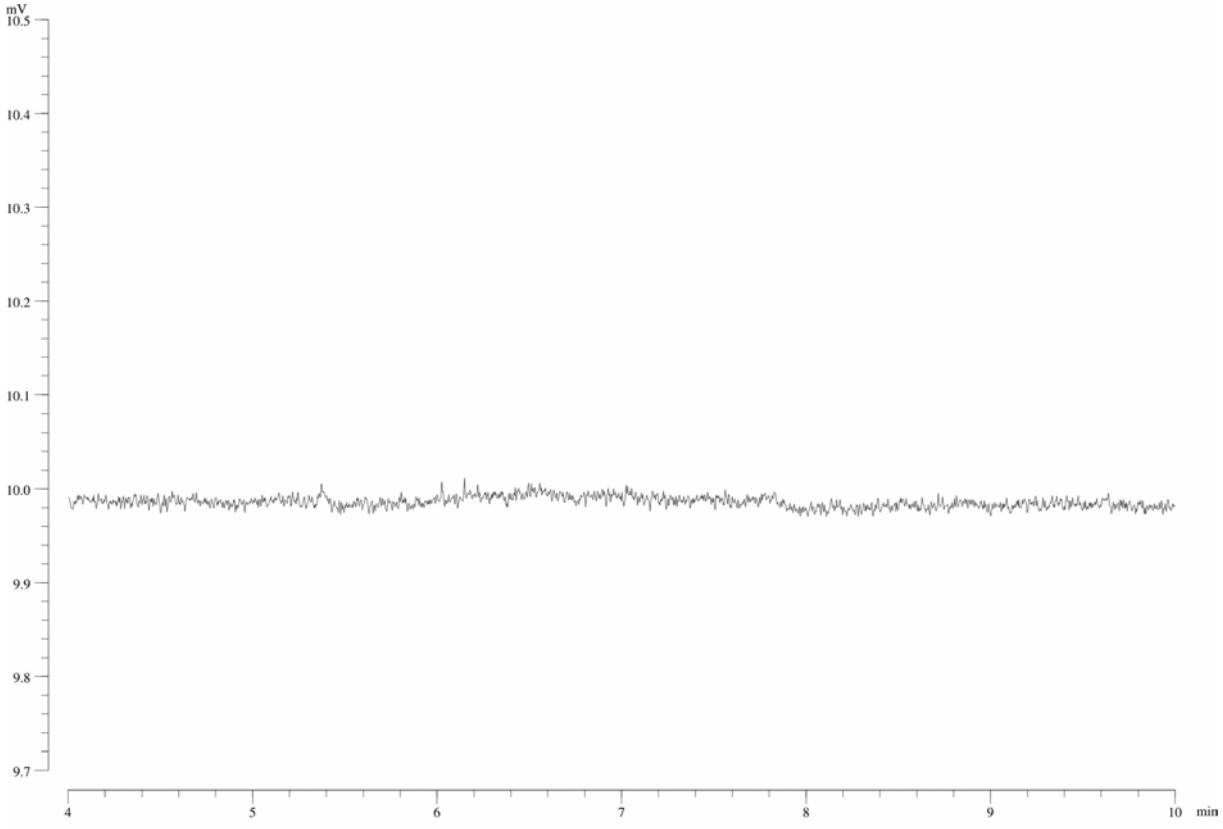

Analysis: [GC_LABOR]P513B06 ,11, 1 Samplename: E50169/1-GC_TM40-1 aquired on 28-Nov-2001 20:05:41 Channel: 17 reported on 29-JAN-2002 11:45:47.19 from user LEISTNER5

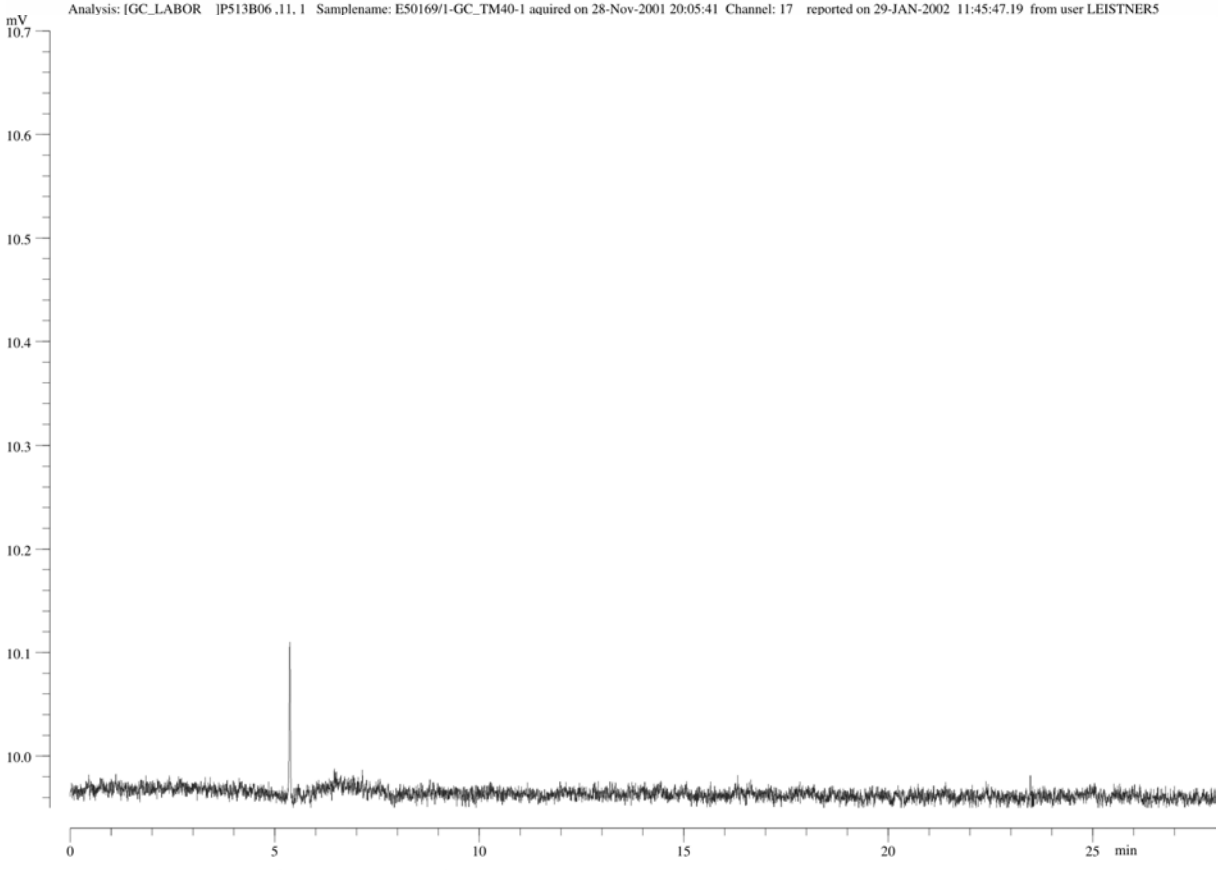

Analysis: [GC_LABOR]P513B06 ,12, 1 Samplename: E50168/1-GC_TM40-1 aquired on 28-Nov-2001 20:35:41 Channel: 17 reported on 5-DEC-2001 15:59:25.32 from user LEISTNER5

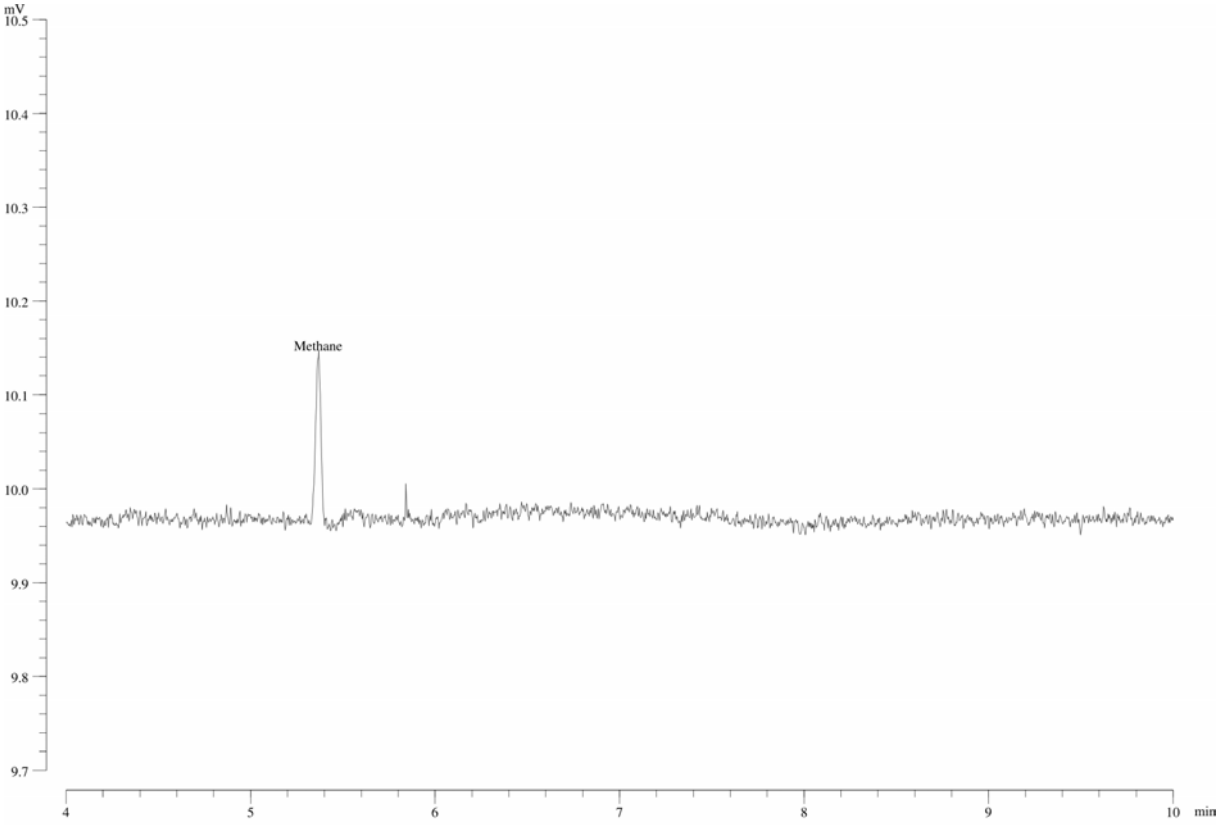

Analysis: [GC_LABOR]P513B06 ,13, 1 Samplename: E50167/1-GC_TM40-1 aquired on 28-Nov-2001 21:05:41 Channel: 17 reported on 29-JAN-2002 11:45:49.39 from user LEISTNER5

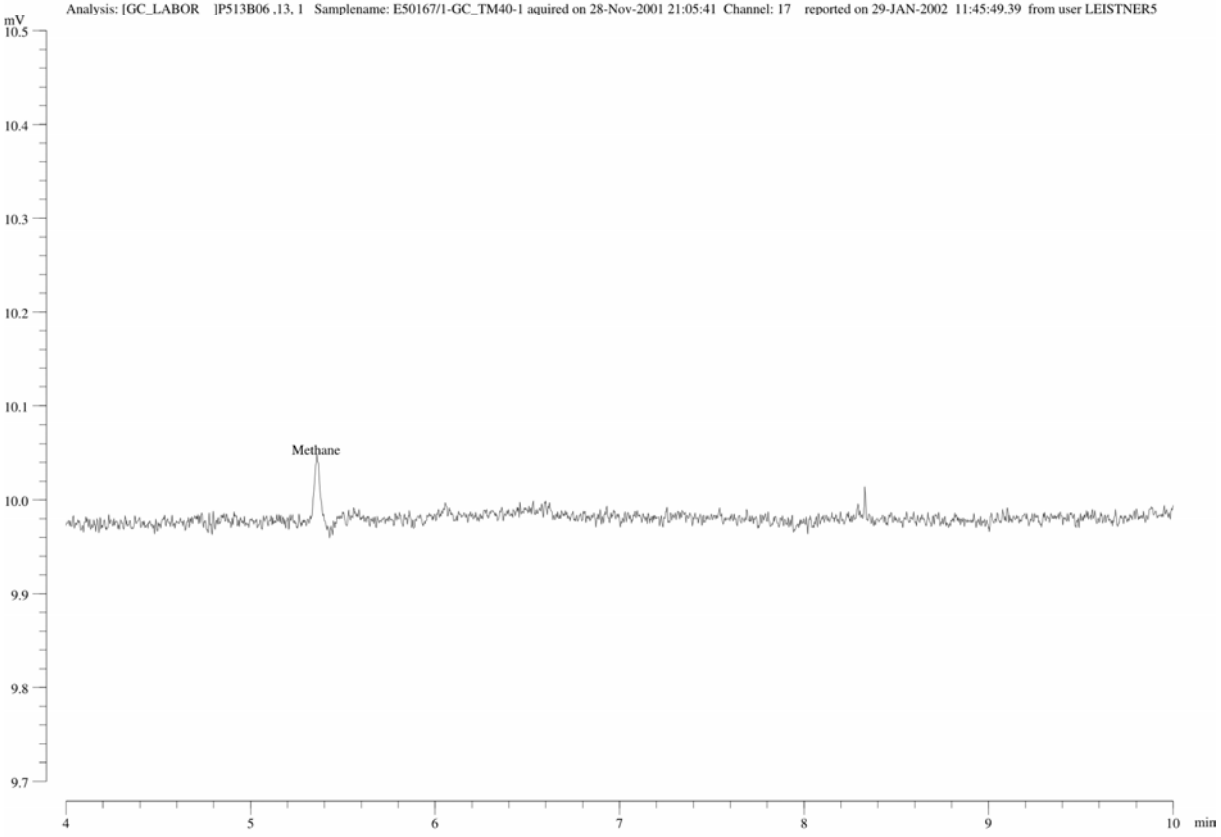

Analysis: [GC_LABOR]P513B06 ,14, 1 Samplename: E50226/1-GC_TM40-1 aquired on 28-Nov-2001 21:35:41 Channel: 17 reported on 29-JAN-2002 11:45:50.46 from user LEISTNER5

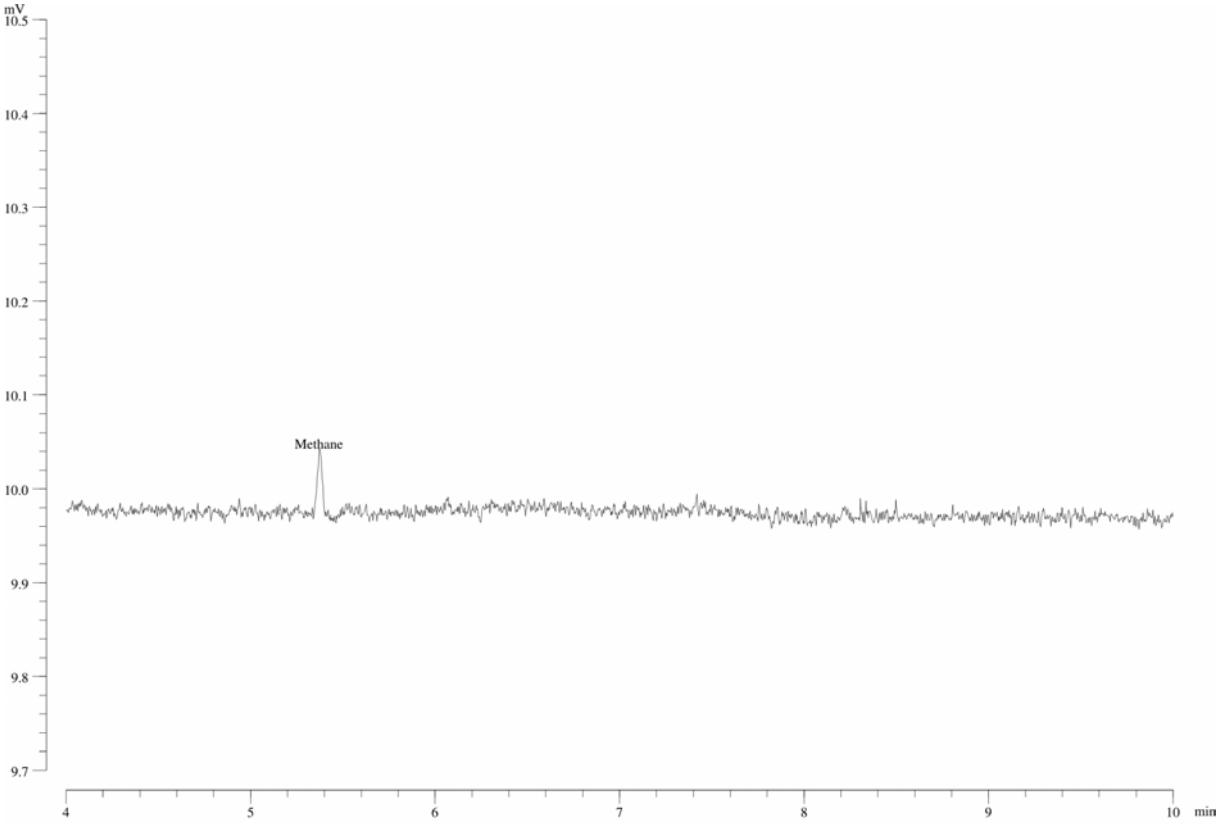

Analysis: [GC_LABOR]P513B06 ,15, 1 Samplename: E50225/1-GC_TM40-1 aquired on 28-Nov-2001 22:05:41 Channel: 17 reported on 29-JAN-2002 11:45:51.55 from user LEISTNER5

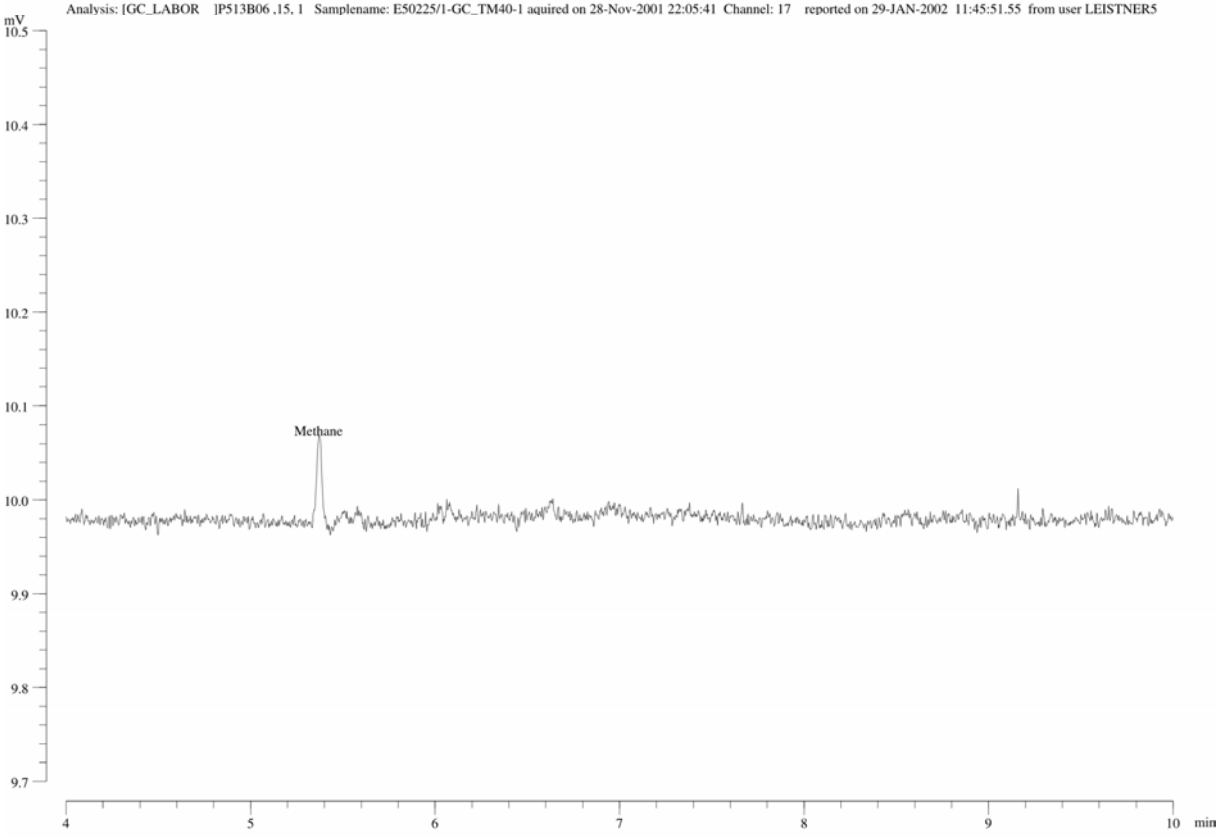

Analysis: [GC_LABOR]P513B06 ,16, 1 Samplename: E50224/1-GC_TM40-1 aquired on 28-Nov-2001 22:35:41 Channel: 17 reported on 29-JAN-2002 11:45:52.66 from user LEISTNER5

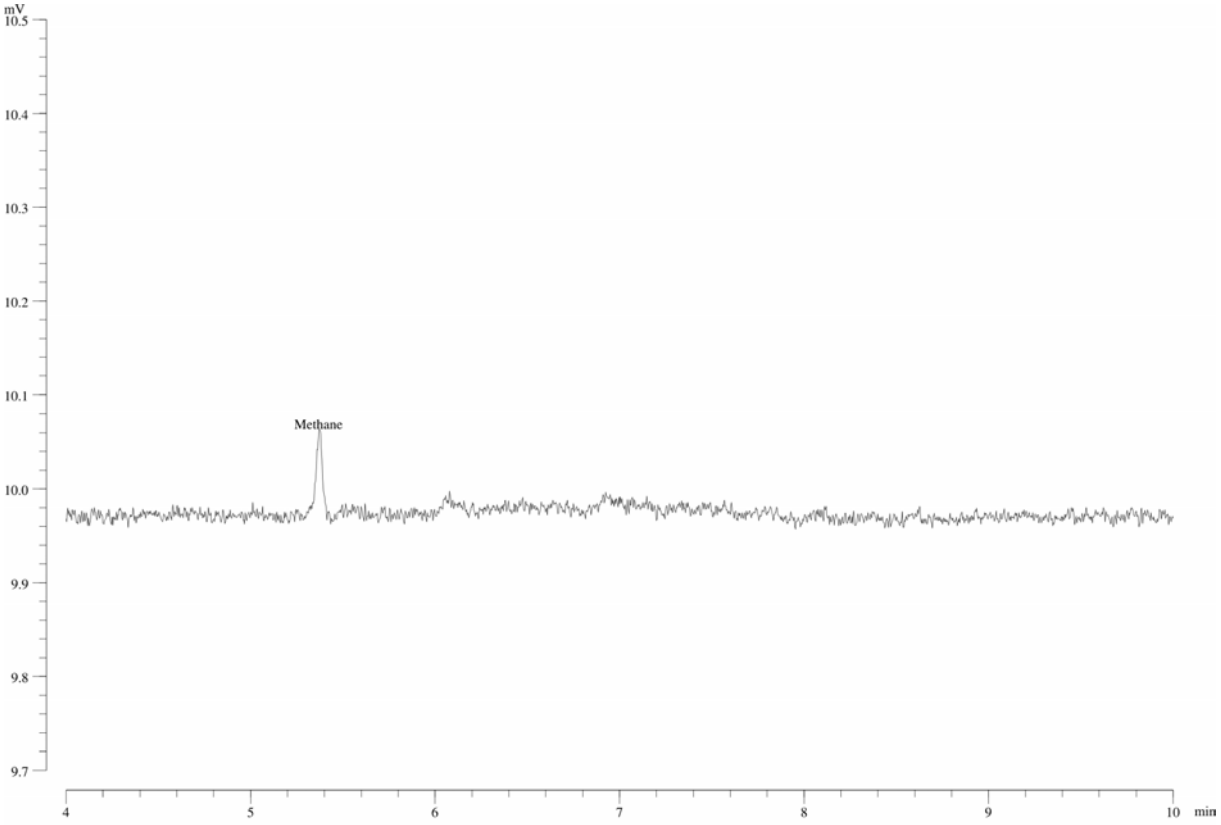

Analysis: [GC_LABOR]P513B06 ,17, 1 Samplename: E50223/1-GC_TM40-1 aquired on 28-Nov-2001 23:05:41 Channel: 17 reported on 29-JAN-2002 11:45:53.74 from user LEISTNER5

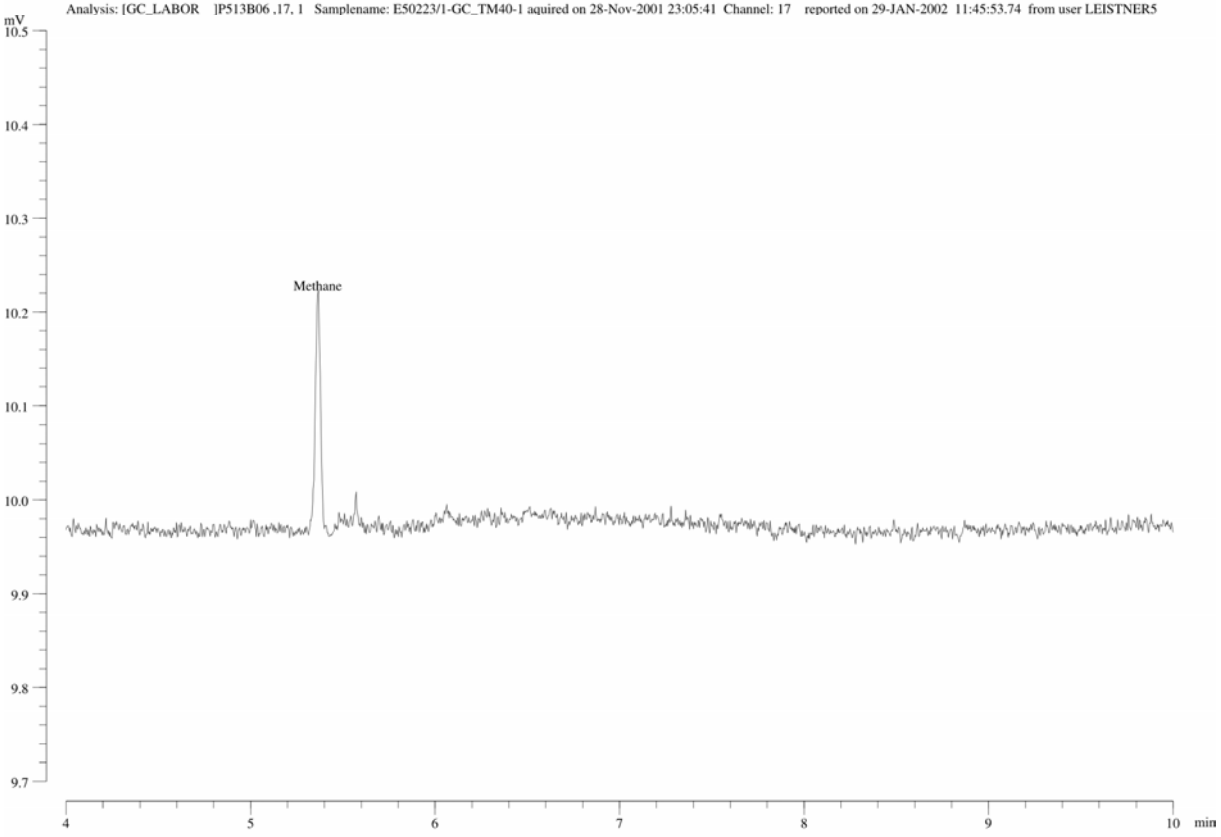

Analysis: [GC_LABOR]P513B06 ,18, 1 Samplename: E50221/1-GC_TM40-1 aquired on 28-Nov-2001 23:35:41 Channel: 17 reported on 29-JAN-2002 11:45:54.83 from user LEISTNER5

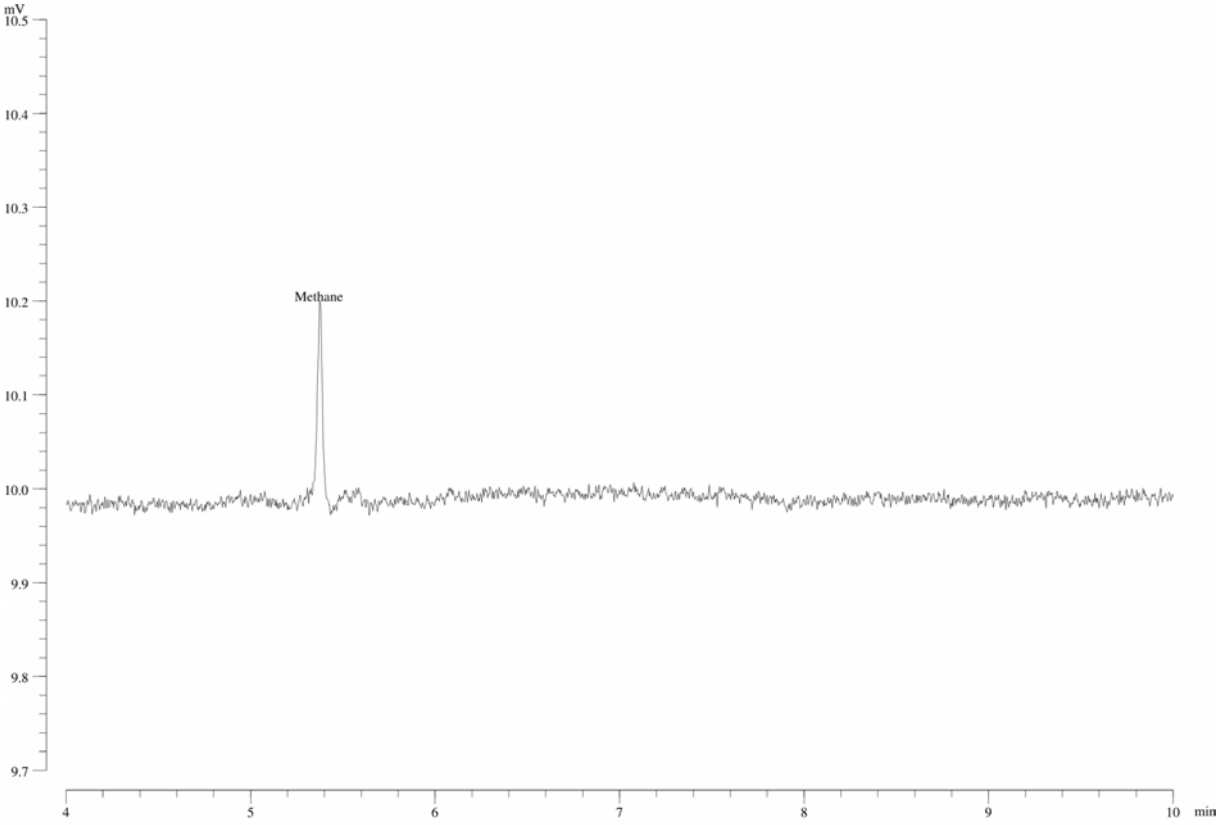

Analysis: [GC_LABOR]P513B06 ,19, 1 Samplename: E50220/1-GC_TM40-1 aquired on 29-Nov-2001 00:05:41 Channel: 17 reported on 29-JAN-2002 11:45:56.11 from user LEISTNER5

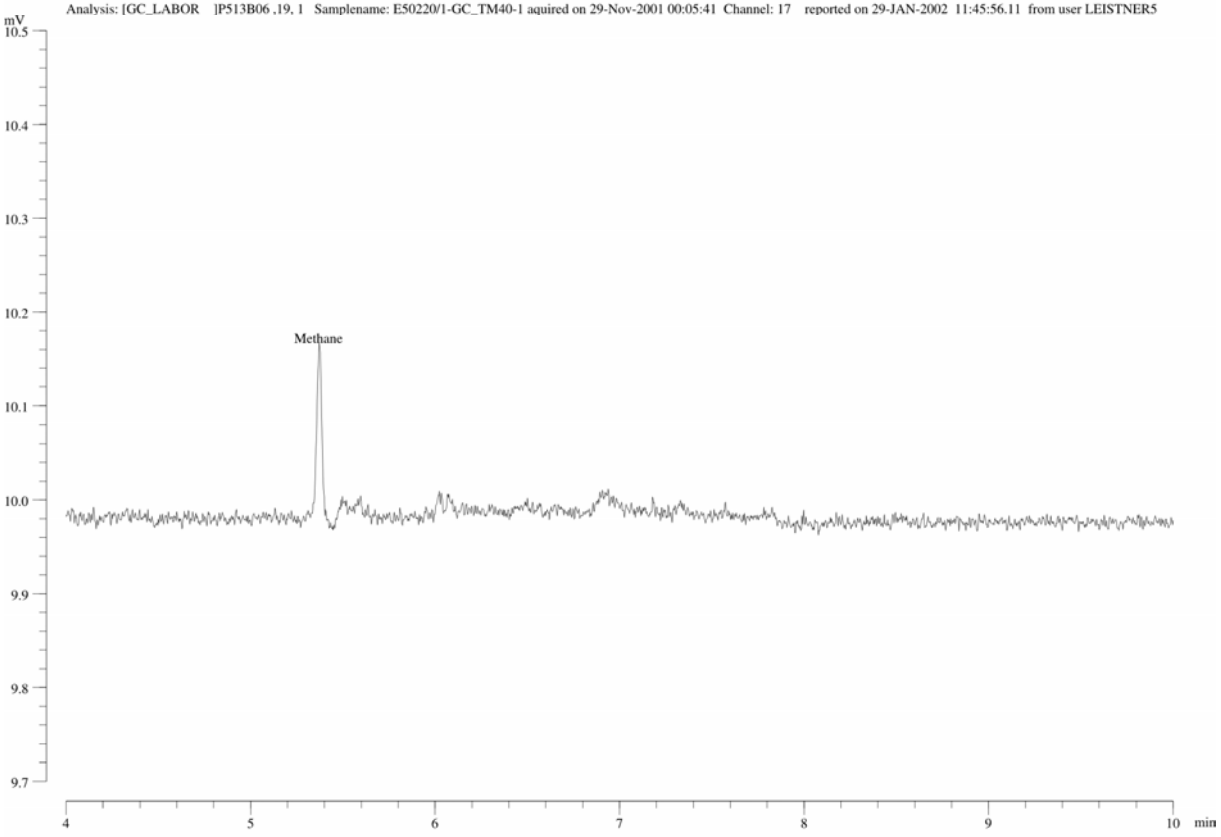

Analysis: [GC_LABOR]P513B06 ,20, 1 Samplename: E50219/1-GC_TM40-1 aquired on 29-Nov-2001 00:35:41 Channel: 17 reported on 29-JAN-2002 11:45:57.20 from user LEISTNER5

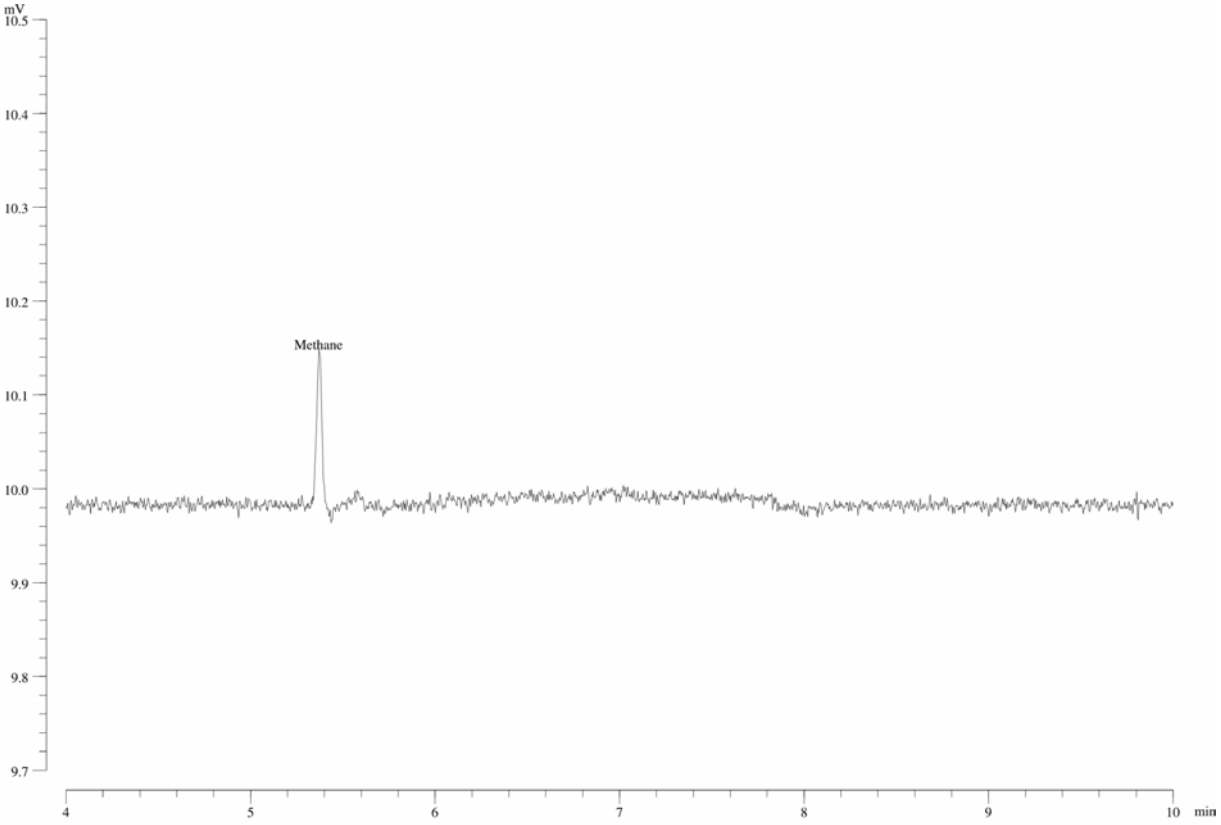

Analysis: [GC_LABOR]P513B06 ,21, 1 Samplename: E50218/1-GC_TM40-1 aquired on 29-Nov-2001 01:05:41 Channel: 17 reported on 29-JAN-2002 11:45:58.31 from user LEISTNER5

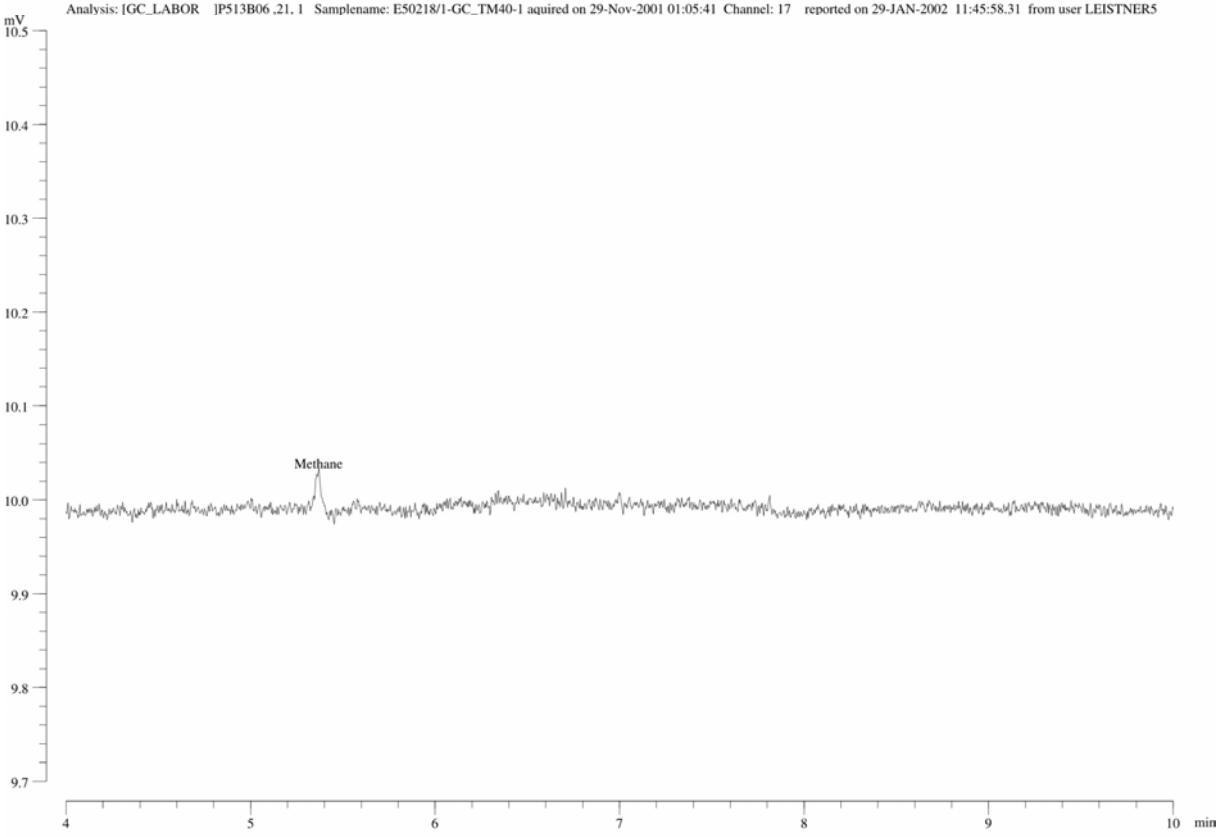

Analysis: [GC_LABOR]P513B06 ,22, 1 Samplename: E50217/1-GC_TM40-1 aquired on 29-Nov-2001 01:35:41 Channel: 17 reported on 29-JAN-2002 11:45:59.39 from user LEISTNER5

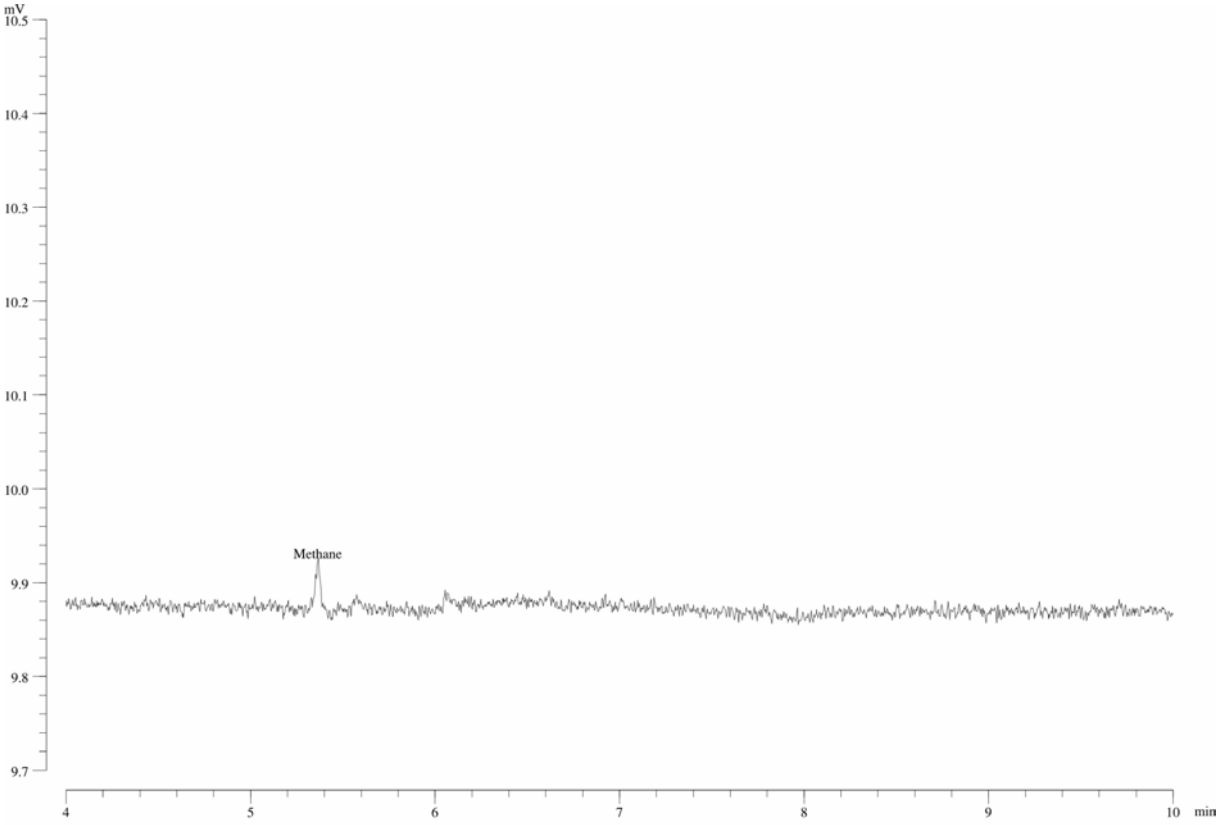

Analysis: [GC_LABOR]P513B06 ,23, 1 Samplename: E50216/1-GC_TM40-1 aquired on 29-Nov-2001 02:05:41 Channel: 17 reported on 29-JAN-2002 11:46:00.47 from user LEISTNER5

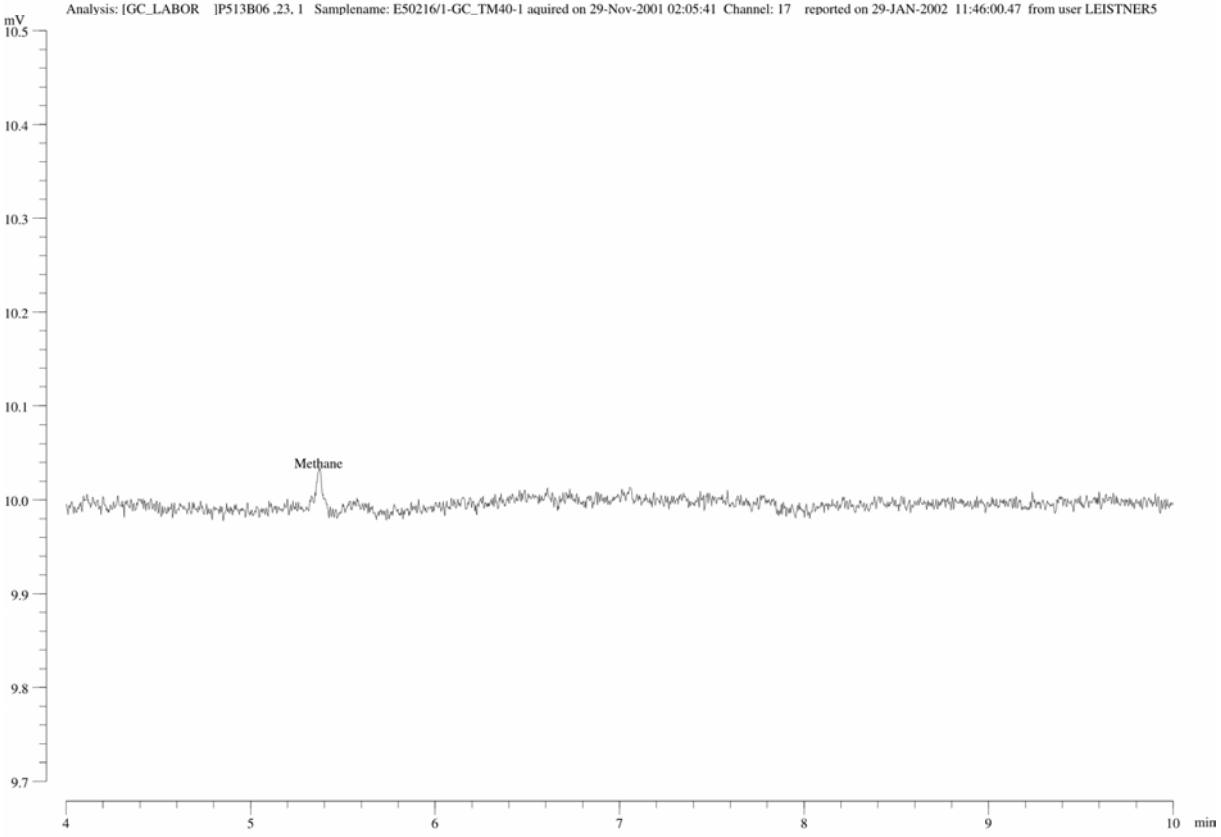

Analysis: [GC_LABOR]P513B06 ,24, 1 Samplename: E50215/1-GC_TM40-1 aquired on 29-Nov-2001 02:35:41 Channel: 17 reported on 29-JAN-2002 11:46:01.59 from user LEISTNER5

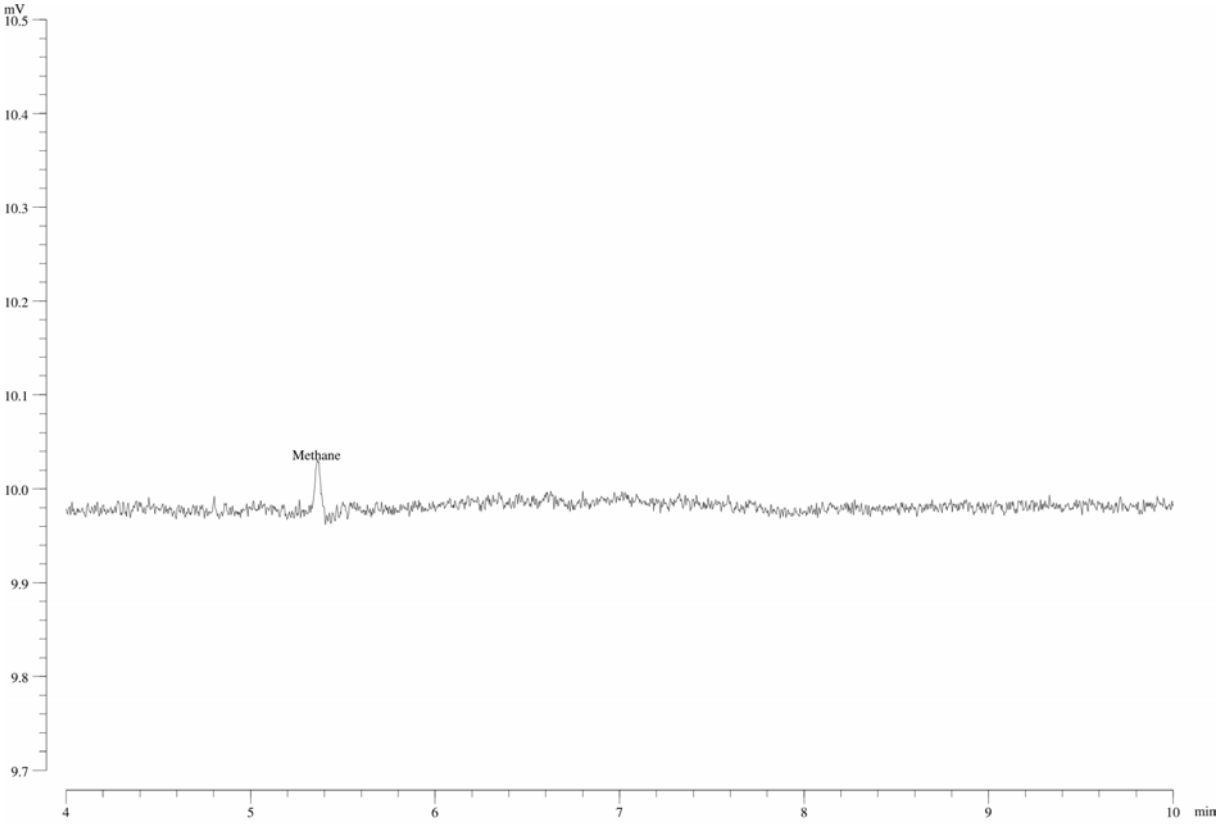

Analysis: [GC_LABOR]P513B06 ,25, 1 Samplename: E50214/1-GC_TM40-1 aquired on 29-Nov-2001 03:05:41 Channel: 17 reported on 29-JAN-2002 11:46:02.67 from user LEISTNER5

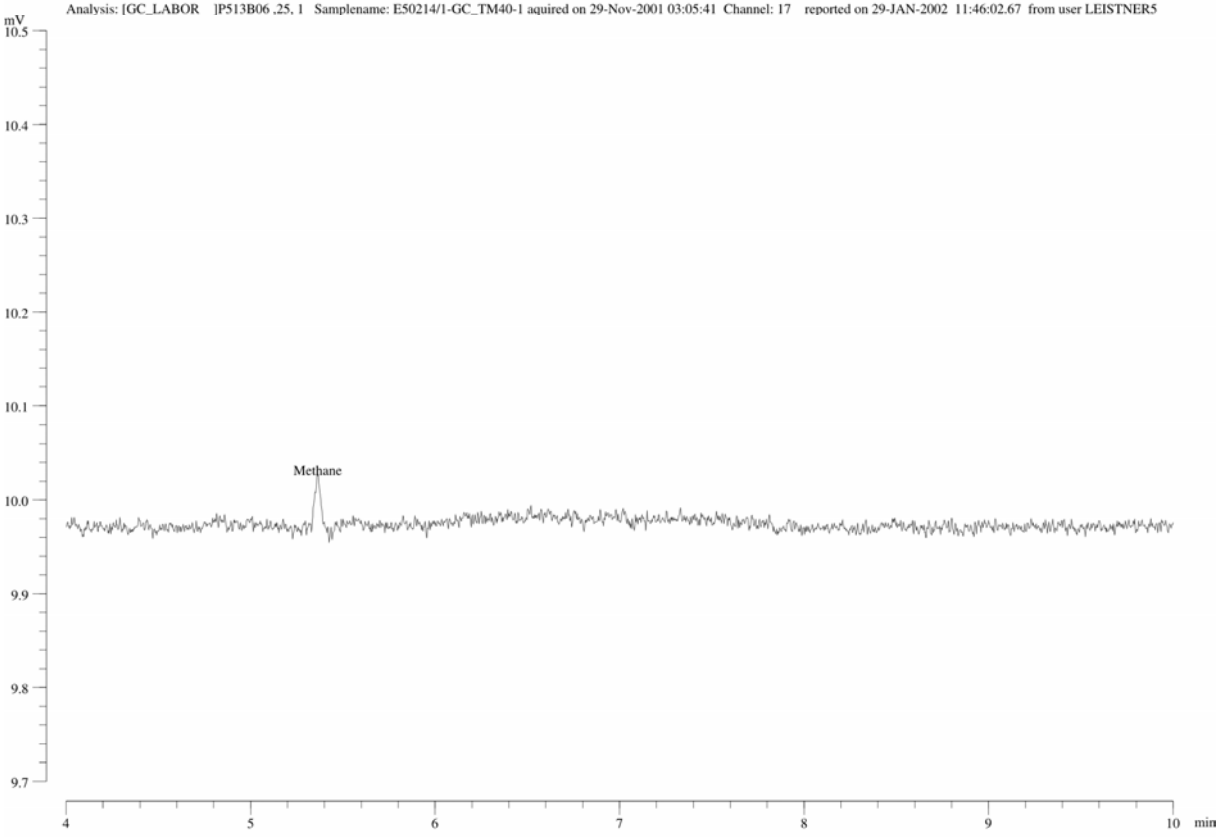

Analysis: [GC_LABOR]P513B06 ,26, 1 Samplename: E50213/1-GC_TM40-1 aquired on 29-Nov-2001 03:35:41 Channel: 17 reported on 29-JAN-2002 11:46:03.74 from user LEISTNER5

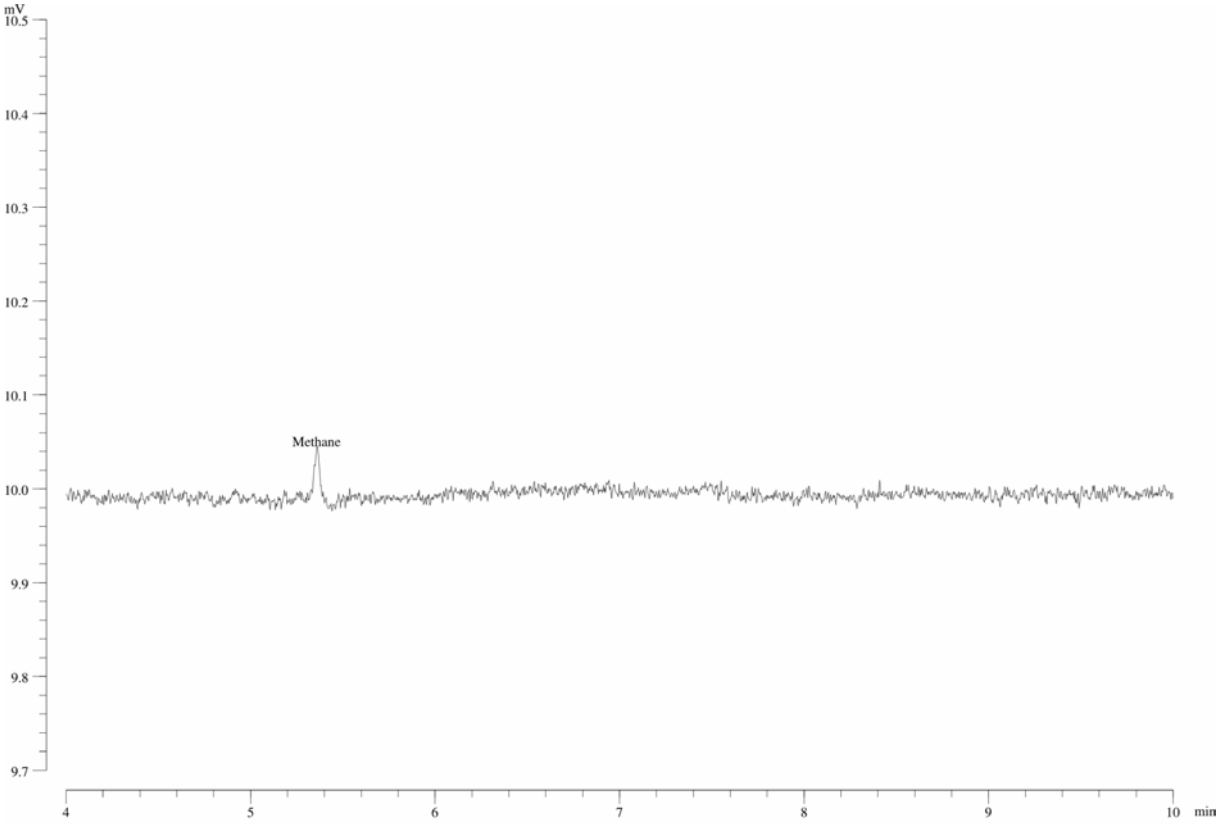

Analysis: [GC_LABOR]P513B06 ,27, 1 Samplename: E50212/1-GC_TM40-1 aquired on 29-Nov-2001 04:05:41 Channel: 17 reported on 29-JAN-2002 11:46:04.79 from user LEISTNER5

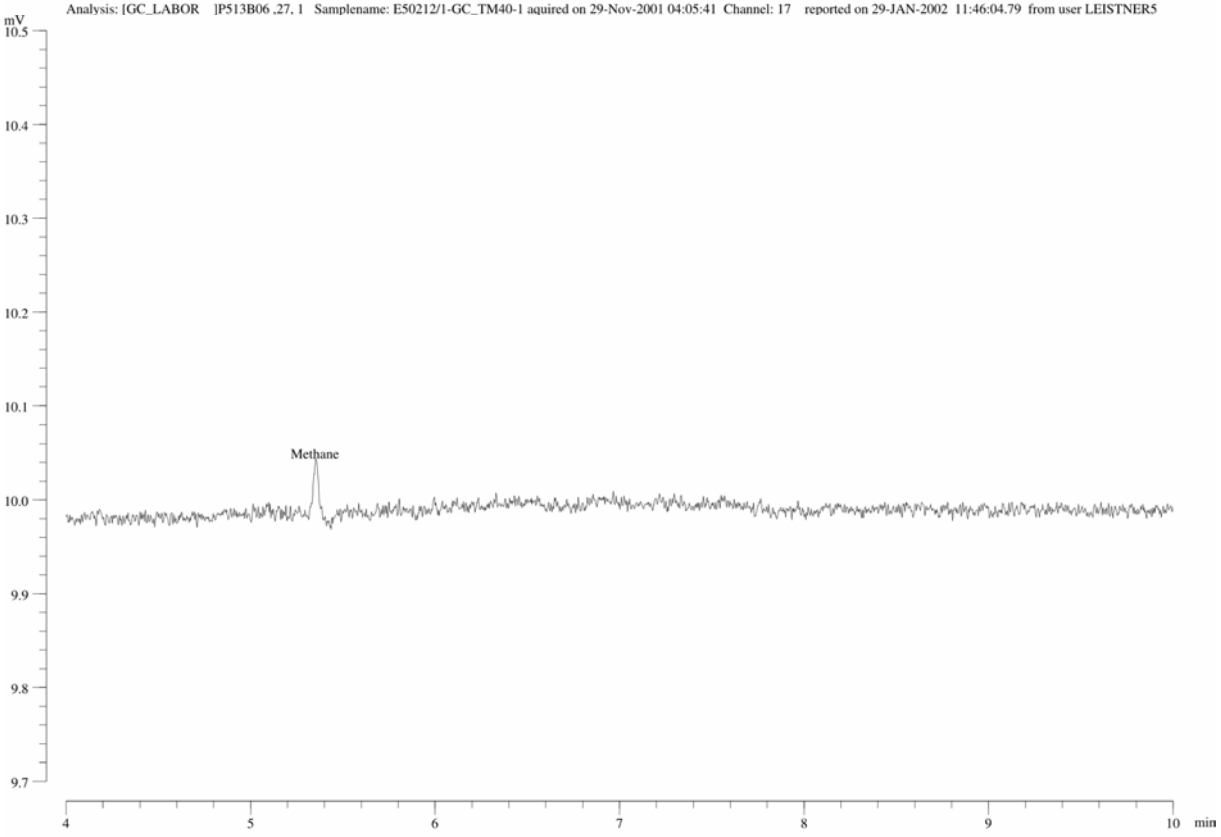

Analysis: [GC_LABOR]P513B06 ,28, 1 Samplename: E50211/1-GC_TM40-1 aquired on 29-Nov-2001 04:35:41 Channel: 17 reported on 29-JAN-2002 11:46:05.88 from user LEISTNER5

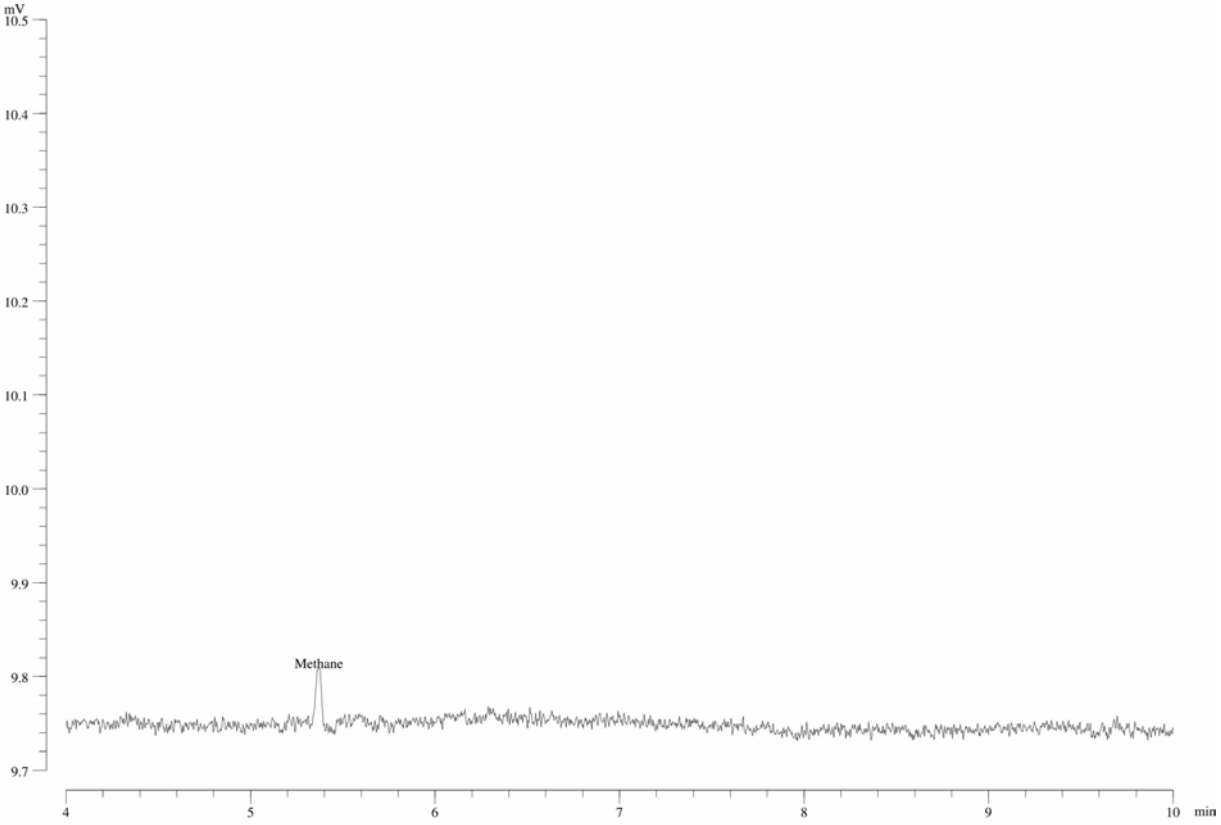

Analysis: [GC_LABOR]P513B06 ,29, 1 Samplename: E50210/1-GC_TM40-1 aquired on 29-Nov-2001 05:05:41 Channel: 17 reported on 29-JAN-2002 11:46:07.23 from user LEISTNER5

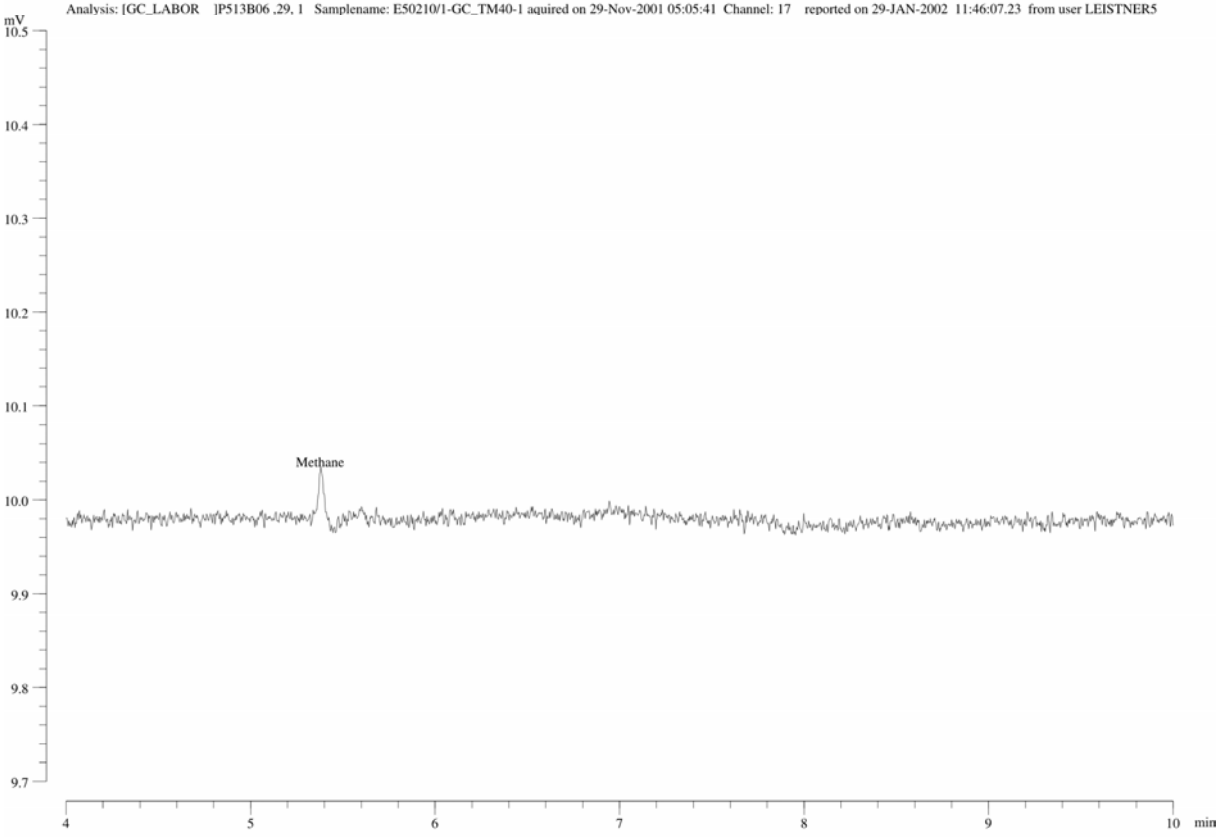

Analysis: [GC_LABOR]P513B06 ,30, 1 Samplename: E50209/1-GC_TM40-1 aquired on 29-Nov-2001 05:35:41 Channel: 17 reported on 29-JAN-2002 11:46:08.33 from user LEISTNER5

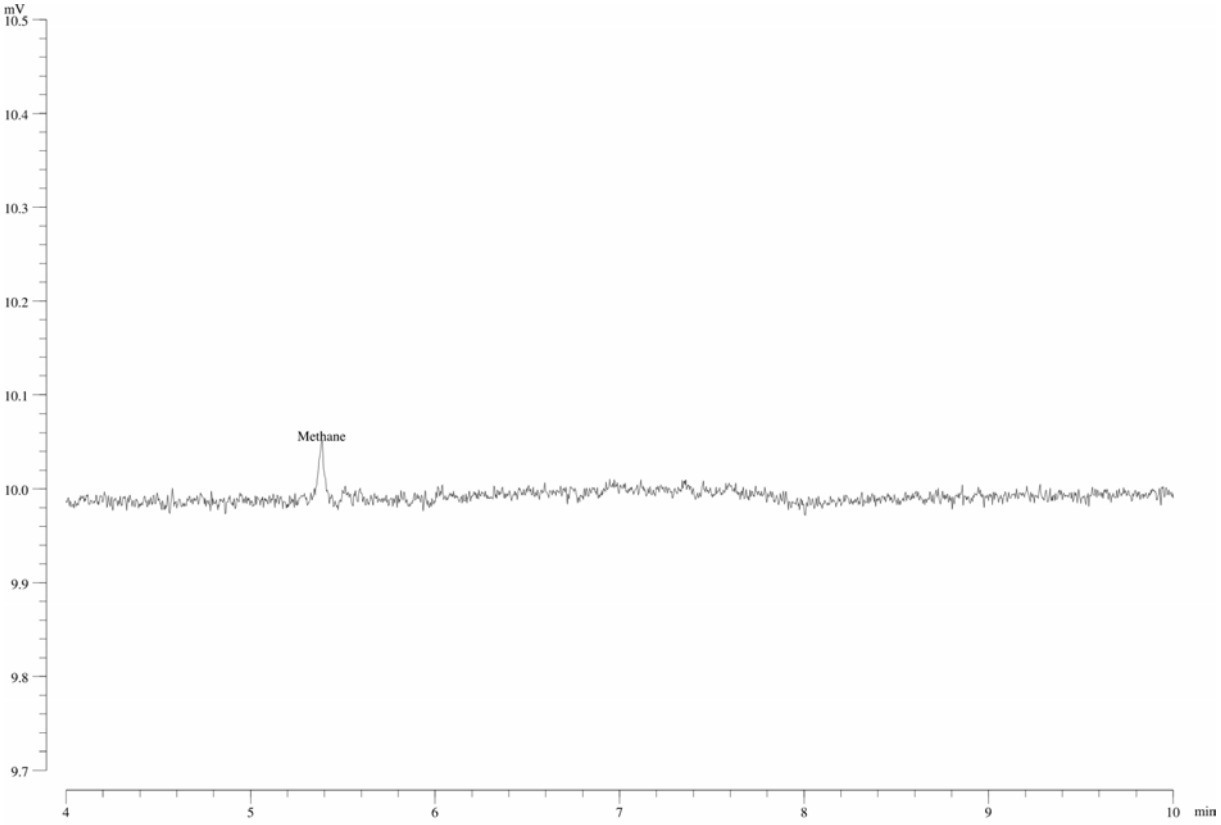

Analysis: [GC_LABOR]P513B06 ,31, 1 Samplename: E50208/1-GC_TM40-1 aquired on 29-Nov-2001 06:05:41 Channel: 17 reported on 29-JAN-2002 11:46:09.45 from user LEISTNER5

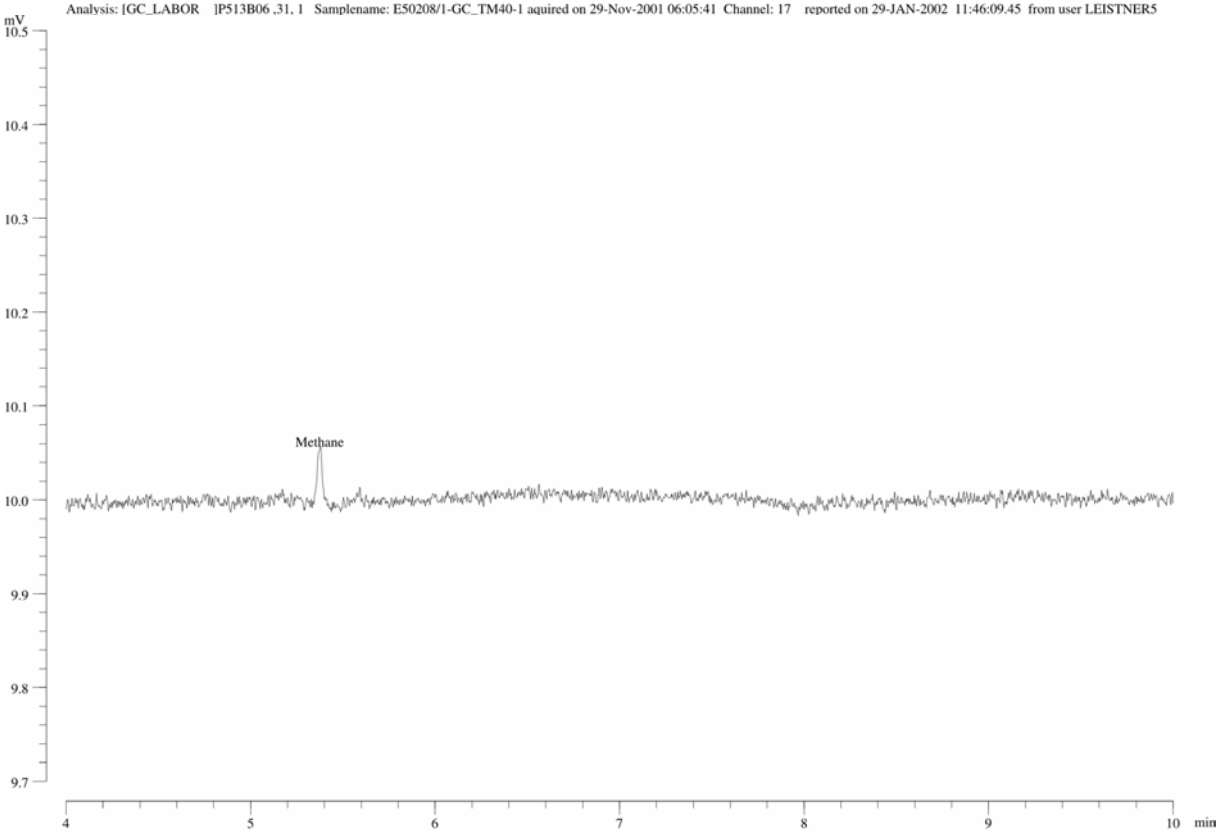

Analysis: [GC_LABOR]P513B06 ,32, 1 Samplename: E50207/1-GC_TM40-1 aquired on 29-Nov-2001 06:35:41 Channel: 17 reported on 29-JAN-2002 11:46:10.52 from user LEISTNER5

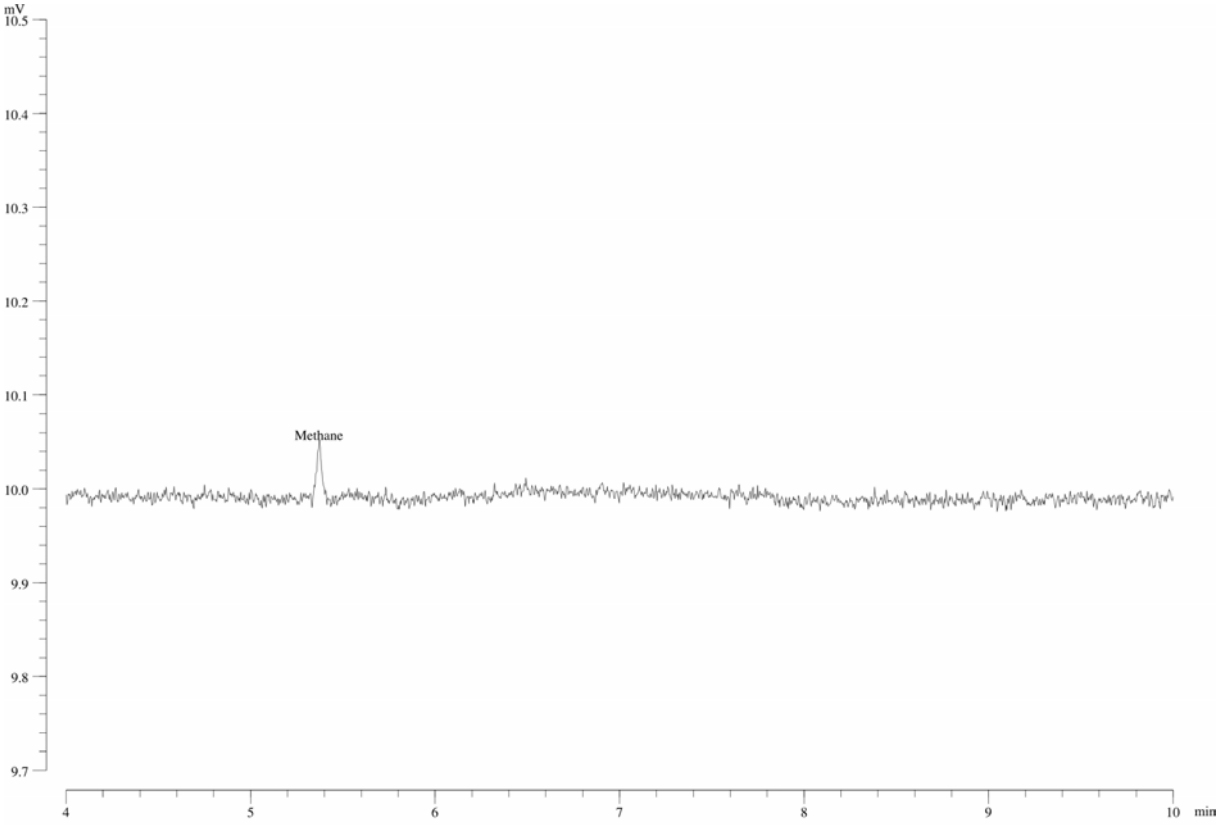

Analysis: [GC_LABOR]P513B06 ,33, 1 Samplename: E50206/1-GC_TM40-1 aquired on 29-Nov-2001 07:05:41 Channel: 17 reported on 29-JAN-2002 11:46:11.65 from user LEISTNER5

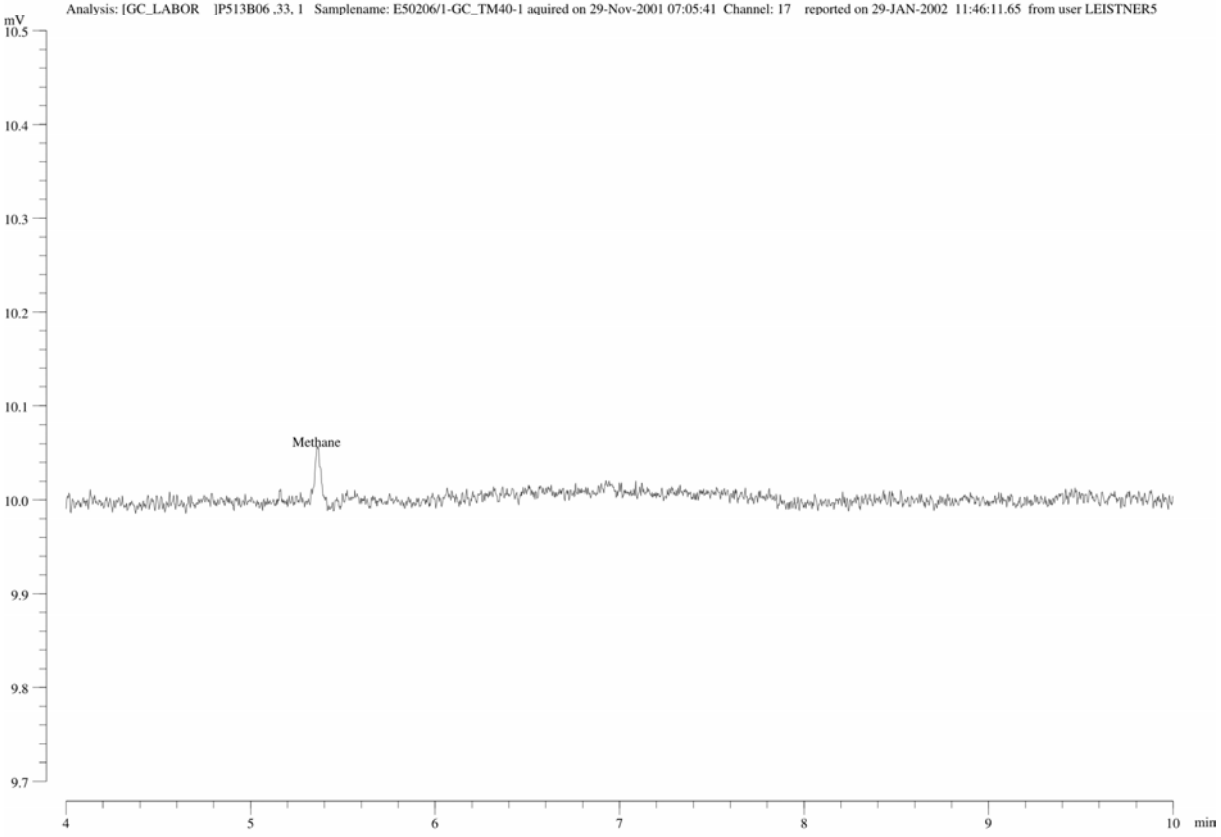

Analysis: [GC_LABOR]P513B06 ,34, 1 Samplename: E50205/1-GC_TM40-1 aquired on 29-Nov-2001 07:35:41 Channel: 17 reported on 29-JAN-2002 11:46:12.75 from user LEISTNER5

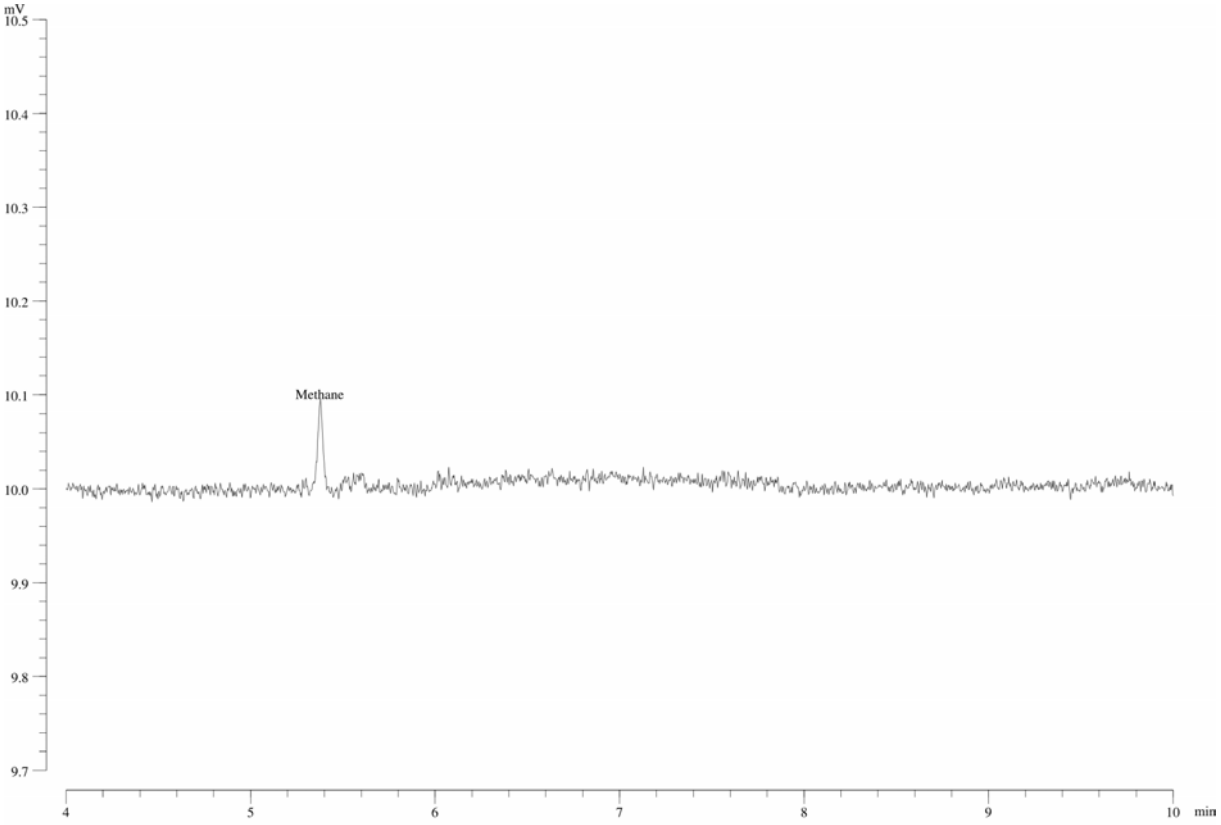

Analysis: [GC_LABOR]P513B06 ,35, 1 Samplename: E50204/1-GC_TM40-1 aquired on 29-Nov-2001 08:05:41 Channel: 17 reported on 29-JAN-2002 11:46:13.83 from user LEISTNER5

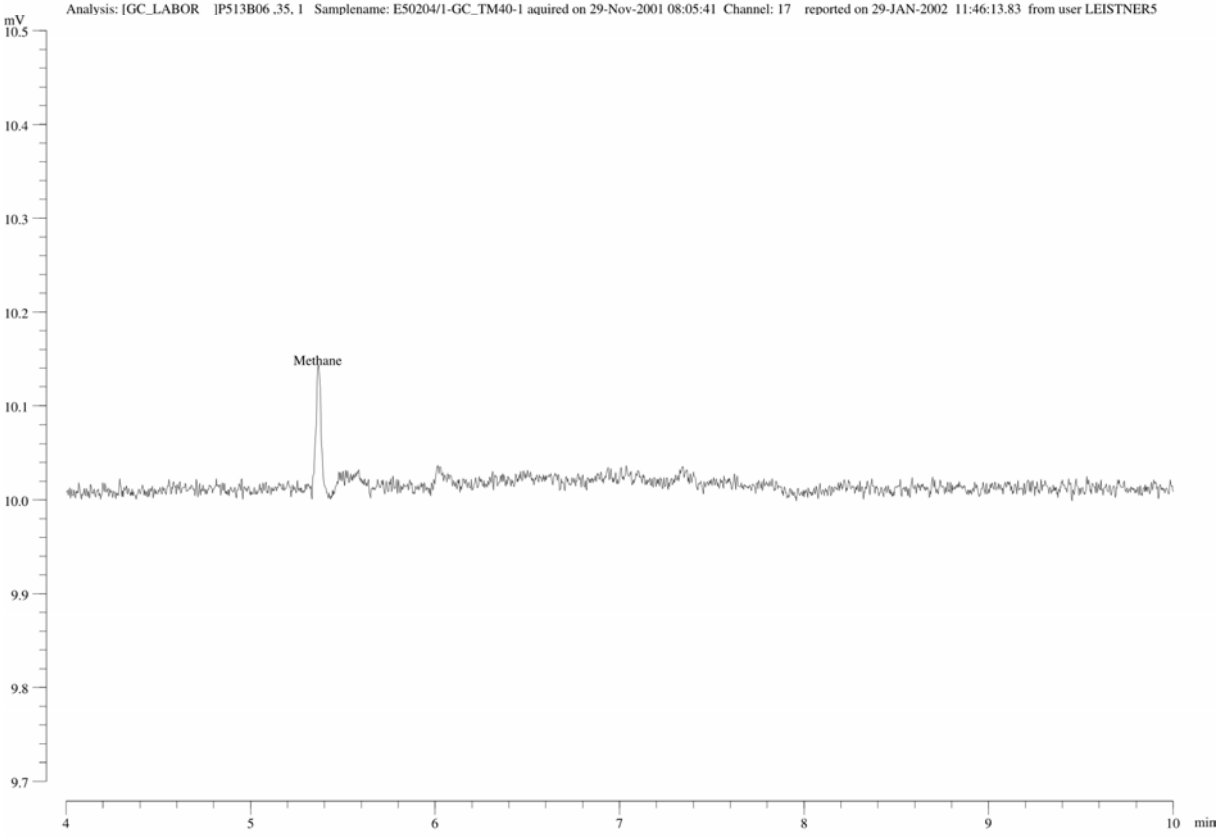

Analysis: [GC_LABOR]P513B06 ,36, 1 Samplename: E50203/1-GC_TM40-1 aquired on 29-Nov-2001 08:35:41 Channel: 17 reported on 29-JAN-2002 11:46:14.90 from user LEISTNER5

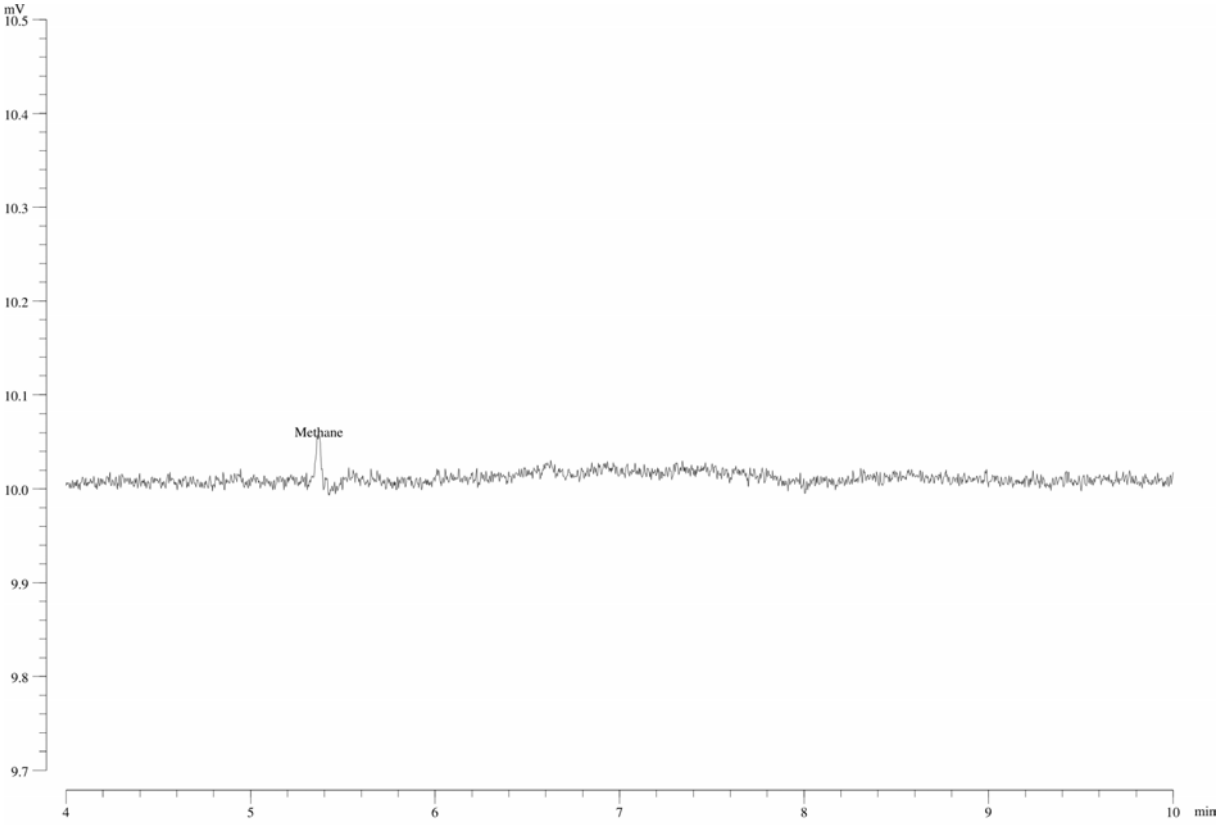

Analysis: [GC_LABOR]P513B06 ,37, 1 Samplename: E50202/1-GC_TM40-1 aquired on 29-Nov-2001 09:05:41 Channel: 17 reported on 29-JAN-2002 11:46:15.95 from user LEISTNER5

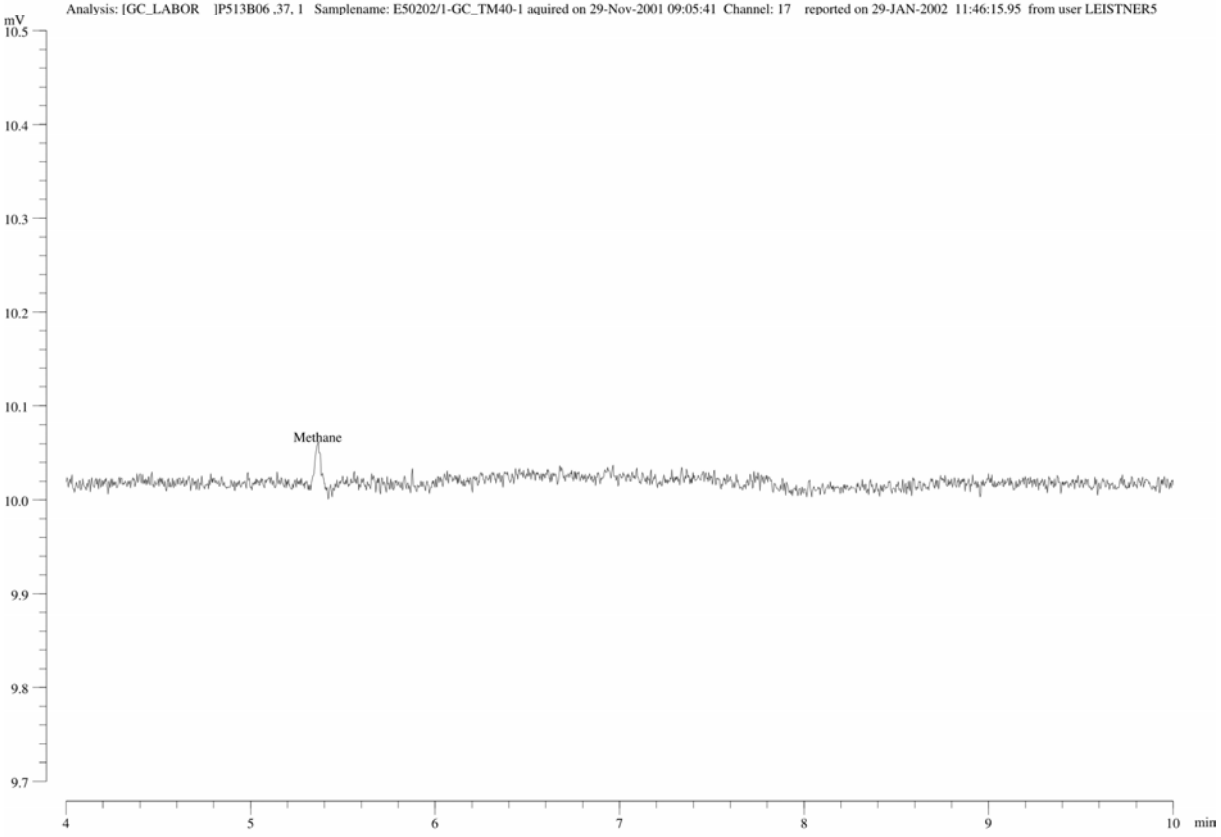

Analysis: [GC_LABOR]P513B06 ,38, 1 Samplename: E50201/1-GC_TM40-1 aquired on 29-Nov-2001 09:35:41 Channel: 17 reported on 29-JAN-2002 11:46:16.99 from user LEISTNER5

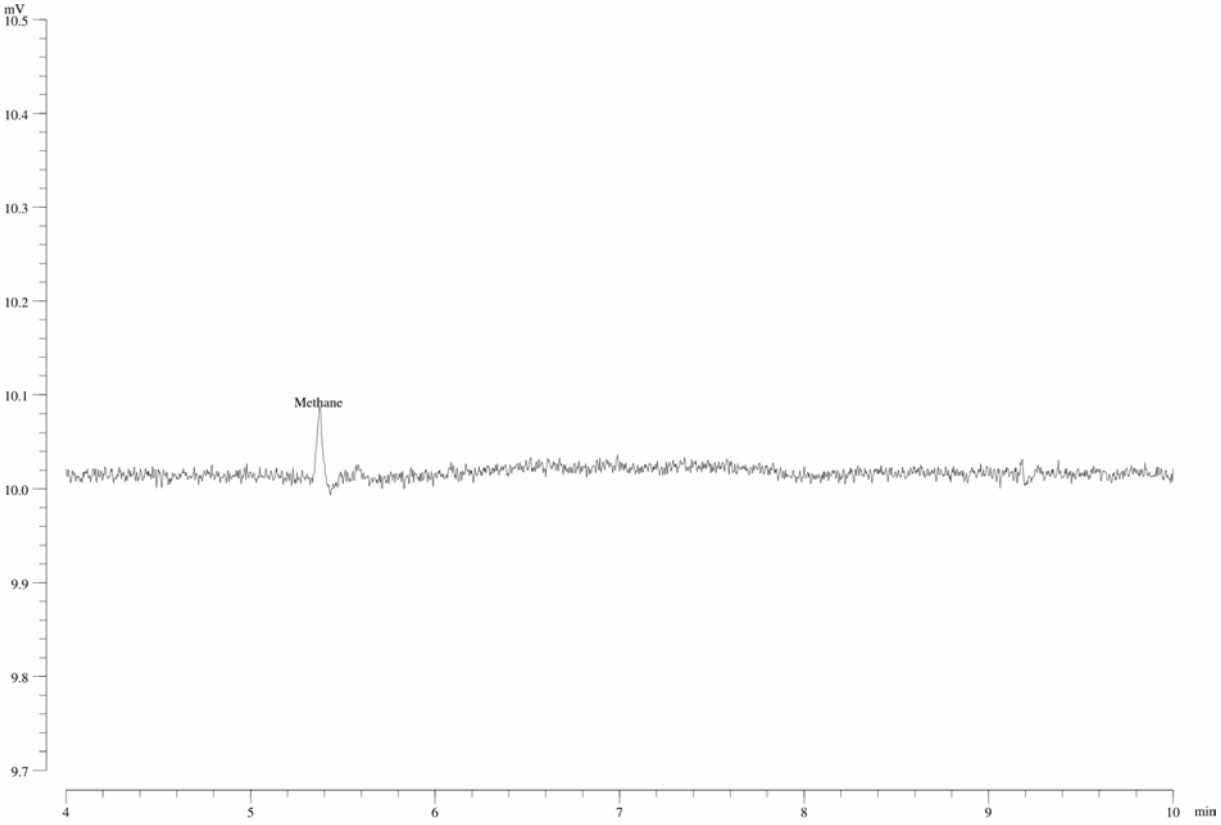

Analysis: [GC_LABOR]P513B06 ,39, 1 Samplename: E50200/1-GC_TM40-1 aquired on 29-Nov-2001 10:05:41 Channel: 17 reported on 29-JAN-2002 11:46:18.31 from user LEISTNER5

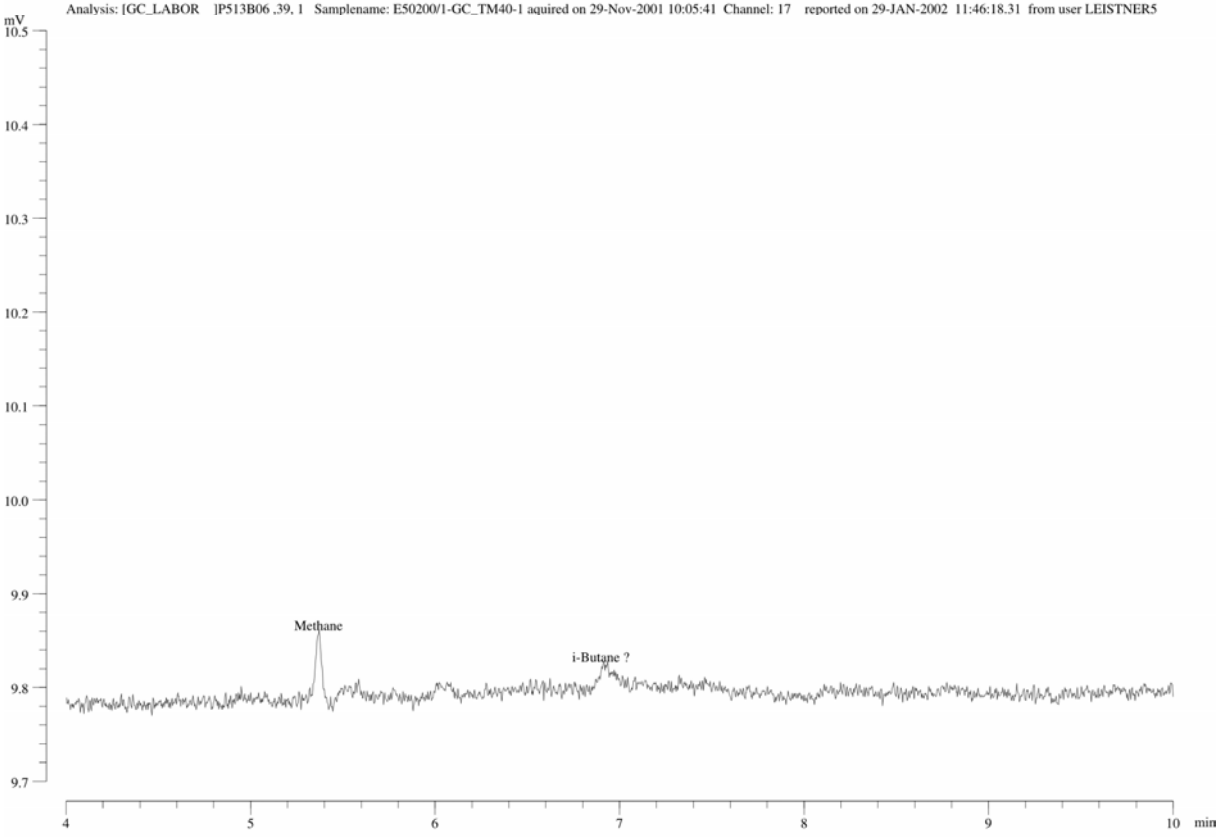

Analysis: [GC_LABOR]P513B06 ,40, 1 Samplename: E50199/1-GC_TM40-1 aquired on 29-Nov-2001 10:35:41 Channel: 17 reported on 29-JAN-2002 11:46:19.43 from user LEISTNER5

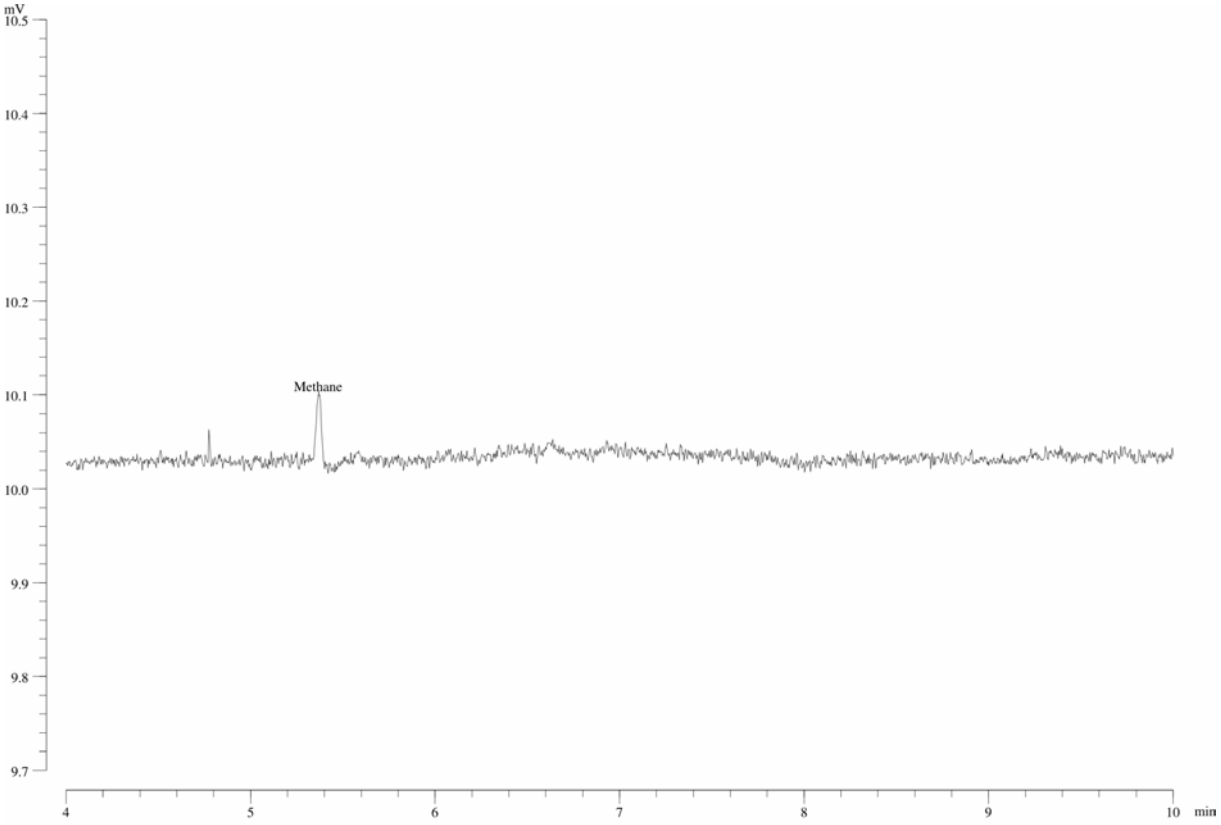

Analysis: [GC_LABOR]P513B06 ,41, 1 Samplename: E50227/1-GC_TM40-1 aquired on 29-Nov-2001 12:30:30 Channel: 17 reported on 29-JAN-2002 11:46:20.51 from user LEISTNER5

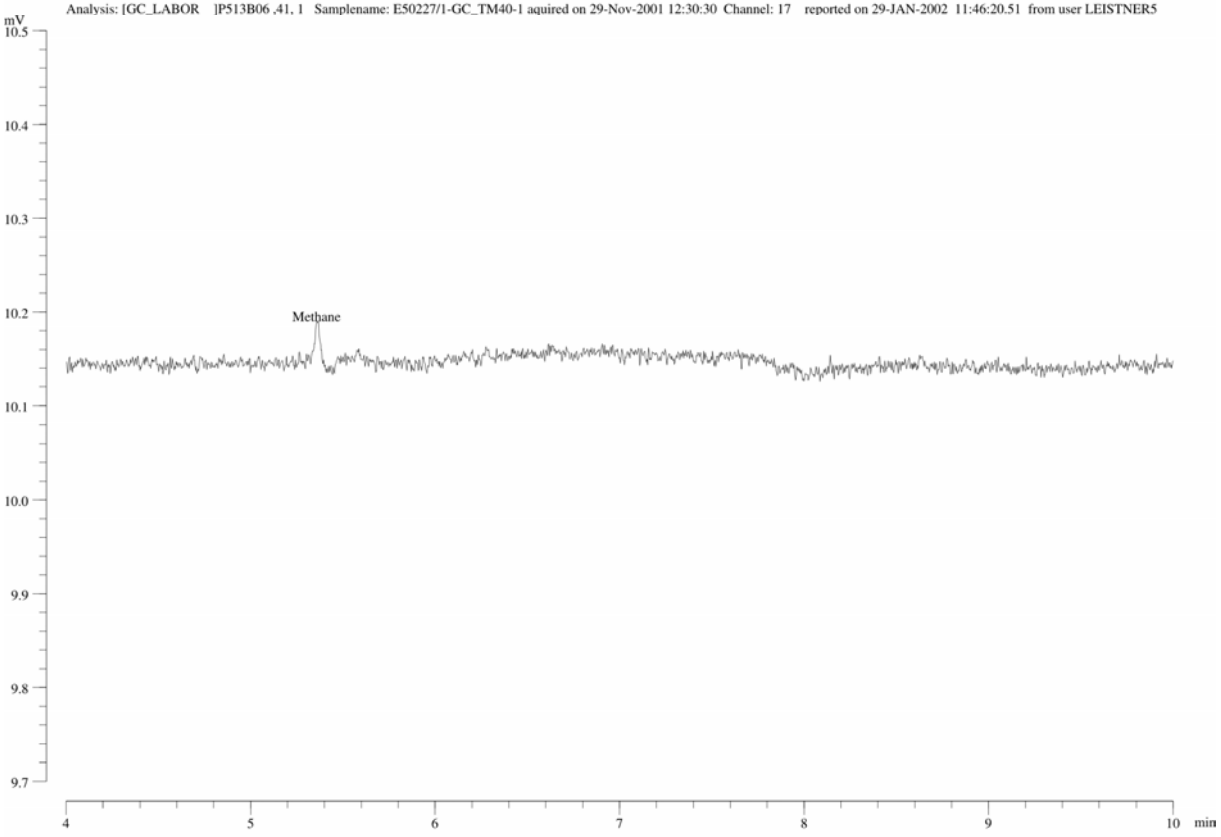

Analysis: [GC_LABOR]P513B06 ,42, 1 Samplename: E50228/1-GC_TM40-1 aquired on 29-Nov-2001 13:21:33 Channel: 17 reported on 29-JAN-2002 11:46:21.57 from user LEISTNER5

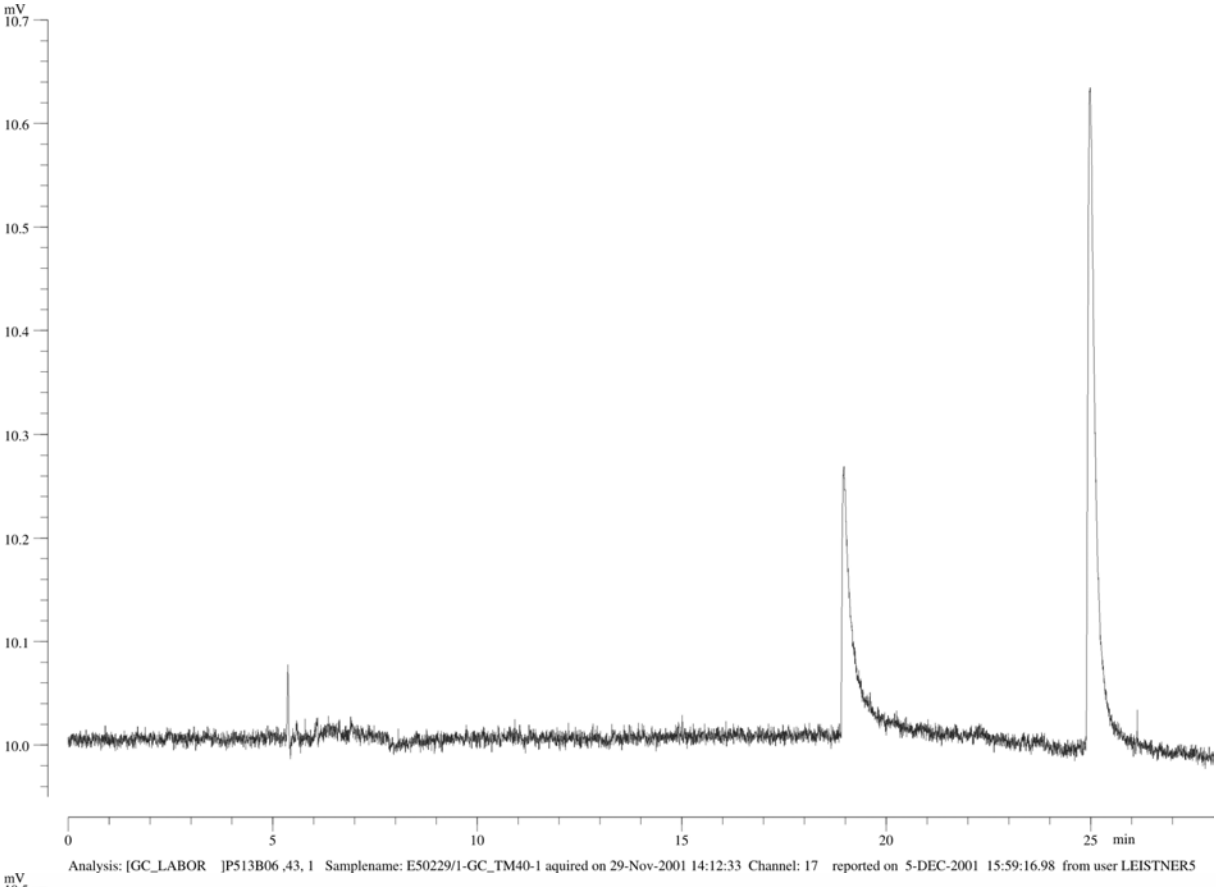
mV
10.7
10.6
10.5
10.4
10.3
10.2
10.1
10.0
0
5
10
15
20
25
min
Analysis: [GC_LABOR]P513B06 ,43, 1 Samplename: E50229/1-GC_TM40-1 aquired on 29-Nov-2001 14:12:33 Channel: 17 reported on 5-DEC-2001 15:59:16.98 from user LEISTNER5

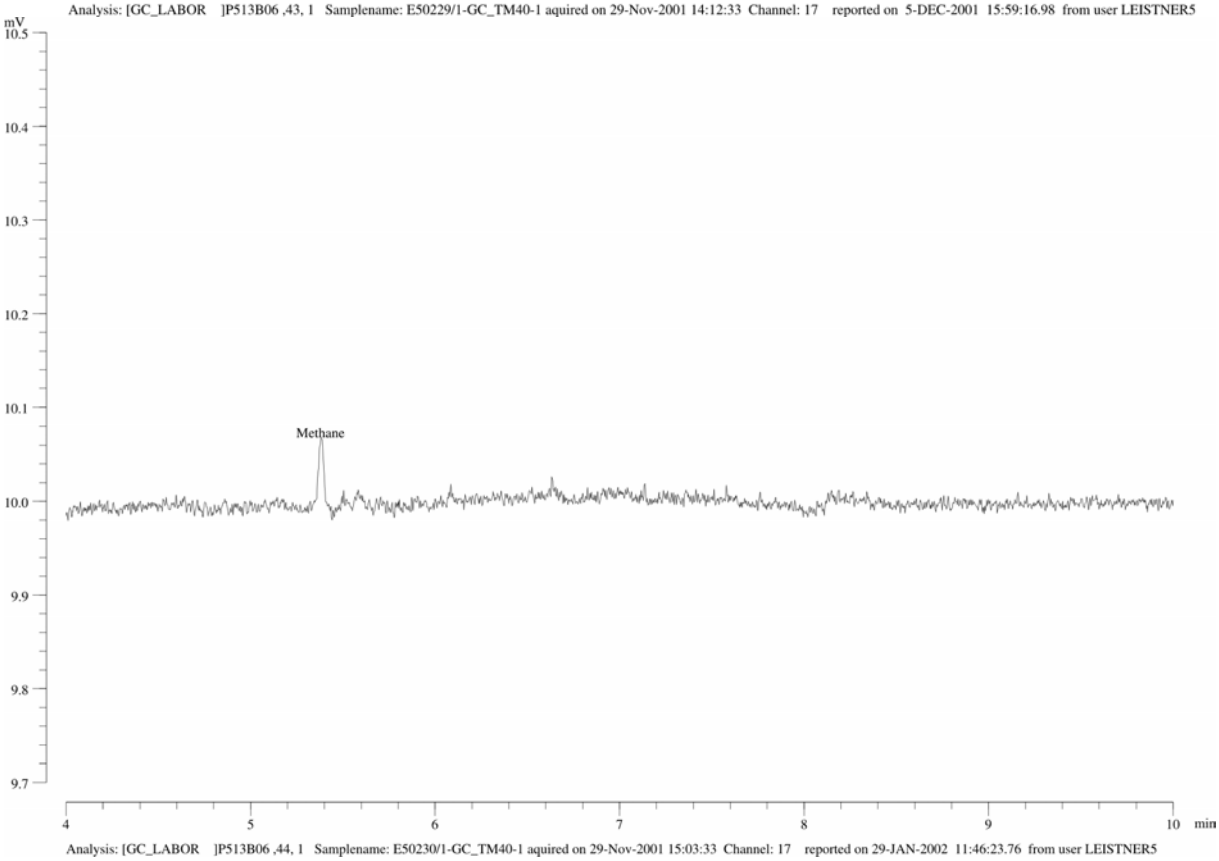
mV
10.5
10.4
10.3
10.2
10.1
10.0
9.9
9.8
9.7
Methane
4
5
6
7
8
9
10
min
Analysis: [GC_LABOR]P513B06 ,44, 1 Samplename: E50230/1-GC_TM40-1 aquired on 29-Nov-2001 15:03:33 Channel: 17 reported on 29-JAN-2002 11:46:23.76 from user LEISTNER5

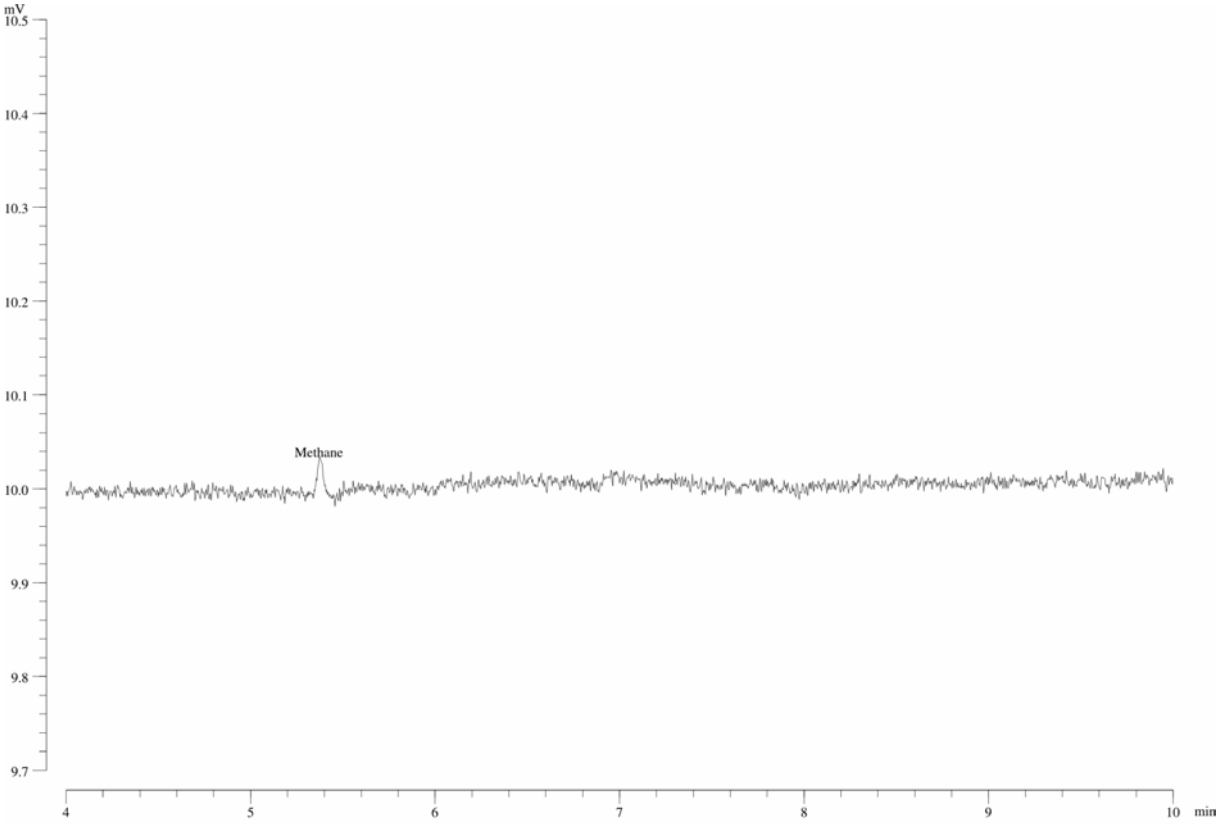

Analysis: [GC_LABOR]P513B06 ,45, 1 Samplename: E50231/1-GC_TM40-1 aquired on 29-Nov-2001 15:54:33 Channel: 17 reported on 29-JAN-2002 11:46:24.84 from user LEISTNER5

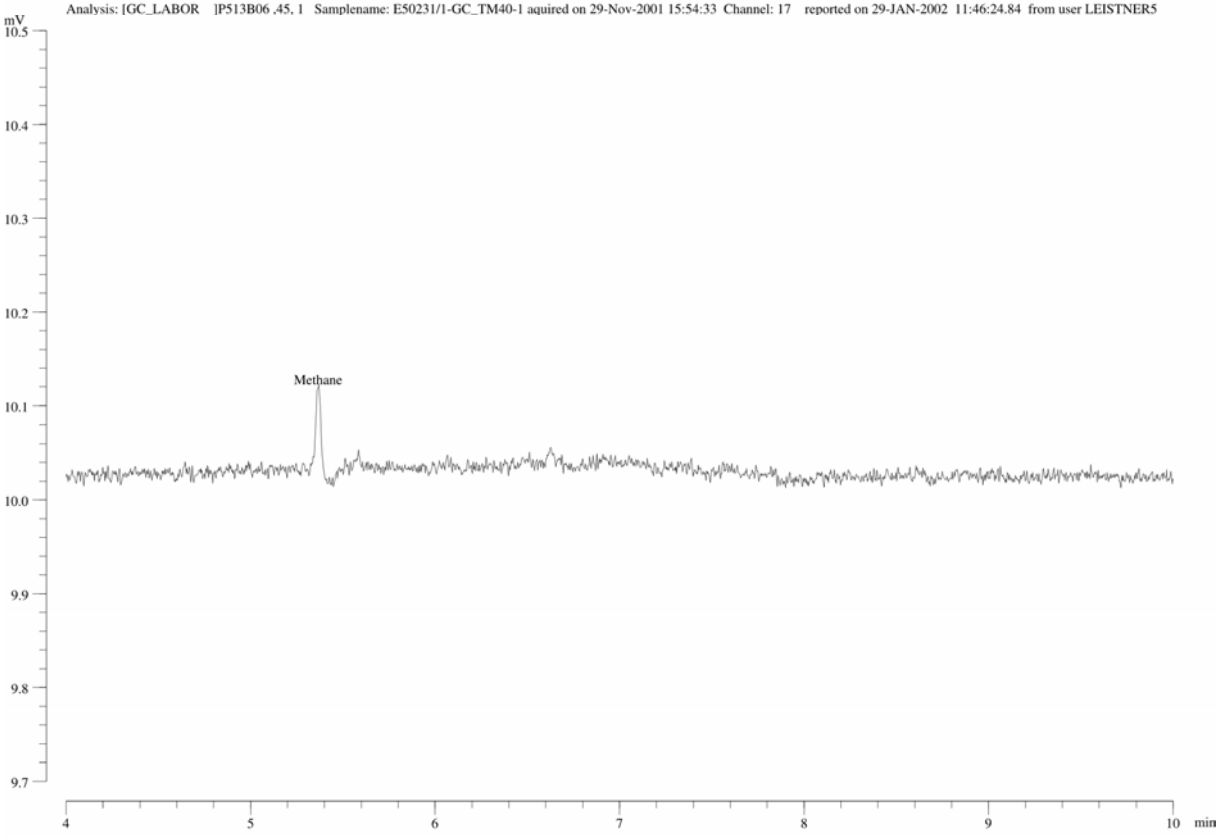

Analysis: [GC_LABOR]P513B06 ,46, 1 Samplename: E50232/1-GC_TM40-1 aquired on 29-Nov-2001 16:45:33 Channel: 17 reported on 29-JAN-2002 11:46:25.91 from user LEISTNER5

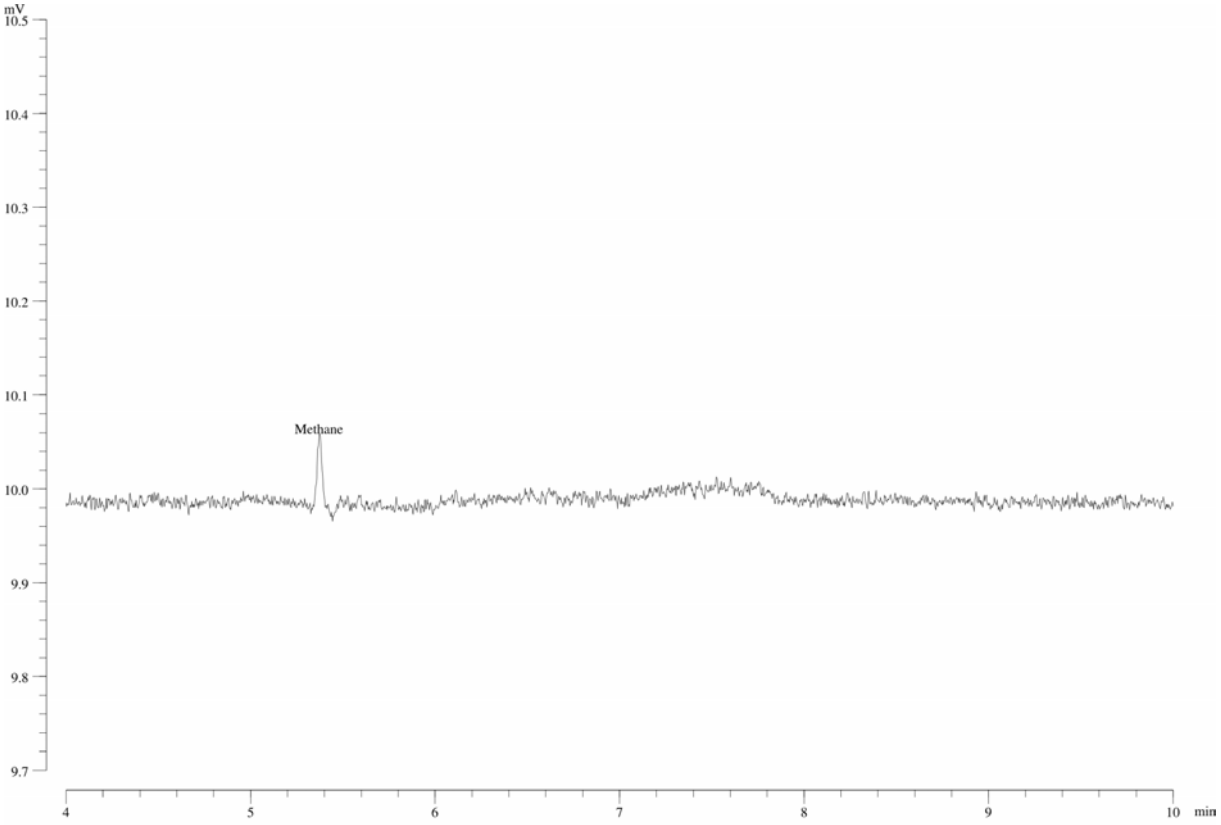

Analysis: [GC_LABOR]P513B06 ,47, 1 Samplename: E50233/1-GC_TM40-1 aquired on 29-Nov-2001 17:36:33 Channel: 17 reported on 29-JAN-2002 11:46:27.01 from user LEISTNER5

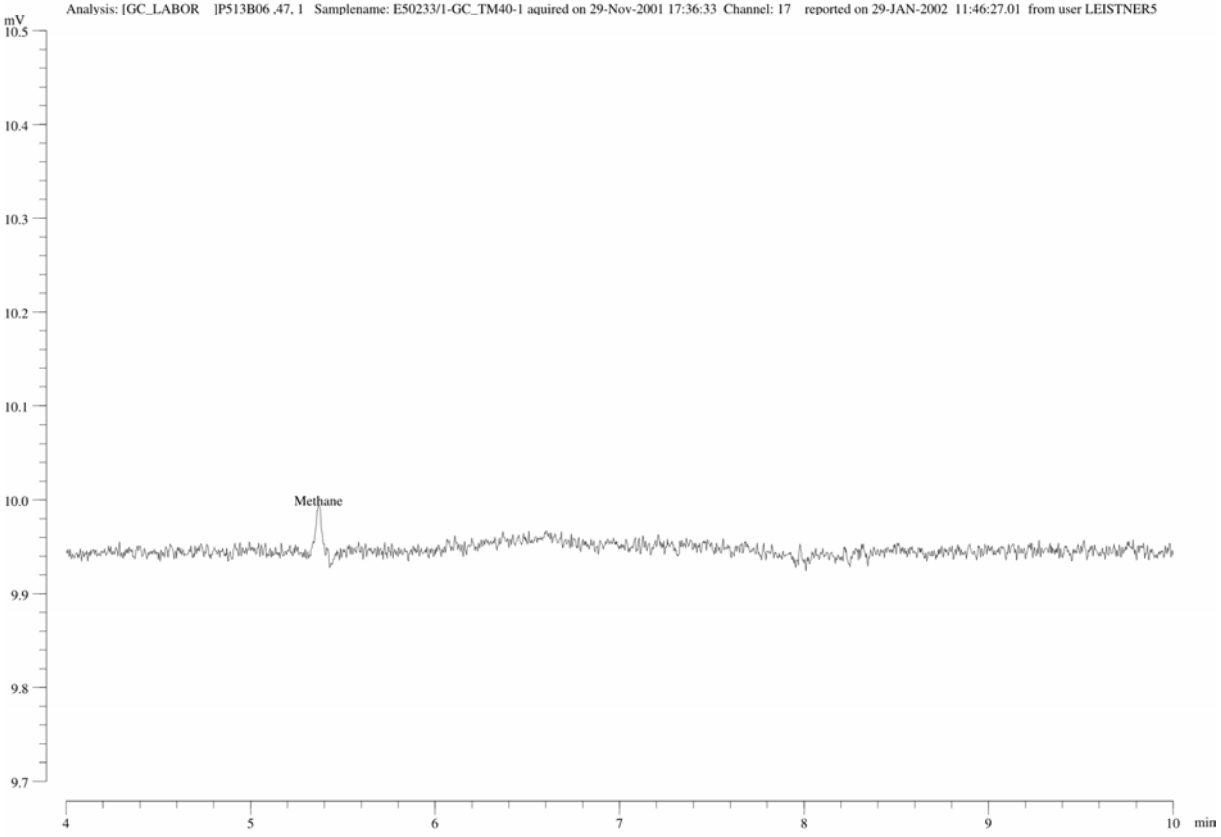

Analysis: [GC_LABOR]P513B06 ,48, 1 Samplename: E50234/1-GC_TM40-1 aquired on 29-Nov-2001 18:27:33 Channel: 17 reported on 29-JAN-2002 11:46:28.13 from user LEISTNER5

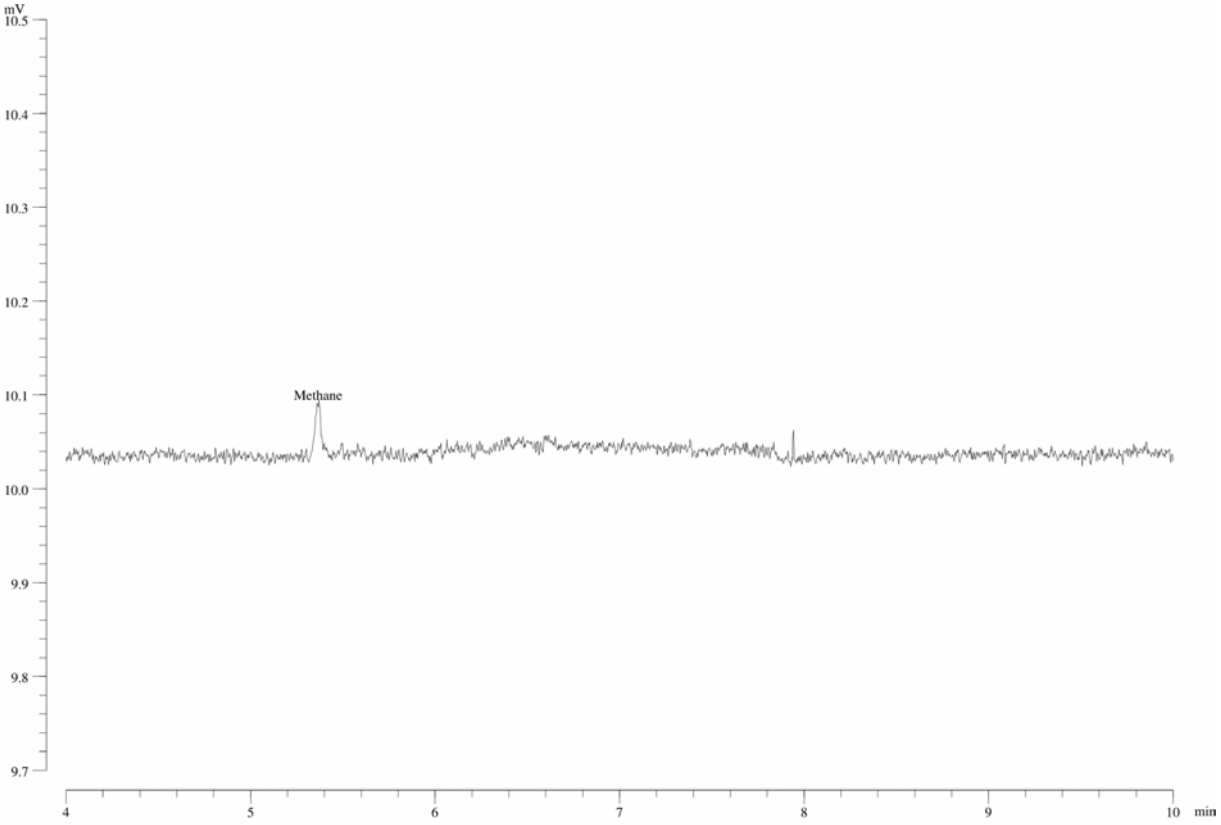

Analysis: [GC_LABOR]P513B06 ,49, 1 Samplename: E50235/1-GC_TM40-1 aquired on 29-Nov-2001 19:18:33 Channel: 17 reported on 29-JAN-2002 11:46:29.18 from user LEISTNER5

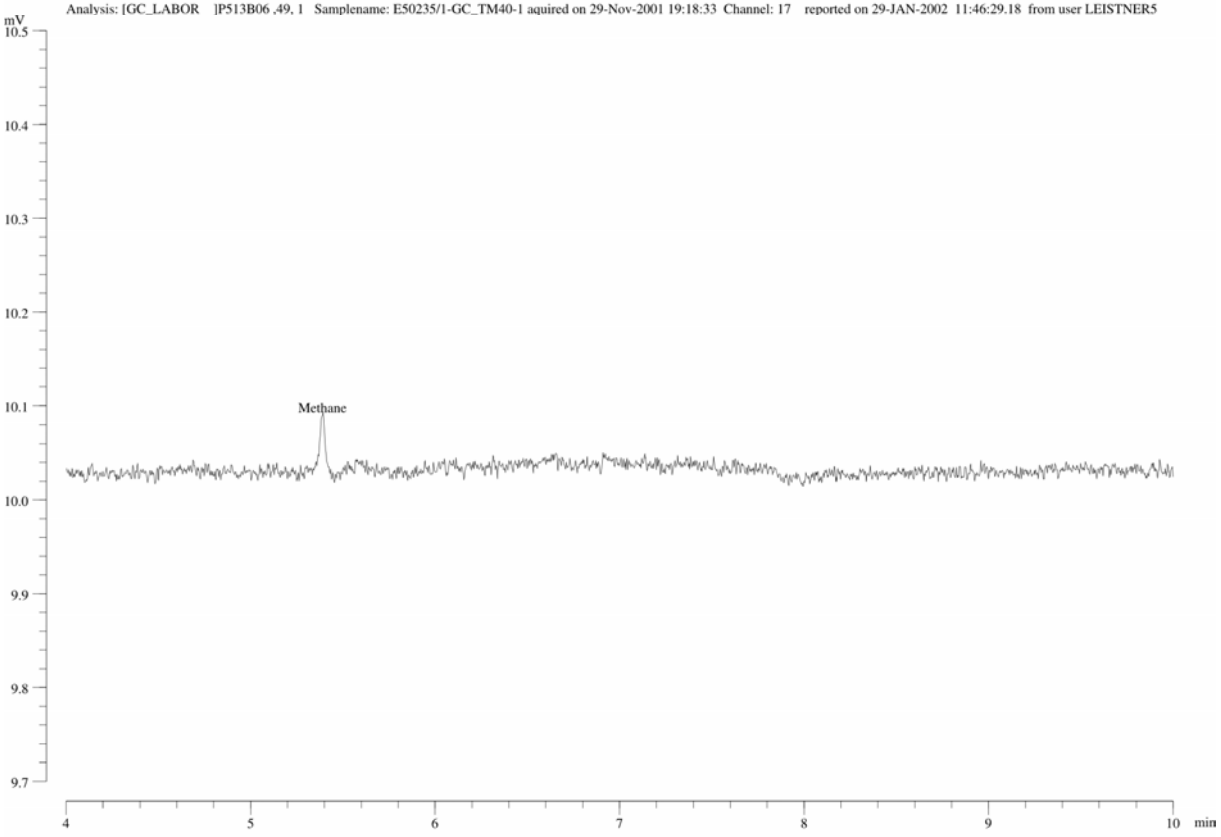

Analysis: [GC_LABOR]P513B06 ,50, 1 Samplename: E50236/1-GC_TM40-1 aquired on 29-Nov-2001 20:09:33 Channel: 17 reported on 29-JAN-2002 11:46:30.44 from user LEISTNER5

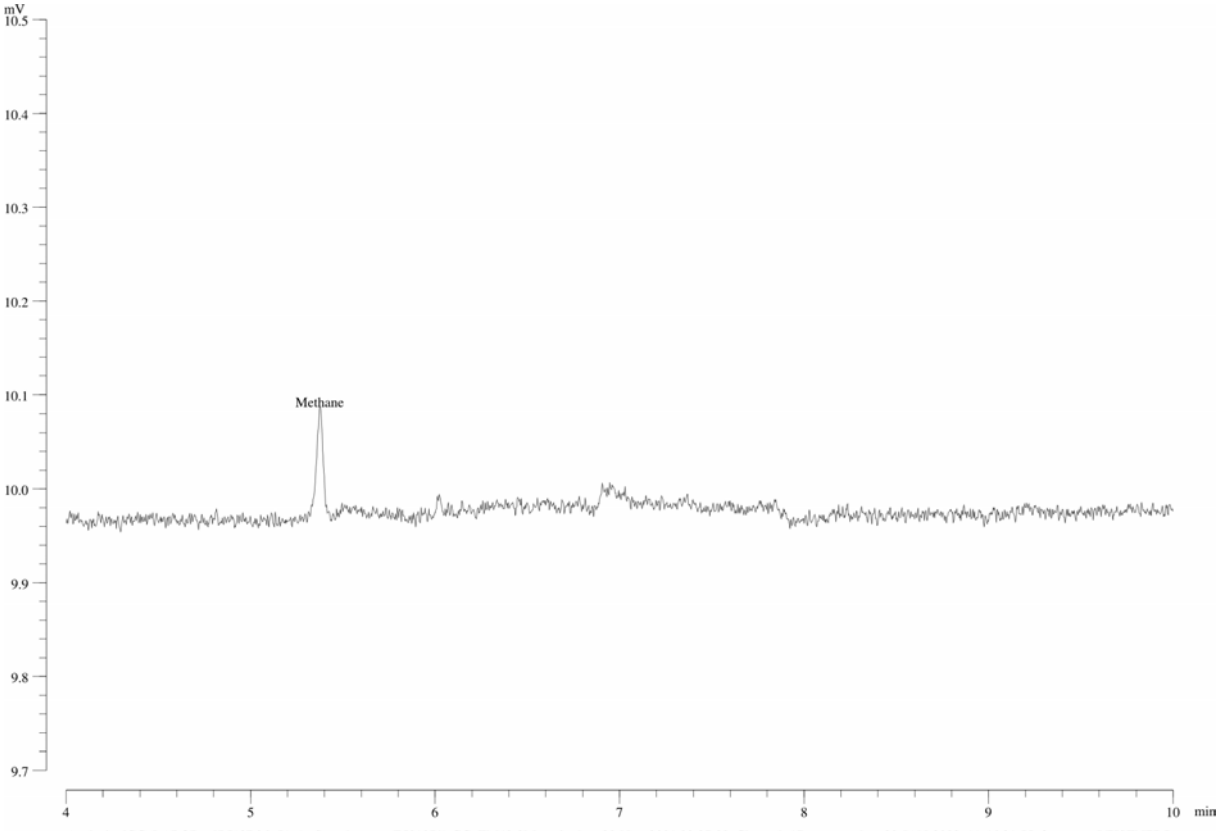

Analysis: [GC_LABOR]P513B06 ,51, 1 Samplename: E50197/1-GC_TM40-2M aquired on 30-Nov-2001 09:27:09 Channel: 17 reported on 29-JAN-2002 11:46:31.55 from user LEISTNER5

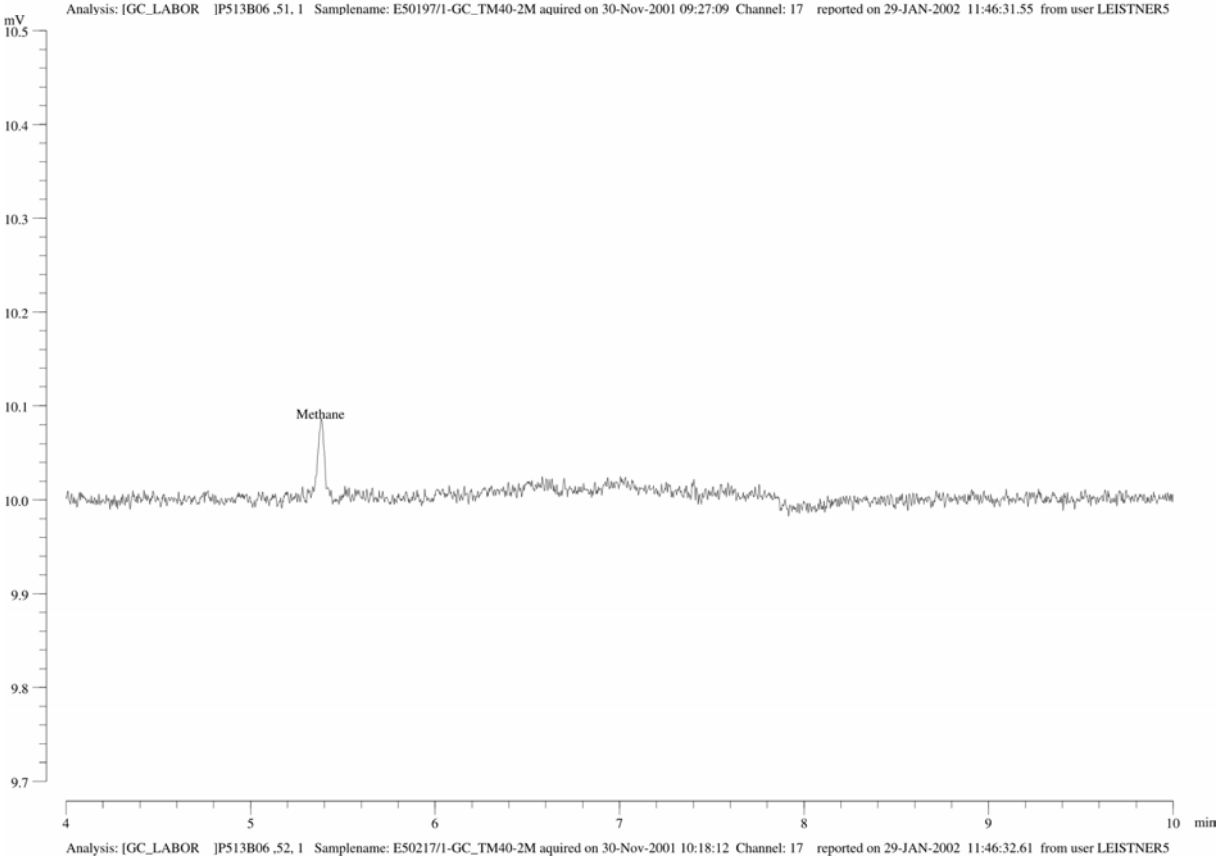

Analysis: [GC_LABOR]P513B06 ,52, 1 Samplename: E50217/1-GC_TM40-2M aquired on 30-Nov-2001 10:18:12 Channel: 17 reported on 29-JAN-2002 11:46:32.61 from user LEISTNER5

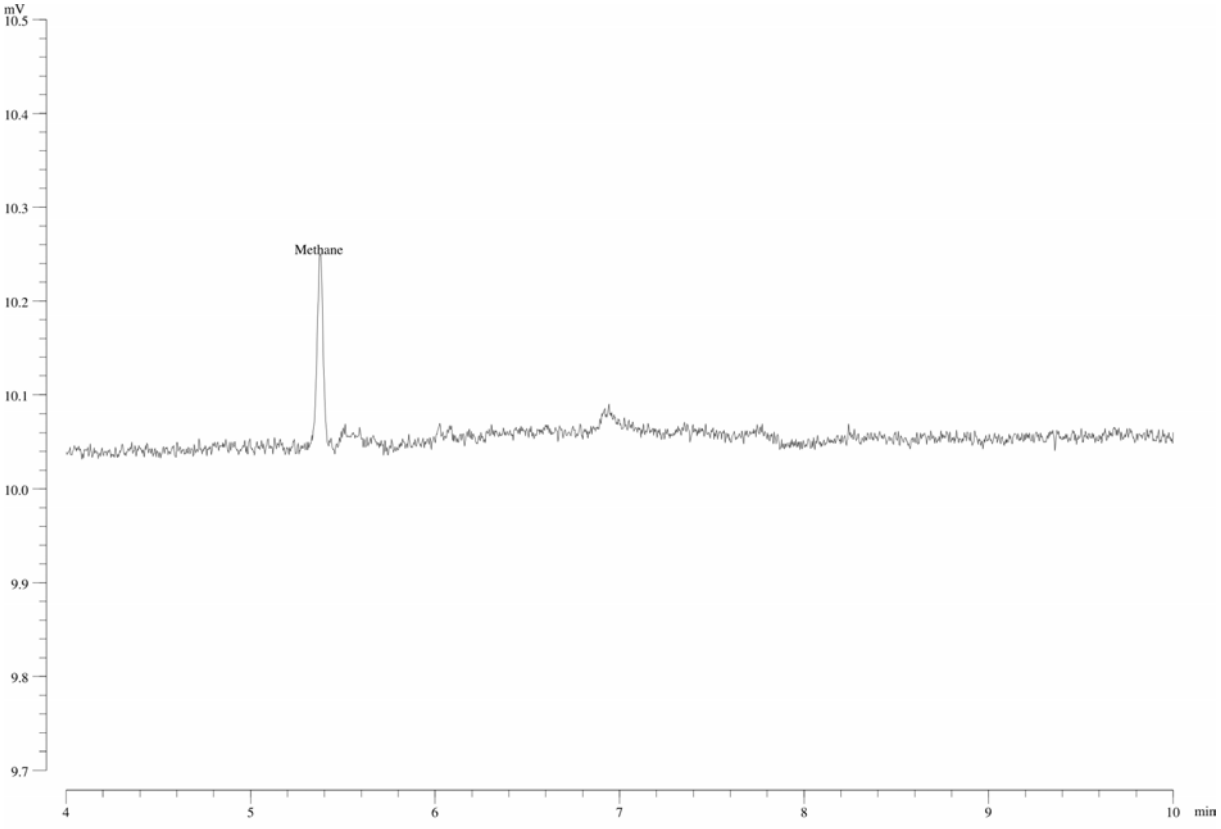

Analysis: [GC_LABOR]P513B06 ,53, 1 Samplename: E50221/1-GC_TM40-2M aquired on 30-Nov-2001 11:09:12 Channel: 17 reported on 29-JAN-2002 11:46:33.69 from user LEISTNER5

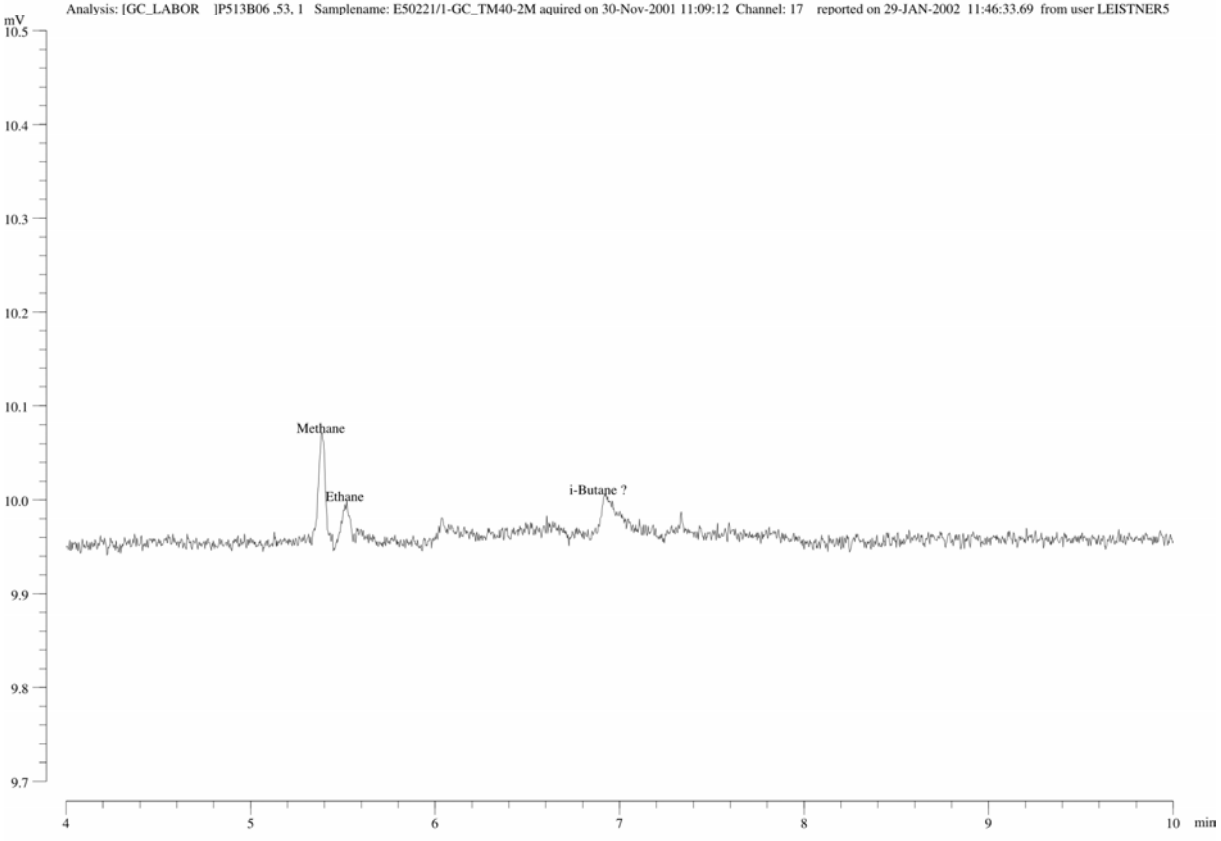

Analysis: [GC_LABOR]P513B06 ,54, 1 Samplename: E50224/1-GC_TM40-2M aquired on 30-Nov-2001 12:00:12 Channel: 17 reported on 29-JAN-2002 11:46:34.75 from user LEISTNER5

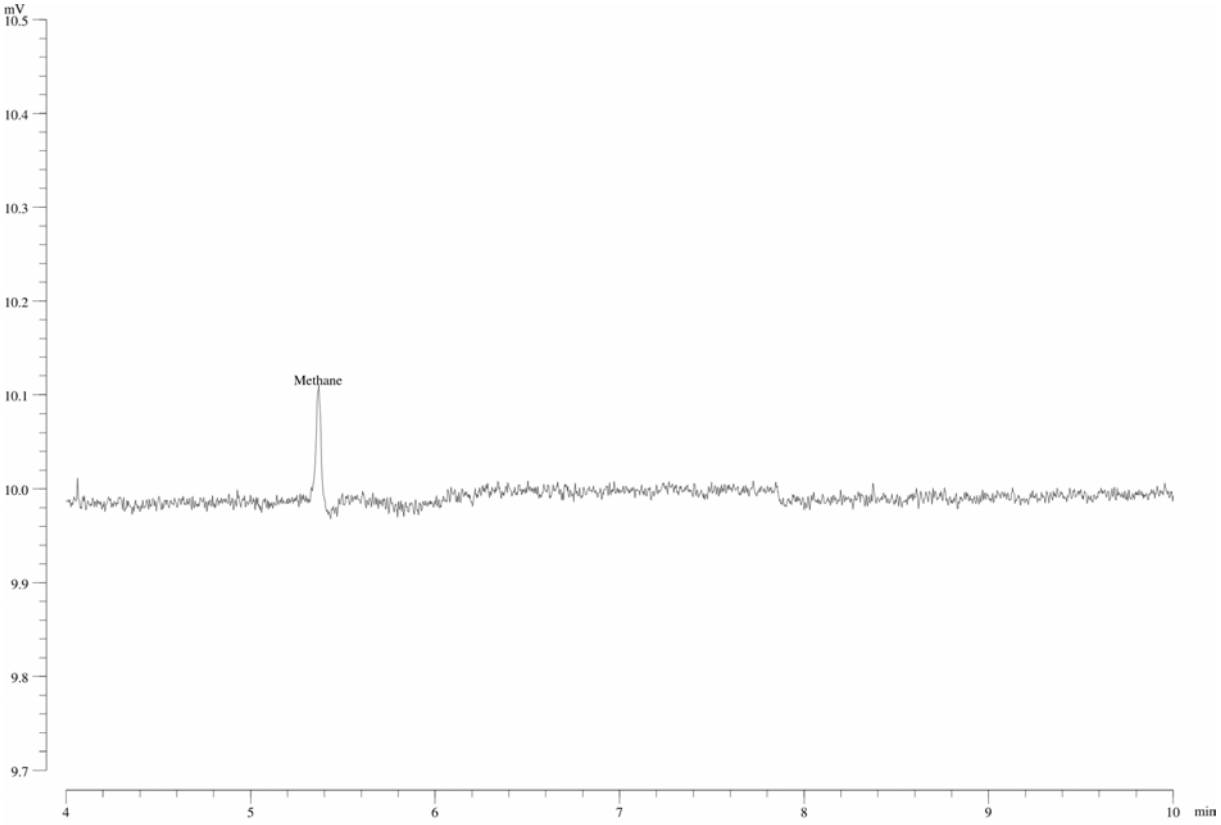

Analysis: [GC_LABOR]P513B06 ,55, 1 Samplename: E50176/2-GC_TM40-1M aquired on 3-Dec-2001 12:54:44 Channel: 17 reported on 29-JAN-2002 11:46:35.82 from user LEISTNER5

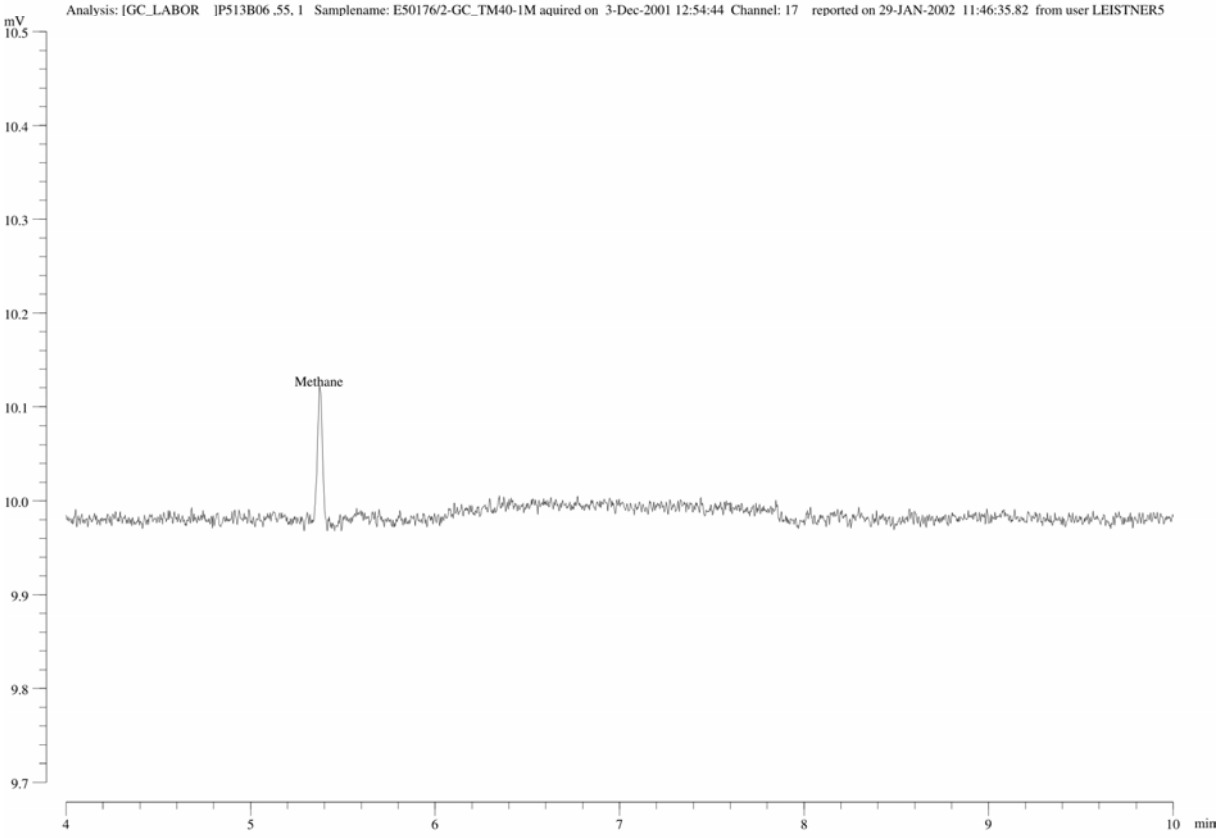

Analysis: [GC_LABOR]P513B06 ,56, 1 Samplename: E50177/2-GC_TM40-1M aquired on 3-Dec-2001 13:45:47 Channel: 17 reported on 29-JAN-2002 11:46:36.89 from user LEISTNER5

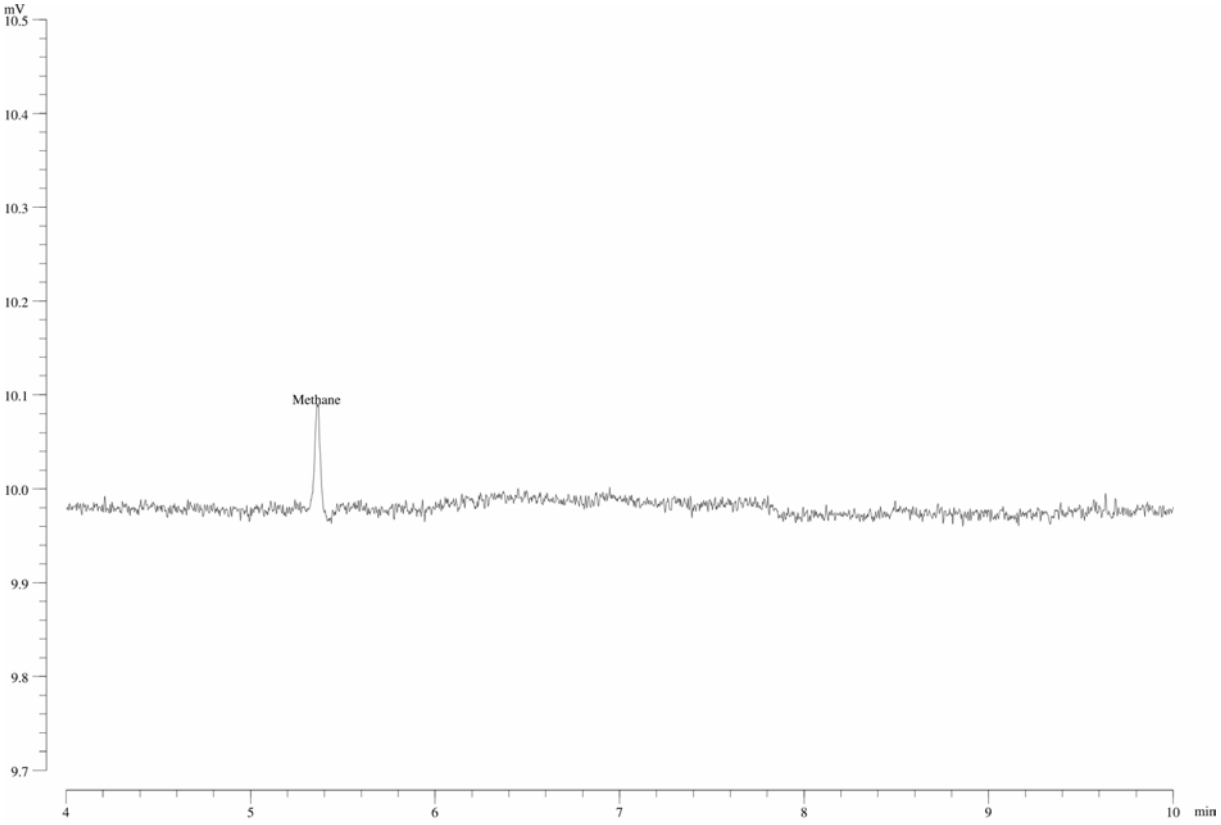

Analysis: [GC_LABOR]P513B06 ,57, 1 Samplename: E50178/2-GC_TM40-1M aquired on 3-Dec-2001 14:36:47 Channel: 17 reported on 29-JAN-2002 11:46:38.05 from user LEISTNER5

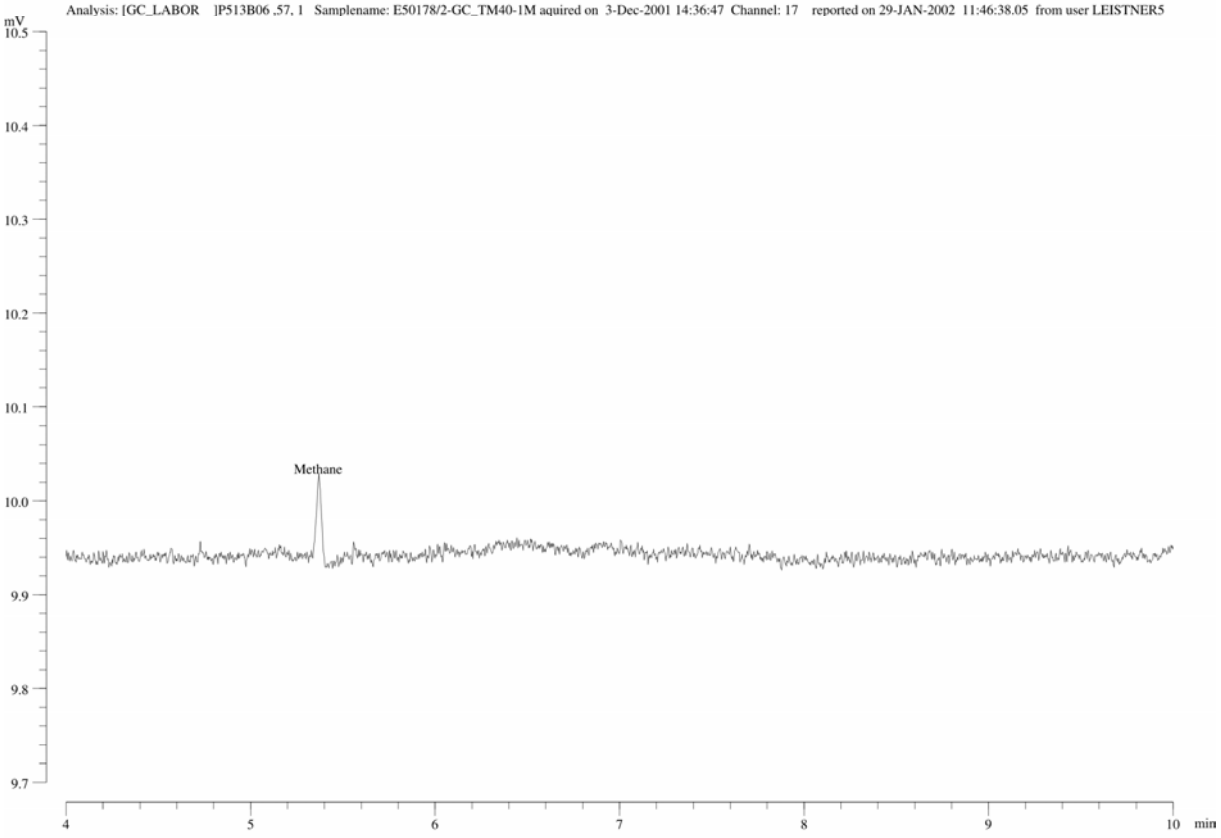

Analysis: [GC_LABOR]P513B06 ,58, 1 Samplename: E50179/2-GC_TM40-1M aquired on 3-Dec-2001 15:27:47 Channel: 17 reported on 29-JAN-2002 11:46:39.10 from user LEISTNER5

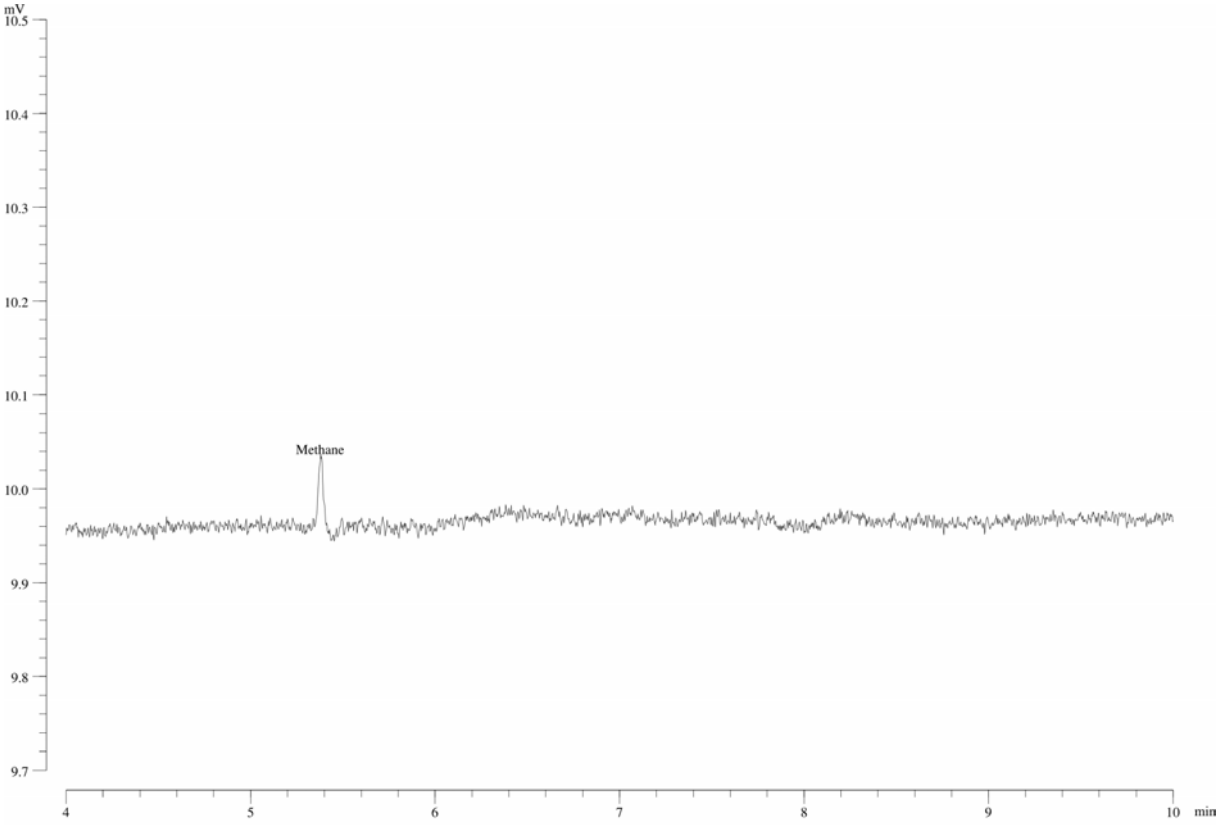

Analysis: [GC_LABOR]P513B06 ,59, 1 Samplename: E50180/2-GC_TM40-1M aquired on 3-Dec-2001 16:18:47 Channel: 17 reported on 29-JAN-2002 11:46:40.15 from user LEISTNER5

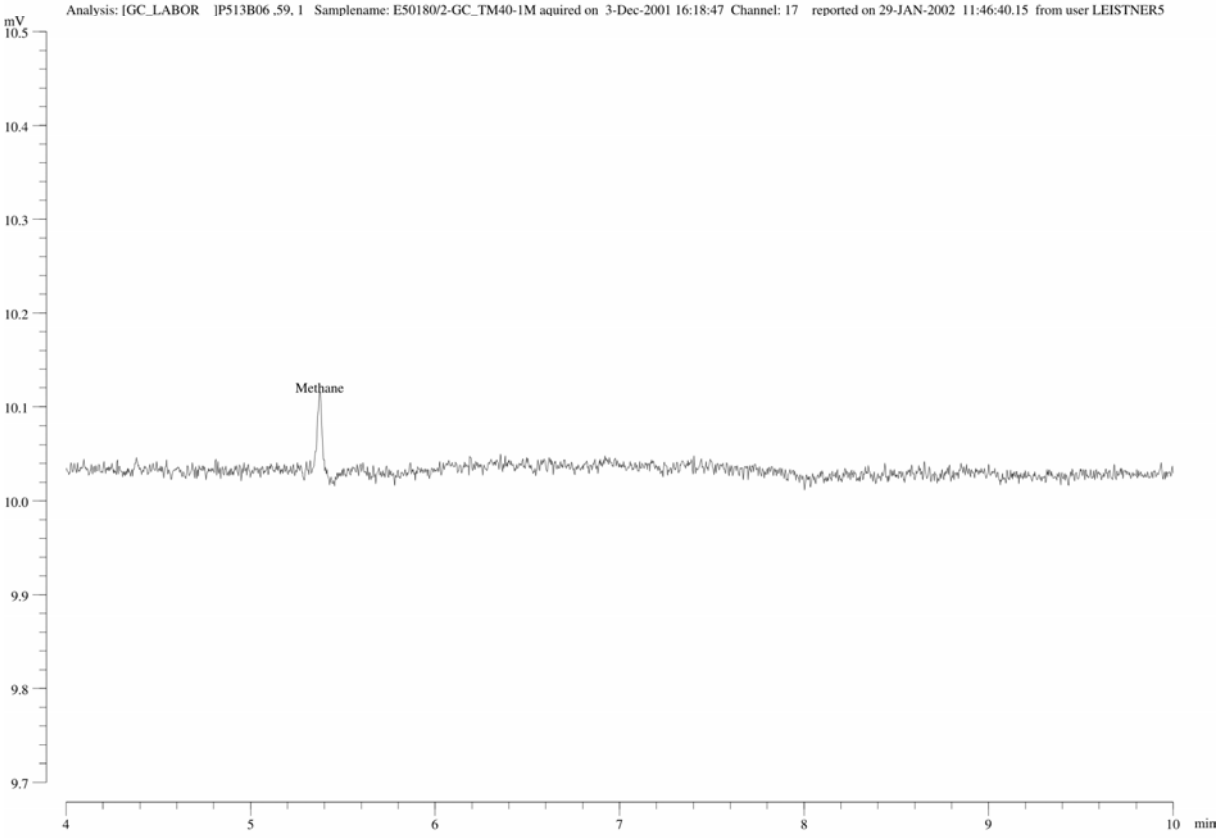

Analysis: [GC_LABOR]P513B06 ,60, 1 Samplename: E50181/2-GC_TM40-1M aquired on 3-Dec-2001 17:09:47 Channel: 17 reported on 29-JAN-2002 11:46:41.42 from user LEISTNER5

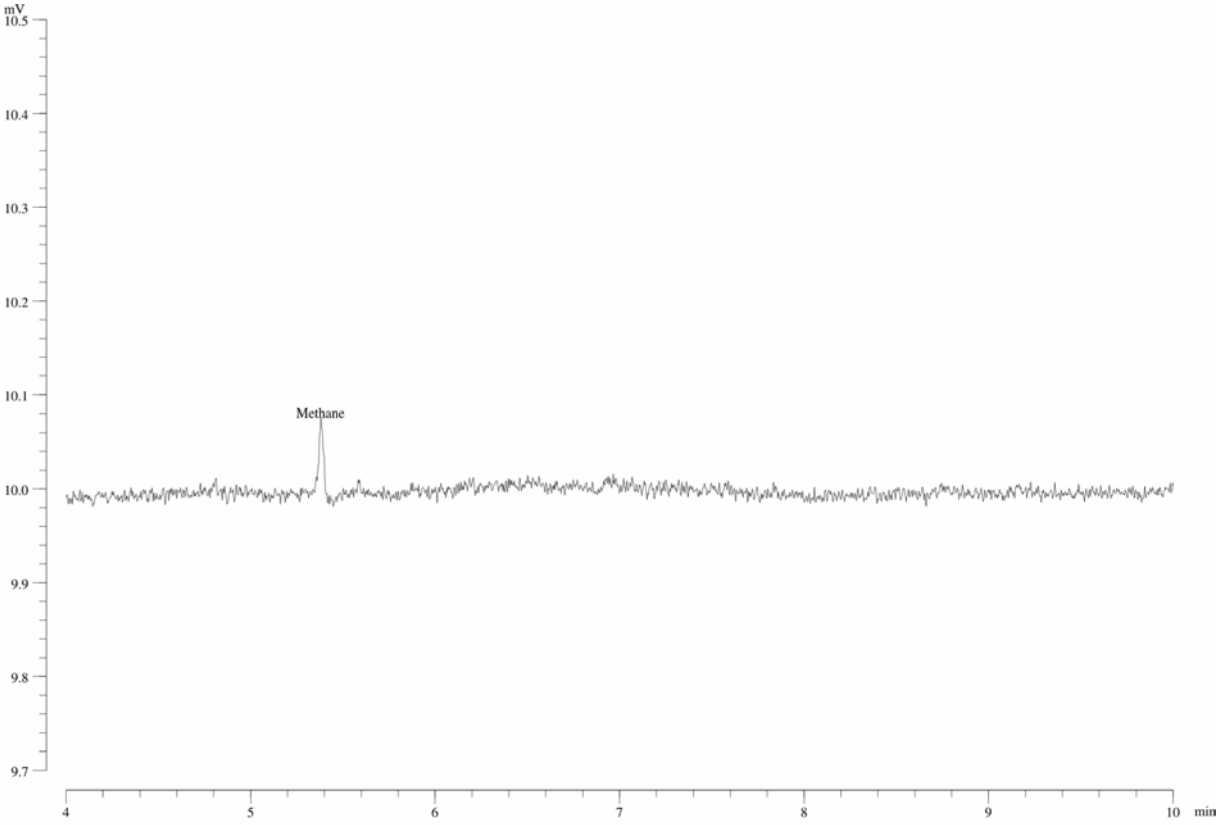

Analysis: [GC_LABOR]P513B06 ,61, 1 Samplename: E50182/2-GC_TM40-1M aquired on 3-Dec-2001 18:00:47 Channel: 17 reported on 29-JAN-2002 11:46:42.47 from user LEISTNER5

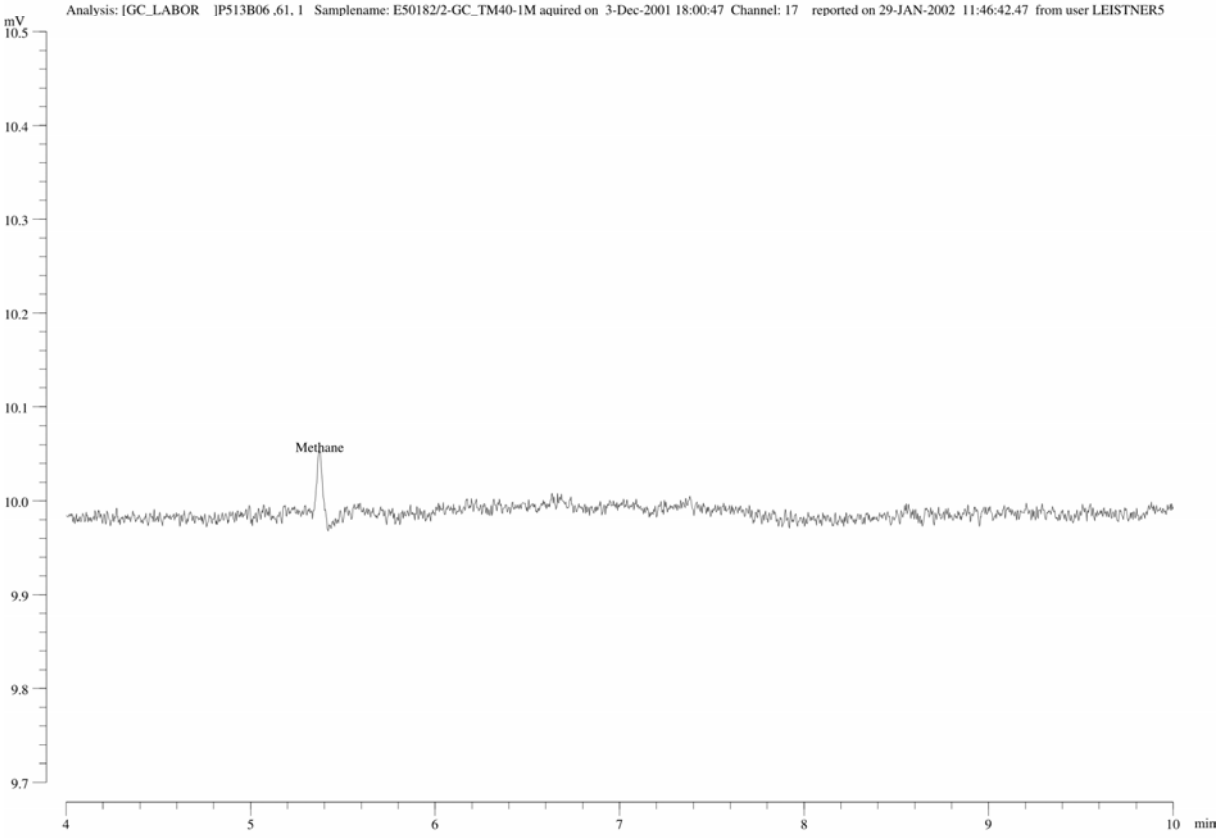

Analysis: [GC_LABOR]P513B06 ,62, 1 Samplename: E50183/2-GC_TM40-1M aquired on 3-Dec-2001 18:51:47 Channel: 17 reported on 29-JAN-2002 11:46:43.54 from user LEISTNER5

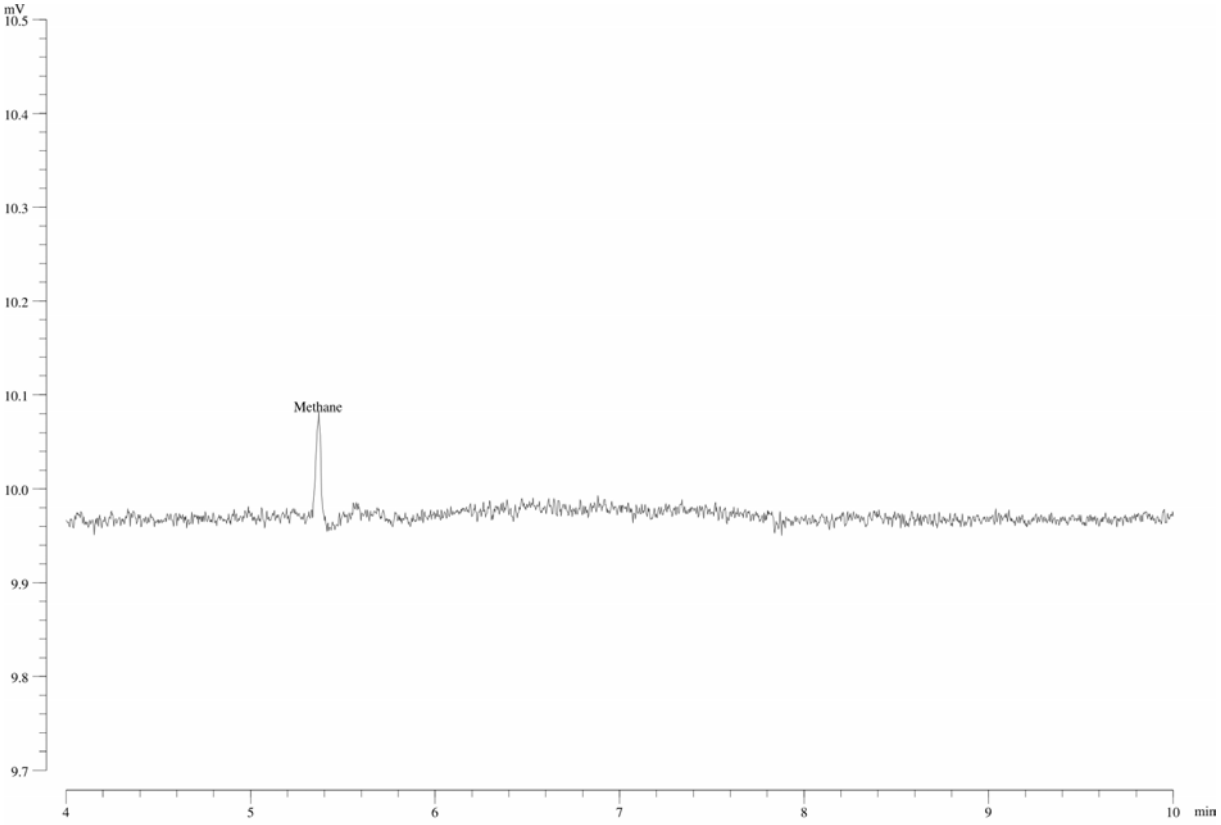

Analysis: [GC_LABOR]P513B06 ,63, 1 Samplename: E50184/2-GC_TM40-1M aquired on 3-Dec-2001 19:42:47 Channel: 17 reported on 29-JAN-2002 11:46:44.58 from user LEISTNER5

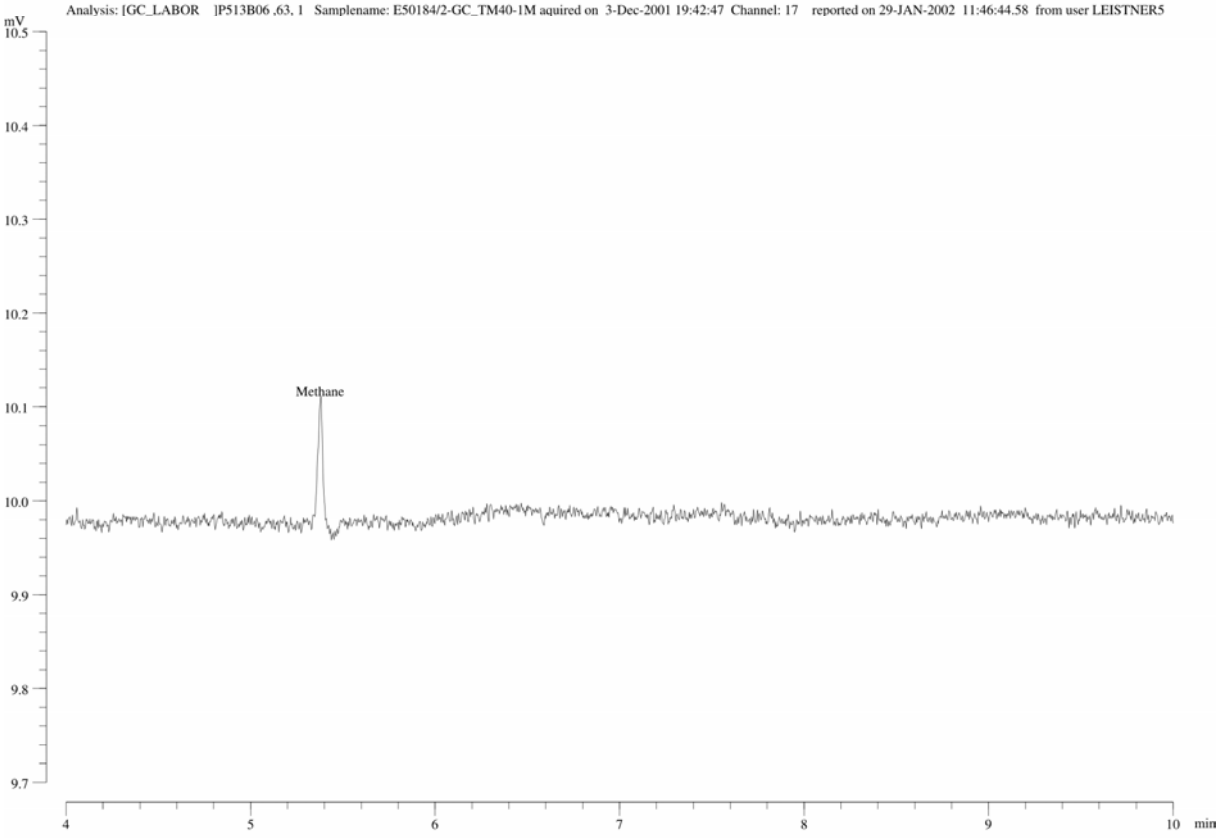

Analysis: [GC_LABOR]P513B06 ,64, 1 Samplename: E50185/2-GC_TM40-1M aquired on 3-Dec-2001 20:33:47 Channel: 17 reported on 29-JAN-2002 11:46:45.68 from user LEISTNER5

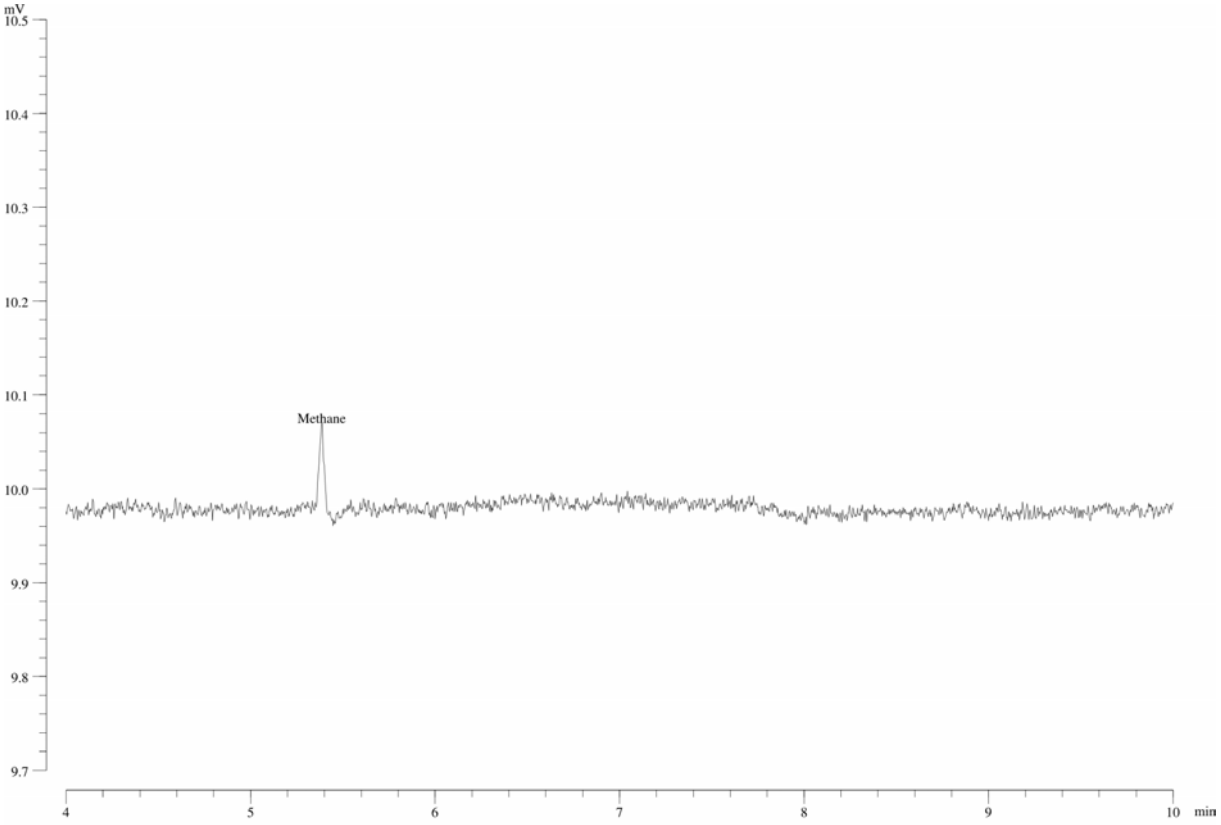

Analysis: [GC_LABOR]P513B06 ,65, 1 Samplename: E50186/2-GC_TM40-1M aquired on 3-Dec-2001 21:24:47 Channel: 17 reported on 29-JAN-2002 11:46:46.76 from user LEISTNER5

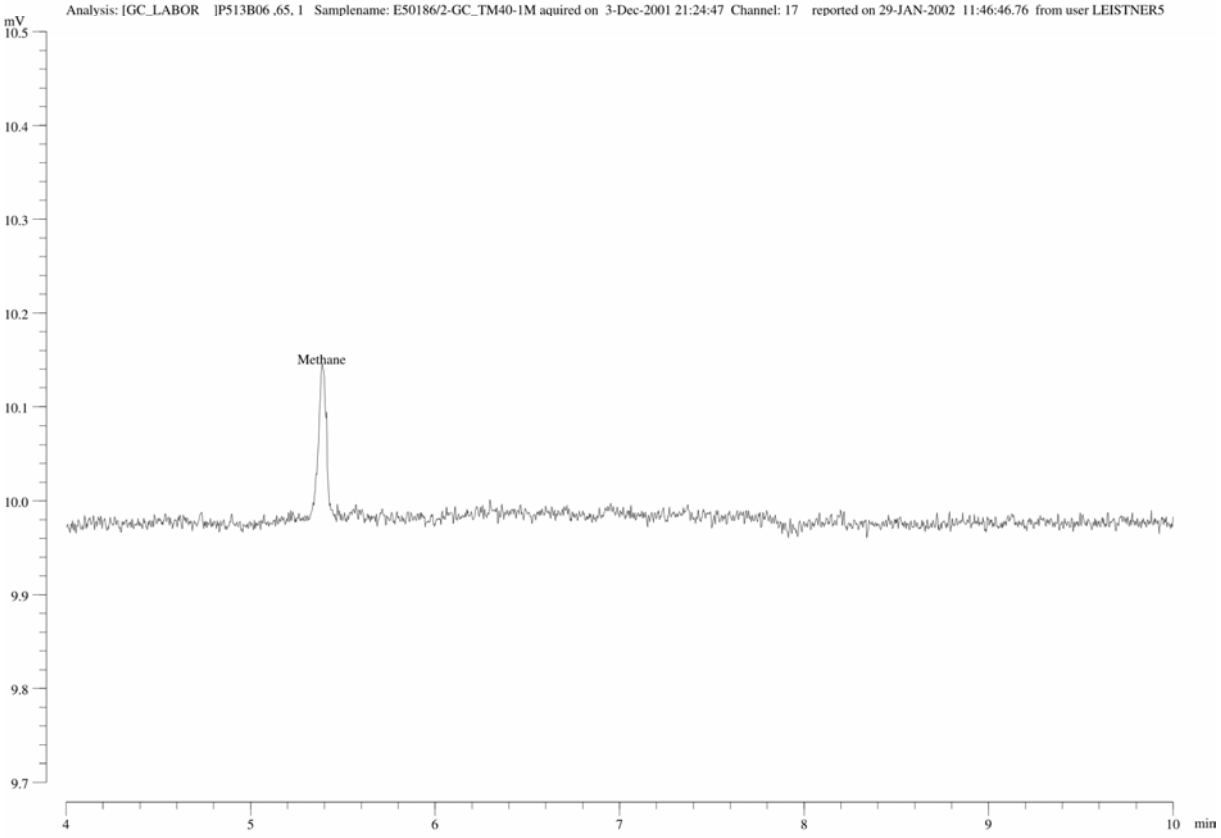

Analysis: [GC_LABOR]P513B06 ,66, 1 Samplename: E50166/0-GC_TM40-1M aquired on 3-Dec-2001 22:15:47 Channel: 17 reported on 29-JAN-2002 11:46:47.81 from user LEISTNER5

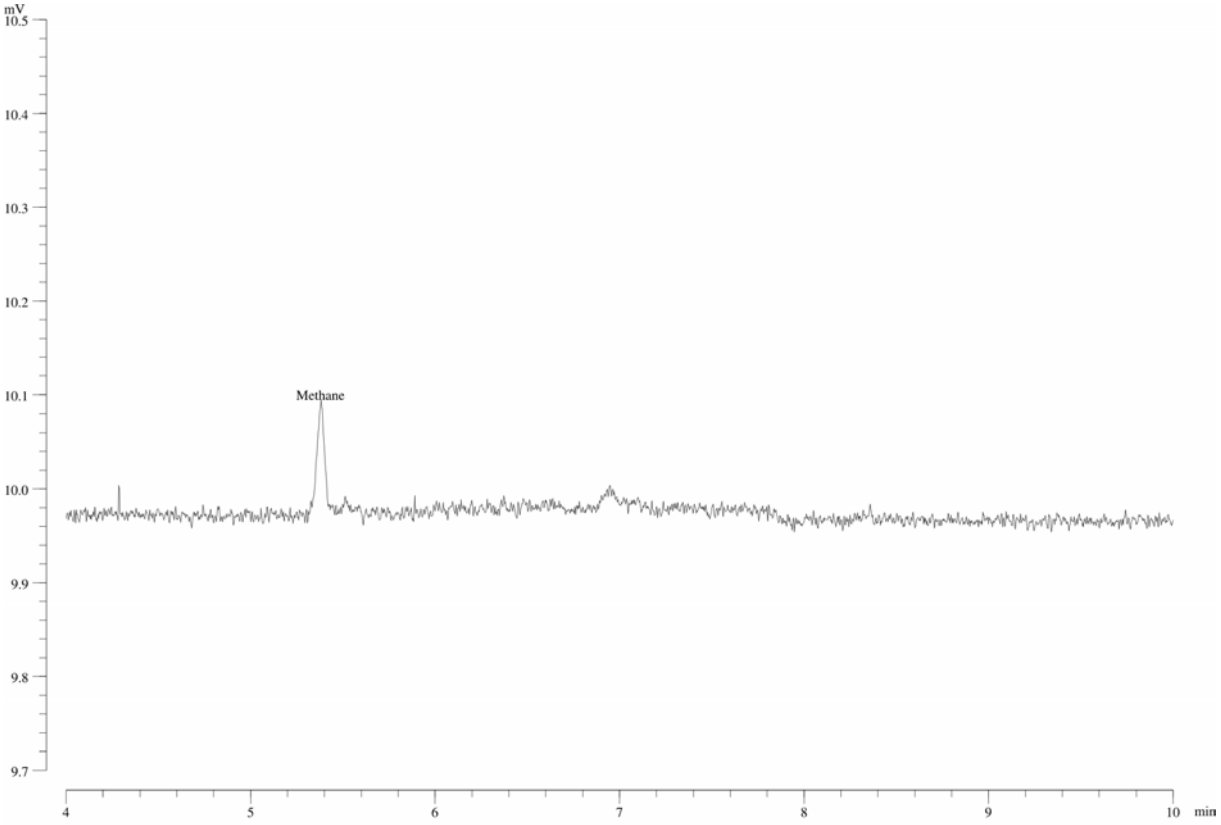

Analysis: [GC_LABOR]P513B06 ,67, 1 Samplename: E50173/0-GC_TM40-1M aquired on 3-Dec-2001 23:06:47 Channel: 17 reported on 29-JAN-2002 11:46:48.83 from user LEISTNER5

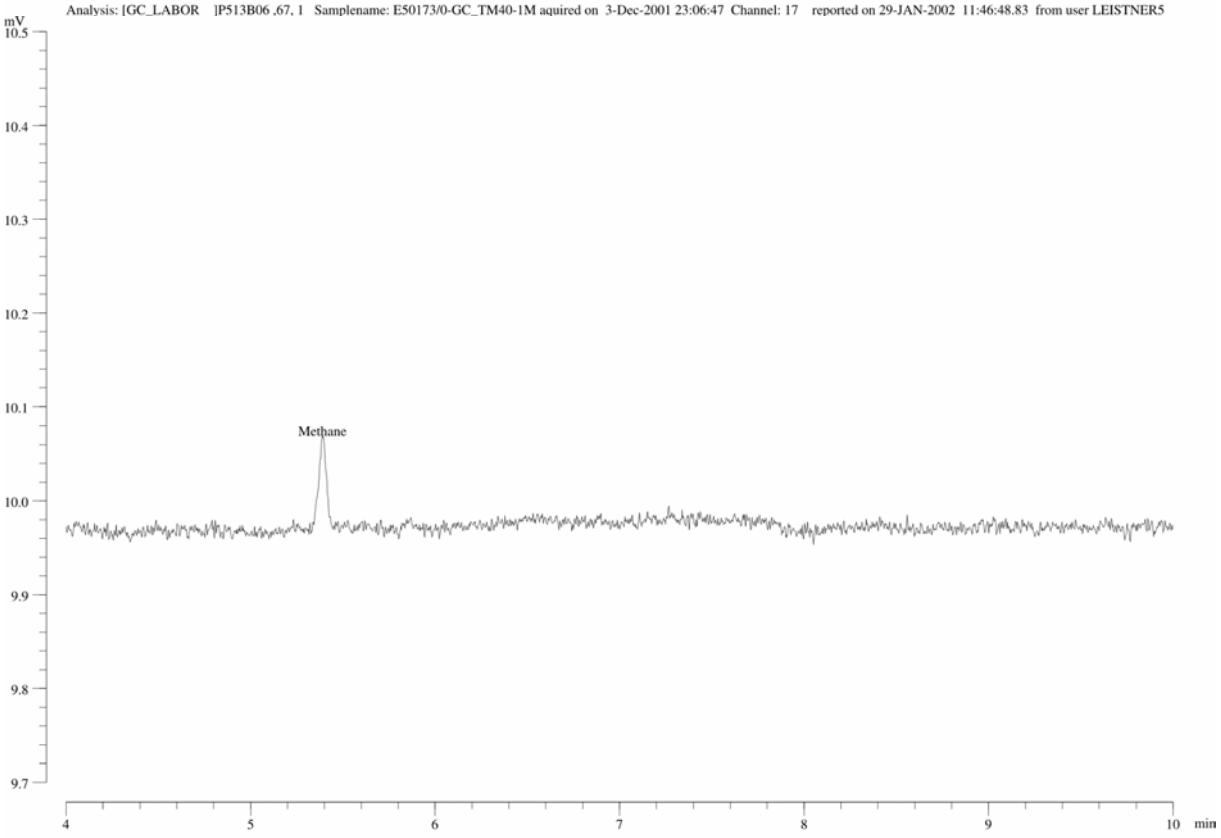

Analysis: [GC_LABOR]P513B06 ,68, 1 Samplename: AufkleberGC_TM40-1M aquired on 3-Dec-2001 23:57:47 Channel: 17 reported on 29-JAN-2002 11:46:49.88 from user LEISTNER5

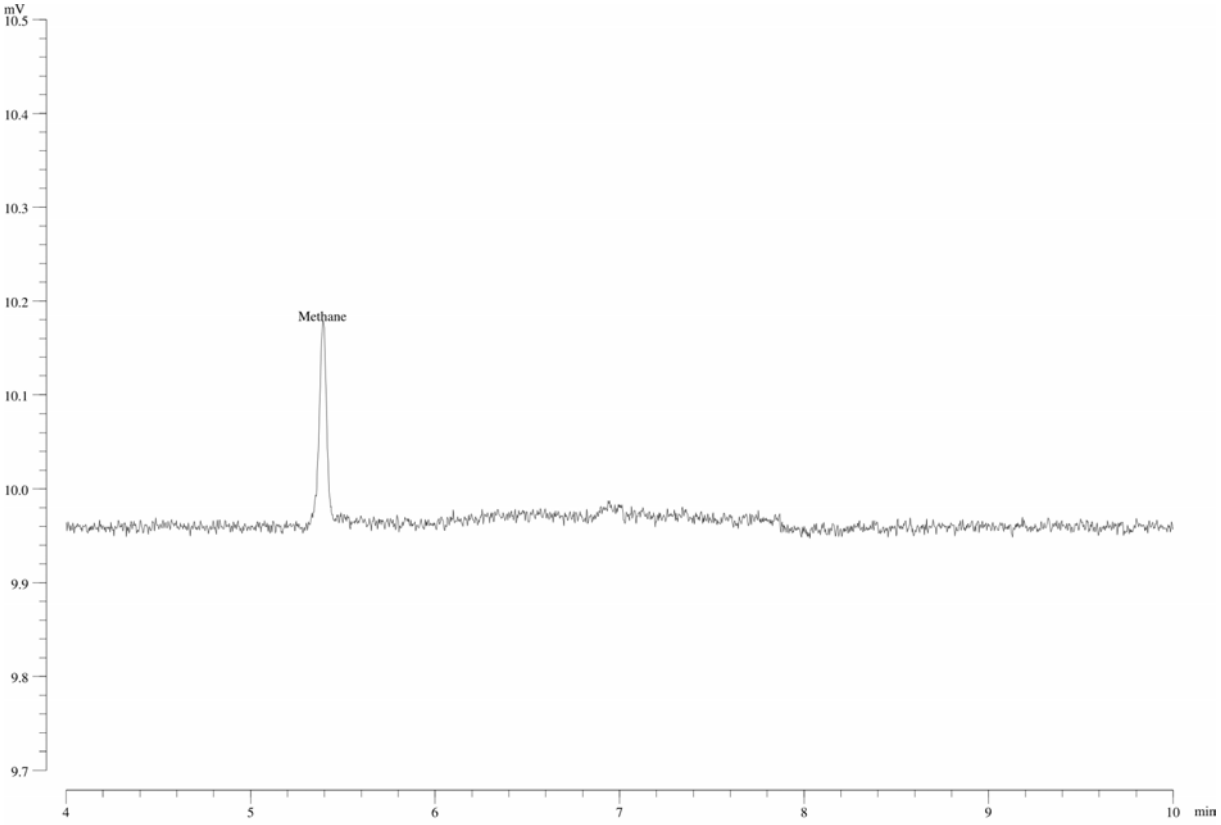

Analysis: [GC_LABOR]P513B06 ,69, 1 Samplename: E50175/1-GC_TM40-1M aquired on 4-Dec-2001 12:28:07 Channel: 17 reported on 29-JAN-2002 11:46:50.91 from user LEISTNER5

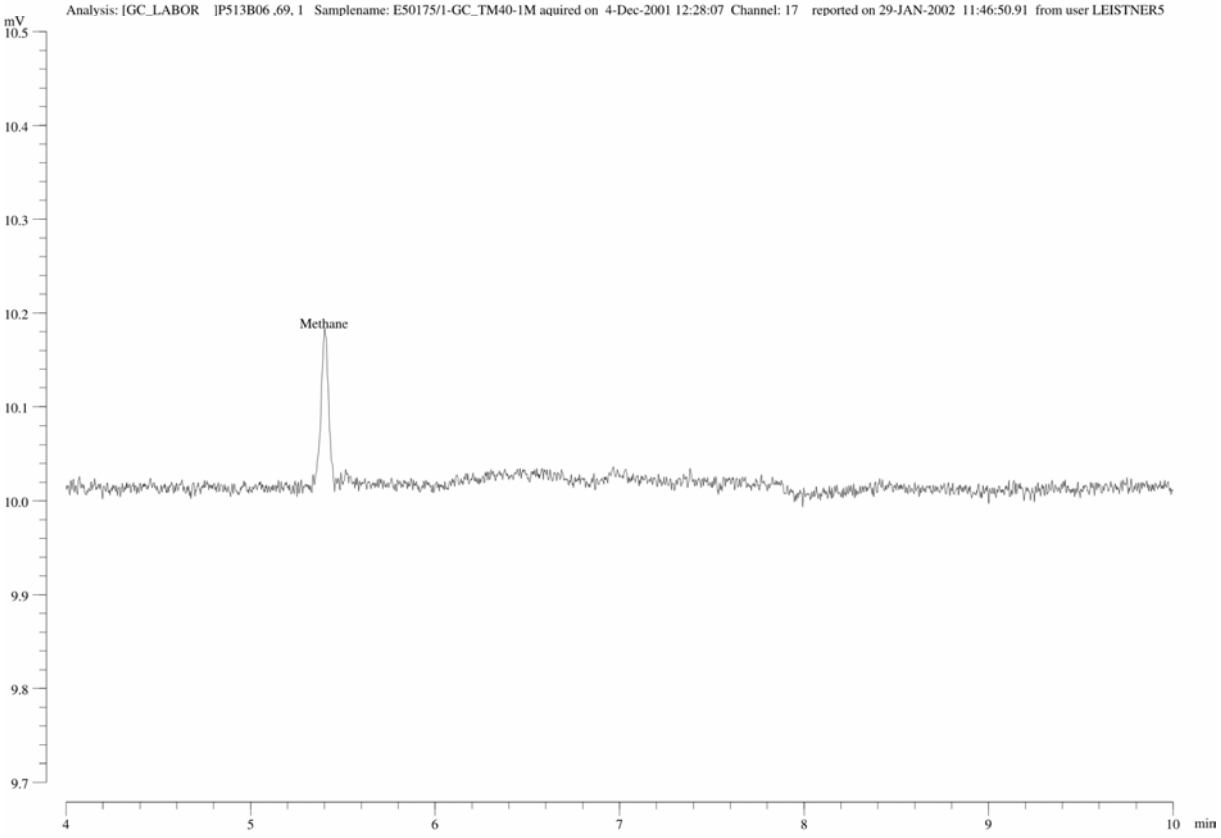

Analysis: [GC_LABOR]P513B06 ,70, 1 Samplename: E50196/1-GC_TM40-1M aquired on 4-Dec-2001 13:19:10 Channel: 17 reported on 29-JAN-2002 11:46:52.24 from user LEISTNER5

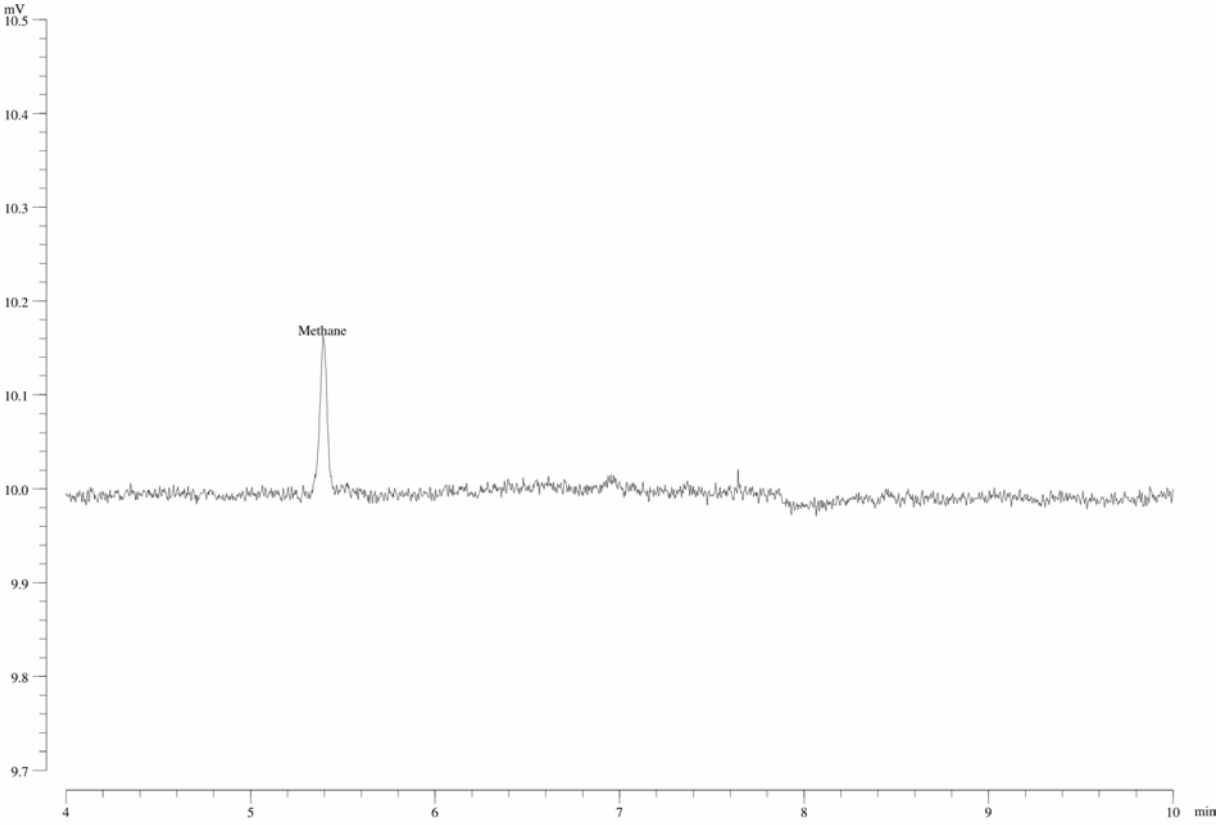

Analysis: [GC_LABOR]P513B06 ,71, 1 Samplename: E50222/1-GC_TM40-1M aquired on 4-Dec-2001 14:10:10 Channel: 17 reported on 29-JAN-2002 11:46:53.30 from user LEISTNER5

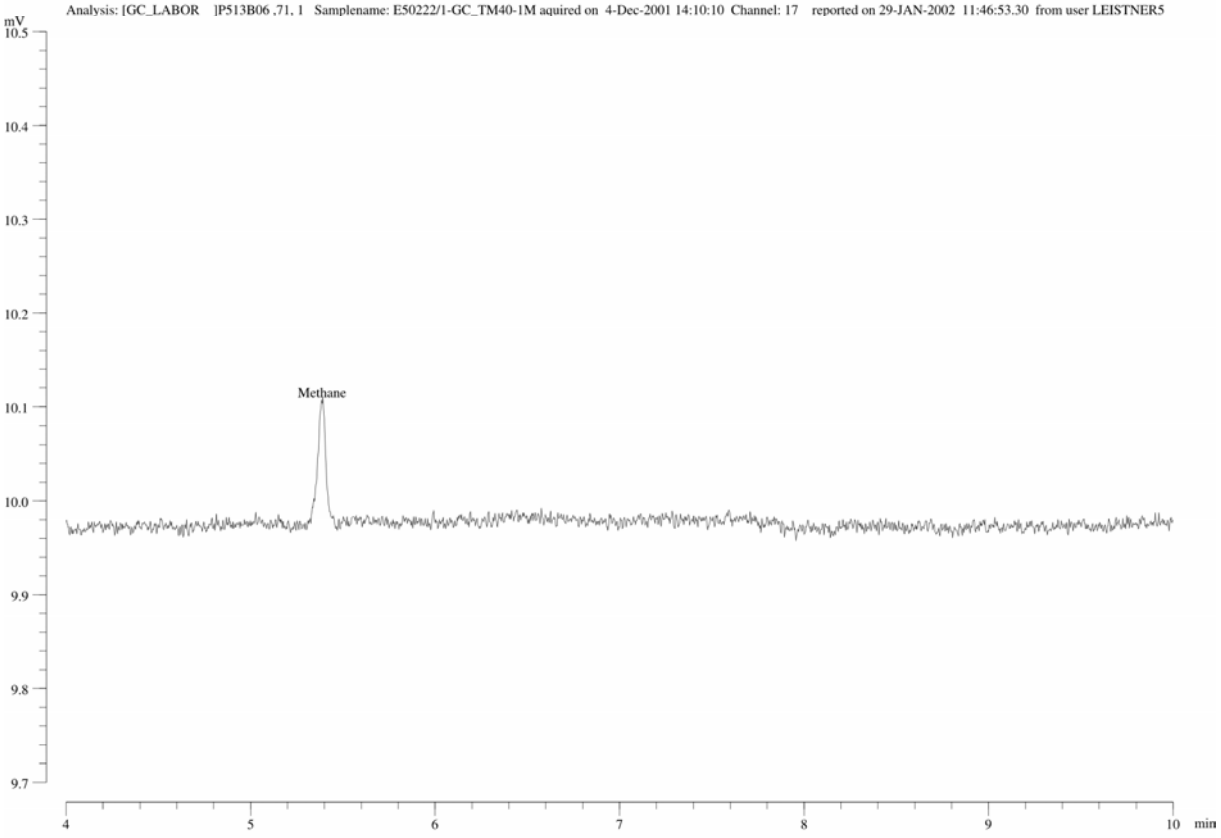

Analysis: [GC_LABOR]P513B06 ,72, 1 Samplename: E50237/1-GC_TM40-1M aquired on 4-Dec-2001 15:01:10 Channel: 17 reported on 29-JAN-2002 11:46:54.34 from user LEISTNER5

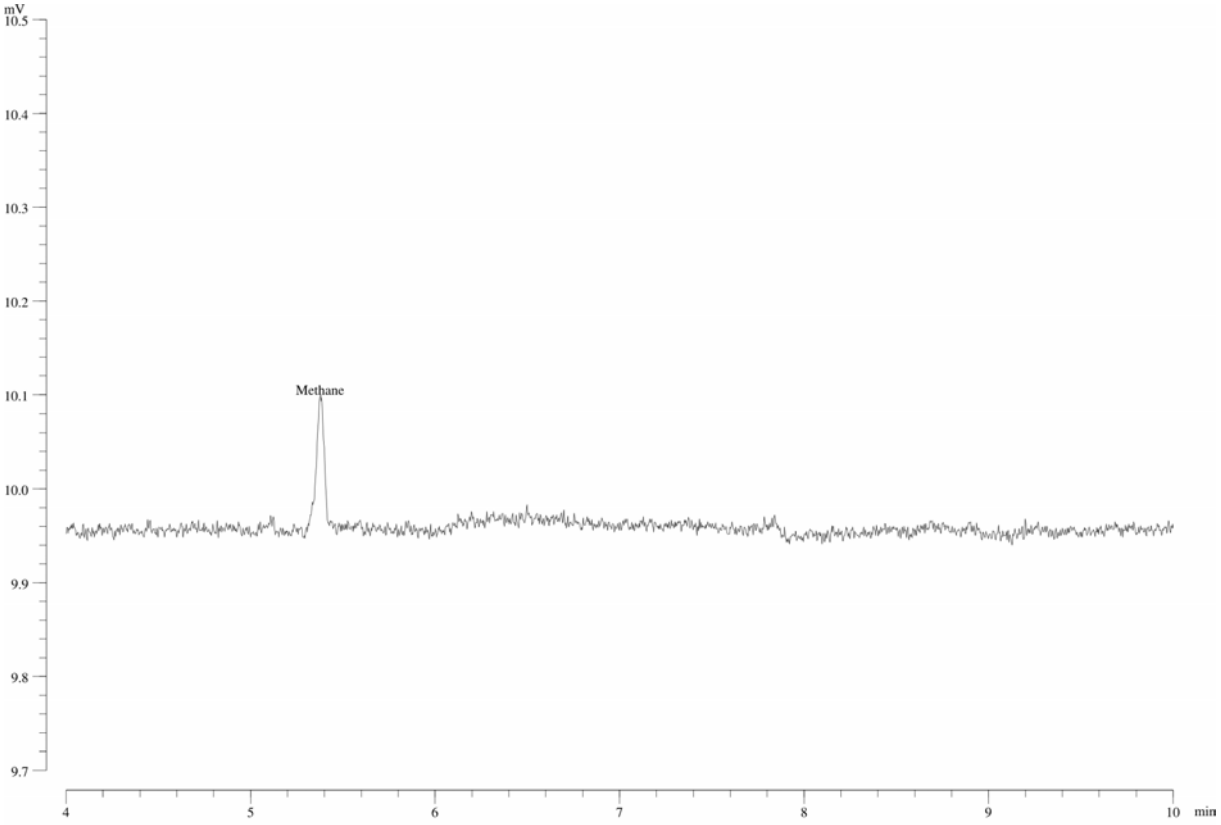

Analysis: [GC_LABOR]P513B06 ,73, 1 Samplename: E50238/1-GC_TM40-1M aquired on 4-Dec-2001 15:52:10 Channel: 17 reported on 29-JAN-2002 11:46:55.38 from user LEISTNER5

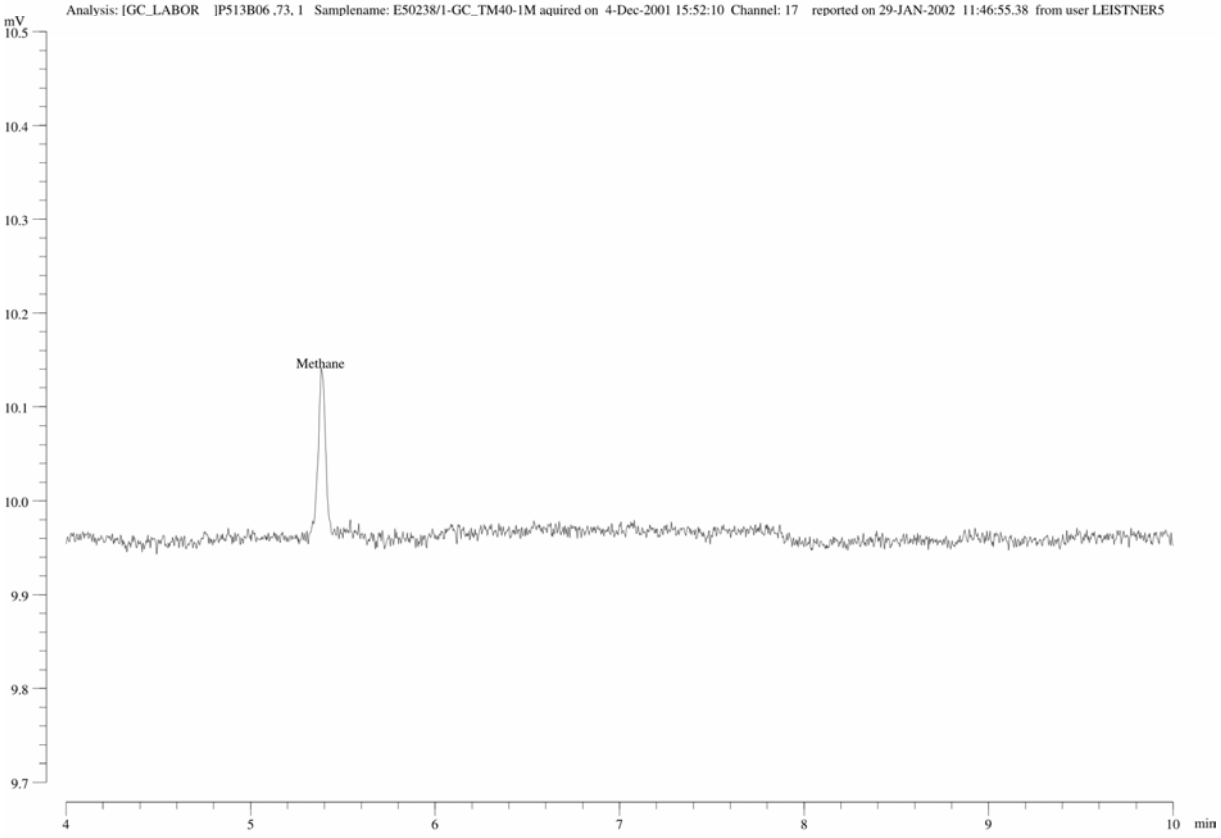

Analysis: [GC_LABOR]P513B06 ,74, 1 Samplename: E50239/1-GC_TM40-1M aquired on 4-Dec-2001 16:43:10 Channel: 17 reported on 29-JAN-2002 11:46:56.43 from user LEISTNER5

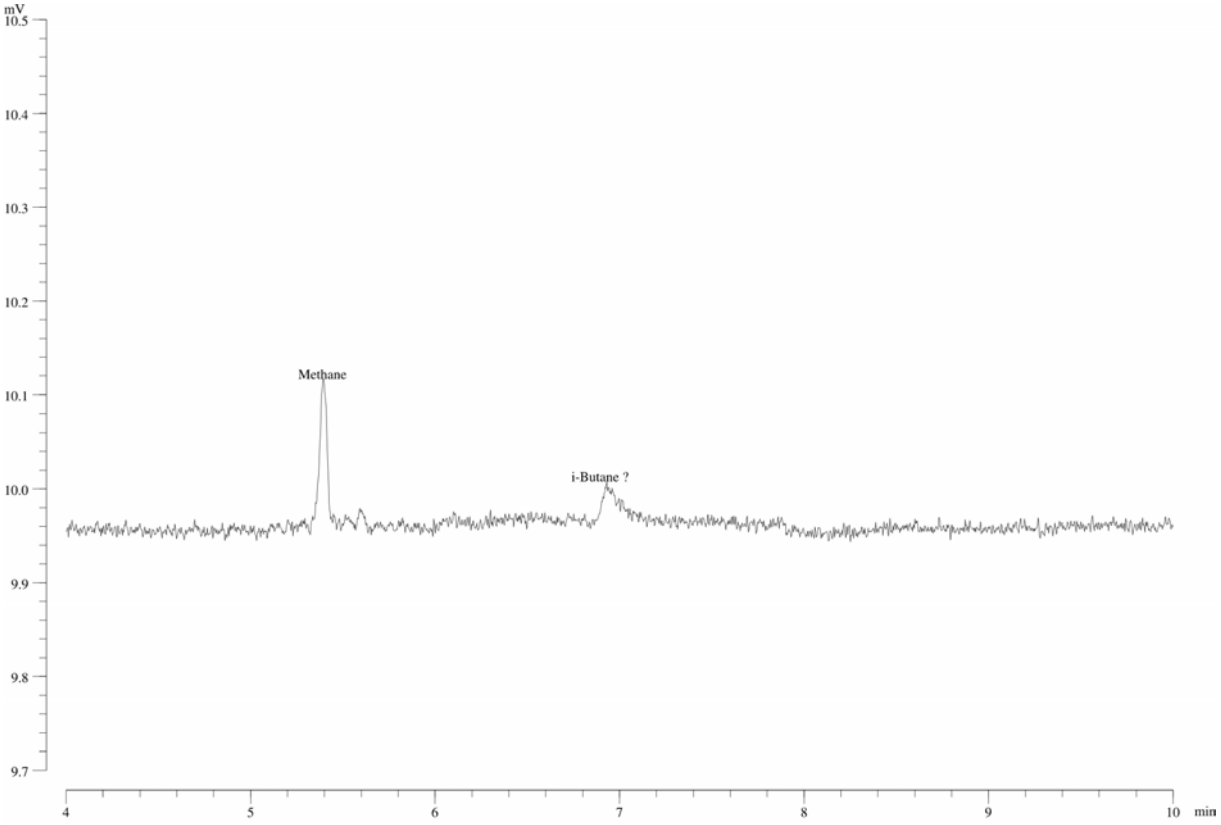

Analysis: [GC_LABOR]P513B06 ,75, 1 Samplename: E50240/1-GC_TM40-1M aquired on 4-Dec-2001 17:34:10 Channel: 17 reported on 29-JAN-2002 11:46:57.47 from user LEISTNER5

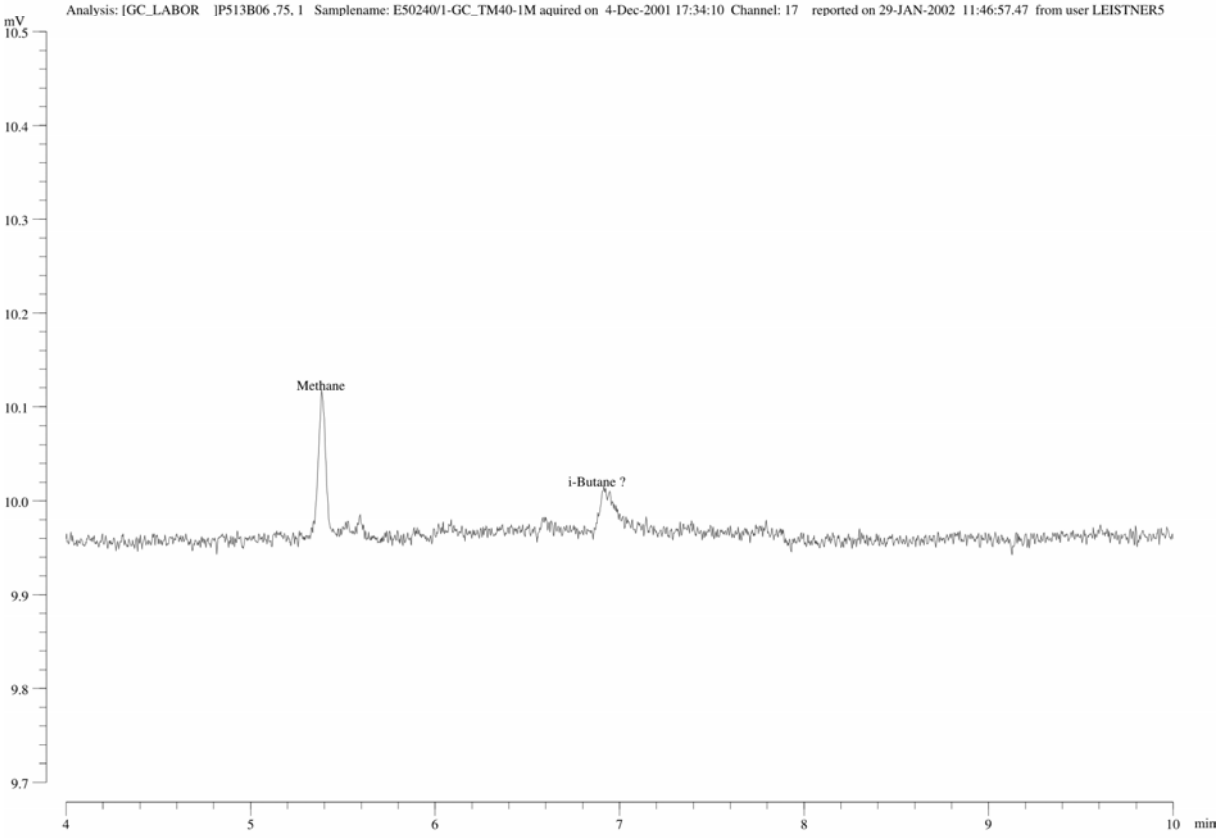

Analysis: [GC_LABOR]P513B06 ,76, 1 Samplename: E50241/1-GC_TM40-1M aquired on 4-Dec-2001 18:25:09 Channel: 17 reported on 29-JAN-2002 11:46:58.54 from user LEISTNER5

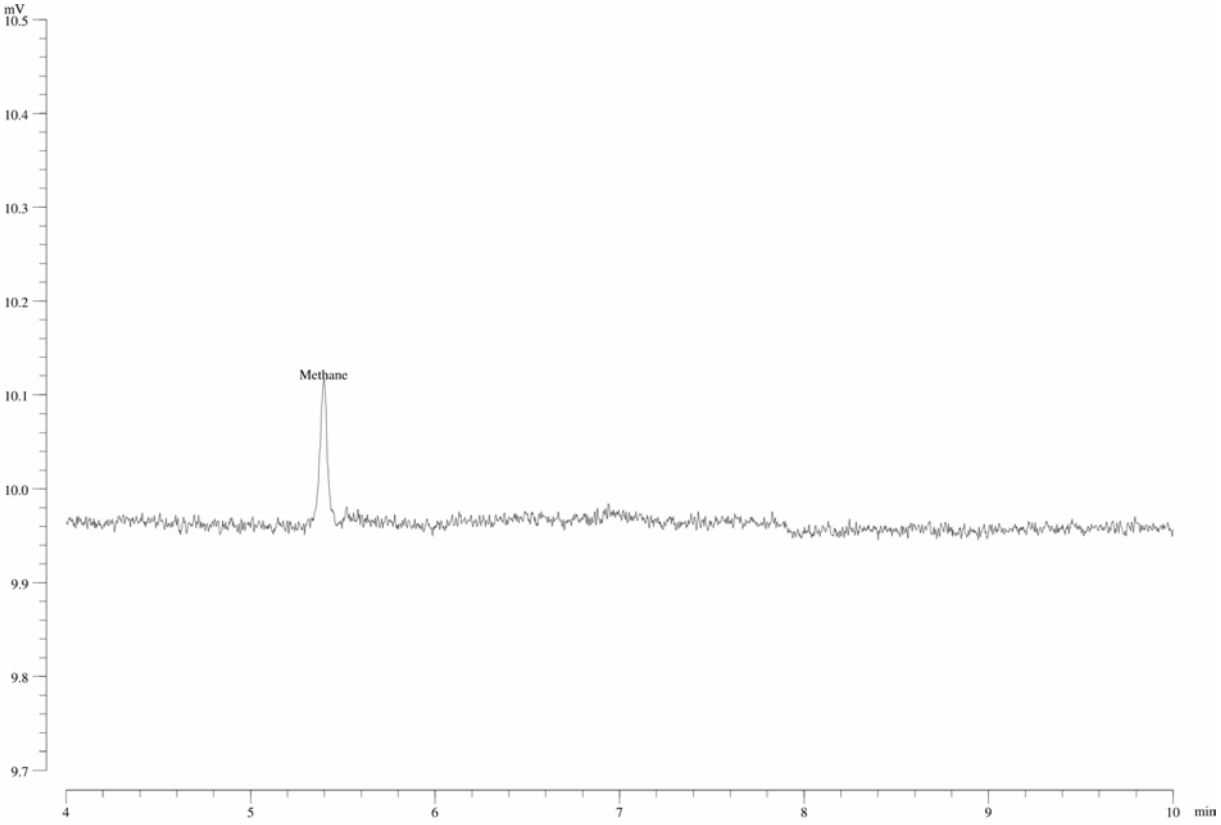

Analysis: [GC_LABOR]P513B06 ,77, 1 Samplename: E50242/1-GC_TM40-1M aquired on 4-Dec-2001 19:16:09 Channel: 17 reported on 29-JAN-2002 11:46:59.59 from user LEISTNER5

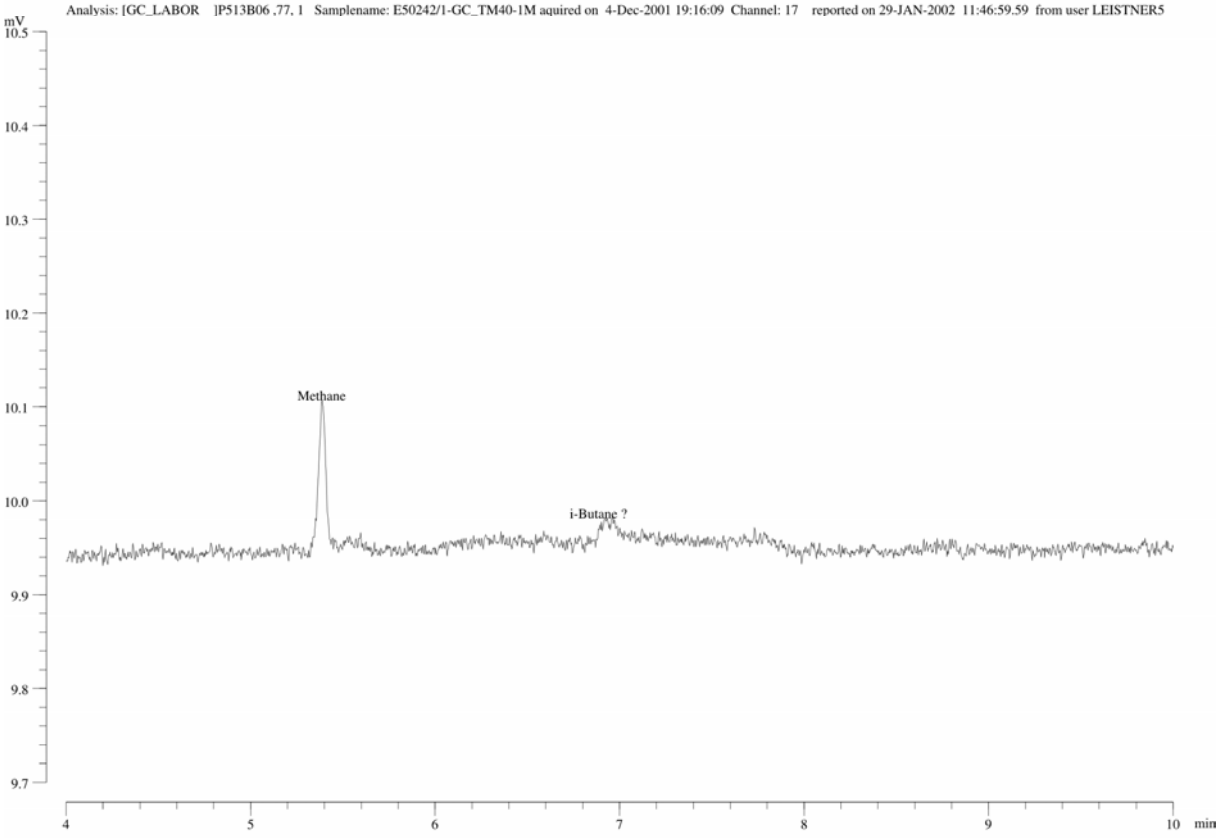

Analysis: [GC_LABOR]P513B06 ,78, 1 Samplename: E50243/1-GC_TM40-1M aquired on 4-Dec-2001 20:07:09 Channel: 17 reported on 29-JAN-2002 11:47:00.61 from user LEISTNER5

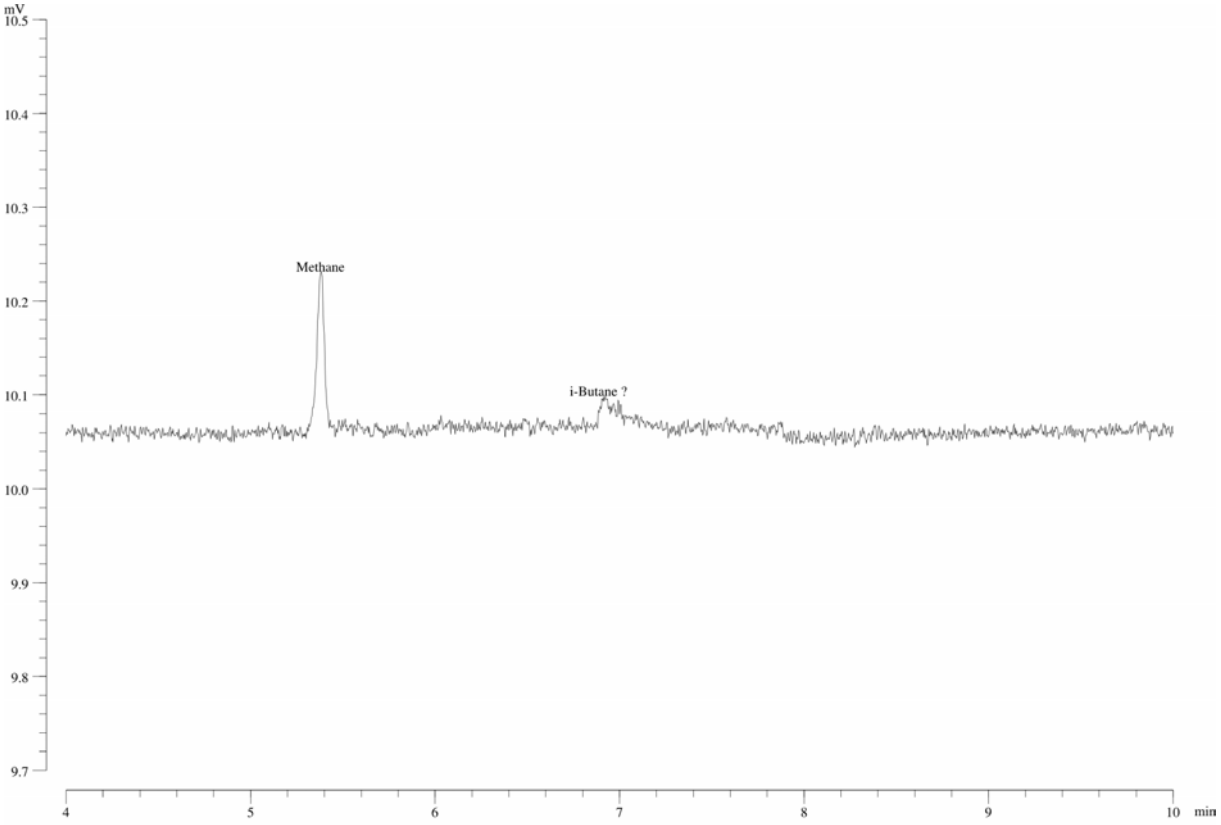

Analysis: [GC_LABOR]P513B06 ,79, 1 Samplename: E50244/1-GC_TM40-1M aquired on 4-Dec-2001 20:58:09 Channel: 17 reported on 29-JAN-2002 11:47:01.67 from user LEISTNER5

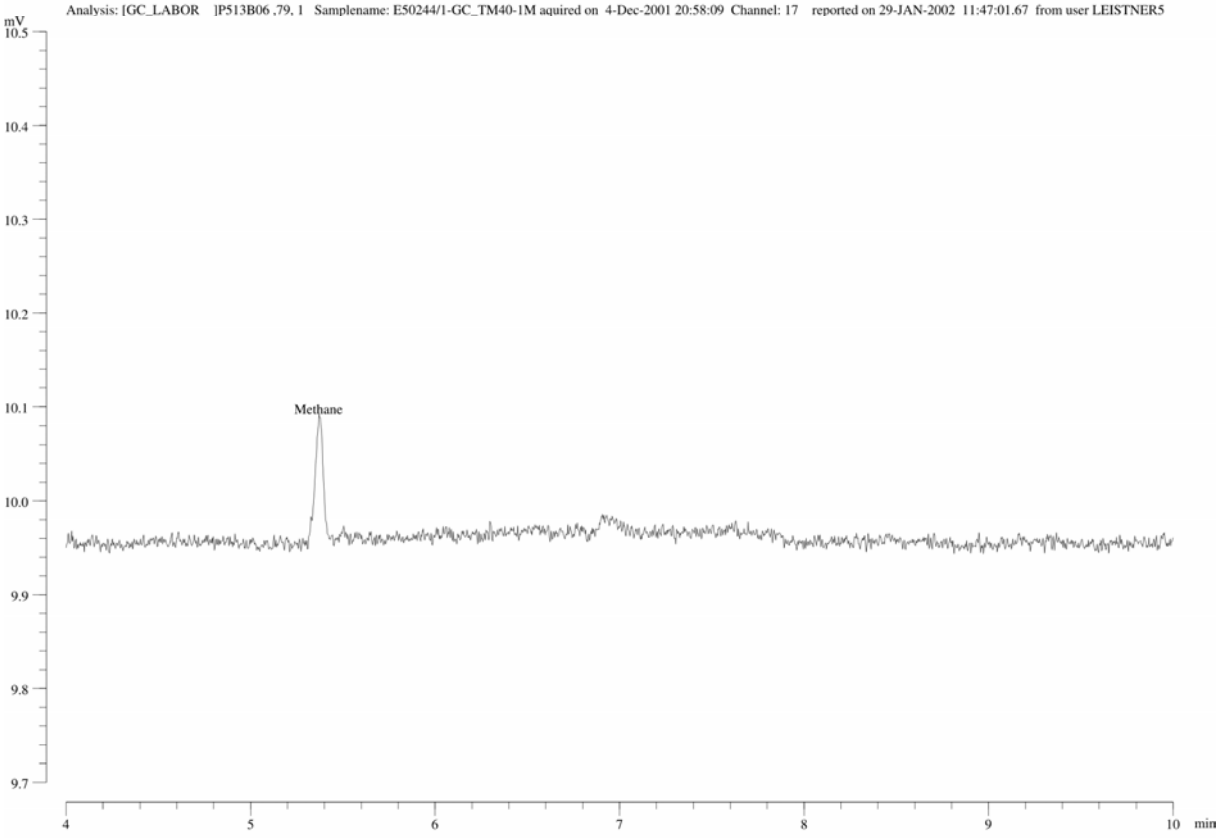

Analysis: [GC_LABOR]P513B06 ,80, 1 Samplename: E50245/1-GC_TM40-1M aquired on 4-Dec-2001 21:49:09 Channel: 17 reported on 29-JAN-2002 11:47:02.90 from user LEISTNER5

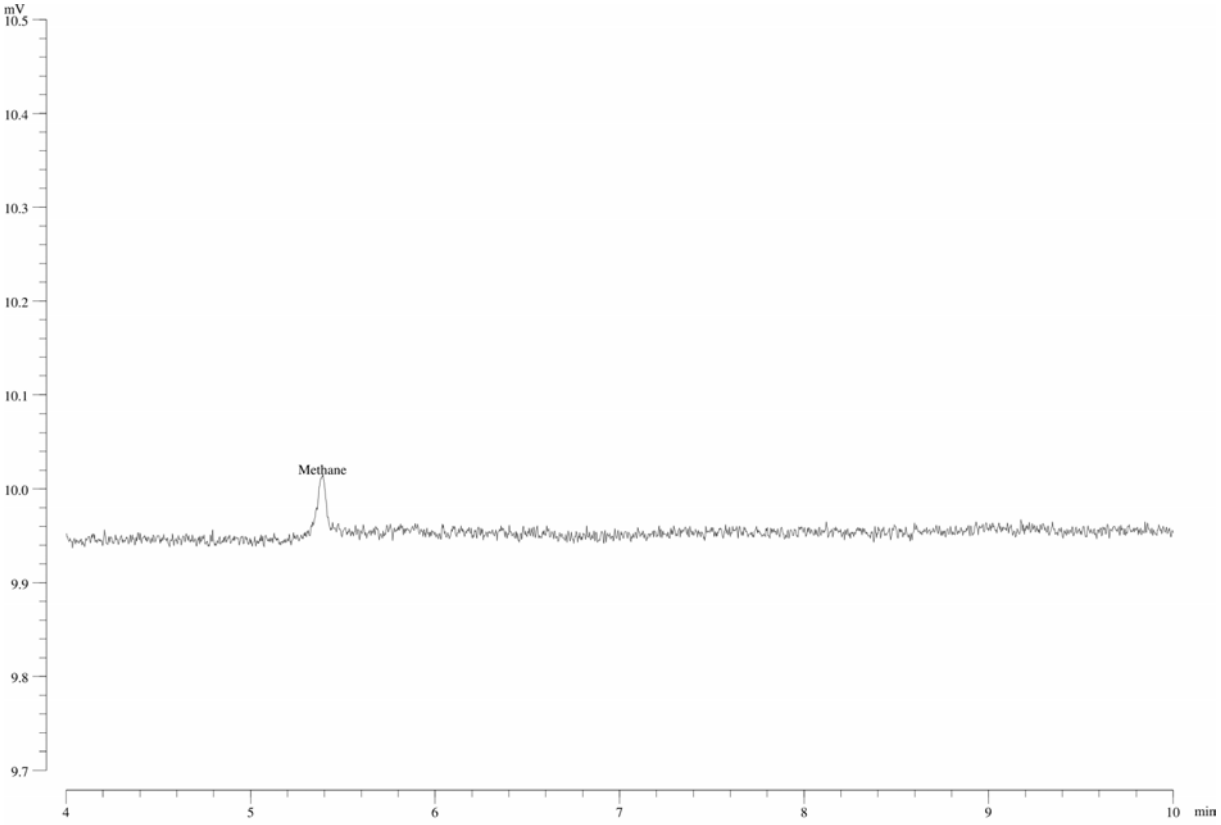

Analysis: [GC_LABOR]P513B06 ,81, 1 Samplename: E50527/1-GC_TM40-1M aquired on 23-Jan-2002 13:54:50 Channel: 17 reported on 29-JAN-2002 11:47:03.94 from user LEISTNER5

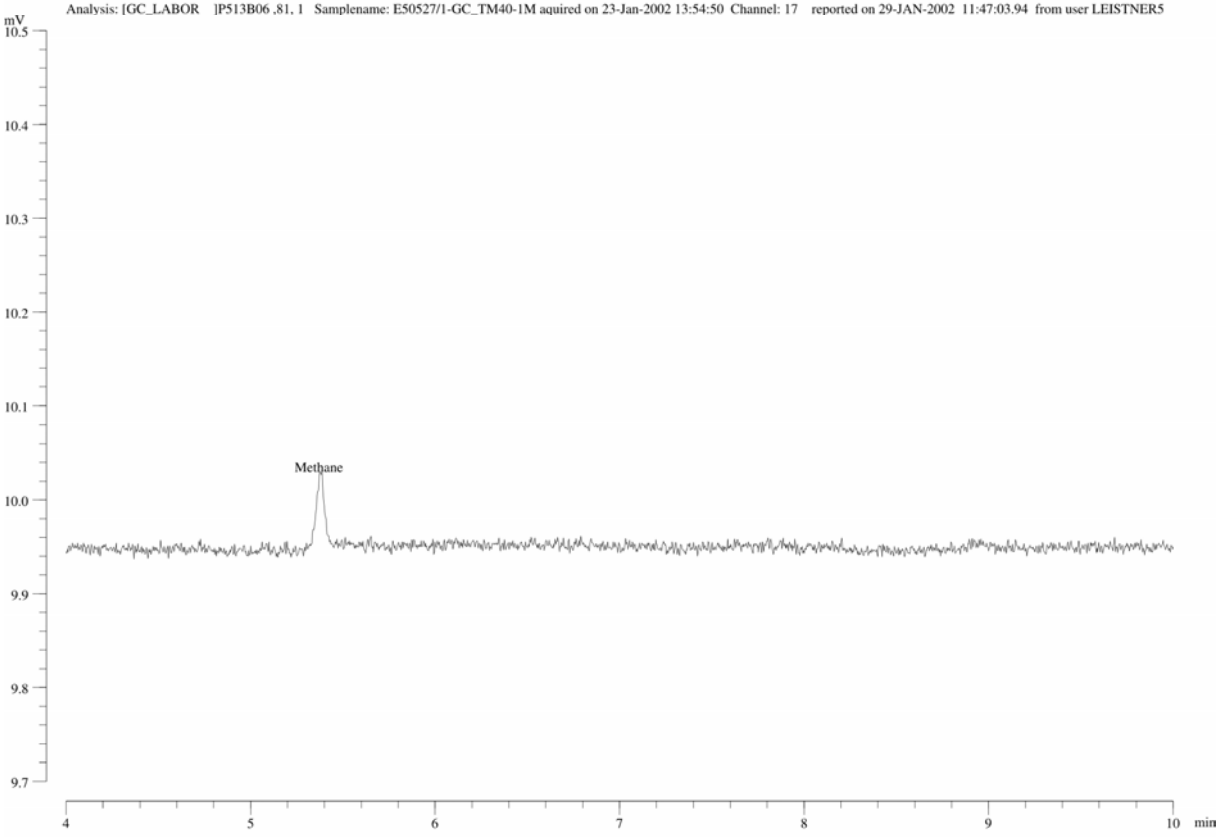

Analysis: [GC_LABOR]P513B06 ,82, 1 Samplename: E50527/2-GC_TM40-1M aquired on 23-Jan-2002 14:45:53 Channel: 17 reported on 29-JAN-2002 11:47:04.96 from user LEISTNER5

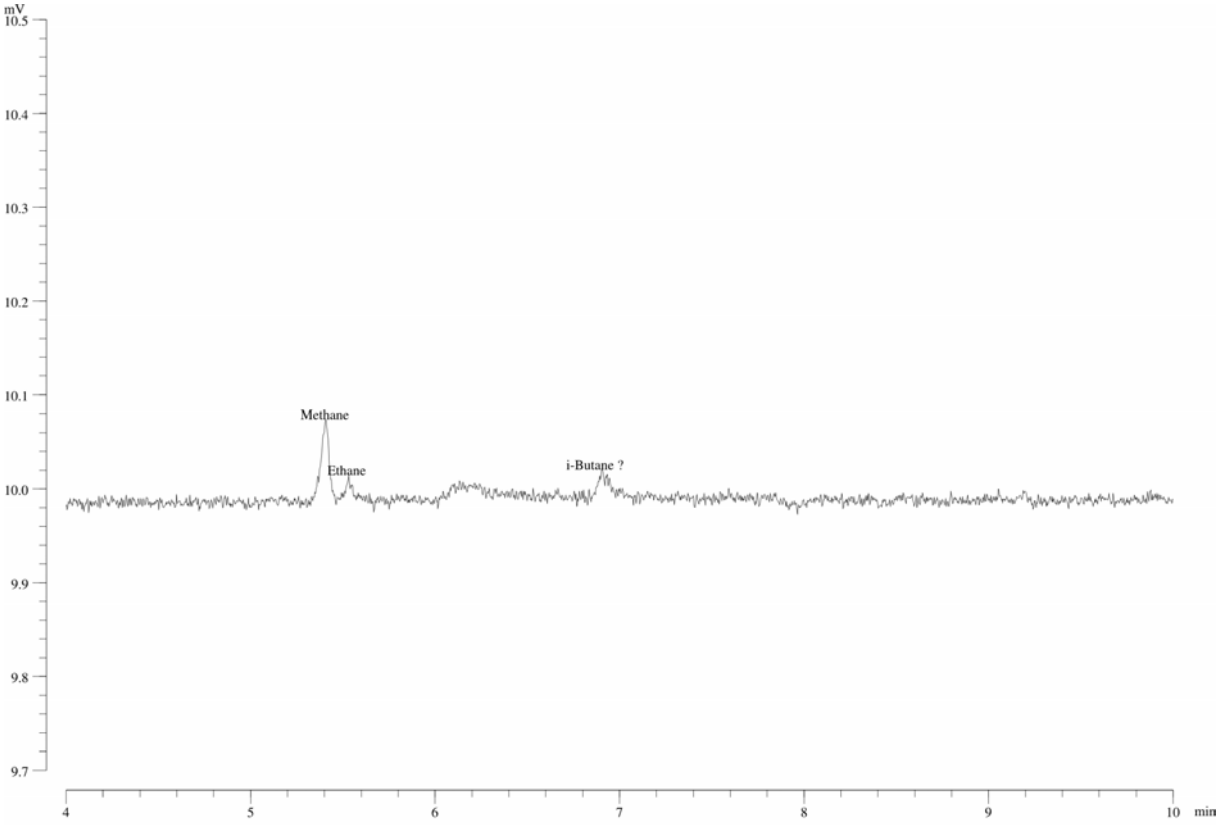

Analysis: [GC_LABOR]P513B06 ,83, 1 Samplename: E50526/1-GC_TM40-1M aquired on 23-Jan-2002 15:36:53 Channel: 17 reported on 29-JAN-2002 11:47:05.99 from user LEISTNER5

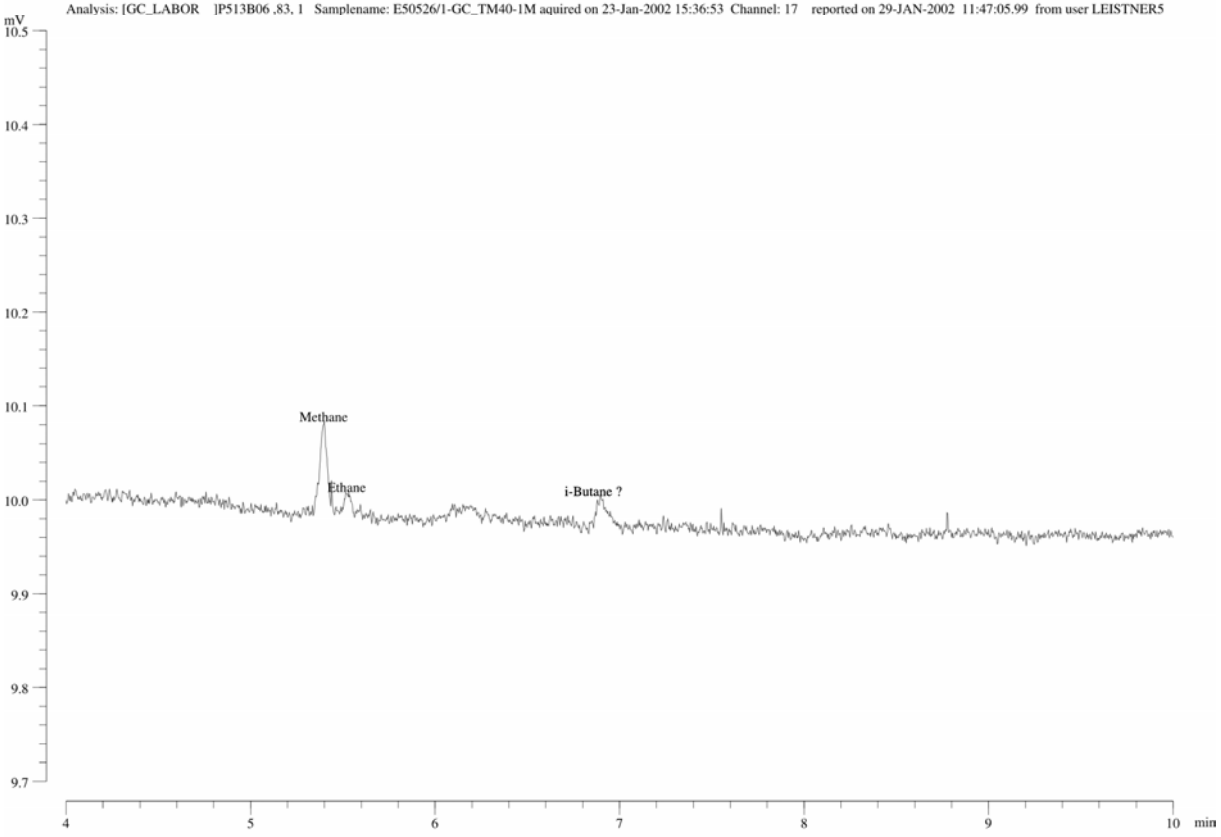

Analysis: [GC_LABOR]P513B06 ,84, 1 Samplename: E50526/2-GC_TM40-1M aquired on 23-Jan-2002 16:27:53 Channel: 17 reported on 29-JAN-2002 11:47:07.03 from user LEISTNER5

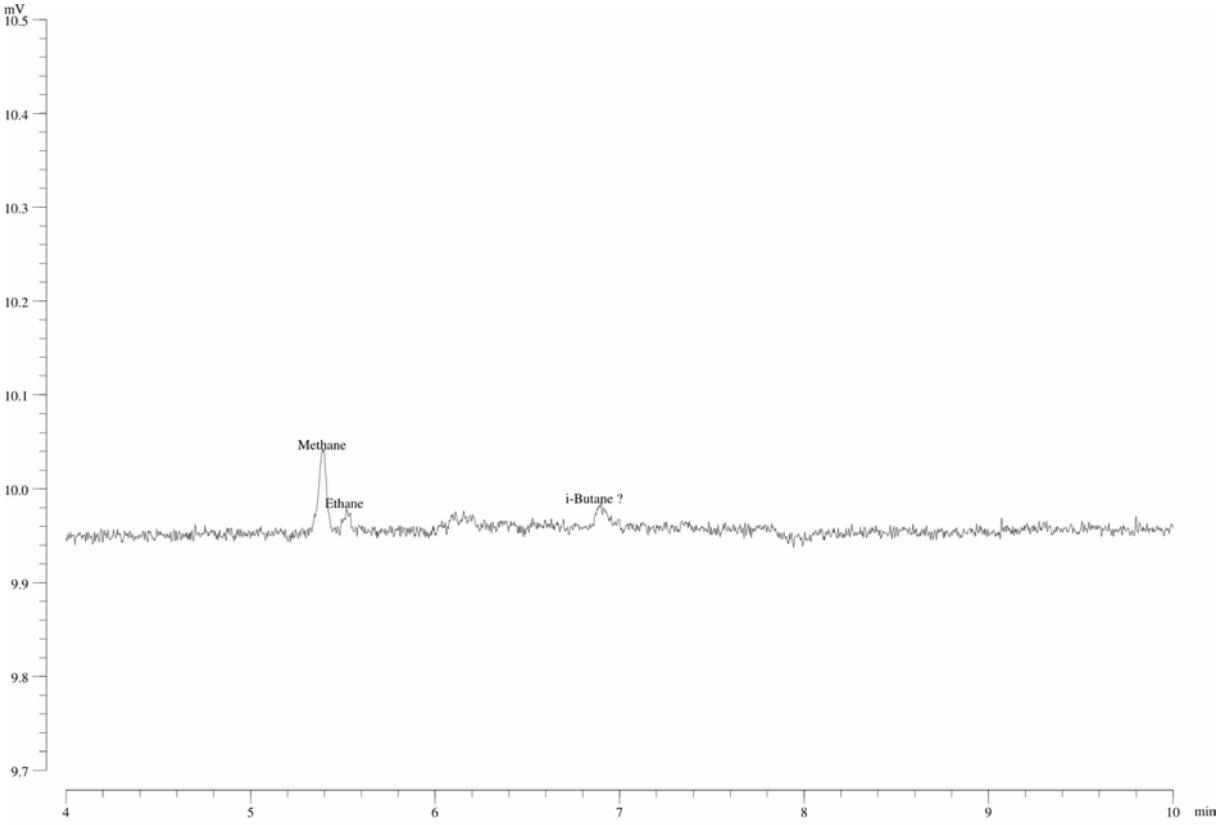

Analysis: [GC_LABOR]P513B06 ,85, 1 Samplename: E50526/3-GC_TM40-1M aquired on 23-Jan-2002 17:18:53 Channel: 17 reported on 29-JAN-2002 11:47:08.16 from user LEISTNER5

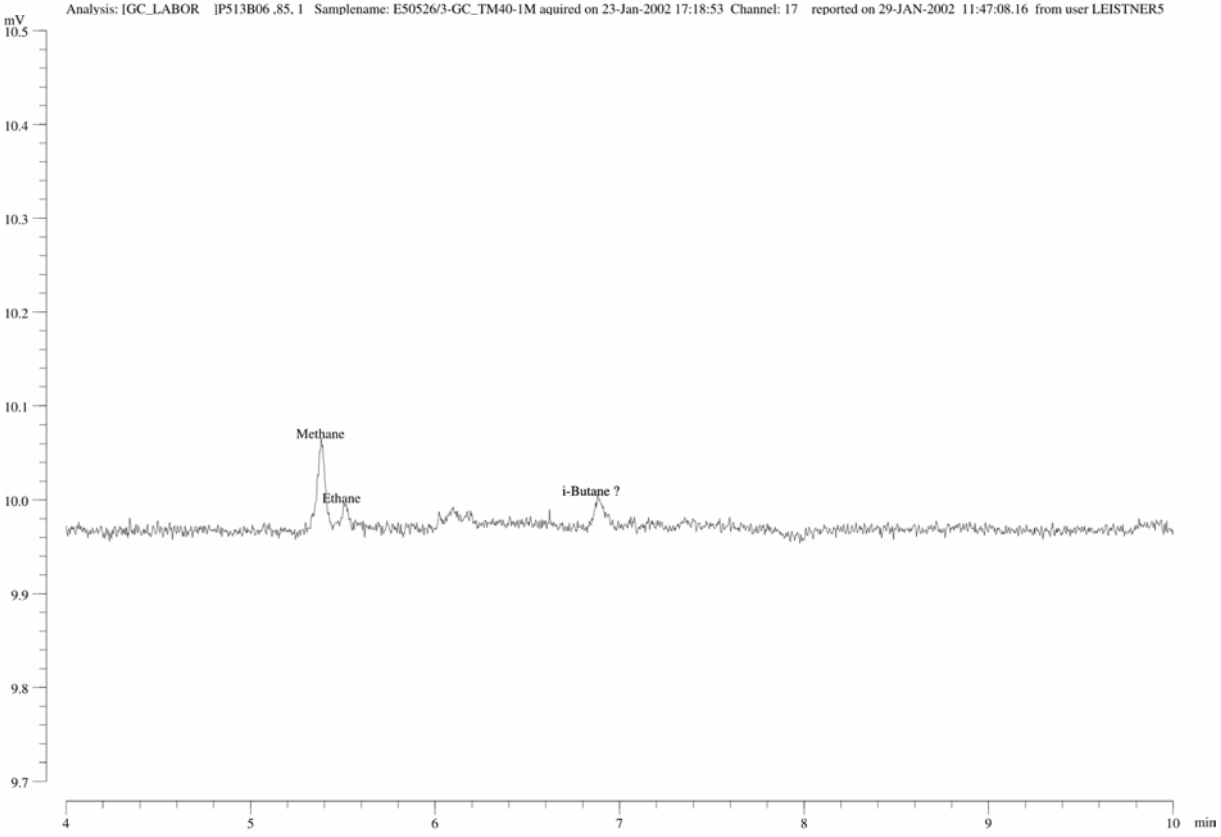

Analysis: [GC_LABOR]P513B06 ,86, 1 Samplename: E50526/4-GC_TM40-1M aquired on 23-Jan-2002 18:09:53 Channel: 17 reported on 29-JAN-2002 11:47:09.23 from user LEISTNER5

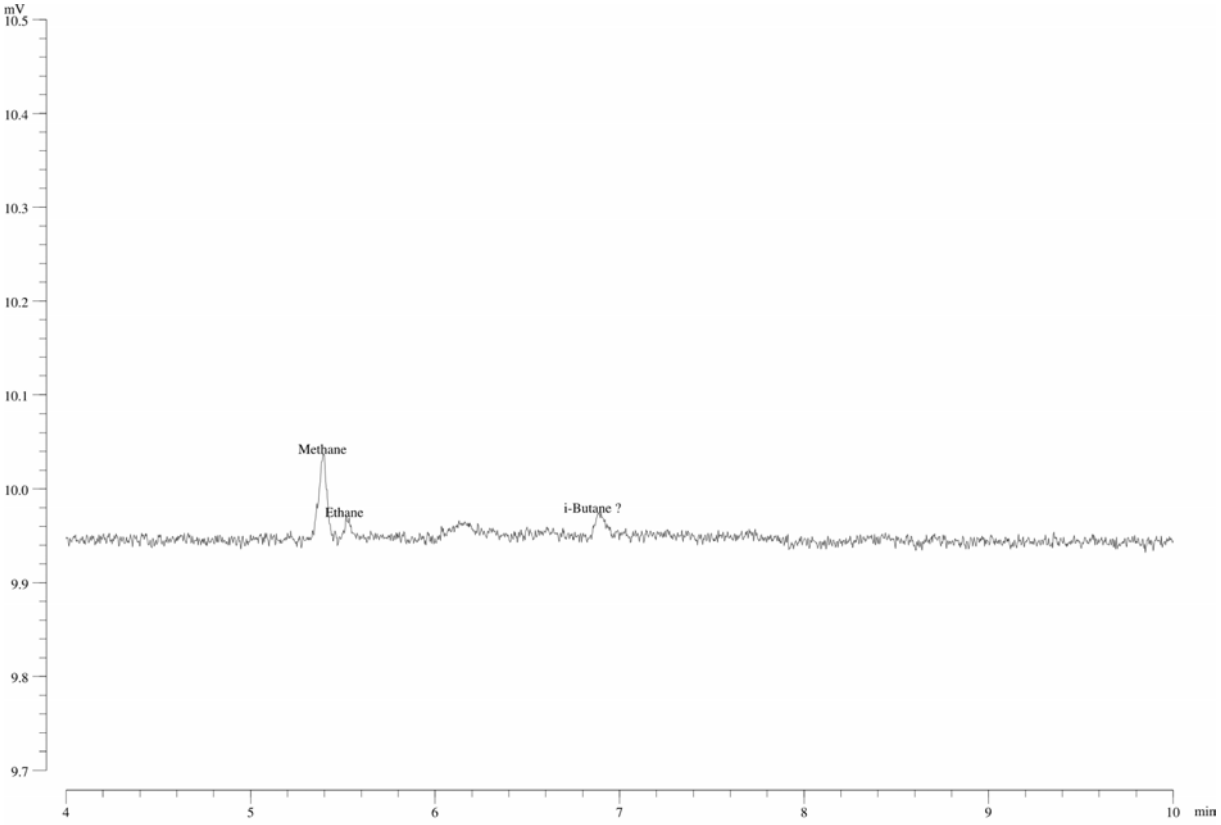

Analysis: [GC_LABOR]P513B06 ,87, 1 Samplename: E50526/5-GC_TM40-1M aquired on 23-Jan-2002 19:00:53 Channel: 17 reported on 29-JAN-2002 11:47:10.27 from user LEISTNER5

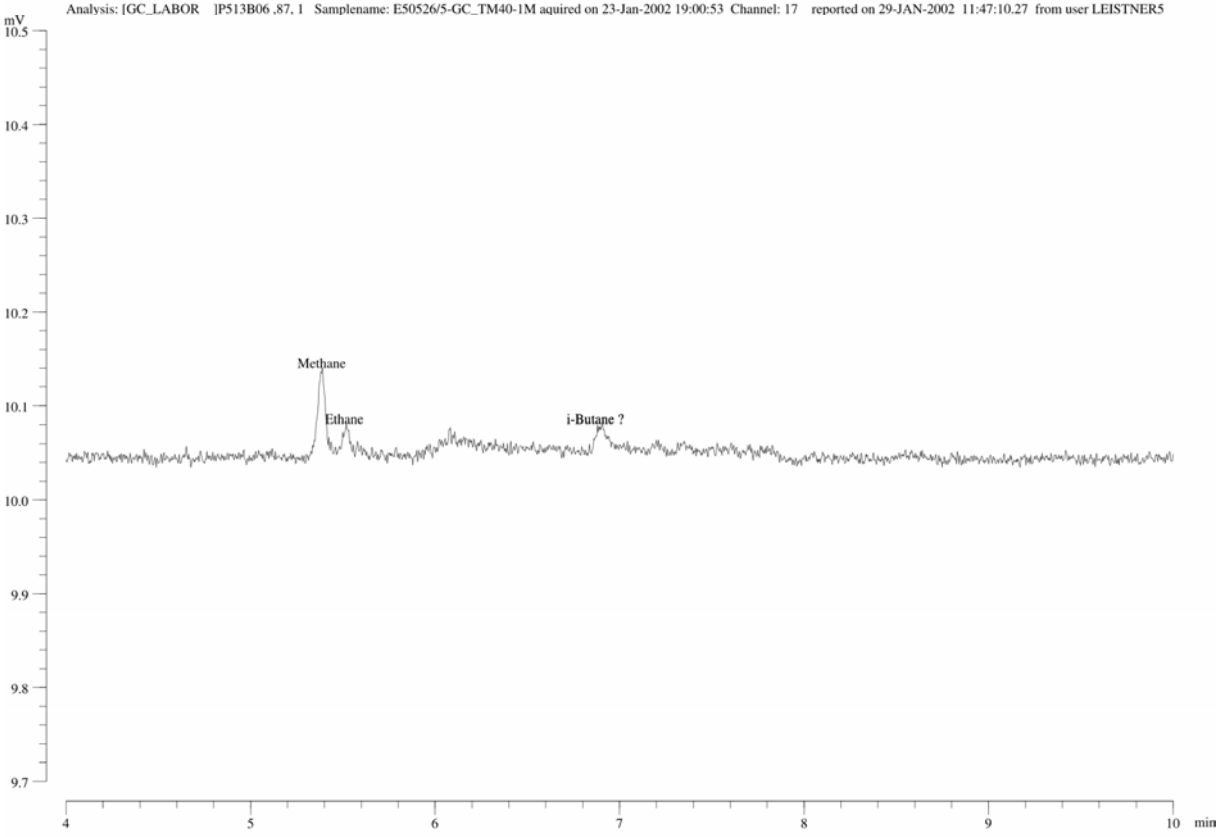

Analysis: [GC_LABOR]P513B06 ,88, 1 Samplename: E50526/6-GC_TM40-1M aquired on 23-Jan-2002 19:51:53 Channel: 17 reported on 29-JAN-2002 11:47:11.31 from user LEISTNER5

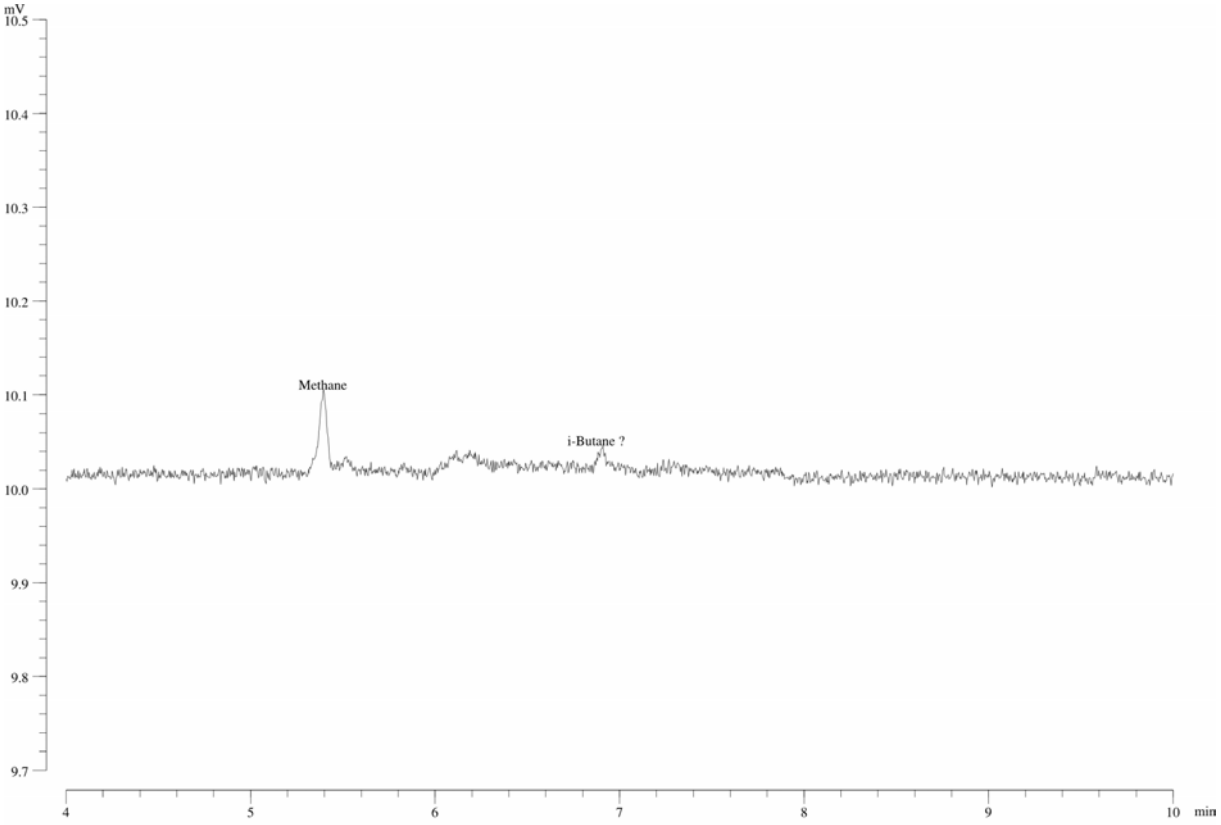

Analysis: [GC_LABOR]P513B06 ,89, 1 Samplename: E50526/7-GC_TM40-1M aquired on 23-Jan-2002 20:42:53 Channel: 17 reported on 29-JAN-2002 11:47:12.39 from user LEISTNER5

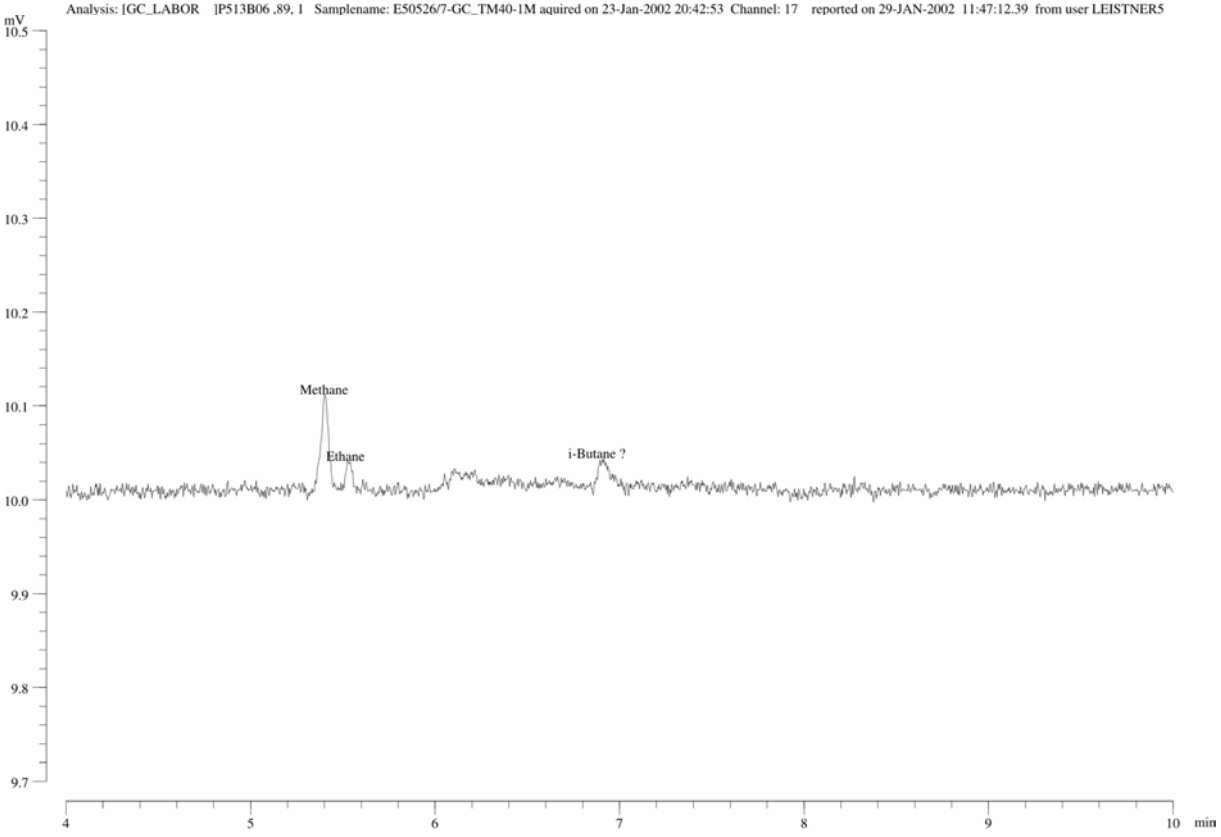

Analysis: [GC_LABOR]P513B06 ,90, 1 Samplename: E50526/8-GC_TM40-1M aquired on 23-Jan-2002 21:33:53 Channel: 17 reported on 29-JAN-2002 11:47:13.65 from user LEISTNER5

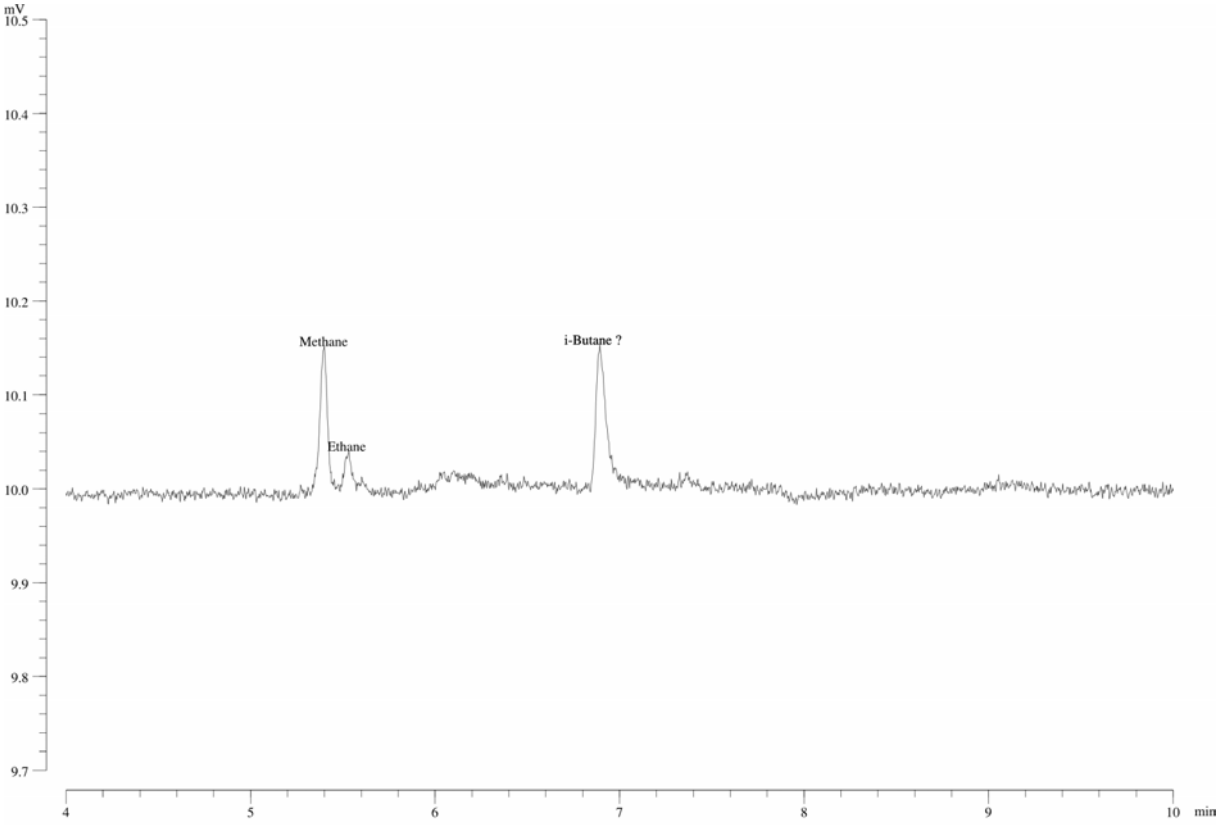

Analysis: [GC_LABOR]P513B06 ,91, 1 Samplename: E50528/1-GC_TM40-1M aquired on 23-Jan-2002 22:24:53 Channel: 17 reported on 29-JAN-2002 11:47:14.74 from user LEISTNER5

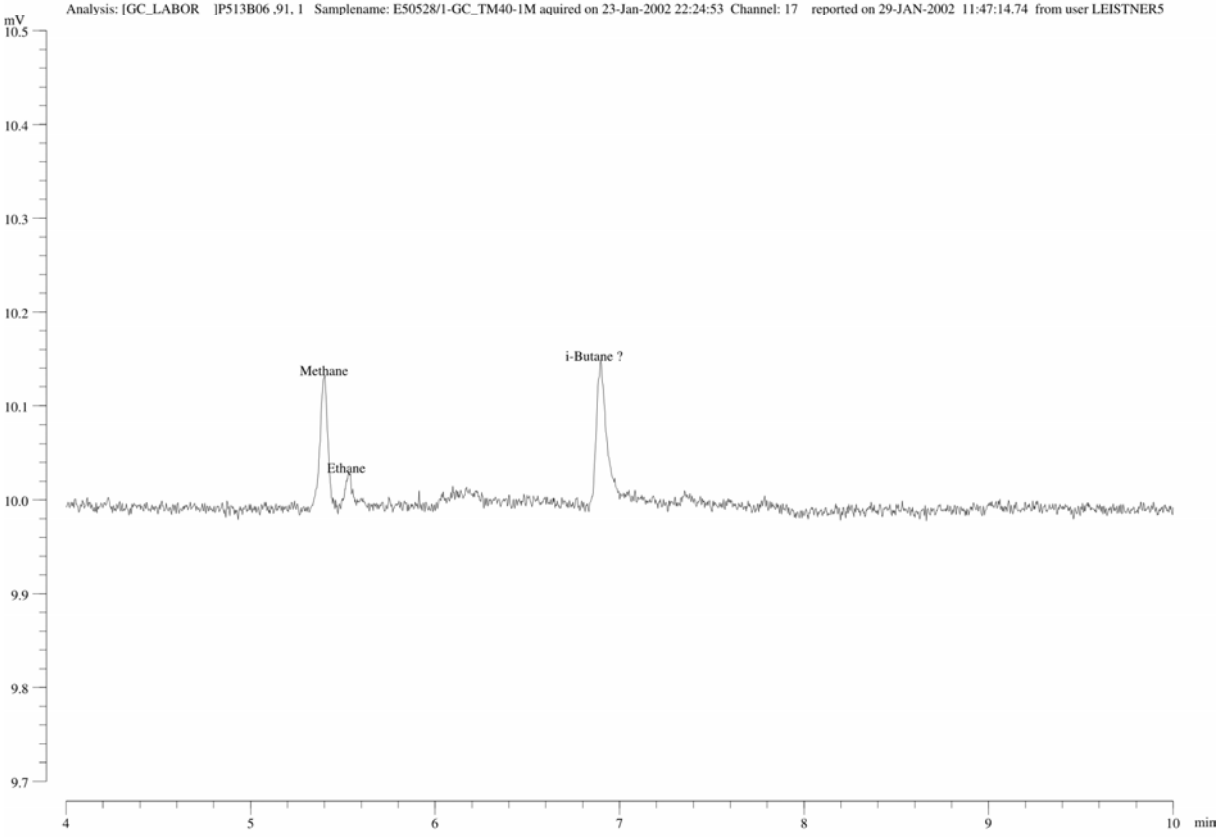

Analysis: [GC_LABOR]P513B06 ,92, 1 Samplename: E50528/2-GC_TM40-1M aquired on 23-Jan-2002 23:15:53 Channel: 17 reported on 29-JAN-2002 11:47:15.82 from user LEISTNER5

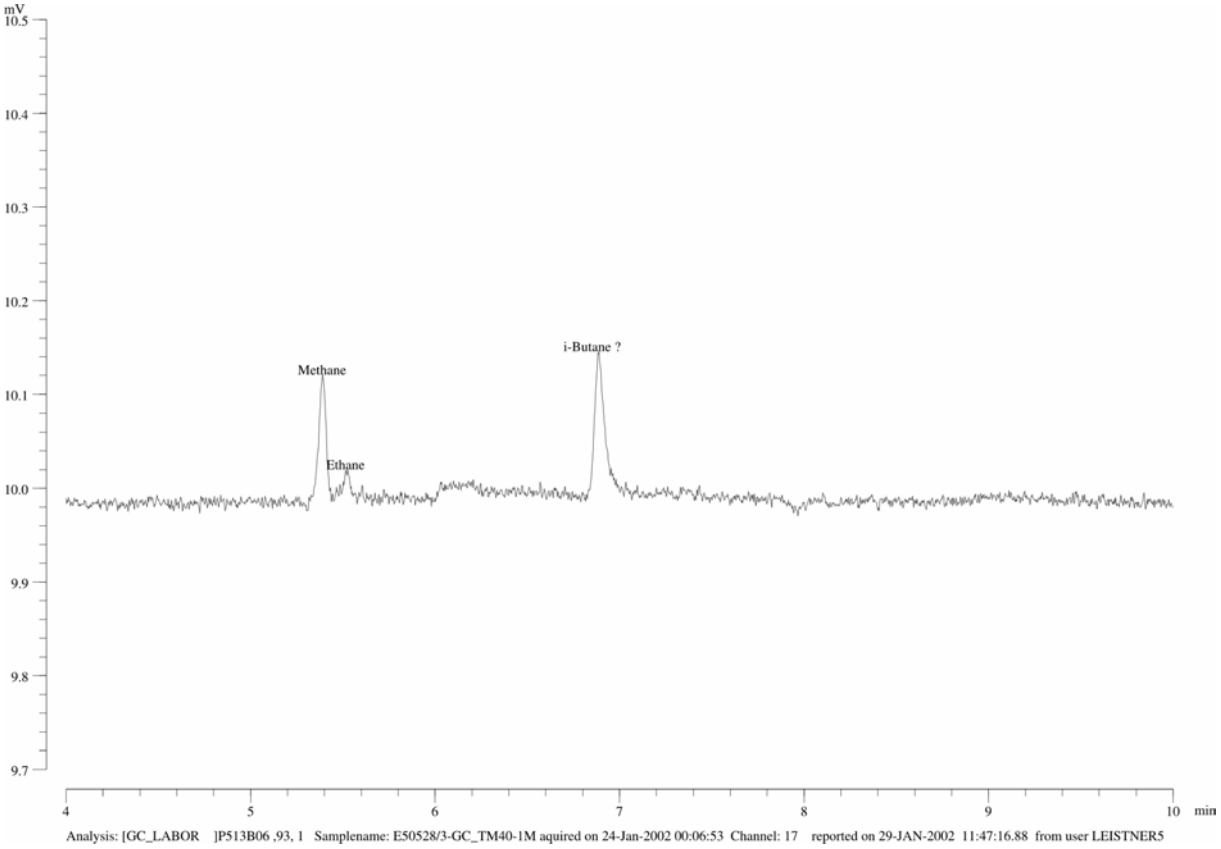
mV
10.5
10.4
10.3
10.2
10.1
10.0
9.9
9.8
9.7
Methane
Ethane
i-Butane ?
4
5
6
7
8
9
10
min
Analysis: [GC_LABOR]P513B06 ,93, 1 Samplename: E50528/3-GC_TM40-1M aquired on 24-Jan-2002 00:06:53 Channel: 17 reported on 29-JAN-2002 11:47:16.88 from user LEISTNER5

8.5 Appendix V: Dynamic Headspace Chromatograms

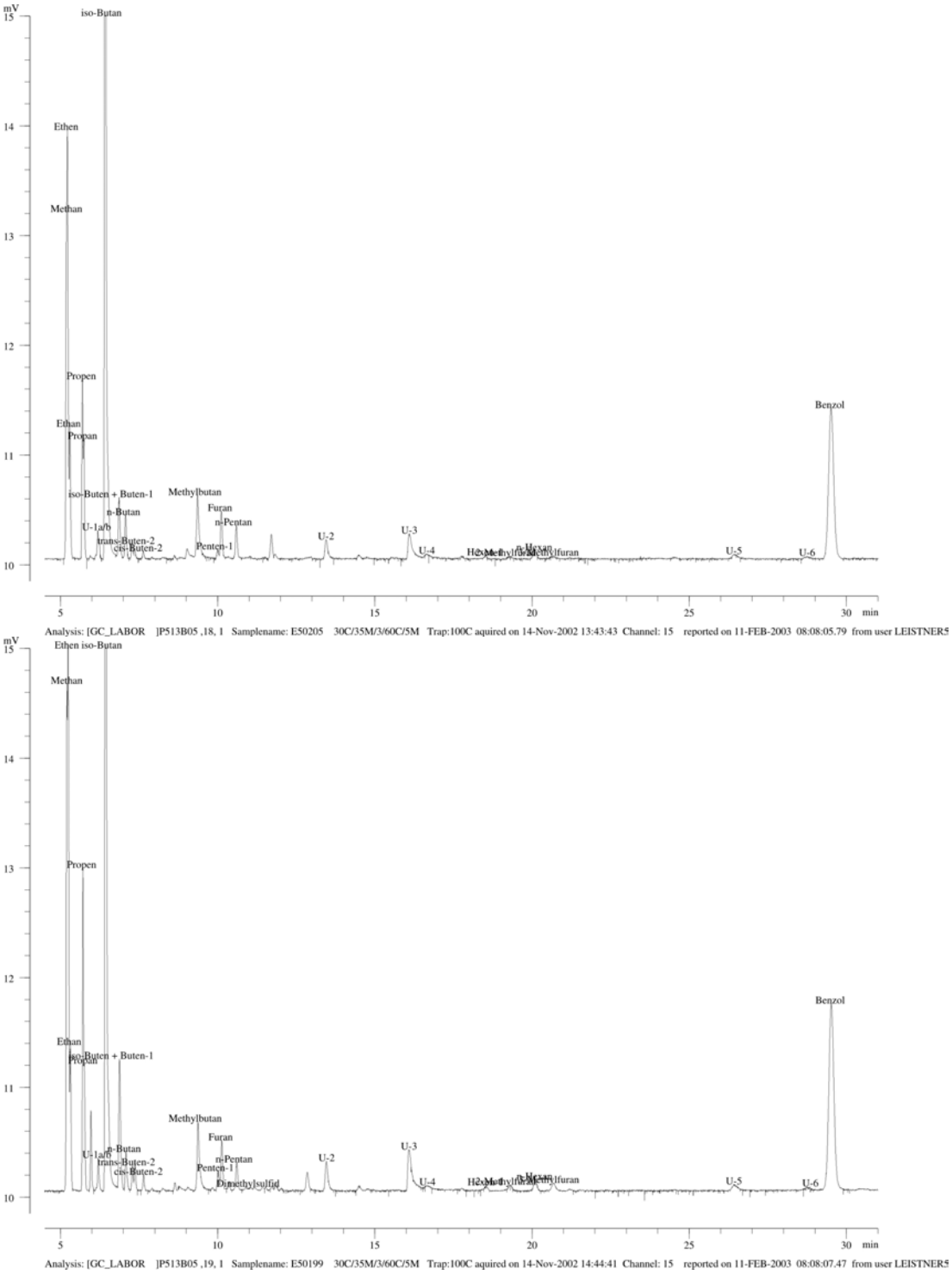

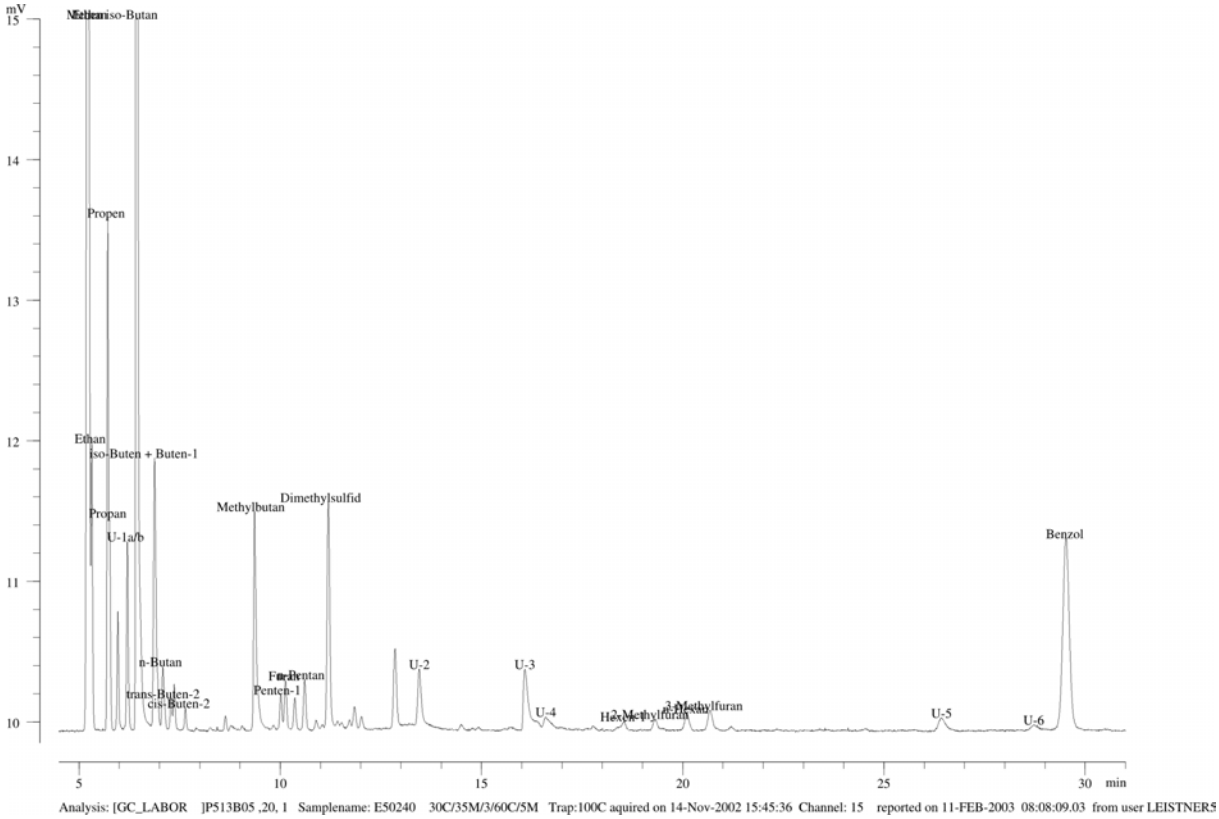
mV
15
14
13
12
11
10
Methan
iso-Butan
Propen
Ethan
iso-Buten + Buten-1
Propan
U-1a/b
Methylbutan
Dimethylsulfid
Benzol
n-Butan
trans-Buten-2
cis-Buten-2
Penten-1
U-2
U-3
U-4
U-5
U-6
5
10
15
20
25
30
min
Analysis: [GC_LABOR]P513B05 ,20, 1 Samplename: E50240 30C/35M/3/60C/5M Trap:100C aquired on 14-Nov-2002 15:45:36 Channel: 15 reported on 11-FEB-2003 08:08:09.03 from user LEISTNER5

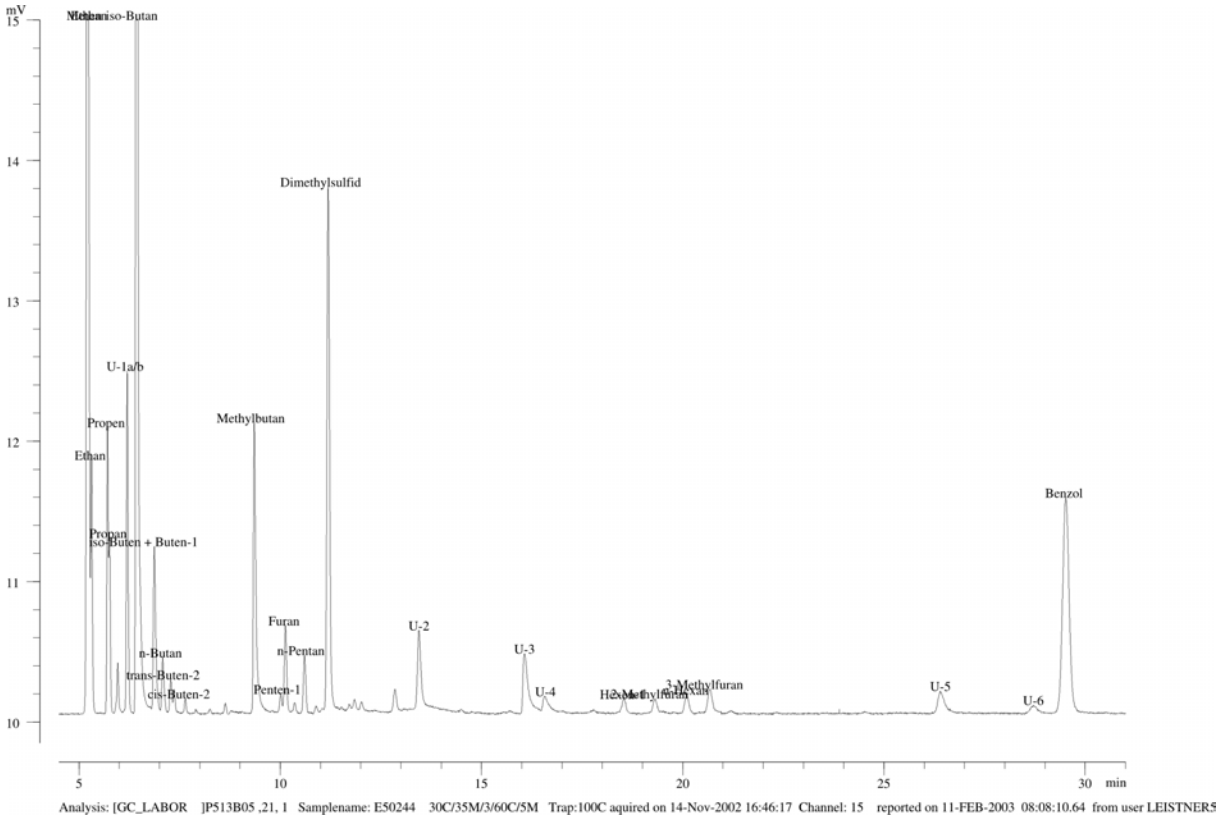
mV
15
14
13
12
11
10
Methan
iso-Butan
Dimethylsulfid
U-1a/b
Propen
Methylbutan
Ethan
Benzol
Propan
iso-Buten + Buten-1
Furan
n-Pentan
n-Butan
trans-Buten-2
cis-Buten-2
Penten-1
U-2
U-3
U-4
U-5
U-6
5
10
15
20
25
30
min
Analysis: [GC_LABOR]P513B05 ,21, 1 Samplename: E50244 30C/35M/3/60C/5M Trap:100C aquired on 14-Nov-2002 16:46:17 Channel: 15 reported on 11-FEB-2003 08:08:10.64 from user LEISTNER5

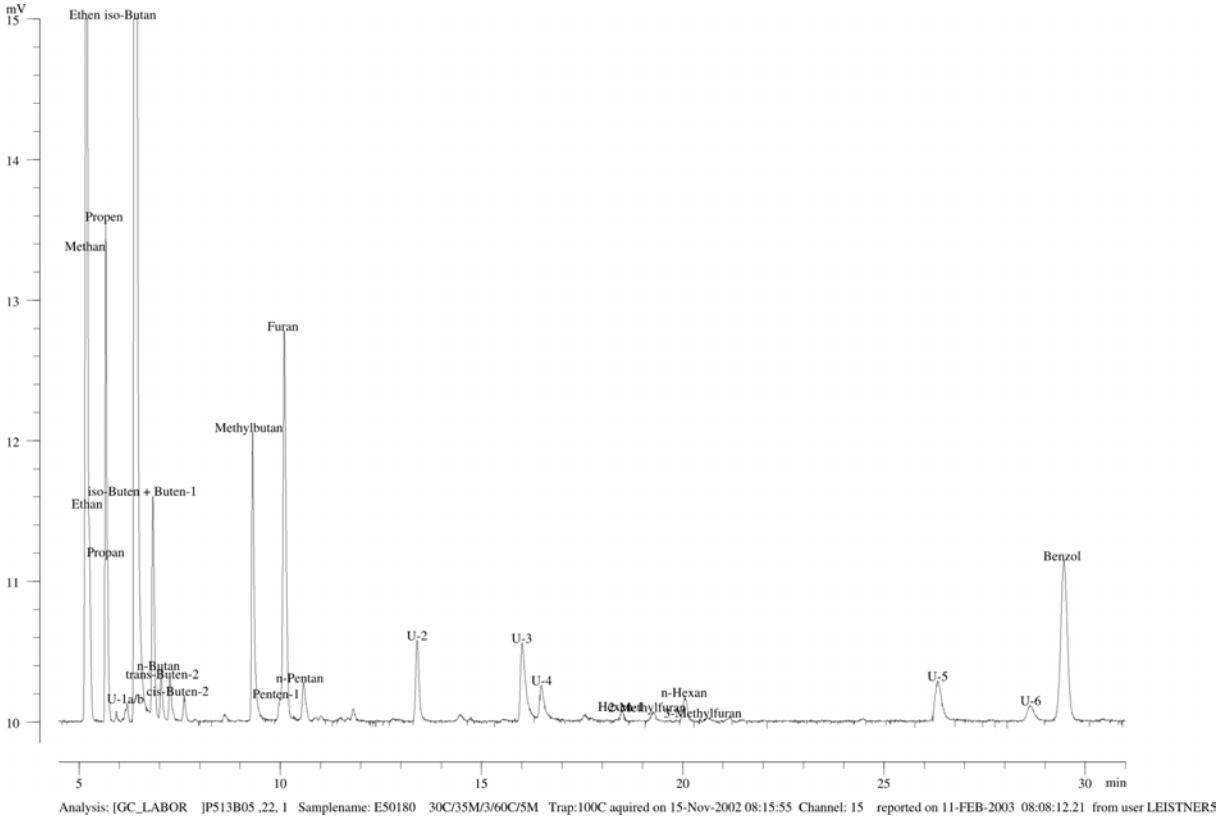
mV
15
14
13
12
11
10
Ethen
iso-Butan
Propen
Methan
Furan
Methylbutan
iso-Buten + Buten-1
Ethan
Propan
Benzol
U-2
U-3
n-Butan
trans-Buten-2
cis-Buten-2
n-Pentan
Penten-1
U-4
U-5
n-Hexan
U-6
5
10
15
20
25
30
min
Analysis: [GC_LABOR]P513B05 ,22, 1 Samplename: E50180 30C/35M/3/60C/5M Trap:100C aquired on 15-Nov-2002 08:15:55 Channel: 15 reported on 11-FEB-2003 08:08:12.21 from user LEISTNER5

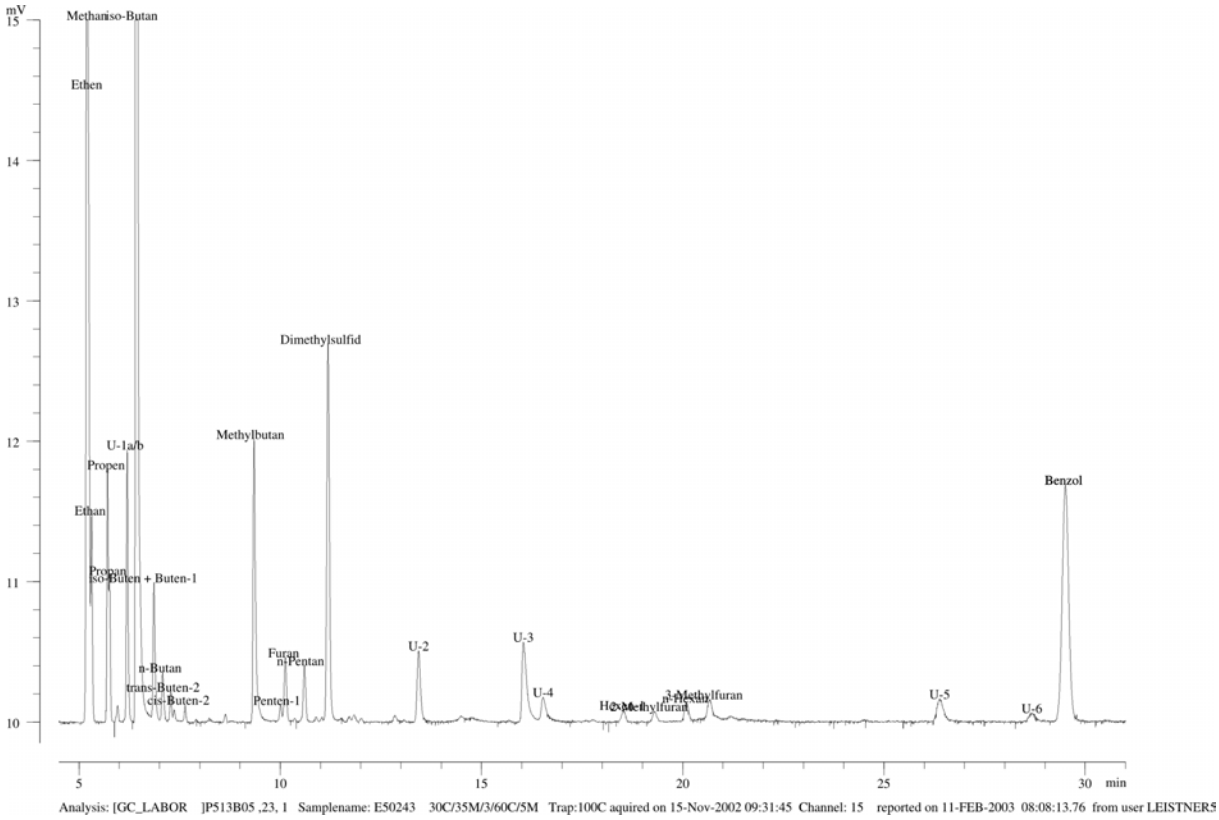
mV
15
14
13
12
11
10
Methan
iso-Butan
Ethen
Dimethylsulfid
Methylbutan
U-1a/b
Propen
Benzol
Ethan
Propan
iso-Buten + Buten-1
U-2
U-3
Furan
n-Pentan
n-Butan
trans-Buten-2
cis-Buten-2
Penten-1
U-4
3-Methylfuran
U-5
U-6
5
10
15
20
25
30
min
Analysis: [GC_LABOR]P513B05 ,23, 1 Samplename: E50243 30C/35M/3/60C/5M Trap:100C aquired on 15-Nov-2002 09:31:45 Channel: 15 reported on 11-FEB-2003 08:08:13.76 from user LEISTNER5

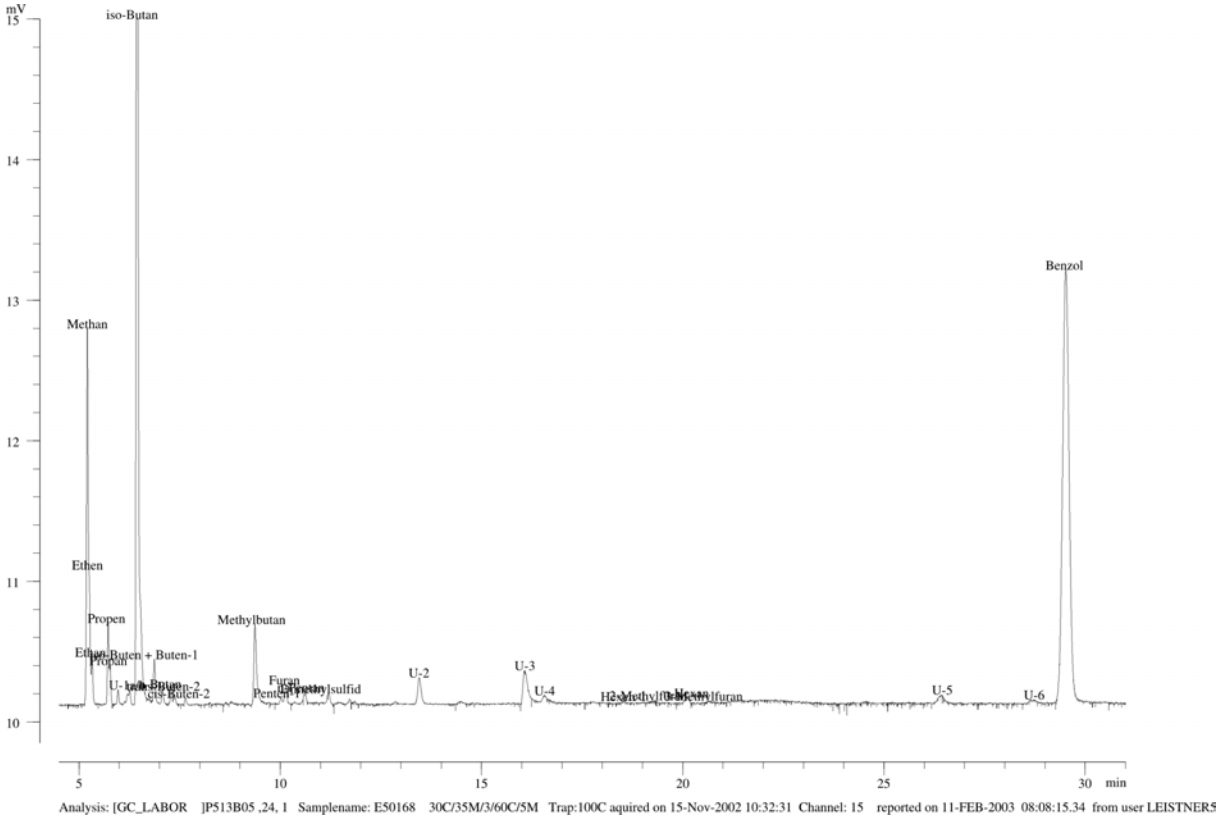

Analysis: [GC_LABOR]P513B05 ,24, 1 Samplename: E50168 30C/35M/3/60C/5M Trap:100C aquired on 15-Nov-2002 10:32:31 Channel: 15 reported on 11-FEB-2003 08:08:15.34 from user LEISTNER5

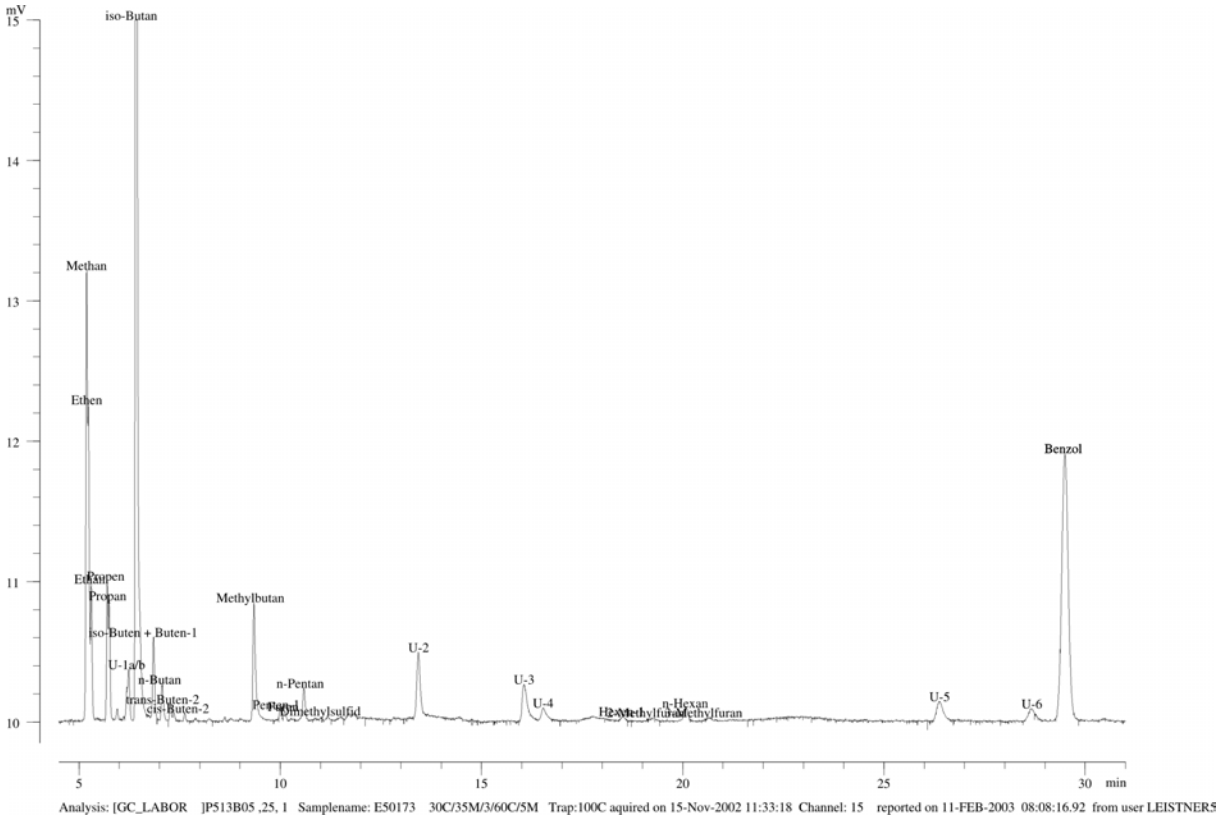

Analysis: [GC_LABOR]P513B05 ,25, 1 Samplename: E50173 30C/35M/3/60C/5M Trap:100C aquired on 15-Nov-2002 11:33:18 Channel: 15 reported on 11-FEB-2003 08:08:16.92 from user LEISTNER5

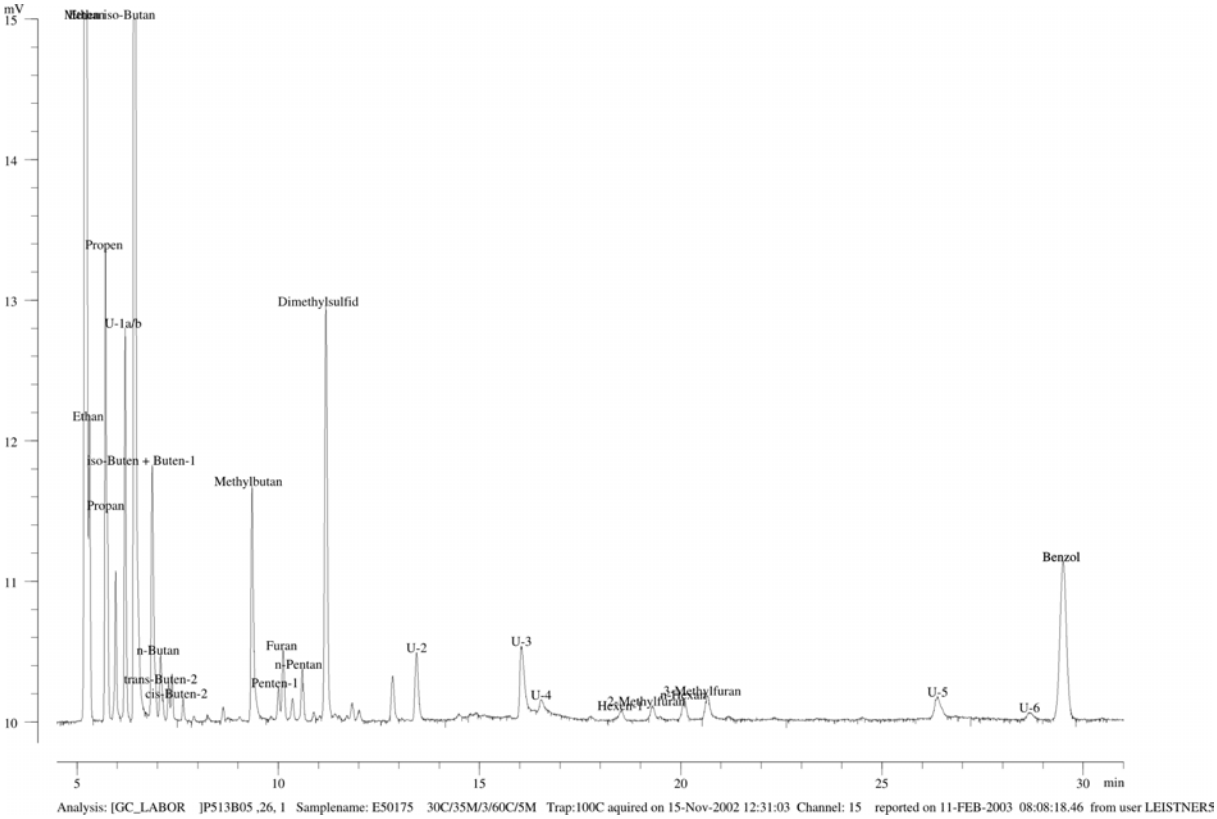
mV
15
14
13
12
11
10
Methan
iso-Butan
Propen
Dimethylsulfid
U-1a/b
Ethan
iso-Buten + Buten-1
Methylbutan
Propan
Benzol
n-Butan
Furan
n-Pentan
U-2
U-3
trans-Buten-2
cis-Buten-2
Penten-1
U-4
Hexen-1
2-Methylfuran
3-Methylfuran
U-5
U-6
5
10
15
20
25
30
min
Analysis: [GC_LABOR]P513B05 ,26, 1 Samplename: E50175 30C/35M/3/60C/5M Trap:100C aquired on 15-Nov-2002 12:31:03 Channel: 15 reported on 11-FEB-2003 08:08:18.46 from user LEISTNER5

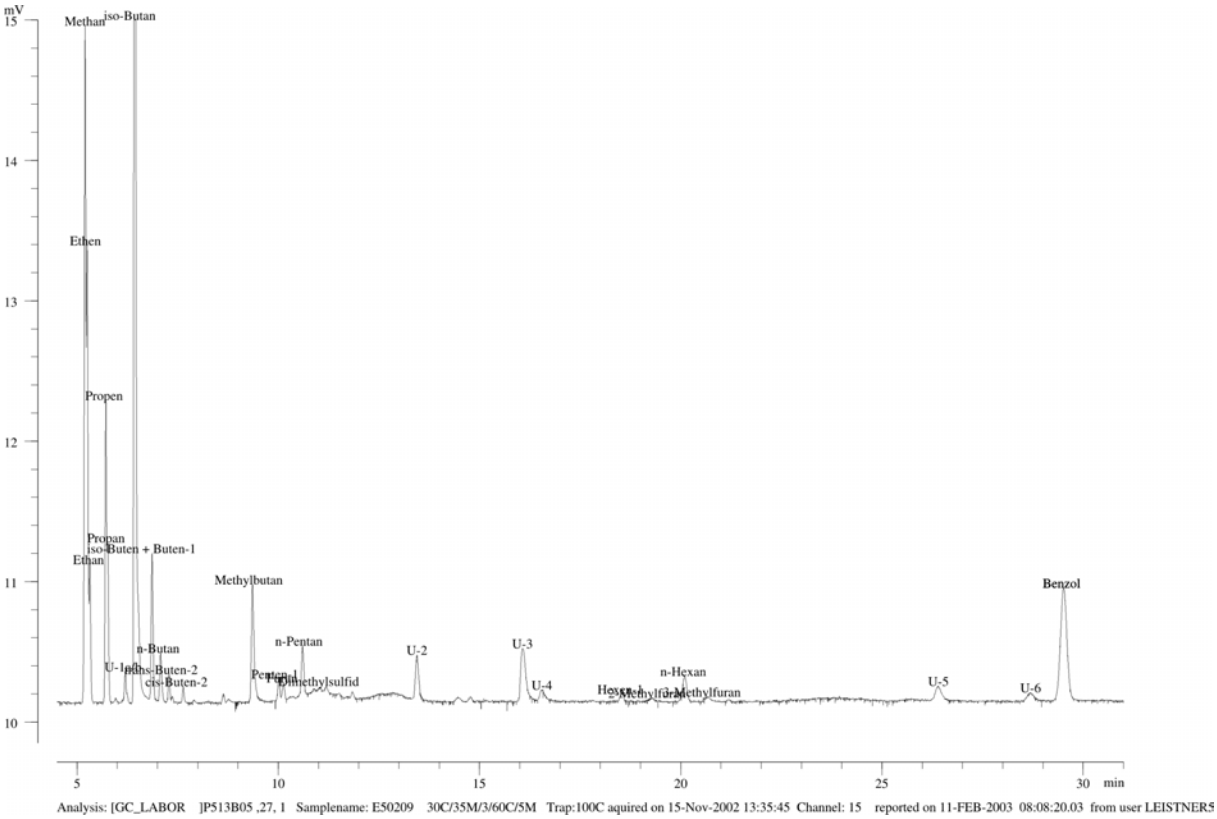
mV
15
14
13
12
11
10
Methan
iso-Butan
Ethen
Propen
Propan
iso-Buten + Buten-1
Ethan
Methylbutan
Benzol
n-Butan
n-Pentan
U-2
U-3
U-1a/b
trans-Buten-2
cis-Buten-2
Penten-1
Dimethylsulfid
U-4
n-Hexan
Hexen-1
2-Methylfuran
3-Methylfuran
U-5
U-6
5
10
15
20
25
30
min
Analysis: [GC_LABOR]P513B05 ,27, 1 Samplename: E50209 30C/35M/3/60C/5M Trap:100C aquired on 15-Nov-2002 13:35:45 Channel: 15 reported on 11-FEB-2003 08:08:20.03 from user LEISTNER5

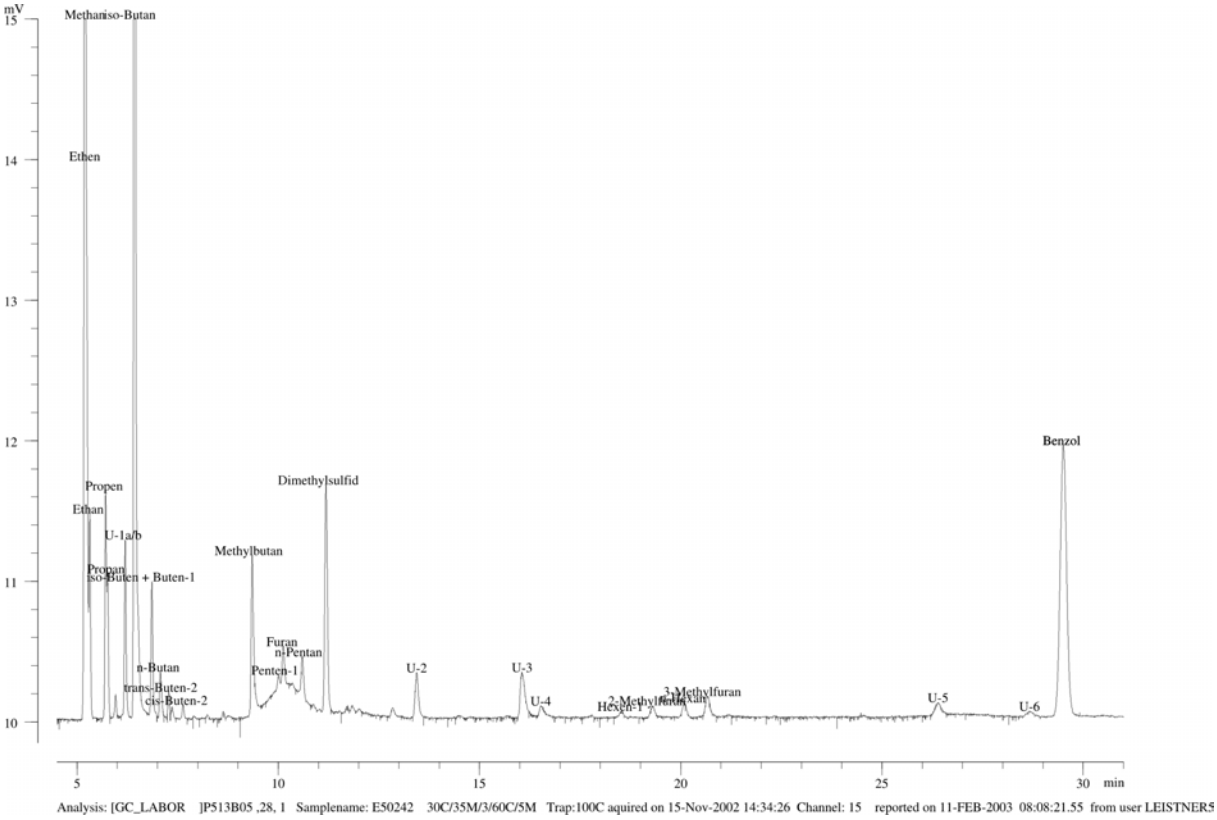
mV
15
14
13
12
11
10
Methan
iso-Butan
Ethen
Propen
Ethan
U-1a/b
Propan
iso-Buten + Buten-1
Methylbutan
Dimethylsulfid
Furan
n-Pentan
Penten-1
n-Butan
trans-Buten-2
cis-Buten-2
U-2
U-3
U-4
Hexen-1
2-Methylfuran
3-Methylfuran
U-5
U-6
Benzol
5
10
15
20
25
30
min
Analysis: [GC_LABOR]P513B05 ,28, 1 Samplename: E50242 30C/35M/3/60C/5M Trap:100C aquired on 15-Nov-2002 14:34:26 Channel: 15 reported on 11-FEB-2003 08:08:21.55 from user LEISTNER5

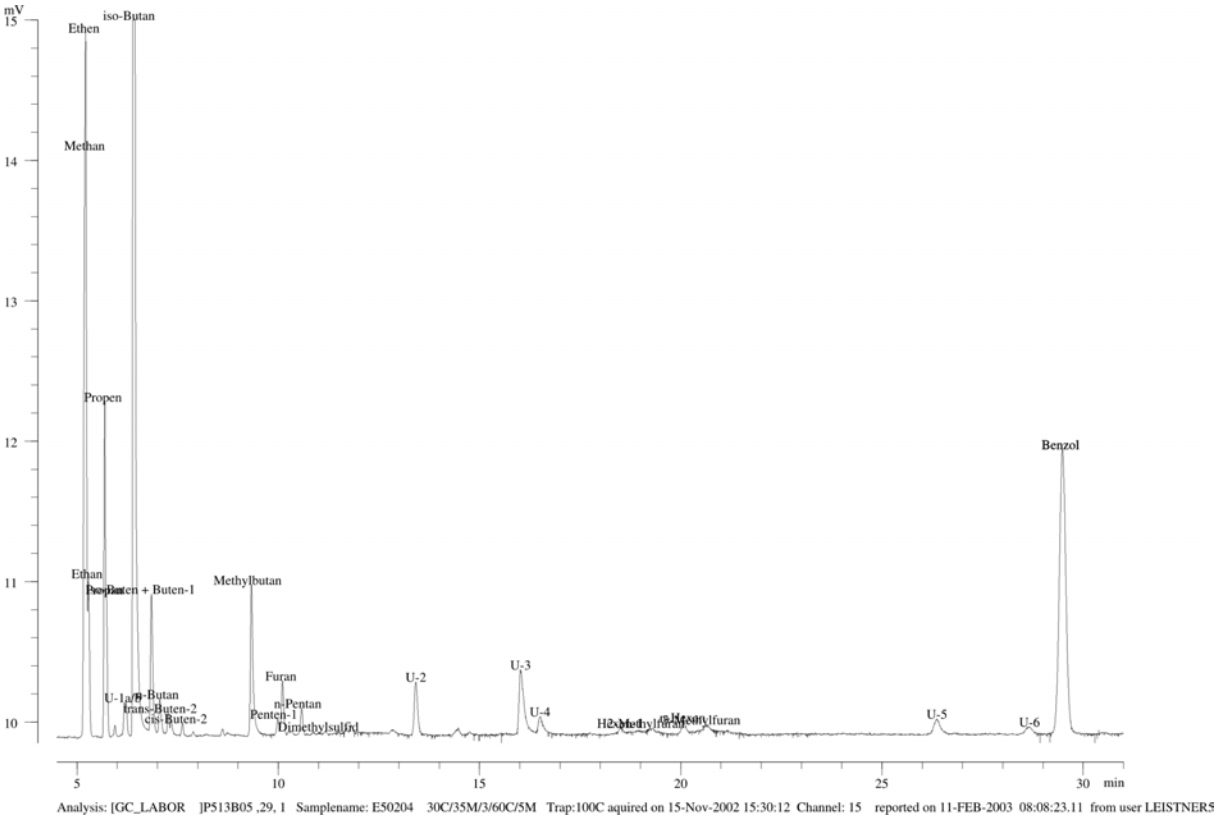
mV
15
14
13
12
11
10
iso-Butan
Ethen
Methan
Propen
Ethan
Buten + Buten-1
Methylbutan
Furan
U-2
U-3
U-1a/b
n-Butan
trans-Buten-2
cis-Buten-2
n-Pentan
Penten-1
Dimethylsulfid
U-4
U-5
U-6
Benzol
5
10
15
20
25
30
min
Analysis: [GC_LABOR]P513B05 ,29, 1 Samplename: E50204 30C/35M/3/60C/5M Trap:100C aquired on 15-Nov-2002 15:30:12 Channel: 15 reported on 11-FEB-2003 08:08:23.11 from user LEISTNER5

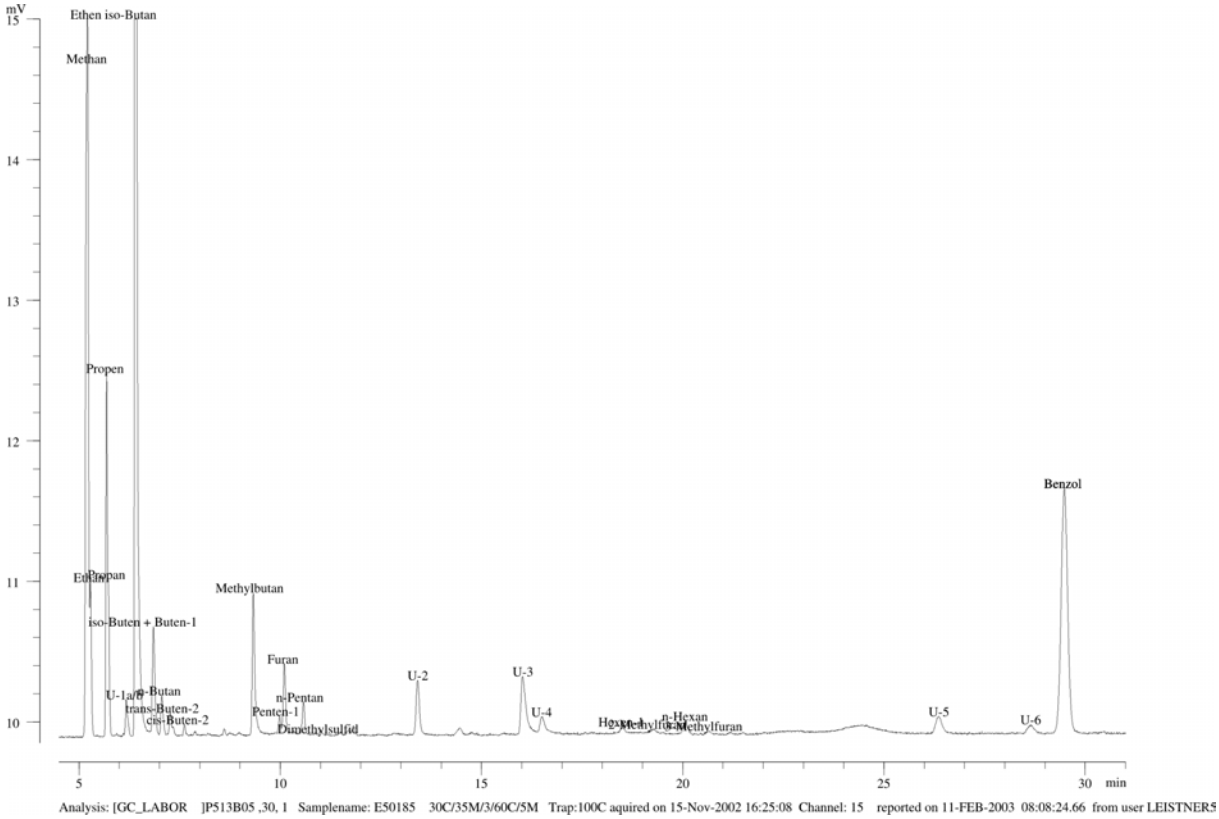
mV
15
14
13
12
11
10
Ethen
iso-Butan
Methan
Propen
Ethan
Propan
iso-Buten + Buten-1
Methylbutan
Furan
U-2
U-3
U-1a/b
n-Butan
trans-Buten-2
cis-Buten-2
n-Pentan
Penten-1
Dimethylsulfid
U-4
Hexen-1
2-Methylfuran
n-Hexan
3-Methylfuran
U-5
U-6
Benzol
5
10
15
20
25
30
min
Analysis: [GC_LABOR]P513B05 ,30, 1 Samplename: E50185 30C/35M/3/60C/5M Trap:100C aquired on 15-Nov-2002 16:25:08 Channel: 15 reported on 11-FEB-2003 08:08:24.66 from user LEISTNER5

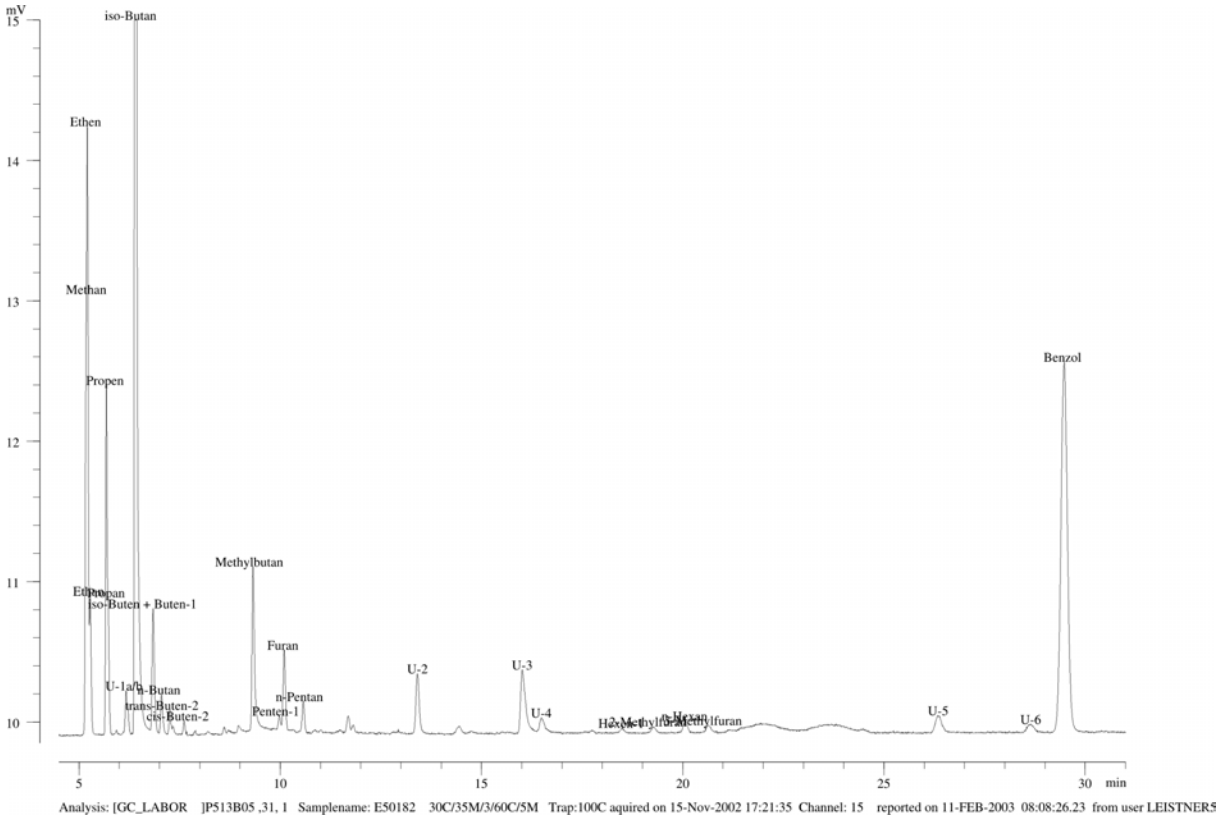
mV
15
14
13
12
11
10
iso-Butan
Ethen
Methan
Propen
Ethan
Propan
iso-Buten + Buten-1
Methylbutan
Furan
U-2
U-3
U-1a/b
n-Butan
trans-Buten-2
cis-Buten-2
n-Pentan
Penten-1
U-4
Hexen-1
2-Methylfuran
n-Hexan
3-Methylfuran
U-5
U-6
Benzol
5
10
15
20
25
30
min
Analysis: [GC_LABOR]P513B05 ,31, 1 Samplename: E50182 30C/35M/3/60C/5M Trap:100C aquired on 15-Nov-2002 17:21:35 Channel: 15 reported on 11-FEB-2003 08:08:26.23 from user LEISTNER5

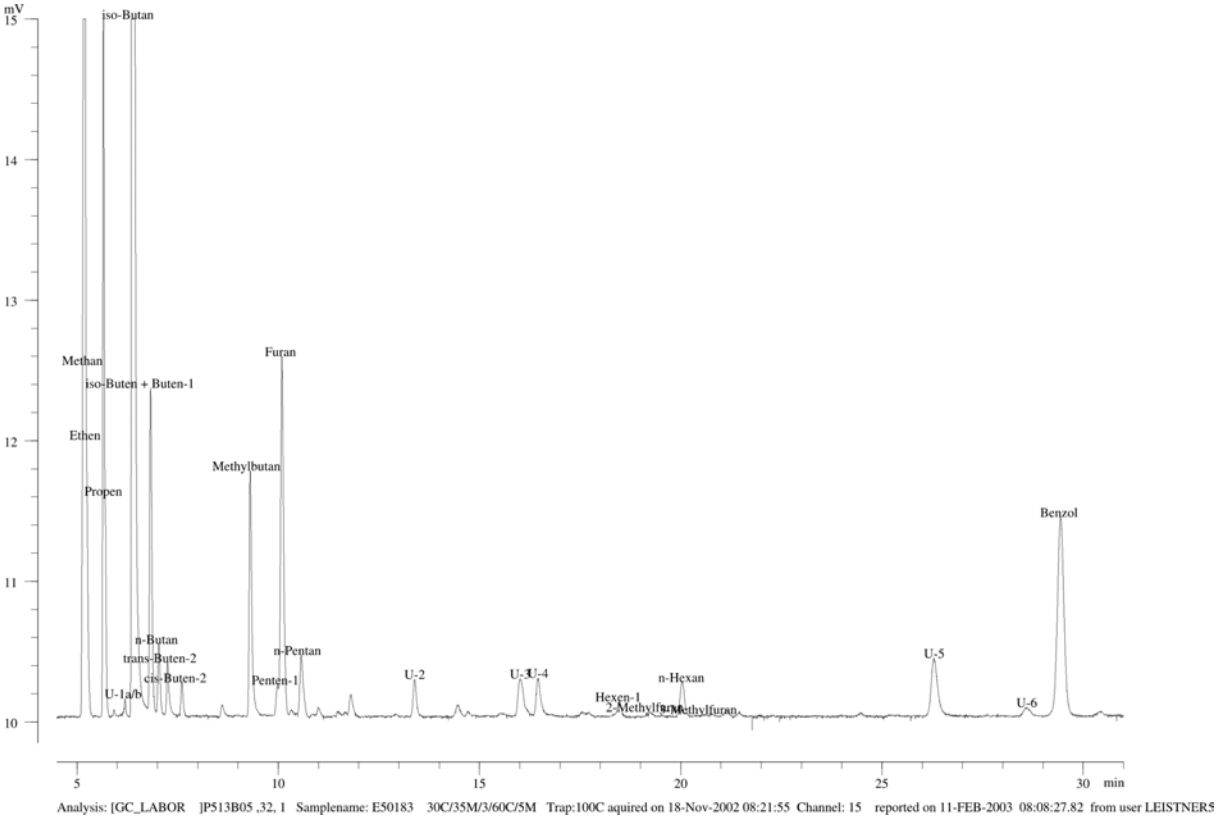
mV
15
14
13
12
11
10
iso-Butan
Methan
iso-Buten + Buten-1
Ethen
Propen
Furan
Methylbutan
n-Butan
trans-Buten-2
cis-Buten-2
U-1a/b
Penten-1
n-Pentan
U-2
U-3
U-4
Hexen-1
n-Hexan
2-Methylfuran
U-5
U-6
Benzol
5
10
15
20
25
30
min
Analysis: [GC_LABOR]P513B05 ,32, 1 Samplename: E50183 30C/35M/3/60C/5M Trap:100C aquired on 18-Nov-2002 08:21:55 Channel: 15 reported on 11-FEB-2003 08:08:27.82 from user LEISTNER5

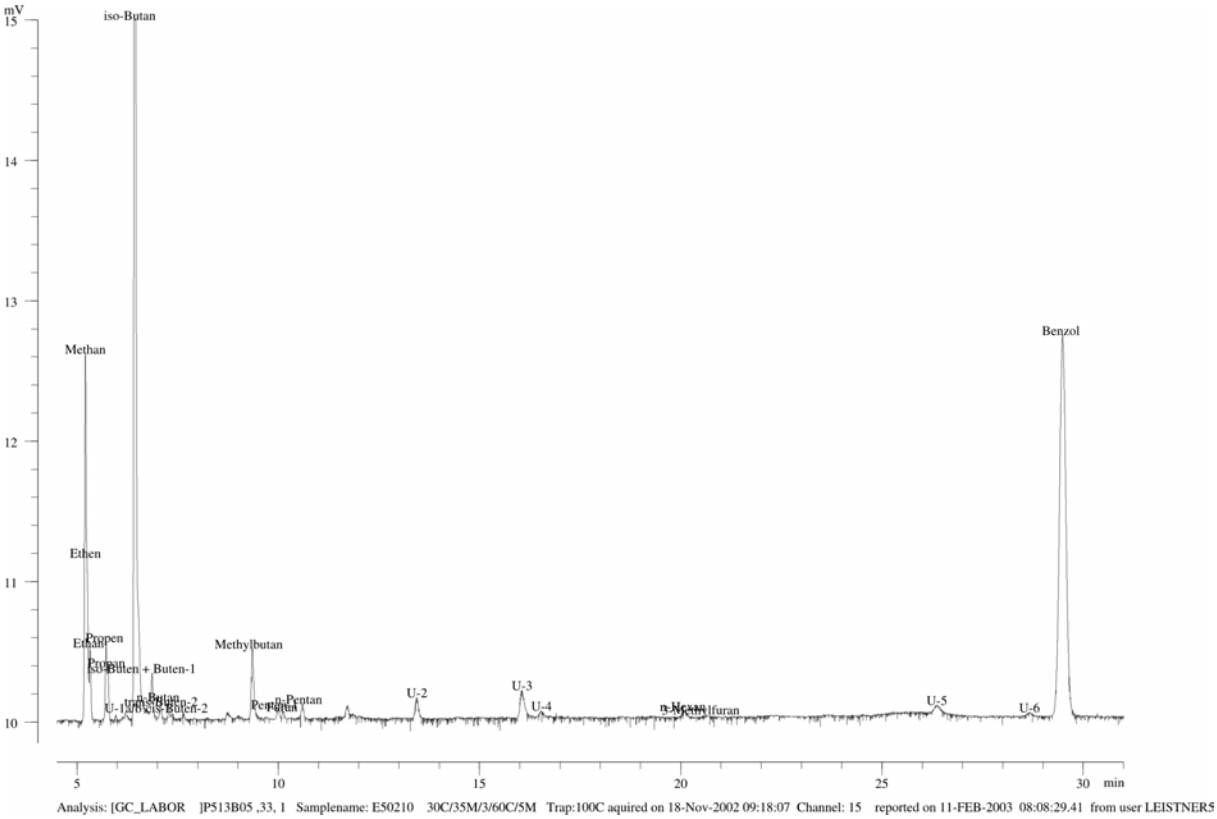
mV
15
14
13
12
11
10
iso-Butan
Methan
Ethen
Propen
Methylbutan
Buten + Buten-1
n-Butan
trans-Buten-2
cis-Buten-2
n-Pentan
U-2
U-3
U-4
U-5
U-6
Benzol
5
10
15
20
25
30
min
Analysis: [GC_LABOR]P513B05 ,33, 1 Samplename: E50210 30C/35M/3/60C/5M Trap:100C aquired on 18-Nov-2002 09:18:07 Channel: 15 reported on 11-FEB-2003 08:08:29.41 from user LEISTNER5

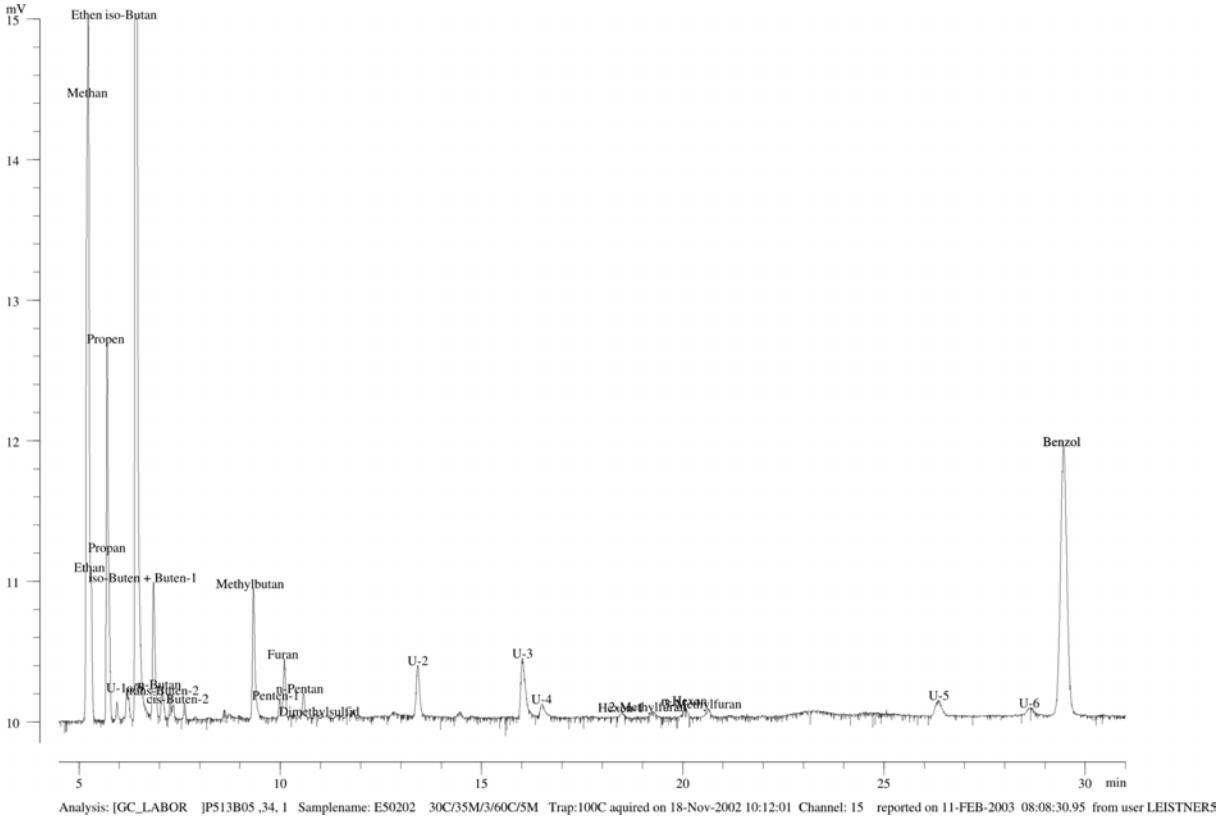

Analysis: [GC_LABOR]P513B05 ,34, 1 Samplename: E50202 30C/35M/3/60C/5M Trap:100C aquired on 18-Nov-2002 10:12:01 Channel: 15 reported on 11-FEB-2003 08:08:30.95 from user LEISTNER5

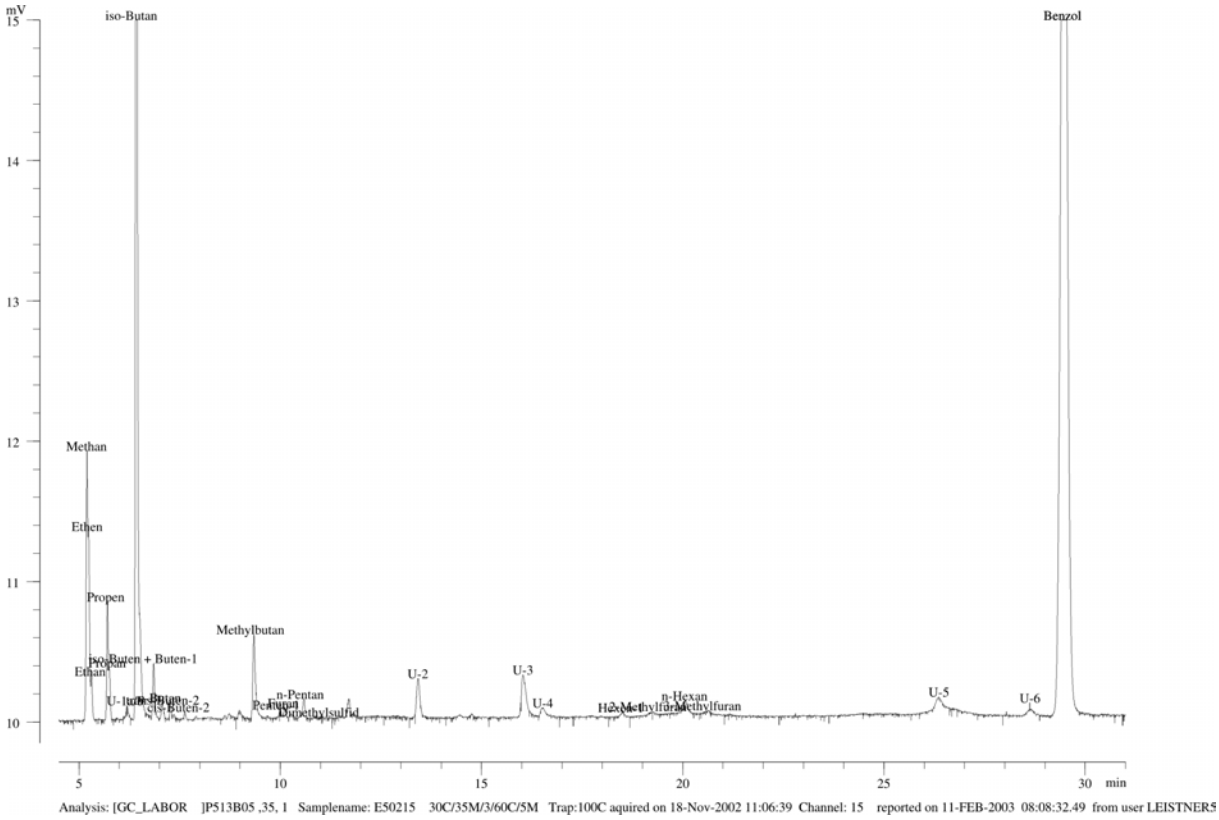

Analysis: [GC_LABOR]P513B05 ,35, 1 Samplename: E50215 30C/35M/3/60C/5M Trap:100C aquired on 18-Nov-2002 11:06:39 Channel: 15 reported on 11-FEB-2003 08:08:32.49 from user LEISTNER5

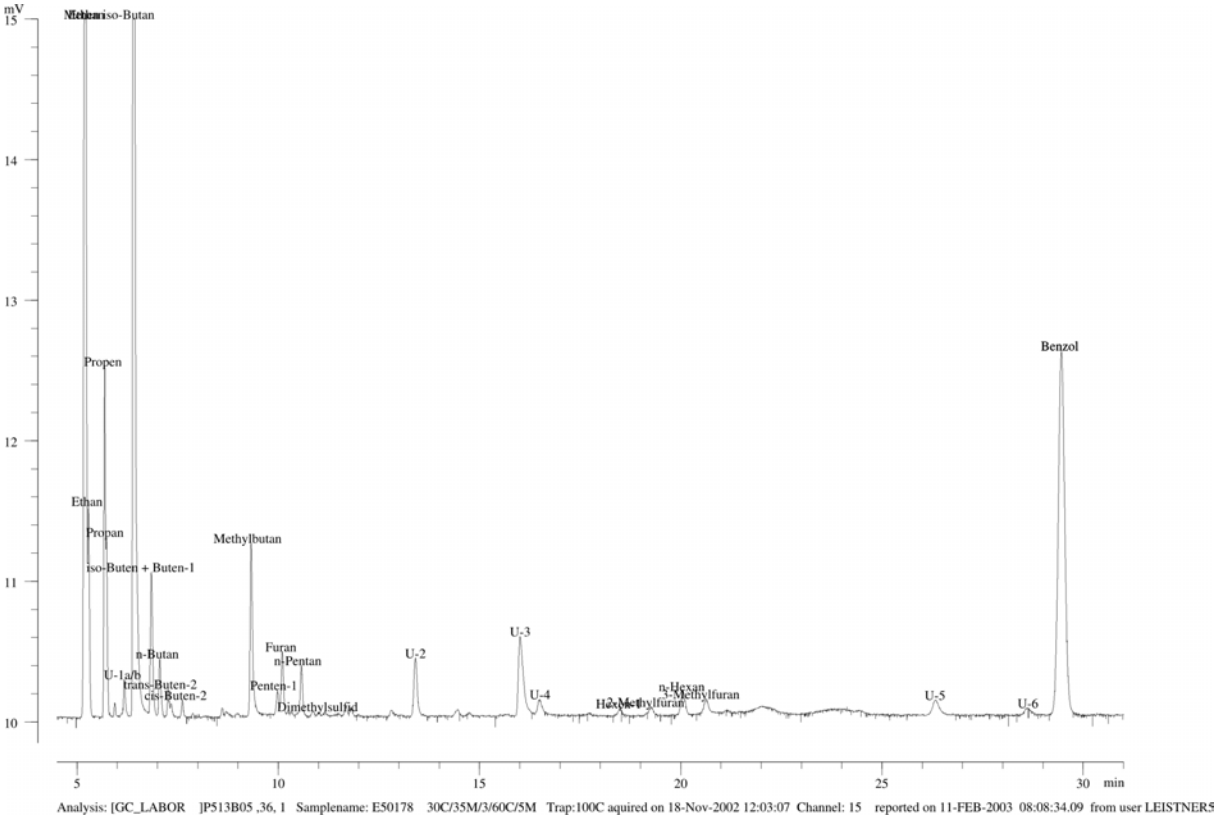
mV
15
14
13
12
11
10
iso-Butan
Propen
Ethan
Propan
Methylbutan
iso-Buten + Buten-1
n-Butan
U-1a/b
trans-Buten-2
cis-Buten-2
Furan
n-Pentan
Penten-1
Dimethylsulfid
U-2
U-3
U-4
n-Hexan
3-Methylfuran
U-5
U-6
Benzol
5
10
15
20
25
30
min
Analysis: [GC_LABOR]P513B05 ,36, 1 Samplename: E50178 30C/35M/3/60C/5M Trap:100C aquired on 18-Nov-2002 12:03:07 Channel: 15 reported on 11-FEB-2003 08:08:34.09 from user LEISTNER5

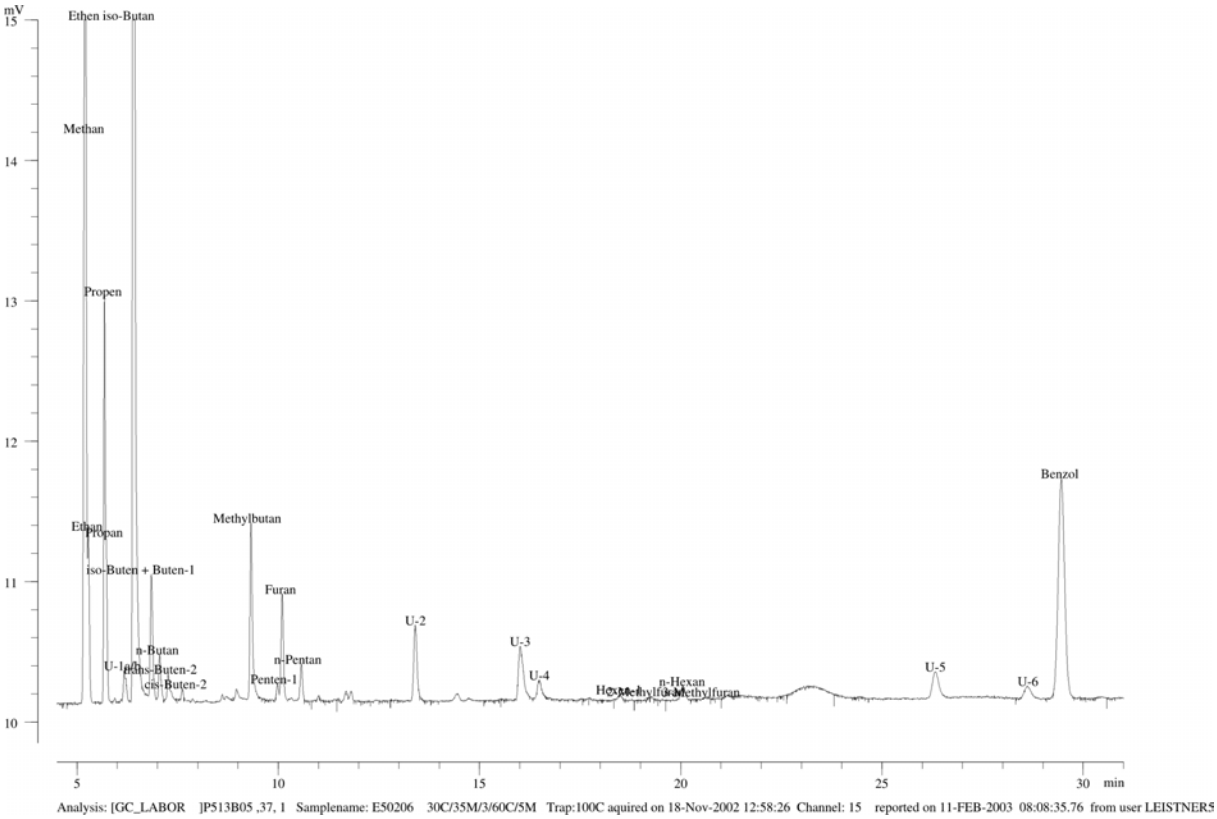
mV
15
14
13
12
11
10
Ethen
iso-Butan
Methan
Propen
Ethan
Propan
Methylbutan
iso-Buten + Buten-1
Furan
n-Butan
U-1a/b
trans-Buten-2
cis-Buten-2
n-Pentan
Penten-1
U-2
U-3
U-4
n-Hexan
3-Methylfuran
U-5
U-6
Benzol
5
10
15
20
25
30
min
Analysis: [GC_LABOR]P513B05 ,37, 1 Samplename: E50206 30C/35M/3/60C/5M Trap:100C aquired on 18-Nov-2002 12:58:26 Channel: 15 reported on 11-FEB-2003 08:08:35.76 from user LEISTNER5

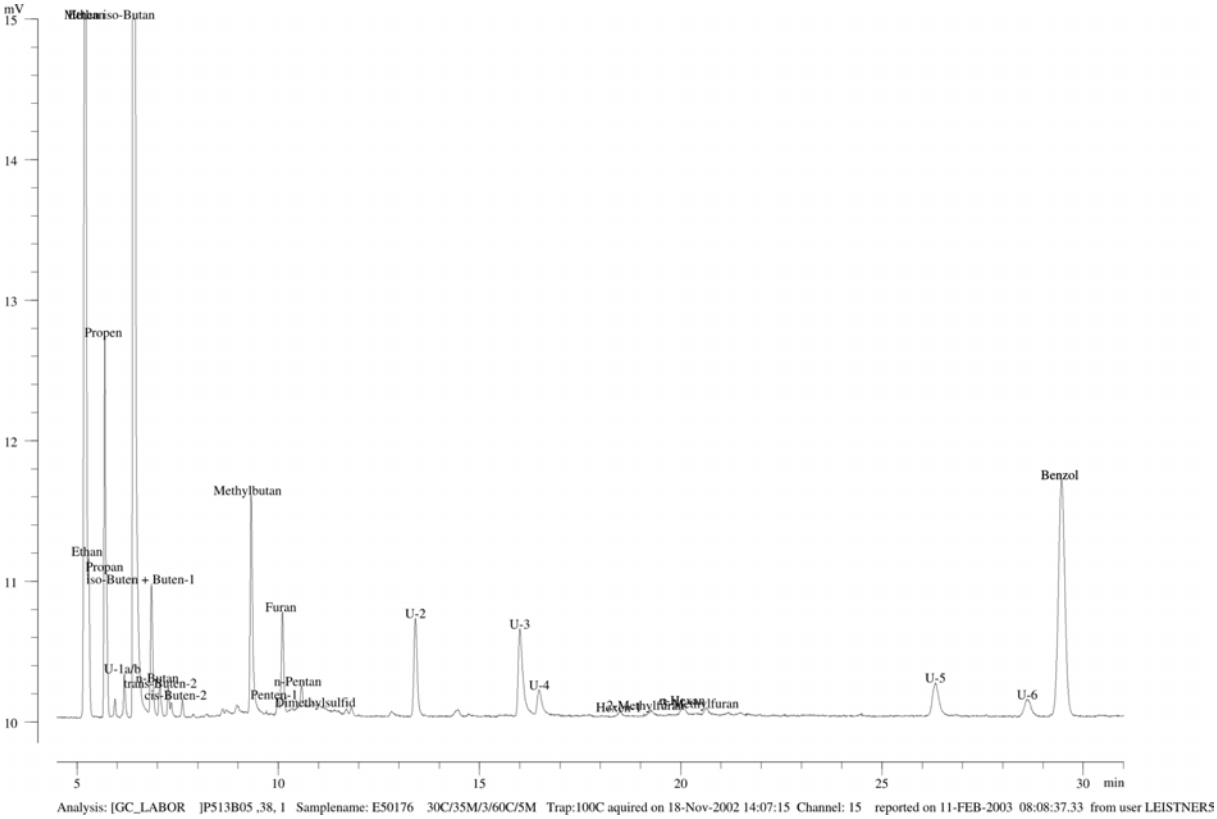

Analysis: [GC_LABOR]P513B05 ,38, 1 Samplename: E50176 30C/35M/3/60C/5M Trap:100C aquired on 18-Nov-2002 14:07:15 Channel: 15 reported on 11-FEB-2003 08:08:37.33 from user LEISTNER5

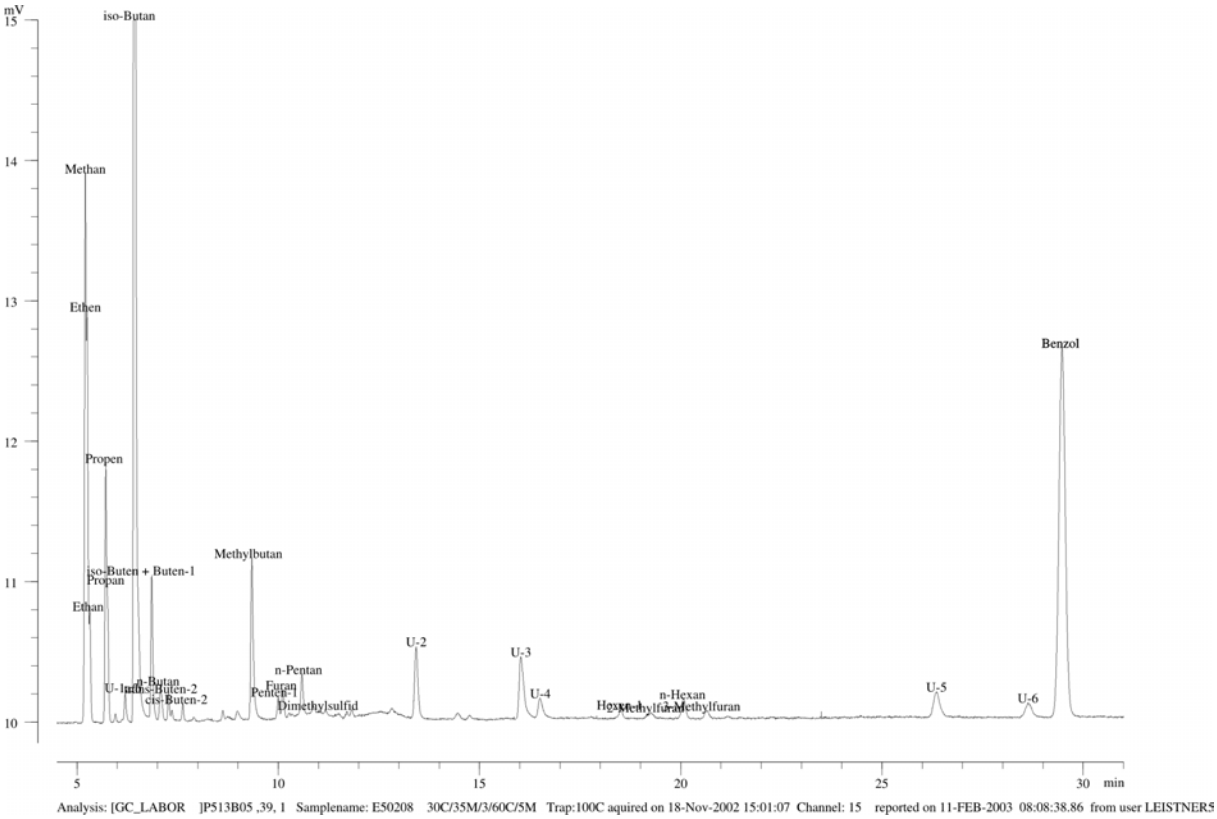

Analysis: [GC_LABOR]P513B05 ,39, 1 Samplename: E50208 30C/35M/3/60C/5M Trap:100C aquired on 18-Nov-2002 15:01:07 Channel: 15 reported on 11-FEB-2003 08:08:38.86 from user LEISTNER5

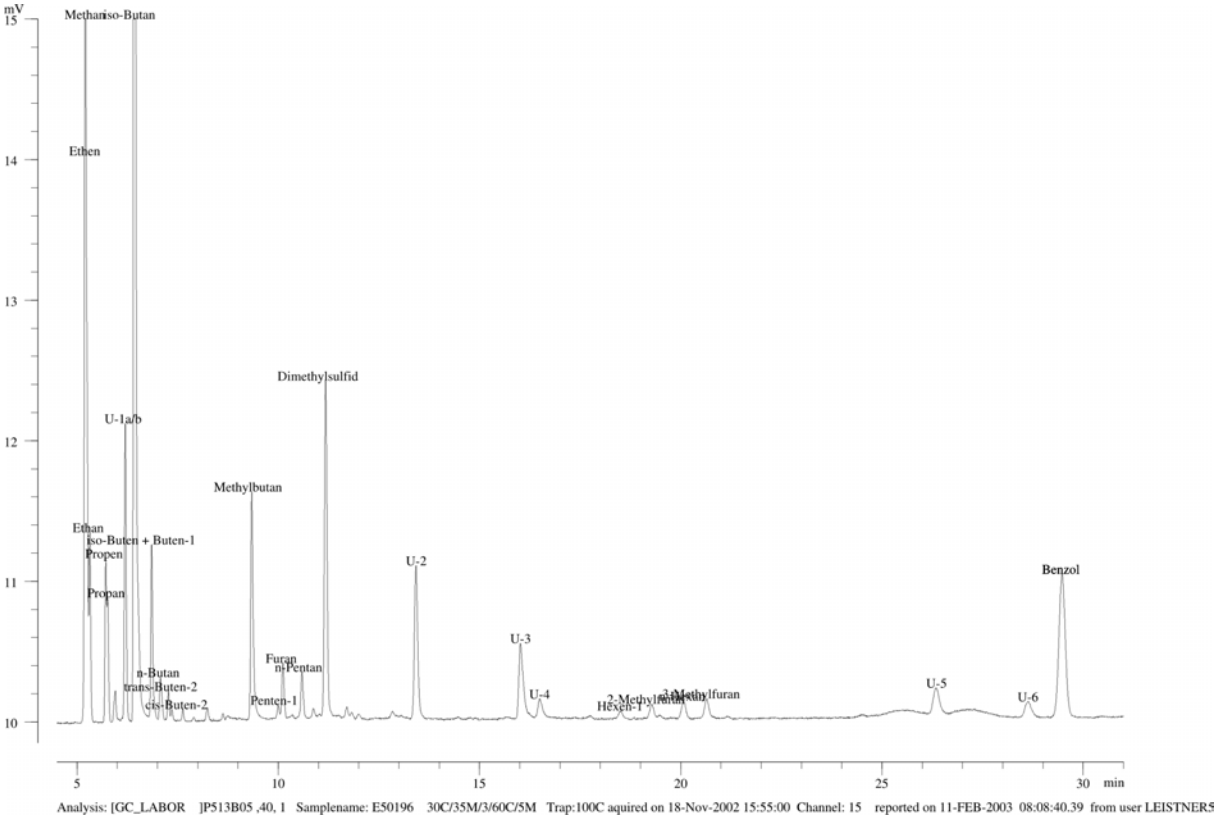
mV
15
14
13
12
11
10
Methan
iso-Butan
Ethen
Dimethylsulfid
U-1a/b
Methylbutan
Ethan
iso-Buten + Buten-1
Propen
U-2
Benzol
Propan
U-3
Furan
n-Pentan
n-Butan
trans-Buten-2
U-4
U-5
U-6
cis-Buten-2
Penten-1
Hexen-1
2-Methylfuran
5
10
15
20
25
30
min
Analysis: [GC_LABOR]P513B05 ,40, 1 Samplename: E50196 30C/35M/3/60C/5M Trap:100C aquired on 18-Nov-2002 15:55:00 Channel: 15 reported on 11-FEB-2003 08:08:40.39 from user LEISTNER5

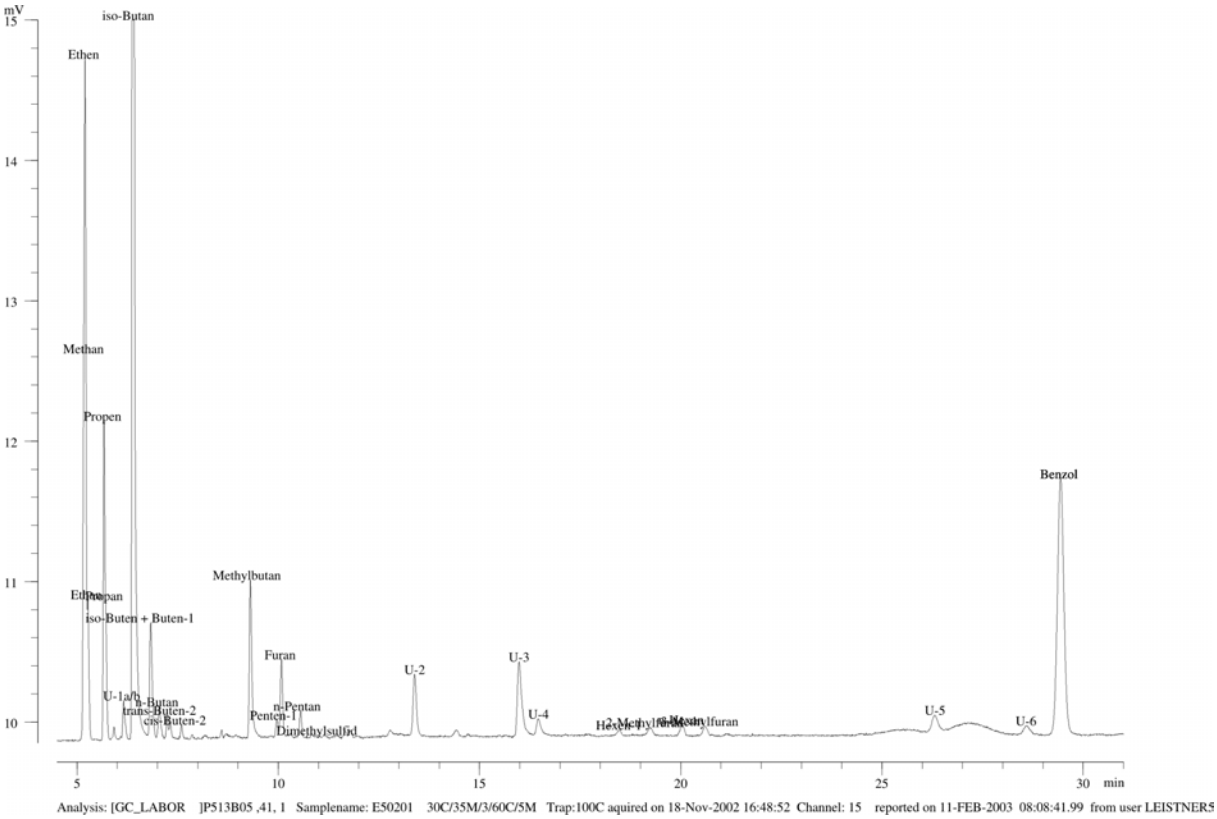
mV
15
14
13
12
11
10
iso-Butan
Ethen
Methan
Propen
Benzol
Methylbutan
Ethan
Propan
iso-Buten + Buten-1
Furan
U-2
U-3
U-1a/b
n-Butan
n-Pentan
trans-Buten-2
Penten-1
U-4
U-5
U-6
cis-Buten-2
Dimethylsulfid
Hexen-1
2-Methylfuran
5
10
15
20
25
30
min
Analysis: [GC_LABOR]P513B05 ,41, 1 Samplename: E50201 30C/35M/3/60C/5M Trap:100C aquired on 18-Nov-2002 16:48:52 Channel: 15 reported on 11-FEB-2003 08:08:41.99 from user LEISTNER5

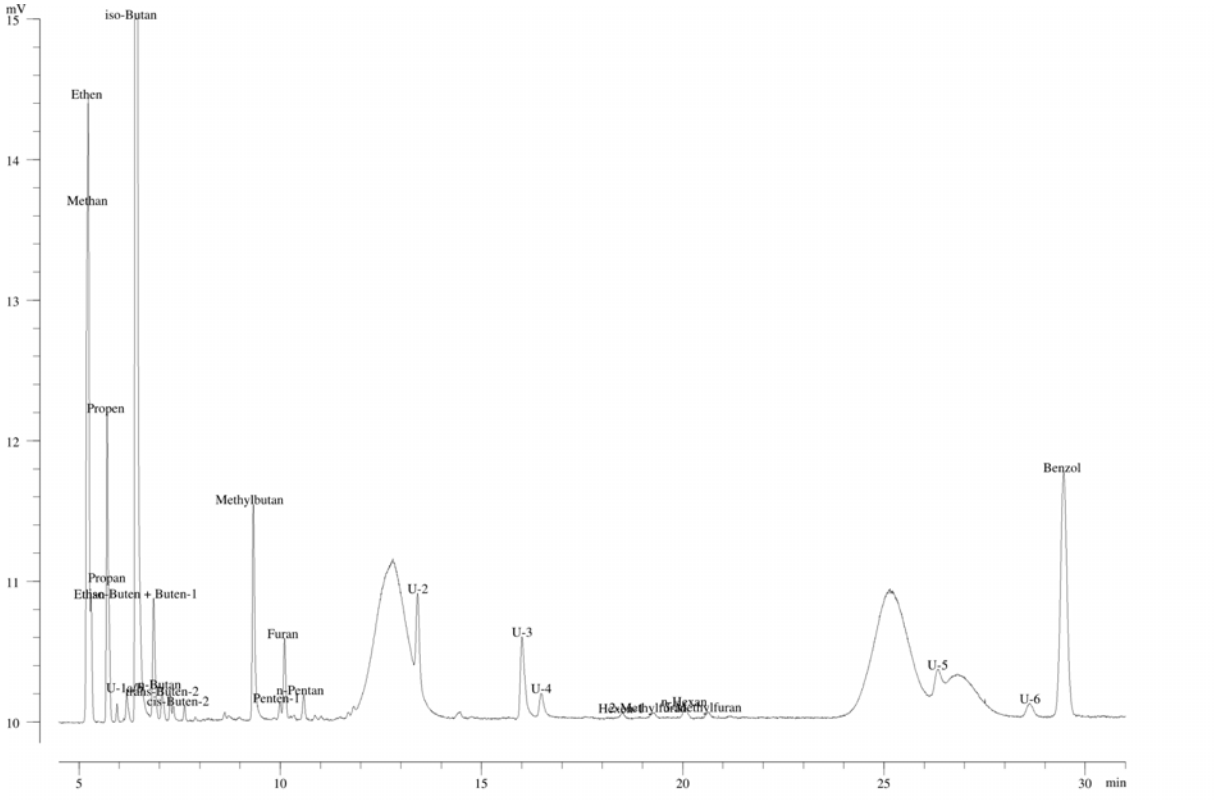
mV
15
14
13
12
11
10
iso-Butan
Ethen
Methan
Propen
Methylbutan
Propan
Ethan
Buten + Buten-1
Furan
U-2
U-3
U-4
U-5
U-6
Benzol
n-Butan
trans-Buten-2
cis-Buten-2
Penten-1
n-Pentan
Hexen-1
n-Hexan
5
10
15
20
25
30
min
Analysis: [GC_LABOR]P513B05 ,42, 1 Samplename: E50179 30C/35M/3/60C/5M Trap:100C aquired on 18-Nov-2002 17:43:03 Channel: 15 reported on 11-FEB-2003 08:08:43.70 from user LEISTNER5

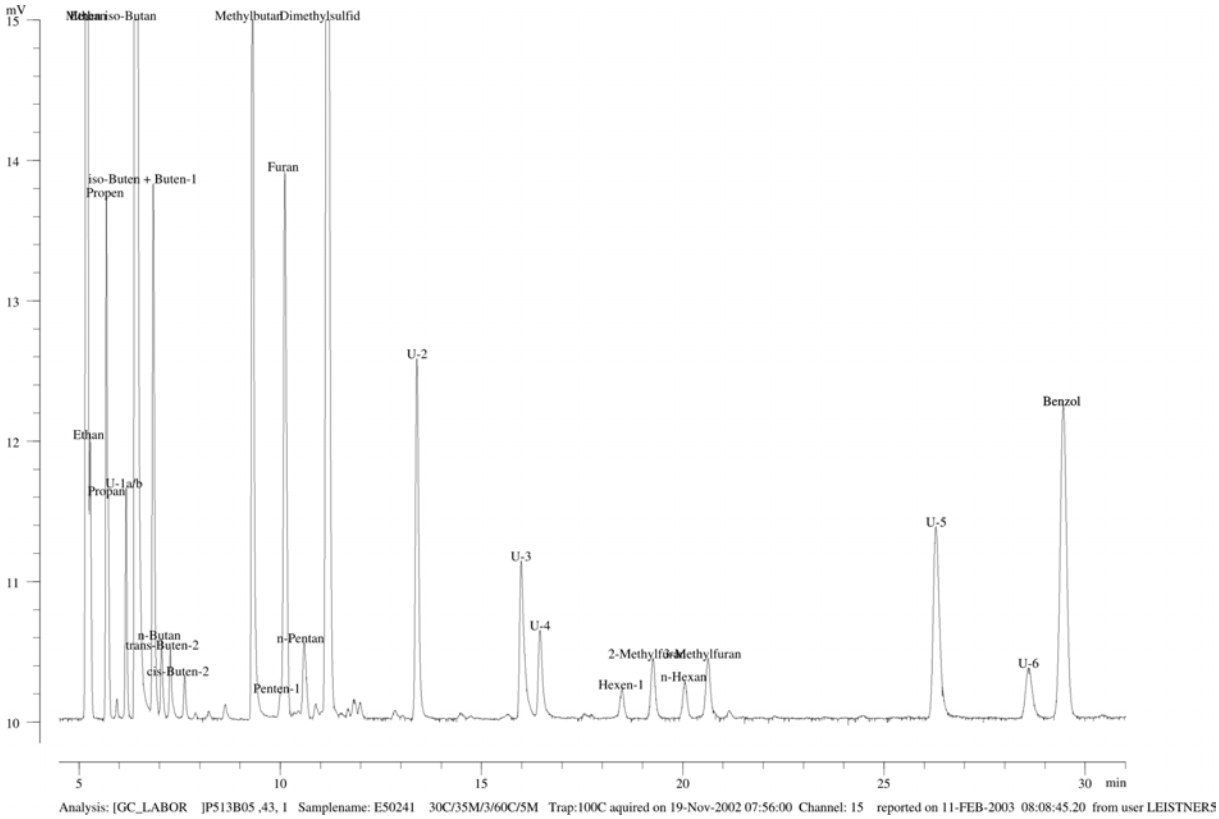
mV
15
14
13
12
11
10
iso-Butan
Methylbutan
Dimethylsulfid
Furan
iso-Buten + Buten-1
Propen
U-2
Benzol
Ethan
U-1a/b
Propan
U-5
U-3
U-4
n-Butan
trans-Buten-2
n-Pentan
cis-Buten-2
Penten-1
Hexen-1
n-Hexan
U-6
5
10
15
20
25
30
min
Analysis: [GC_LABOR]P513B05 ,43, 1 Samplename: E50241 30C/35M/3/60C/5M Trap:100C aquired on 19-Nov-2002 07:56:00 Channel: 15 reported on 11-FEB-2003 08:08:45.20 from user LEISTNER5

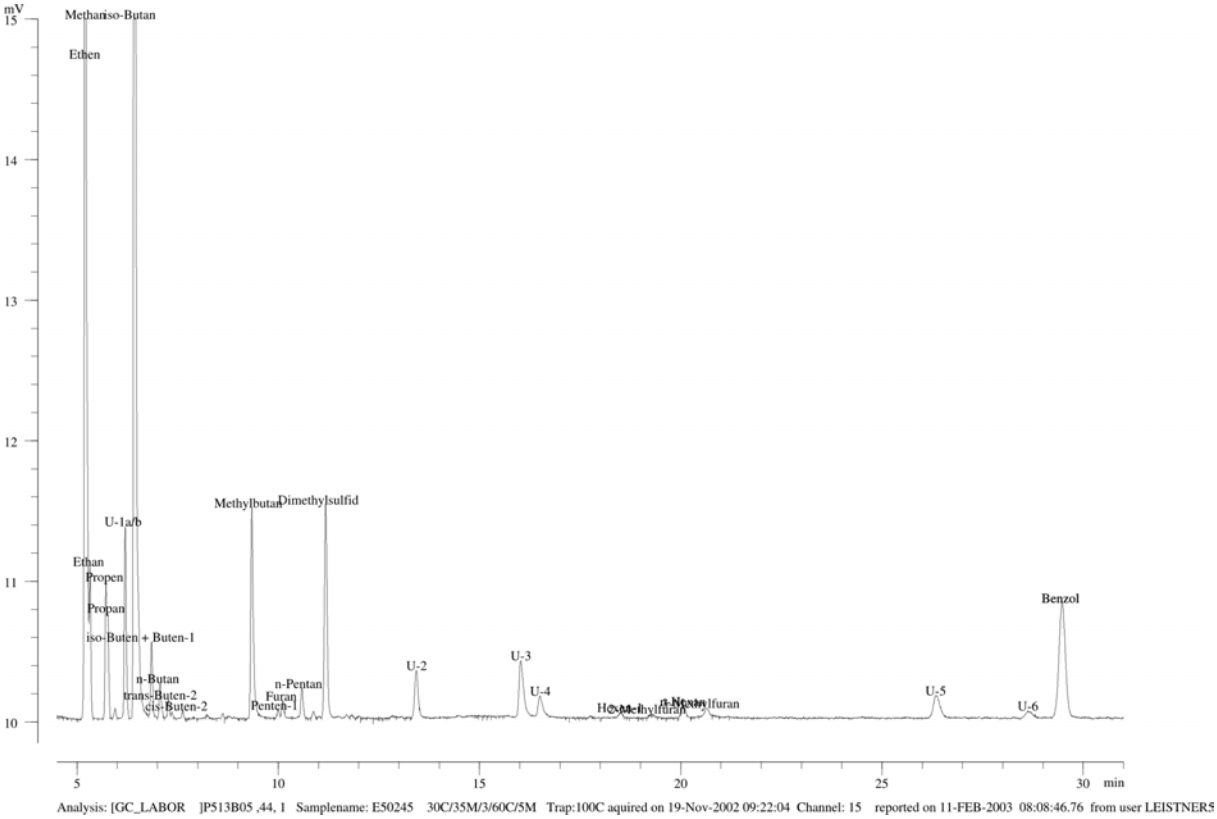
mV
15
14
13
12
11
10
Methan
iso-Butan
Ethen
Methylbutan
Dimethylsulfid
U-1a/b
Ethan
Propen
Propan
iso-Buten + Buten-1
n-Butan
trans-Buten-2
cis-Buten-2
n-Pentan
Furan
Penten-1
U-2
U-3
U-4
U-5
U-6
Benzol
5
10
15
20
25
30
min
Analysis: [GC_LABOR]P513B05 ,44, 1 Samplename: E50245 30C/35M/3/60C/5M Trap:100C aquired on 19-Nov-2002 09:22:04 Channel: 15 reported on 11-FEB-2003 08:08:46.76 from user LEISTNER5

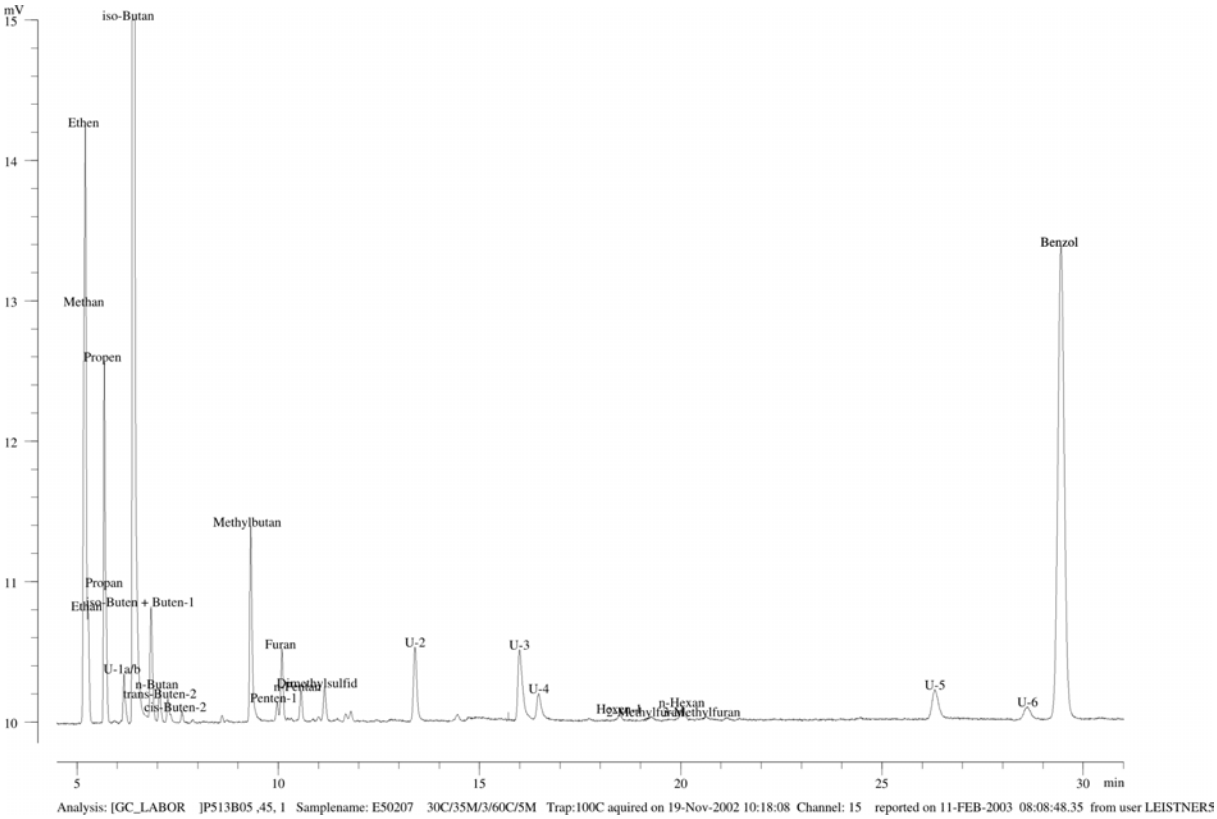
mV
15
14
13
12
11
10
iso-Butan
Ethen
Benzol
Methan
Propen
Methylbutan
Propan
Ethan
iso-Buten + Buten-1
Furan
U-2
U-3
U-1a/b
n-Butan
trans-Buten-2
cis-Buten-2
Penten-1
U-4
U-5
U-6
5
10
15
20
25
30
min
Analysis: [GC_LABOR]P513B05 ,45, 1 Samplename: E50207 30C/35M/3/60C/5M Trap:100C aquired on 19-Nov-2002 10:18:08 Channel: 15 reported on 11-FEB-2003 08:08:48.35 from user LEISTNER5

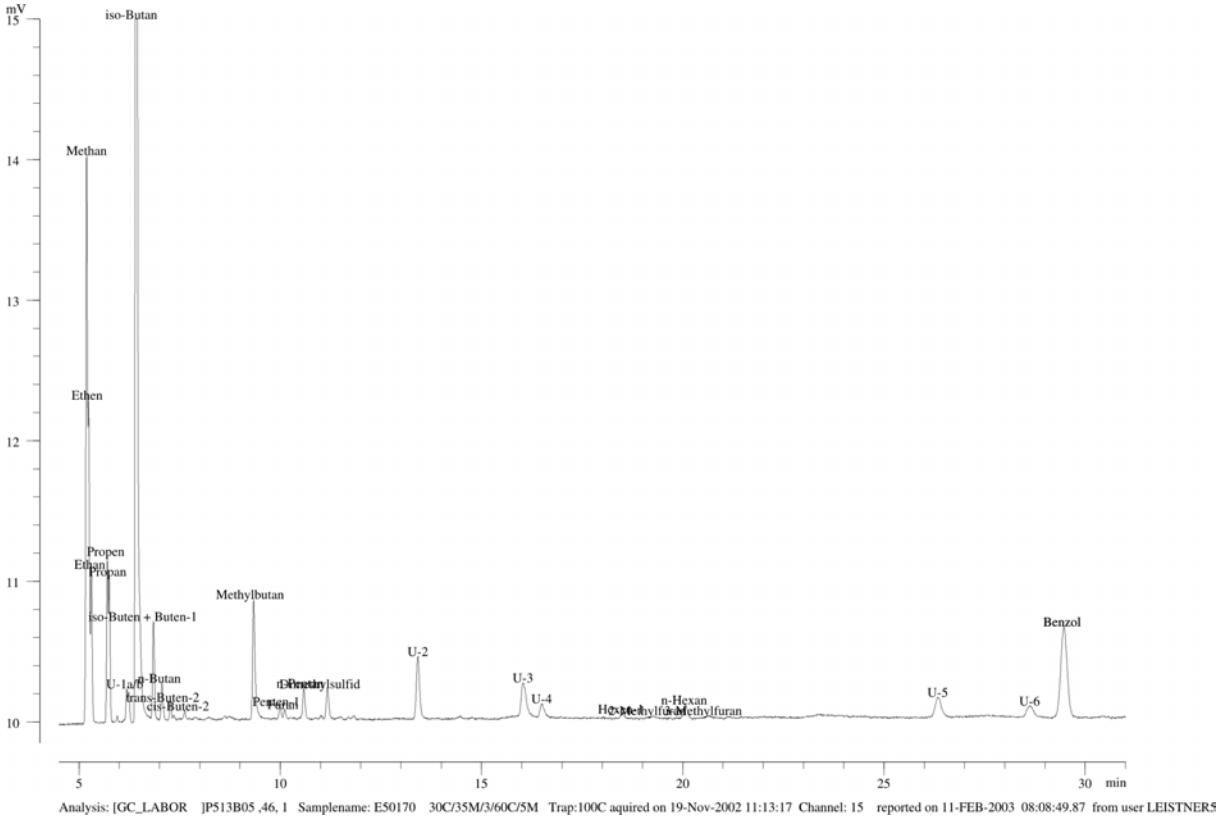

Analysis: [GC_LABOR]P513B05 ,46, 1 Samplename: E50170 30C/35M/3/60C/5M Trap:100C aquired on 19-Nov-2002 11:13:17 Channel: 15 reported on 11-FEB-2003 08:08:49.87 from user LEISTNER5

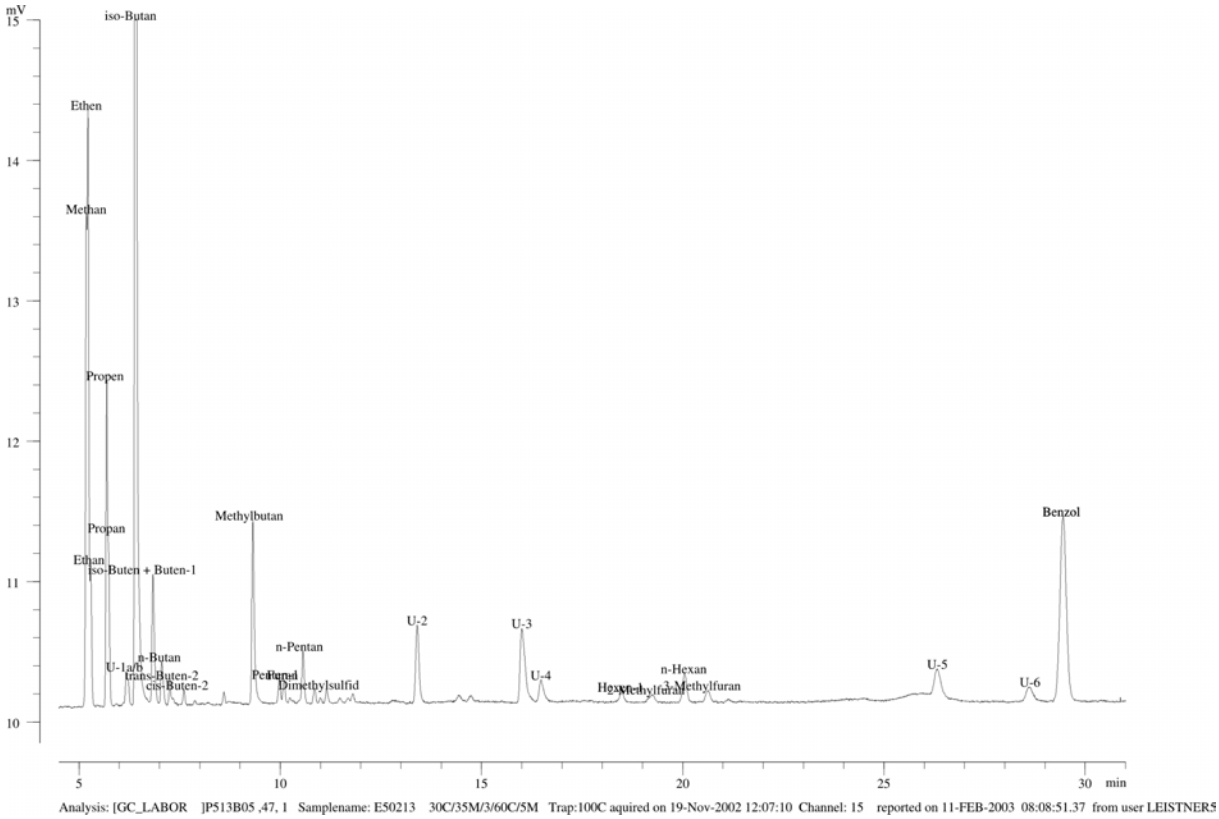

Analysis: [GC_LABOR]P513B05 ,47, 1 Samplename: E50213 30C/35M/3/60C/5M Trap:100C aquired on 19-Nov-2002 12:07:10 Channel: 15 reported on 11-FEB-2003 08:08:51.37 from user LEISTNER5

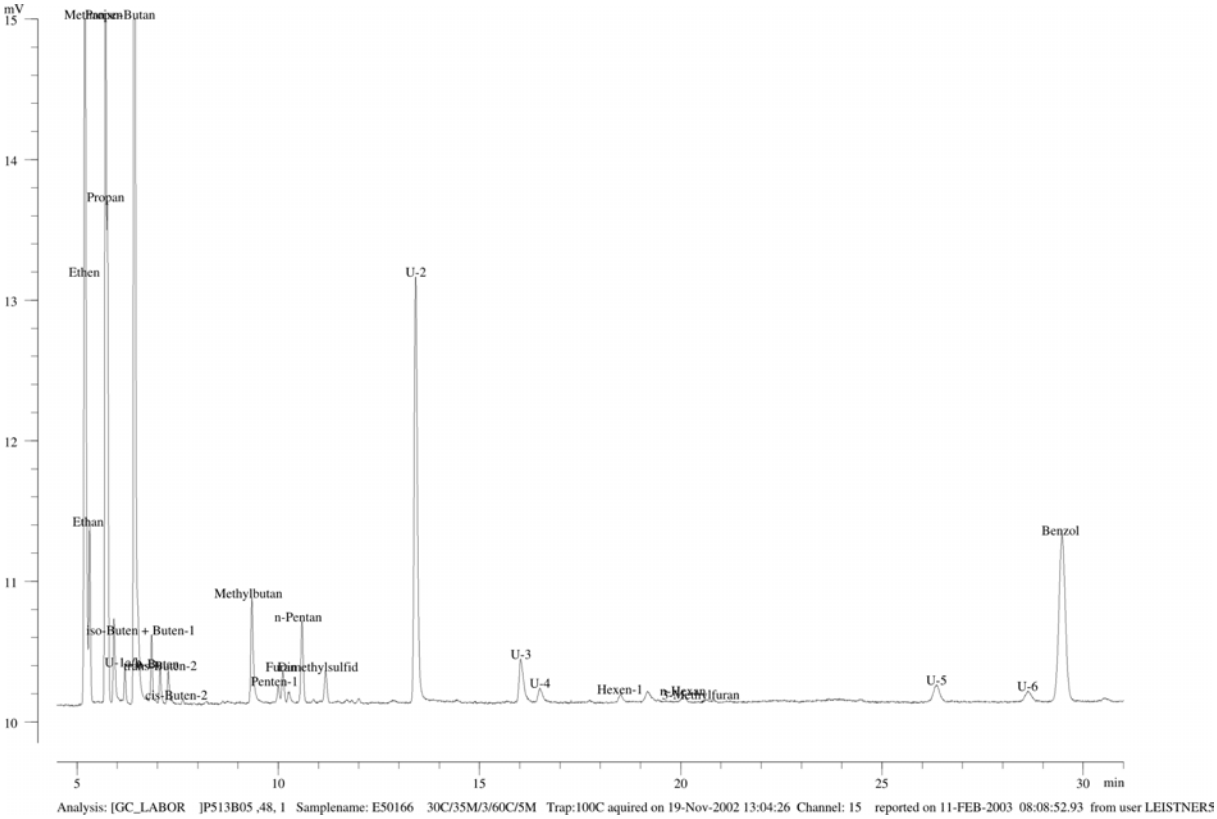
mV
15
14
13
12
11
10
Methan
Propan
Butan
Ethen
Ethan
U-2
Benzol
Methylbutan
n-Pentan
iso-Buten + Buten-1
U-3
U-4
U-5
U-6
Hexen-1
Penten-1
cis-Buten-2
5
10
15
20
25
30
min
Analysis: [GC_LABOR]P513B05 ,48, 1 Samplename: E50166 30C/35M/3/60C/5M Trap:100C aquired on 19-Nov-2002 13:04:26 Channel: 15 reported on 11-FEB-2003 08:08:52.93 from user LEISTNER5

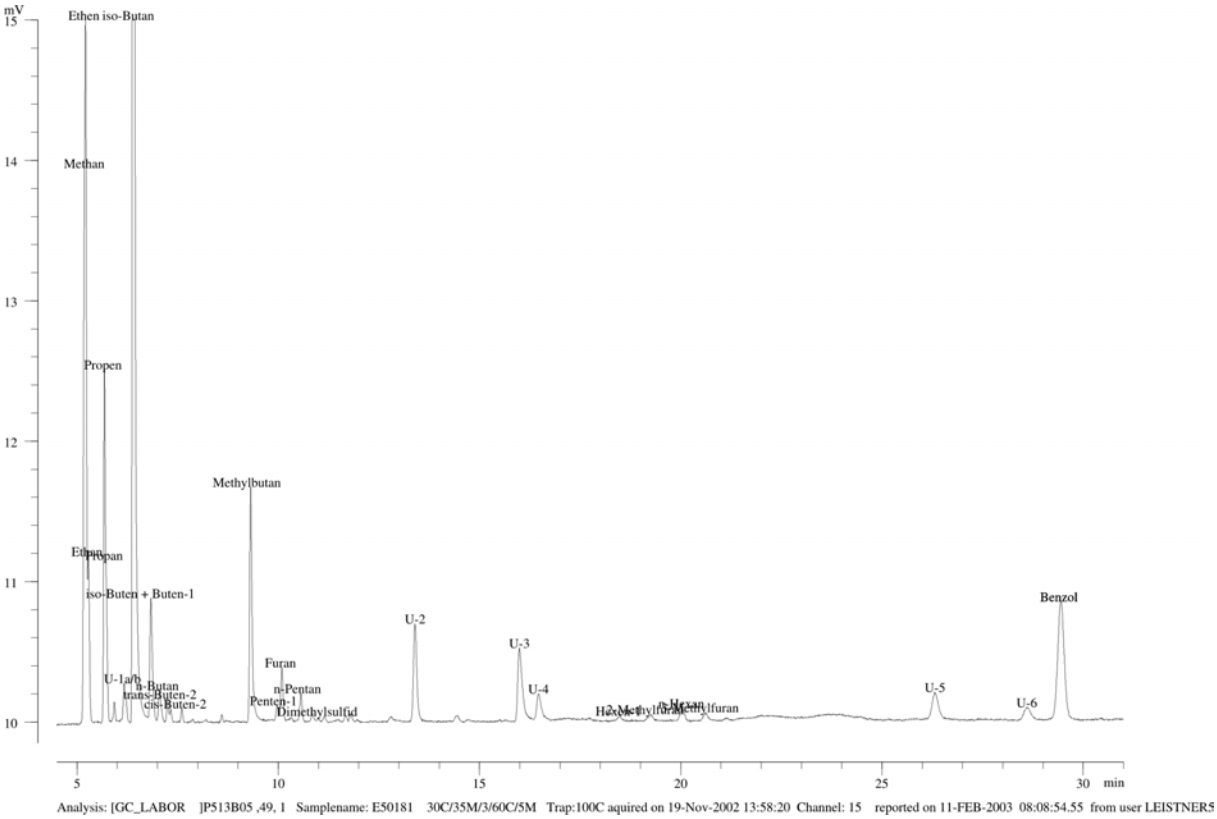
mV
15
14
13
12
11
10
Ethen iso-Butan
Methan
Propen
Methylbutan
Propan
iso-Buten + Buten-1
Benzol
U-2
U-3
Furan
U-1a/b
n-Butan
n-Pentan
trans-Buten-2
U-4
U-5
U-6
cis-Buten-2
Penten-1
Dimethylsulfid
5
10
15
20
25
30
min
Analysis: [GC_LABOR]P513B05 ,49, 1 Samplename: E50181 30C/35M/3/60C/5M Trap:100C aquired on 19-Nov-2002 13:58:20 Channel: 15 reported on 11-FEB-2003 08:08:54.55 from user LEISTNER5

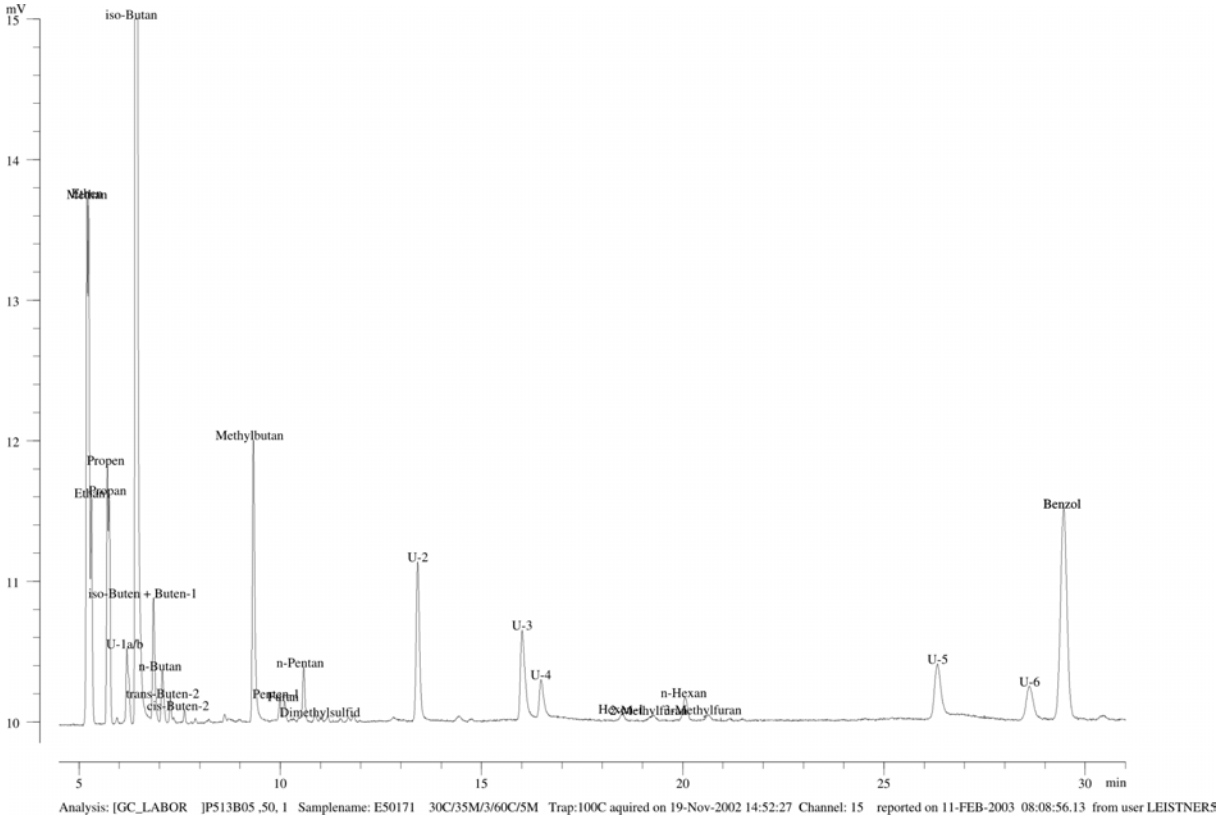
mV
15
14
13
12
11
10
iso-Butan
Methylbutan
Propen
Ethan
Propan
iso-Buten + Buten-1
U-1a/b
n-Butan
trans-Buten-2
cis-Buten-2
n-Pentan
Dimethylsulfid
U-2
U-3
U-4
n-Hexan
Methylfuran
U-5
U-6
Benzol
5
10
15
20
25
30
min
Analysis: [GC_LABOR]P513B05 ,50, 1 Samplename: E50171 30C/35M/3/60C/5M Trap:100C aquired on 19-Nov-2002 14:52:27 Channel: 15 reported on 11-FEB-2003 08:08:56.13 from user LEISTNER5

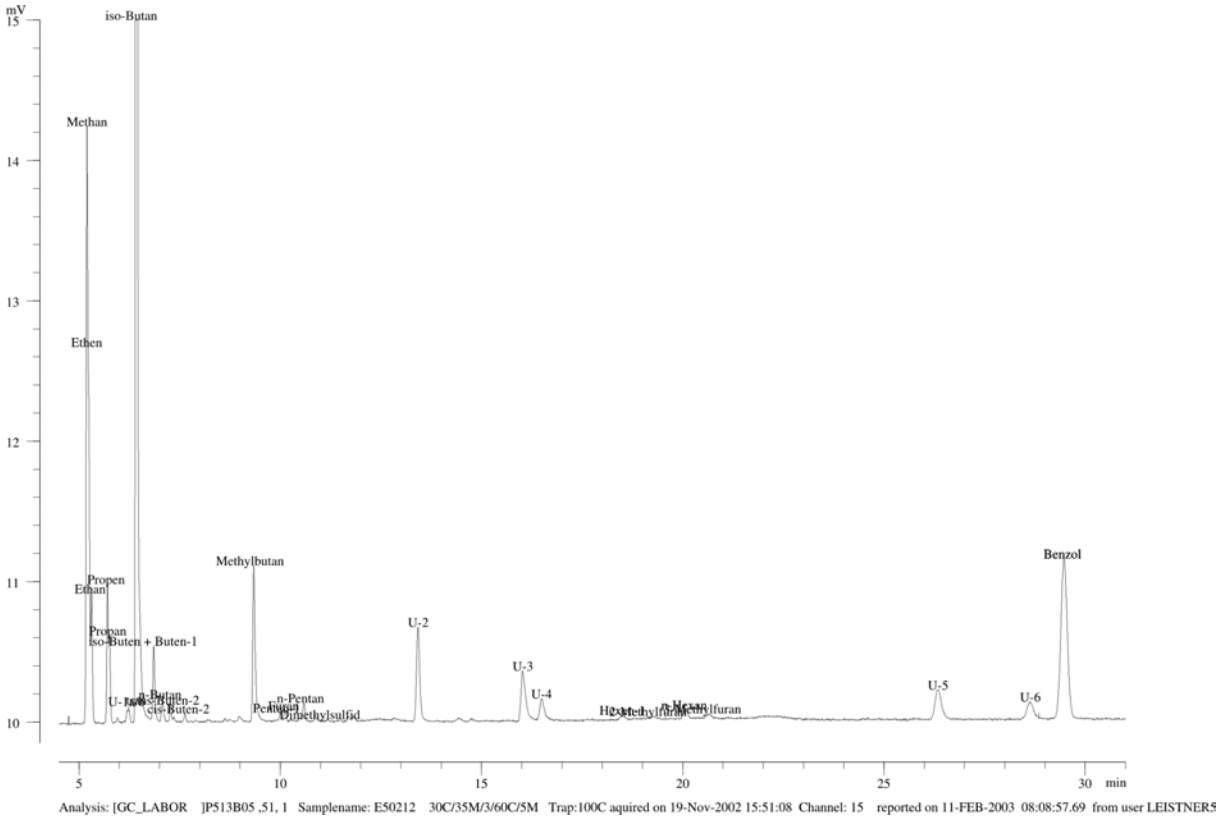
mV
15
14
13
12
11
10
iso-Butan
Methan
Ethen
Propen
Ethan
Propan
iso-Buten + Buten-1
cis-Buten-2
n-Pentan
Dimethylsulfid
Methylbutan
U-2
U-3
U-4
U-5
U-6
Benzol
5
10
15
20
25
30
min
Analysis: [GC_LABOR]P513B05 ,51, 1 Samplename: E50212 30C/35M/3/60C/5M Trap:100C aquired on 19-Nov-2002 15:51:08 Channel: 15 reported on 11-FEB-2003 08:08:57.69 from user LEISTNER5

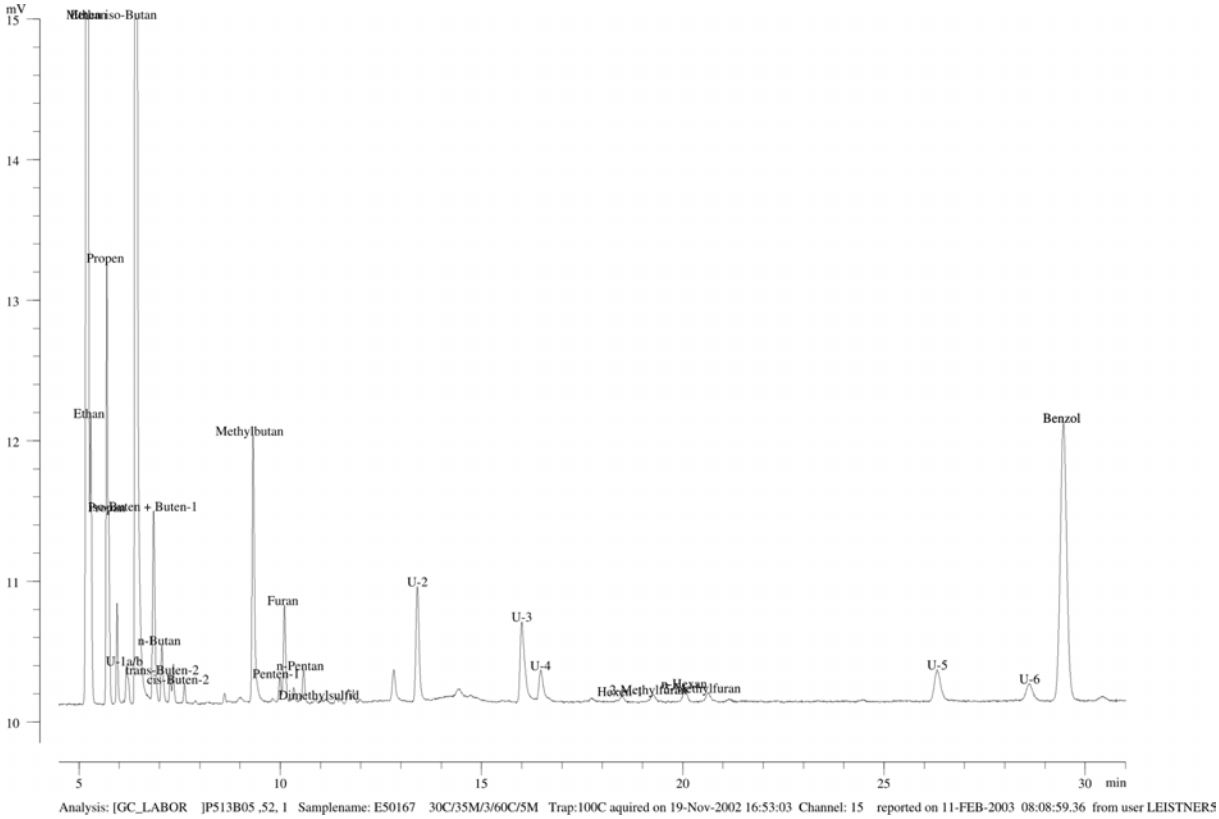
mV
15
14
13
12
11
10
Methaniso-Butan
Propen
Ethan
Methylbutan
Buten + Buten-1
Furan
U-2
U-3
n-Butan
U-1a/b
trans-Buten-2
cis-Buten-2
n-Pentan
Penten-1
Dimethylsulfid
U-4
U-5
U-6
Benzol
5
10
15
20
25
30
min
Analysis: [GC_LABOR]P513B05 ,52, 1 Samplename: E50167 30C/35M/3/60C/5M Trap:100C aquired on 19-Nov-2002 16:53:03 Channel: 15 reported on 11-FEB-2003 08:08:59.36 from user LEISTNER5

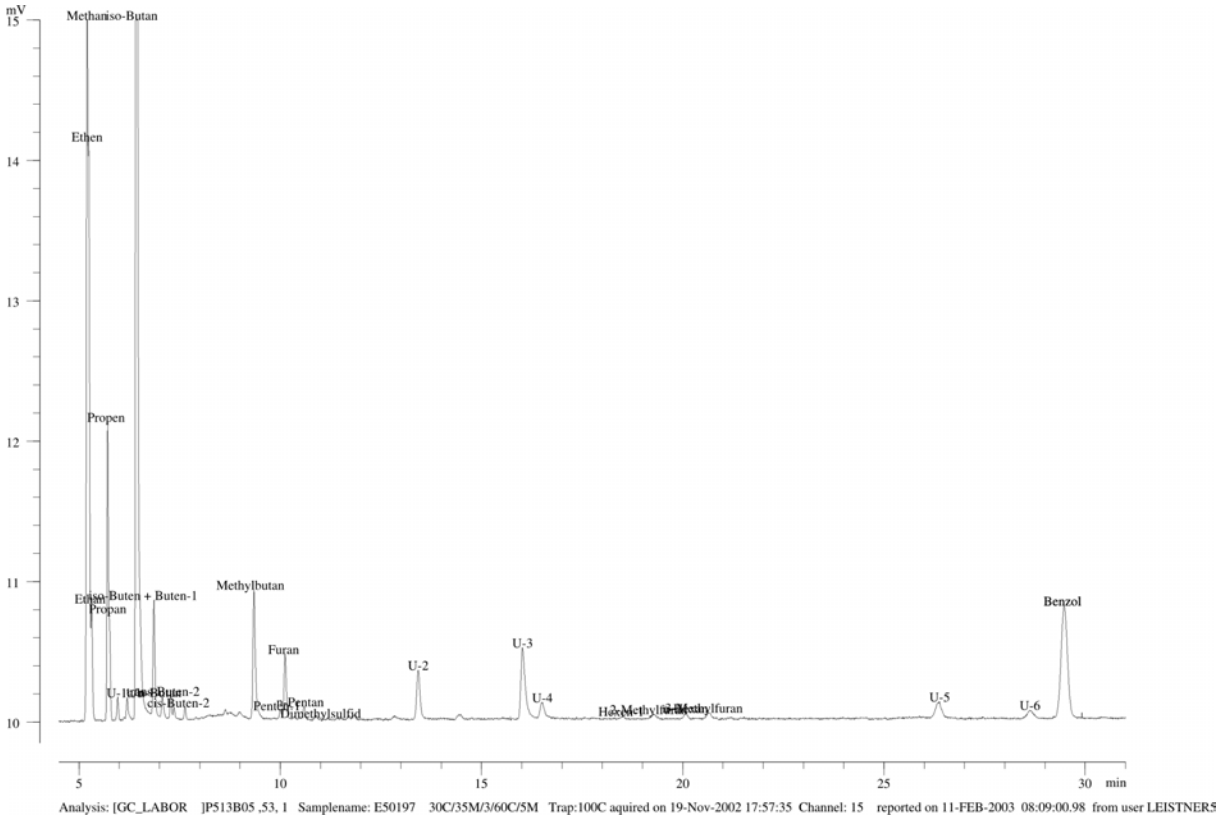
mV
15
14
13
12
11
10
Methaniso-Butan
Ethen
Propen
Methylbutan
Buten + Buten-1
Propan
Furan
U-2
U-3
U-4
U-5
U-6
Benzol
5
10
15
20
25
30
min
Analysis: [GC_LABOR]P513B05 ,53, 1 Samplename: E50197 30C/35M/3/60C/5M Trap:100C aquired on 19-Nov-2002 17:57:35 Channel: 15 reported on 11-FEB-2003 08:09:00.98 from user LEISTNER5

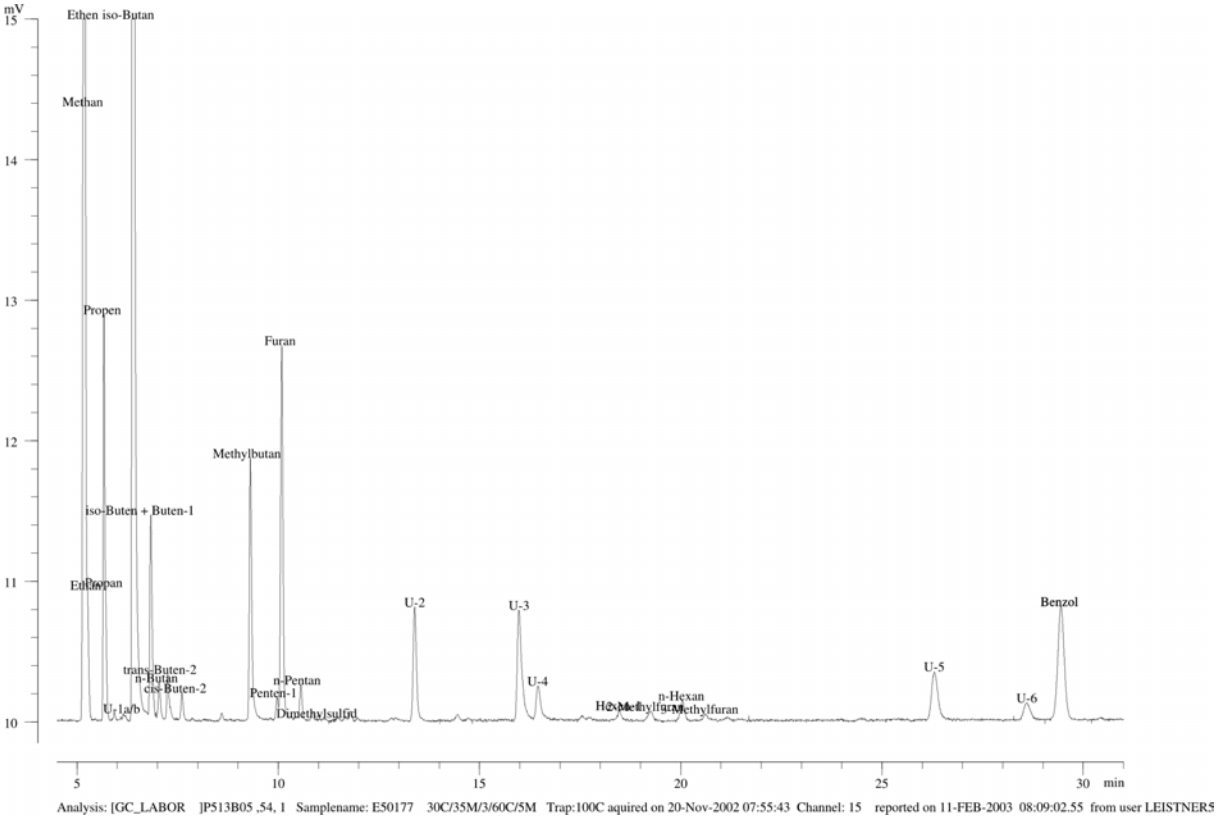

Analysis: [GC_LABOR]P513B05 ,54, 1 Samplename: E50177 30C/35M/3/60C/5M Trap:100C aquired on 20-Nov-2002 07:55:43 Channel: 15 reported on 11-FEB-2003 08:09:02.55 from user LEISTNER5

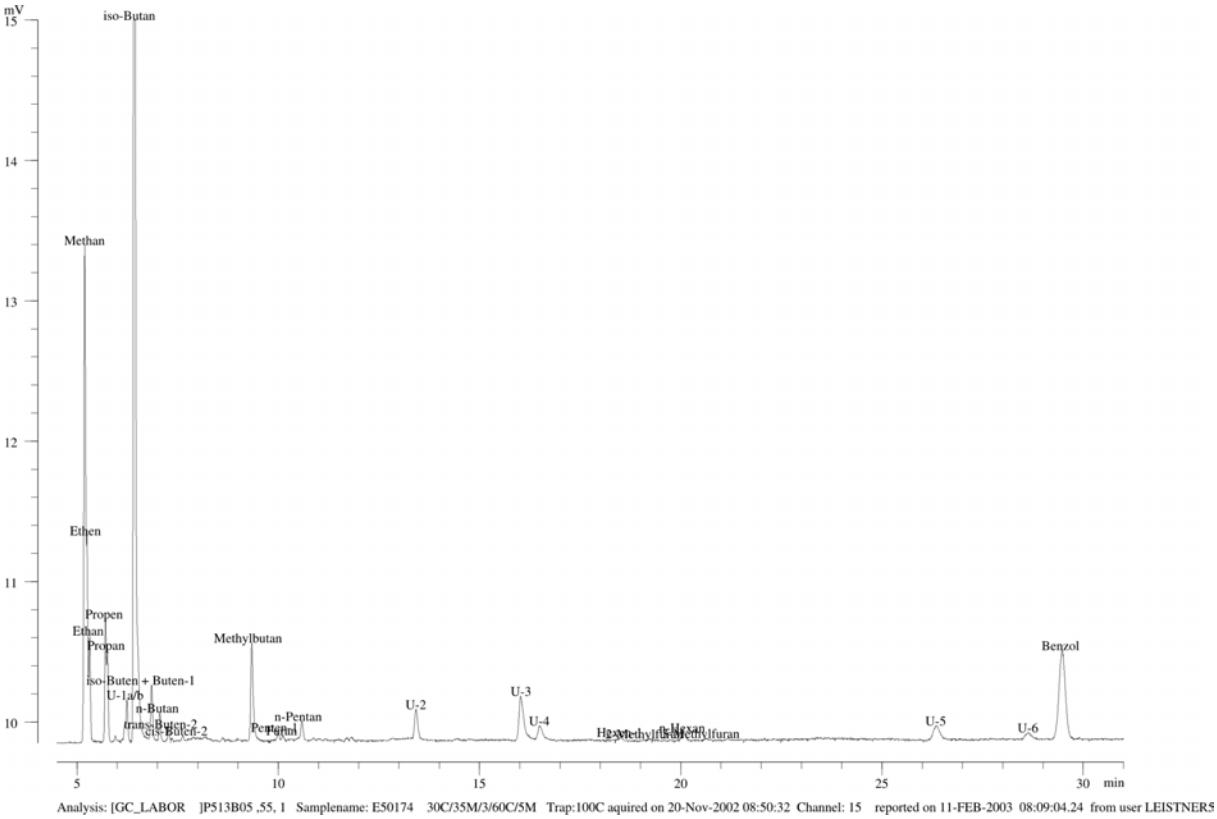

Analysis: [GC_LABOR]P513B05 ,55, 1 Samplename: E50174 30C/35M/3/60C/5M Trap:100C aquired on 20-Nov-2002 08:50:32 Channel: 15 reported on 11-FEB-2003 08:09:04.24 from user LEISTNER5

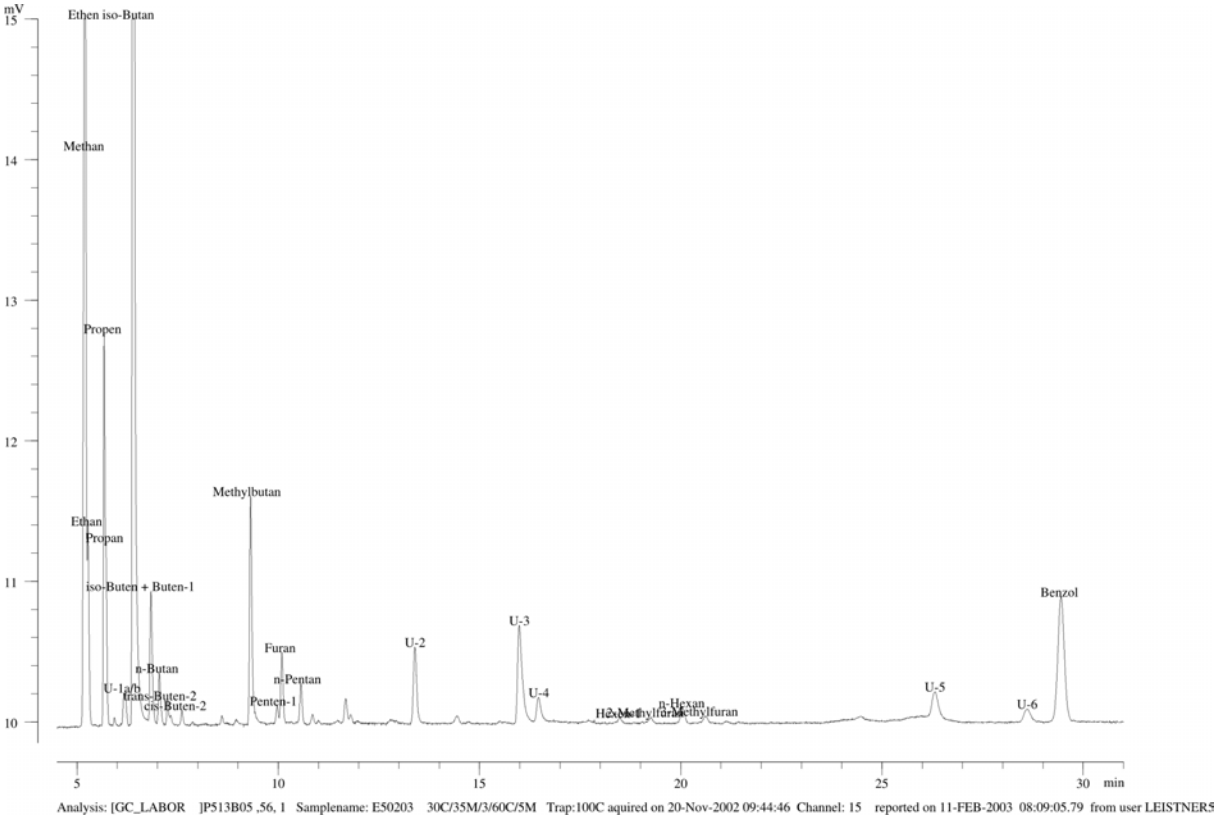
mV
15
14
13
12
11
10
Ethen
iso-Butan
Methan
Propen
Methylbutan
Ethan
Propan
iso-Buten + Buten-1
Benzol
U-3
U-2
Furan
n-Butan
n-Pentan
U-1a/b
trans-Buten-2
cis-Buten-2
Penten-1
U-4
U-5
U-6
n-Hexan
5
10
15
20
25
30
min
Analysis: [GC_LABOR]P513B05 ,56, 1 Samplename: E50203 30C/35M/3/60C/5M Trap:100C aquired on 20-Nov-2002 09:44:46 Channel: 15 reported on 11-FEB-2003 08:09:05.79 from user LEISTNER5

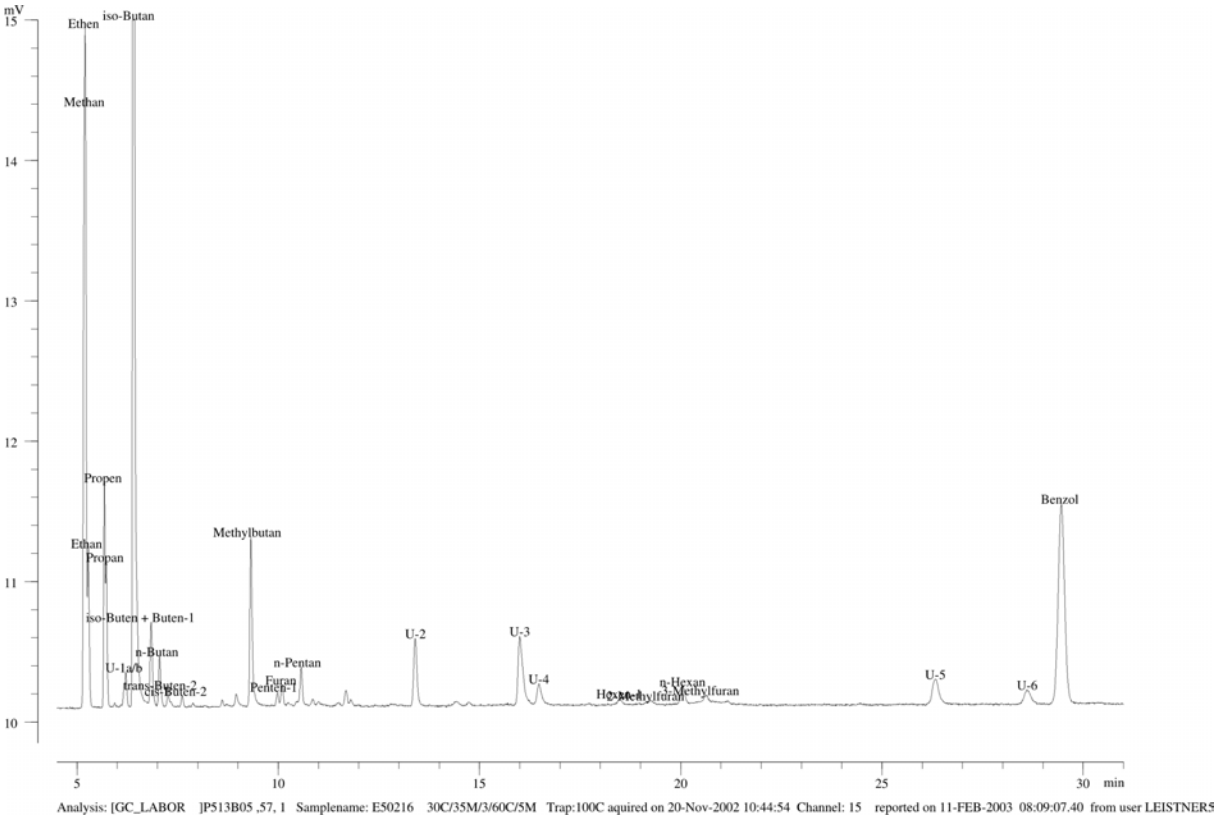
mV
15
14
13
12
11
10
Ethen
iso-Butan
Methan
Propen
Benzol
Methylbutan
Ethan
Propan
iso-Buten + Buten-1
U-2
U-3
n-Butan
n-Pentan
U-1a/b
Furan
U-4
U-5
U-6
n-Hexan
5
10
15
20
25
30
min
Analysis: [GC_LABOR]P513B05 ,57, 1 Samplename: E50216 30C/35M/3/60C/5M Trap:100C aquired on 20-Nov-2002 10:44:54 Channel: 15 reported on 11-FEB-2003 08:09:07.40 from user LEISTNER5

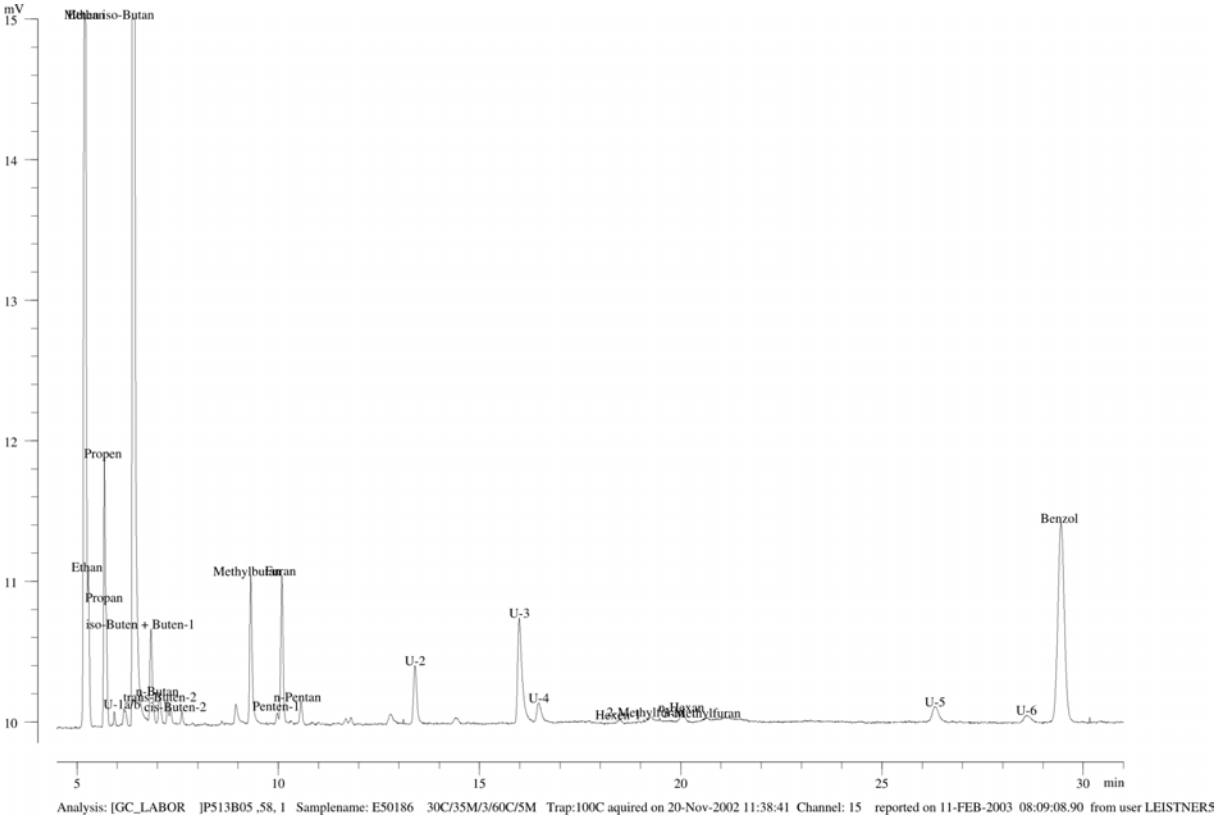
mV
15
14
13
12
11
10
iso-Butan
Propen
Ethan
Propan
iso-Buten + Buten-1
n-Butan
trans-Buten-2
cis-Buten-2
U-1a/b
Methylbutan
Furan
n-Pentan
Penten-1
U-2
U-3
U-4
Hexen-1
2-Methylfuran
n-Hexan
3-Methylfuran
U-5
U-6
Benzol
5
10
15
20
25
30
min
Analysis: [GC_LABOR]P513B05 ,58, 1 Samplename: E50186 30C/35M/3/60C/5M Trap:100C aquired on 20-Nov-2002 11:38:41 Channel: 15 reported on 11-FEB-2003 08:09:08.90 from user LEISTNER5

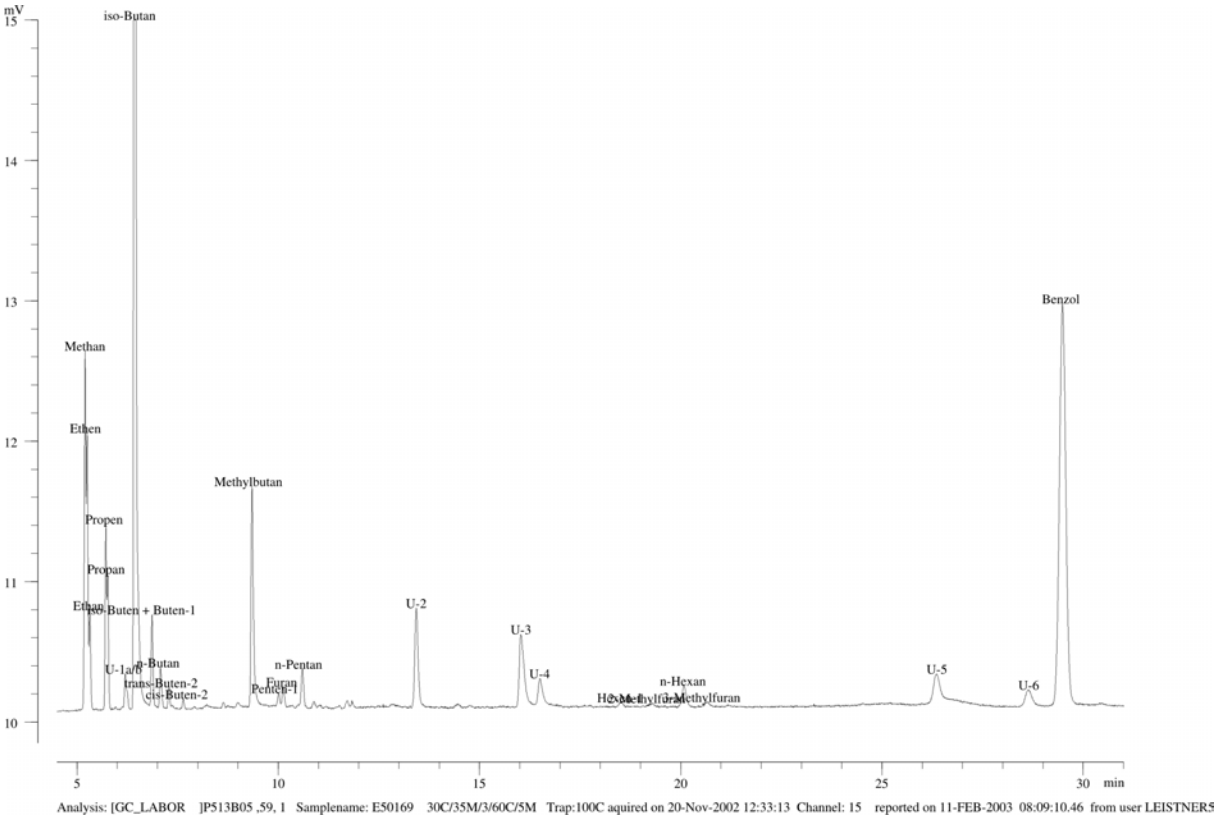
mV
15
14
13
12
11
10
iso-Butan
Methan
Ethen
Methylbutan
Propen
Propan
Ethan
iso-Buten + Buten-1
U-1a/b
n-Butan
trans-Buten-2
cis-Buten-2
n-Pentan
Furan
Penten-1
U-2
U-3
U-4
n-Hexan
U-5
U-6
Benzol
5
10
15
20
25
30
min
Analysis: [GC_LABOR]P513B05 ,59, 1 Samplename: E50169 30C/35M/3/60C/5M Trap:100C aquired on 20-Nov-2002 12:33:13 Channel: 15 reported on 11-FEB-2003 08:09:10.46 from user LEISTNER5

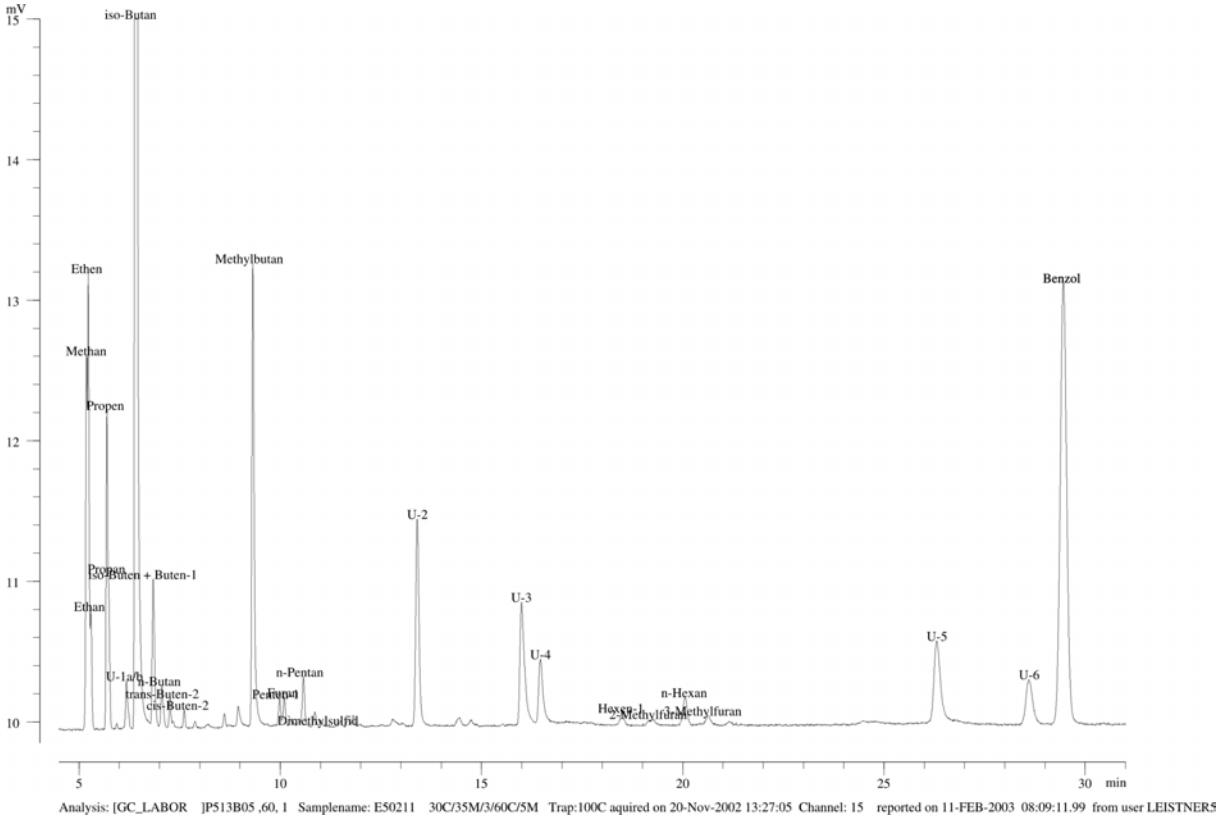
mV
15
14
13
12
11
10
iso-Butan
Ethen
Methan
Propen
Propan
iso-Buten + Buten-1
Ethan
U-1a/b
n-Butan
trans-Buten-2
cis-Buten-2
Methylbutan
n-Pentan
Pentan-1
Dimethylsulfid
U-2
U-3
U-4
Hexen-1
2-Methylfuran
3-Methylfuran
n-Hexan
U-5
U-6
Benzol
5
10
15
20
25
30
min
Analysis: [GC_LABOR]P513B05 ,60, 1 Samplename: E50211 30C/35M/3/60C/5M Trap:100C aquired on 20-Nov-2002 13:27:05 Channel: 15 reported on 11-FEB-2003 08:09:11.99 from user LEISTNER5

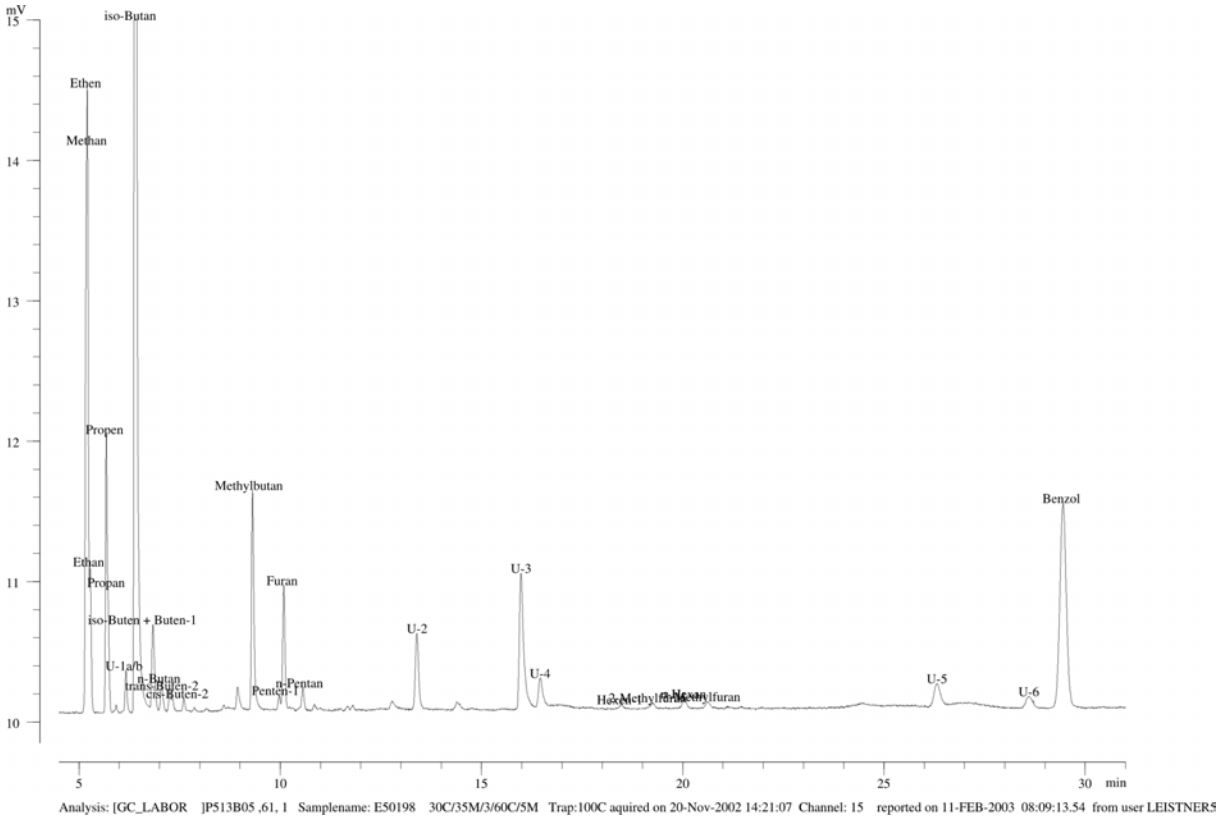
mV
15
14
13
12
11
10
iso-Butan
Ethen
Methan
Propen
Ethan
Propan
iso-Buten + Buten-1
U-1a/b
n-Butan
cis-Buten-2
Methylbutan
Furan
Penten-1
n-Pentan
U-2
U-3
U-4
2-Methylfuran
n-Hexan
U-5
U-6
Benzol
5
10
15
20
25
30
min
Analysis: [GC_LABOR]P513B05 ,61, 1 Samplename: E50198 30C/35M/3/60C/5M Trap:100C aquired on 20-Nov-2002 14:21:07 Channel: 15 reported on 11-FEB-2003 08:09:13.54 from user LEISTNER5

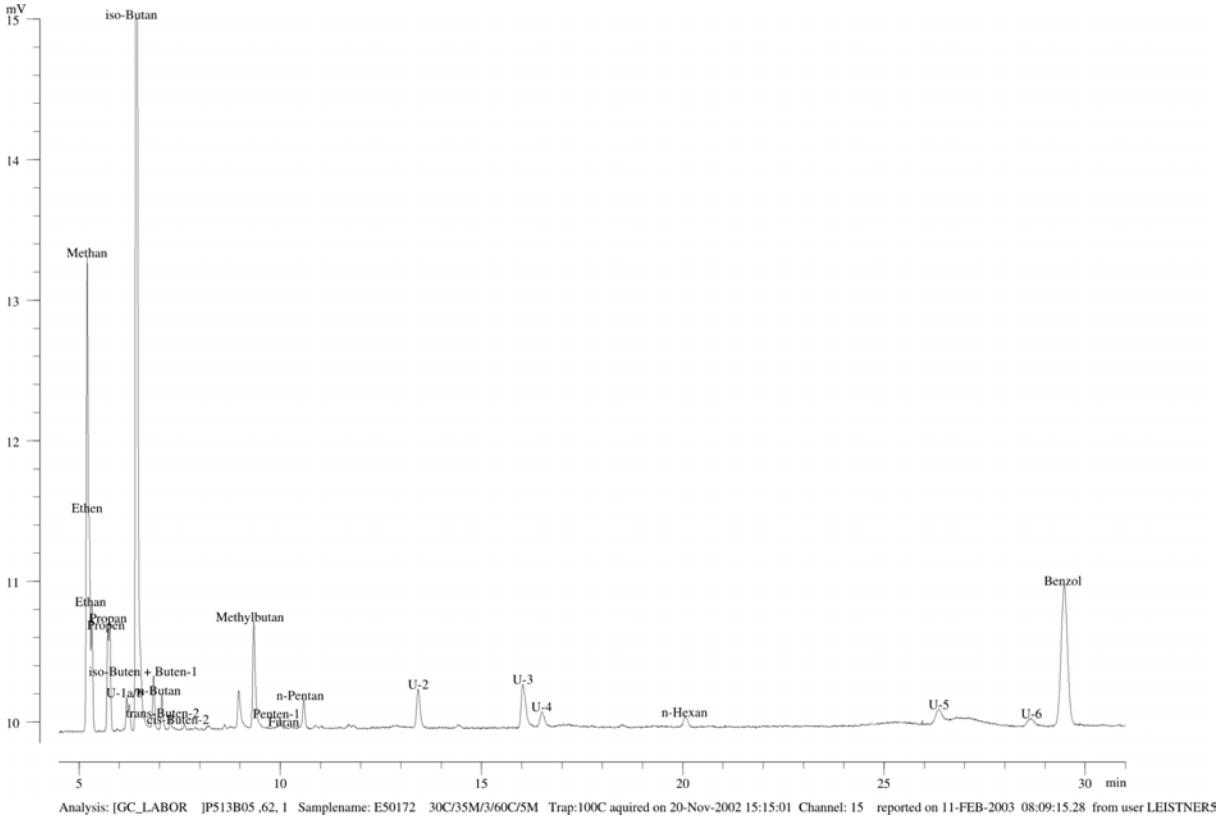
mV
15
14
13
12
11
10
iso-Butan
Methan
Ethen
Ethan
Propan
Propen
Methylbutan
iso-Buten + Buten-1
U-1a/b
n-Butan
trans-Buten-2
cis-Buten-2
Penten-1
Furan
n-Pentan
U-2
U-3
U-4
n-Hexan
U-5
U-6
Benzol
5
10
15
20
25
30
min
Analysis: [GC_LABOR]P513B05 ,62, 1 Samplename: E50172 30C/35M/3/60C/5M Trap:100C aquired on 20-Nov-2002 15:15:01 Channel: 15 reported on 11-FEB-2003 08:09:15.28 from user LEISTNER5

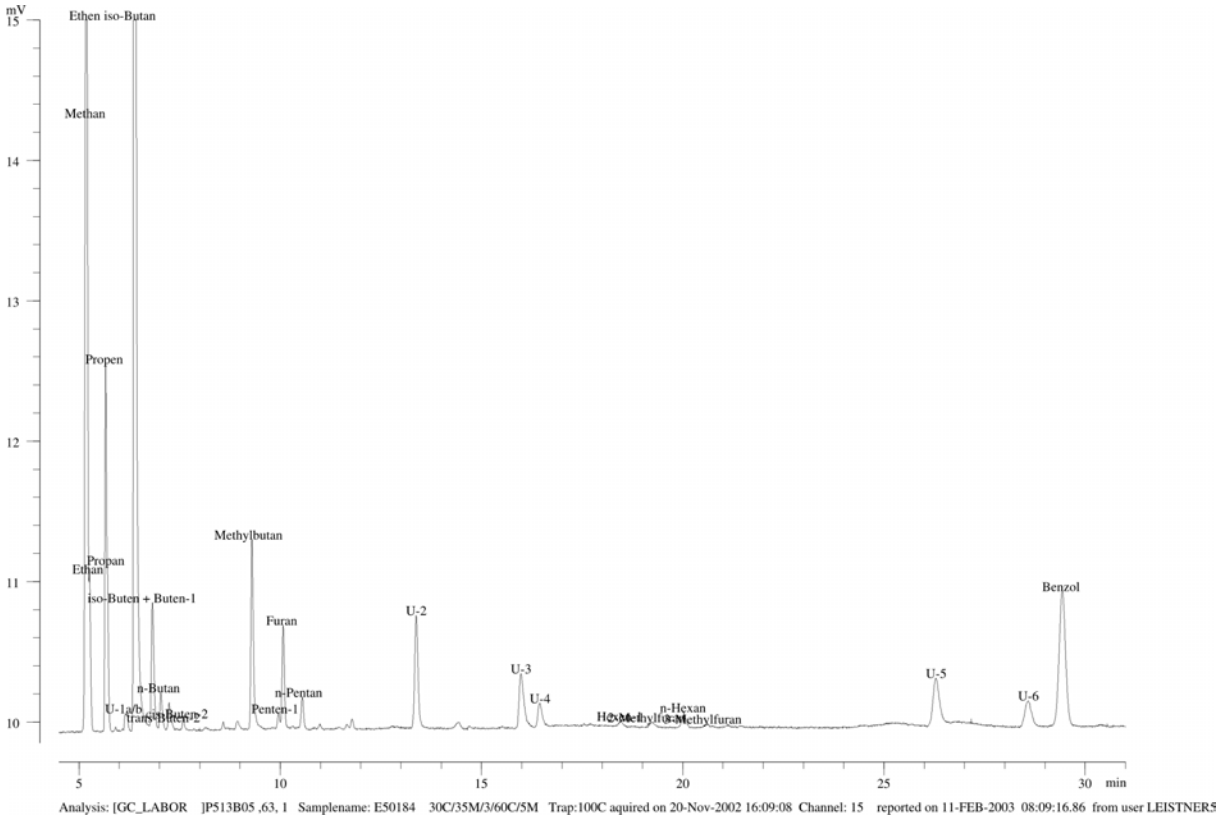
mV
15
14
13
12
11
10
Ethen
iso-Butan
Methan
Propen
Methylbutan
Propan
Ethan
iso-Buten + Buten-1
Furan
U-2
U-3
U-4
U-5
U-6
Benzol
n-Butan
U-1a/b
trans-Buten-2
Penten-1
n-Pentan
n-Hexan
Methylfuran
5
10
15
20
25
30
min
Analysis: [GC_LABOR]P513B05 ,63, 1 Samplename: E50184 30C/35M/3/60C/5M Trap:100C aquired on 20-Nov-2002 16:09:08 Channel: 15 reported on 11-FEB-2003 08:09:16.86 from user LEISTNER5

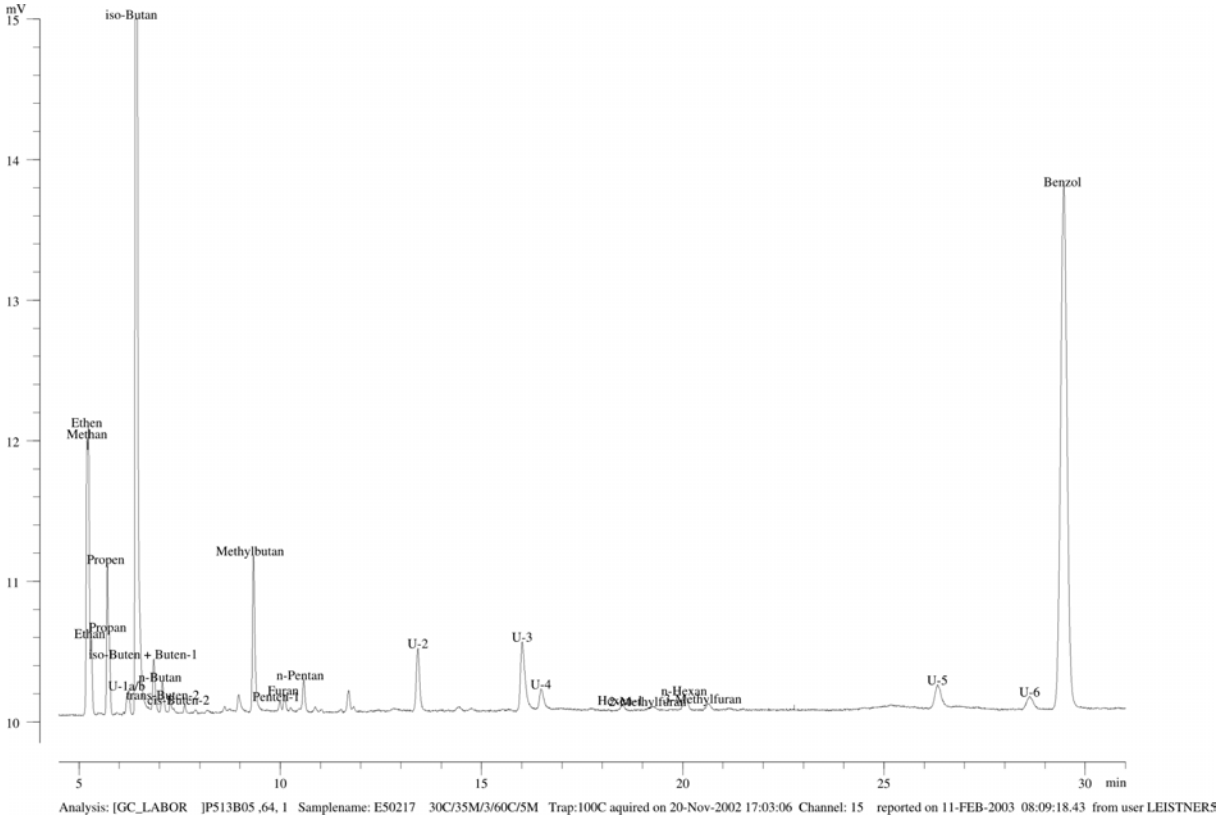
mV
15
14
13
12
11
10
iso-Butan
Benzol
Ethen
Methan
Propen
Methylbutan
Propan
Ethan
iso-Buten + Buten-1
U-2
U-3
n-Butan
n-Pentan
U-4
U-5
U-6
Furan
Penten-1
n-Hexan
5
10
15
20
25
30
min
Analysis: [GC_LABOR]P513B05 ,64, 1 Samplename: E50217 30C/35M/3/60C/5M Trap:100C aquired on 20-Nov-2002 17:03:06 Channel: 15 reported on 11-FEB-2003 08:09:18.43 from user LEISTNER5

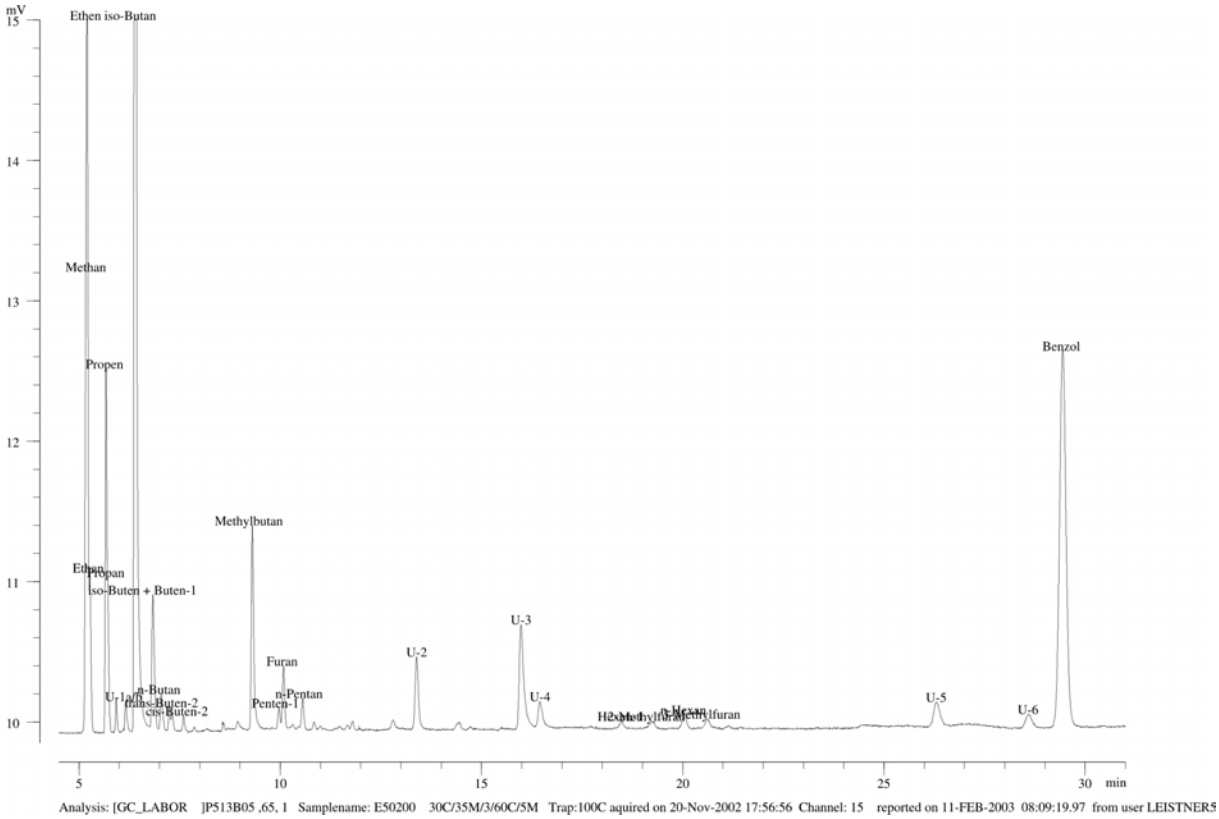
mV
15
14
13
12
11
10
Ethen iso-Butan
Benzol
Methan
Propen
Methylbutan
Ethan
Propan
iso-Buten + Buten-1
U-3
U-2
Furan
n-Butan
n-Pentan
U-4
U-5
U-6
Penten-1
5
10
15
20
25
30
min
Analysis: [GC_LABOR]P513B05 ,65, 1 Samplename: E50200 30C/35M/3/60C/5M Trap:100C aquired on 20-Nov-2002 17:56:56 Channel: 15 reported on 11-FEB-2003 08:09:19.97 from user LEISTNER5

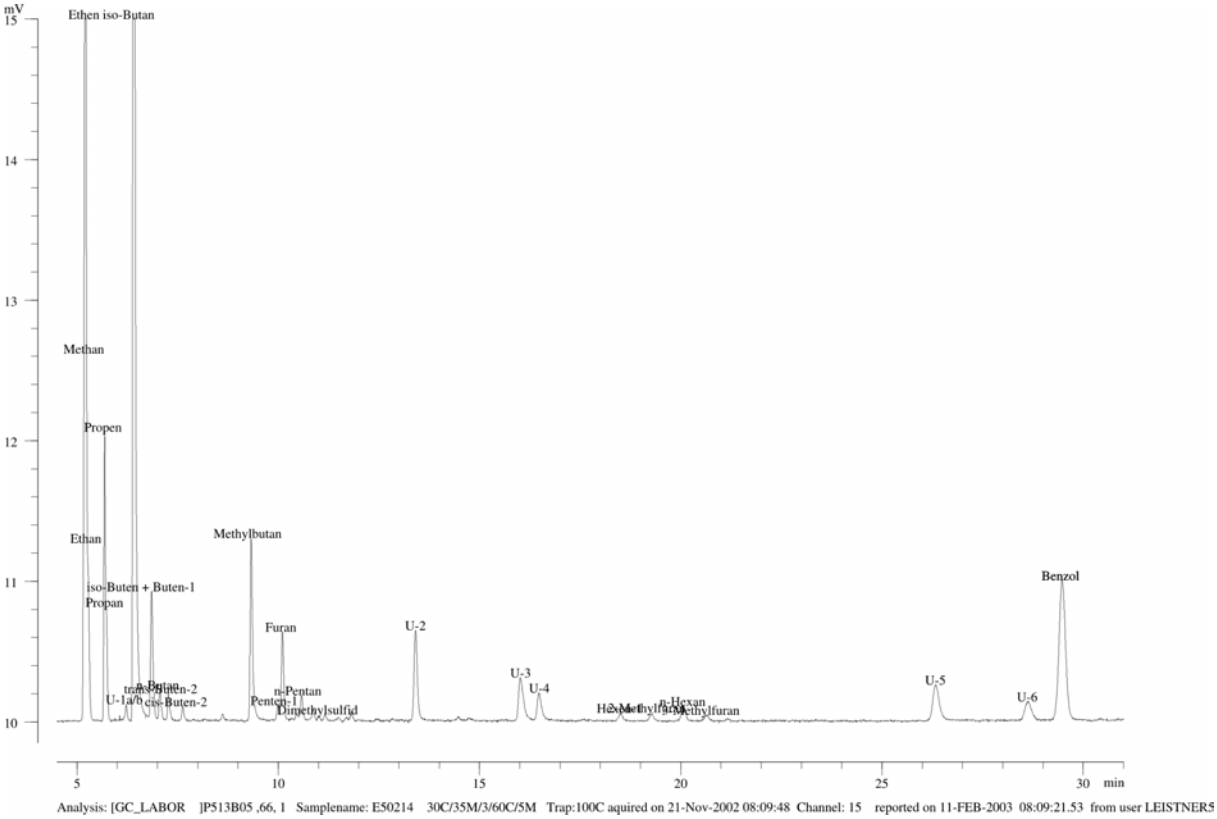
mV
15
14
13
12
11
10
Ethen
iso-Butan
Methan
Propen
Ethan
iso-Buten + Buten-1
Propan
Methylbutan
Furan
U-2
U-3
U-4
U-5
U-6
Benzol
n-Butan
trans-Buten-2
U-1a/b
cis-Buten-2
n-Pentan
Penten-1
Dimethylsulfid
n-Hexan
5
10
15
20
25
30
min
Analysis: [GC_LABOR]P513B05 ,66, 1 Samplename: E50214 30C/35M/3/60C/5M Trap:100C aquired on 21-Nov-2002 08:09:48 Channel: 15 reported on 11-FEB-2003 08:09:21.53 from user LEISTNER5

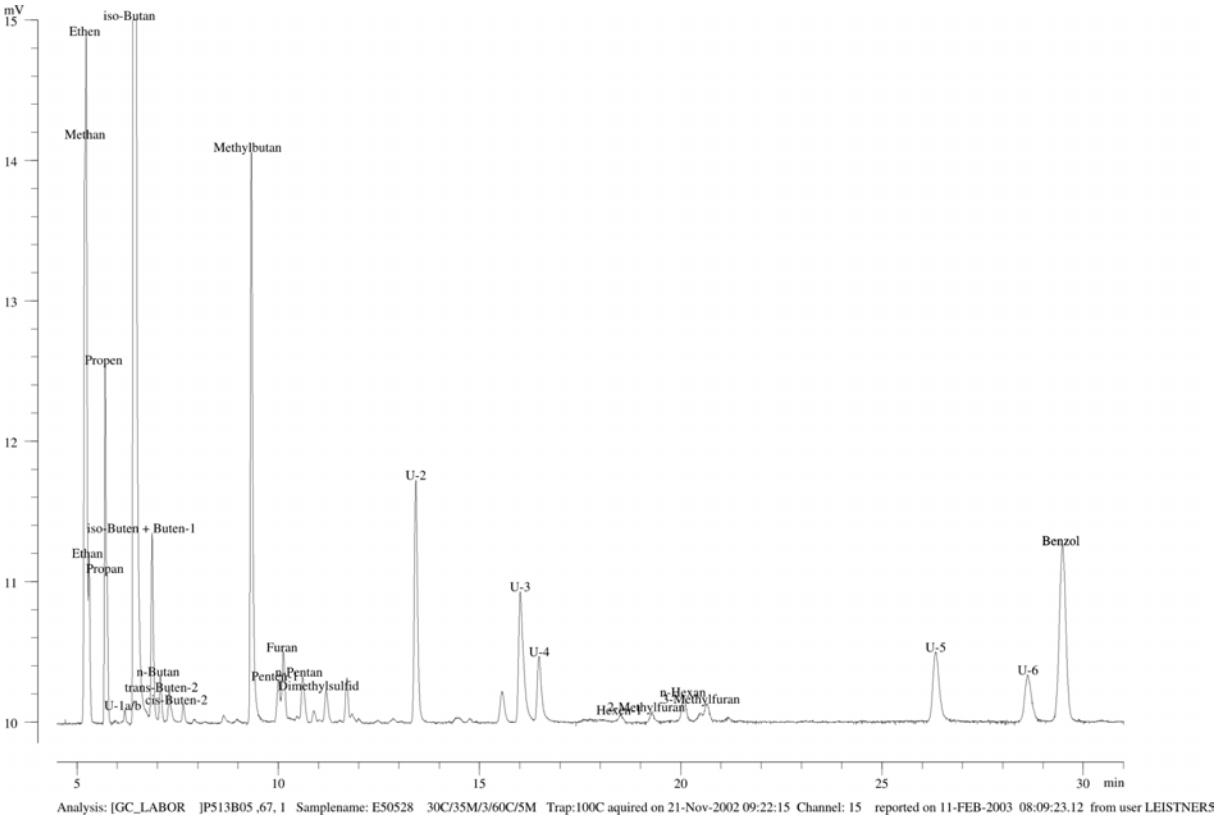
mV
15
14
13
12
11
10
iso-Butan
Ethen
Methan
Methylbutan
Propen
U-2
iso-Buten + Buten-1
Ethan
Propan
Benzol
U-3
U-4
U-5
U-6
Furan
n-Butan
trans-Buten-2
U-1a/b
cis-Buten-2
n-Pentan
Penten-1
Dimethylsulfid
n-Hexan
5
10
15
20
25
30
min
Analysis: [GC_LABOR]P513B05 ,67, 1 Samplename: E50528 30C/35M/3/60C/5M Trap:100C aquired on 21-Nov-2002 09:22:15 Channel: 15 reported on 11-FEB-2003 08:09:23.12 from user LEISTNER5

German	Englisch (IUPAC)
Methan	methane
Ethen	ethene
Ethan	ethane
Propen	propene
Propan	propane
U-1a/b	
iso-Butan	methylpropane
iso-Buten + Buten-1	methylpropene +1-butene
n-Butan	n-butane
trans-Buten-2	trans-2-butene
cis-Buten-2	cis-2-butene
Methylbutan	methylbutane
Penten-1	1-pentene
Furan	furane
n-Pentan	n-pentane
Dimethylsulfid	dimethylsulphide
U-2	
U-3	
U-4	
Hexen-1	1-hexene
2-Methylfuran	2-methylfurane
n-Hexan	n-hexane
3-Methylfuran	3-methylfurane
U-5	
U-6	
Benzol	benzene